



**HAL**  
open science

# Transmission of Alzheimer pathology in murine and primate models: from proteinopathies to neuronal and cognitive impairments

Suzanne Lam

► **To cite this version:**

Suzanne Lam. Transmission of Alzheimer pathology in murine and primate models: from proteinopathies to neuronal and cognitive impairments. Neuroscience. Université Paris-Saclay, 2021. English. NNT: 2021UPASL063 . tel-03656231

**HAL Id: tel-03656231**

**<https://theses.hal.science/tel-03656231>**

Submitted on 2 May 2022

**HAL** is a multi-disciplinary open access archive for the deposit and dissemination of scientific research documents, whether they are published or not. The documents may come from teaching and research institutions in France or abroad, or from public or private research centers.

L'archive ouverte pluridisciplinaire **HAL**, est destinée au dépôt et à la diffusion de documents scientifiques de niveau recherche, publiés ou non, émanant des établissements d'enseignement et de recherche français ou étrangers, des laboratoires publics ou privés.

Transmission de la pathologie Alzheimer à des  
modèles murins et primates :  
des protéinopathies aux atteintes neuronales et  
cognitives

*Transmission of Alzheimer pathology in murine and  
primate models: from proteinopathies to neuronal and  
cognitive impairments*

**Thèse de doctorat de l'université Paris-Saclay**

École doctorale n°568

Signalisations et réseaux intégratifs en biologie (BIOSIGNE)

Spécialité de doctorat : Sciences de la vie et de la santé

Université Paris-Saclay, CEA, CNRS, Molecular Imaging Research Center

Laboratoire des Maladies Neurodégénératives

92265, Fontenay-aux-Roses, France

Faculté de Médecine

**Thèse présentée et soutenue à Paris-Saclay,  
le 06/10/2021, par**

**Suzanne LAM**

**Composition du Jury**

**Michel BOTTLAENDER**

Directeur de recherche, CEA Paris-Saclay

Président

**Sylvie CLAEYSEN**

Directrice de recherche, INSERM, Université de Montpellier

Rapporteur & Examinatrice

**Nicolas SERGEANT**

Directeur de recherche, INSERM, Université de Lille

Rapporteur & Examineur

**Claire PAQUET**

Professeure, Praticien hospitalier, Université Paris-Diderot

Examinatrice

**Direction de la thèse**

**Marc DHENAIN**

Directeur de recherche, CNRS, CEA Paris-Saclay

Directeur de thèse

**Jean-Luc PICQ**

Professeur des Universités, Université Paris 8

Co-Directeur de thèse



## ACKNOWLEDGMENTS

---

Je tiens à remercier les membres du jury Michel Bottlaender, Sylvie Claeysen, Nicolas Sergeant et Claire Paquet pour avoir accepté d'examiner mon travail de thèse. En particulier, je remercie Sylvie Claeysen et Nicolas Sergeant pour leur rôle de rapporteur.

Merci également à la Fondation pour la recherche médicale pour son soutien financier m'ayant permis de poursuivre mon travail de thèse pendant une année supplémentaire.

Je remercie aussi Philippe Hantraye, Romina Aron-Badin, Emmanuel Brouillet et Gilles Bonvento pour leur accueil au sein de MIRCen et du Laboratoire des maladies neurodégénératives.

Un grand merci à Marc Dhenain, mon directeur de thèse, et à Jean-Luc Picq, mon co-directeur de thèse, pour leur confiance et leur encadrement durant ces quatre années. Merci aussi à toute l'équipe, en particulier à Anne-Sophie Hérard et Fanny Petit dont l'aide et les nombreux conseils m'ont été plus que précieux. Merci aussi à tous les collaborateurs de l'Institut du Cerveau et du Centre de Recherche Lille Neurosciences & Cognition pour leur aide et leur contribution au projet.

Enfin, merci à tous les membres de MIRCen pour leur bienveillance et leur bonne humeur.



# TABLE OF CONTENTS

---

<b>ABBREVIATIONS.....</b>	<b>7</b>
<b>LIST OF FIGURES.....</b>	<b>9</b>
<b>LIST OF TABLES.....</b>	<b>11</b>
<b>INTRODUCTION .....</b>	<b>13</b>
<b>1. Alzheimer’s disease .....</b>	<b>15</b>
<b>1.1. Epidemiology .....</b>	<b>15</b>
<b>1.2. Etiology and risk factors .....</b>	<b>16</b>
1.2.1. Genetic factors.....	16
1.2.2. Vascular factors.....	18
1.2.3. Psychosocial factors .....	18
<b>1.3. Clinical signs.....</b>	<b>19</b>
1.3.1. Memory impairment.....	19
1.3.2. Instrumental, executive and attention deficits .....	20
1.3.3. Behavioral and psychiatric changes.....	20
<b>1.4. AD diagnosis .....</b>	<b>20</b>
1.4.1. Clinical diagnosis .....	21
1.4.2. Neuropathological diagnosis .....	23
<b>1.5. AD biomarkers .....</b>	<b>27</b>
1.5.1. Amyloid biomarkers .....	30
1.5.2. Tau biomarkers .....	31
1.5.3. Neurodegeneration biomarkers .....	33
<b>1.6. AD therapeutic management.....</b>	<b>35</b>
1.6.1. Current symptomatic treatments .....	35
1.6.2. Promising disease-modifying treatments.....	36
<b>1.7. Pathophysiology .....</b>	<b>38</b>
1.7.1. Amyloidosis .....	38
1.7.2. Tauopathy .....	46
1.7.3. Neuroinflammation.....	52
1.7.4. Synaptopathy .....	60

1.7.5. Neurodegeneration.....	67
<b>1.8. Animal models of AD.....</b>	<b>68</b>
1.8.1. Transgenic models .....	68
1.8.2. Spontaneous models.....	72
1.8.3. The gray mouse lemur: an emerging model of AD pathology.....	77
<b>2. Sporadic AD heterogeneity.....</b>	<b>85</b>
<b>2.1. Clinical subtypes of AD .....</b>	<b>85</b>
2.1.1. Pure amnesic temporal AD .....	85
2.1.2. Posterior cortical atrophy .....	86
2.1.3. Logopenic primary progressive aphasia .....	86
2.1.4. Frontal AD variant .....	86
<b>2.2. Atrophy-defined subtypes of AD.....</b>	<b>87</b>
2.2.1. Limbic-predominant.....	88
2.2.2. Hippocampal sparing .....	89
2.2.3. Minimal brain atrophy .....	89
<b>2.3. Rapidly progressive AD.....</b>	<b>90</b>
2.3.1. Clinical presentation .....	90
2.3.2. Predictors of disease progression rate .....	91
2.3.3. Biomarker profile .....	92
2.3.4. Neuropathology .....	92
<b>3. Prion diseases .....</b>	<b>95</b>
<b>3.1. Epidemiology and etiology of human prion diseases.....</b>	<b>95</b>
3.1.1. Sporadic prion diseases .....	95
3.1.2. Genetic prion diseases .....	95
3.1.3. Acquired prion diseases.....	96
<b>3.2. Clinical phenotypes and diagnosis .....</b>	<b>96</b>
3.2.1. Sporadic CJD.....	96
3.2.2. Genetic prion diseases .....	97
3.2.3. Acquired prion diseases .....	97
<b>3.3. Neuropathology.....</b>	<b>97</b>
<b>3.4. Physiopathology .....</b>	<b>97</b>
3.4.1. PrP <sup>C</sup> and its physiological functions .....	97

3.4.2. Pathological prion PrP <sup>Sc</sup> properties.....	98
<b>4. Prion-like hypothesis of AD .....</b>	<b>101</b>
<b>4.1. Structural properties of amyloids .....</b>	<b>101</b>
<b>4.2. Stability and resistance to inactivation .....</b>	<b>101</b>
<b>4.3. Self-propagation through seeding.....</b>	<b>102</b>
<b>4.4. Seeding experiments .....</b>	<b>104</b>
4.4.1. Nature of the seeding agents.....	104
4.4.2. Impact of the host.....	112
4.4.3. Impact of local environment.....	116
4.4.4. A $\beta$ and tau cross-seeding.....	117
4.4.5. Functional impacts of A $\beta$ and tau seeding.....	118
<b>4.5. Spreading.....</b>	<b>119</b>
4.5.1. A $\beta$ .....	119
4.5.2. Tau.....	122
<b>4.6. Strains.....</b>	<b>126</b>
4.6.1. A $\beta$ .....	127
4.6.2. Tau.....	129
<b>4.7. Infectivity.....</b>	<b>131</b>
<b>OBJECTIVES.....</b>	<b>137</b>
<b>RESULTS .....</b>	<b>141</b>
<b>1. Relationships between cognitive, synaptic and neuropathological changes in AD brain-inoculated mice.....</b>	<b>143</b>
<b>1.1. Context, objectives &amp; abstract.....</b>	<b>143</b>
<b>1.2. Article .....</b>	<b>144</b>
<b>1.3. Complementary data.....</b>	<b>204</b>
1.3.1. Distinct neuroanatomical pathways are affected by tau pathology following AD brain extracts inoculation .....	204
1.3.2. Cognitive alterations cannot solely be explained by a dose effect .....	207
1.3.3. Characterization of A $\beta$ pathology in rpAD and clAD patients .....	208
<b>2. Encephalopathy induced by AD brain inoculation in a non-human primate .....</b>	<b>211</b>
<b>2.1. Context, objectives &amp; abstract.....</b>	<b>211</b>
<b>2.2. Article .....</b>	<b>212</b>



3.	<b>Transmission of A<math>\beta</math> and tau pathologies is associated with cognitive impairments in a primate</b> .....	<b>253</b>
3.1.	<b>Context, objectives &amp; abstract</b> .....	<b>253</b>
3.2.	<b>Article</b> .....	<b>254</b>
	<b>DISCUSSION</b> .....	<b>287</b>
1.	<b>The APP/PS1dE9 mouse model</b> .....	<b>289</b>
1.1.	<b>Transmission of AD-like neuropathological lesions after AD brain extract inoculation</b> .....	<b>290</b>
1.1.1.	A $\beta$ and tau pathologies.....	290
1.1.2.	Neuroinflammation.....	291
1.2.	<b>Transmission of heterogeneous cognitive and synaptic profiles after the inoculation of different AD brain extracts</b> .....	<b>292</b>
1.2.1.	Alteration of specific cognitive functions.....	292
1.2.2.	Synaptic alterations.....	293
1.3.	<b>Relationships between neuropathological lesions</b> .....	<b>294</b>
1.4.	<b>Mechanistic hypothesis for heterogeneous phenotypes</b> .....	<b>295</b>
2.	<b>The mouse lemur primate model</b> .....	<b>298</b>
2.1.	<b>First transmission of an AD-like phenotype in a primate</b> .....	<b>298</b>
2.1.1.	A $\beta$ and tau pathologies.....	298
2.1.2.	Neuroinflammation.....	301
2.1.3.	Cognitive impairments.....	301
2.1.4.	Morphological and neuronal alterations.....	302
2.2.	<b>Relationships between induced pathological hallmarks</b> .....	<b>303</b>
2.3.	<b>Implications for human pathology</b> .....	<b>304</b>
	<b>CONCLUSION &amp; PERSPECTIVES</b> .....	<b>307</b>
	<b>REFERENCES</b> .....	<b>311</b>
	<b>ANNEXES</b> .....	<b>359</b>
	Annex I - Additional publication.....	373
	Annex II - Scientific production.....	373
	Annex III - Abstract.....	374

## ABBREVIATIONS

---

AD: Alzheimer's disease  
AICD: APP intracellular domain  
AMPA:  $\alpha$ -amino-3-hydroxy-5-methylisoxazole-4-propionic acid  
APOE: apolipoprotein E  
APP: amyloid protein precursor  
A $\beta$ :  $\beta$ -amyloid peptide  
BDNF: brain-derived neurotrophic factor  
CAA: cerebral amyloid angiopathy  
CBD: corticobasal degeneration  
CERAD: consortium to establish a registry for Alzheimer's disease  
clAD: classical form of Alzheimer's disease  
CNS: central nervous system  
CSF: cerebrospinal fluid  
CTF: C-terminal membrane fragment  
DAMP: danger-associated molecular pattern  
DMN: default-mode network  
fAD: familial Alzheimer's disease  
FDA: Food and Drug Administration  
FDG: fluorodeoxyglucose  
FTD: frontotemporal dementia  
GWAS: genome-wide association studies  
IL: interleukin  
LRP1: low-density lipoprotein receptor-related protein 1  
LTD: long-term depression  
LTP: long-term potentiation  
MAPT: microtubule-associated protein tau  
MCI: mild-cognitive impairment  
MMSE: mini mental state examination  
mpi: months post-inoculation

MRI: magnetic resonance imaging

MTBD: microtubule-binding domain

NDAN: non-demented individual with AD neuropathology

NfL: neurofilament light chain

NFT: neurofibrillary tangle

NINCDS-ADRDA: National Institute of Neurological and Communicative Diseases and Stroke – Alzheimer's Disease and Related Disorders Association

NLRP3: NOD-, LRR- and pyrin domain- containing 3

NMDA: N-methyl-D-aspartate

NMR: nuclear magnetic resonance

NT: neuropil thread

PART: primary age-related tauopathy

PET: positron emission tomography

PHF: paired-helical filaments

PiB: Pittsburg compound B

PRD: proline-rich domain

PRNP: prion protein gene

PrP<sup>c</sup>: cellular protease-resistant prion protein

PSEN: presenilin

PSP: progressive supranuclear palsy

RAGE: receptor for advanced glycation end product

ROI: region of interest

ROS: reactive oxygen species

rpAD: rapidly evolving form of Alzheimer's disease

SF: straight filaments

SNAP: suspected non-Alzheimer's pathophysiology

SUVR: standardized uptake value ratio

TDP-43: TAR-DNA-binding protein 43

TNF $\alpha$ : tumor necrosis factor  $\alpha$

TREM2: triggering receptor expressed on myeloid cells 2

# LIST OF FIGURES

---

<b>Figure 1:</b> Genetic landscape of Alzheimer’s disease .....	16
<b>Figure 2:</b> Alzheimer’s disease continuum .....	21
<b>Figure 3:</b> Thal phases for amyloid plaque deposition pattern .....	24
<b>Figure 4:</b> Braak stages for tau deposition pattern .....	25
<b>Figure 5:</b> Model of Alzheimer’s disease biomarker temporal evolution .....	28
<b>Figure 6:</b> Model depicting the evolution of tau and A $\beta$ depositions in AD .....	29
<b>Figure 7:</b> Association between <sup>11</sup> C-labeled PiB and Thal phases across the AD spectrum .....	30
<b>Figure 8:</b> Fluor 18 labeled-MK-6240 binding patterns in PiB-positive patients recapitulates the neuropathological staging of NFTs.....	32
<b>Figure 9:</b> Gray matter atrophy according to AD pathological progression.....	33
<b>Figure 10:</b> APP metabolism through the non-amyloidogenic and amyloidogenic pathways..	39
<b>Figure 11:</b> A $\beta$ deposits in AD brains .....	41
<b>Figure 12:</b> Cerebral amyloid angiopathy .....	42
<b>Figure 13:</b> The amyloid cascade hypothesis .....	45
<b>Figure 14:</b> Tau isoforms in the human brain.....	46
<b>Figure 15:</b> Tau deposits in AD brains.....	50
<b>Figure 16:</b> Reactive glia is associated with A $\beta$ plaques and NFTs in AD .....	52
<b>Figure 17:</b> Microglial morphological changes upon activation .....	53
<b>Figure 18:</b> Amyloid plaque deposition spontaneously occurs in fAD-mutant huAPP mice but not in huAPP <sub>wt</sub> mice. ....	69
<b>Figure 19 :</b> The gray mouse lemur ( <i>Microcebus murinus</i> ) .....	76
<b>Figure 20:</b> Cerebral atrophy in the aged mouse lemur .....	79
<b>Figure 21:</b> A $\beta$ deposition in aged mouse lemurs .....	80
<b>Figure 22:</b> Tau pathology in an aged mouse lemur .....	81
<b>Figure 23:</b> Amyloid-plaque associated glia in the mouse lemur brain .....	82
<b>Figure 24:</b> Atrophy-defined subtypes of AD .....	88
<b>Figure 25:</b> Comparison of disease duration between rpAD and clAD patients. ....	90
<b>Figure 26:</b> Amyloid fibril formation.....	103

<b>Figure 27:</b> Kinetics of the amyloid seeding process with and without exposure to preformed seeds.....	104
<b>Figure 28:</b> Development of A $\beta$ and tau pathologies in transgenic mice following AD brain inoculation.....	105
<b>Figure 29:</b> A $\beta$ deposition in the brain of AD, MCI, NDAN and aged control individuals and APP/PS1dE9 mice inoculated with these extracts .....	106
<b>Figure 30:</b> Tau deposition in the brain of AD, CBD and PSP patients and non-transgenic mice inoculated with these extracts.....	107
<b>Figure 31:</b> Brain extracts from transgenic mouse models induce A $\beta$ and tau pathologies following inoculation in mice .....	108
<b>Figure 32:</b> Dose-dependent acceleration of A $\beta$ and tau pathologies .....	109
<b>Figure 33:</b> A $\beta$ seeding-ability of brain extracts is abolished after formic acid treatment and immunodepletion.....	110
<b>Figure 34:</b> Synthetic A $\beta$ and tau can potently induce pathologies .....	111
<b>Figure 35:</b> A $\beta$ and tau pathologies in NHPs following AD brain inoculation .....	113
<b>Figure 36:</b> <i>De novo</i> induction of A $\beta$ and tau pathologies .....	114
<b>Figure 37:</b> Differences in A $\beta$ deposition following brain extracts inoculation in different brain regions of APP23 mice.....	116
<b>Figure 38:</b> Spatiotemporal spreading of A $\beta$ pathology along neuroanatomical pathways... ..	120
<b>Figure 39:</b> Spatiotemporal spreading of tau pathology to interconnected regions.....	123
<b>Figure 40:</b> Potential mechanisms underlying tau transcellular spreading .....	126
<b>Figure 41:</b> Distinct rates of disease progression and vascular deposits associated with various A $\beta$ strains.....	128
<b>Figure 42:</b> Distinct regional vulnerabilities and spreading rates associated with various tau strains .....	130
<b>Figure 43:</b> Iatrogenic A $\beta$ transmission associated with tau pathology in humans .....	133
<b>Figure 44:</b> Context-free and context-rich memory pathways .....	204
<b>Figure 45:</b> Quantification of tau pathology in context-free and context-rich memory pathways .....	206
<b>Figure 46:</b> Novel object recognition performances following the inoculation of Ctrl or AD brain extracts with normalized phospho-tau181 levels.....	207
<b>Figure 47:</b> Characterization of A $\beta$ deposition in rpAD and cIAD patients.....	209

## LIST OF TABLES

---

<b>Table 1:</b> ABC scores for AD neuropathological changes .....	26
<b>Table 2:</b> Overview of ATN biomarkers .....	27
<b>Table 3:</b> Reported cases of A $\beta$ iatrogenic transmission in humans, with or without tau pathology.....	135



# **INTRODUCTION**





# 1. Alzheimer's disease

---

Alzheimer's disease (AD) is a progressive neurodegenerative disorder and the most common form of dementia worldwide. The vast majority of AD cases are characterized by a late-onset, affecting people over 65 years old. Its etiology remains unclear but increasing evidence strongly points to the role of multiple risk factors in the development of the disease.

AD patients progressively develop cognitive alterations including memory loss as well as behavioral and psychiatric symptoms that ultimately affect their quality of life. Additionally, their gradual loss of autonomy results in a greater dependence on caregivers and high economic costs to society.

The definitive diagnosis of AD is based on the association between clinical signs evoking an AD-type dementia and typical neuropathological changes occurring in the brain. These include extracellular amyloid plaques and intracellular neurofibrillary tangles, respectively resulting from  $\beta$ -amyloid peptides and tau proteins misfolding and abnormal aggregation. Neuroinflammatory and neurodegenerative processes also characterize AD pathology.

To this day, most available treatments are symptomatic and used to temporarily improve cognitive functions without slowing the progression of the disease ("2021 Alzheimer's disease facts and figures," 2021). Recently in 2021, the first monoclonal antibody directed against A $\beta$  aggregates has been approved by the Food and Drug Administration (FDA) although its benefits remain limited (Cavazzoni, 2021).

To address this major public health challenge, several animal models have been developed over the last decades in an attempt to better characterize AD pathology.

## 1.1. Epidemiology

AD is a major public health issue of the 21<sup>st</sup> century with devastating impacts on individuals, caregivers and societies. It is the commonest cause of dementia among the elderly, accounting for an estimated 60% to 80% of all cases. In 2021, AD was reported to affect 44 million people worldwide, including 1.1 million individuals in France ("2021 Alzheimer's disease facts and figures," 2021; Dumurgier and Sabia, 2020). As life expectancy increases and the population

## 1. Alzheimer's disease

ages, these numbers are expected to double by 2050 (Hebert et al., 2001). Indeed, both AD prevalence and incidence increase dramatically with age, rising respectively from 5.3% and 0.4% among 65 to 74 years old, to 34.6% and 7.6% among people age 85 and older ("2021 Alzheimer's disease facts and figures," 2021).

### 1.2. Etiology and risk factors

AD is a multifactorial disorder which greatest risk factor is age. Although its etiology remains unclear, it is likely driven by a complex interplay between genetic, biological and psychosocial factors across the lifespan.

#### 1.2.1. Genetic factors

Several genetic factors have been identified, but only a small proportion of AD cases can directly be attributed to specific gene mutations. In most cases, it is assumed that multiple risk factors act in concert to increase the risk for AD (Figure 1).

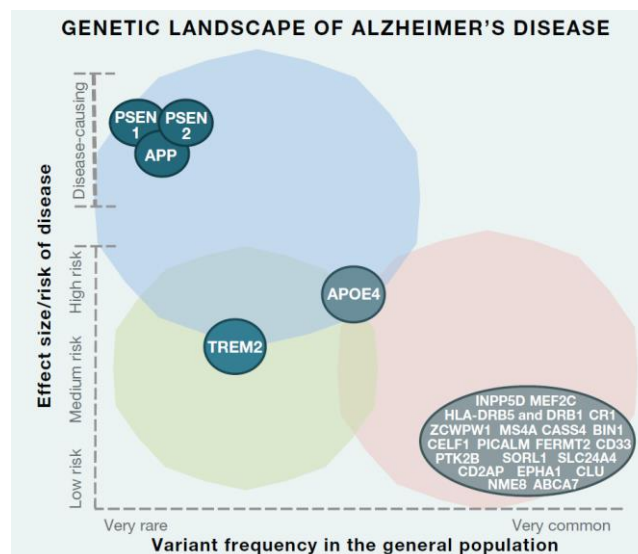


**Figure 1: Genetic landscape of Alzheimer's disease**

Familial AD-associated genes, including disease causing mutations in amyloid precursor protein (APP), presenilin 1 (PSEN1) and presenilin 2 (PSEN2) and high risk factor APOE $\epsilon$ 4 are represented in the blue area. Common variants with low risk for AD are presented in the orange area. The first rare variant with intermediate risk for AD, *i.e.* triggering receptor expressed on myeloid cells 2 (TREM2), is shown in the green area (Guerreiro et al., 2013).

### 1.2.1.1. Familial AD

Early-onset familial AD (fAD) represents 2 to 5% of all AD cases (Blennow et al., 2006). fAD cases are caused by rare autosomal dominant mutations in the amyloid precursor protein (APP), presenilin 1 (PSEN1) or presenilin 2 (PSEN2) genes involved in  $\beta$ -amyloid ( $A\beta$ ) metabolism (Mayeux, 2003). These mutations have a high penetrance and result in an increase in  $A\beta_{42}$  relative levels, promoting its aggregation and leading to the early-onset of AD, typically between the ages of 30 and 60 (Hardy and Selkoe, 2002; Mayeux and Stern, 2012).

### 1.2.1.2. Susceptibility genes

The vast majority of AD cases occur on an apparently sporadic basis and are characterized by a late-onset, as they usually occur after 65 years old. Despite the absence of identified mutations directly causing the disease, family history is a well-established risk factor for sporadic AD. Indeed, heritability has been evaluated at approximately 80% (Gatz et al., 2006) and first-degree relatives of AD patients have a greater risk to develop AD dementia than the general population (Green 2002). Additionally, genome-wide association studies (GWAS) have identified many susceptibility genes and highlighted the importance of genetic polymorphism in the development of AD. Among them, the apolipoprotein E (APOE) and the microglia-associated triggering receptor expressed on myeloid cells 2 (TREM2) genes show the highest risk for AD (**Figure 1**) (Guerreiro et al., 2013).

#### *1.2.1.2.1. Apolipoprotein E gene (APOE)*

The APOE gene is the most important susceptibility gene and was shown to influence both late-onset sporadic AD and early-onset fAD (Kunkle et al., 2019; Pastor et al., 2003). Polymorphism in the APOE gene results in three allelic variants ( $\epsilon 2$ ,  $\epsilon 3$  and  $\epsilon 4$ ), each one associated with specific impacts on  $A\beta$  metabolism, accumulation and clearance in the brain and cerebrovasculature (Verghese et al., 2011). Additionally, the ApoE protein is involved in lipid homeostasis, notably by acting as a cholesterol transporter in the brain, as well as in synaptic activity, neuroinflammation and response to neuronal injury (Verghese et al., 2011). In the general population, the  $\epsilon 3$  allele is the most frequent. In contrast, it is estimated that around 80% of familial and 65% of sporadic late-onset AD patients carry the  $\epsilon 4$  allele, compared to 30% of control subjects (Corder et al., 1993; Verghese et al., 2011). The  $\epsilon 4$  allele

## 1. Alzheimer's disease

---

increases the risk for AD by three-fold in heterozygotes and twelve-fold in homozygotes (Holtzman et al., 2012), as opposed to the  $\epsilon 2$  allele which is associated with a decreased risk. Moreover, each copy of the  $\epsilon 4$  allele reduces the age of AD onset by nearly 10 years (Corder et al., 1993). Overall, approximately 15-20% of AD cases are attributable to the  $\epsilon 4$  allele (Qiu et al., 2004).

### *1.2.1.2.2. Triggering receptor expressed on myeloid cells 2 (TREM2)*

More than 30 AD risk loci have been identified and over 50% of them have been implicated in microglial and innate immune cell function (Shi and Holtzman, 2018). Particularly, rare variants in the TREM2 gene have been identified as important risk factors for AD (Colonna and Butovsky, 2017). The R47H loss-of-function mutation is the most clearly associated with AD and increases the risk for AD by approximately three-fold (Jonsson et al., 2013). Interestingly, it has been suggested that this mutant likely impairs TREM2-mediated microglial function by altering A $\beta$  peptide phagocytosis, clearance and plaque compaction (Dourlen et al., 2019).

### **1.2.2. Vascular factors**

The vascular hypothesis of AD is supported by strong evidence from epidemiologic, neuroimaging and neuropathological studies. Cerebrovascular diseases, such as stroke, increase the risk of dementia by two-fold and have been associated with the occurrence of cognitive impairment, possibly resulting from the destruction of brain parenchyma, hypoperfusion and A $\beta$  accumulation (Honig et al., 2003; Mayeux and Stern, 2012). Furthermore, cardiovascular comorbidities at midlife including hypercholesterolemia and uncontrolled hypertension, as well as obesity and tobacco use also increase the risk of dementia in later life (Kivipelto et al., 2001; Whitmer et al., 2005). Similarly, type 2 diabetes increases the risk of developing AD by two-fold (Mayeux and Stern, 2012).

### **1.2.3. Psychosocial factors**

Psychosocial factors have also been associated with the risk of developing AD dementia. Evidence suggests that higher education, social engagement, mental and physical activities in late life could have a protective effect against dementia (Fratiglioni et al., 2004; Stern, 2006). Interestingly, neuroimaging studies have shown that a greater participation in cognitively

stimulating activities across the lifespan is correlated with a decrease in hippocampal atrophy rate (Valenzuela et al., 2008) and reduced A $\beta$  plaque deposition (Landau et al., 2012).

The reserve hypothesis has emerged from these associations and posits that psychosocial factors can participate in enhancing an individual's cognitive reserve. As opposed to brain reserve which reflects brain anatomy (*i.e.* the number of neurons and synapses), cognitive reserve is an indicator of brain function that encompasses the notions of neural reserve (*i.e.* the susceptibility of brain networks to disruption) and neural compensation (*i.e.* brain plasticity and ability to activate alternative networks to compensate disrupted ones) (Stern, 2009, 2002). Accordingly, similar amounts of brain pathology should not have the same effects on different individuals, as the ones with a higher cognitive reserve can more effectively cope with brain pathological changes (Stern, 2012). Higher cognitive reserve has indeed been associated with a 46% risk reduction of developing dementia (Stern, 2012) and recent evidence suggest that it also attenuates the risk of dementia in APOE $\epsilon$ 4 carriers (Dekhtyar et al., 2019). However, once AD first symptoms appear, patients with high cognitive reserve show a more rapid decline suggesting that in these individuals, clinical manifestations emerge at a more advanced stage of the disease (Stern et al., 1999).

### **1.3. Clinical signs**

AD is characterized by an insidious onset and a progressive impairment of cognitive functions disrupting daily life activities and resulting in a complete loss of autonomy. AD cardinal symptoms typically include memory loss, alterations in instrumental and executive functions, attention deficits as well as behavioral and psychological changes. However, AD is clinically heterogeneous and atypical presentations can also emerge from its various subtypes (see § 2. **Sporadic AD heterogeneity**).

#### **1.3.1. Memory impairment**

Memory impairment is the earliest and most common sign of AD. Memory can be divided into short-term memory, associated with working memory, and long-term memory. The latter is composed of:

## 1. Alzheimer's disease

---

- Non-declarative or implicit memory, including procedural memory associated with unconsciously acquired and automatically retrieved information to perform learned cognitive and motor skills;
- Declarative or explicit memory, associated with the conscious storage and recollection of information that can be expressed verbally. It encompasses semantic memory, *i.e.* general knowledge such as facts and theoretical concepts, and episodic memory, *i.e.* personal experiences associated to a specific spatiotemporal context.

In AD, working and episodic memory are typically disrupted at early stages as patients show difficulties in learning new information (Jahn, 2013).

### **1.3.2. Instrumental, executive and attention deficits**

Alterations in instrumental functions characterize AD patients who gradually develop language impairment (aphasia), alterations in voluntary motor skills (apraxia) and perception deficits (agnosia). Executive dysfunction moreover manifests with challenges in planning, decision-making, problem-solving and impaired judgment. Additionally, patients also display spatial and temporal disorientation ("2021 Alzheimer's disease facts and figures," 2021; Blennow et al., 2006).

### **1.3.3. Behavioral and psychiatric changes**

Behavioral modifications typically occur in AD patients. They can manifest early in the disease and include changes in mood and personality, depression and apathy. Furthermore, patients may become agitated, aggressive and psychotic with signs of delusions and hallucinations as the disease progresses (Li et al., 2014).

## **1.4. AD diagnosis**

As pathological changes occur in the brain prior to clinical manifestations, the most recent diagnostic criteria include preclinical phases of AD and are based on biomarker evaluation along with clinical, neurological and psychiatric examination. Nonetheless, the definitive diagnosis of AD is based on the association between clinical signs evoking AD-related

dementia and typical neuropathological changes observed in the postmortem brain (McKhann et al., 2011).

### 1.4.1. Clinical diagnosis

#### 1.4.1.1. AD continuum

The spectrum of AD spans from the appearance of asymptomatic brain changes to dementia and symptoms interfering with daily life. AD continuum is divided into three main phases: preclinical AD characterized by biomarker-positive changes without symptom occurrence, mild cognitive impairment (MCI) characterized by subtle cognitive changes that do not interfere with everyday activities and AD dementia which can be qualified as mild, moderate or severe depending on the impact of the symptoms on everyday activities (**Figure 2**). The rate of conversion from one stage to another highly varies between individuals and is influenced by many risk factors, including age, genetics and biologics (“2021 Alzheimer’s disease facts and figures,” 2021). However, it is worth mentioning that not all patients presenting with AD-related brain changes go on to develop AD, nor do all MCI patients convert to dementia. Interestingly, it has been estimated that approximately 15% of MCI individuals develop dementia within two years and 32% within five years (“2021 Alzheimer’s disease facts and figures,” 2021).

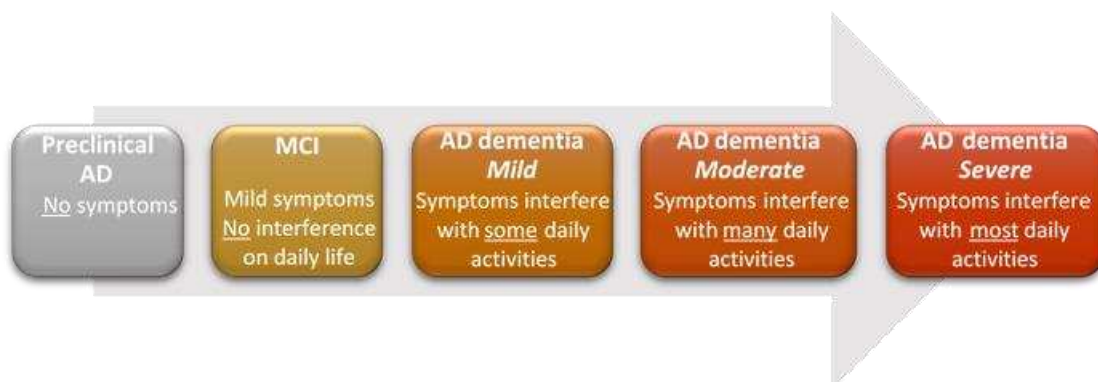


**Figure 2: Alzheimer’s disease continuum**

AD continuum is divided into three main phases: preclinical AD characterized by biomarker-positive changes without symptom occurrence, mild cognitive impairment (MCI) associated with mild cognitive changes without interference on daily life and AD dementia, qualified as mild, moderate or severe, according to the severity of symptom interference on everyday activities. Adapted from (“2021 Alzheimer’s disease facts and figures,” 2021).



### 1.4.1.2. Clinical criteria

AD clinical diagnosis relies on the interview of the patient and their relatives as well as clinical and physical examination. Standardized neuropsychological tests including the Mini-Mental State Examination (Folstein et al., 1975) and the Clinical Dementia Rating (Hughes et al., 1982) are routinely used to assess cognitive decline.

#### *1.4.1.2.1. Criteria for a dementia syndrome*

The diagnosis of dementia is based on the National Institute of Neurological and Communicative Diseases and Stroke – Alzheimer's Disease and Related Disorders Association (NINCDS-ADRDA) criteria revised in 2011 (McKhann et al., 2011) and the Diagnostic and Statistical Manual of Mental Disorders (DSM-V) criteria. It can be made in the presence of cognitive or behavioral symptoms that interfere with daily life and lead to a decline in comparison with previous performances. Additionally, cognitive deficits should not be better explained by other mental disorders (American Psychiatric Association, 2013; McKhann et al., 2011).

According to the 2011 NINCDS-ADRDA criteria, cognitive impairment should involve at least two of the following symptoms: difficulty in learning or remembering new information, executive dysfunction such as impaired reasoning or poor judgment, visuospatial or language deficits, changes in mood or personality (McKhann et al., 2011). In comparison, the DSM-V posits that dementia, also referred to as major neurocognitive disorder, is characterized by a significant cognitive decline affecting one or more cognitive domains including learning and memory, language, executive function, complex attention, perceptual-motor or social cognition (American Psychiatric Association, 2013).

As opposed to dementia, MCI is characterized by very mild cognitive symptoms such as subtle alterations in memory and thinking, without a significant impact on everyday life.

#### *1.4.1.2.2. Criteria of AD-related dementia*

The diagnosis of AD-related dementia can be made with different levels of certainty ranging from definitive to probable and possible AD. The definitive diagnosis of AD dementia relies on the presence of both AD clinical dementia and AD core lesions observed in the postmortem brain (see § 1.4.2. Neuropathological diagnosis). Probable AD dementia is associated with an

insidious onset and clear evidence of gradual worsening of cognitive functions. Possible AD dementia diagnosis should be made when the core clinical criteria for AD dementia are met but are associated with an atypical course of progression, insufficient documentation of progressive decline or evidence for mixed pathology (American Psychiatric Association, 2013; McKhann et al., 2011).

Additionally, blood tests and neuroimaging can be performed in the differential diagnosis to exclude alternative causes of dementia including Lewy body diseases, frontotemporal lobar degeneration (FTD), vascular and metabolic dementia and brain tumor (Lane et al., 2018).

### 1.4.1.3. Biomarker-based evaluation of AD neuropathological changes

Neuropathological changes associated with AD progression can be assessed *in vivo* using biomarkers that reflect amyloid pathology (A), tau burden (T) and neurodegeneration (N) (see § 1.5. AD biomarkers). AD preclinical stage is characterized by the presence of both amyloid and tau deposits (A+, T+, N-), while symptomatic stages appear as neurodegeneration begins (A+, T+, N+) (Jack et al., 2018). Using biomarkers, MCI or dementia can be attributed to underlying AD pathology with high, intermediate or low likelihood (Lane et al., 2018).

### 1.4.2. Neuropathological diagnosis

Postmortem brain neuropathological examination remains the gold standard for defining AD. According to the 2012 National Institute on Aging-Alzheimer's Association Guidelines, the definitive diagnosis of AD is based on the morphology, density and neuroanatomical distribution of amyloid plaques, neurofibrillary tangles (NFTs) and neuritic plaques observed through a variety of histological staining. Indeed AD is characterized by the highly stereotyped spreading of amyloid plaques and NFTs throughout the brain as described by Thal and Braak staging schemes, respectively. Together with the semiquantitative evaluation of neuritic plaques based on the Consortium to Establish a Registry for AD (CERAD) criteria, the level of AD neuropathological changes are summarized by an ABC scoring system that helps in the definite diagnosis of AD.

### 1.4.2.1. Thal phases

Amyloid plaques first appear in the neocortex (Thal phase 1), before expanding to the allocortex, including the entorhinal cortex, hippocampus and cingulate gyrus (Thal phase 2). In Thal phase 3, amyloid deposits reach the subcortical nuclei, including the striatum, the cholinergic nuclei of the basal forebrain as well as the thalamus and hypothalamus. The brainstem is affected in phase 4, including the substantia nigra, reticular formation, inferior and superior colliculi, while the cerebellum and the brainstem pons, including the raphe nuclei and locus coeruleus, begin to display A $\beta$  lesion during phase 5 (**Figure 3**) (Thal et al., 2015, 2002). Of note, cognitively unimpaired individuals can often manifest Thal 1-3 amyloid phases (DeTure and Dickson, 2019).

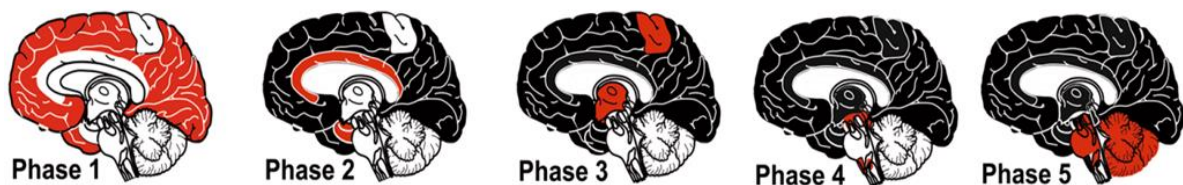


**Figure 3: Thal phases for amyloid plaque deposition pattern**

Thal phases are based on the progressive deposition of amyloid plaques in the neocortex (phase 1), the allocortex and limbic regions (phase 2), diencephalon and basal ganglia (phase 3), brainstem (phase 4) and cerebellum and brainstem pons (phase 5). Adapted from (Thal et al., 2015).

### 1.4.2.2. Braak stages

NFT and neuropil thread (NT) deposition begin in the transentorhinal cortex with lesions appearing in the perirhinal region (Braak stage I) and the entorhinal region (Braak stage II). In Braak stage III, ghost tangles begin to develop in the transentorhinal cortex whereas NFTs spread to the CA1 region of the hippocampus and the subiculum, as well as to the magnocellular nuclei of the basal forebrain and anterodorsal nucleus of the thalamus. In Braak stage IV, NFTs can be observed in the CA4 region of the hippocampus. The basolateral nuclei of the amygdala along with parts of the putamen and accumbens nucleus display both NFTs and NTs. Additionally, neuritic plaques (NP) appear in the corticomедial complex. In stage V, NTs and ghost tangles become more abundant in affected areas and NPs appear in CA1. The

isocortex and temporal lobes are involved, and most association cortices become affected by stage VI. The primary sensory cortex displays NTs and some NFTs, and the primary motor cortex mainly displays NPs in layer III. Moreover, the thalamic anteroventral and reticular nuclei, the hypothalamus, striatum and substantia nigra become involved (**Figure 4**) (Braak et al., 2006; Braak and Braak, 1991).

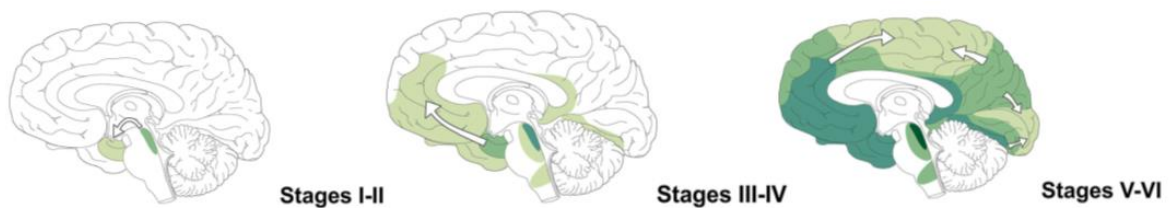


**Figure 4: Braak stages for tau deposition pattern**

Tau deposition begins in the transentorhinal cortex, affecting the perirhinal (stage I) and entorhinal regions (stage II). In Braak stage III, NFTs spread to the hippocampal formation, basal forebrain and thalamus. Braak stage IV is associated with the involvement of the amygdala, putamen and accumbens nucleus. In stage V, the isocortex and temporal lobes are involved and most association cortices become affected by stage VI. Adapted from (Goedert et al., 2014).

#### 1.4.2.3. Neuritic plaque CERAD score

Neuritic plaque frequency is determined using a semiquantitative scoring system elaborated by the Consortium to Establish a Registry for AD (CERAD). Four levels of neuritic plaque density are described in the CERAD standardized protocol: none, sparse, moderate and frequent.

Coupled with patient age and a clinical history of dementia, the CERAD score reflects the level of certainty regarding AD diagnosis, ranging from “no evidence of AD” to “possible AD”, “probable AD” and “definite AD” (Mirra et al., 1991).

#### 1.4.2.4. ABC scoring system

The ABC scoring system relies on the semiquantitative measures of AD neuropathological changes based on amyloid Thal phase (A), NFT Braak stage (B) and neuritic plaque CERAD score (C). The combination of A, B and C scores reflects the degree of AD-associated lesion changes that can range from no change to low, intermediate or high changes (**Table 1**) (Montine et al., 2012).

## 1. Alzheimer's disease

A A $\beta$ Thal phase	C Neuritic plaque CERAD score	B NFT Braak stage		
		0 or I-II	III-IV	V-VI
0	None	No		
1-2	None to sparse	Low		
	Moderate to frequent	Low	Intermediate	Intermediate
3	None to frequent			
4-5	None to sparse	Low	Intermediate	High
	Moderate to frequent			

**Table 1: ABC scores for AD neuropathological changes**

The assessment of AD neuropathological changes based on amyloid Thal phase (A), NFT Braak stage (B) and neuritic plaque CERAD score (C) results in an ABC score. This score reflects the degree of AD-associated lesion changes that can range from no change to low, intermediate or high changes (in grey). Adapted from (Montine et al., 2012).

It is worth mentioning that 20 to 40% of non-demented individuals display enough amyloid plaques and NFTs to validate a neuropathological diagnosis of AD (Blennow et al., 2006). In symptomatic patients, intermediate and high ABC scores provide an adequate explanation for cognitive impairment or dementia. However, the presence of comorbidities should also be evaluated as they could account for the clinical deficits (Montine et al., 2012). Indeed, mixed pathology defined as the co-occurrence of other neurodegenerative disorders (including Lewy bodies diseases, TAR-DNA-binding protein 43 (TDP-43) proteinopathies and argyrophilic grain disease) and/or non-degenerative pathologies (including cerebrovascular and metabolic diseases), is frequently observed in AD patients and can contribute to dementia (Rahimi and Kovacs, 2014). As a result, only one third of definite AD patients have pure Alzheimer pathology (Lim et al., 1999). Interestingly, brain regions affected by AD neuropathological changes are also vulnerable to the pathological deposition of other proteins such as  $\alpha$ -synuclein and TDP-43 (DeTure and Dickson, 2019). Around 70% of sporadic AD patients display  $\alpha$ -synuclein-positive lesions in the amygdala and limbic regions (Hamilton, 2000) and patients with fAD associated with mutations in presenilin genes develop increased levels of Lewy body pathologies (Leverenz et al., 2006; Snider et al., 2005).

## 1.5. AD biomarkers

A biomarker is defined as a quantifiable characteristic that can be used as an indicator of normal biological processes, pathogenic processes or response to an exposure or intervention (Califf, 2018). The association of various biomarkers assessed in biofluids, *e.g.* cerebrospinal fluid (CSF) and blood, or through imaging, can yield a highly sensitive and specific diagnostic tool for AD. Their clinical application is however still limited. They can be used to help for the diagnosis of unusual forms of AD (*e.g.* in young subjects) and are also used to enroll patients in clinical trials.

As AD pathology begins decades before symptom onset, a recent shift occurred in AD definition from a syndromal to a biological construct. AD is considered as a continuum and its progression can be evaluated in living patients using biomarkers reflecting its core lesions *e.g.* amyloid pathology (A), tau pathology burden (T) and neurodegeneration (N) (**Table 2**) (Jack et al., 2018).

	Biofluid biomarker	Imaging biomarker
<b>(A)</b> <b>Amyloid pathology</b>	- A $\beta$ <sub>42</sub> - A $\beta$ <sub>42</sub> /A $\beta$ <sub>40</sub> ratio	Amyloid PET
<b>(T)</b> <b>Tau pathology</b>	Phospho-tau	Tau PET
<b>(N)</b> <b>Neurodegeneration</b>	Total tau	- Anatomic MRI - FDG PET

**Table 2: Overview of ATN biomarkers**

AD pathological progression can be assessed *in vivo* using biofluid and imaging biomarkers of amyloid pathology (A), tau pathology (T) and neurodegeneration (N). Adapted from (Jack et al., 2018).

The ATN biomarker profile results from the binarization (normal – or abnormal +) of each of the three biomarker groups previously mentioned. Depending on their ATN profile, and independently of any clinical signs, patients can be categorized into three groups: individuals with normal AD biomarkers (A-T-N-), individuals in the AD continuum (any A+ profile, *e.g.* A+T-N-, A+T+N-, A+T+N+, A+T-N+) or as suspected non-Alzheimer's pathophysiology (SNAP) cases

## 1. Alzheimer's disease

(i.e. normal amyloid but abnormal tau and/or neurodegeneration A-T+N-, A-T-N+, A-T+N+) (Jack et al., 2018).

Many models of AD biomarker evolution have been proposed. In accordance with the amyloid cascade hypothesis, Jack and colleagues have proposed the hypothetical model displayed in **Figure 5**. In this model, amyloid biomarkers first appear in biofluids and imaging, followed by CSF tau changes, cerebral atrophy detected by magnetic resonance imaging (MRI) and cerebral metabolism abnormalities assessed by positron emission tomography (PET) imaging. Cognitive impairment appear last in the progression of the disease. A range of cognitive response can be observed and depends on each individual's risk profile (Jack and Holtzman, 2013).

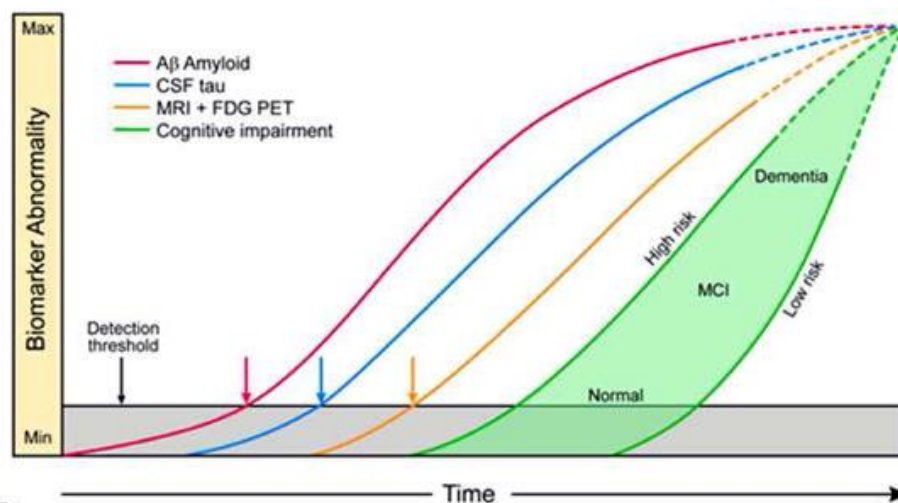


**Figure 5: Model of Alzheimer's disease biomarker temporal evolution**

Amyloid biomarkers (red) first appear, followed by CSF tau modifications (blue), cerebral atrophy in MRI and cerebral metabolism abnormalities in PET imaging (yellow). Cognitive impairment appear last in the progression of the disease (green area). A range of cognitive response can be observed and depends on each individual's risk profile, shifting to the left for those with low cognitive reserve and to the right for those with high cognitive reserve (Jack and Holtzman, 2013).

Interestingly, Duyckaerts and colleagues have proposed another model in which tau pathology starts before A $\beta$  deposition (Duyckaerts et al., 2015). They suggest that such pathology belongs to the AD continuum, as opposed to being a separate disease entity referred to as "primary age-related tauopathy" (PART) (Crary et al., 2014). In this model, tau deposits are

first found in the entorhinal cortex and hippocampus in the absence of A $\beta$  pathology, and are later observed in the isocortex along with A $\beta$  deposits (**Figure 6**) (Duyckaerts et al., 2015).

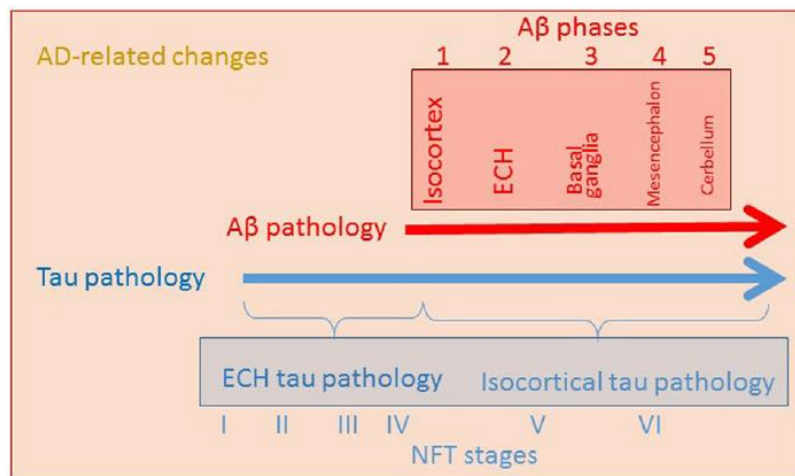


**Figure 6: Model depicting the evolution of tau and A $\beta$  depositions in AD**

According to this model, AD continuum is first characterized by the occurrence of tau lesions in the entorhinal cortex and hippocampus (ECH) (NFT stages I to III or IV) in the absence of A $\beta$  pathology (phase 0). Tau pathology later spreads to the isocortex (NFT stages V and VI) where A $\beta$  deposits can also be found (phase 1 or higher) (Duyckaerts et al., 2015).

Among the most studied biomarkers, CSF and plasma measures reflect the balance between amyloid and tau production and clearance at a specific time, without any information on the specific localization of the changes. Conversely, imaging biomarkers can reveal the accumulation and propagation of protein deposits in the brain over time, *e.g.* A $\beta$  and tau spatiotemporal depositions, through PET imaging. Moreover, the topographical severity of neurodegeneration can be evaluated using MRI and fluorodeoxyglucose (FDG)-PET, but their use can be limited by expense and availability. Compared to lumbar puncture, drawing blood is technically easier, safer, less invasive and inexpensive. However, blood biomarkers present with the disadvantage of being expressed in very low concentrations therefore requiring highly sensitive analytical techniques and are not yet validated AD biomarkers.



### 1.5.1. Amyloid biomarkers

#### 1.5.1.1. A $\beta$ -PET imaging

Amyloid progressive aggregation can be visualized with PET imaging using compounds that bind to A $\beta$  fibrillary forms. Pittsburgh Compound B (PiB) labeled with carbon 11 was the first ligand available (**Figure 7**).

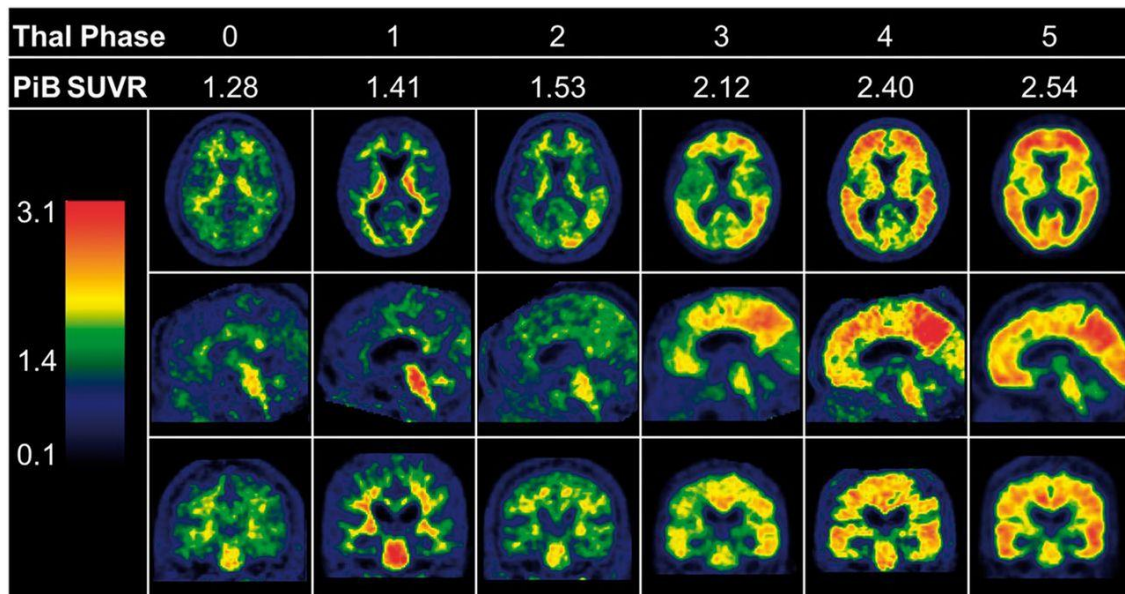


**Figure 7: Association between carbon 11-labeled PiB and Thal phases across the AD spectrum**

Increasing PiB-PET positivity assessed by the standardized uptake value ratio (SUVR) is observed with each subsequent Thal amyloid phase (Murray et al., 2015).

PiB-PET however presents multiple technical limitations, including a 20-minute half-life and structural constraints including an on-site cyclotron. In addition, it shows poor specificity to detect MCI patients that would eventually transition to AD (Marcus et al., 2014). More recently, some fluor-18 labeled fluorinated tracers (florbetaben, flutemetamol) with strong correlations with postmortem amyloid deposition and PiB, as well as longer half-lives showed good sensitivity and specificity values in predicting AD progression, including from MCI to full-blown AD (Martínez et al., 2017a, 2017b).

### 1.5.1.2. Biofluid measurements of A $\beta$

Given its direct interactions with the interstitial fluid, the CSF reflects the pathophysiological changes occurring in the brain of AD patients. In AD, as A $\beta$  progressively aggregates into plaques, lower amounts are secreted in the extracellular space and in the CSF resulting in a decrease in A $\beta_{42}$  load (Blennow and Zetterberg, 2018). Indeed, AD patients display a 50% decrease in CSF A $\beta_{42}$  but, although effective to discriminate AD from cognitively unimpaired individuals, this marker has limited sensitivity and specificity for discriminating AD from non-AD dementias (Forlenza et al., 2015; Olsson et al., 2016). Conversely, the CSF A $\beta_{42}$ /A $\beta_{40}$  ratio yields high predictive value (85% sensitivity and 82% specificity) for the differential diagnosis of dementia as it normalizes A $\beta_{42}$  levels to total amyloid load, reliably represented by A $\beta_{40}$  levels. A $\beta_{40}$  is indeed the main amyloid species in the CSF and therefore, normalization to A $\beta_{40}$  concentrations takes into account interindividual variability in amyloid production (Biscetti et al., 2019). Additionally, and regardless of which tracer is used, CSF A $\beta_{42}$ /A $\beta_{40}$  ratio highly correlates with amyloid PET imaging (Hansson et al., 2019).

Plasma A $\beta_{42}$ /A $\beta_{40}$  ratio reflects with high accuracy the CSF A $\beta_{42}$ /A $\beta_{40}$  ratio and positivity in amyloid PET suggesting a blood-brain transportation mechanism of A $\beta$  (Schindler et al., 2019). However, compared to amyloid-negative individuals, amyloid-positive patients show a 50% decrease in the CSF A $\beta_{42}$ /A $\beta_{40}$  ratio (Olsson et al., 2016) whereas the plasmatic ratio only decreases by 14-20% (Ovod et al., 2017; Schindler et al., 2019).

## 1.5.2. Tau biomarkers

### 1.5.2.1. Tau PET-imaging

The development of tau ligands as a mean to detect tau deposition using PET imaging is limited by the multiple conformational changes occurring for tau. Off-target binding and retention in the striatal region have been observed with the first developed ligands ([ $^{18}$ F] AV1451 or T-807). However recently, new promising PET tracers without off-target binding were developed and showed promising results in improving diagnostic accuracy ([ $^{18}$ F] PI-2620 or [ $^{18}$ F] MK-6240) (Khoury and Ghossoub, 2019) (**Figure 8**).

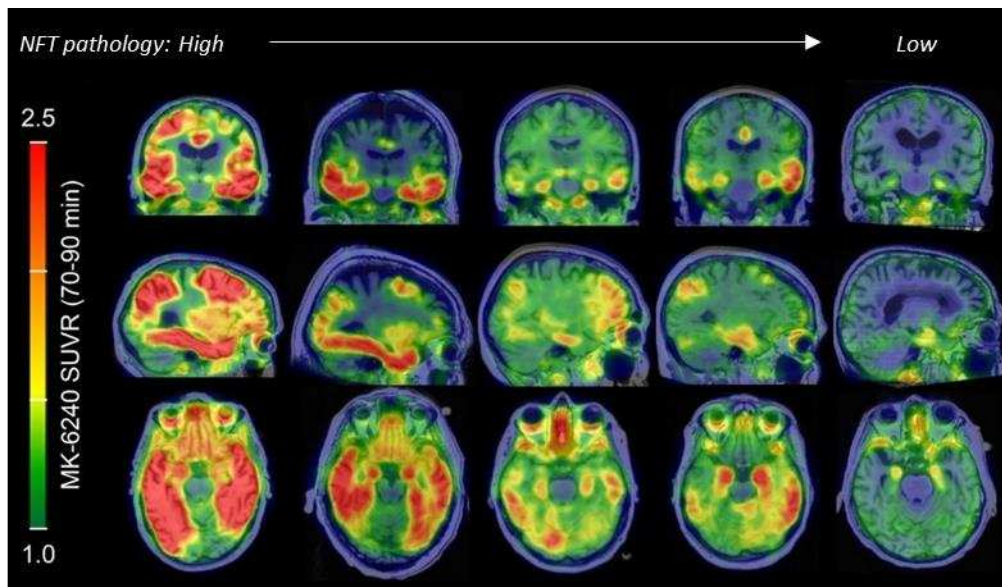


**Figure 8: Fluor 18 labeled-MK-6240 binding patterns in PiB-positive patients recapitulates the neuropathological staging of NFTs**

Fluor 18 labeled-MK-6240 SUVR imaging in PiB-positive individuals, 70 to 90 minutes after tracer injection, is consistent with the neuropathological staging of neurofibrillary tangles observed in AD (from high pathology on the left, to low pathology on the right) (Adapted from Betthausen et al., 2019).

### 1.5.2.2. Biofluid measurements of phospho-tau

CSF phospho-tau likely reflects tau phosphorylation state and tangle formation. It is a predictive marker of AD-associated tau pathology and increases in preclinical AD, while only subtle changes of A $\beta$  pathology are observed. CSF phospho-tau 181, 231 and 199 levels can equally discriminate AD from other neurodegenerative diseases and non-demented controls (Hempel et al., 2004). AD is associated with a 200% increase in phospho-tau CSF concentrations reflecting tau burden (Forlenza et al., 2015). CSF phospho-tau217 shows a better correlation with tau PET assessed by [18F] flortaucipir uptake. Furthermore, CSF phospho-tau217 outperforms phospho-tau181 for the differential diagnosis of AD and PET amyloid-positive patient identification (Barthélemy et al., 2020) and may increase earlier than CSF phospho-tau181 in response to A $\beta$  pathology (Janelidze et al., 2020b).

Plasma phospho-tau181 levels changes occur before symptom onset and increase as AD clinical severity progresses (Mielke et al., 2018; Suárez-Calvet et al., 2020). They also show a

good correlation with phospho-tau181 levels in the CSF, amyloid and tau PET, cerebral atrophy and glucose hypometabolism (Mattsson et al., 2016; Mielke et al., 2018). Interestingly, changes in plasma phospho-tau181 occur after CSF and plasma A $\beta$  changes but before amyloid and tau PET suggesting that plasma phospho-tau181 may reflect early A $\beta$ -related tau changes and could be useful to estimate disease stage (Janelidze et al., 2020a; Palmqvist et al., 2019). Furthermore, elevated phospho-tau181 levels can predict the conversion to AD dementia in MCI and cognitively unimpaired individuals (Janelidze et al., 2020a).

### 1.5.3. Neurodegeneration biomarkers

#### 1.5.3.1. Structural magnetic resonance imaging (MRI)

Brain atrophy assessed by structural MRI is a validated marker of neurodegeneration. Gray matter volume and cortical thickness evaluated on regional and global scales are classically used to estimate atrophy (Jagust, 2018). AD patients display a typical atrophy pattern, first affecting the medial temporal lobe, in particular the hippocampus and entorhinal cortex (Jouttonen et al., 1999), followed by cortical regions along a temporo-parieto-frontal trajectory, while sensorimotor and visual areas are usually spared until late disease stages (**Figure 9**) (Chandra et al., 2019; Matsuda, 2012; Pini et al., 2016).

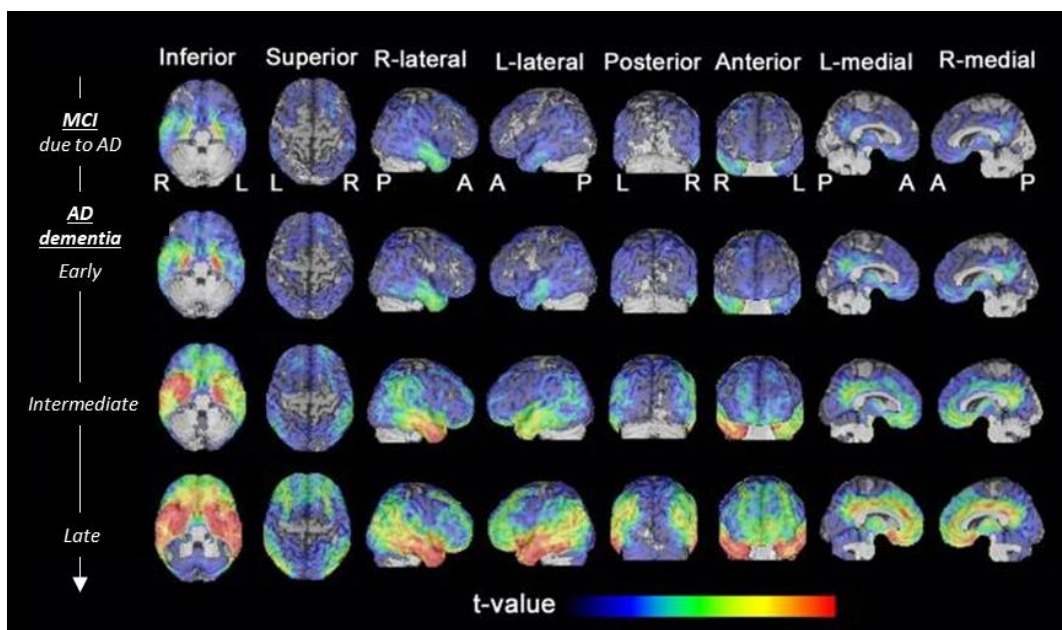


**Figure 9: Gray matter atrophy according to AD pathological progression**

Brain atrophy assessed by voxel-based morphometry analysis first affects medial temporal structures in MCI and early AD patients. As the disease progresses, it further extends to lateral

temporal, parietal and frontal cortices. R: right, L: left, P: posterior, A: anterior. (Adapted from Matsuda, 2012).

Interestingly, this topographical progression correlates with disease progression and clinical signs (Pini et al., 2016), as well as Braak staging scheme (Braak and Braak, 1991; Matsuda, 2012). Sensitivity and specificity are excellent to differentiate AD from healthy individuals (above 90% for both) but decreases to around 80% when discriminating AD from other dementias (Bloudek et al., 2011).

### 1.5.3.2. FDG-PET imaging

PET techniques can also evaluate neuronal injury by using the glucose analogue  $^{18}\text{F}$ -fluorodeoxyglucose (FDG) to map brain glucose metabolism. Metabolic deficits in AD reflect alterations in neuronal activity and are widely assumed to reveal synaptic dysfunction although they could also be associated with disturbance in glial cell function (Jagust, 2018). Glucose uptake locally decreases in the posterior cingulate cortex and temporo-parietal regions of AD patients as well as MCI patients that later convert to AD (Anchisi et al., 2005). As for structural imaging, sensitivity and specificity are excellent to differentiate AD from healthy individuals (above 90% for both) but decreases when discriminating AD from non-AD dementias as it reflects nonspecific neurodegenerative processes (Bloudek et al., 2011).

### 1.5.3.3. Biofluid measurements of total tau and neurofilament light chain

The evaluation of total tau in the CSF provides information regarding neurodegeneration but is not specific to AD. Indeed, increased levels of CSF total tau occur as a result of both chronic and acute neuronal degeneration as observed in Creutzfeldt-Jakob disease (Skillbäck et al., 2014) as well as following acute stroke (Hesse et al., 2001) or traumatic brain injury (Ost et al., 2006). AD is associated with a 300% increase in total tau CSF concentrations reflecting neuronal injury (Forlenza et al., 2015). Moreover, higher levels of CSF total tau and phospho-tau predict faster clinical deterioration (Wallin et al., 2010).

CSF and plasmatic neurofilament light chain (NfL) evaluation has recently emerged as a promising marker of neurodegeneration and disease progression. In presymptomatic fAD patients, serum NfL is predictive for rate of cortical atrophy and cognitive alterations (Preische et al., 2019). In sporadic AD patients, increase in plasma NfL correlates with amyloid and tau PET and reflects neuronal injury (Mattsson et al., 2019).

## **1.6. AD therapeutic management**

Currently approved therapies for AD are mainly symptomatic. They are used to temporarily manage cognitive symptoms and dysfunction in global activities without affecting disease progression. Efficacy is however modest and their medical benefits has been evaluated as insufficient by the French National Health Authority in 2016 (HAS, 2016). The need for disease-modifying therapies that can modulate the course of the disease is critical. For this purpose, clinical research has mainly focused on anti-A $\beta$  and anti-tau therapies (Vaz and Silvestre, 2020), leading to the FDA approval of the first disease-modifying therapy targeting A $\beta$  pathology in 2021 (Cavazzoni, 2021).

### **1.6.1. Current symptomatic treatments**

Symptomatic treatments for AD include cholinesterase inhibitors and N-methyl-D-aspartate (NMDA) receptor antagonists.

#### **1.6.1.1. Cholinesterase inhibitors**

Acetylcholine plays a crucial role in attention, learning and memory. During the course of AD, cholinergic neurons are destroyed, leading to an overall reduction in brain cholinergic transmission. Acetylcholinesterase inhibitors reverse this deficiency by preventing acetylcholine hydrolysis in the synaptic cleft therefore enhancing cholinergic neurotransmission. Three acetylcholinesterase inhibitors with similar efficacy and tolerance are currently used in mild to moderate AD: donepezil, rivastigmine and galantamine (Long and Holtzman, 2019).

#### **1.6.1.2. N-methyl-D-aspartate receptor antagonists**

Memantine is a low-affinity non-competitive NMDA receptor antagonist. It is used in moderate to severe AD for which it has shown modest efficacy and safety profile. Although its exact mechanism of action is unclear, it may act by decreasing glutamate-mediated neurotoxicity by preventing NMDA receptor overactivation, thus reducing calcium influx and restoring synaptic function (Breijyeh and Karaman, 2020; Long and Holtzman, 2019).

### **1.6.2. Promising disease-modifying treatments**

#### 1.6.2.1. Anti-A $\beta$ therapies

The amyloid cascade hypothesis postulates that A $\beta$  accumulation and aggregation into plaques initiates a cascade of events leading to AD pathology (Selkoe and Hardy, 2016). Thus, different strategies have been explored in an attempt to reduce A $\beta$  parenchymal levels and limit its toxicity, including:

- Reducing A $\beta$  production through the amyloidogenic pathway, using  $\beta$ -secretase inhibitors,  $\gamma$ -secretase inhibitors or modulators and  $\alpha$ -secretase promoters;
- Preventing A $\beta$  aggregation, using agents that bind to soluble A $\beta$  peptides and inhibit their aggregation into oligomers, fibrils and plaques;
- Promoting A $\beta$  clearance through immunotherapy, which can either be “active”, when A $\beta$  or its fragments are injected to stimulate the patient immune system, or “passive”, when monoclonal antibodies directed against A $\beta$  and its aggregates are used.

Compounds decreasing A $\beta$  production and aggregation have all failed to show clinical benefits. However, recently in June 2021, and for the first time since 2003, the FDA has approved the use of a new drug in AD (Cavazzoni, 2021). Aducanumab (Biogen), a monoclonal antibody directed against soluble and insoluble aggregates of A $\beta$  (Arndt et al., 2018), was shown to reduce A $\beta$  plaques burden measured by PET-imaging, decrease phospho-tau CSF levels and have beneficial effects on cognition, function and behavior (Cummings et al., 2021). In parallel, the efficacy of other immunotherapies is still under evaluation, including phase II/III trials with preclinical AD participants (amilomotide CAD106, Novartis/Amgen) or phase III trials with prodromal to mild AD patients (gantenerumab RO4909832, Hoffmann-La Roche and BAN2401 Eisai/Biogen) (Vaz and Silvestre, 2020).

Interestingly, sodium oligomannate (GV-971), a marine-derived oligosaccharide that was shown to reduce A $\beta$  aggregation, restore the gut microbial profile and lessen brain immune cell infiltration and inflammation in animal models, also demonstrated solid and consistent cognition improvement in a phase III trial conducted in China (Wang et al., 2019).

### 1.6.2.2. Anti-tau therapies

As the severity of cognitive impairment strongly correlates with tau pathology, as opposed to A $\beta$  (Duyckaerts et al., 1997a), recent efforts have focused on anti-tau therapies and aim to:

- Prevent tau abnormal hyperphosphorylation, notably through the inhibition of the glycogen synthase kinase 3 $\beta$ ;
- Prevent tau aggregation;
- Stabilize microtubules, to compensate for physiological tau loss-of-function;
- Promote tau clearance, through active and passive immunization.

Most anti-tau treatments are still in the early stages of clinical trials. Notably, a phase III trial evaluating the efficacy of leuco-méthylthinium (TauRx therapeutics) in preventing tau aggregation in mild to moderate AD is ongoing, as well as phase II trials testing anti-tau vaccines in mild AD (AADvac1, Axon neuroscience) and anti-tau antibodies in prodromal to mild AD (gosuranemab BIIB092/BMS-986168 Biogen, tilavonemab ABBV-8E12/C2N8E12 AbbVie, semorinemab RO7105705 Genentech/AC Immune, zagotenemab LY3303560 Eli Lilly) (Vaz and Silvestre, 2020).

AD drug development has a 99.6% failure rate (Cummings et al., 2014), highlighting the need for new approaches and a better understanding of AD pathophysiology. Interestingly, it has been suggested that treatments may be more beneficial in preclinical stages before neurodegeneration begins. Thus, the development of new biomarkers, validated both in animal models and humans, is still required to insure an early diagnosis. In addition to clinical diagnosis, AD biomarker confirmation should systematically be used to include patients in clinical trials to produce more homogeneous groups. In early phases, brain penetration and target engagement proof-of-concept should moreover be provided (Briggs et al., 2016; Cummings, 2018). Finally, the use of appropriate endpoints is essential to identify effective drugs. In AD trials the most clinically significant endpoint is cognitive improvement. However, the most widely used tests lack sensitivity to reliably measure subtle changes in cognitive function (Elmaleh et al., 2019; Posner et al., 2017). Given the complexity of AD pathology, recent evidence suggests that combination therapies aimed at multiple targets, *e.g.* A $\beta$  and tau but also neuroinflammation and oxidative stress, may be more effective than monotherapies (Cummings et al., 2019).



### 1.7. Pathophysiology

Extracellular amyloid plaque deposition and intraneuronal accumulation of hyperphosphorylated tau are the main neuropathological hallmarks of AD. However, AD is a complex disease that also involves vascular aggregates of A $\beta$ , neuroinflammatory processes, synaptic alterations and neurodegeneration.

#### 1.7.1. Amyloidosis

##### 1.7.1.1. Amyloid protein precursor processing

A $\beta$  peptides are the main component of senile plaques and result from the proteolytic cleavage of the transmembrane APP, an integral membrane protein with a single transmembrane domain that is especially expressed at the synapses of neurons (Agostinho et al., 2015). It is involved in neuronal homeostasis including neuronal development, signaling and intracellular transport but also in synaptic development (Chen et al., 2017). The imbalance in APP metabolism and APP cleavage products may contribute to amyloid pathology and neuronal dysfunction in AD.

Depending on the enzymatic cascade that is involved, APP processing can follow two alternative pathways, either non-amyloidogenic or amyloidogenic. APP is first cleaved either by  $\alpha$ -secretase (non-amyloidogenic) or by  $\beta$ -secretase (amyloidogenic) releasing an N-terminal ectodomain from the cell surface (sAPP $\alpha$  or sAPP $\beta$ , respectively) and generating a C-terminal membrane fragment (83-amino acid CTF $\alpha$  or 99-amino acid CTF $\beta$ , respectively). The  $\gamma$ -secretase complex, which is composed of four protein subunits (*i.e.* presenilin, nicastrin, presenilin enhancer 2 and anterior pharynx-defective 1) further cleaves the CTFs to produce a C-terminal fragment called APP intracellular domain (AICD) along with non-pathogenic P3 and A $\beta$  peptides in the non-amyloidogenic pathway or different pathogenic A $\beta$  species in the amyloidogenic pathway (**Figure 10**). The most commonly generated pathogenic A $\beta$  peptides are A $\beta$ <sub>1-40</sub> and A $\beta$ <sub>1-42</sub>, the latter being more toxic with a greater propensity to aggregate because of two additional hydrophobic residues in C-terminus (Yoshiike et al., 2003). A $\beta$  production predominantly occurs in endosomes and its release is regulated both by pre- (Cirrito et al., 2005) and post-synaptic (Verges et al., 2011) activity.

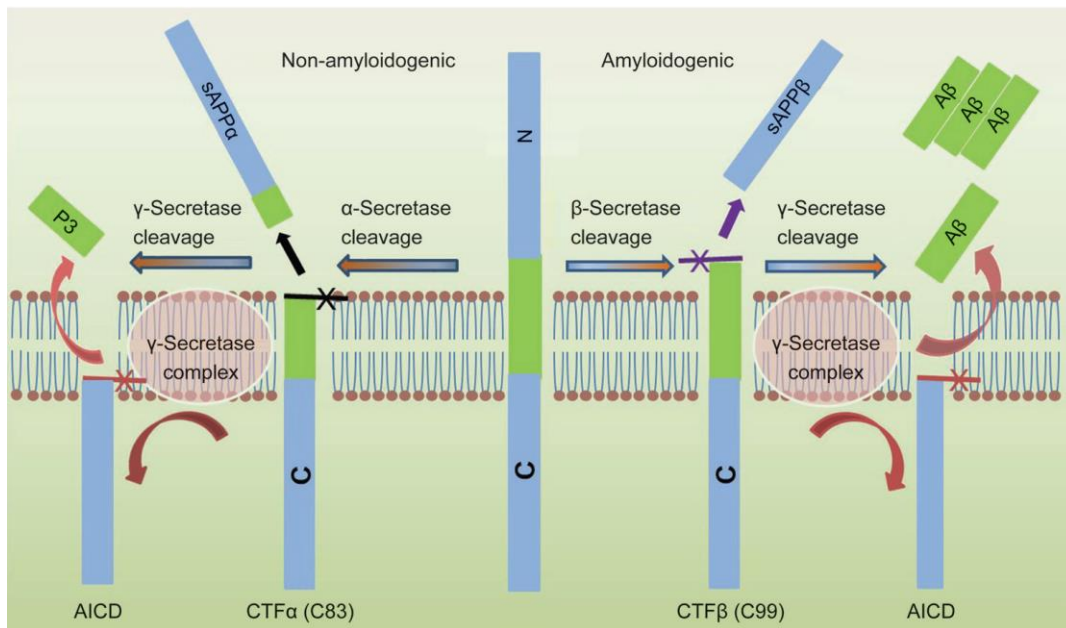


**Figure 10: APP metabolism through the non-amyloidogenic and amyloidogenic pathways**

APP is first cleaved either by  $\alpha$ -secretase (non-amyloidogenic) or by  $\beta$ -secretase (amyloidogenic) releasing an N-terminal ectodomain from the cell surface (sAPP $\alpha$  or sAPP $\beta$ , respectively) and generating a C-terminal membrane fragment (83-amino acid CTF $\alpha$  or 99-amino acid CTF $\beta$ , respectively). The  $\gamma$ -secretase complex further cleaves the CTFs into a C-terminal fragment called APP intracellular domain (AICD) and either non-pathogenic P3 and A $\beta$  peptides in the non-amyloidogenic pathway, or pathogenic A $\beta$  species in the amyloidogenic pathway (Chen et al., 2017).

Many processes are involved to maintain a proper balance in A $\beta$  production and elimination. A $\beta$  clearance can be mediated by the release of various proteases. Metalloendopeptidases insulin-degrading enzyme and neprilysin which are thought to preferentially participate in monomer degradation (Leissring et al., 2003) and their proteolytic activity is promoted by ApoE, with ApoE2 being the most effective isoform, as opposed to ApoE4 which is the less effective one (Jiang et al., 2008). As for A $\beta$  insoluble forms, metalloprotease-9 was shown to be effective in A $\beta$ <sub>1-40</sub> and A $\beta$ <sub>1-42</sub> fibrils and plaques degradation (Yan et al., 2006). In addition, cell-mediated clearance (*e.g.* by microglia) and active transport across the blood-brain barrier regulated by the receptor for advanced glycation end product (RAGE) (Deane et al., 2003) and low-density lipoprotein receptor-related protein 1 (LRP1) (Shibata et al., 2000) also participate in A $\beta$  regulation. Moreover, glial cells can release ApoE proteins into the brain interstitial fluid

where they can interact with A $\beta$  and promote its cellular clearance and conversion into insoluble fibrils (Holtzman, 2001).

### 1.7.1.2. A $\beta$ structural conformations

A $\beta$  peptides are heterogeneous in size and can range from 37 to 49 residues. A $\beta$  monomers are secreted by cells and can progressively assemble into oligomers, protofibrils and fibrils that can eventually aggregate into plaques in the brain parenchyma and vasculature. However, aggregation pathways highly depend on A $\beta$  primary amino acid sequence and intermolecular interactions (Bitan et al., 2003).

A $\beta$  monomers are highly hydrophobic 4 kDa-proteins that tend to self-aggregate into larger amyloid species. They are mainly associated with an  $\alpha$ -helix conformation (Agrawal and Skelton, 2019) and the conversion to a  $\beta$ -sheet structure depends on their C-terminal region (Mirza et al., 2014).

Soluble A $\beta$  oligomeric assemblies can range from low molecular weight oligomers including dimers, trimers and tetramers, to higher molecular weight species such as hexamers and dodecamers. Nuclear magnetic resonance (NMR) studies revealed that A $\beta$  oligomers display a mixed parallel and anti-parallel  $\beta$ -sheet structure (Yu et al., 2009). It has been suggested that oligomers are kinetic intermediates in the formation of amyloid fibrils (Harper et al., 1997) and potent inducers of A $\beta$  plaque formation (Langer et al., 2011).

X-ray diffraction data show that A $\beta$  fibrils are highly ordered and form a characteristic cross  $\beta$ -sheet pattern (Sunde et al., 1997). Fibrils are typically 5 to 15 nm wide and can be several microns long (Iadanza et al., 2018). However, A $\beta$  fibrils structural polymorphism has been widely reported in AD patients (Kollmer et al., 2019; Lu et al., 2013; Qiang et al., 2017), leading to various amyloid plaque morphologies (Condello et al., 2018; Watts et al., 2014).

### 1.7.1.3. A $\beta$ deposits in AD brains

In AD, A $\beta$  pathology can be found in the brain parenchyma, as extracellular amyloid plaques and neuritic plaques, intracellular deposits and in blood vessels leading to cerebral amyloid angiopathy (CAA).

### 1.7.1.3.1. A $\beta$ plaques

Plaques are mainly composed of highly fibrillogenic A $\beta$ <sub>1-42</sub> although other A $\beta$  species can also be detected (Walker, 2020). Plaque morphological appearance is heterogeneous and can result from genetic mutations, amyloid polymorphism as well as depend on their anatomical distribution (Thal et al., 2006a). However, they are classically divided into two main categories: diffuse plaques and dense core plaques.

Diffuse plaques are amorphous amyloid deposits with ill-defined limits that are negative for amyloid binding dyes. They are usually not associated with activated glial cells nor with neuritic components although some diffuse neuritic plaques can be observed in advanced stages of AD (Dickson, 1997; Serrano-Pozo et al., 2011a) (**Figure 11A**).

Dense core plaques consist of dense reticular or radiating compact dense amyloid that is highly positive to amyloid dyes (Thal et al., 2006a) (**Figure 11B**).

### 1.7.1.3.2. Neuritic plaques

Neuritic plaques usually have a central core of radiating amyloid fibrils surrounded by a halo of dystrophic neurites with activated glia, tau filaments and A $\beta$  oligomers (Masters and Selkoe, 2012; Thal et al., 2006a) (**Figure 11C**). In addition, degenerating mitochondria and lysosomes can accumulate in abnormal neurites (Serrano-Pozo et al., 2011a). Dense core plaques with tau-positive neurites are closely associated with neurodegeneration and cognitive decline (Knowles et al., 1999).

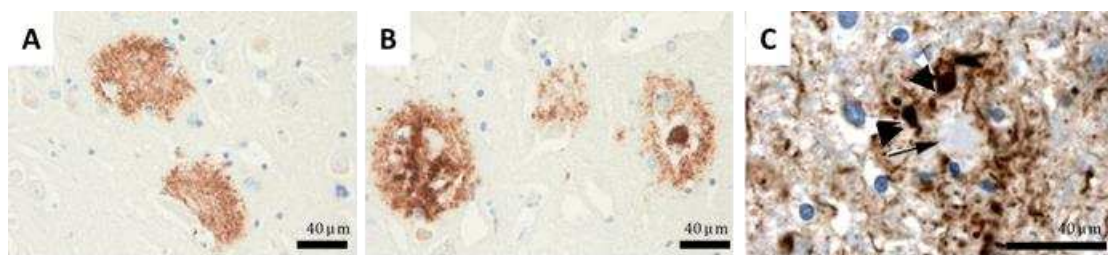


**Figure 11: A $\beta$  deposits in AD brains**

Diffuse (A) and dense core (B) amyloid plaques stained by anti-A $\beta$  antibodies. (C) Neuritic plaque with tau-positive processes revealed by AT8 immunostaining (arrowheads) in contact with the amyloid core (arrow). Scale bars : 40  $\mu$ m. Adapted from (DeTure and Dickson, 2019; Duyckaerts et al., 2009).

### 1.7.1.3.3. Intracellular A $\beta$

In AD brains, A $\beta$  can accumulate within neurons, and more specifically in multivesicular bodies (Takahashi et al., 2002). This accumulation has been associated with synaptic morphological alterations (Takahashi et al., 2002) and appears to precede plaque and tangle formation (Gouras et al., 2000).

### 1.7.1.3.4. Cerebral amyloid angiopathy

In addition to A $\beta$  parenchymal deposition, approximately 80% of AD cases display some level of cerebral amyloid angiopathy (CAA). Thioflavin-S and Congo red-positive A $\beta$  deposits, mainly composed of A $\beta$ <sub>1-40</sub>, can be found in the tunica media of leptomeningeal arteries and cortical capillaries, small arterioles and arteries, particularly in the parietal and occipital cortices (**Figure 12**) (Serrano-Pozo et al., 2011a). Two types of CAA have been described: type 1 CAA involves capillaries, arterioles and small arteries, whereas type 2 CAA mainly affects large arteriolar vessels but spares capillaries (DeTure and Dickson, 2019).

Accumulation of A $\beta$  may result from impaired perivascular clearance of A $\beta$  and blood-brain barrier dysfunction leading to its deposition within the vessel wall (Magaki et al., 2018). Amyloid deposition in the microvasculature can cause physical disruption and lead to hemorrhages (Charidimou et al., 2012). In mice, A $\beta$  can be responsible for a decrease in cerebral blood flow by recruiting adherent neutrophils to occlude capillaries (Cruz Hernández et al., 2019) and activate pericytes that release reactive oxygen species (Nortley et al., 2019).

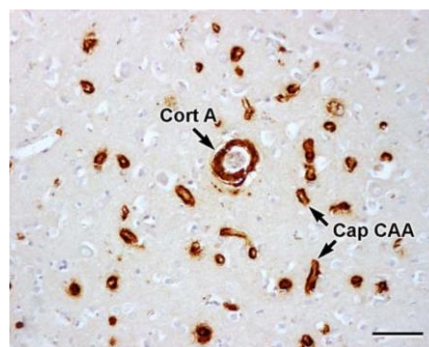


**Figure 12: Cerebral amyloid angiopathy**

Cerebral amyloid angiopathy affecting a cortical artery (Cort A) and its capillary bed (Cap CAA), revealed by anti-A $\beta$  immunohistochemistry. Scale bar: 10  $\mu$ m. (Weller et al., 2009).

#### 1.7.1.4. A $\beta$ conformation-dependent toxicity

Polymorphism in A $\beta$  peptides has been associated with distinct biological and toxic properties. Although some level of toxicity has been reported for each amyloid species, mounting evidence suggest that soluble oligomers are the most toxic species, as opposed to insoluble aggregates.

In humans, amyloid plaque load weakly correlates with clinical signs in late-onset AD (McLean et al., 1999) and approximately one third of the elderly population displays cerebral A $\beta$  deposition without cognitive alterations (Aizenstein et al., 2008). Conversely, cognitive status strongly correlates with A $\beta$  oligomers cerebral (McLean et al., 1999; Tomic et al., 2009) and plasmatic levels (Meng et al., 2019). In addition, patients in early stages of AD display increased levels of soluble A $\beta$  oligomers in synapses (Bilousova et al., 2016) as well as in the CSF (Herskovits et al., 2013) before plaque formation.

Several studies conducted on animal models have shown that A $\beta$  oligomers derived from AD brains can alter synaptic structure and activity by inducing a loss of dendritic spines, inhibiting long-term potentiation (LTP) and enhancing long-term depression (LTD), as opposed to amyloid plaque cores (Shankar et al., 2008; Walsh et al., 2002). Interestingly, high molecular weight oligomers, which are prevalent in AD brains, can cause hippocampal LTP impairment and activate microglial responses in wild-type mice only once they are dissociated into lower molecular weight oligomers (of approximately 8 to 70 kDa) (Yang et al., 2017). Moreover, intracerebroventricular injection, in mice, of high molecular weight A $\beta$  oligomers was shown to induce a transient memory impairment as opposed to low molecular weight A $\beta$  oligomers which induced a rapid and persistent cognitive deficit in addition to synaptic dysfunction (Figueiredo et al., 2013). These results were also shown in rat models in which the intracerebroventricular injection of soluble oligomers, including dimers and dodecamers can alter memory performances (Lesné et al., 2006; Shankar et al., 2008). Strong evidence indeed suggests that A $\beta$ \*56 dodecamers are critically involved in early AD as their presence correlates with synaptic alteration, neuronal injury and pathological forms of soluble tau in humans (Lesné et al., 2013), along with memory impairment in animal models (Lesné et al., 2006). One study has shown that both fibrillar and oligomeric A $\beta$ <sub>1-42</sub> species can induce spatial learning impairment when infused into the lateral ventricles. However, cognitive deficits,

neurodegeneration and neuroinflammation were more severe in oligomer-infused rats (He et al., 2012).

Altogether, these studies suggest that soluble oligomers rather than insoluble fibrils or plaques are the main responsible species for neuronal and glial alterations that underlie synaptic failure and cognitive impairment in AD (Ferreira et al., 2015). Fibrillar amyloid plaques may sequester toxic oligomers, or serve as reservoirs of soluble bioactive oligomers, and their disassembly into small active amyloid species could contribute to local synaptotoxicity (Shankar et al., 2008).

### 1.7.1.5. Amyloid cascade hypothesis

The amyloid cascade hypothesis has dominated the field of AD research for many years and provided the intellectual framework for therapeutic investigations. It is based on the discovery that all dominant mutations causing early-onset fAD occur in genes altering A $\beta$  accumulation. APP mutations within the A $\beta$  sequence increase the self-aggregating properties of A $\beta$  whereas mutations in presenilin genes involved in  $\gamma$ -secretase proteolytic activity increase the A $\beta$ <sub>1-42</sub>/A $\beta$ <sub>1-40</sub> ratio (Chávez-Gutiérrez et al., 2012). Moreover, the  $\epsilon$ 4 allele of the APOE gene, the strongest genetic risk factor for late-onset AD, has been shown to alter A $\beta$  clearance and promote A $\beta$  deposition (Liu et al., 2017). Interestingly, the APP A673T icelandic mutation which reduces the amyloidogenic processing of APP and decreases A $\beta$  aggregation protects against AD, therefore providing compelling evidence in support of the amyloid hypothesis (Maloney et al., 2014).

Genetic studies and biomarker-based longitudinal evaluations have shown that amyloid pathology occurs years prior to other AD manifestations. As previously described, A $\beta$  accumulation can induce synaptotoxicity, neuroinflammation and oxidative injury. Moreover, whereas early A $\beta$  accumulation can progressively lead to tau deposition in APP mutant bearing patients, mutations in tau genes do not induce A $\beta$  aggregation in patients with FTD (Selkoe and Hardy, 2016), which further supports the amyloid hypothesis of AD. A $\beta$  oligomers greatly enhance the seeding and aggregation of tau *in vitro* (Shin et al., 2019) and were shown to trigger tau hyperphosphorylation at AD-relevant epitopes and lead to neuritic degeneration (Jin et al., 2011). Several studies also suggest that amyloid pathology promotes the spreading of tau from the entorhinal cortex to the neocortex (Bennett et al., 2017; Pontecorvo et al.,

2019). Interestingly,  $A\beta$  accumulation rate has been associated with the onset of tau deposition, while tau progression predicts the onset of cognitive decline (Hanseeuw et al., 2019). In addition, cognitive decline in AD begins as NFTs spread from the entorhinal cortex into the neocortex already exhibiting amyloid lesions (Price et al., 2009; Price and Morris, 1999). Major events leading to AD pathology according to the amyloid cascade hypothesis are summarized in **Figure 13**.

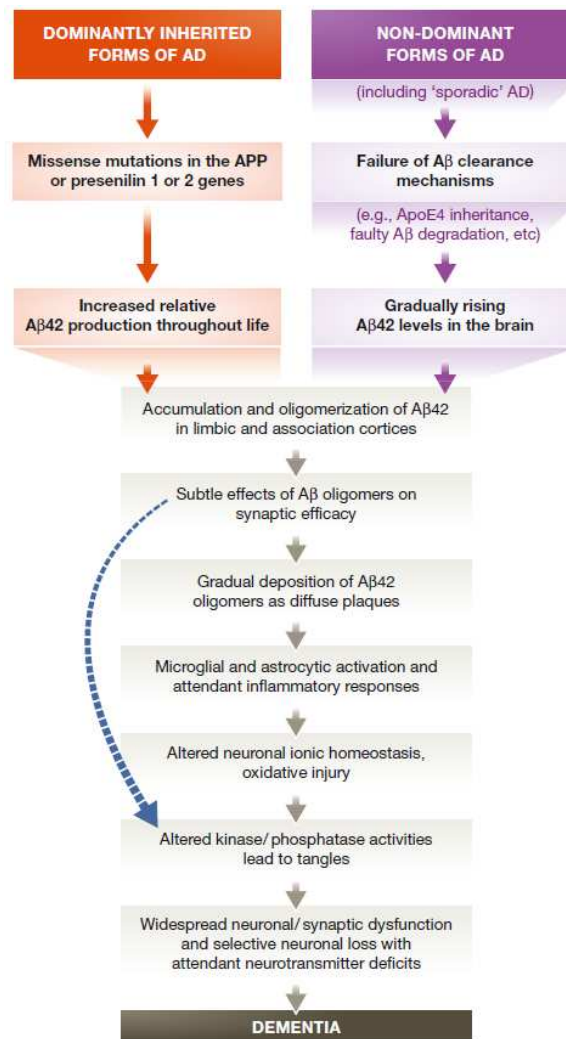


**Figure 13: The amyloid cascade hypothesis**

According to the amyloid cascade hypothesis, AD pathology begins with an increase in  $A\beta_{42}$  levels in the brain. It is followed by its progressive oligomerization and aggregation into amyloid plaques, leading to neuroinflammation, alterations of neuronal ionic homeostasis and oxidative injury, tau pathology and widespread neuronal and synaptic dysfunction and loss eventually leading to dementia. The curved blue arrow indicates a potential direct effect of  $A\beta$  oligomers on microglial and astrocytic activations, tau pathology, as well as on synaptic/neuronal alterations (Selkoe and Hardy, 2016).



Some evidence however oppose the amyloid cascade hypothesis. Aside from the many studies showing that A $\beta$  accumulation does not correlate with neuronal loss and cognitive decline, many individuals can present with significant A $\beta$  deposition in their brain without other AD pathological hallmarks (DeTure and Dickson, 2019). Moreover, some studies suggest that tau intraneuronal inclusions may occur before plaque formation in the brain (Braak et al., 2013; Duyckaerts et al., 2015) and dendritic tau has been observed in regions without A $\beta$  accumulation (Braak and Del Tredici, 2011). Multiple failures in clinical trials with therapeutics targeting A $\beta$  suggest that preventing amyloid pathology may not be sufficient to prevent AD pathological development as suggested by the amyloid cascade hypothesis.

### 1.7.2. Tauopathy

#### 1.7.2.1. Tau gene and isoforms

Tau is a microtubule-associated protein encoded by the MAPT gene, which is found on chromosome 17 and comprises 16 exons. The alternative splicing of exons 2, 3 and 10 yields six distinct isoforms in the human adult brain, ranging from 352 to 441 amino acids and differing by the absence (0N) or presence of one (1N) or two (2N) inserts in N-terminal and by three (3R) or four (4R) microtubule-binding repeat domains in C-terminal (Goedert et al., 1989; Guo et al., 2017) (**Figure 14**).

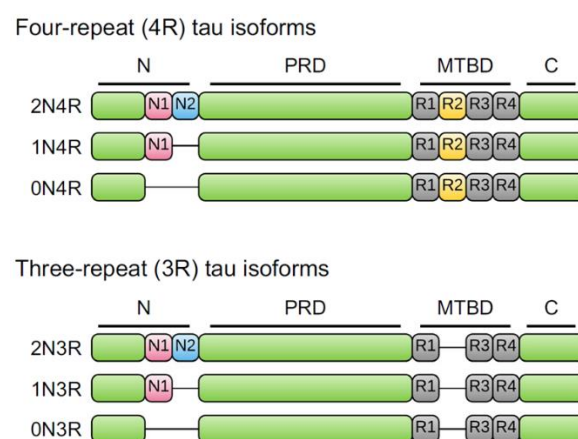


**Figure 14: Tau isoforms in the human brain.**

The alternative splicing of exon 2 and 3 leads to the absence (0N) or presence of one (1N) or two (2N) inserts in the N amino-terminal region of tau. Near the C-terminal end of tau, the alternative splicing of exon 10 in the microtubule-binding domain (MTBD) results in the

---

presence or absence of the second repeat, leading to 3R or 4R isoforms. The proline-rich domain (PRD) represents the central region of tau. Adapted from (Guo et al., 2017).

All six isoforms (0N3R, 0N4R, 1N3R, 1N4R, 2N3R and 2N4R) are likely to have distinct functions as they are differentially expressed during brain development. Interestingly, the expression of distinct sets of tau isoforms in different neuronal populations is associated with different tauopathies. Notably, AD is characterized by the abnormal accumulation of 3R and 4R isoforms in a one-to-one ratio whereas in other tauopathies, either 3R or 4R isoforms are over-expressed (Guo et al., 2017). Immunoblotting of AD brains shows the presence of a typical triplet of tau proteins with apparent molecular weights of 60, 64 and 68 kDa, as well as a minor 72-74 kDa band (Buée et al., 2000; Greenberg and Davies, 1990).

#### 1.7.2.2. Tau protein structure and physiological functions

Tau is primarily expressed in neurons, and to a lesser extent in astrocytes and oligodendrocytes. Intraneuronal distribution is polarized as tau is mainly located within axons (Guo et al., 2017).

Tau can be divided into four functional domains: the N-terminal projection domain, proline-rich domain (PRD), the microtubule-binding domain (MTBD) and the C-terminal tail (Figure 14). All tau regions are involved in microtubule assembly and stabilization and therefore participate in the maintenance of neuronal architecture and polarization. As microtubule networks mediate axonal transport systems, tau also plays a pivotal role in regulating neuronal functions through its influence on the motor proteins, dynein and kinesin, involved in protein and organelle axonal transport (Dixit et al., 2008). Moreover, it has been shown that the PRD modulates tau signaling functions, can interact with DNA and RNA, including by preserving DNA integrity and participating in DNA repair mechanisms, and is involved in neuronal cytoskeleton maintenance (Guo et al., 2017; Violet et al., 2014).

Evidence suggests that tau may participate in synaptic plasticity, through its involvement in brain-derived neurotrophic factor-induced spine growth (Chen et al., 2012) and long-term depression in the hippocampus (Kimura et al., 2014). During adult neurogenesis, tau plays a crucial role in the maturation and migration of newborn hippocampal granule neurons, the formation of post-synaptic densities, dendritic spines and mossy fiber terminals as well as the

acute stress-induced selective cell death of immature granule neurons (Fuster-Matanzo et al., 2009; Pallas-Bazarra et al., 2016).

### 1.7.2.3. Tau post-translational modifications

Tau can undergo multiple post-translational modifications including phosphorylation, acetylation, truncation, glycosylation, glycation, nitration and ubiquitination. In particular, tau phosphorylation and acetylation have emerged as dominant post-translational modifications in AD.

Tau can be phosphorylated at 85 different residues (Guo et al., 2017) but its phosphorylation sites are mainly localized in the proline-rich and C-terminal tail regions (Liu et al., 2007). Under physiological conditions, phosphorylation regulates tau affinity to bind microtubules and therefore its ability to promote tubulin assembly (Buée et al., 2000). In AD brains, phosphorylated tau load is increased by three to four-fold compared to normal brains (Ksiezak-Reding et al., 1992). This is partly due to an imbalance between kinases and phosphatases activity as it has been shown that phosphatase activity is reduced by 20 and 40%, respectively in the gray and white matter of AD patients (Gong et al., 1993). Tau hyperphosphorylation can potentially result in conformational modifications, changes in protein charges and ultimately to its self-aggregation. Moreover, hyperphosphorylated tau can aggregate with normal tau, therefore decreasing its binding affinity for microtubules (Alonso et al., 1994). This results in the loss of tau physiological functions, promotes its self-aggregation into pathological filaments and eventually compromise proper axonal transport and synaptic plasticity (Muralidar et al., 2020). Additionally, tau phosphorylation can prevent its degradation by the proteasome (Dickey et al., 2007).

Tau acetylation at specific lysine residues is also associated with AD pathology and its distribution pattern is similar to hyperphosphorylated tau (Irwin et al., 2012). It has been shown to prevent phospho-tau degradation (Min et al., 2010), impair tau-mediated microtubule stabilization and promote tau aggregation into fibrils (Trzeciakiewicz et al., 2017). However, depending on the acetylation site, aggregation may also be reduced (Yao et al., 2018).

#### 1.7.2.4. Tau structural conformation

Tau is highly soluble and natively unfolded in its monomeric form although its second and third MTBD repeats have a propensity to form  $\beta$ -sheets and are considered as drivers of tau abnormal self-assembly (Mukrasch et al., 2009). Free cytoplasmic tau adopts a “paperclip” conformation, with closely associated N and C terminal regions (Jeganathan et al., 2006).

Under pathological conditions, tau proteins can undergo conformational changes and self-aggregate into  $\beta$ -sheet structures known as paired helical filaments (PHF). PHFs, that include all six isoforms of tau, consist of two small filaments of 10 nm diameter forming a helical structure of 10-20 nm-wide with a crossover distance of 80 nm (Braak et al., 1986; Crowther, 1991). Straight filaments (SF) can also be found in AD brains, in which they are 10-15 nm in diameter (Crowther, 1991), whereas other tauopathies are characterized by 10 nm-wide straight half filaments (DeTure and Dickson, 2019). The core of PHFs and SFs consists of two identical protofilaments comprising tau residues 306–378 within the microtubule-binding domain. It is associated with a combined cross- $\beta$ / $\beta$ -helix structure defining the seed for tau aggregation (Fitzpatrick et al., 2017).

#### 1.7.2.5. Tau deposits in AD

##### *1.7.2.5.1. Neurofibrillary tangles*

Neurofibrillary lesions comprise PHFs and SFs aggregated within neuronal cell bodies (**Figure 15A**). Several factors may participate in their development including genetic mutations (Pittman et al., 2006), neuroinflammation (Yoshiyama et al., 2007) and A $\beta$ -mediated toxicity. Misfolded A $\beta$  can indeed enhance the aggregation and seeding properties of tau (Bennett et al., 2017; He et al., 2018), possibly by increasing glycogen synthase kinase 3 $\beta$  and cyclin-dependent kinase 5 activities (Engmann and Giese, 2009).

Ghost tangles appear as remnant of degenerated neurons which contained NFTs (**Figure 15A**). They consist of extracellular tau filaments and fragments that have undergone substantial proteolysis (Mroczko et al., 2019).

### 1.7.2.5.2. Neuropil threads

Neuropil threads (NTs) are mainly dendritic elements with tau filaments, including PHFs and SFs, that are thought to originate from NFT-bearing neurons (**Figure 15A**) (DeTure and Dickson, 2019). NTs represent 85-90% of cortical tau pathology (Mitchell et al., 2000).

### 1.7.2.5.3. Neuritic corona of senile plaques

As described in § 1.7.1.3.2. *Neuritic plaques*, tau can also accumulate in axonal processes forming the neuritic corona of A $\beta$  plaques (**Figure 15B**) (Duyckaerts et al., 2009).

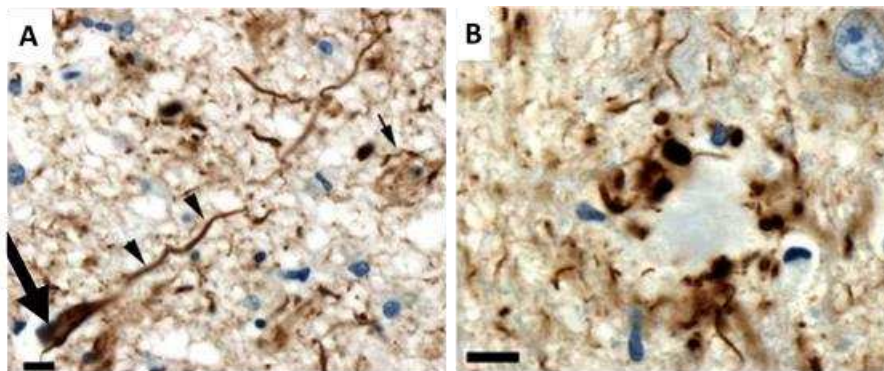


**Figure 15: Tau deposits in AD brains.**

(A) AT8-positive tau pathology accumulates intracellularly the form of neurofibrillary tangles (wide arrow), within the dendritic shaft as neuropil threads (arrowheads) or in the extracellular space as ghost tangles (small arrow). (B) Neuritic corona containing tau-positive elements (tau polyclonal antibody). Scale bars: 10  $\mu$ m. Adapted from (Duyckaerts et al., 2009).

### 1.7.2.6. Tau conformation-dependent toxicity

As NFT burden correlates with clinical decline and disease severity, tau fibrils have long been considered to be the main neurotoxic species in the AD brain (Nelson et al., 2012). Dominantly inherited mutations in MAPT lead to FTD with parkinsonism linked to chromosome 17, therefore supporting that tau alterations can induce neurodegeneration and dementia (Ghetti et al., 2015). In primary age-related tauopathy (PART), patients develop tau deposits in the entorhinal cortex and medio-temporal lobes with minimal A $\beta$  deposits, and only patients with severe tau burden display cognitive alterations (Besser et al., 2019; Cray et al., 2014).

Despite strong correlations, neurodegeneration far exceeds NFT burden in AD (Gómez-Isla et al., 1997). In transgenic mice expressing the P301L tau mutation, tau suppression led to cognitive function recovery and prevented neuronal loss, despite the induction of tangle pathology (SantaCruz et al., 2005). This suggests that NFTs may not be necessary nor sufficient to induce neuronal dysfunction. Moreover, tangles were shown to form after cognitive decline and neurodegeneration onsets in different models (Mroczko et al., 2019). Therefore, it has been suggested that NFTs may constitute a neuronal protective response through the sequestration of soluble oligomeric species (Spires-Jones et al., 2009).

More recently, several lines of evidence have suggested that tau oligomers are the most deleterious forms of tau. Oligomers have been detected in AD brains (Lasagna-Reeves et al., 2012b), including in cortical synapses (Henkins et al., 2012), and were correlated with memory loss in a mouse model of tauopathy (Berger et al., 2007). The subcortical injection of recombinant full-length human tau protein into mice disrupted memory, synaptic and mitochondrial functions, as opposed to tau fibrils and monomers (Lasagna-Reeves et al., 2011). Moreover, impairment of LTP and memory have been observed upon exposure to tau oligomers, either exogenously administered in mice (recombinant or extracted from AD brains) or expressed in transgenic mice overexpressing human tau. This effect was independent from A $\beta$  oligomer levels (Fá et al., 2016). Interestingly, tau trimers were shown to be toxic at nanomolar concentrations and represent the minimal propagation unit that may spontaneously be internalized and seed further intracellular aggregates therefore mediating the progression of tau pathology through the brain (Tian et al., 2013).

### 1.7.2.7. Tau hypothesis

Although the amyloid hypothesis has prevailed for decades, neuropathological data suggest that tau pathology begins about a decade prior to A $\beta$  plaques, therefore arguing that A $\beta$  is unlikely to be the initial cause of sporadic AD (Braak and Del Trecidi, 2015; Duyckaerts et al., 2015). Recently, Arnsten et al. hypothesized that cortical tau pathology may develop in selected and extensively interconnected glutamatergic projection neurons, with unique properties leading to tau abnormal phosphorylation and seeding. Consequently, phospho-tau may participate in APP metabolism towards the amyloidogenic pathway (Arnsten et al., 2021). Even if tau pathology can be frequently observed in cognitively unimpaired individuals, it is

also highly correlated with cognitive decline and neurodegeneration in AD patients as opposed to A $\beta$  (Braak and Del Tredici, 2015; Nelson et al., 2012). Recently, compelling evidence however suggested that rather than a linear model in which one pathology initiates the other, A $\beta$  and tau most likely act in synergy to drive AD progression (Busche and Hyman, 2020).

### 1.7.3. Neuroinflammation

Growing evidence suggests that immune mediators play a crucial role in regulating AD pathology. Indeed, neuroinflammation characterized by morphological and functional changes in microglial and astrocytic cells is a prominent feature in AD brains, in which reactive glia associates with both A $\beta$  plaques and tangles (**Figure 16**) (Serrano-Pozo et al., 2011b).

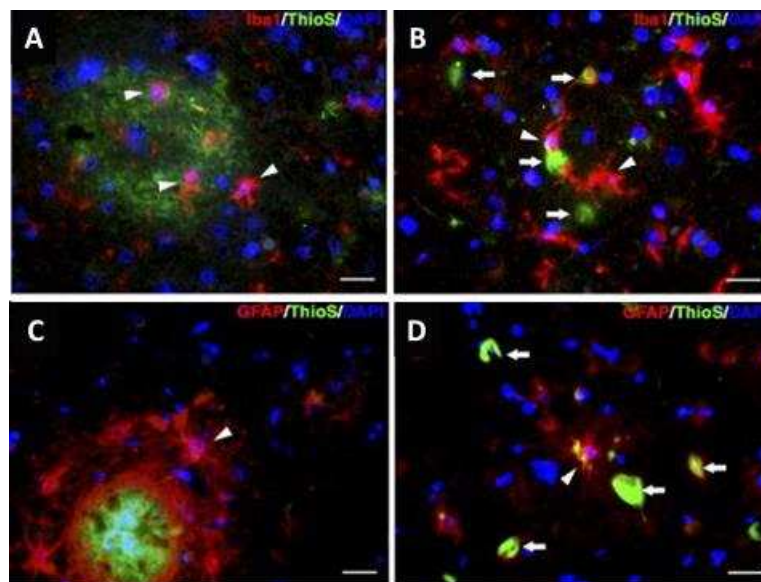


**Figure 16: Reactive glia is associated with A $\beta$  plaques and NFTs in AD**

Triple staining for Iba1 or GFAP (red), thioflavin-S (green) and DAPI (blue) in an AD brain. Thioflavin-S binds to  $\beta$ -sheets associated with amyloid structures such as A $\beta$  and tau. Reactive microglia (Iba1-positive, A-B) and astrocytes (GFAP-positive, C-D) are closely associated with dense core plaques (A and C, respectively) and NFTs (B and D, respectively). Scale bars: 20  $\mu$ m. Adapted from (Serrano-Pozo et al., 2011b).

#### 1.7.3.1. Microgliosis

##### 1.7.3.1.1. *Generalities and physiological functions of microglia*

Microglia are the innate immune cells and resident macrophages of the central nervous system (CNS). They are highly ramified cells that dynamically scan their environment to maintain brain homeostasis. They engage in a mutual and continuous interaction with their

surroundings and can initiate an immune response following exposure to CNS insults (such as misfolded protein aggregates considered as danger-associated molecular patterns or DAMPs), as well as respond to environmental stimuli, including neuronal activity and neurotransmitter release (Abiega et al., 2016). Microglia undergo morphological and functional changes upon activation, including shortening of their processes with swelling of the soma (**Figure 17**), and modifications in secretory mediators.

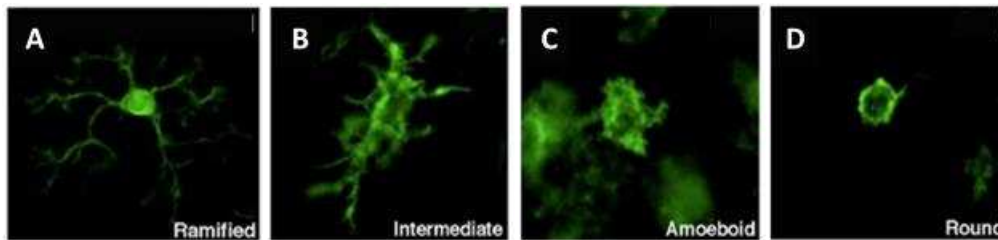


**Figure 17: Microglial morphological changes upon activation**

Photomicrographs of Iba1-positive microglial cells with various phenotypes representing different activation states: ramified (A), intermediate (B), amoeboid (C) and round (D). Adapted from (Thored et al., 2009).

Multiple physiological roles of microglia have been described both in the developing and mature CNS. During neurodevelopment, microglia contribute to neural circuit modeling by engulfing and removing neurons and synapses (Frost and Schafer, 2016). Synaptic pruning involves the classical complement cascade, as synapses are tagged with C1q (mainly produced by microglia), opsonized by C3b and subsequently engulfed by microglia (Schafer et al., 2012). In the adult brain, microglia are crucial regulators of activity-dependent synaptic plasticity, learning and memory, as well as neurogenesis (Gemma and Bachstetter, 2013; Schafer et al., 2013). Under physiological conditions, microglia-induced neuronal apoptosis is coupled with phagocytosis to ensure proper elimination of excessive neurons during the proliferation and development of neurons (Abiega et al., 2016; Brown and Neher, 2014).

#### *1.7.3.1.2. Microglia in the context of AD*

Genetic studies have identified many risk genes for AD, most of which are selectively or preferentially expressed by microglial cells (e.g. TREM2 or CR1 gene variants). These studies argue that proper microglial function protects against AD whereas impairment in microglial



functions may be involved in AD onset and progression. Indeed, rare variants in TREM2 gene, such as the R47H loss-of-function mutation, have been reported as major risk factors for AD as they impair the expression of the cell surface protein TREM2 and alter its binding with phospholipids (Colonna and Butovsky, 2017; Jonsson et al., 2013).

Evidence suggest that microglia are versatile cells with different functional states that may have counteracting effects in the early and late stages of AD (Hansen et al., 2018). In humans and animal models, they can surround amyloid plaques and contribute to their elimination in acute phases, but can also induce neuroinflammation and neurodegeneration through the excessive release of inflammatory cytokines during chronic activation. Human data suggest that microglia may have a protective role during early prodromal phases of AD with MCI patients showing a longitudinal reduction in microglial activation while microglial activity positively correlates with cognitive scores and brain volume (Fan et al., 2017). Conversely, microglial activation is increased in AD patients and correlates with glucose hypometabolism. These changes are associated with a disruption in frontal connectivity suggesting a deleterious effect of microglial activation on synaptic function (Tondo et al., 2020). Taken together, these data suggest a bimodal activation of microglia with a protective effect in preclinical/prodromal phases of AD and proinflammatory deleterious effects during clinical stages (Fan et al., 2017).

### *1.7.3.1.3. A $\beta$ and microglia-mediated toxicity*

Evidence suggests that A $\beta$ -induced microglial activation occurs early in AD and that chronic activation may result in an excessive release of inflammatory mediators in the symptomatic stages of the disease (Hansen et al., 2018).

The release of free radicals caused by increasing accumulation of A $\beta$  can lead to microglial activation through oxidative stress-related mechanisms (D. G. Walker et al., 2002). Moreover, several microglial membrane receptors can bind A $\beta$  and cause microglial activation. Notably, type 1 scavenger receptor A, chemokine-like receptor 1 and complement receptors are involved in amyloid uptake and clearance (Chen et al., 2017; Doens and Fernández, 2014). On the contrary, A $\beta$  binding to the receptor for advanced glycation end product (RAGE) leads to oxidative stress (Yan et al., 1996), secretion of proinflammatory mediators such as interleukin-1 $\beta$  (IL-1 $\beta$ ) and tumor necrosis factor  $\alpha$  (TNF $\alpha$ ) and induces synaptic dysfunction (Chen et al., 2017; Origlia et al., 2010). In endothelial cells of the brain, A $\beta$  and RAGE interactions lead to

vascular inflammatory responses, suggesting that A $\beta$ -induced neuroinflammation may play a significant role in the pathogenesis of CAA (Suo et al., 1998). Interestingly, *in vitro* co-culture experiments have shown that both A $\beta$ <sub>1-42</sub> low molecular weight oligomers and fibrils can activate microglia into a pro-inflammatory phenotype but, depending on the peptide conformation, differential secretory profiles associated with different neurotoxicities were reported (Sondag et al., 2009).

The release of pro-inflammatory mediators such as TNF $\alpha$  or IL-1 $\beta$ , caused by the presence of protein aggregates has been associated with neurodegeneration. In the presence of misfolded or aggregated proteins such as A $\beta$  (Halle et al., 2008; Lučiūnaitė et al., 2019, p. 3) and tau (Stancu et al., 2019), microglia can activate the NLRP3 (NOD-, LRR- and pyrin domain-containing 3) inflammasome, a protein complex that increases the cleavage and activity of caspase-1 and the release of IL-1 $\beta$  (Heneka et al., 2018). In turn, studies have shown that the NLRP3 inflammasome has a crucial role in the development, progression and exacerbation of amyloid (Heneka et al., 2013; Venegas et al., 2017) and tau (Ising et al., 2019; Stancu et al., 2019) pathologies. Interestingly, the intracerebral injection of brain homogenates containing A $\beta$  fibrils in transgenic mice induced an NLRP3 inflammasome-dependent tau pathology (Ising et al., 2019). Caspase activity is strongly increased in MCI patients as well as AD patients suggesting that the NLRP3 inflammasome activation is an early event in AD pathogenesis (Heneka et al., 2018).

Mounting evidence argues that aging or genetic susceptibility (*e.g.* TREM2 mutations) can compromise microglial protective function and lead to a decrease in amyloid uptake (Hansen et al., 2018; Hellwig et al., 2015; Krabbe et al., 2013; Orre et al., 2014). Indeed, AD brains display age-associated microglial morphological and functional changes, including impaired phagocytosis and motility (Mosher and Wyss-Coray, 2014). This results in increased amyloid toxicity and tau occurrence (Dejanovic et al., 2018; Lee et al., 2021; Leyns et al., 2019). In particular, the TREM2-associated R47H mutant likely impairs microglial function by altering amyloid peptide phagocytosis, clearance and plaque compaction (Dourlen et al., 2019; Wang et al., 2016). Recent studies suggest that TREM2 mutants moreover prevent microglial clustering around amyloid plaques, leading to more diffuse plaques and increased neuritic damage (Wang et al., 2016). Evidence in transgenic mice and human brains have indeed shown that microglia can compact A $\beta$  aggregates in dense core plaques, therefore forming a

neuroprotective barrier around them, reducing their toxicity and preventing neuritic dystrophy (Condello et al., 2015; Yuan et al., 2016) and plaque-associated disruption in neuronal connections through dendritic spine loss (Zhao et al., 2017). Co-cultures of microglia and cortical neurons have shown that proliferating amoeboid microglia attenuate A $\beta$ -mediated neurotoxicity through phagocytosis and release of neurotrophic factor whereas differentiated process-bearing microglia induce neuronal toxicity (Tsay et al., 2013). Dystrophic microglia have been observed in aged human brains further suggesting that AD may develop in the context of altered microglial function (Streit et al., 2009).

### *1.7.3.1.4. Tau and microglia-mediated toxicity*

Activated microglia and increased proinflammatory mediators are associated with tau pathology in AD brains. Indeed, tau seeds are consistently found in reactive microglia of human tauopathy and AD cases (Hopp et al., 2018). However, whether aberrant neuroinflammation is responsible for tau pathology or whether microglia react in response to tau toxicity is still debated (Leyns and Holtzman, 2017).

Cumulative evidence suggest the implication of microglia in initiating and aggravating tau pathology as well as accelerating neurodegeneration. Neuroinflammation induced by the injection of lipopolysaccharide was shown to promote tau hyperphosphorylation in 3xTg (Kitazawa et al., 2005) and wild-type mice (Gardner et al., 2016). Along with synaptic alterations, prominent microglial activation has been observed prior to tangle formation in the hippocampus of 3-month-old P301S transgenic mice, therefore demonstrating that microgliosis can precede tau deposition. Moreover, immunosuppression attenuated tau pathology therefore suggesting a mechanistic link between early microglial activation and tau pathological progression (Yoshiyama et al., 2007). However in this model, despite the absence of tau deposits, robust tau seeding activity was detected as early as at 1.5 months of age suggesting that tau seeds may first trigger microglial activation that in turn further accelerates tau pathology by promoting tangle formation (Holmes et al., 2014). Interestingly, TREM2-deficiency in Thy-Tau22 mice was shown to be associated with reduced microglial activation and increased tau accumulation at late stages of the disease suggesting a dual role of microglia in tau pathology according to disease stage (Vautheny et al., 2021).

Microglial secreted factors were also shown to play a role in tau pathology. Indeed, IL-1 $\beta$ , which is cleaved into its active form downstream of NLRP3 inflammasome activation, promotes tau hyperphosphorylation, is associated with reduced levels of presynaptic protein synaptophysin *in vitro* (Li et al., 2003) and participates in cognitive alterations *in vivo* (Kitazawa et al., 2011). Secretion of TNF $\alpha$  by microglia can lead to tau aggregation in neurites through reactive oxygen species formation (Gorlovoy et al., 2009), and chronic overexpression of TNF $\alpha$  in 3xTg mice exacerbates tau pathology and neuronal death (Janelins et al., 2008).

Furthermore, several studies have involved microglia in tau cell-to-cell spread throughout the brain, either by endocytosis (*e.g.* microglial uptake) or by exocytosis (*e.g.* tau release in exosomes) (Asai et al., 2015). Indeed, several studies have shown that microglia can phagocytose and degrade tau (Brelstaff et al., 2018; de Calignon et al., 2012; Hopp et al., 2018; Luo et al., 2015), but that they may do so inefficiently and secrete it back to the extracellular space, therefore participating in the spreading of bioactive tau seeds (Hopp et al., 2018). In a model of tau propagation based on the injection of an adeno-associated virus in the entorhinal cortex, tau rapidly spread from the entorhinal cortex to the dentate gyrus, suggesting a trans-synaptic propagation of tau. However, the depletion of microglia and inhibition of exosome synthesis markedly reduced tau deposition in the dentate gyrus, therefore suggesting a key role of microglia in tau propagation (Asai et al., 2015).

Disparate data on the role of TREM2 have emerged in mouse models of tau pathology, with TREM2 deletion associated with either neuroprotective effects in PS19 (Leyns et al., 2017) and Thy-tau22 mice (Vautheny et al., 2021) or neurotoxic effects in hTau mice (Bemiller et al., 2017). In humans, microglia associated with amyloid plaques and neuritic pathology express high levels of TREM2. TREM2 levels correlated with phosphorylated tau loads as well as caspase 3 apoptosis marker and a decrease in presynaptic SNAP25 protein (Lue et al., 2015).

Interestingly, studies have also suggested a detrimental role of tau on microglia. Indeed, soluble tau extracted from the hippocampus of AD patients or Thy-tau mice was shown to drive microglial degeneration *in vitro* (Sanchez-Mejias et al., 2016). During aging and AD, dystrophic or senescent microglia, rather than activated microglia, are associated with tau pathology (Davies et al., 2017; Streit et al., 2009). Indeed, microglia in AD brains are characterized by a decrease in cell count, fragmented and dystrophic processes with spheroid, a reduced area of surveillance and an alteration in spatial distribution (Sanchez-Mejias et al.,

2016). Tau pathology can lead to the accumulation of senescent microglia and astrocytes, but it has been suggested that in turn, senescent cells can also contribute to the initiation and progression of tau pathology. Indeed, the clearance of senescent microglial and astrocytes was shown to prevent tau hyperphosphorylation and deposition, neuronal loss and associated cognitive alterations (Bussian et al., 2018).

Overall, cumulative evidence support the dual role of microglia-associated neuroinflammation in the early and late phases of AD, during which disruption in microglial-mediated clearance mechanisms are thought to occur.

### 1.7.3.2. Astrocytosis

#### *1.7.3.2.1. Generalities and physiological functions of astrocytes*

Astrocytes are neural cells of ectodermal, neuroepithelial origin (Verkhatsky et al., 2010) and are thought to be the most prevalent cell type in the brain (Sofroniew and Vinters, 2010). They function in territorial domains, which are non-overlapping functional territories connected to the vasculature and synapses and in which they exert control over many brain functions. Astrocytes are indeed involved in brain homeostasis by providing trophic and metabolic support to neurons, maintaining ionic balance, regulating the blood-brain barrier through contacts with endothelial cells and pericytes, and modulating the CSF flow. Moreover, they are involved in neuronal networks as they promote synapse formation and plasticity through thrombospondin secretion and phagocytosis. They also participate in neurotransmitter uptake and recycling, including glutamate, GABA and ATP (Vasile et al., 2017).

Astrocytes are morphologically and functionally heterogeneous (Arranz and De Strooper, 2019). They can manifest a wide range of activation states associated with distinct effects on disease onset and progression (Matias et al., 2019).

#### *1.7.3.2.2. Astrocytes in the context of AD*

In AD, astrocytes undergo multiple morphological and functional changes. Both atrophic and hypertrophic reactive astrocytes occur at early stages and precede plaque and tangle formation (Rodríguez-Arellano et al., 2016). In late stages, they can be found in the close vicinity of amyloid plaques where they produce abnormal intercellular calcium waves (Verkhatsky et al., 2016).

Atrophic astrocytes are characterized by a reduction in soma volume and processes. The decrease in their morphological complexity reflects a reduction of their territorial domains likely leading to the impairment of their homeostatic functions (Rodríguez-Arellano et al., 2016). On the other hand, reactive astrocytes display a large soma and thicker processes, and highly express the glial fibrillar acidic protein (GFAP) (Arranz and De Strooper, 2019). Reactive astrocytes have been classified into two categories, A1 and A2 astrocytes, depending on their gene expression pattern and the initiating injury. A1 astrocytes are activated by neuroinflammation, notably activated microglia, and are characterized by the release of neurotoxic factors and upregulation of genes involved in the complement cascade, including complement component C3. Moreover, they lose their neurosupportive functions and their ability to promote synaptogenesis and phagocytosis (Liddelow et al., 2017). Conversely, neuroprotective A2 astrocytes are activated by ischemia and secrete neurotrophic factors and thrombospondins involved in synaptic maintenance (Arranz and De Strooper, 2019).

A recent study further categorized astrocytes into mild and severe reactive astrocytes depending on their level of morphological changes and toxicity. Severe reactive astrocytes release excessive amounts of hydrogen peroxide responsible for microglial activation, neurodegeneration, tau pathology and cognitive alterations (Chun et al., 2020).

Additionally, a new population of Gfap-high state astrocytes, called “disease-associated astrocytes” was recently identified in mice and AD brains. Their appearance was associated with a decrease in the homeostatic Gfap-low state astrocyte population. Interestingly, in disease-associated astrocytes, an upregulation of genes involved in endocytosis, the complement cascade and A $\beta$  production and accumulation was observed (Habib et al., 2020).

A $\beta$  can bind to several astrocytic receptors including RAGE and activate intracellular signaling pathways such as the NF $\kappa$ B pathway that results in the release of proinflammatory mediators, such as IL-1 $\beta$ , IL-6, inducible nitric oxide synthase (iNOS) and TNF $\alpha$ . Moreover, A $\beta$ -induced reactive astrocytes can impair mitochondrial functions, increase oxidative stress, disrupt calcium homeostasis and reduce glutamate uptake leading to excitotoxicity (González-Reyes et al., 2017). Altogether, these stimuli are toxic to neurons and can furthermore stimulate A $\beta$  production in astrocytes. Indeed, a variety of cellular stressors can upregulate the machinery for A $\beta$  production present in reactive astrocytes, which were shown to express increased levels of APP,  $\beta$ -secretase and  $\gamma$ -secretase. This suggests that astrocytes may also contribute

to amyloid load in AD, through the production and secretion of A $\beta$  (Frost and Li, 2017). However, astrocytes have also been implicated in the clearance of A $\beta$  and tau through the glymphatic system, a pathway in which contacts between astrocytic end feet and the vasculature enable the elimination of toxic elements, including pathological proteins (Rasmussen et al., 2018). Moreover, astrocytes surrounding plaques display a phagocytic phenotype and were shown to engulf dystrophic neurites (Gomez-Arboledas et al., 2018). Astrocytes express several A $\beta$ -degrading proteases including neprilysin and metalloendopeptidases 2 and 9, and can promote A $\beta$  clearance by secreting ApoE for which they are the primary source in the brain (Ries and Sastre, 2016).

Altogether, the role of neuroinflammation in AD has gained increasing interest over the past few years. Recent data indeed highlight the importance of glial complex and dual interactions with neurons in the AD continuum.

### **1.7.4. Synaptopathy**

In AD, the collapse of neural networks results from neuronal and synaptic degeneration. Synaptic loss occurs at early stages in AD and MCI, prior to neuronal loss (Forner et al., 2017; Scheff et al., 2006). It is the best correlate to cognitive decline (Terry et al., 1991).

#### **1.7.4.1. Synaptic functions and alterations in AD**

Synaptic plasticity is central in learning and memory functions and involves both long-term potentiation (LTP) and its counterpart long-term depression (LTD). LTP is a long-lasting strengthening of synaptic transmission that can occur both at the pre- and postsynaptic compartments. The early phase of LTP is characterized by the persistent activation of kinases leading to changes in  $\alpha$ -amino-3-hydroxy-5-methylisoxazole-4-propionic acid (AMPA) receptors. In late-LTP, persistence in kinase activation and increase in calcium levels regulate gene expression and lead to protein synthesis, including elements involved in spine formation (Spires-Jones and Hyman, 2014). LTD, as opposed to LTP, is a long-lasting weakening of synaptic transmission, including the transmission mediated by AMPA receptors, which is the most affected in AD. It can be triggered through the activation of glutamate receptors, in particular N-methyl-D-aspartate (NMDA) receptors and metabotropic glutamate receptors (mGluRs). LTD is particularly essential for cognitive flexibility (Collingridge et al., 2010).

In AD, the mechanisms associated with synaptic damage might involve axonal transport impairments, as suggested by the altered expression of genes associated with synaptic structural elements, vesicle trafficking and release, neurotransmitter receptors and receptor trafficking (Overk and Masliah, 2014). Aside from synaptic loss, changes in LTP and LTD involved in synaptic plasticity are crucial in AD-associated cognitive alterations.

A $\beta$  and tau have been observed at the synapse, and appear to have both physiological and pathological implications in synaptic functions (Spires-Jones and Hyman, 2014).

#### 1.7.4.2. A $\beta$ -mediated synaptotoxicity

The APP processing machinery can be found at the synapse and is modulated by synaptic activity, which supports the idea that APP and/or A $\beta$  may be involved in normal synaptic function (Spires-Jones and Hyman, 2014).

However, many studies have shown that A $\beta$  can induce both morphological and functional alterations on synapses, which is consistent with elevated A $\beta$  oligomers synaptic levels in AD patients (Bilousova et al., 2016). Experimentally, plaque-bearing mice show a decrease in dendritic spine density, and more particularly near plaques, due to structural plasticity alterations (Spires-Jones and Hyman, 2014). A $\beta$  oligomers derived from the extracellular plaque halo were shown to accumulate both in pre- and postsynaptic terminals (Pickett et al., 2016), but were more abundant at excitatory synapses including those with NMDA receptors involved in synaptic plasticity and memory (Koffie et al., 2009; Lacor et al., 2007). In addition, oligomers in the vicinity of amyloid plaques were negatively correlated with synaptic density (Koffie et al., 2009). Overall, these data further suggest that plaques may act as reservoirs of A $\beta$  oligomers, which were shown to induce synaptic loss, thereby leading to neuronal network alterations (Mucke and Selkoe, 2012).

Several rodent studies have shown that A $\beta$  oligomers extracted from AD brains can alter synaptic structure and activity by inducing a loss of dendritic spines, inhibiting LTP and enhancing LTD, and alter memory function (Figueiredo et al., 2013; Lesné et al., 2006; Shankar et al., 2008; Walsh et al., 2002; Yang et al., 2017). Oligomers can therefore interfere with brain connectivity by altering dendritic spine morphology and function which is known to associate with cognitive decline in AD (Dorostkar et al., 2015; Lacor et al., 2007).



## 1. Alzheimer's disease

---

Furthermore, soluble A $\beta$  can bind to several cell surface receptors and transduce neurotoxic signaling pathways. Studies have shown that LTP impairment is associated with A $\beta$  oligomer binding with the cellular prion protein PrP<sup>c</sup> (Laurén et al., 2009), and that in dendritic spines, this complex can activate the Fyn kinase and induce tau hyperphosphorylation (Larson et al., 2012). A $\beta$  can also bind AMPA receptors therefore impairing glutamatergic transmission and its association with NMDA receptors can moreover disturb calcium homeostasis (Pozueta et al., 2013). Interestingly, A $\beta$ -mediated mGluR5 activation decreases the fragile X mental retardation protein-mediated repression of APP translation therefore increasing postsynaptic intracellular calcium levels, sAPP $\alpha$  secretion and inducing the amyloidogenic  $\beta$ -secretase pathway and amyloid production (Chen et al., 2017; Sokol et al., 2011).

Elevation in calcium levels and downstream activation of calcineurin appear central in A $\beta$ -mediated synaptotoxicity. Indeed, calcium concentration changes have a direct impact on synaptic plasticity, LTP and LTD, notably through NMDA receptors and mGluRs (Shankar et al., 2008; Spires-Jones and Hyman, 2014; Yang et al., 2017). Calcium dyshomeostasis can promote AMPA and NMDA receptor internalization and was also associated with alterations of dendritic spine cytoskeleton (Pozueta et al., 2013).

A $\beta$  oligomers can also alter synaptic vesicle cycling, including the trafficking, release and recycling steps (Chen et al., 2019). In particular, they can impair NMDA receptors trafficking, therefore interfering with proper neurotransmitter release, altering synaptic homeostasis and consequently contribute to synaptic loss and cognitive impairment (Fagiani et al., 2019; Park et al., 2013).

Interestingly, synapses and their activation state can influence A $\beta$  pathology as well. Chronic reduction in synaptic activity reduces plaque burden, inhibits A $\beta$  secretion and promotes its intraneuronal accumulation, but also leads to synaptic loss and exacerbates memory impairment (Tampellini et al., 2011, 2010). Conversely, chronic activation enhances plaque formation (Yamamoto et al., 2015), promotes A $\beta$  secretion and degradation via neprilysin, reduces intraneuronal A $\beta$  and increases synaptic protein levels (Tampellini et al., 2011, 2009).

### 1.7.4.3. Tau-mediated synaptotoxicity

Given its role in maintaining proper neuronal projections and synaptic transmission in the healthy brain, tau acts as a major regulator of synaptic function (Chong et al., 2018). The

---

presence of tau at the synapse was observed under both physiological and pathological conditions (Pooler et al., 2014).

As for amyloid plaques, NFTs can accumulate in some individuals without cognitive dysfunction. However, the aberrant accumulation of soluble phospho-tau species, ranging from monomers to high molecular weight multimeric forms, into the synaptic compartment was associated with dementia (Perez-Nievas et al., 2013). Additionally, in mild cognitive impairment, cognitive status correlates with pre-fibrillar tau rather than NFTs (Mufson et al., 2014). In transgenic mice, neurodegeneration, synaptic loss and behavioral alterations can occur independently from NFT pathology (Andorfer et al., 2005; Yoshiyama et al., 2007), further suggesting that pre-fibrillar soluble oligomeric tau species are more synaptotoxic than aggregated NFTs. Exposure to tau oligomers, either recombinant, extracted from AD brains or in transgenic mice overexpressing human tau can indeed disrupt memory, as well as synaptic and mitochondrial functions in mice (Fá et al., 2016; Lasagna-Reeves et al., 2011).

In addition, a reduction in tau phosphorylation through kinase inhibition decreases its seeding activity and attenuates synaptic loss and LTP impairment in tau mouse models (Seo et al., 2017). In mice expressing human wild-type tau, tau levels correlate with reduced LTP, cognitive alterations and downregulation of synaptic protein expression (Alldred et al., 2012; Polydoro et al., 2009). Spine morphology was moreover altered as the amount of thin spines increased, as opposed to mushroom-shaped ones that are thought to mediate more stable synaptic connections crucial for memory formation (Dickstein et al., 2010).

By altering axonal transport, tau pathological accumulation may modulate mitochondria and receptor trafficking to synapses. This results in the impairment of synaptic vesicle release and can potentially lead to a die-back of axons as a result of decreased ATP production and calcium buffering (Forner et al., 2017). Indeed as for A $\beta$ , pathological tau may be involved in calcium dysregulation and mediate presynaptic dysfunction (Moreno et al., 2016).

Tau localizes both in the pre- and postsynaptic compartments, but the presence of phospho-tau and tau oligomers in synaptosomes is more frequently observed in AD brains (Tai et al., 2012). Pathogenic tau can bind to presynaptic vesicles via its N-terminal domain and the transmembrane protein synaptogyrin-3, therefore impairing synaptic vesicle mobility and release, and subsequently altering neurotransmission (McInnes et al., 2018; Zhou et al., 2017).

The missorting of tau from the axonal to the somatodendritic compartment is considered pathologic. In mice, it leads to synaptic degeneration and dendritic spine loss, impairs mitochondrial transport (Thies and Mandelkow, 2007) and disrupts synaptic function by altering NMDA and AMPA glutamate receptor trafficking and synaptic anchoring (Hoover et al., 2010). Synaptic activity increases tau secretion into the extracellular space (Yamada et al., 2014) and its phosphorylation, which can enhance its mislocalization into dendritic spines and postsynaptic terminals (Frandemiche et al., 2014).

### 1.7.4.4. A $\beta$ and tau synergy at the synapse

A growing body of evidence suggests that A $\beta$  and tau might have a synergic role in altering normal synaptic functions.

In human AD brains and transgenic rat cortices, synaptic A $\beta$  oligomers can be detected at early stages of the disease, while phospho-tau increases in the synaptic compartment at late stages. Throughout the course of AD pathology, early synaptic alterations may be mediated by A $\beta$  whereas tau contribution to synaptic damage becomes more preponderant in late stages and subsequently leads to dementia (Hyman, 2011).

The chronology of A $\beta$  and tau accumulation at the synapse suggests that oligomeric A $\beta$  may drive phosphorylated tau accumulation and synaptic spread (Bilousova et al., 2016). Indeed, it has been suggested that A $\beta$  oligomers can lead to a local rise in cytosolic calcium and drive tau hyperphosphorylation and aggregation into NFTs (Ittner et al., 2010) as well as its missorting into dendrites (Zempel et al., 2010). This in turn leads to impaired axonal transport, synaptic degeneration and functional alteration.

A positive feedback loop between A $\beta$  and tau has been hypothesized, in which A $\beta$  initiates tau pathology, which in turn aggravates A $\beta$  toxicity (Bloom, 2014). Several studies suggest that tau may mediate A $\beta$ -induced synaptotoxicity (Ittner et al., 2010). Indeed, *in vitro*, tau knockout in neurons prevents A $\beta$ -associated spine loss and microtubule degradation (Zempel et al., 2010). The A $\beta$ -associated elevation of intracellular calcium can activate the CAMKK2-AMPK kinase pathway, which mediates the synaptotoxic effects of A $\beta$  oligomers through tau phosphorylation (Mairet-Coello et al., 2013). Moreover, dendritic tau can mediate A $\beta$  toxicity by interacting with the Fyn kinase at the postsynapse. This interaction leads to the phosphorylation and binding of NMDA receptors to the postsynaptic density protein 95 (PSD-

95), strengthening glutamate excitatory signals which in turn enhances A $\beta$  toxicity (Haass and Mandelkow, 2010; Ittner et al., 2010). In addition, removing endogenous tau was shown to prevent A $\beta$ -induced cognitive alterations (Spires-Jones and Hyman, 2014).

#### 1.7.4.5. Neuroinflammation-mediated synaptotoxicity

Neuroinflammation may also play a critical role in synaptic impairment. Indeed, microglia are modulators of neurodegeneration through the phagocytosis of synaptic elements and the release of neurotoxic mediators. Although human genetic data suggest that proper microglial function protects against AD, considerable evidence also suggest the detrimental roles of microglia in synaptic loss. Indeed, many studies put forward that the aberrant activation of developmental microglia-associated synaptic pruning mechanisms may mediate synaptic loss in AD. Moreover, synaptic density reduction was shown to correlate with the internalization of the postsynaptic marker homer by microglial cells (Hong et al., 2016).

The involvement of the complement cascade in microglia-associated synaptotoxicity has been widely studied. The expression profile of complement proteins shows low baseline levels of C1q and C3 expression all throughout life, except for a significant upregulation during development and normal aging (Rajendran and Paolicelli, 2018). In mice, C1q depletion leads to a reduction in microglial activation and in synaptic loss, supporting the detrimental role of C1q on neuronal integrity (Fonseca et al., 2004).

In human AD brains, complement upregulation was associated with amyloid plaques, as well as neurofibrillary tangles and dystrophic neurites (Zanjani et al., 2005). C1q can tag tau-affected synapses, leading to microglial engulfment and synaptic loss in mice (Dejanovic et al., 2018). It was suggested that tau may induce local apoptotic mechanisms leading to phosphatidylserine exposure on synapses, to which C1q can bind (Païdassi et al., 2008) and act as a “eat-me” signal to microglia (Brelstaff et al., 2018).

Interestingly, prior to plaque deposition in mouse models, microglia were shown to mediate early synaptic loss through the complement pathway when exposed to soluble A $\beta$  oligomers (Hong et al., 2016). A $\beta$  oligomers can indeed upregulate C3 expression in microglia, which promotes the removal of synapses. Conversely, C3-mediated impairment of microglial phagocytic function has been reported at late stages of the disease when amyloid plaques are abundant (Lian et al., 2016). *In vitro*, acute C3 activation promotes microglial phagocytosis, as

opposed to chronic exposure to C3 (Lian et al., 2016). These studies highlight the importance of disease stage in complement-mediated regulation of microglial phagocytosis.

Activated microglia can also induce the phosphorylation and upregulation of AMPA receptors, resulting in excitotoxicity, synaptic degeneration and dendritic spine loss (Centonze et al., 2009). Dysregulation in microglial activity can moreover increase the release of neurotoxic mediators, such as TNF $\alpha$ , nitric oxide and IL-6, which can ultimately promote synaptic degeneration (Wang et al., 2015) and reduce the release of soluble factors critical for synaptic plasticity and function such as the brain-derived neurotrophic factor (BDNF) (Parkhurst et al., 2013).

In addition, microglia can trigger the conversion of astrocytes into a neurotoxic "A1" state through the release of C1q, TNF and IL-1 $\alpha$  (Liddel et al., 2017). A1 reactive astrocytes can act in synergy with microglia by upregulating the expression of complement proteins and participate in synaptic and neuronal dysfunction by reducing trophic support and impair clearance (Liddel et al., 2017; Zamanian et al., 2012). Interestingly, astrocyte-mediated synaptic pruning and C1q accumulation were shown to be highly dependent on APOE alleles, as APOE $\epsilon$ 2 knock-in mice showed reduced C1q levels (which may represent the amount of senescent synapses) and enhanced phagocytosis, as opposed to APOE $\epsilon$ 4 knock-in mice (Chung et al., 2016). Compared to wild-type mice, astrocytes in tau P301S transgenic mice expressed less thrombospondin 1, a major survival and synaptogenic factor, therefore suggesting that tau can also mediate synaptic loss by impairing astrocytic functions (Sidoryk-Wegrzynowicz et al., 2017). Moreover, in cultured hippocampal neurons tau oligomer accumulation within astrocytes can disrupt calcium signaling and gliotransmitter release (including ATP), thereby resulting in a decrease in synaptic vesicle release as well as pre- and postsynaptic protein expression (Piacentini et al., 2017).

Altogether, these data highlight the complementary roles of A $\beta$ , tau and neuroinflammation in the impairment of synaptic function observed in AD.

### 1.7.5. Neurodegeneration

Neuronal loss is another hallmark of AD. Although it parallels NFT development, it is a better correlate of cognitive alterations than tau pathology (Gómez-Isla et al., 1997). The neurodegenerative processes involved in normal ageing and AD are qualitatively different and distinct patterns of neuronal loss have been reported (Brun and Englund, 1981; West et al., 1994). Progressive neurodegeneration begins during AD preclinical phases, before plaque and tangle formation (Mukhin et al., 2017), in specific vulnerable brain regions such as the CA1 region of the hippocampus and the entorhinal cortex, which are relatively spared during normal ageing (Gómez-Isla et al., 1996; West et al., 1994). Neuronal density then decreases in the temporal, frontal and parietal cortices, followed by other brain regions in late-stage AD, including the olfactory bulbs, amygdala, basal nucleus of Meynert, substantia nigra, locus coeruleus and dorsal raphe nucleus (Mukhin et al., 2017).

Alterations in postnatal neurogenesis and increased neuronal death are both involved in AD-related neuronal loss (Mukhin et al., 2017). A $\beta$  and tau are thought to act in concert to mediate neurodegeneration notably by altering calcium homeostasis. Indeed given their soluble and diffusible properties, A $\beta$  oligomers can interact with membranes, compromise the lipid bilayer integrity as well as disrupt membrane potential and ionic homeostasis notably by generating calcium-permeable pores (Di Scala et al., 2016). Calcium dyshomeostasis may induce mitochondrial dysfunction and subsequent oxidative stress and neuronal apoptosis (Canevari et al., 2004). A $\beta$  aggregation has been associated with the disruption of respiratory electron transport chain complexes and oxidative damage mediated by the release of reactive oxygen species (Bobba et al., 2013; Manczak et al., 2006). These phenomenon were also observed in synaptic mitochondria and may therefore alter neurotransmitter release (Du et al., 2010). Moreover, generation of nitric oxide as a response to A $\beta$  exposure has been implicated in mitochondrial fragmentation, synaptic loss and subsequent neuronal damage, in part via the nitrosylation of dynamin-related protein 1 (Cho et al., 2009). It has been suggested that pathological A $\beta$  and tau intraneuronal accumulation may also cause endoplasmic reticulum stress and induce apoptosis mediated by calpains and caspases (Bernales et al., 2012; Nakagawa et al., 2000). Furthermore, through the release of neurotoxic factors during neurogenesis, microglial cells have also been implicated in neuronal apoptosis (Brown and Neher, 2014).

### **1.8. Animal models of AD**

Animal models are essential to investigate AD pathology and for the translation of drug trial findings from bench to bedside. The proper selection and validation of animal models ideally relies on three main criteria (Tadenev and Burgess, 2019):

- Construct validity, *i.e.* similar etiological origins and underlying pathophysiological mechanisms;
- Face (or phenomenological) validity, *i.e.* similar phenotypes, including biology and symptomatology;
- Predictive validity, *i.e.* similar responses to clinically effective interventions, including drug administration.

However, no preclinical model can currently reproduce the full spectrum of AD pathology. Here, we will present an overview of rodent transgenic models and spontaneous models of AD.

#### **1.8.1. Transgenic models**

The emergence of transgenic models has allowed many advances in the understanding of AD pathology. Most of them are rodents that overexpress human genes, thereby leading to the artificial development of amyloid and tau pathologies. They present with many advantages as they are well characterized, easy to handle and breed as well as cost-effective, therefore allowing the study of large cohorts.

##### **1.8.1.1. Transgenic mouse models of amyloidosis**

The sequence of wild-type murine APP differs from the human APP in three amino acids within the A $\beta$  sequence (R5G, Y10F, H13R) preventing its aggregation into plaques (Drummond and Wisniewski, 2017). Amyloid plaque formation in mice therefore requires the expression of human APP.

The human wild-type APP model (huAPP<sub>wt</sub>) expresses a non-mutated form of the human APP gene (under the control of the platelet-derived growth factor  $\beta$  chain promoter) leading to a high A $\beta$ <sub>1-42</sub> production in neurons. However, this model does not spontaneously develop amyloid plaques, as opposed to mice expressing human APP bearing fAD-related mutations (Mucke et al., 2000) (**Figure 18**).

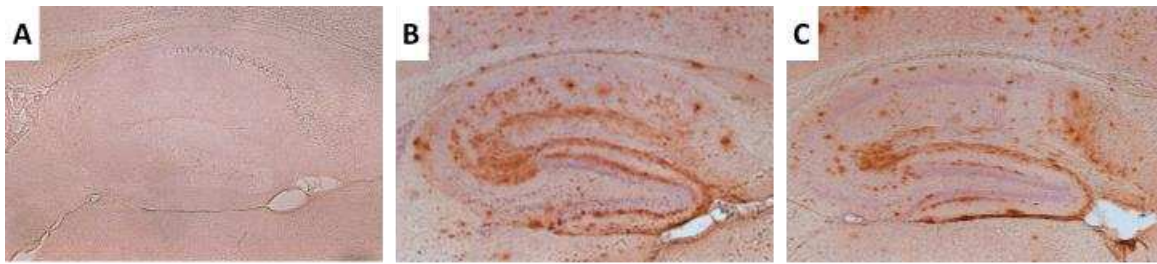


**Figure 18: Amyloid plaque deposition spontaneously occurs in fAD-mutant huAPP mice but not in huAPP<sub>wt</sub> mice.**

Hippocampal sections of huAPP<sub>wt</sub> (A), huAPP<sub>Ind</sub> bearing the fAD 717<sub>V→F</sub> mutation (B) and huAPP<sub>Sw,Ind</sub> bearing the fAD 717<sub>V→F</sub> and 670/671<sub>KM→NL</sub> mutations (C). Amyloid plaques were stained with the 3D6 antibody. Adapted from (Mucke et al., 2000).

In fAD-mutant huAPP models, neuritic plaques, gliosis, synaptic alterations (Games et al., 1995) and neuronal loss (Masliah et al., 1996) have been reported.

Similarly, it has been shown that the co-expression of mutated APP and presenilin 1 genes leads to a more severe pathology. This resulted in the generation of models exhibiting different pathological and behavioral characteristics associated with different time courses, depending on the mutations, the promoter and the background strain that were involved. Overall, these models develop a heavy load of amyloid plaques associated with gliosis. They display various levels of cognitive impairment that can be associated with synaptic alterations and neuronal loss in some models. However, tau lesions were usually sparse and in the form of pre-tangles rather than neurofibrillary tangles (Drummond and Wisniewski, 2017).

The APP/PS1dE9 model expresses a humanized APP gene with the Swedish K670N/M671L mutations and a human PS1 gene lacking exon 9 (Jankowsky et al., 2004) under the mouse prion promoter and on a C57BL/6J background. These mutations lead to an increase in amyloid production and in the A $\beta$ <sub>42/40</sub> ratio. This model begins to develop amyloid plaques by 4 months of age with a progressive increase in plaque deposition until 12 months of age, both in the cortex and hippocampus (Garcia-Alloza et al., 2006a). Secondly to A $\beta$ , insoluble hyperphosphorylated tau aggregates, including PHFs, have been reported around amyloid deposits at 18 months old (Metaxas et al., 2019). Neuroinflammation accompanies the development of amyloid plaques (Kamphuis et al., 2012). Synaptic alterations were observed at three months of age with a decrease in pre- and postsynaptic markers colocalization linked



to microglial activation (Hong et al., 2016), and with LTP deficits by 6 months (Viana da Silva et al., 2016). Deficits in contextual (Kilgore et al., 2010) and spatial memory (Volianskis et al., 2010) have been reported at 6 and 12 months respectively, along with alterations in spontaneous behaviors such as nest building and burrowing (Janus et al., 2015).

### 1.8.1.2. Transgenic mouse models of tauopathy

The lack of sequence homology between murine and human tau is thought to be involved in the fact that mouse do not spontaneously develop neurofibrillary tangles. Indeed, adult mice express a unique 4R tau isoform, as opposed to the human tau protein that exists under six isoforms, with both 3R and 4R isoforms (Andorfer et al., 2003).

Tau knock-in mice (hTau) express all six isoforms of the human wild-type tau protein, but lack the murine tau protein as its presence may interfere with human tau accumulation (Duff et al., 2000). This model develops hyperphosphorylated tau and an age-dependent mislocalization of tau from the axonal to the somatodendritic compartment. Moreover, tau pathology shows a regional distribution similar to humans, with the majority of the pathology observed in the neocortex and hippocampus (Andorfer et al., 2003). Tau aggregates are observed in the forms of PHFs by 9 months and NFTs by 15 months of age (Andorfer et al., 2005). Extensive neurodegeneration can be observed in this model but is not clearly correlated with tau fibrillary accumulation, suggesting that cell death can occur independently from NFT accumulation (Andorfer et al., 2005). Moreover, age-dependent cognitive and synaptic deficits precede neurodegeneration as both object recognition and spatial memory are altered and electrophysiological dysfunctions at the Schaffer collateral to CA1 pyramidal cell synapses are reported by 12 months (Polydoro et al., 2009).

Most transgenic mouse models of tauopathy were engineered to overexpress the MAPT gene bearing FTD-associated mutations, such as the P301L or P301S mutations. They develop NFTs and neurodegeneration, as well as synaptic deficits and cognitive impairment. However, they also display significant motor impairment as tau pathology develops in the spinal cord and brainstem, thus interfering with behavioral evaluation and limiting their relevance in translational research (Puzzo et al., 2014).

Moreover, most models develop widespread tau pathology that do not reflect the stereotyped pattern of progression observed in AD (Braak and Braak, 1991). An AD-like

progression of tau was reproduced in the rTgEC model, in which the overexpression of the human 4R tau gene with the P301L mutation was restricted to the entorhinal cortex. Indeed, progressive tau pathology was observed in the form of Gallyas-positive NFT-like aggregates in the entorhinal cortex at 18 months and followed by hyperphosphorylated tau accumulation in the dentate gyrus and CA1 region of the hippocampus by 24 months of age (de Calignon et al., 2012).

### 1.8.1.3. Transgenic mouse models of amyloidosis and tauopathy

Transgenic mice overexpressing mutated forms of APP, MAPT and PS1 were also designed to produce more complete models that recapitulate both amyloid and tau lesions. Among them, the 3xTg mouse bearing the APP Swedish K670N/M671L, MAPT P301L and PS1 M146V mutations is the most widely used. 3xTg mice develop age-related intracellular and extracellular amyloid followed by NFTs in the hippocampus and cortex (Oddo et al., 2003). Synaptic and cognitive alterations occur before plaque and NFT formation in this model (Billings et al., 2005). Astrogliosis has also been reported (Caruso et al., 2013). However, the appearance of these AD-like lesions is heterogeneous and shows high variability depending on the breeding laboratory. Moreover, the applications of the 3xTg mouse model remain limited as this model is based on the non-physiological overexpression of mutated proteins that only reflect some aspects of fAD or FTD.

### 1.8.1.4. Transgenic rat models

Fewer transgenic rats were developed to model amyloid and tau pathologies. As for mice, the expression of fAD-related mutations in APP and/or PS1 genes has been used to induce extensive amyloid plaque pathology in rats. The TgF344-AD rat line was generated on a Fisher 344 background and expresses the Swedish mutant human APP and the human PS1 lacking exon 9 genes, both driven by the mouse prion promoter. Rats develop an age-dependent amyloidosis in the forms of amyloid plaques, amyloid angiopathy, intraneuronal deposits and soluble oligomers. Greater similarities with humans in the rat MAPT tau sequence resulted in the development of NFT-like lesions, in aged rats without any tau mutations, both in the close proximity of amyloid plaques and in regions without amyloid deposition. Neuronal loss and behavioral changes, including hyperactivity, spatial learning and memory deficits, were

## 1. Alzheimer's disease

---

reported by 16 months of age. Reactive microglia and astrocytes were increased at 6 months of age, before amyloid deposition (Cohen et al., 2013).

Transgenic rat models of tauopathy are rarely described. Recently, the R962-hTau line expressing the human 2N4R tau isoform with the P301S mutation under the control of the mouse CAMKII $\alpha$  promoter was generated. Rats displayed an age-dependent accumulation of aggregated tau inclusions, neurodegeneration associated with cerebral atrophy and neuronal loss, as well as activated microglia and astrocytes. Cognitive deficits in the novel object recognition, Morris water maze and fear conditioning tasks were reported at advanced tau pathology stages (Malcolm et al., 2019).

Although useful to evaluate specific pathological features, most transgenic models only recapitulate parts of AD lesions and do not display widespread amyloid and tau pathologies. In addition, the non-physiological overexpression of mutated genes and potential interactions with endogenous proteins, needed to induce pathological features, poorly reflect the human pathology phenotype. Therefore, the translational value of these transgenic models remains limited.

### **1.8.2. Spontaneous models**

Many animal species can spontaneously develop AD-like lesions as they age. Among them, common degus, dogs and non-human primates were the most characterized.

#### **1.8.2.1. Common degu**

The common degu (*Octodon degus*) is a small rodent endemic in central Chile. It is the only known wild-type rodent that naturally develops AD-like lesions with age. Its A $\beta$  sequence is highly homologous to humans, with a single amino acid substitution. The old common degu can spontaneously develop amyloid deposits, both in cortical regions and in the hippocampus (Braidy et al., 2015), as well as intracellular tau, NFTs and astrocytosis. Moreover, synaptic impairment and deficits in spatial and object recognition memory correlate with A $\beta$  oligomer loads and tau hyperphosphorylation (Ardiles et al., 2012). However, contradictory studies have shown that common degus in captivity do not always develop these lesions with age (Steffen et al., 2016).

### 1.8.2.2. Dogs

Dogs have the same A $\beta$  sequence as humans and can develop both amyloid plaques and vascular deposits starting at 8-9 years old (Schütt et al., 2016; Uchida et al., 1991). The majority of amyloid plaques are diffuse and follow a progressive pattern of distribution starting from the prefrontal cortex to temporal and occipital cortical regions (Head et al., 2000), which parallels human pathology. Moreover, A $\beta$  oligomer load increases with age while the CSF A $\beta_{42}$ /A $\beta_{40}$  ratio decreases and is a good predictor of cerebral amyloidosis (Head et al., 2010). As for tau pathology, a limited number of cognitively impaired dogs were shown to develop pre-tangles, but not NFTs, and accumulate hyperphosphorylated tau in synaptosomes (Smolek et al., 2016). In addition, aged dogs can display cortical and hippocampal atrophy (Tapp et al., 2004).

### 1.8.2.3. Non-human primates

Non-human primates (NHPs) have the advantage of being phylogenetically close to humans and show many similarities with them in terms of physiology, neuroanatomy and behavioral complexity. In addition, A $\beta$  and tau proteins are highly homologous in NHPs and humans. Aged NHPs can replicate the human aging process and develop AD-like pathological features, although they do not manifest the full phenotype of AD.

#### *1.8.2.3.1. Great apes*

Technical constraints such as a long lifespan (up to 60 years for chimpanzees and gorillas) and ethical concerns resulted in very few studies characterizing the neurobiological process of aging in great apes.

Senile plaques and amyloid angiopathy have been reported in various great apes including chimpanzees (*Pan troglodytes*) (Gearing et al., 1994), gorillas (*Gorilla gorilla*) (Kimura et al., 2001; Márquez et al., 2008) and orangutans (Gearing et al., 1997). Overall, vascular amyloidosis appears to predominate over parenchymal plaque deposition, which is usually very sparse. Old chimpanzees can display similar levels of cerebral insoluble A $\beta$  than AD patients. However, NHP amyloid proteins might have specific biophysical properties that are different to humans as suggested by a lower affinity for the PiB benzothiazole imaging agent (Rosen et al., 2011).

## 1. Alzheimer's disease

---

The presence of NFTs in great apes remains unclear. Some tau deposits were reported in the gorilla (Márquez et al., 2008) and one case report has revealed cortical AD-like PHFs following a stroke in an aged chimpanzee that displayed several human AD risk factors such as obesity and hypercholesterolemia (Rf et al., 2008).

Cognitive impairment and more specifically spatial memory alteration has also been reported in aged chimpanzees (Lacreuse et al., 2014).

### *1.8.2.3.2. Old world monkeys*

Spontaneous age-related parenchymal and vascular deposition of amyloid has been observed in aged rhesus monkeys (*Macaca mulatta*) (Poduri et al., 1994; Uno et al., 1996) as well as cynomolgus monkeys (*Macaca fascicularis*) (Nakamura et al., 1998) with variability among animals. As opposed to humans, plaques were mainly composed of A $\beta$ <sub>40</sub> (Gearing et al., 1996; Sani et al., 2003). Aged rhesus monkeys mainly displayed diffuse plaques although some compact cortical plaques have been described in the eldest (after 29 years) as well (Sani et al., 2003). Swollen neurites and gliosis (microglial and/or astrocytic activations) have been reported around plaques (Poduri et al., 1994).

A neocortical to allocortical spreading of amyloid plaques, starting from association cortical areas to paralimbic and limbic cortical regions has been reported in old rhesus monkey (Sani et al., 2003), similar to human pathology (Thal et al., 2006b). Deposition in subcortical regions were located within the striatum and the caudate nucleus. However, another report suggested that amyloid plaque deposition follows a pattern specific to each individual (Sloane et al., 1997), further supporting the high variability of amyloid pathology among rhesus monkeys. As opposed to amyloid spreading in AD, the hippocampus is usually reported as free of plaques and only a few neuritic plaques are usually observed in aged rhesus monkeys (Sloane et al., 1997).

Occasional abnormally phosphorylated tau depositions were observed in the brains of rhesus monkeys (Härtig et al., 2000) and cynomolgus monkeys (Oikawa et al., 2010), but NFTs were not reported. Interestingly, age-related pathological tau progression has also been observed in old baboons (Schultz et al., 2000), with abnormally phosphorylated tau proteins described in both neurons and glial cells (Schultz et al., 2001).

Cortical thickness remains stable with age and no evidence of neurodegeneration has been reported in the neocortex nor in the hippocampal formation. No change in astrocytic and microglial densities were observed either (Peters and Kemper, 2012). Aging however impacts the synaptic organization of the cerebral cortex as a significant decrease in excitatory and inhibitory synapses (Peters et al., 2008) along with a loss of dendritic spines (Kabaso et al., 2009) from the upper layers of the prefrontal cortex were correlated with cognitive impairment. A significant reduction in nerve fibers from white matter tracts in the splenium of the corpus callosum, the fornix and the anterior commissure has been correlated with increasing age and cognitive decline (Peters and Kemper, 2012).

Old-world monkeys can develop cognitive deficits with age. Notably, recognition and spatial memory alterations (Herndon et al., 1997), decrease in performances in reversal learning (Lai et al., 1995) and set-shifting (Moore et al., 2006) can appear in middle-aged rhesus monkeys, in their early twenties. Interestingly, novel object recognition deficits in old rhesus macaques have been associated with hyperactivity in the CA3 region of the hippocampus, compared to adult animals (Thomé et al., 2016). No correlation has been reported between cognitive status and amyloid plaque burden (Sloane et al., 1997).

#### *1.8.2.3.3. New world monkeys*

Some parenchymal plaques and mostly amyloid angiopathy were found in the brains of aged squirrel monkeys (*Saimiri sciureus*) (Elfenbein et al., 2007) and marmosets (*Callithrix jacchus*). In the former species, histological studies have shown that amyloid lesions were composed of both A $\beta$ <sub>40</sub> and A $\beta$ <sub>42</sub> and were particularly abundant in the neocortex, whereas only a few lesions were found in the amygdala and the hippocampus (Elfenbein et al., 2007). For the marmoset, association cortical regions were predominantly affected followed by less lesions in the paralimbic cortex (Geula et al., 2002). Vascular A $\beta$  deposits were found to affect arteries, arterioles and capillaries in the squirrel monkey (Elfenbein et al., 2007).

As in great apes and old world monkeys, no significant tau pathology has been observed in the brains of new world monkeys although a few neurons bearing abnormally phosphorylated tau were observed in aged squirrel monkeys (Elfenbein et al., 2007). Moreover, dystrophic microglia in aged marmosets were shown to be associated with hyperphosphorylated tau (Rodríguez-Callejas et al., 2016).

## 1. Alzheimer's disease

---

Alterations in the prefrontal cortex functions were observed in the squirrel monkey, as suggested by impaired cognitive response inhibition, that was moreover correlated with an increase in white matter volume (Lyons et al., 2004).

### *1.8.2.3.4. Prosimians : the gray mouse lemur*

Technical constraints associated with the need for specific housing facilities, breeding and long lifespan have led to limited studies in NHPs. The gray mouse lemur (*Microcebus murinus*) model presents with many advantages including, their small body size and a relatively short life expectancy of approximately twelve years in captivity. Additionally, it can be easily bred and kept in captivity at low costs (Pifferi et al., 2019) (**Figure 19**).



**Figure 19** : The gray mouse lemur (*Microcebus murinus*)

As the mouse lemur was the primate species used in this PhD thesis, the following paragraphs of the **Animal models of AD chapter** will be exclusively dedicated to its presentation.

### **1.8.3. The gray mouse lemur: an emerging model of AD pathology**

#### **1.8.3.1. Generalities on the mouse lemur**

The gray mouse lemur belongs to the *Strepsirrhini* suborder, the *Lemuriformes* infraorder and the *Cheirogaleidae* family originating from Madagascar. It is one of the smallest primates in the world with a body length of approximately 15 cm and a 60 to 80 g body weight (Pifferi et al., 2019). The mouse lemur is an arboreal species which vertical jump can reach up to 33±4 cm (Legreneur et al., 2010). It is a nocturnal and solitary forager that frequently rests in groups during daytime. Its diet is omnivorous and mainly composed of fruits and insects.

The mouse lemur is very sensitive to photoperiodic variations and shows a high phenotypic plasticity allowing its adaptation to fluctuating environmental conditions. During the 6 months of the cool and dry season, characterized by a short photoperiod, low temperatures and limited food resources, the mouse lemur adapts to its hostile environment by developing energy saving strategies. It is a heterothermic species that can go into daily torpor, a state of decreased activity associated with reduced body temperature, hypometabolism and increased fat deposits. Conversely, during the hot rainy season, characterized by a long photoperiod, elevated temperatures and food abundance, physical activity increases along with metabolic rate whereas its body weight decreases (Pifferi et al., 2019).

The mouse lemur reproductive activity is seasonal, with the summer corresponding to the mating period. Various physiological and hormonal changes occur: increase in testicle size, functional spermatogenesis and high testosterone levels in the males, entry in the ovulatory period, rupture of the vulva membrane in the females (Eberle and Kappeler, 2004; Perret, 1997). Following a two-months gestation period, females give birth to 1 to 3 offspring per litter with a weaning period of 6 to 8 weeks (Perret, 2005). The transition into adulthood occurs at 6 to 8 months of age together with sexual maturity and the first signs of ageing appear at approximately 6 years old.

In its natural biotope, the mouse lemur lifespan is relatively short (approximately 3 to 4 years) because of food restriction, parasitism and high predation by hawks and snakes (Lutermann et al., 2006). However, mouse lemurs can live up to 12 years in captivity, allowing the study of sensorimotor, endocrine, physiological and cerebral alterations that occur as they age. As these alterations are similar to modifications occurring in humans, the mouse lemur appears



## 1. Alzheimer's disease

---

as a privileged model to study physiological and pathological ageing processes and their consequences on brain function. Indeed, it is an emerging model in the study of AD pathology since it is estimated that around 20% of aged individuals display AD-like pathological changes (Languille et al., 2012).

### 1.8.3.2. AD-related genes similarities with humans

Genes associated with fAD have been partially sequenced in *Microcebus murinus*. The mouse lemur APP, PS1 and PS2 genes have respectively a 100, 95.3 and 95.6% sequence homology with their human counterparts (Calenda et al., 1998, 1996; Silhol et al., 1996). Of note, differences in presenilin amino acid sequences do not correspond to known mutations in fAD (Bons et al., 2006). Mouse lemurs are APOE $\epsilon$ 4 homozygotes, and this allele presents a 92.7% homology with the human sequence, differing by a single nucleotide (Calenda et al., 1995).

Interestingly, transcriptomic studies have highlighted the differential expression of various genes involved in the regulation of protein synthesis in lemurs undergoing normal ageing compared to animals presenting an AD-like pathology (Abdel Rassoul et al., 2010).

### 1.8.3.3. Cognitive alterations

During their normal ageing process and with the same 10% prevalence as in humans over 65, mouse lemurs can develop cognitive deficits with progressive alterations in executive functions and declarative memory (Languille et al., 2012). Additionally, a decline in attention and visual discrimination has been reported among aged subjects (Bons et al., 2006; Schmidtke et al., 2020), as opposed to procedural memory which is relatively spared (Languille et al., 2012; Steenland et al., 2016).

### 1.8.3.4. Brain morphological and functional changes

Aged lemurs can develop a massive brain atrophy associated with cerebral ventricle dilation (Bons et al., 2006; Kraska et al., 2011) (**Figure 20**).

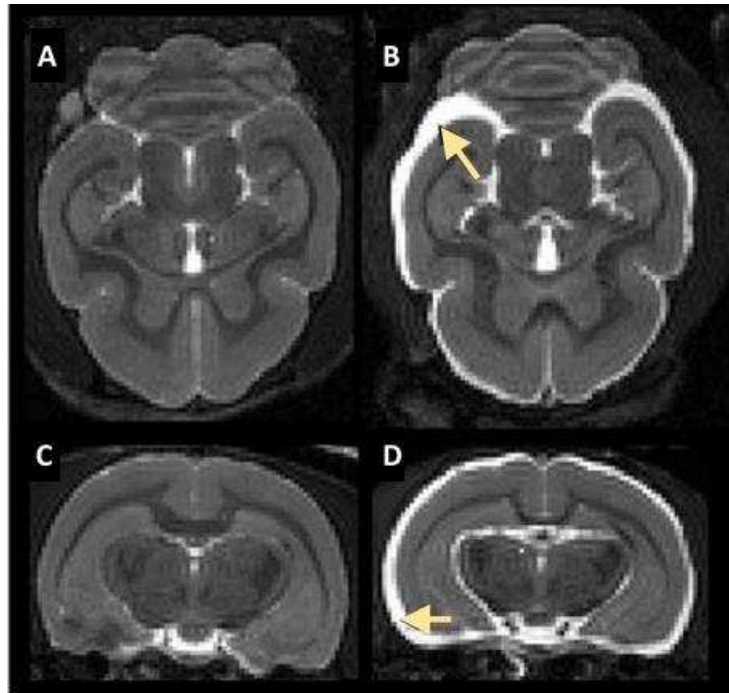


**Figure 20: Cerebral atrophy in the aged mouse lemur**

Axial (A-B) and coronal (C-D) MRIs from a young 5.5-year-old lemur (on the left) and an aged 8.8-year-old lemur (on the right). Atrophy in the aged animal was measured through the evaluation of the CSF volume (arrow) (Kraska et al., 2011).

Similarly to humans, interindividual variability can be observed among mouse lemurs. Interestingly, some aged animals can develop specific alterations reminiscing of an AD-like pathological process. Indeed, in some cases, old lemurs show septal and medial temporal atrophy, including in the hippocampus and the entorhinal cortex, regions that are normally spared during physiological ageing. These lesions are respectively correlated with executive dysfunction and spatial memory impairment (Picq et al., 2012).

Additionally, glucose metabolism alterations have been reported following blood examination (Djelti et al., 2016) and PET functional imaging (Dorieux, 2012). As in humans, impaired fasting blood glucose was correlated with cerebral atrophy and cognitive impairment in middle-aged animals, suggesting the role of metabolic alterations as a risk factor for pathological ageing (Djelti et al., 2016; Geijselaers et al., 2015).

Finally, functional MRI studies have highlighted that aged lemurs can display alterations in the default-mode network, which is also predominantly impaired in AD patients (Garin et al., 2021).

### 1.8.3.5. Neuropathological lesions

Neuropathologically, AD-type lesions can also be found in some aged animals and their presence has been correlated with the severity of brain atrophy (Kraska et al., 2011).

#### *1.8.3.5.1. A $\beta$ pathology*

Parenchymal A $\beta$  plaques are predominantly observed in cortical regions, more specifically in occipital and parietal cortices, and can occasionally expand to the hippocampus, amygdala, thalamus and brainstem. Both diffuse and dense core plaques can be found, as well as intracellular deposits. Additionally, vascular deposits are observed in the wall of leptomeningeal vessels, cortical arterioles and capillaries in 30% of aged animals (Languille et al., 2012) (**Figure 21**). Most cortical plaques are A $\beta_{42}$ -immunopositive whereas only a subset is positive for A $\beta_{40}$  (Mestre-Francés et al., 2000).

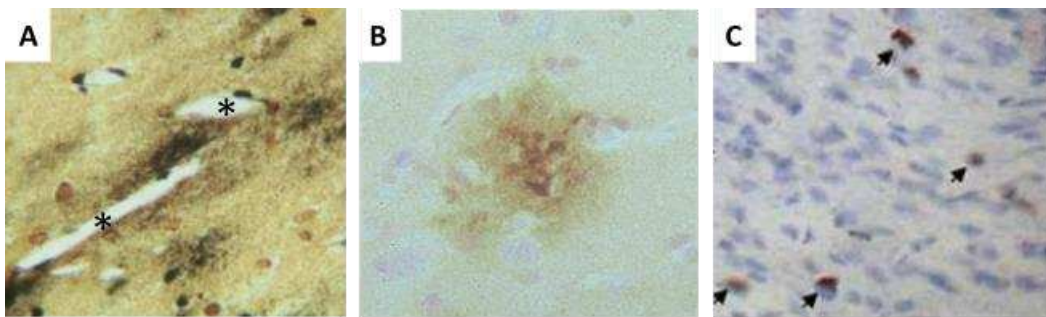


**Figure 21: A $\beta$  deposition in aged mouse lemurs**

Extracellular diffuse (A) and dense core (B) plaques, or intracellular amyloid deposits (C) in aged mouse lemurs. The symbol \* indicates the lumen of arterioles (Bons et al., 2006; Kraska et al., 2011).

In aged lemurs, low A $\beta_{40}$  plasmatic levels have been associated with white matter and subcortical atrophy (Gary et al., 2018), and inversely correlated with cerebral A $\beta$  intracellular levels (Roy et al., 2015). Additionally, poor performance in discrimination tasks in old age has been shown to predict A $\beta$  accumulation (Schmidtke et al., 2020).

#### *1.8.3.5.2. Tau pathology*

Abnormally aggregated tau proteins can be found both in young adults and aged animals (**Figure 22**). However, the prevalence and density of tau-positive accumulation increase with

age. Additionally, an age-related regional progression of tau pathology has been observed with lesions appearing early in the neocortex and affecting the subiculum, entorhinal cortex and amygdala of animals over 8 years. Interestingly, in animals of 8 years or more, these lesions occur with a density comparable to that seen in AD patients (Bons et al., 2006; Giannakopoulos et al., 1997). However, tau lesions are morphologically and biochemically different from NFTs in AD brains. Indeed, they are mainly localized in the soma and neurites of neurons from the frontal and occipital cortices, and only some of them are labeled with human anti-PHF antibodies (Bons et al., 1995).

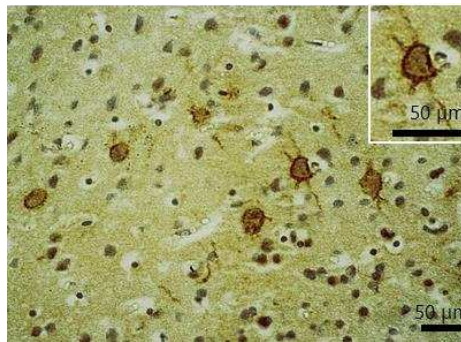


**Figure 22: Tau pathology in an aged mouse lemur**

Tau protein-immunoreactive accumulations in the parietal cortex of an old 6-year-old mouse lemur (Giannakopoulos et al., 1997).

During ageing, a change of conformation and stabilization in the tau hyperphosphorylation state leads to an increase in the apparent molecular weight of tau variants, shifting from 52-54, 64 and 67 kDa to 60 and 70kDa variants. Interestingly, the 60 kDa variant is recognized by PHF-directed antibodies suggesting the presence of AD-type epitopes in the mouse lemur brain (Delacourte et al., 1995).

Of note, no correlation has been reported between A $\beta$  and tau lesion densities (Giannakopoulos et al., 1997).

#### *1.8.3.5.3. Gliosis*

Activated microglia and astrocytes have been associated with amyloid plaques (Bons et al., 2006; Giannakopoulos et al., 1997) (**Figure 23**). Additionally, in the presence of A $\beta$  plaques, GFAP levels were shown to increase by two-fold (Languille et al., 2012).

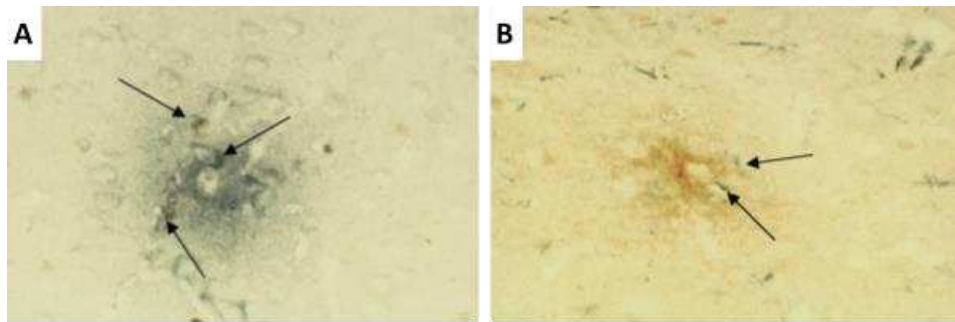


**Figure 23: Amyloid-plaque associated glia in the mouse lemur brain**

Double immunolabeling revealed (A) microglia (anti-ferritin labeling) and (B) astrocytes (anti-GFAP) in the area of amyloid plaques (anti-A $\beta_{42}$ ) (Bons et al., 2006).

### *1.8.3.5.4. Synaptic alterations*

A dramatic loss of basal ganglia cholinergic neurons is commonly found in aged animals, reaching 40% in the accumbens nucleus, 70% in the caudate nucleus and 80% in the globus pallidus. Remaining neurons show an altered morphology with the shortening of neuritic processes, lack of ramifications and large vacuoles in the soma (Languille et al., 2012). The most severely affected animals also show A $\beta$  plaques, tau-positive deposits, poor cognitive performances and altered behavior associated with a loss of biorhythm (Bons et al., 2006). Additionally, a decrease in catecholaminergic and serotonergic neurons has also been reported in old animals, albeit to a lesser extent (Bons et al., 2006).

Interestingly, the administration of currently approved cognitive enhancers, *i.e.* the acetylcholinesterase inhibitor donepezil and the NMDA receptor antagonist memantine, in mouse lemurs, can prevent sleep-induced cognitive deficits, highlighting the translational potential of the mouse lemur model (Rahman et al., 2017).

### 1.8.3.6. Advantages and limits of the mouse lemur model

The mouse lemur clearly appears as an emerging model of AD as many aspects of its pathological ageing process resemble sporadic AD pathology. It naturally models biological heterogeneity and spontaneously develops AD-like lesions at an advanced age, including cognitive deficits, morphological and functional brain alterations associated with synaptic changes, A $\beta$  and tau deposition and neuroinflammation. As in sporadic AD, these lesions are not associated with specific mutations in APP or presenilin genes. Moreover, mouse lemurs

can show altered social interactions with stereotyped behavior such as isolation and aggressiveness, loss of normal circadian rhythmicity and display impaired olfaction with olfactory brain structures showing structural degeneration, A $\beta$  deposition and gliosis (Bons et al., 2006). As in humans, aged animals show impaired cognitive function along with brain atrophy, age-related A $\beta$  and tau pathologies and loss of cholinergic neurons (Bons et al., 2006). However, the mouse lemur model also has several limitations. Biologically, mouse lemurs exhibit particularities that oppose them to humans such as being nocturnal and highly photoperiodic species with marked seasonal phenotypes (Languille et al., 2012). The neuroanatomy of the mouse lemur brain is characterized by a size that is similar to the rat brain (approximately 23 mm long, 18 mm wide and 1.7g weight) and a distinct macroscopic organization with reduced cortical surface in comparison with other primates (Bons et al., 1998; Le Gros Clark, 1931). Furthermore, the pattern of brain atrophy observed during aging is different as it begins in the frontal cortex and progresses to the temporoparietal and occipital regions (Kraska et al., 2011), while in AD medial temporal structures are first affected followed by the lateral temporal, inferior parietal and orbitofrontal regions (Rasero et al., 2017). Finally, the distribution of A $\beta$  and tau deposits sharply contrasts with humans as lesions are mainly found in cortical regions as opposed to the hippocampus which is largely spared (Giannakopoulos et al., 1997). This suggests a differential neuronal vulnerability to pathological protein accumulation in mouse lemurs. Additionally, these AD-type lesions only spontaneously develop after 6 years of age and in approximately 20% of mouse lemurs (Bons et al., 1992). As for rodent and other NHP models, the occurrence of these lesions should be experimentally accelerated to facilitate their characterization.

In conclusion, although available models do not fully reproduce the complete spectrum of AD, some are able to recapitulate several aspects of AD pathology. More specifically, NHPs appear to have an important translational value in AD research due to their genetic and biological proximity with humans. Of note, the mouse lemur could be considered as a good compromise between rodent and higher primate models.

To promote the occurrence of AD pathology in animal models, genetic manipulation has been widely used but other procedures have also been undertaken. In particular, the prion-like hypothesis of AD posits that A $\beta$  and tau pathological aggregates can induce the misfolding and

pathological conversion of native proteins. Thus, over the last decades, new paradigms were established to induce widespread A $\beta$  and tau pathologies through the intracerebral injection of A $\beta$  and tau pathological proteins, either synthetic or extracted from the brains of human AD patients or transgenic models. These inoculated models provide a unique opportunity to re-examine relationships between AD core lesions and downstream neurodegenerative processes (see **§ 4.4. Prion-like hypothesis of AD – Seeding experiments**). During my PhD thesis, we investigated the impacts of human AD brain extracts inoculations in two complementary models, well-characterized in our laboratory, namely, the APP/PS1dE9 mouse model and the mouse lemur primate model (see **Results chapter**).

---

## 2. Sporadic AD heterogeneity

---

AD is a heterogeneous disorder characterized by different genotypes and phenotypes. In the context of sporadic AD, multiple pathophysiological outcomes associated with different clinical presentations can be observed, dividing sporadic AD into multiple subtypes.

### 2.1. Clinical subtypes of AD

AD is commonly characterized as a late-onset amnesic-predominant disorder. However, various atypical subtypes have been clinically identified, including both amnesic and non-amnesic variants. They differ from typical AD in their cognitive profile, age of onset and rate of disease progression. Indeed, while the atypical amnesic variant is associated with a late onset and slower rates of decline than typical AD, non-amnesic AD variants are characterized by an early onset, faster rates of decline and an APOE $\epsilon$ 4 negative genotype (Scheltens et al., 2017, 2016). These non-amnesic atypical variants, *e.g.* visuospatial (including posterior cortical atrophy; PCA), language (including logopenic primary progressive aphasia; LPA) and frontal variants, account for approximately 14% of AD cases (Galton et al., 2000). Interestingly, each clinical variant is also characterized by specific focal patterns of brain hypometabolism/hypoperfusion reflecting the involvement of different functional networks. Additionally, distinct patterns of A $\beta$  and tau deposition can also be observed in each subtype (Lam et al., 2013) and the most atrophied and hypometabolic regions greatly overlap with the ones showing the most severe tau deposition (Lehmann et al., 2013).

#### 2.1.1. Pure amnesic temporal AD

Pure amnesic AD patients show isolated defects of episodic and semantic memory while visuospatial and executive functions are relatively spared (Butters et al., 1996). Cerebral hypoperfusion is prominent in the mesial temporal lobes and absent in temporo-parietal regions usually affected in typical AD (Cappa et al., 2001). Neuropathologically, pure amnesic AD patients may correspond to a subset of late-onset cases with NFTs restricted to limbic areas, even at late stages of the disease (Armstrong et al., 2000).



### **2.1.2. Posterior cortical atrophy**

PCA clinical phenotype is characterized by predominant visuospatial and visuoperceptual alterations (Karantzoulis and Galvin, 2011; Scialò et al., 2019). Right parietal hypometabolism with reduced FDG uptake can be observed in the right ventral default mode, right executive-control and higher-order visual networks (Lehmann et al., 2013). Tau regional distribution differs from typical AD cases as NFT occurrence in occipital regions is more frequent (Karantzoulis and Galvin, 2011; Scialò et al., 2019). Moreover, differences in the molecular architecture of misfolded A $\beta$  was also observed between PCA and typical AD, using luminescent conjugated oligothiophenes binding to amyloids (Rasmussen et al., 2017).

### **2.1.3. Logopenic primary progressive aphasia**

LPA is a language variant associated with a slow speech rate, impaired single-word retrieval in spontaneous speech as well as sentence comprehension and repetition deficits. As opposed to other primary progressive aphasias, grammar and articulation are preserved (Gorno-Tempini et al., 2008). Gray matter atrophy or hypoperfusion can be observed in left posterior temporal and inferior parietal regions (Gorno-Tempini et al., 2008), as well as a trend towards lower FDG uptake in the left language network (Lehmann et al., 2013). Interestingly, sentence repetition and comprehension deficits were positively correlated with A $\beta$  neocortical load (Leyton et al., 2011). LPA patients moreover display greater tangle deposition in left hemisphere language regions and higher neocortical-to-entorhinal tangle ratio than typical AD cases (Gefen et al., 2012).

### **2.1.4. Frontal AD variant**

The frontal variant is a very rare early-onset subtype associated with predominant behavioral alterations and executive dysfunction, illustrated by poor performances in tests evaluating frontal lobe function (Karantzoulis and Galvin, 2011; Scialò et al., 2019). Bilateral atrophy in temporo-parietal regions can be observed, as opposed to the frontal cortex that is mostly spared by neurodegeneration (Ossenkoppele et al., 2015). However, NFT load in the frontal cortex is approximately ten-fold higher than in typical AD, whereas A $\beta$  burden remains similar (Johnson et al., 1999).

## **2.2. Atrophy-defined subtypes of AD**

Based on neuroimaging and neuropathological studies, four AD subtypes associated with distinct atrophy patterns were identified. Patients were classified as typical AD, limbic-predominant, hippocampal sparing or minimal atrophy AD, with respective frequency of 55, 21, 17 and 15% (**Figure 24**) (Ferreira et al., 2020, 2017; Persson et al., 2017). Moreover, patterns of brain hypometabolism and atrophy match in these subtypes, with each subtype associated with a distinct pattern of brain network disruption, presumably reflecting the differential spread of NFTs (Ferreira et al., 2020, 2019). Indeed, tau-PET imaging shows a strong regional association with AD clinical and anatomical heterogeneity, as opposed to A $\beta$  imaging (Ossenkoppele et al., 2016). Additionally, subtypes also differ in their age of onset, sex distribution, education level, global cognitive status, APOE $\epsilon$ 4 genotype and CSF biomarker levels (Ferreira et al., 2020). Disease duration is comparable between these four subtypes (Ferreira et al., 2020).

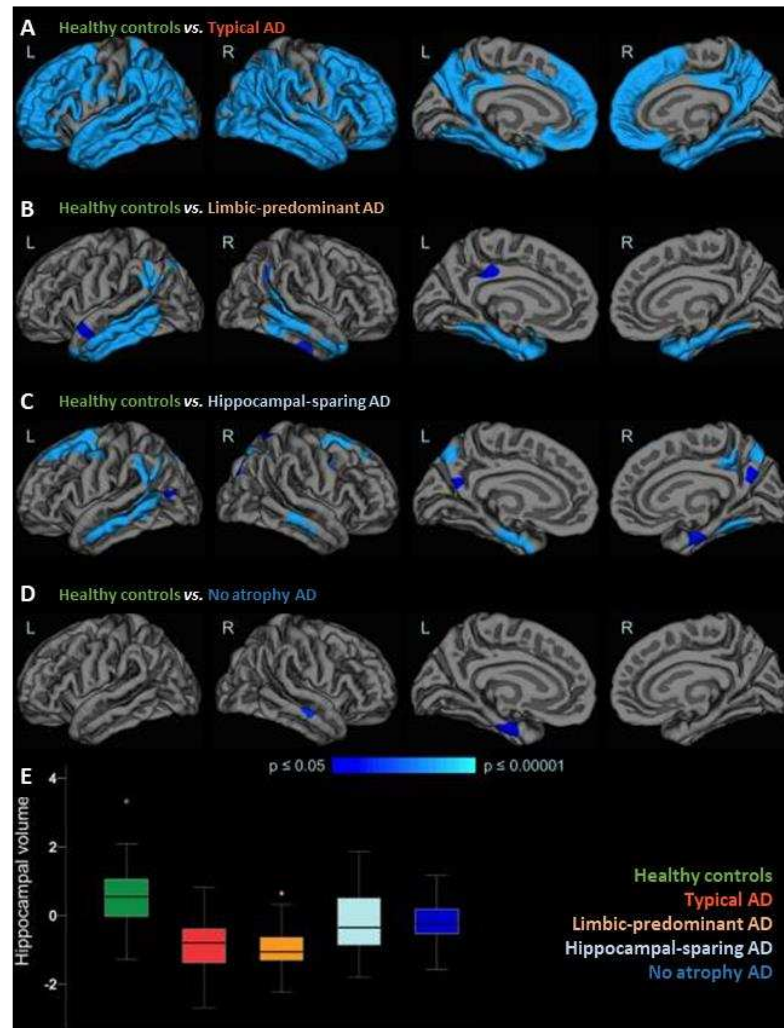


**Figure 24: Atrophy-defined subtypes of AD**

(A-D) Cortical maps of differences in thickness when comparing MRIs from healthy controls with MRIs from different AD subtypes, after controlling for age, gender, education level and APOEε4 status. Atrophy significance level is illustrated by the colored bar showing various shades of blue. Lateral (the first two images on the left of each row) and medial (the two images on the right of each row) views of both the left (L) and right (R) hemispheres are shown for each subtype. (E) Boxplot of the average hippocampal volume controlling for total intracranial volume, age, education level and APOEε4 status. Data are presented as median and confidence intervals. Adapted from (Ferreira et al., 2017).

### 2.2.1. Limbic-predominant

The limbic-predominant variant is associated with a late-onset and slow disease progression (Ferreira et al., 2020). APOEε4 carriers and females are more frequently affected (Ferreira et al., 2020). Compared with typical AD, patients display greater amyloid PET binding in the

medial frontal and parietal cortices (Ferreira et al., 2020). Tau pathology assessed by PET-imaging affects both temporal lobes, as well as the posterior cingulate (Whitwell et al., 2018). Moreover, while typical AD is characterized by NFT deposition both in the hippocampus and association cortex, limbic-predominant AD patients mainly display tau deposits in the hippocampus with relative sparing of the cortex (Murray et al., 2011). In addition, vascular pathologies such as hypertensive arteriopathy seem to play an important role in the pathophysiology (Ferreira et al., 2020).

### **2.2.2. Hippocampal sparing**

Hippocampal sparing AD is a non-amnestic variant characterized by the earliest disease onset among atrophy-defined AD subtypes (Ferreira et al., 2020). It is the most aggressive form, associated with higher levels of neurodegeneration, the highest rate of decline and younger age at death (Ferreira et al., 2020; Na et al., 2016). APOE $\epsilon$ 4 non carriers and males are more frequently affected (Ferreira et al., 2020). Hippocampal sparing AD patients have the highest level of education or cognitive reserve in comparison with other atrophy-defined subtypes (Ferreira et al., 2020).

CSF biomarker evaluation revealed that hippocampal-sparing AD patients show lower A $\beta$ <sub>42</sub> but higher phospho-tau levels than typical AD, and increased CSF total tau compared to limbic-predominant AD suggesting more severe neurodegeneration (Ferreira et al., 2020). Neuropathologically, A $\beta$  deposition evaluated by Florbetapir-PET imaging is more severe in the frontal and parietal cortices compared to typical and limbic-predominant AD (Hwang et al., 2015). Moreover, patients rather show increased levels of NFTs in the association cortex whereas the medial temporal lobe, including the hippocampus, is largely spared (Murray et al., 2011). The contribution of CAA in hippocampal sparing AD pathology appears to be strong (Ferreira et al., 2018a). Interestingly, hippocampal-sparing AD is more commonly associated with atypical non-amnestic subtypes such as PCA, LPA and the frontal variant of AD, than other atrophy-defined AD subtypes (Ferreira et al., 2020).

### **2.2.3. Minimal brain atrophy**

Minimal atrophy AD shows comparable disease severity with other AD subtypes, despite the lack of widespread atrophy (Ferreira et al., 2018a; Persson et al., 2017). Compared to hippocampal-sparing AD, patients can display similar disease severity but no brain atrophy or

## 2. Sporadic AD heterogeneity

minimal brain atrophy, possibly due to lower cognitive reserve (Ferreira et al., 2018a; Persson et al., 2017). Indeed, minimal atrophy AD patients display higher levels of phospho-tau and total tau in their CSF, compared to other subtypes (Ferreira et al., 2018a). Neurodegeneration occurring at a molecular level, but not macroscopically, may therefore be sufficient to cause clinical deterioration in these patients (Ferreira et al., 2018b). As for the hippocampal-sparing subtype, CAA seems to play an important role in the pathophysiology of minimal atrophy AD (Ferreira et al., 2018a).

### 2.3. Rapidly progressive AD

Disease progression rate, including survival time and rate of cognitive decline, can also be used to define AD subtypes. Among patients referred to prion disease pathology surveillance centres with clinical suspicion of Creutzfeldt-Jakob disease (CJD) because of a rapidly progressing dementia and additional focal neurological symptoms, the rapidly progressive form of AD (rpAD) has been identified following post mortem studies. AD is indeed the most frequent differential diagnosis of CJD (Chitras et al., 2011) and it has been estimated that rpAD, which clinically and neuropathologically differs from typical/classical AD, approximately accounts for 10 to 30% of all AD cases (Schmidt et al., 2011).

#### 2.3.1. Clinical presentation

rpAD is associated with an aggressive phenotype, characterized by a rapid clinical decline akin to CJD and a short disease duration from onset to death. Indeed, while classical AD (clAD) is characterized by a mean survival time of 8 to 10 years and a MMSE score decline of 3 points per year, rpAD cases are defined by a disease duration of less than 3 years and an annual decrease of 6 points in the MMSE cognitive test (Schmidt et al., 2011) (**Figure 25**).

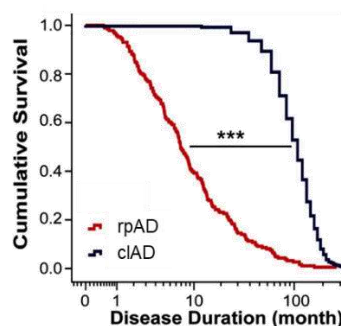


**Figure 25: Comparison of disease duration between rpAD and clAD patients.**

Kaplan-Meier cumulative survival analysis of rpAD cases, initially referred to National Prion Disease Pathology Surveillance Centre (rpAD, n=186), and classical/typical AD cases (clAD, n = 2605). \*\*\* $p < 0.001$ , log rank Mantel-Cox and generalized Wilcoxon test. Adapted from (Cohen et al., 2015).

In contrast with typical/classical AD, rpAD cases are characterized by the early impairment of the frontal lobe (Mann et al., 1992; Tosto et al., 2015). Indeed, early executive dysfunction (Buccione et al., 2007; Mann et al., 1992; Tosto et al., 2015) along with extrapyramidal signs such as rigidity, motor impairment, myoclonus, gait disturbances and language deficits notably distinguish rpAD from classical AD (Cohen et al., 2016; Portet et al., 2009; Scarmeas et al., 2005). Other clinical manifestations of rpAD patients include cerebellar ataxia, akinetic mutism, a positive Babinski sign, aphasia and hallucinations (Schmidt et al., 2010).

### **2.3.2. Predictors of disease progression rate**

Studies comparing baseline cognitive profiles of slowly and rapidly progressing AD patients have highlighted that, despite similar ADAS-Cog and MMSE scores, a faster rate of decline was associated with poorer performances on neuropsychological tests, especially memory, attention, mental control, fluency and visuospatial construction evaluations (Buccione et al., 2007; Marra et al., 2000; Seidl and Massman, 2016; Tosto et al., 2015). Deficits in executive functions (Buccione et al., 2007; Mann et al., 1992; Tosto et al., 2015) and early motor and extrapyramidal signs (Portet et al., 2009; Scarmeas et al., 2005) have also been observed in rapid progressors. Moreover, many studies have reported a younger age at onset and lower APOE $\epsilon$ 4 frequency in rpAD cases (Abu-Rumeileh et al., 2018, p.; Cohen et al., 2015; Pillai et al., 2018).

Conflicting data however implicate comorbidities (including cardiovascular diseases and diabetes) and demographic variables (such as education and sex) as predictors of cognitive decline speed (Bowler et al., 1998; Cohen et al., 2015; Ito et al., 2011; Schmidt et al., 2011; Seidl and Massman, 2016).

### **2.3.3. Biomarker profile**

Region-specific hypometabolism assessed by FDG-PET has been associated with rapidly progressing AD cases, involving the left angular and temporal cortices (Ba et al., 2017) as well as the frontal cortex (Mann et al., 1992).

Compared with typical AD patients, higher CSF levels of phospho-tau and total tau and lower A $\beta$ <sub>42</sub> CSF burden have been reported in rpAD cases (Schmidt et al., 2011). However, conflicting results have also been observed with CSF levels of A $\beta$  and tau pathology being comparable in both cases despite a lower phospho-tau/total tau ratio (Ba et al., 2017). Additionally, the presence of the 14-3-3 protein, a marker of rapid neurodegeneration usually associated with prion diseases, is more frequently observed in rpAD (Schmidt et al., 2011, 2010). An elevation in specific proinflammatory cytokines, *e.g.* IL-13, TNF $\alpha$  and G-CSF, has also been reported in the serum of rpAD patients (Stoeck et al., 2014).

### **2.3.4. Neuropathology**

The distribution of A $\beta$  plaques and NFTs appear to be similar in rpAD and classical AD (Cohen et al., 2015; Schmidt et al., 2012), although A $\beta$ <sub>42</sub> deposition is more prominent in the posterior cingulate cortex of rpAD patients (Cohen et al., 2015).

Interestingly, A $\beta$ <sub>42</sub> conformational heterogeneity was correlated with the rate of clinical decline by Cohen and colleagues (Cohen et al., 2015). Structural heterogeneity was assessed by evaluating differences in the domain display and stability under denaturing conditions. In the posterior cingulate cortex and hippocampus, rpAD brains presented higher levels of particles composed of 30 to 100 monomers and fewer particles of less than 30 monomers, with more exposed N- and C-termini than typical AD brains. Higher levels of conformers with low stability can also be found in rpAD cases, suggesting that these species may be more susceptible to dissociation *in vivo*, therefore facilitating A $\beta$  spreading (Cohen et al., 2015). In addition, solid-state NMR studies revealed that rpAD patients exhibit highly heterogeneous A $\beta$ <sub>40</sub> fibril morphology as opposed to typical AD and PCA brains that display a predominant A $\beta$ <sub>40</sub> fibril structure (Qiang et al., 2017). Altogether, these studies further support the role of different A $\beta$  conformers in AD pathogenesis.

Furthermore, A $\beta$  plaque proteomic composition shows a distinctive pattern of protein expression in rpAD. Indeed compared with typical AD cases, rpAD-associated plaques showed

higher levels of neuronal proteins and lower levels of astrocytic ones. Interestingly, proteins involved in synaptic vesicle release were particularly abundant suggesting the involvement of synaptic dysfunction in A $\beta$  pathological progression (Drummond et al., 2017). Additionally, PrP expression and localization differs between slowly and rapidly progressing AD cases resulting in differences in the PrP interactome which may affect AD pathophysiology (Zafar et al., 2017).





## 3. Prion diseases

---

Prion diseases or transmissible spongiform encephalopathies are a group of fatal neurodegenerative disorders affecting both humans and animals. They are caused by an unconventional agent, known as proteinaceous infectious particle or prion (Prusiner, 1982). Prion diseases are characterized by conformational changes occurring in the prion protein leading to its misfolding from a normal cellular isoform ( $\text{PrP}^{\text{C}}$ ) to a pathological isoform referred to as  $\text{PrP}^{\text{Sc}}$ , in reference to scrapie, a naturally occurring prion disease in sheep and goats. Other prion diseases affecting animals include transmissible mink encephalopathy, chronic wasting disease in mule deer and elk, bovine spongiform encephalopathy (BSE) and feline spongiform encephalopathy (Collinge, 2005).

### **3.1. Epidemiology and etiology of human prion diseases**

Human prion diseases can be classified according to their etiology and clinicopathological phenotype. They can be caused by rare sporadic events, inherited mutations in the human prion protein gene (PRNP) or acquired through dietary exposure or iatrogenic contamination.

#### **3.1.1. Sporadic prion diseases**

The majority of human prion disease cases occur sporadically as Creutzfeldt-Jakob disease (CJD), which represents approximately 85% of all prion disease cases (Wadsworth et al., 2003). It is assumed that sporadic CJD cases may arise spontaneously through somatic PRNP mutations or through the stochastic conversion of  $\text{PrP}^{\text{C}}$  to  $\text{PrP}^{\text{Sc}}$ . However, it has been shown that methionine and valine homozygosity at codon 129 of PRNP predisposes to sporadic CJD and is relevant to incubation period (Deslys et al., 1994; Palmer et al., 1991).

#### **3.1.2. Genetic prion diseases**

Genetic prion diseases account for approximately 10 to 15% of human prion disease cases (Wadsworth et al., 2003). Over 50 autosomal dominant pathogenic mutations in PRNP have been identified, each one leading to various clinical phenotypes and associated with familial forms of prion diseases such as familial CJD, Gerstmann-Sträussler-Scheinker disease (GSS) and fatal familial insomnia (FFI) (Jones and Mead, 2020; Wadsworth et al., 2003).

#### **3.1.3. Acquired prion diseases**

Several acquired forms of prion diseases have been identified. Most notably, over 3000 cases of Kuru acquired through ritual endocannibalism amongst the Fore linguistic group of the Eastern Highlands of Papua New Guinea were reported in the 1950s (Collinge et al., 2006). More recently, around 230 cases of variant CJD transmitted through dietary exposure to the BSE agent in cattle were identified, mainly in Europe (Jones and Mead, 2020). Additionally, over 450 cases of iatrogenic CJD have been observed in relation with medical or surgical procedures (Brown et al., 2012). Most cases have arisen as a result of cadaver-derived human growth hormone (c-hGH) injections and dura matter grafts positive for PrP<sup>Sc</sup>, although transmission through corneal transplantation, contaminated electroencephalographic (EEG) electrode intracerebral implantation, exposure to contaminated neurosurgical instruments or blood transfusion have been reported as well (Brown et al., 2012).

As for sporadic CJD, genetic susceptibility to iatrogenic and variant CJD has been identified since most cases occur in individuals homozygous at PRNP polymorphic codon 129 (Collinge, 2005; Collinge et al., 1991; Deslys et al., 1994).

#### **3.2. Clinical phenotypes and diagnosis**

A wide range of clinical presentations is associated with human prion diseases as each disease is characterized by a distinct set of clinical features and rate of evolution. Along with biomarker evaluation (EEG, MRI, CSF 14-3-3 protein) and PRNP analysis, clinical presentation participates in the differential diagnosis of prion diseases.

##### **3.2.1. Sporadic CJD**

Classical sporadic CJD presents with rapidly progressive dementia associated with multifocal neurologic disorders including myoclonus, cerebellar ataxia, cortical blindness, pyramidal and extrapyramidal signs and kinetic mutism (Wadsworth et al., 2003). CSF 14-3-3 is usually elevated and EEG evaluation can reveal periodic triphasic complexes. Death usually occurs within 6 months following disease onset although atypical forms can last over two years (Ironsides et al., 2017).

#### **3.2.2. Genetic prion diseases**

While familial CJD clinical presentation resembles that of classical sporadic CJD, GSS cases predominantly present with cerebellar ataxia associated with pyramidal signs and progressive cognitive decline that does not necessarily result in dementia. FFI is characterized by insomnia, dysautonomia, dementia, pyramidal signs and myoclonus (Ironside et al., 2017; Wadsworth et al., 2003).

#### **3.2.3. Acquired prion diseases**

In Kuru, ataxia is the main clinical feature as opposed to dementia. The early clinical presentation of variant CJD is characterized by psychiatric and sensory disturbances and ataxia, followed by pyramidal and extrapyramidal signs and cognitive decline (Ironside et al., 2017; Wadsworth et al., 2003).

Depending on the route of exposure, iatrogenic CJD clinical presentation can either be similar to sporadic CJD in dura mater graft and neurosurgery cases, or resemble that of Kuru when peripheral routes of contamination are involved (Wadsworth et al., 2003).

### **3.3. Neuropathology**

Post-mortem neuropathological evaluation provides the definite diagnosis of prion disease. Indeed in prion diseases, affected brains are characterized by a classical diagnostic triad of spongiform changes that comprise rounded vacuoles in the gray matter associated with neuronal loss and neuroinflammation involving reactive astrocytes and microglia. Importantly, cerebral PrP<sup>Sc</sup> accumulation is also observed, including in the form of Congo red-positive amyloid plaques (Ironside et al., 2017). However as for their clinical presentation, each prion disease is also characterized by neuropathological specificities that will not be detailed in this manuscript.

### **3.4. Physiopathology**

#### **3.4.1. PrP<sup>C</sup> and its physiological functions**

The normal host-encoded cellular prion protein (PrP<sup>C</sup>) is a glycosylphosphatidylinositol-anchored glycoprotein highly expressed in the CNS, although its expression is ubiquitous. In the CNS, PrP<sup>C</sup> is expressed not only in neurons but also in microglia (Adele-Biassette et al.,

2006), astrocytes (Hartmann et al., 2013) and oligodendrocytes (Bribián et al., 2012). Several studies have shown that PrP<sup>C</sup> is implicated in a wide array of different cellular processes including cell proliferation and adhesion, neuronal excitability and synaptic plasticity, myelin maintenance, antioxidant enzyme modulation, immune function, glucose homeostasis, iron uptake and circadian rhythm regulation (Castle and Gill, 2017). In addition to the putative neurotoxicity associated with PrP<sup>Sc</sup> pathological isoforms, the loss of PrP<sup>C</sup> physiological functions could contribute to the neurodegenerative process observed in prion diseases (Castle and Gill, 2017).

#### **3.4.2. Pathological prion PrP<sup>Sc</sup> properties**

The central physiopathological event in prion diseases is the post-translational conversion of PrP<sup>C</sup> into PrP<sup>Sc</sup>, an abnormally misfolded amyloidogenic isoform. PrP<sup>C</sup> and PrP<sup>Sc</sup> share the same amino acid sequence but differ in their conformational and aggregation states (Collinge, 2005). Indeed, it has been suggested that the prion protein can fluctuate between different conformation states: a dominant native PrP<sup>C</sup> state and one or several conformations that can self-associate into a stable PrP<sup>Sc</sup> structure composed of misfolded monomers. The misfolding process is characterized by the conversion of  $\alpha$ -helices into aggregation-prone  $\beta$ -sheet structures (Pan et al., 1993). Furthermore, the resulting stable PrP<sup>Sc</sup> can act as a “seed”, providing a template for further pathogenic conversion of normal PrP<sup>C</sup>, therefore allowing the auto-catalytic formation of PrP<sup>Sc</sup> and the spreading of the disease from cell to cell (Collinge, 2005).

The initiation of this cascade of events may result from pathogenic PRNP mutations and rare stochastic conformational changes, or can be precipitated by the exposure to pathological seeds of misfolded PrP<sup>Sc</sup>. A landmark in the field was the experimental transmission of Kuru (Gajdusek et al., 1966) and CJD (Gibbs et al., 1968) through the intracerebral inoculation of pathological brain homogenates into non-human primates in the 1960s. Since then, several transmission studies have been conducted in wild type and transgenic animal models, therefore demonstrating the infectivity of prion diseases.

Evidence suggests that prion disease phenotypic diversity relies on the different physicochemical properties of PrP<sup>Sc</sup> isoforms referred to as prion strains (Wadsworth et al., 2003). Indeed, conformational changes into pathological PrP<sup>Sc</sup> isoforms can lead to various

levels of resistance to conventional degradation techniques including heat and proteolysis, as well as detergent insolubility. Biologically, strains are associated with distinct incubation periods, clinical manifestations and neuropathological patterns. In animal models, these properties can be serially transmitted and maintained following multiple inoculations, in a host of both the same and different species (Collinge et al., 1996).



---

## 4. Prion-like hypothesis of AD

---

The prion paradigm has emerged as a unifying pathogenic principle for many age-related neurodegenerative diseases. Indeed, the hypothesis that neurodegenerative diseases such as AD and Parkinson's disease may arise from mechanisms similar to those of prion diseases is based on multiple similarities between them, including the progressive accumulation of misfolded proteins into well-ordered aggregates referred to as "amyloids". In AD, misfolded A $\beta$  and tau proteins indeed share common molecular features and key properties with prions, including the ability to self-propagate and spread to cells and tissues.

### 4.1. Structural properties of amyloids

"Amyloid" is a generic term that encompasses A $\beta$ , tau and prions, among other proteins in a highly thermodynamically stable state. Indeed, as previously described, A $\beta$ , tau and prion proteins can all undergo conformational changes leading to their pathological conversion from a native normal state to a stable misfolded  $\beta$ -sheet-enriched state. Misfolded aggregates can range from small soluble oligomers to large insoluble fibrils (Soto and Pritzkow, 2018), but mounting evidence suggests that PrP<sup>Sc</sup>, A $\beta$  and tau soluble oligomers are the main neurotoxic species (Ferreira et al., 2015; Simoneau et al., 2007; Spires-Jones et al., 2009).

Amyloids are highly ordered protein fibrils that form a characteristic cross- $\beta$ -sheet pattern as monomers assemble into  $\beta$ -sheets with  $\beta$ -strands perpendicularly oriented to the fibril axis and stabilized by hydrogen bonds (Sunde et al., 1997). Solid-state NMR studies have shown that fibrils cross- $\beta$  structures can display a parallel or antiparallel organization (Benzinger et al., 1998; Petkova et al., 2004). Amyloids can be revealed using  $\beta$ -sheet specific dyes such as Congo red and thioflavin under crossed polarized light and are characterized by a cross- $\beta$  X-ray diffraction pattern (Riek and Eisenberg, 2016).

### 4.2. Stability and resistance to inactivation

Similarly to PrP, A $\beta$  and tau aggregates can resist to multiple methods classically used to disrupt the 3D architecture of proteins. Indeed, A $\beta$  and tau seeds can remain bioactive following proteinase-K treatment (Langer et al., 2011; Li et al., 2021), heating at 95°C (Li et al., 2021; Meyer-Luehmann et al., 2006) and formaldehyde fixation (Fritschi et al., 2014a;



Kaufman et al., 2017). As for prions, A $\beta$  can bind on stainless-steel wires and seed A $\beta$  aggregation when intracerebrally implanted in APP transgenic mice (Eisele et al., 2009).

Interestingly, our group showed that A $\beta$  seeds can retain their pathogenic properties in the living brain for up to 18 months even at levels below routine detection (Hérard et al., 2020) (see **Annex**). Indeed, hippocampal extracts from APP null (Ye et al., 2015a) and huAPP mice (Hérard et al., 2020) previously inoculated with AD brains and presenting A $\beta$  levels falling below the detection limit, can potently induce A $\beta$  deposition in APP23 and APP/PS1dE9 mice respectively.

### **4.3. Self-propagation through seeding**

Amyloids are characterized by their seeding properties which give them the inherent ability to self-propagate, *i.e.* to convert native proteins into pathological ones and progressively spread the aggregation process.

The process of amyloid fibril formation follows a sigmoid kinetics and is divided into two main steps: the nucleation phase and the growth phase. During nucleation, monomers misfold into  $\beta$ -sheet-enriched structures that aggregate into a stable oligomeric seed, providing a template for the pathogenic conversion and incorporation of native proteins. The nucleation phase is a rare, slow and thermodynamically unfavorable event characterized by a lag phase, and is therefore the determining step of the amyloid fibril formation process. It is followed by a rapid elongation phase as seeds progressively grow into fibrils by recruiting native monomers. With increasing length, fibrils can undergo fragmentation, either spontaneously or through cellular processes, and generate supplemental seeds. In turn, this accelerates the overall process of fibril formation and increases the rate of disease progression (**Figure 26**) (Jucker and Walker, 2013; Soto and Pritzkow, 2018). Misfolded aggregates silently propagate before reaching a toxic threshold, which ultimately results in progressive cellular dysfunction and clinical disease (Soto and Pritzkow, 2018).

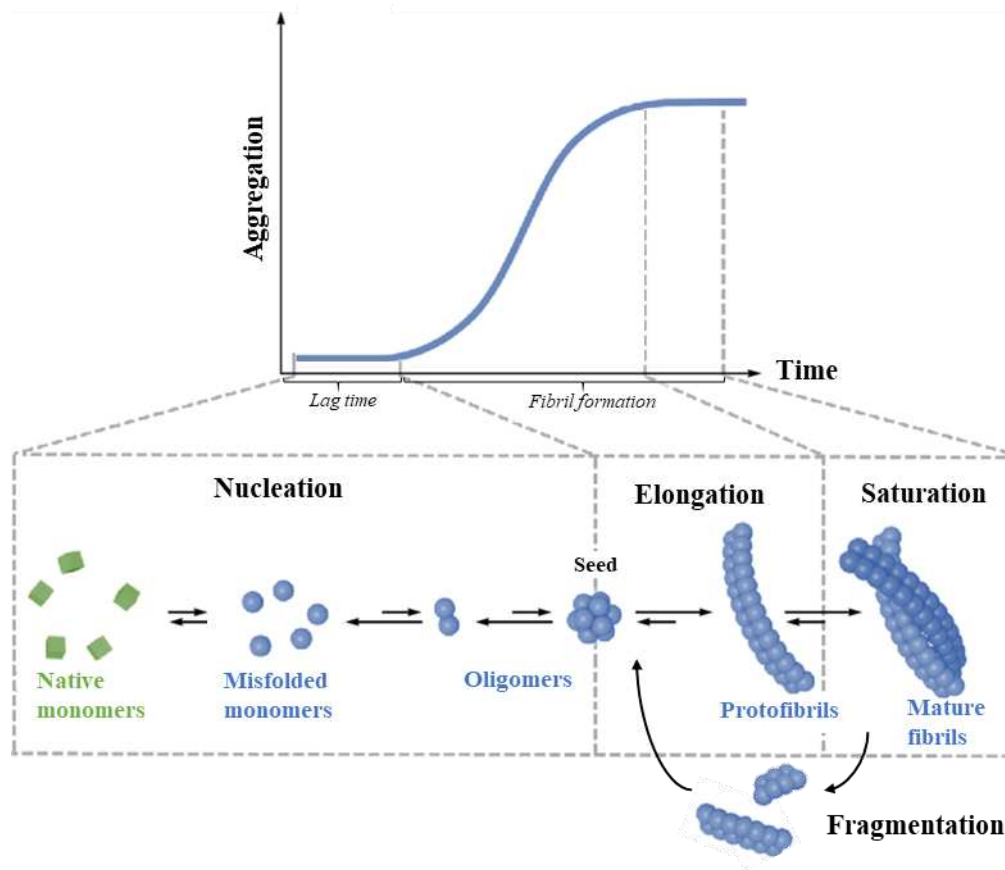


**Figure 26: Amyloid fibril formation**

Amyloid fibril formation follows a sigmoid kinetics and is divided into two main steps: the nucleation phase and the growth phase. During nucleation, native monomers misfold into  $\beta$ -sheet-enriched structures that aggregate into a stable oligomeric seed, providing a template for further pathogenic conversion of native proteins. The nucleation phase is a slow and thermodynamically unfavorable process characterized by a lag phase. It is followed by a rapid growth phase as seeds progressively grow into protofibrils in the elongation phase and fibrils in the saturation phase. With increasing length, fibrils can undergo fragmentation and generate supplemental seeds therefore accelerating the overall process of fibril formation. Adapted from (Kulikova et al., 2015).

Interestingly, as the nucleation phase is the rate-limiting event, bypassing this step through the exogenous administration of preformed seeds was undertaken as it was hypothesized to accelerate the pathological process of amyloid fibril formation (Figure 27). This was first demonstrated in the context of prions, following the successful experimental transmission of Kuru (Gajdusek et al., 1966) and CJD (Gibbs et al., 1968).

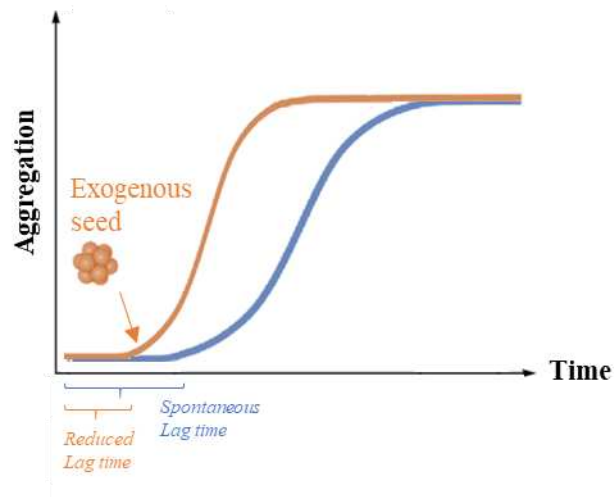


**Figure 27: Kinetics of the amyloid seeding process with and without exposure to preformed seeds**

As the nucleation phase is the rate-limiting event, the exogenous administration of preformed seeds can allow bypassing this step and accelerates the pathological process of amyloid fibril formation.

### **4.4. Seeding experiments**

The concept that A $\beta$  and tau may act in a prion-like manner gave rise to several studies investigating the experimental transmission of AD hallmarks in animal models by exposing them to pathological seeds. It was shown that the transmission of A $\beta$  and tau pathologies highly depends on the nature of the seeding agent and the host. Animal models of seeding present with many advantages as they can greatly accelerate disease onset and help to identify the mechanisms involved in the development and progression of AD pathology.

#### **4.4.1. Nature of the seeding agents**

In a paradigm similar to that used in the study of prion transmission, intracerebral inoculations of human AD brain extracts have been widely used to induce A $\beta$  and tau pathologies in transgenic mice (**Figure 28**) (Boluda et al., 2015; Clavaguera et al., 2013; Kane et al., 2000). Since depositions can only be observed following a lag period, it has been suggested that they do not directly originate from the inoculum itself but rather result from a seeding process (Jucker and Walker, 2011).

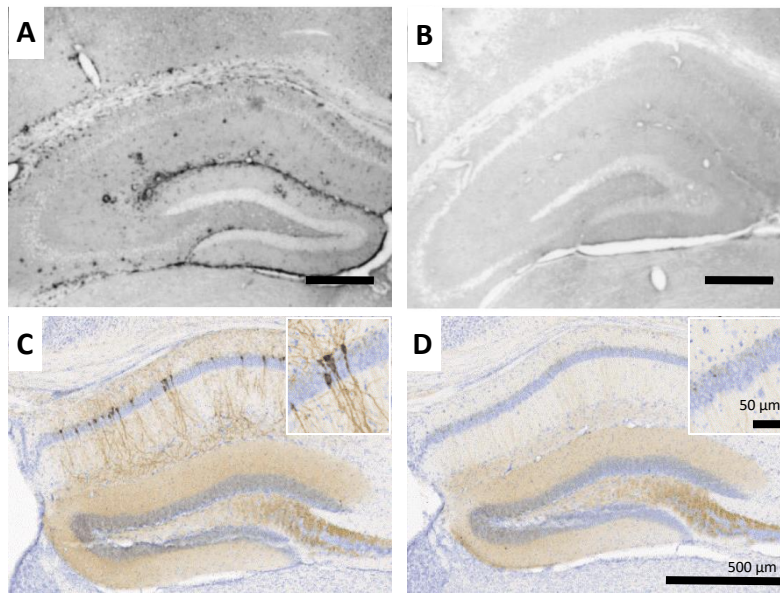


**Figure 28: Development of A $\beta$  and tau pathologies in transgenic mice following AD brain inoculation**

(A) A $\beta$  pathology revealed by 4G8 immunostaining after human AD brain inoculation in Tg2576 mice at 5 months post-inoculation. (B) No A $\beta$  immunoreactivity was observed in age-matched non-transgenic littermates injected with the same AD extract. Scale bars : 500  $\mu$ m. Adapted from (Kane et al., 2000). (C) AD brain inoculation induces tau pathology following a 4 month-incubation period, as opposed to (D) control brain inoculation in tau transgenic mice (AT8 antibody). Scale bars: 500  $\mu$ m and 50  $\mu$ m in inserts. Adapted from (Gary et al., 2019).

**The demonstration that A $\beta$  and tau seeds are responsible for such induced pathology was performed through various methods:**

- (1) Brain extracts from aged control individuals lacking misfolded A $\beta$  and tau proteins do not induce A $\beta$  and tau pathologies (Clavaguera et al., 2013; Kane et al., 2000). In contrast, A $\beta$ -positive brains from AD and MCI patients, as well as non-demented individuals with AD neuropathology (NDAN) can accelerate  $\beta$ -amyloidosis in mice (**Figure 29**) (Duran-Aniotz et al., 2013). Similarly, tau-positive brains from patients with different types of tauopathies can accelerate tau deposition in mice (**Figure 30**) (Boluda et al., 2015; Narasimhan et al., 2017).

#### 4. Prion-like hypothesis of AD

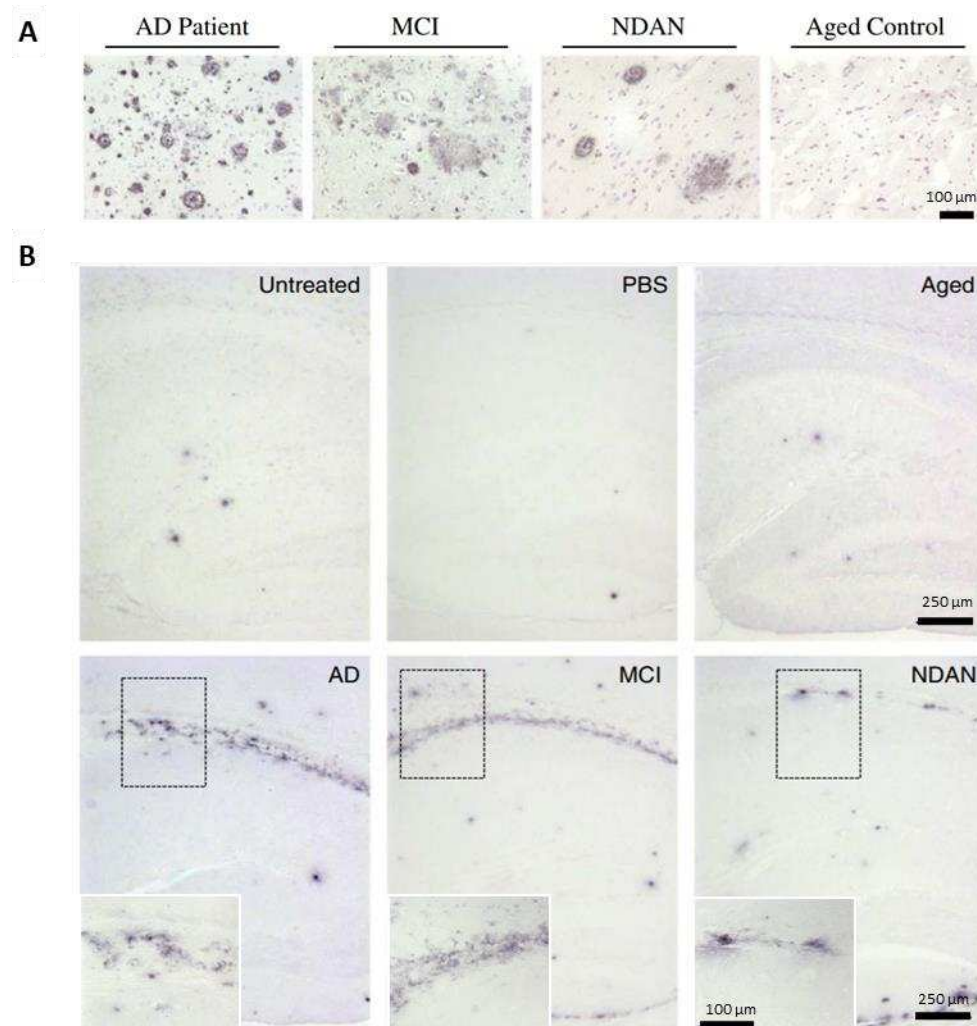


**Figure 29: Aβ deposition in the brain of AD, MCI, NDAN and aged control individuals and APP/PS1dE9 mice inoculated with these extracts**

(A) Aβ deposition patterns in the cingulate cortex of AD, MCI and non-demented patients with AD neuropathology (NDAN) are shown along with an aged control individual (4G8 antibody). Scale bar: 100 μm. (B) Aβ pathology was accelerated in the hippocampal area of 1 month-old APP/PS1dE9 mice inoculated with AD, MCI and NDAN brains after an incubation period of 5 months. Untreated mice and mice inoculated with a phosphate-buffered saline (PBS) solution or aged control individuals did not develop Aβ plaques (4G8 antibody). Adapted from (Duran-Aniotz et al., 2013).

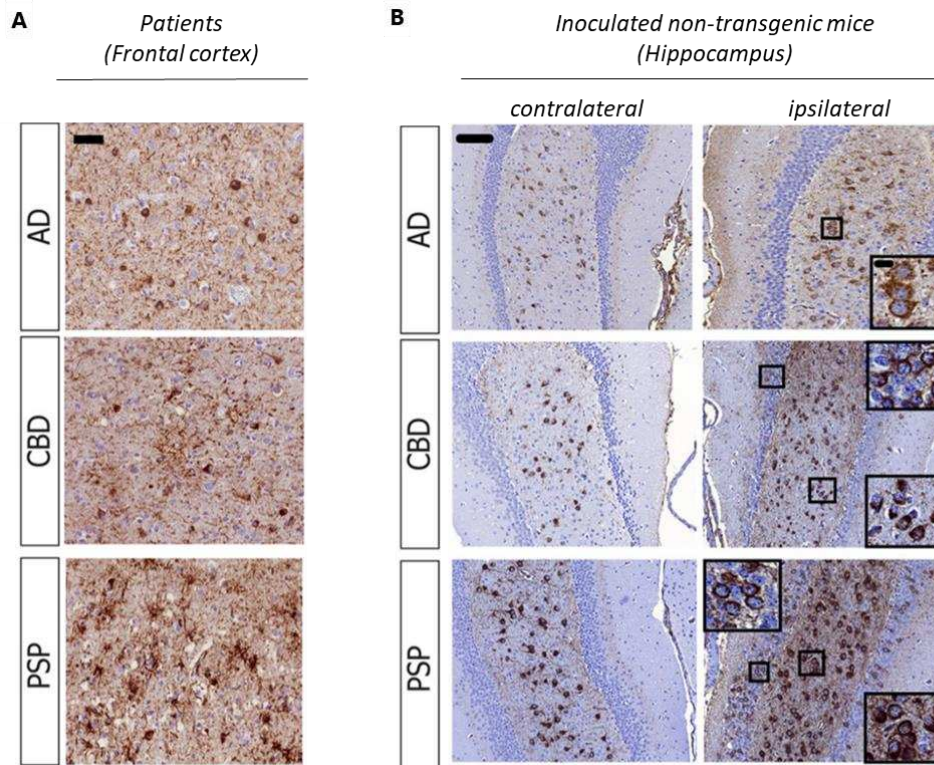


**Figure 30: Tau deposition in the brain of AD, CBD and PSP patients and non-transgenic mice inoculated with these extracts**

(A) Tau pathology in the frontal cortex of AD, corticobasal degeneration (CBD) and progressive supranuclear palsy (PSP) patients (anti-tau monoclonal antibody PHF-1). Scale bar: 50  $\mu\text{m}$ . (B) Seeded tau pathology in non-transgenic mice, 3 months after their inoculations with tau-containing AD, CBD or PSP brain extracts in the dorsal hippocampus and overlying cortex (anti-tau monoclonal antibody AT8). Scale bars: 100  $\mu\text{m}$  and 10  $\mu\text{m}$  in inserts. Adapted from (Narasimhan et al., 2017).

#### 4. Prion-like hypothesis of AD

(2) A $\beta$  or tau-rich brain extracts from transgenic models potently induce A $\beta$  and tau deposition, ruling out the involvement of factors specific to the human brain (**Figure 31**) (Clavaguera et al., 2009; Meyer-Luehmann et al., 2006);

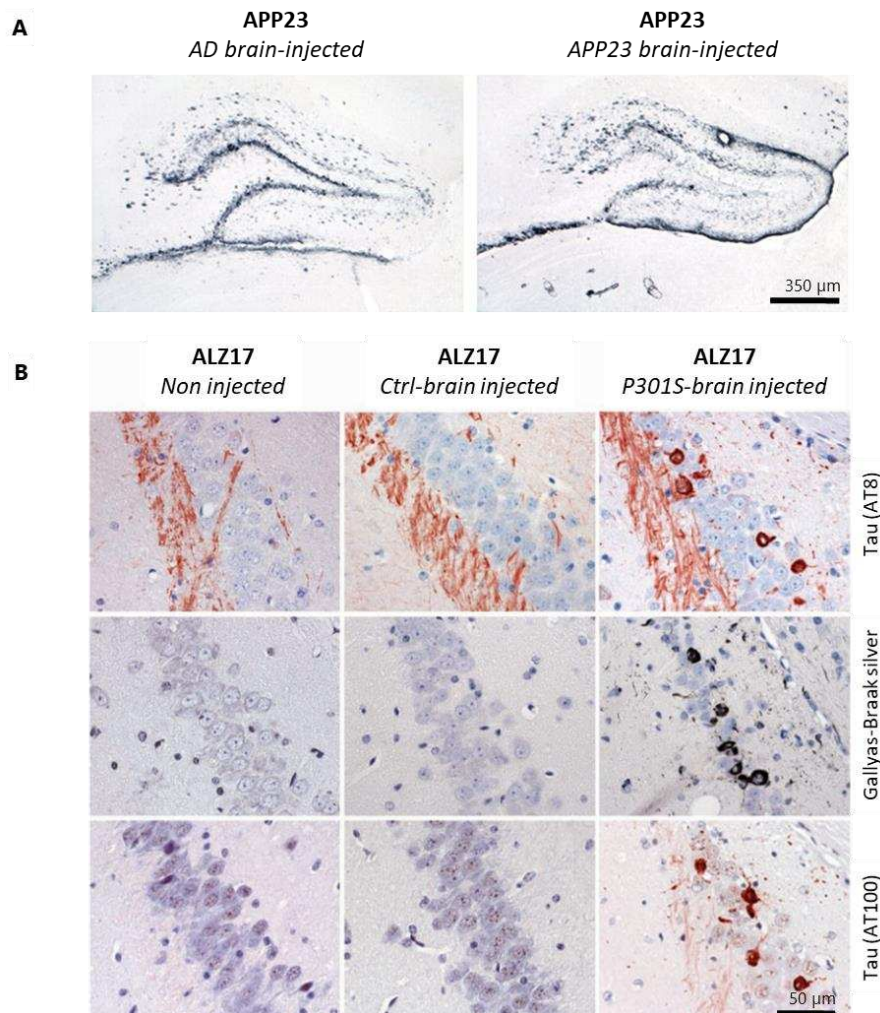


**Figure 31: Brain extracts from transgenic mouse models induce A $\beta$  and tau pathologies following inoculation in mice**

(A) Similar seed-induced A $\beta$  deposition following the inoculation of 10% brain extracts from AD patients or APP23 mice in the hippocampus of young APP23 hosts after a 4-month incubation period. Scale bar: 350  $\mu$ m. Adapted from (Meyer-Luehmann et al., 2006). (B) Tau pathology evaluation in non-injected ALZ17 mice, 3-month-old ALZ17 mice injected with non-transgenic control mouse brains or tau-positive P301S mouse brains following a 15-month incubation period (AT8 and AT100 antibodies, Gallyas-Braak silver staining). Scale bar: 50  $\mu$ m. Adapted from (Clavaguera et al., 2009).

- (3) The severity and extent of the induced pathology depends on the concentration of A $\beta$  (Fritschi et al., 2014b; Morales et al., 2015) and tau seeds (Boluda et al., 2015; Iba et al., 2013) that is injected (**Figure 32**);

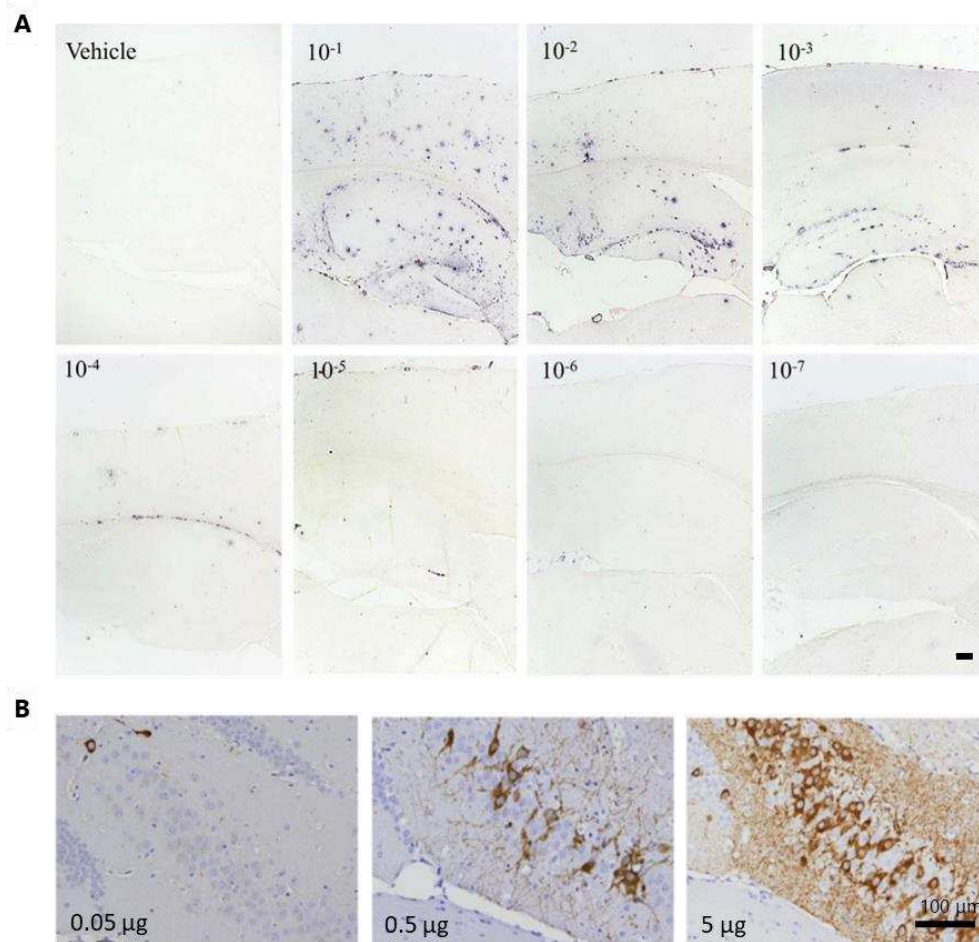


**Figure 32: Dose-dependent acceleration of A $\beta$  and tau pathologies**

(A) Tg2576 mice were injected with the vehicle solution (PBS) or increasing dilutions ( $10^{-1}$  to  $10^{-7}$ ) of a brain homogenate extracted from an aged Tg2576 mouse containing large amounts of A $\beta$  seeds. At approximately 10 months old, animals developed a dose-dependent level of A $\beta$  pathology in accordance with the injected inoculum (4G8 antibody). Scale bar: 200  $\mu$ m. From (Morales et al., 2015). (B) P301S mice inoculated with increasing concentrations of synthetic tau preformed fibrils K18/PL, containing the microtubule-binding repeats with the P301L mutation, displayed a dose-dependant increase in tau deposition after 4 weeks (AT8 antibody). Scale bar: 100  $\mu$ m. Adapted from (Iba et al., 2013).



#### 4. Prion-like hypothesis of AD

---

- (4) AD brain extracts treated with protein denaturing agents such as formic acid (**Figure 33A-B**), or extracts that underwent plasma sterilization do not lead to A $\beta$  pathology (Eisele et al., 2009; Meyer-Luehmann et al., 2006);
- (5) The removal of aggregates using the Aggregate Specific Reagent 1 compound that specifically binds to misfolded protein species reduces the *in vivo* seeding ability of AD brain extracts (Duran-Aniotz et al., 2014);
- (6) Seeding is abolished by the immunodepletion of A $\beta$  (**Figure 33C-D**) (Duran-Aniotz et al., 2014; Meyer-Luehmann et al., 2006) or tau (Clavaguera et al., 2009) from brain extracts;

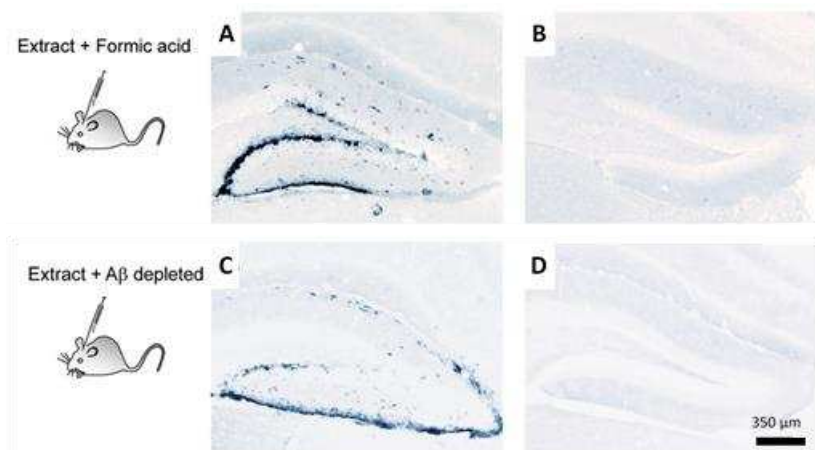


**Figure 33: A $\beta$  seeding-ability of brain extracts is abolished after formic acid treatment and immunodepletion**

(A, C) APP23 brain extracts were inoculated in the hippocampus of 3-month-old APP23 mice leading to A $\beta$  deposition. Seeding ability of the extract was completely abolished following formic acid treatment (B) and A $\beta$  immunodepletion (D). Adapted from (Meyer-Luehmann et al., 2006).

- (7) The inoculation of purified or synthetic A $\beta$  and tau proteins in transgenic mice successfully leads to A $\beta$  (Stöhr et al., 2012) and tau (Falcon et al., 2015; Iba et al., 2013) pathologies respectively, further supporting that A $\beta$  and tau seeds are required and sufficient to induce amyloidosis and tau pathology when inoculated in the appropriate host (**Figure 34**).

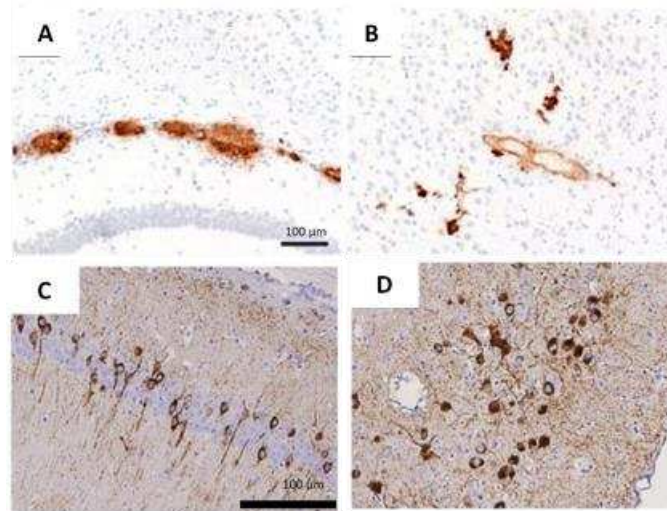


**Figure 34: Synthetic A $\beta$  and tau can potentially induce pathologies**

A $\beta$  deposition in the corpus callosum (A) and thalamus (B) of Tg(APP23:Gfap-luc) mice 330 days following synthetic A $\beta$  aggregates inoculation. Scale bar: 100  $\mu$ m. (Stöhr et al., 2012). Tau pathology in the CA1 (C) and caudal entorhinal cortex (D) of P301S mice 6 months after tau T40/PS fibrils inoculation (MC1 antibody). Scale bar: 100  $\mu$ m. Adapted from (Iba et al., 2013).

However, synthetic proteins are less bioactive than aggregates present in AD brains (Guo et al., 2016; Stöhr et al., 2012). Interestingly, CSF from AD or MCI patients was shown to promote tau pathology in P301S mice following intrahippocampal inoculations (Skachokova et al., 2019). Conversely, attempts to seed A $\beta$  pathology through the inoculation of CSF from AD patients have failed although A $\beta$  levels in CSF samples were 10-fold higher than in brain extracts (Fritschi et al., 2014b). Taken together, these data suggest that cofactors present in the brain, post-translational modifications occurring *in vivo* and/or specific protein conformations may facilitate the seeding of A $\beta$  pathology. Indeed, it was suggested that seeding abilities of synthetic peptides highly depend on the polymerization method (Stöhr et al., 2014). In addition, studies have shown that brain-derived A $\beta$  seeds were more proteinase K-resistant than A $\beta$  synthetic fibrils, highlighting specific properties that characterize each type of seeds according to its origin (Langer et al., 2011).

A $\beta$  seeds extracted from AD brains or aged APP transgenic models consist of multiple A $\beta$  assemblies, ranging from monomers and oligomers to multimers, associated with distinct biochemical properties (Langer et al., 2011). Interestingly, it was shown that following ultracentrifugation of the brain extracts, the amyloidogenic potency of soluble A $\beta$  contained

## 4. Prion-like hypothesis of AD

---

in the supernatant represented up to 30% that of the total extract. Moreover, the fragmentation of insoluble fibrils into soluble seeds through extended sonication also increased the seeding ability and sensitivity to proteinase K of the brain extract (Langer et al., 2011). This suggests that although, to a certain extent, each type of assembly appears to be capable of seeding A $\beta$  deposits, soluble aggregates may be more potent inducers. As for tau, mixed results have emerged from different studies, since both insoluble tau assemblies (Clavaguera et al., 2009) and soluble tau species (Lasagna-Reeves et al., 2012a) have been shown to be more effective in seeding silver-stained tau deposits when compared to each other. Similarly to A $\beta$  fibrils, it is however unclear whether tau fibrils acts as seeds themselves or rather represent a source of smaller soluble seeding-competent fragments.

Finally, Gibbons and colleagues have suggested that seeding potency may depend on the compatibility between the seed and the host. Indeed, whereas AD brain-derived fibrils can more potently seed tau pathology in wild-type mice than synthetic fibrils bearing the P301L mutation, the opposite was observed in P301L transgenic mice (Gibbons et al., 2017).

### 4.4.2. Impact of the host

#### 4.4.2.1. Seeding in different types of animal models

Most experimental transmission studies were carried out on **transgenic rodent models in which the overexpression of human genes** readily leads to A $\beta$  and tau pathologies (Clavaguera et al., 2009; Gary et al., 2019; Kane et al., 2000; Meyer-Luehmann et al., 2006). These studies underline the fact that seeding experiments can **accelerate the onset** of a disease that would have eventually occurred with age.

**In NHP spontaneous models**, following an incubation period of 3.5 to 7 years, marmosets inoculated with AD brain extracts were shown to develop senile plaques and CAA, but not tau deposits (Baker et al., 1994, 1993a, 1993b; Ridley et al., 2006). Interestingly, plaque distribution resembled the pattern of amyloid plaque deposition in aged non-injected controls (Maclean et al., 2000). Recently, our group showed in two independent cohorts of mouse lemur primates that, both A $\beta$  parenchymal and vascular deposits and tau lesions were seedable following AD brain extract intracerebral inoculation (**Figure 35**) (Gary et al., 2019; unpublished data) (see **Results chapter – § 2. Encephalopathy induced by AD brain**

inoculation in a non-human primate and § 3. Transmission of A $\beta$  and tau pathologies is associated with cognitive impairments in a primate).

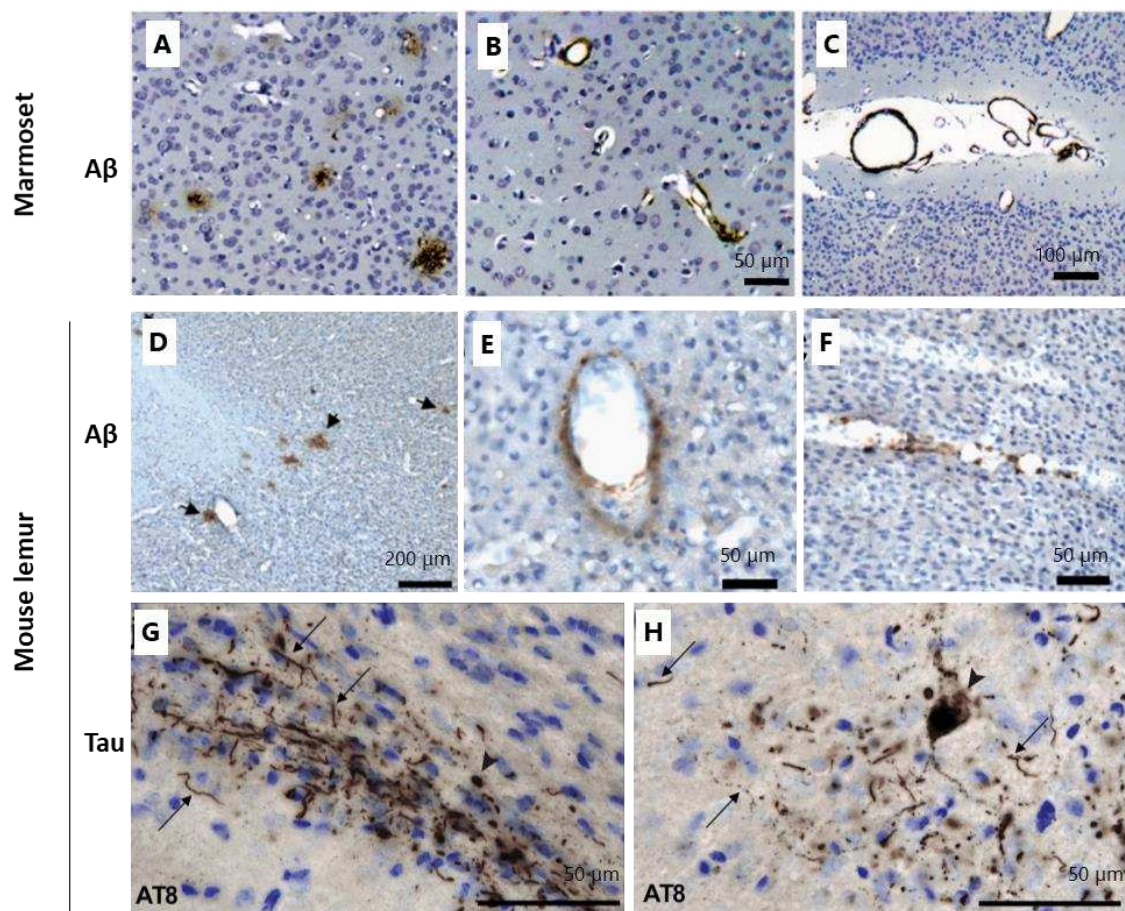


**Figure 35: A $\beta$  and tau pathologies in NHPs following AD brain inoculation**

A $\beta$  pathologies were induced after AD brain inoculation in the forms of parenchymal plaques (A, D) and CAA (B-C and E-F) in marmosets (A-C; 6F/3D antibody) and mouse lemurs (D-F; 4G8 antibody). Tau pathology, including intracellular deposits (arrowheads) and neuropil threads (arrows), was however only detected in mouse lemur primates (AT8 antibody) (G-H). Scale bars: 50  $\mu$ m in A-B, E-H, 100  $\mu$ m in C, 200  $\mu$ m in D. Adapted from (Ridley et al., 2006) and (Gary et al., 2019).

Additionally, it has also been shown that, following brain extract inoculation, **A $\beta$  and tau pathologies can be *de novo* induced in transgenic models** that do not spontaneously develop lesions within their lifespan (Clavaguera et al., 2013; Guo et al., 2016; Morales et al., 2012; Rosen et al., 2012) (**Figure 36**).

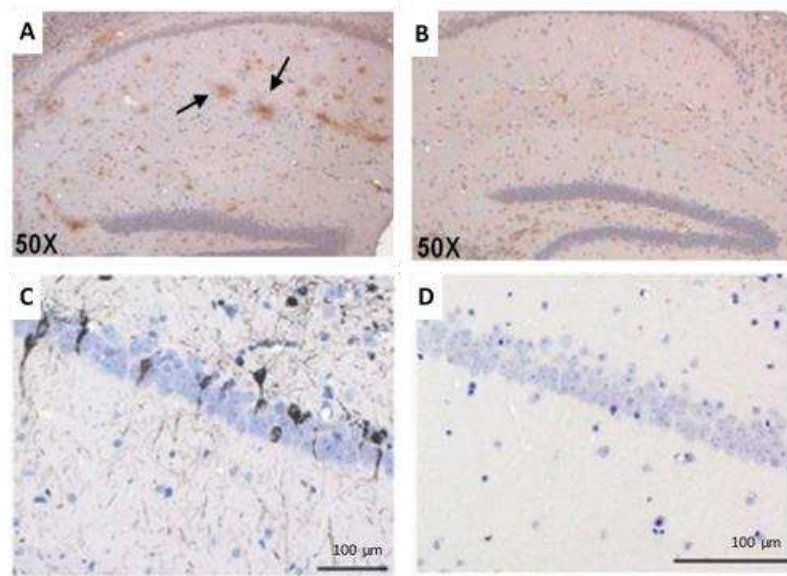


**Figure 36: *De novo* induction of A $\beta$  and tau pathologies**

Induction of A $\beta$  deposits in huAPP mice following AD brain (A) but not Ctrl-brain inoculation (B) (4G8 antibody) (Morales et al., 2012). Tau pathology revealed by Gallyas-Braak silver impregnation following human AD brain inoculation in non-aggregation prone ALZ17 mice at 12 months post-inoculation (C). No pathology was found in ALZ17 mice after tau-negative control brain extract inoculation (D). Scale bars : 100  $\mu$ m. Adapted from (Clavaguera et al., 2013).

Interestingly, ***de novo* induction of tau pathology can also occur in non-transgenic mice**, albeit less severely than in transgenic mice, following the inoculation of AD brain extracts or tau purified from these extracts (Clavaguera et al., 2013; Guo et al., 2016; Saito et al., 2019). The seeding and spreading of tau lesions in non-transgenic mice appear to depend on the source of the seeds, as tau derived from P301S mice brains only seed tau pathology at the injection site (Clavaguera et al., 2009) as opposed to human AD brains which lead to widespread tau deposition (Guo et al., 2016). Overall, these studies suggest that pathological human tau can seed the misfolding of wild-type murine tau, and does so more efficiently than pathological murine tau in non-transgenic mice. Conversely, following the intracerebral inoculation of AD brain extracts, A $\beta$  deposits are not induced in non-transgenic mice as wild-type murine A $\beta$  is not prone to aggregation (**Figure 28B**) (Kane et al., 2000). This highlights the need for compatible endogenous proteins in the host in order to seed a pathology, which is further supported by studies showing that mice immunized for A $\beta$  (Meyer-Luehmann et al. 2006) and tau (Yanamandra et al. 2013; Dai et al. 2017) do not develop A $\beta$  and tau aggregates.

Although the expression of human APP remains necessary, its overexpression may however not be required to seed A $\beta$  pathology in mice. Indeed, a recent study showed that mice expressing physiological levels of humanized APP can develop A $\beta$  deposition following brain-derived A $\beta$  aggregates inoculation (Ruiz-Riquelme et al., 2018). Accordingly, the inoculation of AD brains in APP null mice did not induce A $\beta$  deposits (Ye et al., 2015a). However, A $\beta$  deposition was remarkably reported when brain extracts from these inoculated mice, apparently free of A $\beta$  pathology, were reintroduced into transgenic mice bearing mutant human APP, *i.e.* APP23 (Ye et al., 2015a). These results were recently replicated by our group using huAPP mice that did not develop A $\beta$  deposits following AD brain injections but which brains potently accelerated A $\beta$  pathology when inoculated in APP/PS1dE9 mice (Hérard et al., 2020). These data support that the transmission of A $\beta$  pathology is not only governed by the inoculated sample but also by the host.

### 4.4.2.2. Incubation period

The induction of A $\beta$  and tau pathologies only occurs following a lag period which duration depends on both the nature of the seed and the host (Jucker and Walker, 2011). Indeed, it was shown that when inoculated with brain extracts originating from transgenic models, APP/PS1 mice can develop A $\beta$  deposits within a month as opposed to APP23 hosts for which A $\beta$  pathology was observed after 4 months (Meyer-Luehmann et al., 2006).

### 4.4.2.3. Influence of age

Advanced age is known as the greatest risk factor for AD but how it may impact the development of A $\beta$  and tau deposition remains unclear.

Seeding experiments have provided evidence that A $\beta$  deposition may not be influenced by the age of the host at the time of seeding. Indeed, prior to plaque deposition in their brain at either 3 or 9 months old, transgenic mice were inoculated with aged APP23 brain extracts. Following the same incubation period of 6 months, all mice displayed similar levels of A $\beta$  pathology, despite being young or old at the age of inoculation (Hamaguchi et al., 2012). Conversely, susceptibility to tau seeding appears to increase with age as tau-seeded pathological spreading is more important in wild-type mice aged 15-19 months than in mice aged 2-3 months, although no difference in tau-associated neurodegeneration and neuroinflammation was reported (Guo et al., 2016).

### 4.4.3. Impact of local environment

In addition to the host effect (Heilbronner et al., 2013; Meyer-Luehmann et al., 2006), the morphology and biochemical properties of the seed-induced deposits also appear to depend on the local environment, *e.g.* brain regions in which the inoculation was performed. Indeed, Eisele and colleagues showed that the inoculation of aged APP23 mice brain extracts into different brain regions of young APP23 mice led to differences in the amount and type of A $\beta$  deposition. While injections in the hippocampus and entorhinal cortex induced strong, dense and significantly congophilic plaques, inoculation in the striatum led to lower amyloid loads and mainly induced diffuse deposits (**Figure 37**) (Eisele et al., 2009).

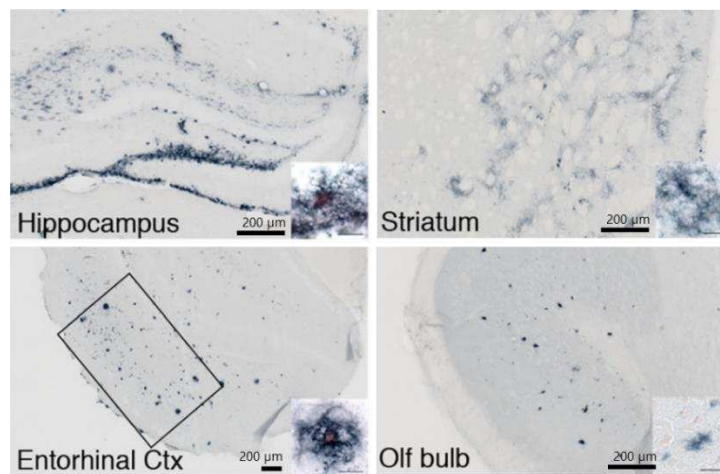


**Figure 37: Differences in A $\beta$  deposition following brain extracts inoculation in different brain regions of APP23 mice**

Differences in A $\beta$  deposition in brain regions (hippocampus, striatum, entorhinal cortex and olfactory bulb) inoculated with aged APP23 mouse brain extracts, in young APP23 mice after a 3 to 6 months incubation period. Scale bars: 200  $\mu$ m. Adapted from (Eisele et al., 2009).

As for A $\beta$ , tau seeding also varies depending on the susceptibility of the injected region to develop tau lesions. Indeed, the inoculation of tau fibrils in the striatum and overlying neocortex led to significant tangle-like accumulations in the neocortex as opposed to the striatum in which tau pathology was barely detected (Iba et al., 2013). In addition, it has been suggested that the initiating region may determine the development of unique tau strains, as distinct biochemical environments may predispose the formation of different pathological conformers (Narasimhan et al., 2017).

Altogether, this suggests that seeded-pathologies highly depend on the underlying properties and susceptibility of inoculated brain regions to develop A $\beta$  and tau pathologies.

#### 4.4.4. **A $\beta$ and tau cross-seeding**

Following the amyloid cascade hypothesis, A $\beta$  has been suggested to trigger tau pathology that subsequently leads to neurodegeneration and functional alterations in AD. It has been suggested that A $\beta$  may increase tau pathology either through direct cross-seeding mechanisms or by altering the local environment which increases tau susceptibility to aggregation.

In APP transgenic mice, AD brain intracerebral inoculation was shown to induce axonal tau hyperphosphorylation close to the injection site (L. C. Walker et al., 2002). Our group showed that in APP/PS1dE9 mice, tau deposition induced by AD brain inoculation could also spread to interconnected brain regions (unpublished data, see **Results chapter – § 1. Relationships between cognitive, synaptic and neuropathological changes in AD brain-inoculated mice**). In addition, in transgenic mice expressing mutant human tau, A $\beta$  synthetic fibrils (Götz et al., 2001) or brain extracts from aged APP23 mice, exhibiting severe A $\beta$  deposits but no tau pathology (Bolmont et al., 2007), can lead to tau neurofibrillary pathology. Conversely, aged APP23 brain extracts do not seed tau pathology in mice expressing non-mutated human tau (Clavaguera et al., 2013).

It has been suggested that interactions between phospho-tau and PrP<sup>C</sup> may be a prerequisite for A $\beta$  to promote tau pathology, suggesting that PrP<sup>C</sup> is a critical mediator in the interplay between A $\beta$  and tau propagation (Gomes et al., 2019). Although mechanisms involved *in vivo* remain unclear, direct cross-seeding between A $\beta$  and tau has been demonstrated *in vitro*, as A $\beta$  seeds can directly promote tau fibrillization in a cell-free assay (Vasconcelos et al., 2016).

Aside from a direct cross-seeding effect, A $\beta$  plaques may also create a unique environment facilitating tau deposition. In double APP23  $\times$  B6/P301L tau transgenic mice, tau pathology was more severe than in single B6/P301L tau mice, and was predominately observed in areas with high A $\beta$  plaque load (Bolmont et al., 2007). In addition, the presence of A $\beta$  deposition was shown to accelerate and promote tau propagation as well as increase tau-induced neuronal loss in rTgTauEC  $\times$  APP/PS1 compared to rTgTauEC mice (Pooler et al., 2015). Interestingly, in A $\beta$  plaque-bearing mice expressing mutant human A $\beta$  and wild-type murine



tau, the inoculation of tau purified from AD brains first leads to tau deposition in dystrophic axons surrounding A $\beta$  plaques, therefore forming neuritic plaque-like lesions before neurofibrillary tangles and neuropil threads (He et al., 2018). However, in the absence of plaques, the inoculation mainly leads to NFTs thus suggesting that A $\beta$  deposition can modulate tau pathology (He et al., 2018). In addition, increased cell vulnerability, neuroinflammation, oxidative stress and kinase activation locally induced by misfolded A $\beta$  may also impact tau accumulation (Morales et al., 2013).

Evidence of tau enhancing A $\beta$  pathology has also been reported. Tau deletion in APP/PS1 transgenic mice was shown to decrease A $\beta$  plaque burden, possibly by reducing  $\beta$ -secretase-mediated APP cleavage, prevent neuronal and synaptic loss and rescue spatial memory and motor deficits (Leroy et al., 2012).

Overall, and as mentioned in **§ 1.7.4.4. A $\beta$  and tau synergy at the synapse**, A $\beta$  and tau may form a positive feedback loop, in which A $\beta$  initiates tau pathology, which in turn further aggravates A $\beta$  toxicity (Bloom, 2014).

#### **4.4.5. Functional impacts of A $\beta$ and tau seeding**

Little research has addressed the functional impacts of seeding experiments. In some studies conducted in rodents, the pathological aggregations of A $\beta$  (Lesné et al., 2006; Shankar et al., 2008; Ziegler-Waldkirch et al., 2018) and tau (He et al., 2018; Lasagna-Reeves et al., 2011; Stancu et al., 2015) have been associated with cognitive alterations. In 3xTg mice, passive immunization targeting tau was shown to rescue cognitive deficits (Dai et al., 2017). In addition, various studies have highlighted the impact of A $\beta$  (Shankar et al., 2008; Walsh et al., 2002) and tau species on hippocampal LTP (Fá et al., 2016; Stancu et al., 2015). Interestingly, LTP and memory impairment following exposure to tau oligomers, either recombinant, extracted from AD brains or expressed in transgenic mice overexpressing human tau, could be observed independently from A $\beta$  oligomer levels in mice (Fá et al., 2016).

In mouse lemurs, our group recently showed for the first time in a primate that AD brain inoculation leads to cognitive alterations, neuronal activity impairments and cerebral atrophy associated with neuronal loss, despite sparse A $\beta$  and tau deposition, therefore suggesting a role for soluble species in the induced functional and morphological alterations (Gary et al., 2019).

Altogether, these studies provide strong evidence that exogenously administered A $\beta$  and tau seeds can act as templates for the misfolding of endogenous proteins, and ultimately lead to functional alterations in the recipient host. Importantly, they also highlight that this process strongly depends on the nature of the seeding agent, the host and the local environment of the seed.

## **4.5. Spreading**

Following their pathological conversion, misfolded seeds were shown to propagate their conformation from cell to cell, between regions of the brain and more widely from the periphery to the brain.

In AD, both A $\beta$  and tau pathologies spread in a highly stereotyped pattern throughout the brain (see § 1.4.2. **Neuropathological diagnosis**). Several studies have therefore argued that axonal transport may be a major mechanism involved in their pathogenic spread. However, the exact contributions of neuronal proximity and neuronal connectivity in the spreading process remain to be elucidated (Jucker and Walker, 2013).

### **4.5.1. A $\beta$**

Despite mounting evidence showing the spreading ability of A $\beta$  seeds, the exact mechanisms that are involved remain unclear. It has been suggested that they most likely implicate both active transportation between synaptically connected regions and passive extracellular diffusion along neuroanatomical pathways.

The occurrence of intraneuronal A $\beta$  in humans and animals as well as studies demonstrating that neurons can internalize and transport A $\beta$  aggregates, suggest that neuronal pathways may be implicated in A $\beta$  spreading (Nath et al., 2012). Additionally, the experimental inoculation of A $\beta$ -rich brain extracts into one region leads to A $\beta$  deposition close to the injection site and progressively in axonally coupled areas, suggesting that A $\beta$  aggregates can propagate in an anterograde manner between connected brain regions (**Figure 38**) (Walker et al., 2016; Ye et al., 2015b).

#### 4. Prion-like hypothesis of AD

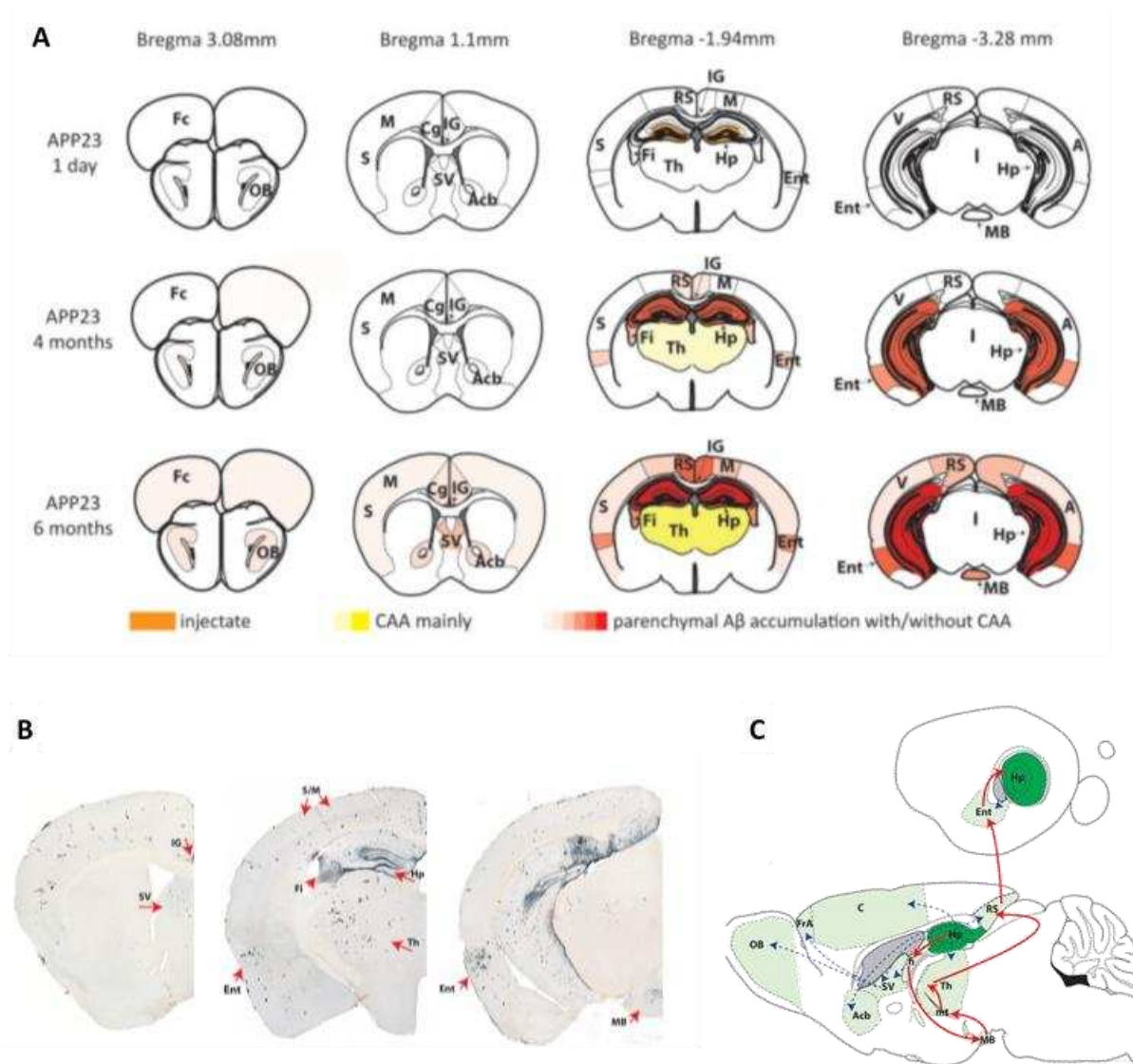


**Figure 38: Spatiotemporal spreading of A $\beta$  pathology along neuroanatomical pathways**

(A) Schematic diagram showing the onset and spreading of A $\beta$  pathology over time, *e.g.* 1 day, 4 and 6 months after A $\beta$ -rich brain extracts inoculation in the dorsal hippocampus of APP23 mice. Both parenchymal plaques and cerebral amyloid angiopathy (CAA) were reported. (B) A $\beta$  pathology at 6 months post-inoculation (anti-A $\beta$  polyclonal antibody CN3). (C) Scheme of A $\beta$  hypothesized spreading pathways after hippocampal seeding. Solid red arrows: Papez circuit, dotted blue arrows: direct outputs pathways from the hippocampus. A, auditory cortex; Acb, nucleus accumbens; C, cerebral cortex; Cg, cingulate cortex; Ent, entorhinal cortex; Fc, frontal cortex; Fi, fimbria; FrA: frontal area; Hp, hippocampal formation; IG, indusium griseum; M, motor cortex; MB, mammillary bodies; mt, mammillothalamic tract; OB, olfactory bulb; PoDG, polymorphic cell layer of the dentate gyrus; RS, retrosplenial cortex; S, somatosensory cortex; SV, septum verum; Th, thalamus; V, visual cortex. Adapted from (Ye et al., 2015b).

---

Importantly, since the majority of seeding experiments are based on hippocampal injections and as most connections between the hippocampus and spreading areas are bidirectional, it is difficult to ascertain if the *in vivo* spreading occurs both in anterograde and retrograde pathways. Interestingly, *in vitro*, the retrograde transport of A $\beta$  monomers and oligomers has been described using microfluidic chambers (Song et al., 2014).

Mechanisms associated with active transportation and propagation of A $\beta$  seeds may also involve extracellular vesicles including exosomes (Eisele and Duyckaerts, 2016; Rajendran et al., 2006), tunneling nanotubes as suggested by *in vitro* experiments (Ollinger et al., 2019), or be mediated by immune cells. Indeed, macrophages can phagocytose A $\beta$  and participate in its propagation, including from the periphery to the brain (Cintron et al., 2015; Eisele et al., 2014).

Selective regional vulnerability to A $\beta$  deposition could also contribute to the characteristic spreading pattern of A $\beta$  pathology, since A $\beta$  production and clearance may differ between brain regions. Additionally, it has been suggested that A $\beta$  tends to accumulate along functional networks, and is particularly abundant in the default-mode network (DMN) (Buckner et al., 2009). The DMN is defined by structural and functional interconnections between several epicenters converging on the posterior cingulate cortex extending into the precuneus, which is strongly associated with the hippocampal formation, and also involves the medial prefrontal cortex, inferior parietal lobule and lateral temporal cortex (Buckner et al., 2008; Greicius et al., 2004). The posterior cingulate cortex is of particular interest as it is considered a prominent hub associated with high connectivity in the brain (Buckner et al., 2009). It is also vulnerable to early amyloid deposition and plays a critical role in memory function (Sperling et al., 2009). Interestingly, important functional connections within the DMN are disrupted in AD, and it has been suggested that A $\beta$  accumulation may, at least in part, be responsible for such impairments, given that A $\beta$  was shown to enhance and alter neuronal activity (Busche and Hyman, 2020; Cirrito et al., 2005; Palmqvist et al., 2017; Sheline et al., 2010; Yamamoto et al., 2015). Alternatively, activity within the DMN could increase an activity- or metabolism-dependent cascade of events leading to A $\beta$  accumulation (Buckner et al., 2008). This is consistent with the hypothesis that if A $\beta$  seeds do not travel trans-synaptically, they may influence their local environment, affecting surrounding neurons and resulting in the increased release of A $\beta$  into synaptically-connected regions (Eisele and Duyckaerts, 2016).

## 4. Prion-like hypothesis of AD

---

Computational models of A $\beta$  spreading have also been developed. One study suggested that A $\beta$  regional accumulation is better predicted when the model is based on structural connectivity measured by diffusion-weighted MRI and that the anterior and posterior cingulate cortices most likely represent the epicenters from which A $\beta$  pathology spreads (Iturria-Medina et al., 2014). A physics-based model however showed that the spreadings of A $\beta$  and tau are better modelled when both anisotropic (*i.e.* neuronal connectivity-based axonal transport) and isotropic diffusion (*i.e.* spatial proximity-based extracellular diffusion) are taken into account, with an extracellular-to-intracellular diffusion ratio of 1:2 (Weickenmeier et al., 2019). Altogether, these data suggest that A $\beta$  spreading is mainly influenced by neuronal connectivity although passive diffusion is also involved.

Finally, as for prions, the systemic administration of A $\beta$  seeds, both by the peritoneal (Eisele et al., 2010) and venous route (Burwinkel et al., 2018), can also result in the intracerebral deposition of A $\beta$ , even in the absence of peripheral APP (Eisele et al., 2014). Interestingly, these routes of administration induce a significant amount of A $\beta$  deposition within the vasculature, suggesting a role for the vascular system (Meyer-Luehmann et al., 2006) or perivascular drainage channels (Thal et al., 2007) as potential propagation routes for A $\beta$  seeds.

### 4.5.2. Tau

#### 4.5.2.1. Experimental evidence for tau spreading

As opposed to A $\beta$ , tau seeding experiments clearly argue for the neuronal connectivity-based model of propagation. Intracerebral inoculation of tau-enriched extracts or synthetic fibrils experiments have indeed shown that tau systematically spreads from the injection site to axonally connected brain regions (**Figure 39**) (Clavaguera et al., 2009; Iba et al., 2013), both through anterograde and retrograde pathways (Sanders et al., 2014; Wu et al., 2013).

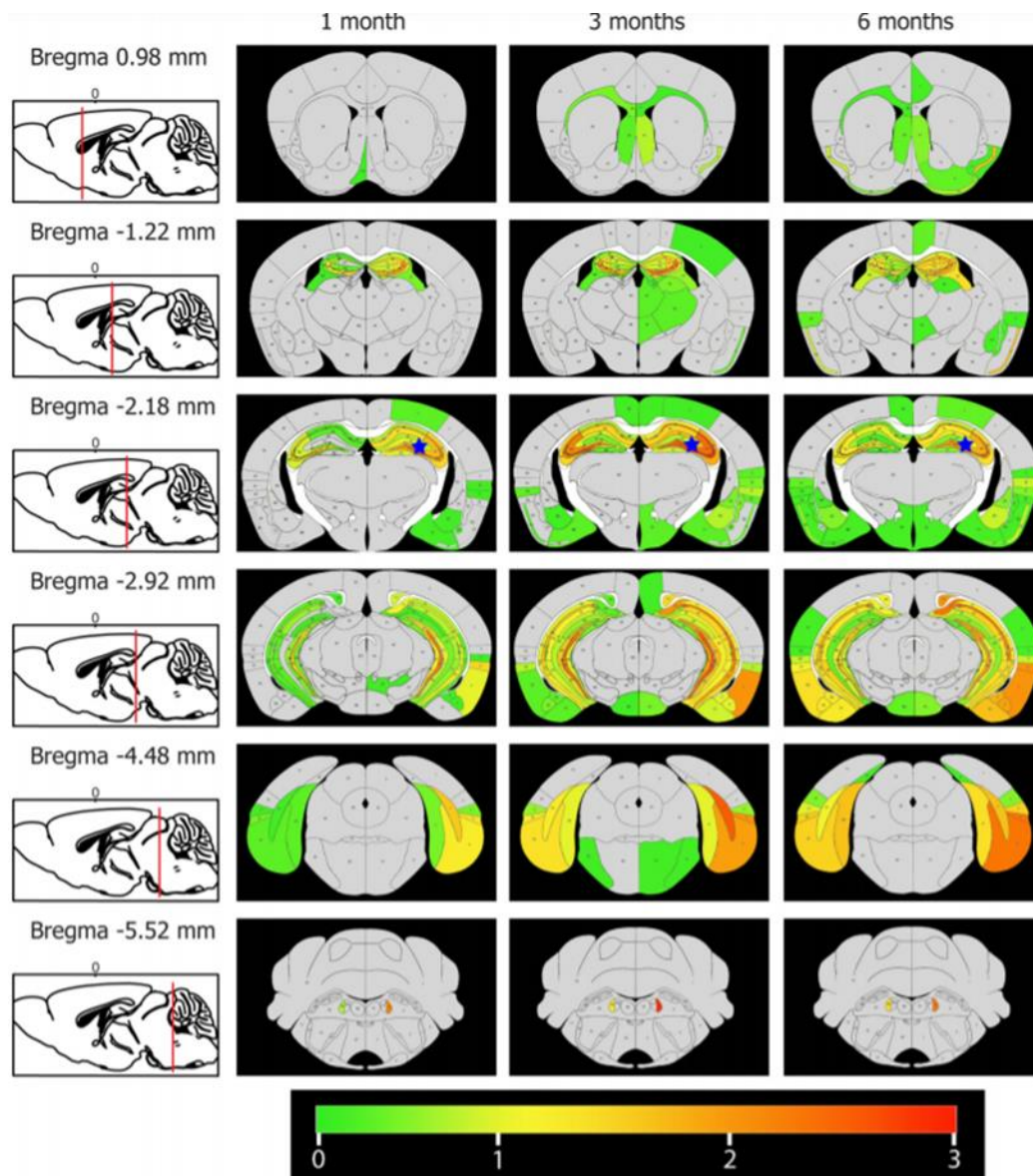


**Figure 39: Spatiotemporal spreading of tau pathology to interconnected regions**

Tau pathology spreading after tau fibril inoculation in the hippocampus of young P301S mice, based on anti-tau MC1 antibody staining. Lesions propagated in a time-dependent manner throughout the hippocampus, followed by interconnected regions, *e.g.* the entorhinal cortex, amygdala, piriform cortices and locus coeruleus. Blue stars indicate the inoculation site. From (Iba et al., 2013).

The spatial distribution of tau pathology was shown to depend on the inoculation site and its neuronal connectome. Thus, inoculation of tau fibrils into the hippocampus eventually leads to tau propagation to the entorhinal cortex, and injections in the striatum and overlying cortex leads to substantial tau deposition in striatum-connected regions such as the substantia

## 4. Prion-like hypothesis of AD

---

nigra and thalamus (Iba et al., 2013). In addition, many groups have studied the entorhinal/hippocampal pathway using transgenic mice in which human tau P301L transgene expression is restricted to the entorhinal cortex. In this model, tau inclusions first appear in the entorhinal cortex before spreading to interconnected regions such as the hippocampus (de Calignon et al., 2012; Liu et al., 2012). At more advanced stages of the disease, entorhinal tau lesions are moreover accompanied by neuronal loss, gliosis and recognition memory alterations (Fu et al., 2016). As opposed to A $\beta$ , tau spreading experiments can also be conducted on non-transgenic mice, therefore overcoming limitations regarding the non-physiological overexpression of mutated proteins and/or regional differences in transgene expression. These studies performed on wild-type mice further support that tau pathology can spread between synaptically connected brain areas (Guo et al., 2016; Narasimhan et al., 2017).

Interestingly in a case report, the disconnection of a small part of the frontal cortex in a patient that later developed AD resulted in the absence of neuritic plaques, neuropil threads and NFTs in that particular region, as opposed to massive A $\beta$  plaques and despite numerous tau lesions in limbic and isocortical regions. This study therefore suggests that as opposed to A $\beta$ , tau spreading mainly relies on axonal connections (Duyckaerts et al., 1997b).

Altogether, these data are consistent with results obtained with a computational model in which the entorhinal cortex was defined as the epicenter from which tau pathology spreads. Models based on functional or structural connectivity showed better predictive performances of tau spatial deposition than the Euclidian distance model based on the extracellular spread of tau pathology (Vogel et al., 2020).

Finally, as for prions and A $\beta$ , it has been shown that intraperitoneal administration of tau aggregates can result in tau intracerebral deposition in transgenic mice, therefore arguing that tau pathology can also spread from the periphery to the brain (Clavaguera et al., 2014).

### 4.5.2.2. Mechanisms underlying tau spreading

Several studies have suggested that tau can spread from neuron to neuron transneuronally and trans-synaptically (Frost et al., 2009). Although the underlying mechanisms are still poorly understood, different cellular pathways have been suggested.

#### 4.5.2.2.1. *Tau release*

Studies have shown that most extracellular tau is released in a free form, either through direct translocation across the plasma membrane or active exocytosis (Merezhko et al., 2018; Mudher et al., 2017). In addition, tau can also be secreted in the extracellular space inside membrane-bound extracellular vesicles such as exosomes and ectosomes (Dujardin et al., 2014; Pérez et al., 2019; Wang et al., 2017). Indeed, vesicles containing tau have been isolated from both transgenic models and humans, including in biofluids (Dujardin et al., 2014; Saman et al., 2012; Wang et al., 2017). In organotypic hippocampal slices, tau-containing exosomes can moreover successfully seed tau aggregation in neurons and microglia therefore suggesting that they may be competent for spreading tau pathology (Wang et al., 2017). Additionally, microglia was shown to spread tau aggregates through exosome secretion (Asai et al., 2015).

*In vitro* studies have suggested that tunneling nanotubes that directly connect the cytoplasm of two cells may also be a mean of tau propagation. However, the occurrence of such structures in the brain and whether transferred seeds can promote tau aggregation in the recipient cell remain to be elucidated (Mudher et al., 2017).

Given the stereotypical pattern of tau deposition in the brain, tau spreading through neural networks may also involve synaptic release mechanisms. Phosphorylated and seed competent tau was indeed shown to be enriched in synapses isolated from AD brains (DeVos et al., 2018). Moreover, neuronal activity can upregulate tau secretion and exacerbate tau pathology *in vivo* (Pooler et al., 2013; Wu et al., 2016; Yamada et al., 2014). This suggests that synaptic activity itself may participate in tau pathological spreading. Taken together, these data support the hypothesis that neuronal connectivity rather than proximity drives tau spreading throughout the brain.

#### 4.5.2.2.2. *Tau uptake*

Free tau can bind several receptors on the cell surface including heparin-sulfate proteoglycans (Holmes et al., 2013) and APP (Takahashi et al., 2015), enabling its internalization through receptor-mediated endocytosis. Tau uptake was also suggested to occur through micropinocytosis (Holmes et al., 2013). A recent study showed that tau monomers and aggregates can access neurons via the lysosome/endosome system. Both forms could be internalized via a rapid dynamin-dependent process typical of endocytosis, but only



#### 4. Prion-like hypothesis of AD

monomers were also taken up by neurons through a slower actin-dependent pathway typical of micropinocytosis (Evans et al., 2018). In addition, passive diffusion may participate in tau internalization into the cytosol as it has been shown to contribute to its secretion (Merezhko et al., 2018).

The hypothesized mechanisms of tau transcellular propagation are recapitulated in **Figure 40**.

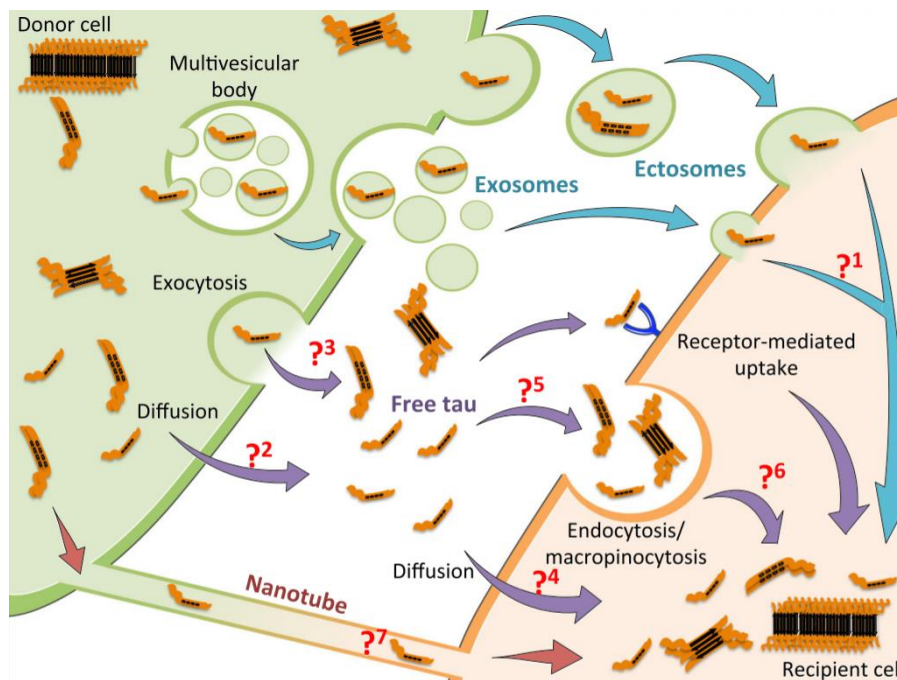


**Figure 40: Potential mechanisms underlying tau transcellular spreading**

Tau may be transferred from a donor cell (green) to a recipient cell (orange) through different mechanisms. Tau may be released in a free form possibly through passive diffusion across the plasma membrane (?<sup>2</sup>) or active exocytosis (?<sup>3</sup>) (violet arrows). It may also be released in the extracellular space within extracellular vesicles, e.g. exosomes and ectosomes (blue arrows), but how tau proteins are later released in the cytoplasm of the recipient cell remains unclear (?<sup>1</sup>). Additionally, tau may enter the recipient cell through passive diffusion (?<sup>4</sup>), non-receptor mediated endocytosis/micropinocytosis (?<sup>5,6</sup>) or by binding to cell surface receptors. *In vitro* experiments have suggested that tau may also travel in tunneling nanotubes directly connecting the cytoplasm of two cells (?<sup>7</sup>, red arrows). From (Mudher et al., 2017).

#### 4.6. Strains

In prion diseases, a critical factor responsible for phenotypic diversity relies on the occurrence of various PrP<sup>Sc</sup> molecular conformations, referred to as strains. Mounting evidence suggest that, like prions, A $\beta$  and tau can fold into distinct conformational variants. Each strain yields

specific structural and functional properties leading to distinct biochemical and biological characteristics such as different seeding and spreading abilities, distribution patterns, disease incubation times and clinical signs. Moreover, strain-specific properties are retained upon serial transmissions (Scialò et al., 2019). The occurrence of distinct A $\beta$  and tau strains may therefore provide a molecular explanation for AD heterogeneity and for distinct tauopathies.

#### 4.6.1. A $\beta$

A $\beta$  structural heterogeneity has been associated with distinct biophysical properties and pathological phenotypes, including lesions with different morphologies and distribution patterns (Thal et al., 2006b), as well as different clinical outcomes, therefore suggesting that different A $\beta$  strains may account for AD heterogeneity.

Several studies have highlighted conformational diversity in A $\beta$  species. Indeed, differences in the molecular architecture of A $\beta$  plaques has been reported in AD patients with various etiological backgrounds, *e.g.* familial or sporadic forms, using luminescent conjugated oligothiophenes binding to amyloids (Rasmussen et al., 2017). Moreover, structural variations in A $\beta$ <sub>40</sub> and A $\beta$ <sub>42</sub> fibrils were demonstrated using solid-state NMR among patients with typical AD, rapidly progressive AD and the posterior cortical atrophy variant (Petkova et al., 2005; Qiang et al., 2017). A $\beta$  originating from patients with different forms of AD could also be associated with distinct stabilities under denaturing conditions, reliably suggesting conformational differences (Cohen et al., 2015; Watts et al., 2014). Finally, A $\beta$ <sub>42</sub> conformational heterogeneity and the rate of cognitive decline were correlated in a study comparing slowly and rapidly progressing sporadic AD cases, further supporting the role of different conformers in AD pathogenesis (Cohen et al., 2015).

Interestingly, the conformational features of A $\beta$  deposits found in human AD brains can be partially replicated in animal models (Condello et al., 2018; Rasmussen et al., 2017). The experimental inoculation of different A $\beta$  strains into transgenic mice has indeed resulted in various patterns of protein aggregation and rates of disease progression (Heilbronner et al., 2013; Watts et al., 2014). Bigenic APP23 mice, which express the luciferase reporter under the control of the GFAP promoter (Tg(APP23:Gfap-luc)), inoculated with brain extracts from familial AD patients bearing the Arctic mutation, developed A $\beta$  lesions more rapidly compared with sporadic AD or familial Swedish AD-inoculated mice. Moreover, vascular deposits had a

#### 4. Prion-like hypothesis of AD

distinctive “furry” morphology and an A $\beta_{38}$ -enriched composition, similar to Arctic AD patients (Watts et al., 2014) (**Figure 41**). Finally, upon serial transmission, these features were maintained from the donor to the inoculated host, providing further evidence for distinct A $\beta$  strains (Watts et al., 2014).

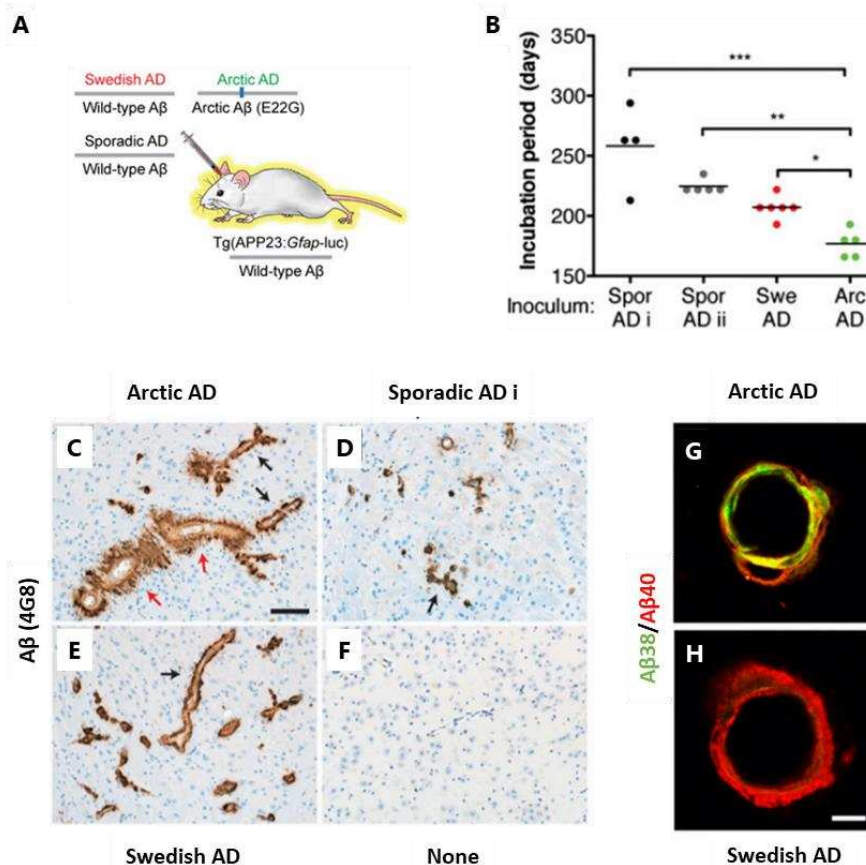


**Figure 41: Distinct rates of disease progression and vascular deposits associated with various A $\beta$  strains**

(A) Bigenic APP23 mice expressing wild-type A $\beta$  and luciferase reporter under the control of the murine GFAP promoter (Tg(APP23:Gfap-luc)) were inoculated with brain extracts from sporadic AD or fAD patients bearing the Swedish or Arctic mutations. The Swedish mutation does not alter the sequence of wild-type A $\beta$  as opposed to the Arctic mutation which produces mutant A $\beta$  (E22G). (B) Incubation periods, determined by bioluminescent imaging of astrocytosis stimulated by A $\beta$  deposition, are lower in Arctic AD-inoculated mice in comparison with all of the other groups. (C-F) A $\beta$  vascular deposits (4G8 antibody) show distinct phenotypes in the thalamus at 330 days post-inoculation. Mice inoculated with the sporadic or Swedish AD extract displayed a thin and compact layer of A $\beta$  deposition in the vasculature (black arrows), whereas Arctic-inoculated mice showed furry A $\beta$  deposits (red arrows). In F, an age-matched non-injected mouse is shown as a control. (G-H) A $\beta$  vascular deposits stained for A $\beta_{38}$  (7-14-4 antibody; green) and A $\beta_{40}$  (11A50- B10 antibody; red) show

distinct compositions, with Arctic AD brain inoculation resulting in A $\beta$ <sub>38</sub>-enriched deposition in blood vessels. Scale bars: 100  $\mu$ m in C-F and 15  $\mu$ m in G-H. Adapted from (Watts et al., 2014).

Interestingly, different synthetic strains of A $\beta$  inoculated into transgenic mice were also shown to induce different loads of A $\beta$  plaques that moreover differed in their A $\beta$ <sub>40</sub>/A $\beta$ <sub>42</sub> composition and morphology (Stöhr et al., 2014). In animal models, APP23 and APP/PS1 mice spontaneously develop A $\beta$  pathologies that differ in plaque morphology and A $\beta$ <sub>40</sub>/A $\beta$ <sub>42</sub> ratio. However, when brain extracts from one model is inoculated into the other, induced A $\beta$  pathological phenotype was influenced both by the host and the source of inoculated seed, suggesting the occurrence of polymorphic A $\beta$  strains (Meyer-Luehmann et al., 2006). Indeed, plaques induced in the receiving host tended to reflect the pathology seen in the model from which the inoculum was extracted. Overall, the APP23 extract led to more diffuse and filamentous plaques compared to smaller and more compact plaques following APP/PS1 extract inoculation. Altogether, this suggests that the molecular composition and conformation of A $\beta$  in APP transgenic mice can be maintained by seeded conversion (Heilbronner et al., 2013).

#### 4.6.2. Tau

The heterogeneity of tau conformers across different tauopathies has been suggested by many groups (Clavaguera et al., 2013; Sanders et al., 2014). In AD, tau structural heterogeneity has been linked to distinct pathological phenotypes, as tau seeding activity and some post-translational modifications were associated with clinical disease severity, therefore suggesting that different tau strains may contribute to AD heterogeneity (Dujardin et al., 2020).

The heterogeneity of tau seeding abilities was moreover demonstrated *in vitro* using real-time quaking induced conversion assays (Kraus et al., 2019). Interestingly, tau strains displaying distinct seeding profiles have been associated with different levels of cytotoxicity (Kaufman et al., 2016). When injected in non-transgenic mice, tau strains displayed different seeding potencies and cell-type specificities, as only seeds associated with specific tauopathies - *e.g.* progressive supranuclear palsy (PSP) and corticobasal degeneration (CBD) but not AD - could induce tau aggregation in astrocytes and oligodendrocytes (Narasimhan et al., 2017).

#### 4. Prion-like hypothesis of AD

Interestingly, when brain homogenates from patients with different tauopathies are injected in wild-type mice, ALZ17 mice transgenic for wild-type human tau or P301S mice, specific tau lesions reminiscent of the corresponding human disorder are induced (Boluda et al., 2015; Clavaguera et al., 2013). Various patterns of protein aggregation, selective seeding of different brain areas reflecting regional vulnerability to tau pathology as well as different rates of tau spreading along neuronal networks were moreover detected in P301S mice inoculated with different tau strains (**Figure 42**) (Kaufman et al., 2016).

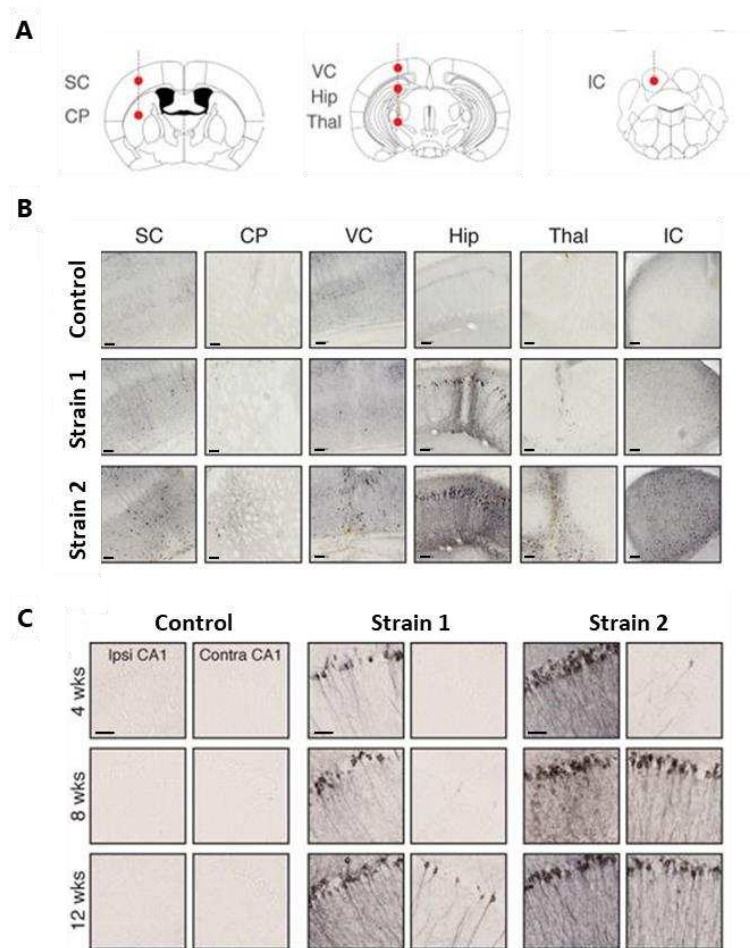


**Figure 42: Distinct regional vulnerabilities and spreading rates associated with various tau strains**

(A) P301S mice were injected unilaterally in the sensory cortex (SC), caudate/putamen (CP), visual cortex (VC), hippocampus (Hip), thalamus (Thal) and inferior colliculus (IC) with different strains of tau or a negative control. (B) Inoculated regions showed various levels of tau (AT8 antibody) accumulation depending on the inoculum (negative control or distinct tau strains) at 5 weeks post-inoculation. (C) Ipsi- and contralateral CA1 4, 8 and 12 weeks (wks) following inoculation. Strain 2 inoculation led to a faster spread of tau pathology than Strain 1. Scale bars: 100  $\mu$ m in B and 50  $\mu$ m in C. Adapted from (Kaufman et al., 2016).

It has been suggested that the pathobiology underlying selective regional vulnerability may involve complex interactions between genetic and epigenetic factors, as they could modulate neuronal and glial functions, modify misfolded protein clearance and degradation processes, affect cellular uptake and release mechanisms and alter signaling pathways (Jaunmuktane and Brandner, 2020).

Serial inoculation of distinct tau seeds primarily isolated from human brains affected with different tauopathies shows that strains can stably propagate through multiple generations in P301S mice and systematically lead to different pathological phenotypes, *e.g.* deposits that differ in their morphology, cell-type specificity, regional localization and spreading (Sanders et al., 2014). Strain properties are moreover maintained when reintroduced into cell lines (Sanders et al., 2014).

Altogether, these studies exemplify the conformation-dependent template propagation of A $\beta$  and tau aggregates and suggest that specific conformers are responsible for distinct clinical phenotypes, a process that is reminiscent of prion strains (Jucker and Walker, 2013).

#### **4.7. Infectivity**

A key feature of prions is their infectivity, as misfolded prion seeds can easily be transmitted from one organism to another. Transmission from human-derived tissues to cells or animals and transmission between animals of the same species have been widely demonstrated for prions, as well as for A $\beta$  and tau as reported in previous chapters of this manuscript (Jaunmuktane and Brandner, 2020). Inter-human transmission of prion diseases however remains rare, as most cases occurred under unusual and specific circumstances such as ritual cannibalism (Collinge et al., 2006) and exposure to cadaver-derived growth hormone or dura mater contaminated with PrP<sup>Sc</sup> (Brown et al., 2012).

Recently, CJD patients who had received contaminated c-hGH injections (Jaunmuktane et al., 2018) or dura mater grafts (Frontzek et al., 2016) were also found to present significant levels of parenchymal and vascular A $\beta$ . The preponderance of CAA is reminiscent of increased A $\beta$  vascular deposition following peripheral inoculation in mice (Eisele et al., 2010). Histopathological examinations of human brains do not allow to discriminate transmitted A $\beta$  pathologies from familial or sporadic forms (Jaunmuktane and Brandner, 2020). Additionally, some level of tau pathology was also observed in these patients (Cali et al., 2018; Duyckaerts

#### 4. Prion-like hypothesis of AD

---

et al., 2018; Hervé et al., 2018). The analysis of c-hGH and dura mater batches demonstrated the presence of A $\beta$  and tau contaminants in some samples (Duyckaerts et al., 2018; Kovacs et al., 2016; Purro et al., 2018), further supporting the prion-like seeding hypothesis of A $\beta$  and tau. Moreover, the ability of these batches to seed A $\beta$  aggregation was demonstrated *in vivo* as their intracerebral inoculation in transgenic mice expressing a humanized APP led to substantial A $\beta$  plaque deposition, both in the parenchyma and the vasculature (Purro et al., 2018).

Cases of iatrogenic transmission of pathological A $\beta$  have also been reported in patients who did not develop CJD but underwent surgical procedures in their childhood, presumably involving contaminated tools. Such transmission of A $\beta$  pathology, and more particularly CAA, revealed to be fatal in some cases as it resulted in cerebral hemorrhages (Banerjee et al., 2019; Hervé et al., 2018).

Over the past decades, more than 70 cases of A $\beta$  iatrogenic transmission have been reported, including 17 cases of cerebral hemorrhages. Despite the occurrence of some tau lesions in these cases, substantial transmission of tau pathology remains to be ascertained in humans. Very recently, Jaunmuktane and colleagues reported the first evidence of significant tau pathology in humans with iatrogenic A $\beta$  transmission following an incubation period of over 35 years. Patients displayed leptomeningeal and cortical CAA, diffuse and dense core A $\beta$  plaques in the parenchyma as well as neuropil threads, pre-tangles, tangles and neuritic plaques (**Figure 43**). However, whether such tau pathology was iatrogenically transmitted or whether it was a downstream consequence of A $\beta$  pathology remains unclear (Jaunmuktane et al., 2021).

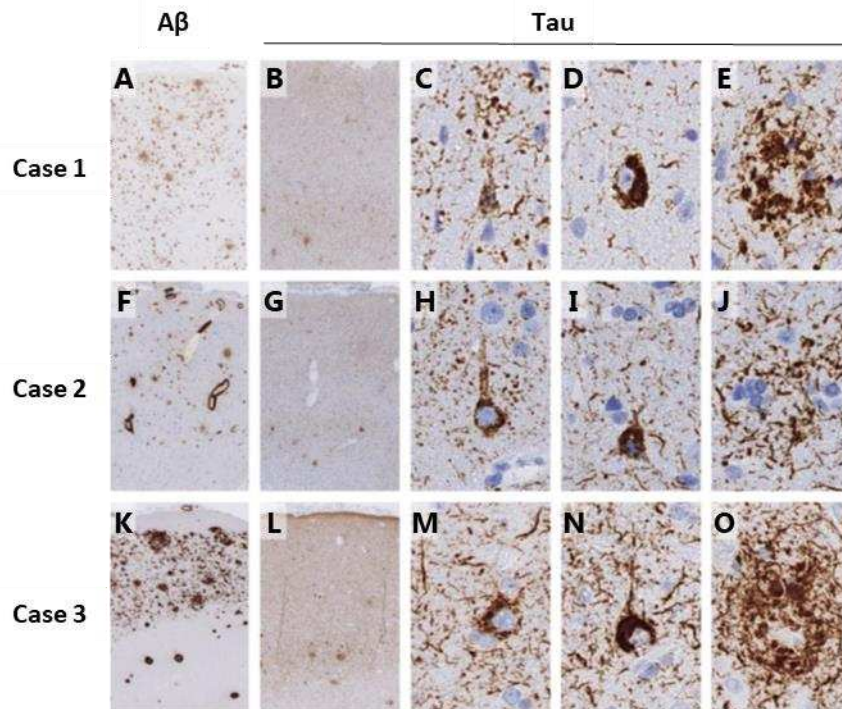


**Figure 43: Iatrogenic A $\beta$  transmission associated with tau pathology in humans**

Overview of A $\beta$  (A, F, K; 6F3D antibody) and tau (B, G, L; AT8 antibody) pathologies, and focus on pretangles (C, H, M), tangles (D, I, N) and neuritic plaques (E, J, O) in three cases of A $\beta$  and potentially tau iatrogenic transmissions following an incubation period of over 35 years (Jaunmuktane et al., 2021).

It has been suggested that the limited number of studies reporting the iatrogenic transmission of tau pathology as opposed to A $\beta$  and PrP<sup>Sc</sup> could, at least in part, be explained by the cellular localization of these proteins. Indeed, A $\beta$  and PrP<sup>Sc</sup> are extracellular and transmembrane proteins as opposed to intracellular tau, therefore making them more readily available for iatrogenic seed transmission (Jaunmuktane and Brandner, 2020).

A summary of published cases reporting A $\beta$  and/or tau transmission in humans is presented in **Table 3**.



#### 4. Prion-like hypothesis of AD

Seed source	Examined cases (n)	A $\beta$ pathology-positive cases		Tau pathology-positive cases	Concomitant pathology	Reference
		Parenchymal	Vascular			
c-hGH	8	4+2 focal	3+1 focal	0	Iatrogenic CJD	(Jaunmuktane et al., 2015a)
	33	12 (12 diffuse, 6 dense core, 5 neuritic)	14	1 with pretangles and phospho-tau in neurites	Iatrogenic CJD	(Ritchie et al., 2017) <sup>1</sup>
	12	4	2	1 with pretangles, NFTs and phospho-tau in neurites	None	(Ritchie et al., 2017) <sup>1</sup>
	24	1	1	3 with NFTs and NTs	Iatrogenic CJD	(Duyckaerts et al., 2018) <sup>2</sup>
	8	2	3	7 with NFTs, 1 with dystrophic neurites	Iatrogenic CJD	(Cali et al., 2018) <sup>3</sup>
Dura mater	1	1	1	-	Iatrogenic CJD	(Simpson et al., 1996)
	1	1	1	0	Iatrogenic CJD	(Preusser et al., 2006)
	16	13	11	11 with threads, pretangles, NFTs or thorn-shaped astrocytes	Iatrogenic CJD	(Hamaguchi et al., 2016)
	7	5	5	0	Iatrogenic CJD	(Frontzek et al., 2016) <sup>4</sup>
	2	2	2	0	Iatrogenic CJD	(Kovacs et al., 2016)
	13	3	8	3 with NFTs, 2 with dystrophic neurites	Iatrogenic CJD	(Cali et al., 2018) <sup>3</sup>
	1	1	1	1 with NFTs	Iatrogenic CJD	(Iwasaki et al., 2018)
	1	1	1	1 with phospho-tau in neurites and NFTs	Cerebral hemorrhage	(Hervé et al., 2018)
	3	2	3	0	Cerebral hemorrhage, seizures	(Banerjee et al., 2019)

	1	1	1	0	Cerebral hemorrhage	(Raposo et al., 2020)
	3	3 (diffuse, dense core)	3	3 with threads, pretangles, NFTs and neuritic plaques (2 with <b>widespread</b> pathologies)	1 Cerebral hematoma 1 Subarachnoid hemorrhage	(Jaunmuktane et al., 2021) <sup>5</sup>
Neurosurgical instruments	4	3 (diffuse, dense core)	4	2 with threads, 1 with NFTs	Cerebral hemorrhage	(Jaunmuktane et al., 2018)
	2	-	2	-	Cerebral hemorrhage	(Hamaguchi et al., 2019) <sup>6</sup>
	1	1	1	1 with phospho-tau positive neurites	Cerebral hemorrhage	(Giaccone et al., 2019) <sup>7</sup>

**Table 3: Reported cases of A $\beta$  iatrogenic transmission in humans, with or without tau pathology.**

Between 1996 and 2021, many cases of A $\beta$  iatrogenic transmission have been reported following cadaver-derived human growth hormone injections, dura-mater grafts and neurosurgery with contaminated tools. Only one study reported significant widespread tau pathology cases, whereas others reported very rare tau lesions. NFT: neurofibrillary tangles.

<sup>1</sup>(Ritchie et al., 2017) Tau pathology was unrelated to areas of A $\beta$  deposition.

<sup>2</sup>(Duyckaerts et al., 2018) Tau-positive cases received radiotherapy in childhood that might have contributed to tau phosphorylation and aggregation. These cases did not develop A $\beta$  pathology. Tau-positive neurites surrounding PrP deposits were detected in all cases but were associated with a prion-related tauopathy.

<sup>3</sup>(Cali et al., 2018) All cases with parenchymal A $\beta$  deposition displayed CAA. Detected tau pathology was most likely age-related.

<sup>4</sup>(Frontzek et al., 2016) All A $\beta$ -positive cases showed both parenchymal and vascular deposits.

<sup>5</sup>(Jaunmuktane et al., 2021) For one of the three cases, the use of cadaver-derived dural graft during neurosurgery is not known.

<sup>6</sup>(Hamaguchi et al., 2019) For these patients, it is unclear whether the neurosurgeries they underwent during childhood involved cadaveric dura mater grafts.

<sup>7</sup>(Giaccone et al., 2019) This is a case report of a 29-year-old man who suffered a traumatic brain injury in childhood and underwent surgery that included dura mater reconstruction. No information is available about the origin of the dura mater, although cadaveric dura grafts were still widely used in Italy at the time of surgery.

#### 4. Prion-like hypothesis of AD

---

These studies raise concerns that iatrogenic transmission could represent a major public health issue. It is however important to stress that, although iatrogenic transmissions of AD neuropathological hallmarks have been described, there is no evidence suggesting that AD *per se* is transmissible in humans, as none of the studied patients presented the full spectrum of AD pathology (Collinge, 2005).

Nonetheless, the implementation of preventive procedures involving non-standard decontamination methods should be considered to ensure the complete removal of misfolded seeds from surgical and laboratory instruments. In addition, it would be interesting to design prospective epidemiological studies to specifically detect cases of misfolded proteins iatrogenic transmission that are associated with very long incubation periods (Jaunmuktane and Brandner, 2020).

# OBJECTIVES



AD is a neurodegenerative disorder characterized by cognitive decline, cerebral atrophy and the aggregation of misfolded A $\beta$  peptides and tau proteins in the brain (Duyckaerts et al., 2009). The iatrogenic transmission of such aggregates in patients exposed to compounds or neurosurgical tools contaminated with A $\beta$  and tau is suspected (Duyckaerts et al., 2018; Hervé et al., 2018; Jaunmuktane et al., 2021, 2015b). Over the past decades, the experimental transmission of A $\beta$  and tau pathologies has been widely demonstrated in transgenic rodent models, through the intracerebral inoculation of proteopathic seeds (Clavaguera et al., 2013; Iba et al., 2013; Meyer-Luehmann et al., 2006; Stöhr et al., 2012). These models are valuable tools to better understand AD pathophysiology and characterize the mechanisms involved in the development and progression of AD cardinal features.

Cognitive deficits are strongly correlated with synaptic impairments in AD patients (Terry et al., 1991). However, the links between these alterations, A $\beta$  and tau pathologies and neuroinflammation are still debated. My **first** objective was to evaluate the relationships between these AD features in an A $\beta$ -plaque bearing mouse model that is not based on the genetic manipulation of tau or microglia, following human AD brain extracts inoculation.

Lesion emergence and functional impacts are highly modulated by the nature of the host and by the properties of the inoculated seeds (Jucker and Walker, 2013). Because of their phylogenetic proximity, NHPs have a brain environment closer to the human brain than that of transgenic mice. Hence, my **second** objective was to evaluate the functional, morphological and histopathological impacts of AD brain extracts inoculations in mouse lemur primates (*Microcebus murinus*).

Despite evidence suggesting the iatrogenic transmission of A $\beta$  and tau pathologies in humans, there is little information regarding the clinical and cognitive impacts associated with such transmission (Jaunmuktane et al., 2021, 2015b). My **third** objective was to characterize A $\beta$  and tau pathological transmissions as well as clinical alterations in mouse lemur primates, after AD brain extracts inoculations. In order to promote the seeding and spreading properties of A $\beta$  and tau seeds, a new stereotactic injection paradigm was developed in this study and validated using two different batches of AD brain extracts.



# RESULTS





---

# 1. Relationships between cognitive, synaptic and neuropathological changes in AD brain-inoculated mice

---

## 1.1. Context, objectives & abstract

AD is characterized by cognitive decline and neuropathological changes including aggregates of misfolded A $\beta$  peptides and tau proteins, neurodegeneration and neuroinflammation (Duyckaerts et al., 2009). However, the relationships between these AD features are still partly unknown. Cognitive deficits are strongly correlated with synaptic impairments in humans (Terry et al., 1991). Studies in animal models have suggested that both A $\beta$  (Selkoe, 2002; Sivanesan et al., 2013) and tau (Dejanovic et al., 2018; Hoover et al., 2010; Pooler et al., 2014) can induce synaptic deficits. They have also suggested that activated microglia surrounding amyloid plaques are responsible for neuronal damage (Colonna and Butovsky, 2017), and that microglia can engulf tau-positive synapses (Dejanovic et al., 2018). However, human genetic evidence, exemplified by the large effect of the loss-of-function TREM2 mutations on AD risk and on microglial function (Dourlen et al., 2019), argues that microglia have a protective function that lowers the incidence of AD.

Previous attempts to elucidate the interactions between all of these AD-associated lesions have mainly implicated transgenic mice overexpressing human A $\beta$  and tau (Bennett et al., 2017; Götz et al., 2001; Pooler et al., 2015) or have used models based on the genetic or chemical manipulation of microglia (Clayton et al., 2021; Lee et al., 2021; Leyns et al., 2019). Based on the prion paradigm, the experimental transmission of A $\beta$  and tau pathologies has been widely demonstrated in transgenic rodent models, through the intracerebral inoculation of either synthetic or brain-derived proteopathic seeds (Clavaguera et al., 2013; Iba et al., 2013; Meyer-Luehmann et al., 2006; Stöhr et al., 2012). These models provide a unique opportunity to reassess relationships between AD core lesions and downstream neurodegenerative processes.

## 1. Relationships between cognitive, synaptic and neuropathological changes in AD brain-inoculated mice

---

In this first article, we aimed to evaluate the relationships between AD hallmarks using a well-characterized mouse model that produces high levels of A $\beta$  but is not transgenic for any human tau. We showed that AD brain extracts intrahippocampal inoculation can induce A $\beta$  deposition as well as Alzheimer-like tau-positive neuritic plaques, neuropil threads and neurofibrillary tangles that spread through the brain. Additionally, in spite of leading to comparable A $\beta$ , tau and microglial pathologies, the inoculation of two different types of AD brain extracts, either originating from patients with slowly (cIAD) or rapidly evolving forms of AD (rpAD), led to different levels of synaptic loss and cognitive impairments. A complementary analysis based on correlative studies further evaluated the relationships between all of these AD features. Synaptic defects in the hippocampus and the perirhinal/entorhinal cortex were associated with the severity of tau pathology and with lower microglial load. Lower cognitive scores were associated with synaptic defects and A $\beta$  load in the hippocampus, as well as with tau pathology in both the hippocampus and the perirhinal/entorhinal cortex. Altogether, our study highlights the multifactorial origin of cognitive deficits, reinforces the major contribution of tau to AD-related neurodegenerative processes and suggests that microglial activity may protect against synaptic loss.

### **1.2. Article**

*Submitted*

*& Available on BioRxiv (<https://www.biorxiv.org/content/10.1101/2021.04.06.438654v1>).*

**Lam S.**, Boluda S. Hérard AS. Petit F., Eddarkaoui S., Cambon K., The Brainbank Neuro-CEB Neuropathology Network, Picq JL., Buée L., Duyckaerts C., Haïk S., Dhenain M. Cognitive, synaptic and neuropathological changes in Alzheimer's brain-inoculated mice.

# Cognitive, synaptic and neuropathological changes in Alzheimer's brain-inoculated mice

**Running Title:** Impacts of Alzheimer-brain inoculation

**Suzanne Lam<sup>1,2</sup>, Susana Boluda<sup>3,4</sup>, Anne-Sophie Hérard<sup>1,2</sup>,**

**Fanny Petit<sup>1,2</sup>, Sabiha Eddarkaoui<sup>5</sup>, Karine Cambon<sup>1,2</sup>,**

**The Brainbank Neuro-CEB Neuropathology Network<sup>4,5</sup>, Jean-Luc Picq<sup>1,2,6</sup>,**

**Luc Buée<sup>5</sup>, Charles Duyckaerts<sup>3,4</sup>, Stéphane Haïk<sup>3,4</sup>, Marc Dhenain<sup>1,2</sup>**

<sup>1</sup> Université Paris-Saclay, CEA, CNRS, Laboratoire des Maladies Neurodégénératives, 18 Route du Panorama, F-92265 Fontenay-aux-Roses, France.

<sup>2</sup> Commissariat à l'Énergie Atomique et aux Énergies Alternatives (CEA), Direction de la Recherche Fondamentale (DRF), Institut François Jacob, MIRCen, 18 Route du Panorama, F-92265 Fontenay-aux-Roses, France

<sup>3</sup> ICM Institut du Cerveau et de la Moelle épinière, CNRS UMR7225, INSERM U1127, Sorbonne Université, Hôpital de la Pitié-Salpêtrière, Paris, France

<sup>4</sup> GIE Neuro-CEB/Neuropathologist Network: Plate-Forme de Ressources Biologiques, Bâtiment Roger Baillet, Hôpital de la Pitié-Salpêtrière, 47-83 boulevard de l'Hôpital, 75651 Paris Cedex 13.

<sup>5</sup> Université de Lille, Inserm, CHU-Lille, Lille Neuroscience & Cognition, Alzheimer & Tauopathies, LabEx DISTALZ, Rue Polonovski, 59045 Lille, France

<sup>6</sup> Laboratory of Cognitive Functioning and Dysfunctioning (DysCo), University of Paris 8, Saint-Denis 93526 cedex, France.

<sup>5</sup> GIE Neuro-CEB: Charles Duyckaerts, Véronique Sazdovitch, Sabrina Leclère-Turbant, and Marie-Claire Artaud-Botté; The national network includes the following neuropathologists: Anne Vital (Bordeaux), Françoise Chapon (Caen), Jean-Louis Kemeny (Clermont-Ferrand), Claude-Alain Maurage & Vincent Deramecourt (Lille), David Meyronet & Nathalie Streichenberger (Lyon), André Maues de Paula (Marseille), Valérie Rigau (Montpellier), Fanny Vandembos-Burel (Nice), Charles Duyckaerts (Paris), Danielle Seilhean (Paris), Véronique Sazdovitch (Paris), Serge Milin (Poitiers), Dan Christian Chiforeanu (Rennes), Annie Laquerrière (Rouen), Béatrice Lannes (Strasbourg), Marie-Bernadette Delisle & Emmanuelle Uro-Coste (Toulouse).

## **Corresponding author**

Marc Dhenain, DVM, PhD

Commissariat à l'Énergie Atomique et aux Énergies Alternatives (CEA), Direction de la Recherche Fondamentale (DRF), Institut François Jacob, MIRCen, 18 Route du Panorama, F-92265 Fontenay-aux-Roses, France

E-mail: [marc.dhenain@cea.fr](mailto:marc.dhenain@cea.fr)

## ABSTRACT

Alzheimer's disease is characterized by lesions including extracellular amyloid- $\beta$  plaques, intracellular tau accumulations, activated microglia around amyloid plaques and synaptic alterations that lead to cognitive impairments. Tau lesions occur in the form of tau-positive aggregates surrounding amyloid- $\beta$  deposits leading to neuritic plaques, neuropil threads, and neurofibrillary tangles. The interactions between these lesions and their contribution to cognitive impairments is still debated.

In this study, through the intrahippocampal inoculation of human Alzheimer-brain extracts into an amyloid- $\beta$  plaque-bearing mouse model, we induced amyloid plaques, Alzheimer-like tau-positive neuritic plaques, neuropil threads and neurofibrillary tangles that spread through the brain, and microgliosis as well as synaptic and cognitive impairments in some animals.

Neuritic plaques, but not other tau-positive lesions, were detected in both non-inoculated and control-brain-inoculated amyloid- $\beta$  plaque-bearing mice. Alzheimer-brain extracts inoculation further increased tau pathology within neuritic plaques. As opposed to the control-brain extract, Alzheimer-brain extracts induced neuropil threads and neurofibrillary tangles next to the inoculation site. These lesions also spread to connected brain regions such as the perirhinal/entorhinal cortex.

Different levels of synaptic loss and cognitive impairments were induced by inoculating two types of Alzheimer-brain extracts originating from slowly (cAD) or rapidly evolving forms of AD (rpAD), although no difference in amyloid- $\beta$  deposition, tau pathology and microgliosis was identified between cAD- and rpAD-inoculated animals.

A complementary analysis investigated relationships between synaptic or cognitive impairments and Alzheimer pathology. Synaptic defects were associated with the severity of tau lesions and with lower microglial load. Lower cognitive scores correlated with synaptic defects as well as with amyloid and tau pathologies in the hippocampus, and with tau lesions in the perirhinal/entorhinal cortex.

Taken together, this study shows that amyloid- $\beta$  deposits are sufficient to induce tau pathology within neuritic plaques in A $\beta$  plaque-bearing mice that do not overexpress tau. Alzheimer-brain extract inoculation however increases tau pathology within neuritic plaques, and induces neuropil threads and neurofibrillary tangles that spread in the brain. Inoculation

of different human Alzheimer-brain extracts leads to different levels of synaptic loss and cognitive impairments. Synaptic loss and cognitive impairments are associated with multiple factors such as the severity of tau lesions and lower microglial activity, as well as amyloid deposition for cognitive changes. These results highlight that microglial activity may protect against synaptic loss.

## **KEYWORDS**

Alzheimer's disease; microglia; synaptotoxicity; tau; transmission

## INTRODUCTION

Alzheimer's disease (AD) core lesions include amyloid- $\beta$  (A $\beta$ ) plaques and intracellular tau accumulations that spread in a highly stereotyped pattern throughout the brain (Braak and Braak, 1991), neuroinflammation including microgliosis (Hansen *et al.*, 2018), and synaptic alterations (Terry *et al.*, 1991). The relationships between these lesions and how they lead to cognitive deficits are still partly unknown. In humans, cognitive impairments are strongly correlated with synaptic deficits (Terry *et al.*, 1991), with neocortical tau pathology but not as well with A $\beta$  plaque load (Bennett *et al.*, 2004; Nelson *et al.*, 2012). Synaptic deficits have been associated with both tau (Hoover *et al.*, 2010; Pooler *et al.*, 2014; Spires-Jones and Hyman, 2014; Dejanovic *et al.*, 2018) and A $\beta$  (Selkoe, 2002; Sivanesan *et al.*, 2013; Spires-Jones and Hyman, 2014) in mice and other experimental models. Microglia are key regulators of AD pathophysiology although their role is still debated. Several evidence (mostly in mouse models) suggest that increased activated microglia surrounding amyloid plaques are responsible for neuronal damage (Colonna and Butovsky, 2017). Also, microglia can engulf synapses in physiological conditions (Paolicelli *et al.*, 2011), as well as tau-positive synapses in pathological conditions (Dejanovic *et al.*, 2018). However, human genetic evidence, exemplified by the lower incidence of AD in individuals with loss-of-function Trem2 mutations that impair microglial activation (Dourlen *et al.*, 2019), argues that microglia have a protective function.

Several studies have attempted to elucidate the interactions between all these elements of AD pathophysiology using transgenic mice overexpressing human A $\beta$  or tau (with or without frontotemporal dementia mutations) (Gotz *et al.*, 2001; Pooler *et al.*, 2015; Bennett *et al.*, 2017). Over the last decade, new paradigms were established to induce widespread A $\beta$  and tau pathologies in mice via the intracerebral injection of human AD brain extracts. These models provide a unique opportunity to assess relationships between AD core lesions and downstream neurodegenerative processes. In this study, we inoculated crude AD brain homogenates as well as control brain homogenates in the hippocampus of mice with high A $\beta$  production. AD brain homogenates increased amyloid load at the inoculation site, increased tau lesions within neuritic plaques and induced neuropil threads and neurofibrillary tangles that spread in connected areas as the perirhinal/entorhinal cortex. Different levels of synaptic impairments and cognitive loss were induced by inoculating two different types of human AD

brain extracts originating from slowly (clAD) or rapidly (rpAD) evolving forms of AD. No differences in amyloid, tau pathology or microgliosis were identified between the clAD- and rpAD-inoculated groups. In a complementary analysis, we investigated relationships between synaptic alterations or cognitive impairments and AD pathology using correlative studies. Synaptic defects were associated with the severity of tau lesions and to lower microglial load. Lower cognitive scores were associated with synaptic defects, amyloid deposits and tau pathology.

## **MATERIAL AND METHODS**

### **Human brain collection and characterization**

Frozen brain samples (parietal cortex) from clinically different sporadic AD patients (four patients with classical slowly evolving forms of AD (clAD, disease duration of 5 to 8 years) and four with a rapidly evolving form of AD (rpAD, disease duration of 6 months to 3 years)) as well as age-matched control individuals (two cases) were collected from a brain donation program of the GIE NeuroCEB and the CNR-prion brain banks. Consent forms were signed by either the patients themselves or their next of kin in their name, in accordance with French bioethics laws. No case of hippocampal sclerosis was reported and all brain samples were PrPSc negative. Samples from clAD and rpAD brains were also negative for  $\alpha$ -synuclein and TDP-43. All brain tissues were assessed by immunohistochemistry, as previously described in Gary et al. 2019 (Gary *et al.*, 2019) (Supplementary Methods 1).

### **Human brain homogenate preparation and characterization**

Parietal cortex samples from each patient were individually homogenized at 10% weight/volume (w/v) in a sterile 1X Dulbecco's phosphate buffer solution in CK14 soft tissue homogenizing tubes at 5000 rpm for 20 sec (Precellys®, Bertin technologies). Individual brain homogenates were then sonicated on ice for 5 sec at 40% amplitude and centrifuged at 3000g for 5 min at +4°C. The resulting supernatant was aliquoted in sterile polypropylene tubes and stored at -80 °C until use. Brain homogenates were then prepared by combining brain extracts from different patients. clAD and rpAD homogenates consisted in a combination of four brain extracts from the patients with clAD and rpAD, respectively. A third homogenate, considered as a control, was prepared from non-demented individuals (Ctrl, n=2 subjects).



Brain homogenates were characterized by biochemistry. A $\beta$  levels were evaluated using the human V-PLEX kit A $\beta$  Peptide Panel 1 (6E10) (MSD®) according to the manufacturer's recommendations (Supplementary Methods 2.1). Total tau and phospho-tau181 were evaluated by ELISA according to the manufacturer's recommendations (Supplementary Methods 2.1). Tau was characterized by western blotting using AT100, 2H9, tau-Nter and tau-Cter antibodies (Supplementary Methods 2.2). Iba1 and GFAP proteins were also quantified by western blots (Supplementary Methods 2.2).

### **Transgenic mice**

Mouse experiments were performed on the APP<sub>swe</sub>/PS1<sub>dE9</sub> mouse model of amyloidosis (Garcia-Alloza *et al.*, 2006). Animals were studied eight or four months after intracerebral inoculation of the brain homogenates (at 8 and 4 months post-inoculation (mpi) respectively, n<sub>Ctrl</sub>=15 and 11, n<sub>clAD</sub>=15 and 14, n<sub>rpAD</sub>=20 and 12). Wild-type littermates injected with the Ctrl brain sample were used as controls for the behavioral tests (at 8 and 4 mpi respectively, n<sub>WT</sub>=12 and 6). All APP<sub>swe</sub>/PS1<sub>dE9</sub> mice were born and bred in our center (Commissariat à l'Énergie Atomique, centre de Fontenay-aux-Roses; European Institutions Agreement #B92-032-02). All animals were randomly assigned to the experimental groups. Males were exclusively used in this study. All experimental procedures were conducted in accordance with the European Community Council Directive 2010/63/UE and approved by local ethics committees (CEtEA-CEA DSV IdF N°44, France) and the French Ministry of Education and Research (A17\_083 authorization).

### **Preparation of brain samples and stereotaxic surgery**

10% Ctrl, clAD or rpAD individual brain homogenates were thawed on ice. Homogenates were then pooled together according to their group and the three resulting combined samples (Ctrl, clAD, rpAD) were sonicated (70% amplitude, 10 sec on/off; Branson SFX 150 cell disruptor sonicator, 3.17mm microtip probe Emerson, Bron) on ice in a sterile environment, extemporaneously before stereotaxic injection. Bilateral injections of brain samples were performed in the dorsal hippocampus of two-month old anesthetised mice (AP -2 mm, DV -2 mm, L +/- 1 mm from bregma, 2 $\mu$ l of sample administered at a 0.2 $\mu$ l/min rate) through a stereotaxic surgical procedure described in Supplementary Methods 3.

### **Behavioral evaluations**

A battery of behavioral tests (elevated plus maze, a novel object recognition task in a V-maze, and a Morris water maze) was conducted at 8 mpi or 4 mpi on APP<sub>swe</sub>/PS1<sub>dE9</sub> mice. Wild-type littermates injected with the Ctrl brain sample were used as controls for the tests. Mice were handled for 2 minutes per day, for 5 days prior to any test. Before each test, mice were habituated to the experimental room for 30 minutes. The experimenter was blind to mouse groups. Performances were recorded using a tracking software (EthoVision XT14, Noldus) (Supplementary Methods 4).

### **Animal sacrifice and brain preparation for histology**

Mice were sacrificed at 8 or 4 mpi, after the behavioural tests, with an intraperitoneal injection of a lethal dose of pentobarbital (100 mg/kg; Exagon, Axience). They were perfused intracardially with cold sterile 0.1M PBS for 4 minutes, at a rate of 8 ml/min. The brain was extracted and post-fixed in 4% paraformaldehyde for 48 hours at +4°C, transferred in a 15% sucrose solution for 24 hours and in a 30% sucrose solution for 48 hours at +4°C for cryoprotection. Serial coronal sections of 40 µm were performed with a microtome (SM2400, Leica Microsystem) and stored at -20°C in a storing solution (glycerol 30%, ethylene glycol 30%, distilled water 30%, phosphate buffer 10%). Free-floating sections were rinsed in a 0.1M PBS solution (10% Sigma-Aldrich® phosphate buffer, 0.9% Sigma-Aldrich® NaCl, distilled water) before use. Washing and incubation steps were performed on a shaker at room temperature unless indicated otherwise.

### **Immunohistochemistry for amyloid, tau, microgliosis and astrogliosis**

Amyloid deposits were evaluated using a 4G8 labelling. Tau was evaluated using AT8 and AT100 labellings. Microgliosis was evaluated using Iba1 and CD68 antibodies. Astrocytes were stained with the GFAP antibody. Staining procedures are described in Supplementary Methods 5. Stained sections were scanned using an Axio Scan.Z1 and segmented using ImageJ-based automatic local thresholding methods to quantify 4G8, AT8, AT100, Iba1 and CD68 immunostainings (Supplementary Methods 5). In addition for the AT8 immunostaining, a quantification of neuritic plaques and AD-like neurofibrillary tangles was performed by manual counting (Supplementary Methods 5). A semi-quantitative analysis of neuropil threads

was also performed by assigning a severity score based on the intensity and extent of AT8-positive staining in each ROI (Supplementary Methods 5).

### **Gallyas silver staining**

Free-floating sections were mounted on Superfrost Plus (Thermo-Scientific®) slides and dried overnight prior to Gallyas staining according to a procedure described in Supplementary Methods 6.

### **Co-stainings of microglia and amyloid plaques**

In order to evaluate microglial load surrounding amyloid plaques, microglia and amyloid plaque co-staining was performed according to a procedure described in Supplementary Methods 7. The method used to quantify microglial load around plaques is described in the same Supplementary Methods 7.

### **Evaluation of synaptic density**

Synaptic density was evaluated in the hippocampus (CA1) and the perirhinal/entorhinal cortex of inoculated mice using a double immunolabelling of presynaptic (Bassoon) and postsynaptic (Homer1) markers. Free-floating sections were permeabilized in a 0.5% Triton X-100/0.1M PBS (Sigma-Aldrich®) solution for 15min. Slices were incubated with Bassoon (Abcam Ab82958, 1/200) and Homer1 (Synaptic systems 160003, 1/400) antibodies diluted in 3%BSA/PBST solution for 24 hours at +4°C. Incubation with secondary antibodies coupled to a fluorochrome (Alexa Fluor) diluted in a 3%BSA/0.1M PBS solution was then performed for 1h at room temperature. Sections were rinsed and mounted on Superfrost Plus (Thermo-Scientific®) slides with the Vectashield® mounting medium with a refractive index of 1.45. Images of stained sections were acquired using a Leica DMI6000 confocal optical microscope (TCS SPE) with a 63x oil-immersion objective (refractive index 1.518) and the Leica Las X software. A confocal zoom of 3 and a pinhole aperture fixed at 1 Airy were applied. Acquisition was performed in sequential mode with a sampling rate of 1024x1024 and a scanning speed of 700 Hz. Image resolution was 60 nm/pixel and the optical section was 0.896 µm. 26 separate planes with a 0.2 µm step were acquired. The excitation wavelengths were 594 nm or 633 nm. Image acquisition in the CA1 region was performed on 4 adjacent slices located between -1.82 mm and -3.28 mm from the bregma, with 2 images per slice. For the perirhinal/entorhinal cortex, 3 adjacent slices located between -3.28 mm and -4.24 mm from the bregma were

analyzed, with 2 images acquired per slice. 3D deconvolution of the images was performed using the AutoQuant X3 software. The deconvoluted 8-bit images were analyzed using the ImageJ software, as described in Gilles et al (Gilles *et al.*, 2017). Briefly, automated 3D segmentation of the staining allowed to determine the volume occupied by Bassoon-positive or Homer-positive objects in the 3D space as well as the localization of the geometrical centroid or center of mass of the objects. Co-localization was determined by the detection of overlapping objects, and depended on the center-to-center distance and the percentage of co-localization volumes for each pair of objects.

### **Statistical analysis**

Statistical analysis was performed using the GraphPad Prism software 8. Kruskal-Wallis test with Dunn's multiple comparisons were performed except when repeated measures were acquired in the behavioral tasks, in which case, a two-way repeated measures ANOVA with the Geisser-Greenhouse correction and Dunnett's multiple comparisons was carried out. Wilcoxon's signed-rank test was used to compare the time spent in the Morris Water maze quadrants with the theoretical value of 15 seconds (25% of trial duration). For comparisons between AD (cIAD and rpAD mice as one AD group) and Ctrl mice, Mann-Whitney tests were conducted. For correlation studies, Spearman correlation test was performed. The significance level was set at  $p < 0.05$ . Data are shown on scattered dot plots with mean  $\pm$  standard error of the mean (s.e.m).

### **Data availability**

The data that support the findings of this study are available from the corresponding author, upon reasonable request.

## **RESULTS**

### **Characterization of human brain homogenates**

We prepared two brain homogenates from sporadic AD patients, with each homogenate consisting of a combination of four brain extracts from patients with either a rapidly evolving form of AD (rpAD) or patients with forms of AD that evolved more slowly (cIAD). A third homogenate, considered as a control, was prepared from non-demented individuals (Ctrl, n=2 subjects). The characteristics of the selected subjects are presented in Supplementary Table 1 and Supplementary Fig. 1-2. The amounts of amyloid, tau and neuroinflammatory proteins

slightly differed between the brain homogenates, as the rpAD homogenate displayed more total tau and phospho-tau181, but less A $\beta$ <sub>38</sub> and A $\beta$ <sub>40</sub> than the clAD one (Supplementary Fig. 2A-F). Iba1 and GFAP levels were similar in the two AD homogenates (Supplementary Fig. 2G-I).

### **Cognitive alterations in AD brain-inoculated mice**

rpAD, clAD, and Ctrl brain homogenates were inoculated bilaterally (2  $\mu$ l/site) in the dorsal hippocampus (CA1) of 2-month-old APP<sub>swe</sub>/PS1<sub>dE9</sub> mice. This model expresses the endogenous murine tau protein isoforms and is not transgenic for any human tau. Inoculated mice were evaluated using a battery of behavioral tests at 8 mpi. An additional group of Ctrl-inoculated wild-type (WT) littermates was used as controls. First, we found that, compared to clAD and Ctrl brain inoculations, rpAD brain inoculation led to novel object recognition deficits as evaluated in an object-recognition task (V-maze test) (Fig. 1A-C). The test was divided into three phases (spread over 3 days). Following an habituation phase in an empty arena on day 1, two identical objects were added to the maze on day 2 (training phase). One of them was eventually removed and replaced by a novel object on day 3 (discrimination phase). Mice from each group showed similar exploratory activity, as suggested by comparable interest in the two identical objects during the training phase on day 2 (Fig. 1A), and similar distance travelled throughout the three days of test (Fig. 1B). During the novel object recognition evaluation on day 3, rpAD mice spent less time exploring the novel object, leading to a significantly lower discrimination index, compared to WT and APP<sub>swe</sub>/PS1<sub>dE9</sub> clAD or Ctrl-inoculated mice (Fig. 1C, respectively, p=0.0018, 0.0082 and 0.0007). Spatial memory was then assessed using the Morris water maze test (Suppl Fig. 3A-C). During the training phase, no difference was observed between the groups suggesting that Ctrl, clAD and rpAD brain inoculations do not differentially impact spatial learning abilities in APP<sub>swe</sub>/PS1<sub>dE9</sub> mice (Supplementary Fig. 3A-B). Spatial memory retention was then evaluated 72 hours after the last training test. All groups performed as well as the WT group by spending more time in the target quadrant than in the opposite one, suggesting that spatial memory is not impaired in APP<sub>swe</sub>/PS1<sub>dE9</sub> Ctrl or AD-inoculated mice (Supplementary Fig. 3C). Moreover, the time spent both in the target quadrant and in the opposite one was significantly different from the theoretical value of 15 seconds, which corresponds to 25% of the trial duration, supporting the idea that all groups successfully memorized the platform location (Supplementary Fig. 3C). Anxiety levels were

also evaluated using the general aversion of rodents to open spaces in the elevated plus maze test, which is a plus-shaped apparatus with two open and two enclosed arms. The different groups did not display differences in the distance travelled, the time spent leaning over the maze, as well as the time spent in open and enclosed arms or at their intersection in the center of the arena (Supplementary Fig. 3D-F). These results suggest that anxiety levels at 8 mpi are neither impacted by the APP<sub>Swe</sub>/PS1<sub>dE9</sub> genotype, nor by the intracerebral inoculation of AD brains. No difference in cognitive performance was observed at 4 mpi (Supplementary Fig. 4A-C, n<sub>Ctrl</sub>=11, n<sub>clAD</sub>=14, n<sub>rpAD</sub>=12, n<sub>WT</sub>=6).

### **Synaptotoxicity in AD brain-inoculated mice**

Synaptic density was then evaluated in the hippocampus (CA1) and the perirhinal/entorhinal cortex of inoculated mice at 8 mpi, using a double immunolabelling of presynaptic (Bassoon) and postsynaptic (Homer) markers. The amount of colocalized punctas, an indicator of synaptic density, was decreased by 30% and 26% in rpAD mice compared to Ctrl and clAD mice, respectively, in the hippocampus (Fig. 1D, respectively p=0.0011 and 0.037). In the perirhinal/entorhinal cortex, lower synaptic density was observed in the rpAD group compared to the Ctrl group but not to the clAD group (Fig. 1E, respectively p=0.001 and 0.13). No difference in synaptic density was found between the Ctrl and clAD groups (Fig. 1D-E). Correlative studies showed that the discrimination index in the V-maze was correlated with synaptic defects in the CA1 (Fig. 1F,  $r_{\text{spearman-hip}}=0.35$ , p=0.02) but not in the perirhinal/entorhinal cortex (Fig. 1G,  $r_{\text{spearman-P/EC}}=0.27$ , p=0.29).

### **Acceleration of A $\beta$ plaque deposition and induction of tau pathologies close to the injection site in AD brain-inoculated mice**

At 8 mpi, AD brain inoculation led to an increase in amyloid plaque deposition in the hippocampus and in the region surrounding the alveus compared to Ctrl brain (Fig. 2, respectively for clAD and rpAD brains, p=0.0005 and p<0.0001 in the hippocampus, p<0.0001 and p<0.0001 in the alveus). The same changes were found at 4 mpi (Supplementary Fig. 4F-G). This suggests that the amyloid increase detected at 8 mpi (Fig. 2) already started at 4 mpi. Three types of tau lesions occur in AD patients: tau-positive aggregates surrounding A $\beta$  deposits leading to neuritic plaques, neuropil threads and neurofibrillary tangles. AD-like

neuritic plaques (NPs) (Fig. 3A, G-J), neuropil threads (NTs) (Fig. 3B), neurofibrillary tangles (NFTs) (Fig. 3C-F) were all recapitulated in AD brain-inoculated APP<sub>Swe</sub>/PS1<sub>dE9</sub> mice.

At 8 mpi, neuritic plaques were detected in the hippocampus of AD- and Ctrl-inoculated mice (Fig. 3G-I, K-L). To further evaluate if human brain inoculation was necessary to induce these lesions, we performed an AT8 staining on old non-inoculated APP<sub>Swe</sub>/PS1<sub>dE9</sub> mice and also observed neuritic plaques (Fig. 3J). Quantification showed that neuritic plaque count was similar in AD- and Ctrl-inoculated mice (Fig. 3K). However, the AT8-positive area stained within neuritic plaques was larger in the two AD-inoculated groups compared to Ctrl animals (Fig. 3G-I and 3L,  $p=0.001$  and  $p<0.0001$ , respectively for cIAD and rpAD mice).

At 8 mpi, compared to the Ctrl-inoculated mice, AD-inoculated mice displayed an overall increase in tau lesions in the hippocampus (Fig. 3M-O, 3S;  $p=0.001$  and  $p<0.0001$  respectively for cIAD and rpAD mice) and in the alveus (Fig. 3P-R, 3T;  $p=0.0035$  and  $p<0.0001$  respectively for cIAD and rpAD mice), as revealed by an AT8-positive immunostaining directed against hyperphosphorylated tau. The same trends, although to a lesser extent, were reported at 4 mpi (Supplementary Fig. 4I-J). In AD-inoculated mice, AT8-positive neuropil threads were induced both in the hippocampus (Fig. 3U,  $p=0.0005$  and  $p<0.0001$  in cIAD and rpAD mice, respectively) and the alveus (Fig. 3V,  $p=0.0036$  and  $p<0.0001$  in cIAD and rpAD mice, respectively) whereas Ctrl-inoculated animals did not present these lesions. Moreover, AT8-positive NFTs were increased in the hippocampus of AD-inoculated mice as opposed to Ctrl-inoculated animals at 8 mpi (Fig. 3W,  $p=0.001$  and  $p<0.0001$  in cIAD and rpAD mice, respectively).

Further evaluation of tau lesions revealed AT100 positive labelling in the forms of neuropil threads (Supplementary Fig. 5A, arrowheads) and NFTs (Supplementary Fig. 5A, arrow) in AD-inoculated mice. Quantification of the AT100 staining showed increased labelling in the alveus of AD-inoculated mice but not in the hippocampus (Supplementary Fig. 5B-C,  $p=0.0007$  and  $0.092$  respectively). Gallyas silver staining revealed neuropil thread labelling (Supplementary Fig. 5D) as well as amyloid plaques (Supplementary Fig. 5E). No quantification was performed as this technique reveals both tau and amyloid lesions.

### **Tau spreading in AD-brain inoculated mice**

We then evaluated A $\beta$  and tau lesions in the perirhinal/entorhinal brain regions that are connected to the hippocampus (Fig. 4A-B). Amyloid load was similar in the perirhinal/entorhinal cortex of rpAD, cIAD and Ctrl mice (Fig. 4C-E, 4I,  $p>0.05$ ). A $\beta$  detected in the perirhinal/entorhinal cortex may thus only reflect the endogenous expression of the peptide in the APP<sub>swe</sub>/PS1<sub>dE9</sub> model. Conversely, overall hyperphosphorylated tau lesions (AT8-positive area) were clearly increased in the perirhinal/entorhinal cortex of AD brain inoculated animals compared to Ctrl-inoculated ones (Fig. 4F-H, 4J,  $p=0.0007$  and  $p=0.0002$ , respectively for cIAD and rpAD mice). Neuritic plaque accumulation was increased in the perirhinal/entorhinal cortex of rpAD-inoculated mice compared to Ctrl mice (Fig. 6K,  $p=0.038$ ). The AT8-positive area stained within neuritic plaques was larger in the perirhinal/entorhinal cortex of the two AD-inoculated groups compared to Ctrl animals suggesting that the neuritic plaques were more reactive in the AD groups (Fig. 6L,  $p=0.0034$  and  $p<0.0001$ , respectively for cIAD and rpAD mice). Neuropil threads and NFTs were detected in the perirhinal/entorhinal cortex of AD-inoculated mice but not in Ctrl-inoculated animals (Fig. 6M, neuropil thread accumulation for cIAD and rpAD mice,  $p=0.0003$  and  $p=0.0002$ ; Fig. 6N, NTF accumulation for cIAD and rpAD mice,  $p=0.005$  and  $p<0.0001$ ). These lesions were mainly found in the external layers II and III of the cortex (Fig 6F-H) that project to the dentate gyrus via the perforant pathway and to the CA1 region via the temporo-ammonic pathway, respectively. On the contrary, internal layers (*e.g.* layers V-VI) that receive projections from the CA1 region were not labelled. Other cortical regions such as the visual cortex also displayed neuropil threads, NFTs and neuritic plaques in cIAD and rpAD mice (Supplementary Fig. 6A-B). As in the hippocampus, AT100 staining revealed tau lesions in the perirhinal/entorhinal cortex (Supplementary Fig. 7A-B) and a statistical difference in AT100-positive staining was detected between the ADs and Ctrl groups (Supplementary Fig. 7C,  $p=0.005$ ). Gallyas staining was also positive for tau lesions (Supplementary Fig. 7D-E) and amyloid plaques (Supplementary Fig. 7D, 7F) in this region.

Studies at 4 mpi revealed an increased level of tau lesions in AD-inoculated mice next to the inoculation site (Supplementary Fig. 4I-J). However, no changes of tau lesions were detected in the perirhinal/entorhinal cortex at 4 mpi (Supplementary Fig. 4K). The increased presence of tau lesions at both sites at 8 mpi in AD-inoculated mice, while tau was not increased at 4



mpi in the perirhinal/entorhinal cortex, suggests that tau gradually spreads through the brain in a time-dependent manner. Consistently with the lack of amyloid spreading at 8 mpi (Fig. 4), no change in amyloid deposition was detected in the perirhinal/entorhinal cortex of Ctrl compared to AD-brain inoculated animals at 4 mpi (Supplementary Fig. 4H).

### **Neuroinflammatory response**

Neuroinflammation was assessed by staining brain tissues using Iba1, a general marker for microglia as well as an anti-CD68 antibody that stains a lysosomal protein expressed at high levels by activated microglia and at low levels by resting microglia. Iba1 and CD68 stainings were positively correlated in the hippocampus and the perirhinal/entorhinal cortex (Supplementary Fig. 8A-B,  $r_{\text{Spearman-hip}}=0.39$  and  $p=0.009$ ,  $r_{\text{Spearman-EC}}=0.53$  and  $p=0.0002$ ). Quantification revealed similar levels of Iba1 (Fig. 5A-B) and CD68 (Fig. 5C-D) stained areas in the hippocampus or perirhinal/entorhinal cortex of cAD, rpAD and Ctrl groups ( $p>0.05$ ; Kruskal-Wallis with Dunn's multiple comparisons).

Visual observation of the stained sections suggested different levels of staining for Iba1 with some animals displaying high Iba1 labelling (Fig. 5G-H) and some others lower staining (Fig. 5K-L). Animals displaying high Iba1 labelling showed abundant activated microglia characterized by beading with spheroidal swellings of the processes and enlarged cell body with dystrophic ramifications (Fig. 5I, arrows) (Sanchez-Mejias *et al.*, 2016). These activated cells formed microglial clusters surrounding A $\beta$  plaques (Fig. 5J). In contrast, mice with low Iba1 labelling (Fig. 5K-L) displayed highly ramified microglia, both close to and far from amyloid plaques (Fig. 5M and 5N respectively), which is consistent with a non-activated phenotype. As for Iba1, some animals displayed high CD68 labelling (Fig. 5O) and some others lower staining (Fig. 5P). Some clusters of CD68-stained microglia surrounded amyloid deposits (Fig. 5Q) while some others were not associated with amyloid deposits (Fig. 5R). Microglial activation was proposed to shield amyloid plaques off from neurons to prevent their toxicity (Condello *et al.*, 2015). Using confocal microscopy, we showed that, as expected, Iba1 stained microglia surrounding amyloid plaques (Supplementary Fig. 8C). We thus evaluated whether microglial load surrounding amyloid plaques differed following the inoculation of various brain extracts. We could not detect any differences in Iba1 staining around plaques in the different groups (Fig. 5E-F,  $p>0.05$ ). This suggests no difference in the shielding effect in our three models of inoculation.

Finally, astrocyte reactivity (GFAP staining) was evaluated and no difference was detected between the groups in the hippocampus and in the perirhinal/entorhinal cortex (Supplementary Fig. 9).

### **Synaptic density is associated with Tau and reduced microglial activation but not with A $\beta$ pathology**

No differences in amyloid (Fig. 2, 4), tau pathology (Fig. 3, 4) or microgliosis (Fig. 5) were identified between the rpAD- or cIAD-inoculated group despite different levels of synaptic impairments (Fig. 1D-E). To further evaluate the origins of synaptic impairments, we took advantage of interindividual heterogeneity to assess the relationships between synaptic density and tau lesions, amyloid pathology and microgliosis. Synaptic density in the hippocampus (CA1) and in the perirhinal/entorhinal cortex was inversely correlated with global tau pathology in the same region (Fig. 6A, 6E,  $r_{\text{spearman-hip}}=-0.37$ ,  $p=0.008$  and  $r_{\text{spearman-P/EC}}=-0.32$ ,  $p=0.03$ ). Synaptic density in the perirhinal/entorhinal cortex was correlated with neuritic plaque count (Fig. 6F,  $r_{\text{spearman-P/EC}}=-0.50$ ,  $p=0.0005$ ), AT8-positive area stained within neuritic plaques (Fig. 6G,  $r_{\text{spearman-P/EC}}=-0.45$ ,  $p=0.001$ ), neuropil threads (Fig. 6H,  $r_{\text{spearman-P/EC}}=-0.43$ ,  $p=0.003$ ), and NFTs (Fig. 6I,  $r_{\text{spearman-P/EC}}=-0.38$ ,  $p=0.011$ ). This suggests that tau contributes to synaptic alterations. Synaptic density was not correlated with amyloid load in the hippocampus nor in the perirhinal/entorhinal cortex (Fig. 6B, 6J,  $p>0.05$ ). A positive correlation was also reported between synapses and Iba1 staining in the hippocampus (Fig. 6C,  $r_{\text{spearman-hip}}=0.50$ ,  $p=0.0002$ ) and between synapses and Iba1 (Fig. 6K,  $r_{\text{spearman-P/EC}}=0.44$ ,  $p=0.0018$ ) or CD68 stainings (Fig. 6L,  $r_{\text{spearman-P/EC}}=0.57$ ,  $p<0.0001$ ) in the perirhinal/entorhinal cortex. No relationship between synapses and GFAP staining was observed in these regions (not shown).

### **Cognitive scores are associated with increased tau and amyloid loads**

Cognitive changes were shown to be associated with synaptic impairments (Fig. 1F-G). We further investigated their relationships with AD pathology. Cognitive scores in the V-maze test were negatively correlated with tau pathology in both the hippocampus and the perirhinal/entorhinal cortex (global tau pathology (Fig. 7A-B,  $r_{\text{spearman-hip}}=-0.35$ ,  $p=0.021$  and  $r_{\text{spearman-P/EC}}=-0.42$ ,  $p=0.0059$ ), AT8-positive area stained within neuritic plaques (Fig. 7C-D,  $r_{\text{spearman-hip}}=-0.37$ ,  $p=0.014$  and  $r_{\text{spearman-P/EC}}=-0.42$ ,  $p=0.006$ ), neuropil threads (Fig. 7E-F,  $r_{\text{spearman-hip}}=-0.44$ ,  $p=0.0039$  and  $r_{\text{spearman-P/EC}}=-0.36$ ,  $p=0.022$ ), NFTs (Fig. 7G-H,  $r_{\text{spearman-hip}}=-0.34$ ,

$p=0.032$  and  $r_{\text{spearman-P/EC}}=-0.40$ ,  $p=0.012$ ). Cognitive scores in the V-maze were also negatively correlated with amyloid load in the hippocampus, but not in the perirhinal/entorhinal cortex (Fig. 8A-B,  $r_{\text{spearman-hip}}=-0.48$ ,  $p=0.001$  and  $r_{\text{spearman-P/EC}}=-0.17$ ,  $p=0.29$ ). Finally, cognitive scores in the V-maze were positively correlated with microglial load stained by Iba1 in the hippocampus and perirhinal/entorhinal cortex (Fig. 8C-D,  $r_{\text{spearman-hip}}=0.34$ ,  $p=0.028$ ;  $r_{\text{spearman-P/EC}}=0.45$ ,  $p=0.003$ ) but not with CD68 staining (Fig. 8E-F,  $r_{\text{spearman-hip}}=0.07$ ,  $p>0.6$ ;  $r_{\text{spearman-P/EC}}=0.16$ ,  $p>0.3$ ). No relationship between cognitive scores and astrocyte-associated GFAP staining was observed (not shown).

## DISCUSSION

Based on the intracerebral inoculation of crude AD brain homogenates into mice with high A $\beta$  production, we produced a highly pathologically relevant AD model which develops amyloid plaques, tau lesions that spread in the brain, and in some cases synaptic and cognitive impairments.

A first part of our study was dedicated to compare the impact of the inoculation of Ctrl and two AD brain extracts (*e.g.* rapidly (rpAD) or slowly evolving forms (clAD) of AD). Comparison of Ctrl versus AD-inoculated mice (rpAD or clAD) showed that as expected (Di Fede *et al.*, 2018; Gary *et al.*, 2019), amyloid load was increased in the hippocampus following AD brain intrahippocampal inoculation.

Neuritic plaques were detected in AD-inoculated mice as well as in Ctrl-inoculated mice. We evaluated neuritic plaques in aged non-inoculated mice and found that they also displayed these lesions. This result is consistent with reports showing that neuritic plaques occur spontaneously with age in APP<sub>Swe</sub>/PS1<sub>dE9</sub> mice (Metaxas *et al.*, 2019). It suggests that  $\beta$ -amyloid plaques, *per se*, are sufficient to induce neuritic plaques. In humans, different forms of amyloid plaques, including non-A $\beta$  ones, can also induce tau lesions in surrounding neurites (Duyckaerts *et al.*, 2018). Our study moved one step forward by showing that the density of tau lesions within neuritic plaques was higher in AD-inoculated mice compared with Ctrl-inoculated animals. Taken together, this highlights that amyloid plaques create a microenvironment that induces tau lesions within neuritic plaques, and that such lesions are amplified by the exposure to human AD brain, presumably because of exogenous pathological tau seeds.

Unlike neuritic plaques, neuropil threads and NFTs were not detected in Ctrl brain-inoculated mice. They were induced next to the inoculation site in the AD-inoculated animals. In addition, they spread from the inoculated site to connected brain regions such as the perirhinal/entorhinal cortex.

Following the comparison between Ctrl- and AD-inoculated mice, we compared mice inoculated with rpAD and cAD brain extracts. We provided the first experimental evidence that the intracerebral inoculation of these different AD brain extracts can induce different levels of synaptic loss and cognitive alterations. Group comparisons however did not show any differences between amyloid, tau or neuroinflammation levels between rpAD or cAD animals. Synaptic/cognitive differences may thus be related to a biological parameter that was not captured by our study, or also emerge from multiple causes.

In a second part of the study, we thus decided to assess relationships between synaptic or cognitive impairments and amyloid, tau, and microgliosis. At 8 mpi, synaptic deficits in the hippocampus (CA1) and the perirhinal/entorhinal cortex were significantly associated with global tau pathology. In the perirhinal/entorhinal cortex, *i.e.* at distance from the inoculation site, they were also correlated with AT8-positive area stained within neuritic plaques, neuropil threads and NFTs. These results, in a model that is not based on tau overexpression, strongly support that tau pathology contributes to synaptic alterations.

Synaptic loss was also associated with a reduction of microgliosis in the hippocampus (for Iba1 staining), but also at distance from the brain extract inoculation site in the perirhinal/entorhinal cortex (for both Iba1 and CD68 stainings). Controversial results are reported in the literature regarding the impact of microglial activation on AD-related neurodegenerative processes. In contradiction with our results, several studies showed that synaptic alterations are associated with increased microglial activation in amyloid-plaque bearing models (Spangenberg *et al.*, 2016) as well as in mice overexpressing human tau (Leyns *et al.*, 2017; Dejanovic *et al.*, 2018). On the contrary, several evidence in mouse models with genetic-related microglial impairments (*e.g.* Trem2 deficient mice) (Leyns *et al.*, 2019; Lee *et al.*, 2021) or models with microglia depletion (Clayton *et al.*, 2021) suggest that microglial activation is protective. Our study supports a protective effect of microglial activation in, for the first time, a mouse model without genetic or chemical manipulation of microglia. In humans, genetic evidence exemplified by the large effect of the loss-of-function Trem2

mutations on AD risk and on microglial function, argues that microglia have a protective function that lowers the incidence of AD (Hansen *et al.*, 2018). In non-genetic cases of AD, some studies (Streit *et al.*, 2009), but not all (Perez-Nievas *et al.*, 2013), also outlined the potential protective function of microglia.

One unexpected finding of our study is the weak association between synaptic changes and amyloid plaques. This does not rule out the well-described link between synaptic alterations and A $\beta$  (Selkoe, 2002; Sivanesan *et al.*, 2013). In our experiments, we studied A $\beta$  plaque-bearing mice and it is possible that A $\beta$ -related impairments of synaptic function occurred in all experimental groups.

Relationships between cognitive impairments and Alzheimer pathology were also assessed in our study. Cognitive alterations at 8 mpi were correlated with synaptic defects in the hippocampus. They were also associated with the severity of amyloid and tau pathologies (overall tau pathology, neuritic plaque counts, AT8-positive area stained within neuritic plaques, neuropil threads, and NFTs) in the hippocampus, with these tau lesions in the perirhinal/entorhinal cortex as well as with lower Iba1-positive microglial load in the hippocampus and perirhinal/entorhinal cortex. This analysis underlines the potential role of amyloid and parameters linked to synaptic changes (tau/microgliosis) in cognitive impairments.

In our study, although synaptic and cognitive differences were found between rpAD and cIAD animals, we did not detect rpAD/cIAD group differences for amyloid, tau or microgliosis. One possible explanation supported by our results is that synaptic and cognitive impairments resulted from multifactorial and interacting causes and that small differences below the significance threshold for several factors (*e.g.* tau, microgliosis, amyloid) might entail dramatic changes in synapse integrity and cognition. Another possibility, that we cannot rule out, is that a biological parameter that was not detected by our experiments had a major contribution to the differences between rpAD and cIAD animals. Neuroinflammatory factors such as C1q, C3 or IL-33 modulate synapse density by altering their formation and elimination (Dejanovic *et al.*, 2018; Litvinchuk *et al.*, 2018; Wilton *et al.*, 2019; Wang *et al.*, 2021). Although we did not attempt here to characterize the cytokinic profiles of our inocula, we cannot rule out that they contained distinct concentrations or panels of pro- and anti-inflammatory cytokines that may have influenced synapse integrity.

The intracerebral inoculation of human brain extracts in mice was shown to provide pathologically relevant AD models. Indeed, injection of either AD brain homogenates (Condello *et al.*, 2015) or highly aggregated human wild-type tau from sarkosyl-insoluble AD brain extracts (Audouard *et al.*, 2016; Guo *et al.*, 2016) can induce tau aggregates in wild-type mice. Moreover, mice with high A $\beta$  production inoculated with sarkosyl-insoluble brain extracts from AD brains display both amyloid and tau pathologies. For the first time here, we used a strategy based on the inoculation of crude AD brain homogenates into mice with high A $\beta$  production to induce tau lesions, amyloid plaques and downstream events including synaptic loss and cognitive impairments. Altogether, this model will be helpful to assess interactions between AD core lesions and neurodegenerative processes, as well as to evaluate new therapies targeting multiple AD hallmarks.

As a conclusion, we showed that tau-positive neuritic plaques, but not other tau lesions, can occur in old non-inoculated A $\beta$  plaque-bearing mice or in mice inoculated with Ctrl brain extracts. We also showed that intracerebral injection of human AD brain extracts into an A $\beta$  plaque-bearing mouse model that does not overexpress tau can recapitulate amyloid and tau lesions (Supplementary Table 2). AD brain extract inoculation increased tau pathology within neuritic plaques, and induced neuropil threads and NFTs that spread in the brain. Inoculation of different human AD brain extracts led to different levels of synaptic loss and cognitive impairments. Synaptic loss was associated with the severity of tau lesions which highlights the contribution of tau to synaptic pathology in a model that does not rely on the genetic manipulation of tau protein. Synaptic defects were also associated with lower microglial load in a model that does not rely on drastic genetic or chemical-based reduction of microglia. This indicates that microglial activity may protect against synaptic loss. Cognitive defects were associated with synaptic impairments, with tau lesions and also with amyloid deposition. Altogether these results highlight the multifactorial origin of cognitive impairments. Finally, the finding that microglial activity may protect against synaptic loss may have potential applications and supports further studies to assess the effect of anti-inflammatory therapies in subjects at risk for Alzheimer's disease.

## **ACKNOWLEDGEMENTS**

We thank Martine Guillermier and Mylène Gaudin for surgical expertise during inoculation of brain extracts to animals. We thank Nicolas Heck for his help in synapse quantification, and

Nicolas Sergeant for a critical review of this article. We thank the donors and the Brain Donation Program of the “The Brainbank Neuro- CEB Neuropathology Network” run by a consortium of Patient Associations: ARSLA (association for research on amyotrophic lateral sclerosis), CSC (cerebellar ataxias), Fondation ARSEP (association for research on multiple sclerosis), France DFT (fronto-temporal dementia), Fondation Vaincre Alzheimer, France Parkinson, with the support of Fondation Plan Alzheimer and IHU A-ICM for providing the brain samples used in this study.

## **FUNDING**

The project was funded by the Association France-Alzheimer. It was performed in a core facility supported by/member of NeurATRIS - ANR-11-INBS-0011. It was also supported by internal funds from the Laboratory of Neurodegenerative Diseases and MIRCent.

## **AUTHOR CONTRIBUTIONS**

S.L., A.S.H., F.P., and M.D. contributed to the study conception and design. N.N.N., C.D. provided the human brain samples. N.N.N., S.L., S.B., C.D. and S.H. characterized the human brain samples. S.L., M.G. and M.G. performed the inoculations in mice. S.L. and K.C. designed and performed cognitive evaluations, A.S.H., F.P., and S.L. designed and performed the immunohistological analysis in animals. A.S.H., S.E., L.B., and S.L. performed biochemical analysis. S.L., A.S.H., and M.D. wrote the manuscript. All authors commented on previous versions of the manuscript. All authors read and approved the final manuscript.

## **COMPETING INTERESTS**

The authors declare no competing interests.

## **REFERENCES**

Audouard E, Houben S, Masaracchia C, Yilmaz Z, Suain V, Authelet M, et al. High-molecular-weight paired helical filaments from Alzheimer brain induces seeding of wild-type mouse tau into an argyrophilic 4R Tau pathology in vivo. *Am J Pathol* 2016; 186(10): 2709-22.

Bennett DA, Schneider JA, Wilson RS, Bienias JL, Arnold SE. Neurofibrillary tangles mediate the association of amyloid load with clinical Alzheimer disease and level of cognitive function. *Arch Neurol* 2004; 61(3): 378-84.

Bennett RE, DeVos SL, Dujardin S, Corjuc B, Gor R, Gonzalez J, et al. Enhanced Tau aggregation in the presence of amyloid beta. *Am J Pathol* 2017; 187(7): 1601-12.

Braak H, Braak E. Neuropathological staging of Alzheimer related changes. *Acta Neuropathol* 1991; 82: 239-59.

Clayton K, Delpech JC, Herron S, Iwahara N, Ericsson M, Saito T, et al. Plaque associated microglia hyper-secrete extracellular vesicles and accelerate tau propagation in a humanized APP mouse model. *Mol Neurodegener* 2021; 16(1).

Colonna M, Butovsky O. Microglia function in the central nervous system during health and neurodegeneration. *Annu Rev Immunol* 2017; 35: 441-68.

Condello C, Yuan P, Schain A, Grutzendler J. Microglia constitute a barrier that prevents neurotoxic protofibrillar Abeta42 hotspots around plaques. *Nat Commun* 2015; 6: 6176.

Dejanovic B, Huntley MA, De Maziere A, Meilandt WJ, Wu T, Srinivasan K, et al. Changes in the synaptic proteome in tauopathy and rescue of Tau-induced synapse loss by C1q antibodies. *Neuron* 2018; 100(6): 1322-+.

Di Fede G, Catania M, Maderna E, Ghidoni R, Benussi L, Tonoli E, et al. Molecular subtypes of Alzheimer's disease. *Sci Rep* 2018; 8: 3269.

Dourlen P, Kilinc D, Malmanche N, Chapuis J, Lambert JC. The new genetic landscape of Alzheimer's disease: from amyloid cascade to genetically driven synaptic failure hypothesis? *Acta Neuropathol* 2019; 138(2): 221-36.

Duyckaerts C, Sazdovitch V, Ando K, Seilhean D, Privat N, Yilmaz Z, et al. Neuropathology of iatrogenic Creutzfeldt-Jakob disease and immunoassay of French cadaver-sourced growth hormone batches suggest possible transmission of tauopathy and long incubation periods for the transmission of Abeta pathology. *Acta Neuropathol* 2018; 135(2): 201-12.

Garcia-Alloza M, Robbins EM, Zhang-Nunes SX, Purcell SM, Betensky RA, Raju S, et al. Characterization of amyloid deposition in the APP<sup>swE</sup>/PS1<sup>dE9</sup> mouse model of Alzheimer disease. *Neurobiol Dis* 2006; 24(3): 516-24.

Gary C, Lam S, Herard AS, Koch JE, Petit F, Gipchtein P, et al. Encephalopathy induced by Alzheimer brain inoculation in a non-human primate. *Acta Neuropathol Commun* 2019; 7(126).

Gilles JF, Dos Santos M, Boudier T, Bolte S, Heck N. DiAna, an ImageJ tool for object-based 3D colocalization and distance analysis. *Methods* 2017; 115: 55-64.

Gotz J, Chen F, van Dorpe J, Nitsch RM. Formation of neurofibrillary tangles in P301l tau transgenic mice induced by Abeta 42 fibrils. *Science* 2001; 293(5534): 1491-5.

Guo JL, Narasimhan S, Changolkar L, He ZH, Stieber A, Zhang B, et al. Unique pathological tau conformers from Alzheimer's brains transmit tau pathology in nontransgenic mice. *J Exp Med* 2016; 213(12): 2635-54.

Hansen DV, Hanson JE, Sheng M. Microglia in Alzheimer's disease. *J Cell Biol* 2018; 217(2): 459-72.

Hoover BR, Reed MN, Su J, Penrod RD, Kotilinek LA, Grant MK, et al. Tau mislocalization to dendritic spines mediates synaptic dysfunction independently of neurodegeneration. *Neuron* 2010; 68(6): 1067-81.

Lee S-H, Meilandt WJ, Xie L, Gandham VD, Ngu H, Barck KH, et al. Trem2 restrains the enhancement of tau accumulation and neurodegeneration by b-amyloid pathology. *Neuron* 2021; 109: 1-19.

Leyns CEG, Gratuze M, Narasimhan S, Jain N, Koscal LJ, Jiang H, et al. TREM2 function impedes tau seeding in neuritic plaques. *Nat Neurosci* 2019; 22(8): 1217-22.

Leyns CEG, Ulrich JD, Finn MB, Stewart FR, Koscal LJ, Serrano JR, et al. TREM2 deficiency attenuates neuroinflammation and protects against neurodegeneration in a mouse model of tauopathy. *Proc Natl Acad Sci USA* 2017; 114(43): 11524-9.



Litvinchuk A, Wan YW, Swartzlander DB, Chen FD, Cole A, Propson NE, et al. Complement C3aR Inactivation Attenuates Tau Pathology and Reverses an Immune Network Deregulated in Tauopathy Models and Alzheimer's Disease. *Neuron* 2018; 100(6): 1337-+.

Metaxas A, Thygesen C, Kempf SJ, Anzalone M, Vaitheeswaran R, Petersen S, et al. Ageing and amyloidosis underlie the molecular and pathological alterations of tau in a mouse model of familial Alzheimer's disease. *Sci Rep* 2019; 9: 15758.

Nelson PT, Alafuzoff I, Bigio EH, Bouras C, Braak H, Cairns NJ, et al. Correlation of Alzheimer disease neuropathologic changes with cognitive status: a review of the literature. *J Neuropath Exp Neur* 2012; 71(5): 362-81.

Paolicelli RC, Bolasco G, Pagani F, Maggi L, Scianni M, Panzanelli P, et al. Synaptic Pruning by Microglia Is Necessary for Normal Brain Development. *Science* 2011; 333(6048): 1456-8.

Perez-Nievas BG, Stein TD, Tai HC, Dols-Icardo O, Scotton TC, Barroeta-Espar I, et al. Dissecting phenotypic traits linked to human resilience to Alzheimer's pathology. *Brain* 2013; 136: 2510-26.

Pooler AM, Noble W, Hanger DP. A role for tau at the synapse in Alzheimer's disease pathogenesis. *Neuropharmacology* 2014; 76: 1-8.

Pooler AM, Polydoro M, Maury EA, Nicholls SB, Reddy SM, Wegmann S, et al. Amyloid accelerates tau propagation and toxicity in a model of early Alzheimer's disease. *Acta Neuropathol Commun* 2015; 3: Article number 14.

Sanchez-Mejias E, Navarro V, Jimenez S, Sanchez-Mico M, Sanchez-Varo R, Nunez-Diaz C, et al. Soluble phospho-tau from Alzheimer's disease hippocampus drives microglial degeneration. *Acta Neuropathol* 2016; 132(6): 897-916.

Selkoe DJ. Alzheimer's disease is a synaptic failure. *Science* 2002; 298(5594): 789-91.

Sivanesan S, Tan A, Rajadas J. Pathogenesis of abeta oligomers in synaptic failure. *Curr Alzh Res* 2013; 10(3): 316e23.

Spangenberg EE, Lee RJ, Najafi AR, Rice RA, Elmore MRP, Blurton-Jones M, et al. Eliminating microglia in Alzheimer's mice prevents neuronal loss without modulating amyloid-beta pathology. *Brain* 2016; 139: 1265-81.

Spires-Jones TL, Hyman BT. The intersection of amyloid beta and tau at synapses in Alzheimer's disease. *Neuron* 2014; 82(4): 756-71.

Streit WJ, Braak H, Xue QS, Bechmann I. Dystrophic (senescent) rather than activated microglial cells are associated with tau pathology and likely precede neurodegeneration in Alzheimer's disease. *Acta Neuropathol* 2009; 118(4): 475-85.

Terry RD, Masliah E, Salmon DP, Butters N, DeTeresa R, Hill R, et al. Physical basis of cognitive alterations in Alzheimer's disease: synapse loss is the major correlate of cognitive impairment. *Ann Neurol* 1991; 30(4): 572-80.

Wang Y, Fu WY, Cheung K, Hung KW, Chen CP, Geng HY, et al. Astrocyte-secreted IL-33 mediates homeostatic synaptic plasticity in the adult hippocampus. *Proc Natl Acad Sci USA* 2021; 118(1).

Wilton DK, Dissing-Olesen L, Stevens B. Neuron-Glia signaling in synapse elimination. *Annu Rev Neurosci* 2019; 42: 107-27.

# FIGURES

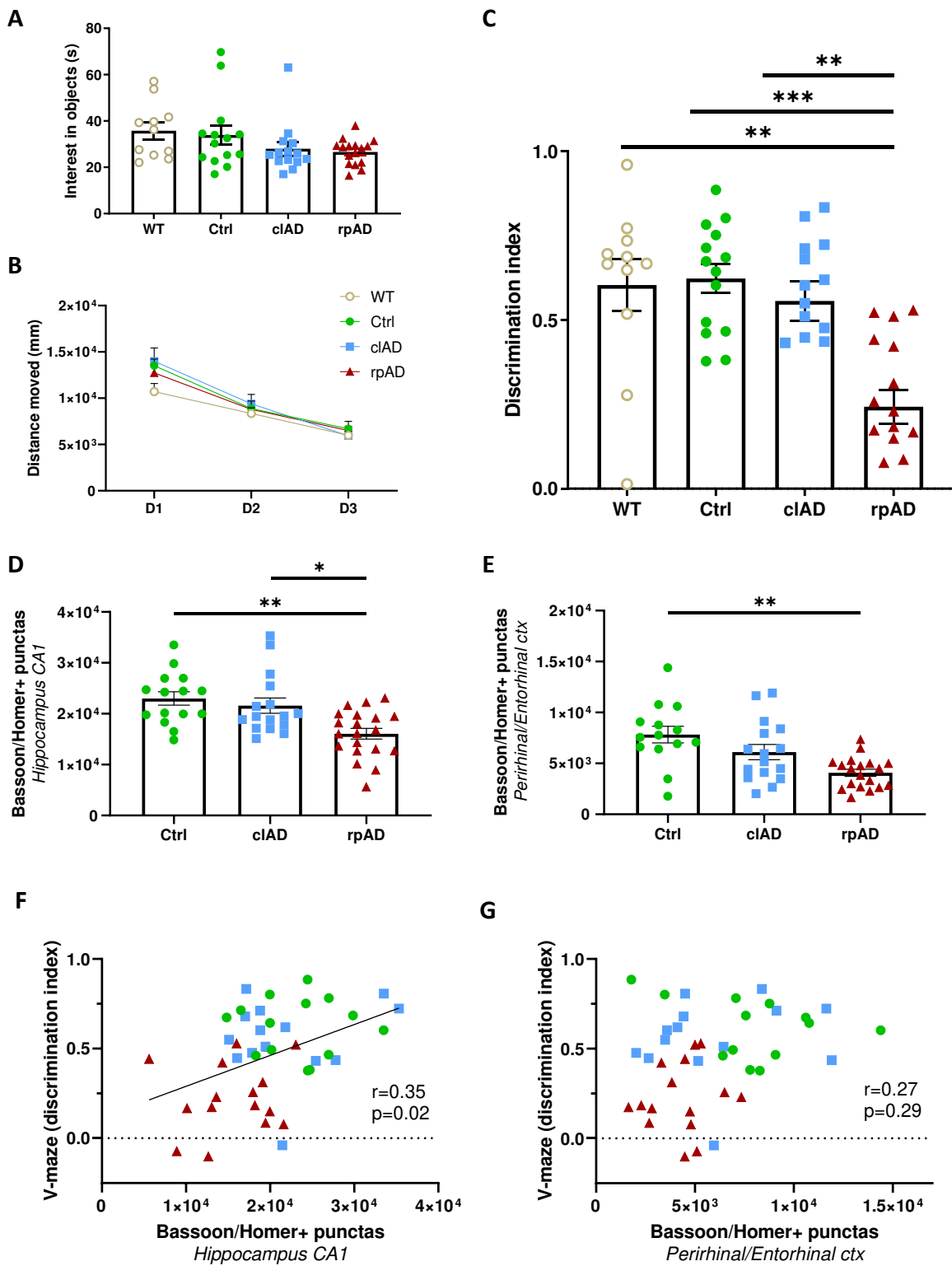


**Figure 1. Object recognition deficits and synaptotoxicity in the rpAD-inoculated mice.**

Object recognition performances were evaluated at 8 mpi in a V-maze. WT mice and APP<sub>swe</sub>/PS1<sub>dE9</sub> mice inoculated with Ctrl, cIAD or rpAD brain extracts had comparable exploratory activity, as suggested by the time spent on exploring the objects (A,  $p > 0.05$ ; Kruskal-Wallis with Dunn's multiple comparisons) and the distance moved throughout the 3-day test (B, for the days:  $F_{(1.75, 89.47)} = 91.97$ ,  $p < 0.0001$ ; for the groups:  $F_{(3, 51)} = 0.89$ ,  $p = 0.45$ ; two-way repeated measures ANOVA with the Geisser-Greenhouse correction and Dunnett's multiple comparisons). During the novel object recognition evaluation, rpAD-inoculated mice spent less time exploring the novel object, as suggested by a lower discrimination index, compared to WT and APP<sub>swe</sub>/PS1<sub>dE9</sub> cIAD or Ctrl-inoculated mice (C, respectively,  $p = 0.0018$ ,  $0.0082$  and  $0.0007$ ; Kruskal-Wallis with Dunn's multiple comparisons). (D-E) Quantification of Bassoon and Homer colocalization revealed a decrease in synaptic density in rpAD mice in the CA1 (D, respectively  $p = 0.0011$  and  $0.037$ ; Kruskal-Wallis with Dunn's multiple comparisons) and perirhinal/entorhinal cortex (E, respectively  $p = 0.001$  and  $0.13$ ; Kruskal-Wallis with Dunn's multiple comparisons), compared to Ctrl and/or cIAD-inoculated mice at 8 mpi. V-maze cognitive scores (discrimination index) were correlated with synaptic defects in the CA1 (F,  $r_{\text{spearman-hip}} = 0.35$ ,  $p = 0.02$ ) but not in the perirhinal/entorhinal cortex (G,  $r_{\text{spearman-P/EC}} = 0.27$ ,  $p = 0.29$ ).  $n_{\text{Ctrl}} = 15$ ,  $n_{\text{cIAD}} = 15$ ,  $n_{\text{rpAD}} = 20$ ,  $n_{\text{WT}} = 12$  mice. \* $p < 0.05$ ; \*\* $p < 0.01$ ; \*\*\* $p < 0.001$ ; Data are shown as mean  $\pm$  s.e.m.

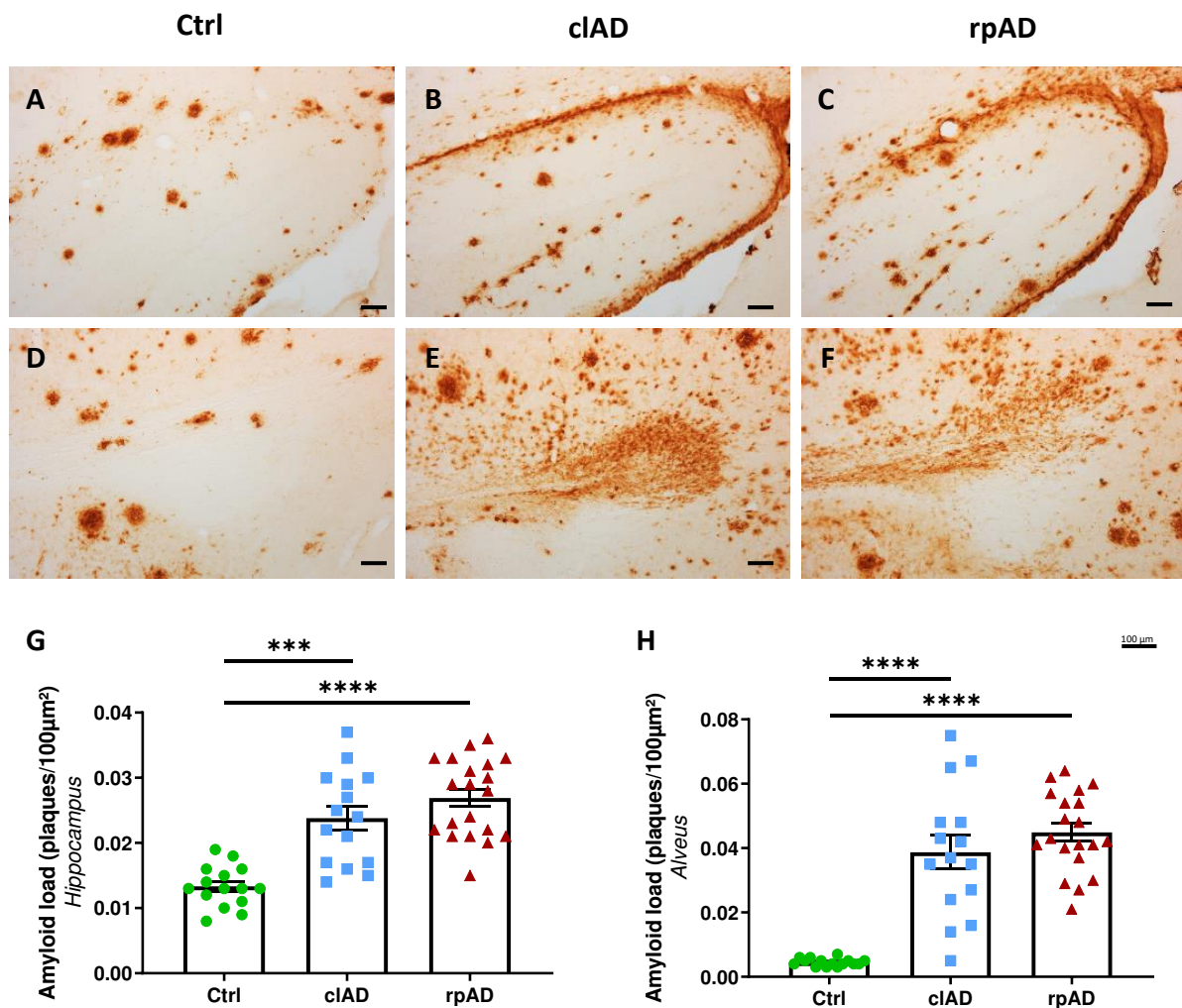


**Figure 2. AD brain inoculation accelerates amyloidosis in  $APP_{swe}/PS1_{dE9}$  mice close to the injection site.** (A-F) Representative images of 4G8 immunolabelling showing amyloid pathology in the hippocampus (A-C) and alveus (D-F) of  $APP_{swe}/PS1_{dE9}$  mice eight months after human brain inoculation. (G-H) Quantification of amyloid load (4G8-positive amyloid plaques per 100  $\mu m^2$ ) revealed that AD (cIAD and rpAD) brain inoculation accelerates amyloid deposition in the hippocampus (G,  $p=0.0005$  and  $p<0.0001$ , respectively) and alveus (H,  $p<0.0001$  and  $p<0.0001$ , respectively). Kruskal-Wallis with Dunn's multiple comparisons. \*\*\* $p<0.001$ ; \*\*\*\* $p<0.0001$ .  $n_{Ctrl}=15$ ,  $n_{cIAD}=15$ ,  $n_{rpAD}=20$  mice. Data are shown as mean  $\pm$  s.e.m. Scale bars = 100  $\mu m$ .

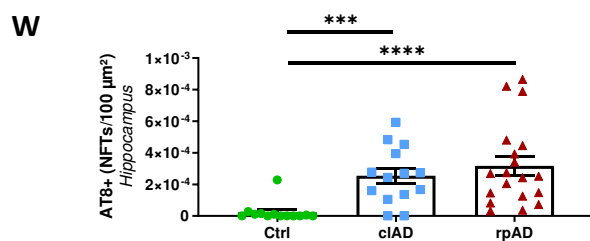
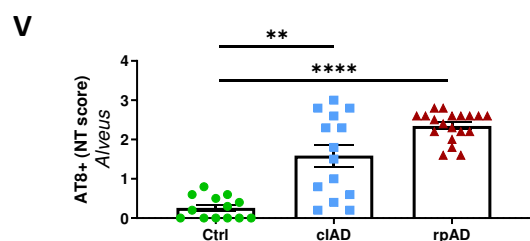
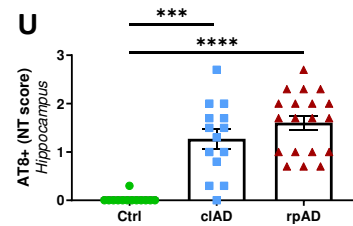
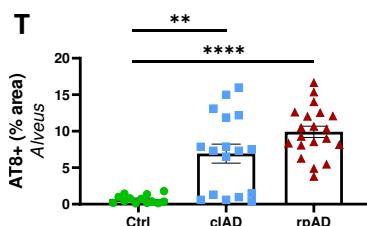
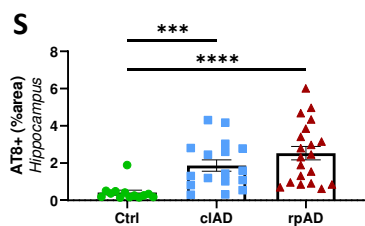
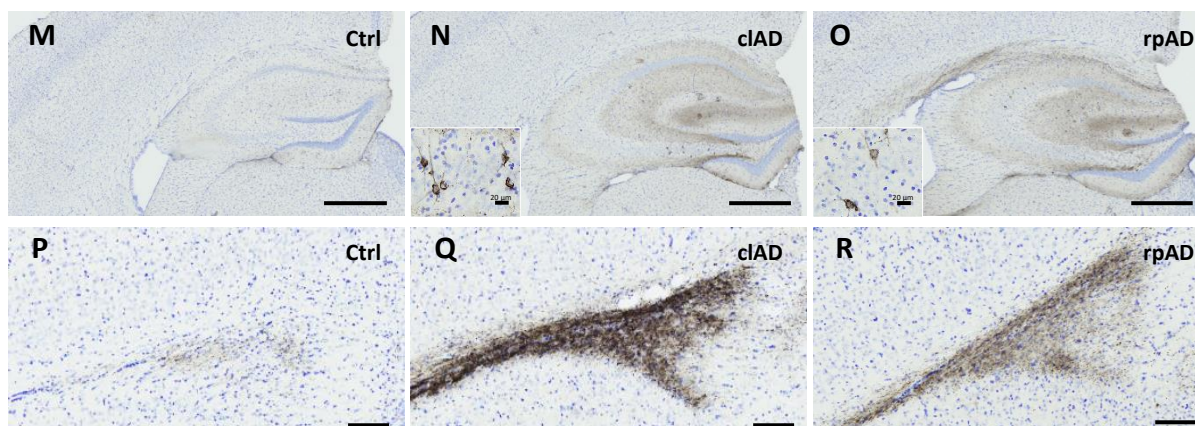
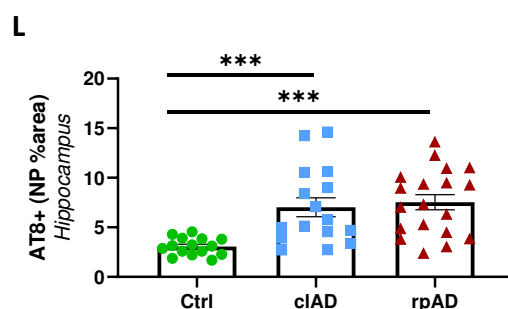
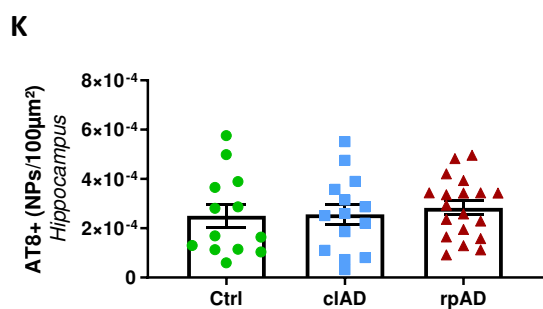
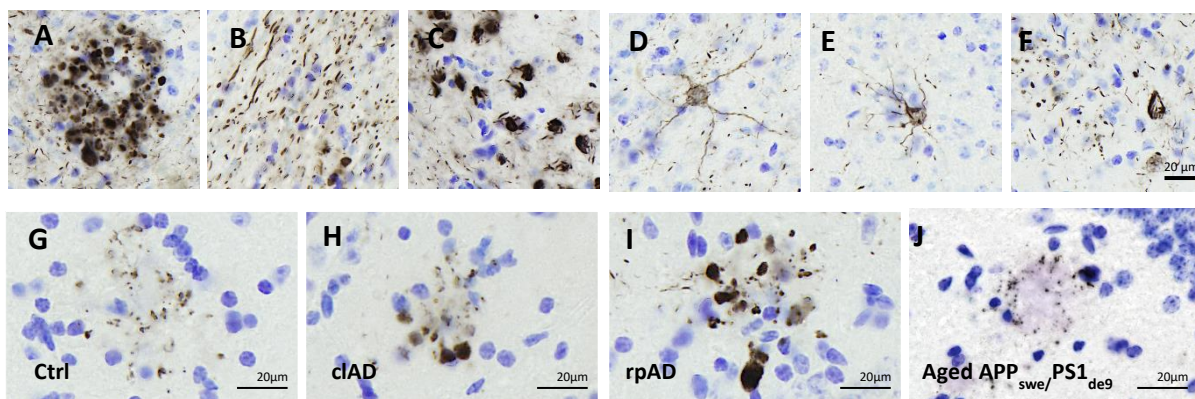


**Figure 3. AD brain inoculation induces tau pathology in APP<sub>swe</sub>/PS1<sub>dE9</sub> mice close to the injection site at 8 mpi.** AT8 immunolabelling revealed tau lesions in the forms of neuritic plaques (A), neuropil threads (B), neurofibrillary tangles (C-F). Representative images of AT8-positive neuritic plaques within the hippocampus of Ctrl- (G) and AD-inoculated (H for clAD, I for rpAD) mice. AT8 immunolabelling of non-inoculated aged APP<sub>swe</sub>/PS1<sub>dE9</sub> mice (24 months old) also revealed neuritic plaques (J). Quantification revealed similar neuritic plaque counts (NPs per 100  $\mu\text{m}^2$  of area) in all groups (K). The AT8-positive area within neuritic plaques (NP %area) was higher in AD-inoculated groups compared to Ctrl animals suggesting that neuritic plaques were more tau-positive in AD groups (L,  $p=0.001$  and  $p<0.0001$ , respectively for clAD and rpAD mice, Kruskal-Wallis with Dunn's multiple comparisons). (M-R) Representative images of AT8 immunolabelling showing tau pathology induction in the dorsal hippocampus (M-O) and alveus (P-R). Quantification of overall AT8-labelled phospho-tau (percentage of AT8-positive area), neuropil thread (NT) scoring and/or NFTs accumulation (AT8-positive NFTs per 100  $\mu\text{m}^2$  of area) in the hippocampus (S, U, W. S:  $p=0.001$  and  $p<0.0001$ . U:  $p=0.0005$  and  $p<0.0001$ . W:  $p=0.001$  and  $p<0.0001$ , respectively for clAD and rpAD mice; Kruskal-Wallis with Dunn's multiple comparisons) and alveus (T, V. T:  $p=0.0035$  and  $p<0.0001$ . V:  $p=0.0036$  and  $p<0.0001$ , respectively for clAD and rpAD mice; Kruskal-Wallis with Dunn's multiple comparisons) showed an increase in tau pathology following clAD and rpAD brain inoculation compared to Ctrl brain. \* $p<0.05$ ; \*\* $p<0.01$ ; \*\*\* $p<0.001$ ; \*\*\*\* $p<0.0001$  (Kruskal-Wallis with Dunn's multiple comparisons test).  $n_{\text{Ctrl}}=15$ ,  $n_{\text{clAD}}=15$ ,  $n_{\text{rpAD}}=20$  mice. Data are shown as mean  $\pm$  s.e.m. Scale bars = 20  $\mu\text{m}$  (A-J and inserts), 500  $\mu\text{m}$  (M-O) and 100  $\mu\text{m}$  (P-R).

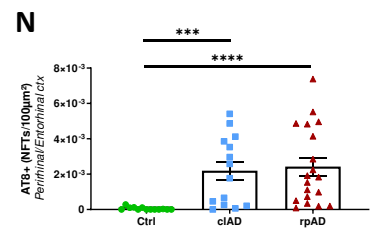
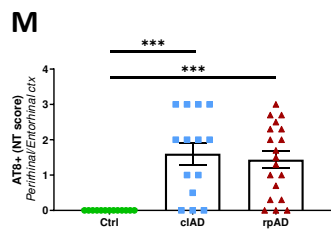
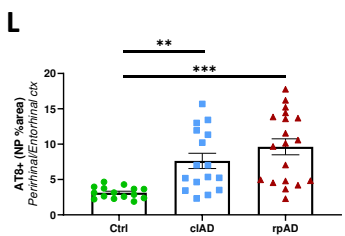
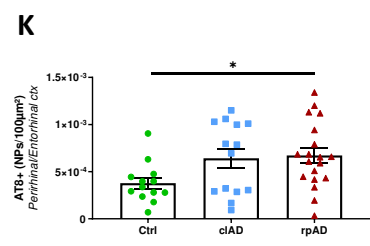
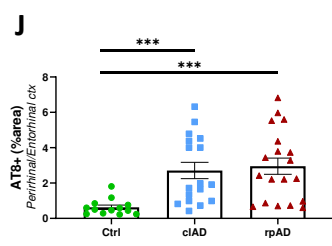
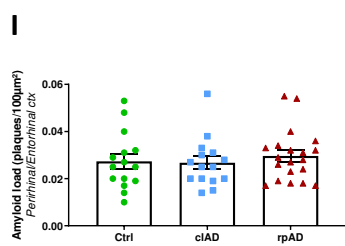
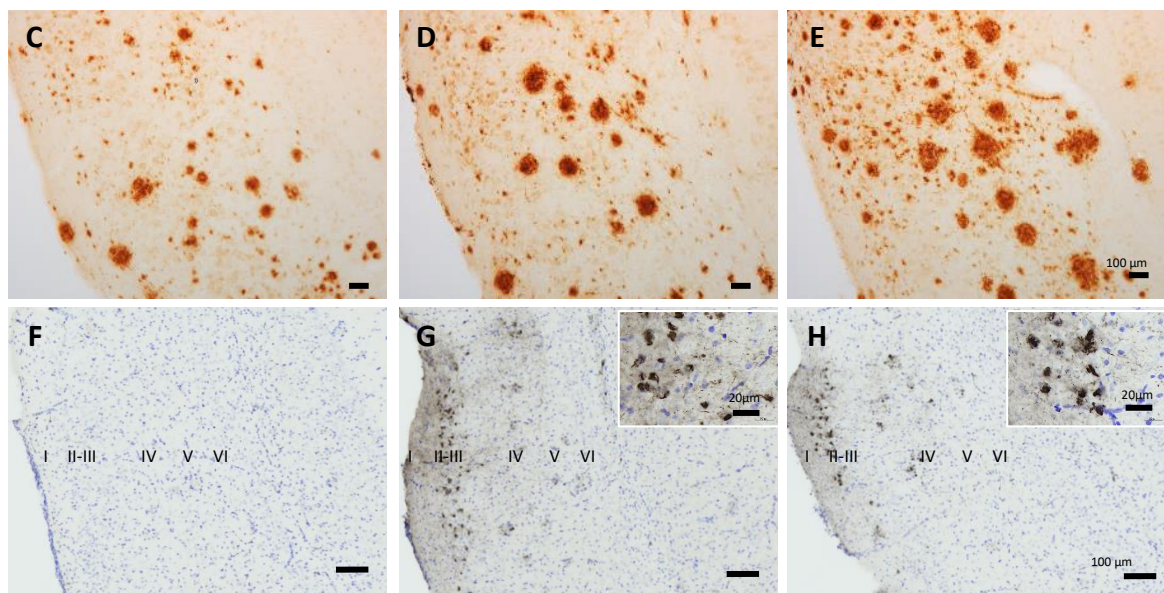
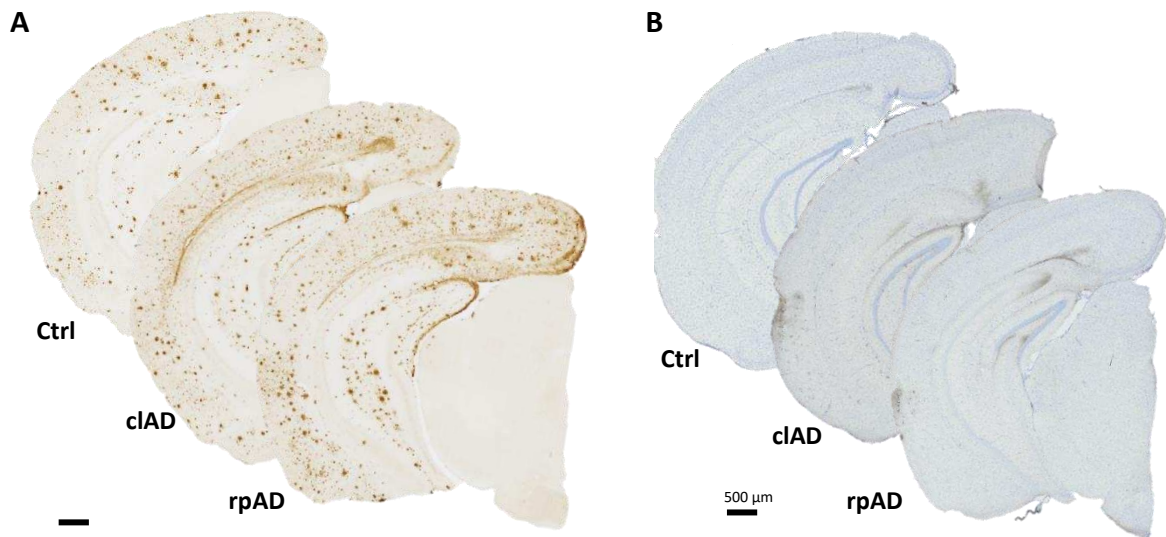


**Figure 4. A $\beta$  and tau pathologies in the perirhinal/entorhinal cortex following AD brain inoculation in APP<sub>swe</sub>/PS1<sub>dE9</sub> mice.** Representative images of the 4G8 immunolabelling showing amyloid pathology (A) and the AT8 immunolabelling showing tau pathology (B) in AD-inoculated APP<sub>swe</sub>/PS1<sub>dE9</sub> mice. Magnified views of amyloid (C-E) and tau (F-H) lesions in the perirhinal/entorhinal cortex. Quantification of amyloid load (I:  $p > 0.05$ ), overall AT8-positive tau lesions (J:  $p = 0.0007$  and  $p = 0.0002$ , respectively for clAD and rpAD mice), neuritic plaque (NPs) count (K:  $p = 0.038$  for rpAD animals versus Ctrl), AT8-positive area stained within neuritic plaques (L:  $p = 0.0034$  and  $p < 0.0001$ , respectively for clAD and rpAD mice), neuropil thread (NTs – M:  $p = 0.0003$  and  $p = 0.0002$ , respectively for clAD and rpAD mice), and NFTs (N:  $p = 0.005$  and  $p < 0.0001$ , respectively for clAD and rpAD mice) in the perirhinal/entorhinal cortex. Kruskal-Wallis with Dunn's multiple comparisons test. \*\*\* $p < 0.001$ ; \*\*\*\* $p < 0.0001$ .  $n_{Ctrl} = 15$ ,  $n_{clAD} = 15$ ,  $n_{rpAD} = 20$  mice. Data are shown as mean  $\pm$  s.e.m. Scale bars = 500  $\mu$ m (A-B), 100  $\mu$ m (C-H) and 20  $\mu$ m in inserts.



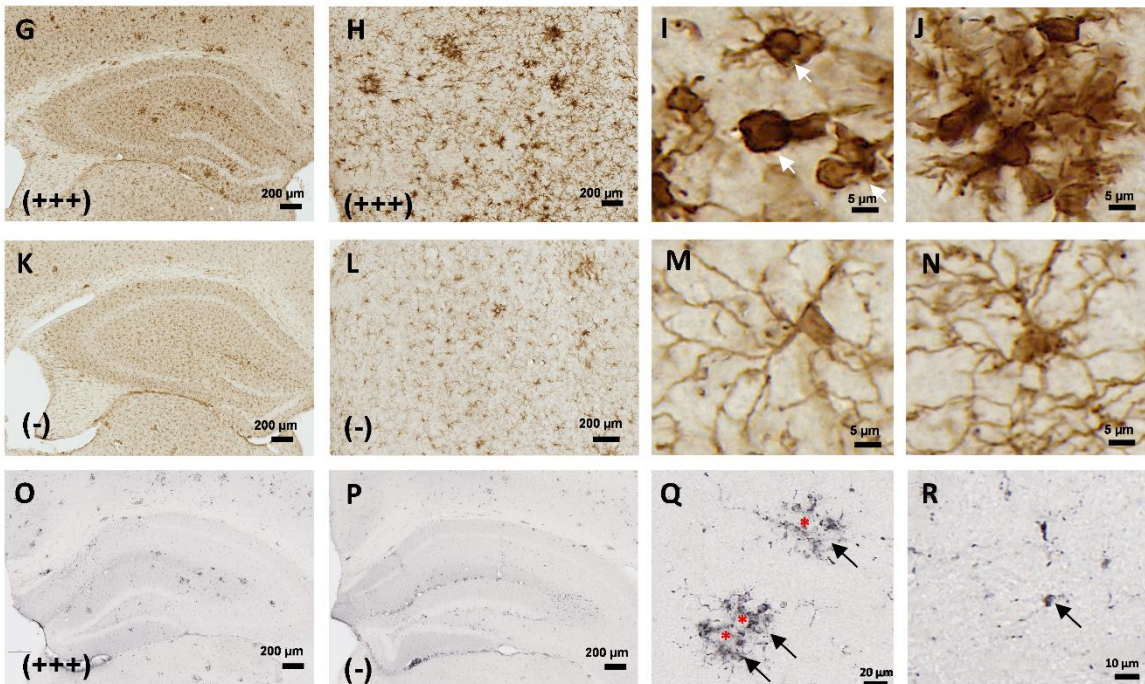
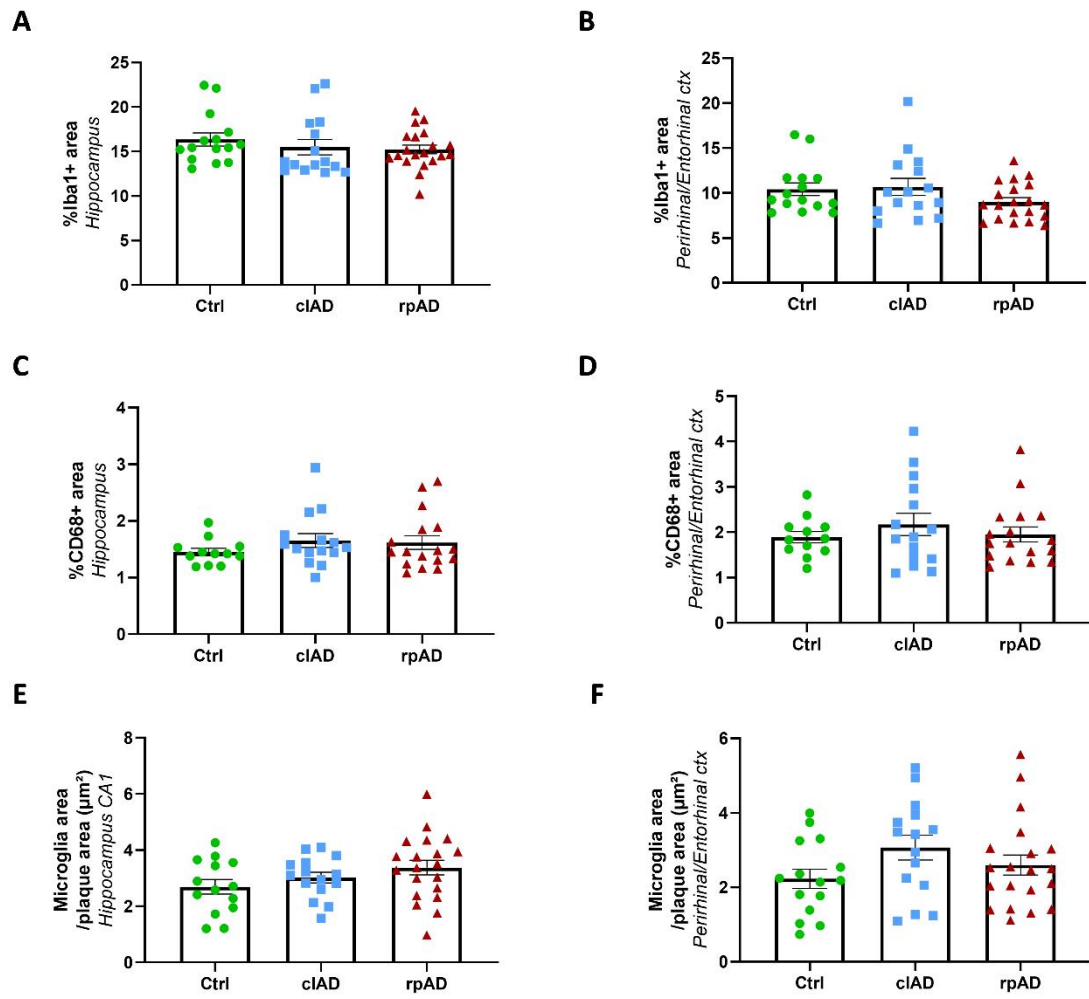
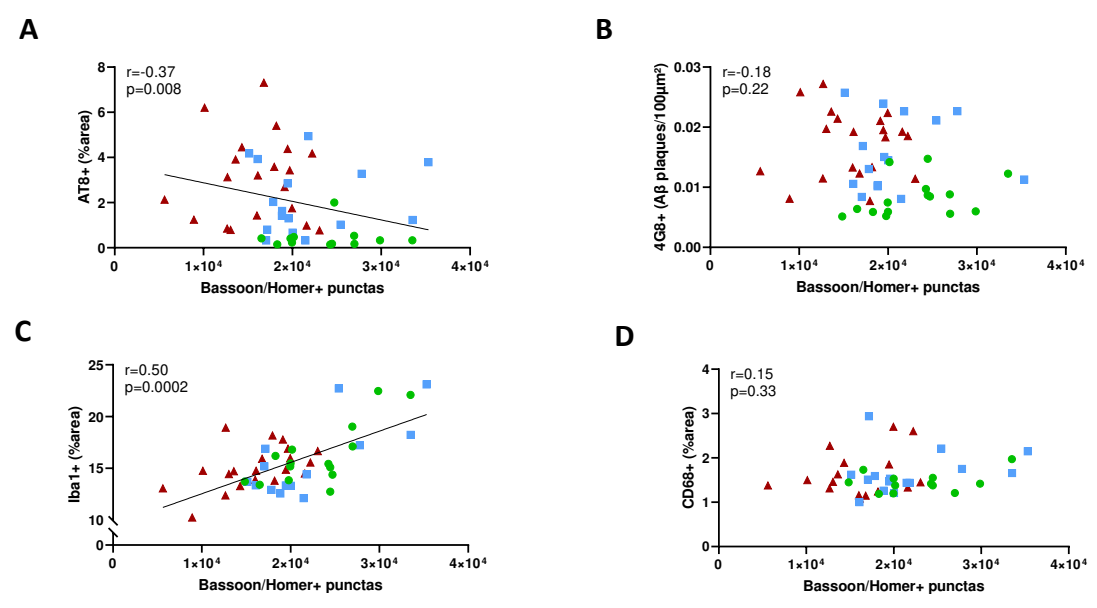


**Figure 5. Microglial activation in AD- and Ctrl-inoculated APP<sub>swe</sub>/PS1<sub>dE9</sub> mice.** Similar levels of Iba1 (A, B) and CD68 (C, D) stained areas in the hippocampus or perirhinal/entorhinal cortex of cAD, rpAD and Ctrl animals (Kruskal-Wallis test). Iba1-positive microglial load surrounding amyloid plaques was also similar in the different groups in both regions (E-F, Kruskal-Wallis test).  $n_{Ctrl}=15$ ,  $n_{cAD}=15$ ,  $n_{rpAD}=20$  mice. Within each group, animals with high and low Iba1 staining were identified. Representative images of one animal with higher Iba1 levels showing abundant staining in the hippocampus (G) and perirhinal/entorhinal cortex (H). Animals with higher Iba1 levels displayed activated microglia characterized by beading with spheroidal swellings of the processes and enlarged cell body with dystrophic ramifications (I, arrows). These activated cells formed microglial clusters surrounding A $\beta$  plaques (J). Animals with lower Iba1 levels (K-L) displayed more cells with a highly ramified profile close to amyloid plaques (M) or far from plaques (N), consistent with a non-activated phenotype. (O-P) Representative images of one animal with higher (O) or lower (P) CD68 staining in the hippocampus. (Q-R) Some clusters of CD68-stained microglia (arrows) surrounded amyloid deposits (\*) (Q) while some others were not associated with amyloid deposits (R).

Hippocampus CA1



Perirhinal/Entorhinal cortex

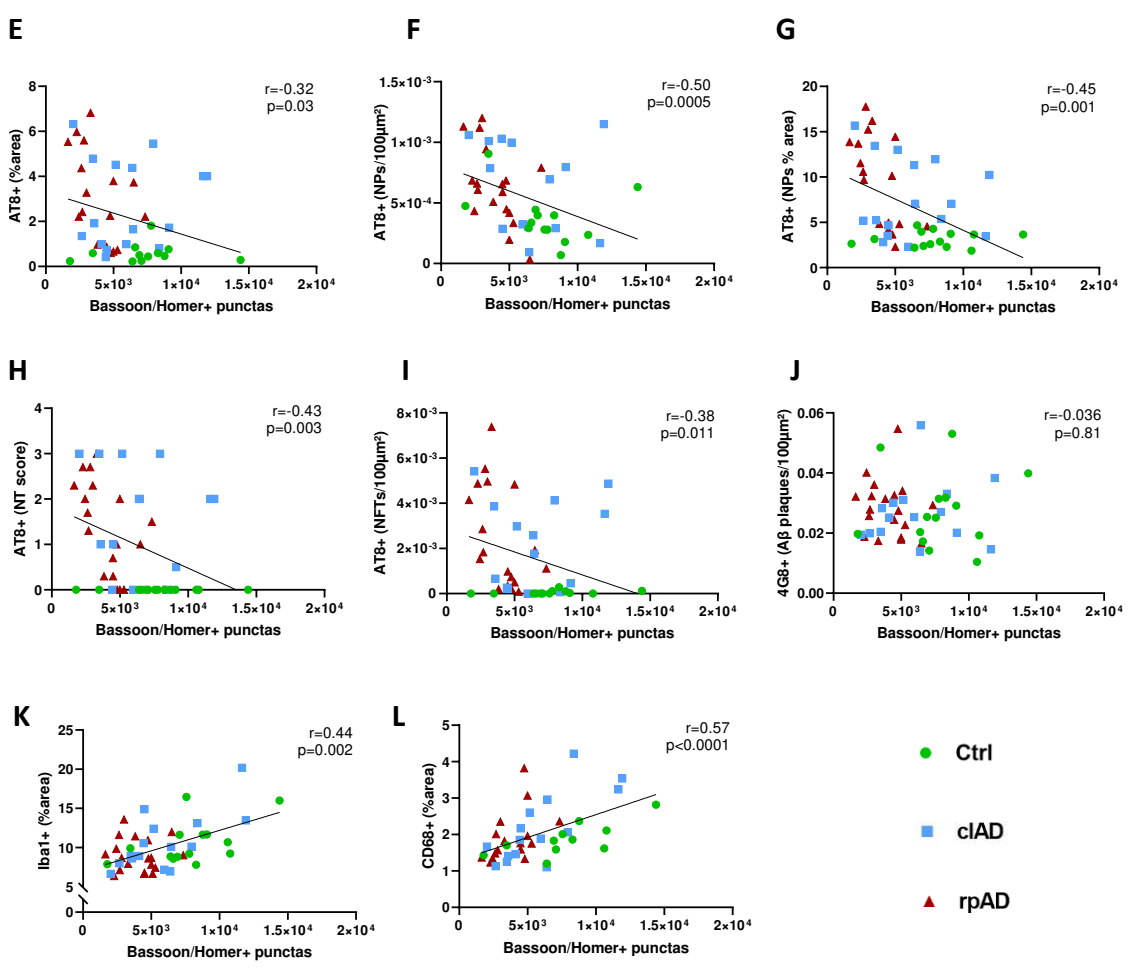
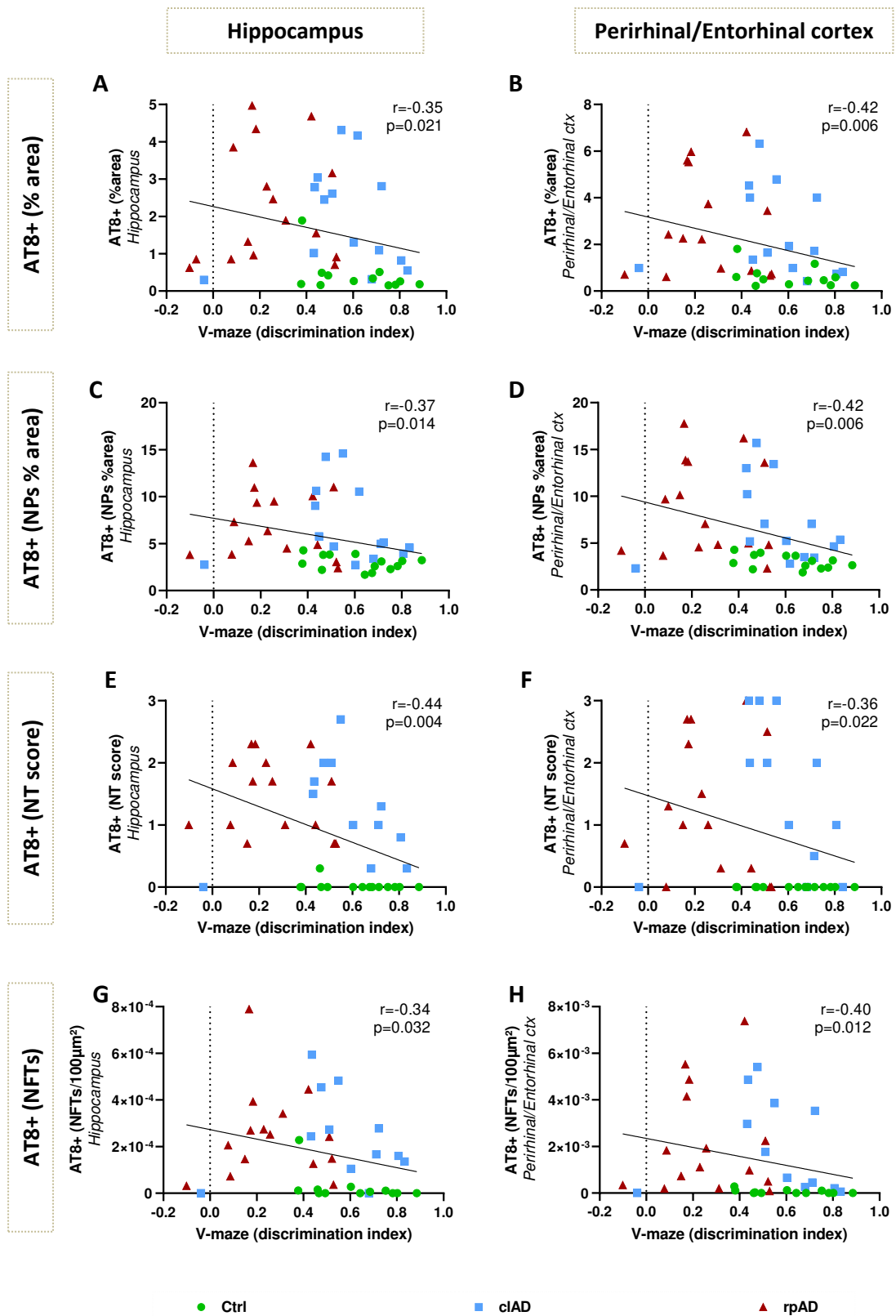


Figure 6. Correlations between synaptic density and tau lesions, A $\beta$  plaque load or microglial activity. Synaptic density (Bassoon/Homer-positive puncta) was negatively

correlated with tau pathology both in the hippocampus (CA1) (A) and the perirhinal/entorhinal cortex (E-I), but not with amyloid pathology (B, J). Interestingly, synaptic density was positively correlated with microglial Iba1 labelling in the hippocampus (C) as well as in the perirhinal/entorhinal cortex (K). Microglial CD68 labelling in the perirhinal/entorhinal cortex (L), but not in the hippocampus (D) was correlated to synaptic density. Spearman's correlations with significance level at  $p < 0.05$ .  $n_{\text{Ctrl}}=15$ ,  $n_{\text{clAD}}=15$ ,  $n_{\text{rpAD}}=20$  mice.



**Figure 7. Correlations between V-maze cognitive scores and tau lesions.** V-maze cognitive scores (discrimination index) were negatively correlated with tau pathology both in the

hippocampus and the perirhinal/entorhinal cortex. (A-B) Overall AT8-positive tau lesions. (C-D) AT8-positive area stained within neuritic plaques. (E-F) Neuropil threads (NT). (G-H) Neurofibrillary tangles (NFTs). Spearman's correlations with significance level at  $p < 0.05$ .  $n_{\text{Ctrl}}=15$ ,  $n_{\text{dAD}}=15$ ,  $n_{\text{rpAD}}=20$  mice.

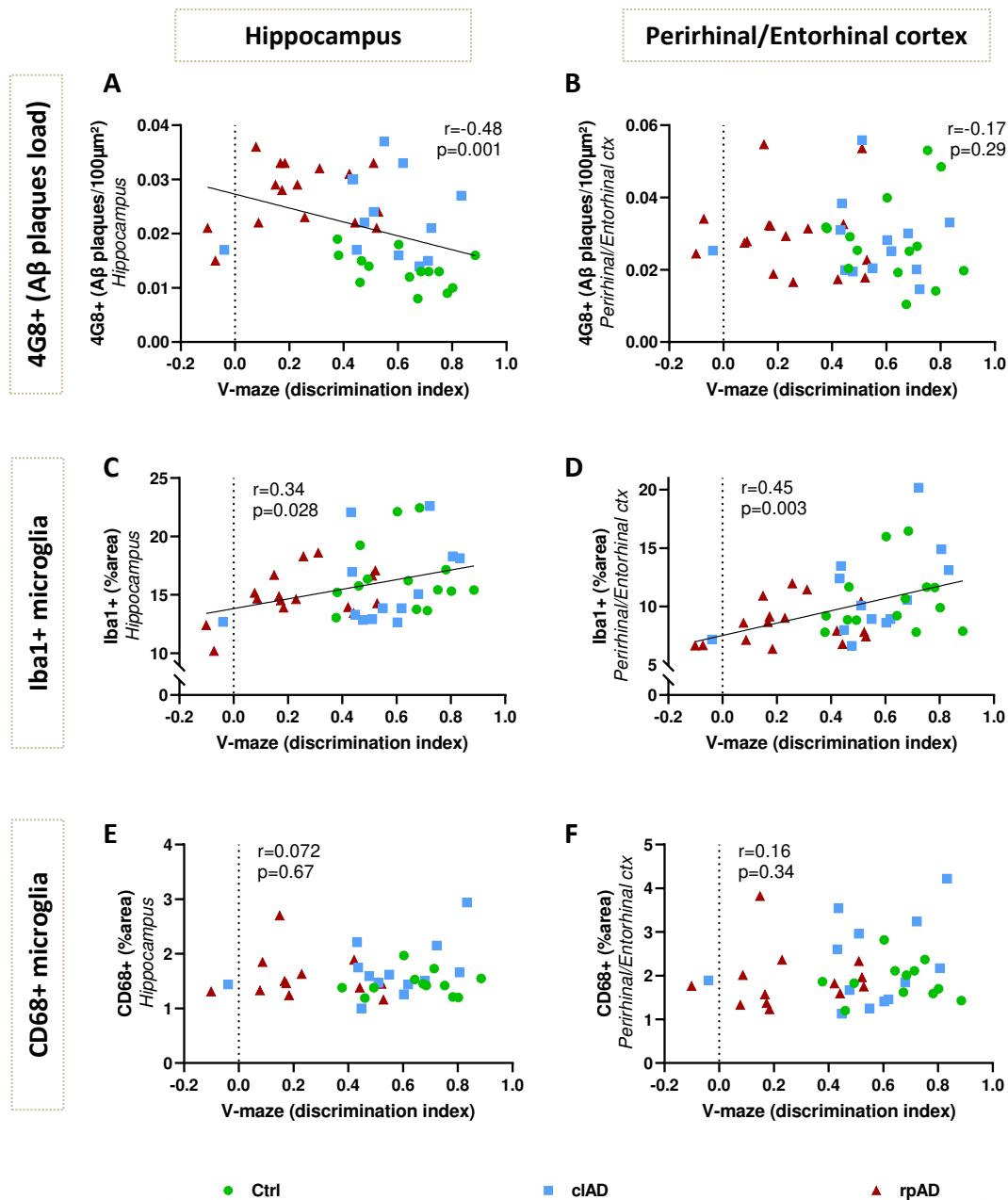


**Figure 8. Correlations between V-maze cognitive scores and amyloid or microgliosis.** V-maze cognitive scores (discrimination index) were correlated with amyloid pathology in the hippocampus (A) but not in the perirhinal/entorhinal cortex (B). Microglial Iba1-positive staining was positively correlated with cognitive scores in both regions (C-D). Microglial CD68-positive staining was however not correlated with cognitive scores in either region (E-F). Spearman's correlations with significance level at  $p < 0.05$ .  $n_{\text{Ctrl}} = 15$ ,  $n_{\text{cIAD}} = 15$ ,  $n_{\text{rpAD}} = 20$  mice.

## SUPPLEMENTARY METHODS

### 1. Immunohistochemistry of human brain samples

All brain tissues were assessed by immunohistochemistry, as previously described in Gary et al. 2019 (Gary *et al.*, 2019). Briefly, 4- $\mu$ m-thick paraffin sections were cut, deparaffinized in xylene, successively rehydrated in ethanol (100, 90, and 70%) and rinsed under running tap water for 10 min before immunohistological staining. They were then incubated in 99% formic acid for 5 min, quenched for endogenous peroxidase with 3% hydrogen peroxide and 20% methanol, and washed in water. Sections were blocked at room temperature (RT) for 30 min in 4% bovine serum albumin (BSA) in 0.05 M tris-buffered saline, with 0.05% Tween 20, pH 8 (TBS-Tween, Sigma). They were then incubated overnight at +4 °C with the 6F3D anti-A $\beta$  antibody (Dako, 1/200), polyclonal anti-tau antibody (Dako, 1/500), monoclonal anti-alpha-synuclein (LB509, Zymed, 1/250), polyclonal anti-TDP43 (Protein Tech Group, 1/1000) routinely used for  $\beta$ -amyloid, tau, alpha-synuclein and TDP43 detection, respectively. Sections were further incubated with a biotinylated secondary antibody for 25 min at room temperature, and the presence of the secondary antibody was revealed by a streptavidin–horseradish peroxidase conjugate using diaminobenzidine (Dako, Glostrup, Denmark). Sliced were counterstained with Harris hematoxylin.

### 2 Characterization of human brain homogenates

Brain homogenates were prepared by combining brain extracts from different patients. cIAD and rpAD homogenates consisted in a combination of four brain extracts from the patients with cIAD and rpAD, respectively. A third homogenate, considered as a control, was prepared from non-demented individuals (Ctrl, n=2 subjects). These brain homogenates were characterized by biochemistry.

#### 2.1. ELISA quantifications

For amyloid protein quantification, all assay-specific material (pre-coated microtiter plate, buffers, antibodies, standard solutions) was provided in the V-PLEX kit A $\beta$  Peptide Panel 1 (6E10) (MSD®). Human brain homogenates were diluted to 1/5 (Ctrl samples) or 1/10 (cIAD and rpAD samples) in the dilution buffer. As described in the manufacturer's protocol, the microtiter plate was blocked for 1 hour at RT with the appropriate buffer. After washing, 25 $\mu$ l



of detection antibody and 25µl of diluted sample or standard were added in duplicate to the wells and incubated under continuous agitation for 2h at RT. Wells were washed and 150µl of reading buffer was added. Plate reading was performed with the MSD Sector Imager 2400 (model 1200) multiplex assay system. Aβ<sub>1-38</sub>, Aβ<sub>1-40</sub> and Aβ<sub>1-42</sub> quantifications were performed with the Discovery Workbench 4.0 MSD® software.

Tau protein quantifications (total tau (InVitrogen KHB0041) and phospho-tau181 (InVitrogen KHB00631)) were performed according to the manufacturer's protocol. Briefly, brain homogenates were diluted to 1/100 and 1/200 in the provided dilution buffer. 50µl of standards or samples, as well as 50µl of detection antibody solution were added to wells and incubated for 14 hours at +4°C. After washing, 100µl of 1X anti-rabbit IgG HRP solution was added for a 30 min incubation period at RT. 100µl of stabilized chromogen were then added to each well for 30 min at RT, in the dark. The reaction was stopped by adding 100µl of Stop solution and the plate was read at 450 nm within the hour. Data were analyzed with GraphPad Prism 7 using the 4PL method. All samples were tested in duplicates.

## 2.2. Western blots

For tau protein extraction, brain homogenates were sonicated on ice for 5 min, centrifuged for 5 min at 3,000g at +4 °C, diluted in 20 mM Tris/2% SDS and sonicated on ice for 5 min. For tau characterization, samples were diluted to 1 µg/µL, diluted in 2X lithium dodecyl sulfate (LDS, Thermo Fisher Scientific) buffer with reducers and heated at +100 °C for 10 min. 15 µg of samples were loaded on a 12% Bis-TrisCriterion™ gel (Bio-Rad) and migrated in MOPS buffer for 1 hour at 165 V on ice. After protein transfer on nitrocellulose sheets, migration and transfer quality were checked with a ponceau S staining. The membrane was saturated for 1 hour at RT, and was then incubated with the AT100 (pT212-pS214, Life technologies MN1060), 2H9 (pS422, 4BioDx 4BDX-1501), tau-Nter (12-21, LB lab-made) or tau-Cter (clone 9F6, LB lab-made) antibodies overnight at +4 °C. A peroxidase coupled secondary anti-rabbit or anti-mouse antibody was then applied for 45 min at RT. Immunoblotting was revealed by ECL. GAPDH (Sigma 9545) was used as a loading control. Operators were blinded to the status of the patients.

For Iba1 and GFAP protein extractions, brain homogenates were sonicated (6 strokes, cycle 0.5, 30% amplitude) in a lysis buffer at a final concentration of 50mM Tris-HCl pH 7.4, 150 mM NaCl, 1% Triton-X-100 supplemented with 1X protease inhibitors (cOmplete™ Mini, EDTA-free

Protease Inhibitor Cocktail, Roche) and 1/100 diluted phosphatase inhibitors (Phosphatase Inhibitor Cocktail 2, Sigma-Aldrich). Samples were centrifuged at 20,000g for 20 minutes at +4°C and the supernatant was collected for further use. Extracted samples were stored at -80°C after evaluation of total protein concentration by a BCA assay (Pierce™). Extracted samples were denatured at +90°C for 5 min in a buffer containing 1X LDS (NuPAGE® LDS sample buffer, Invitrogen) and DTT 1X (NuPAGE® sample reducing agent, Invitrogen). 10 µg of denatured proteins were loaded per well. Samples and the molecular weight marker (Bio-Rad Precision Plus Protein™ Dual Color standards) were loaded on a 4-20% Criterion™ TGX™ gel (Bio-Rad) and migration was performed in a 1X tris-glycine buffer (Bio-Rad) at 120V for 1 hour. Proteins were then transferred to a nitrocellulose membrane using the Trans-Blot® Turbo™ (Biorad) system. Migration and transfer quality were checked with a ponceau S staining. The membrane was then blocked with a TBS/0.1%Tween, 5% milk solution for 1 hour at RT, and incubated with the primary antibody Iba1 (Wako 1919741, 1/2000), GFAP (Dako Z0334, 1/5000) or actin (Sigma A2066, 1/5000) diluted in saturation buffer overnight at +4°C. After washing in TBS/0.1% Tween solution, the membrane was incubated with the appropriate secondary HRP-conjugate antibody diluted to 1/5000 in TBS/0.1%Tween for 1h at RT. The chemiluminescent signal was revealed using the Clarity western ECL (Bio-Rad) kit and the Chemidoc™ MP (Bio-Rad) imaging system. Protein band intensities were quantified on the ImageJ software and normalized by actin expression levels.

### **3 Stereotaxic surgery**

Two month-old APP<sub>swe</sub>/PS1<sub>dE9</sub> and wild-type littermates were anesthetized by an intraperitoneal injection of ketamine (1mg/10g; Imalgène 1000, Merial) and xylazine (0.1mg/10g; 2% Rompun, Bayer Healthcare). Local anesthesia was also performed by a subcutaneous injection of lidocaine at the incision site (1 µl/g; 0.5% Xylovet, Ceva). Mice were placed in the stereotaxic frame (Phymep) and bilateral injections of brain samples were performed in the dorsal hippocampus (AP -2 mm, DV -2 mm, L +/- 1 mm from bregma). Using 34-gauge needles and Hamilton syringes, 2µl of sample were administered at a 0.2µl/min rate. After the injection, needles were kept in place for 5 more minutes before removal and the incision was sutured. The surgical area was cleaned before and after the procedure using povidone iodine (Vétédine, Vétôquinol). Respiration rate was monitored and body temperature was maintained at 37±0.5°C with a heating pad during the surgery. Anesthesia

was reversed with a subcutaneous injection of atipamezole (0.25 mg/kg; Antisedan, Vetoquinol). Mice were placed in a ventilated heating box (25°C) and monitored until full recovery from anesthesia. Postoperative pain management consisted in paracetamol administration in drinking water (1.45ml/20ml of water; Doliprane, Sanofi) during 48 hours.

#### **4 Behavioral evaluations**

Mice were studied using an elevated plus maze, a novel object recognition task in a V-maze, and a Morris water maze. Between each mice, the elevated plus maze and V-maze were cleaned with 10% ethanol and dried. Performances were recorded using a tracking software (EthoVision XT14, Noldus).

##### **4.1. Elevated plus maze**

The elevated plus maze is a plus-shaped apparatus placed at 50 cm above the floor. It consists in four 5 cm-wide and 40 cm-long segments, among which two are open arms (associated with a 150 lux-lighting) and two are enclosed arms (associated with a 15 lux-lighting). Mice were placed at the center of the maze facing an open arm for a 6-min trial. Distance travelled and time spent in each arm were automatically calculated by the software. The time spent leaning over the edge of open arms was scored manually.

##### **4.2. Novel object recognition in the V-maze**

The V-maze arena consisted in two 6 cm-wide, 33.5 cm-long and 15 cm-high black arms forming a V shape and exposed to a 50 lux-lighting. The test was divided into three phases, each one separated by 24 hours. At the beginning of each session, mice were placed at the center of the arena, *i.e.* at the intersection of the arms. During the habituation phase (day 1), mice were free to explore the empty arena for 9 minutes. The distance travelled was automatically recorded as an indicator of their exploratory activity. For the training phase (day 2), two identical objects (bicolor plastic balls) were placed at the end of each arm. Exploratory activity was evaluated as the time spent exploring the objects (manually recorded) and the distance travelled during the 9-minute trial. On the test day (day 3), one familiar object (a bicolor plastic ball) was replaced by a novel one of a different shape and material (a transparent glass flask). Recognition was assessed using a discrimination index, calculated as follows:

*Discrimination index*

$$= \frac{\text{Time exploring the novel object} - \text{Time exploring the familiar object}}{\text{Total exploration time}}$$

It reflects the time spent exploring each object, and therefore, the ability to discriminate a novel object from a familiar, previously explored one. A high discrimination index score reveals that mice spent more time exploring the new object, *i.e.* had less interest in a familiar object, and suggests that their memory is not impaired.

### **4.3. Morris water maze**

An open 122 cm-wide circular swimming arena was maintained at 22°C and exposed to a 400 lux-lighting. The test consisted of three phases during which the arena was divided into four artificial quadrants. At the end of each session, mice were dried with a heated towel before returning to their home cages. During the habituation phase (day 1), mice were trained to find a visible platform to escape from the water. To facilitate its detection, the platform was emerged 0.5 cm above the surface of the water and a colorful cue was placed on it. This phase consisted in four 60-seconds trials, with an inter-trial interval (ITI) of 20-30 minutes. For each trial, the starting point was different as well as the location of the platform. When the mice did not find the platform within the 60 seconds, they were guided to its location and were left on the platform to rest for 30 seconds. The training phase (day 2 to 6) consisted in three daily 60-seconds trials, with 20-30 minutes ITI, for five days. For each trial, the starting point was different whereas the location of the platform remained the same. The platform was hidden 0.5 cm beneath the water surface and the cue previously placed on it was removed. Visual cues were placed around the maze so that mice could spatially navigate to the platform. When the mice did not find the platform within the 60 seconds, they were guided to its location and were left on the platform to rest for 30 seconds. All trials lasted 60 seconds or until the animal located the platform. Escape latency, *i.e.* the time required to find the platform, was evaluated during the habituation and the training phases to assess learning abilities. A probe test (day 7) was performed 72 hours after the last training session to assess spatial long-term memory. During this phase, the platform was removed from the maze. Mice were placed in the water for 60 seconds from a position opposite to the platform. The time spent in each virtual quadrant of the maze was recorded.

## 5 Immunohistochemistry for amyloid, tau, microgliosis, and astrogliosis

Amyloid deposits were evaluated using a 4G8 labelling. Tau was evaluated using AT8 and AT100 labellings. Microgliosis was evaluated using Iba1 and CD68 antibodies. Astrocytes were stained using a GFAP antibody. 4G8 labelling was performed after pretreating brain sections with 70% formic acid (VWR®) for 20 min at RT. AT8 and AT100 labellings were performed after a pretreatment with EDTA 1X citrate (Diagnostic BioSystems®) for 30 min at 95°C. All tissues were then incubated in hydrogen peroxide H<sub>2</sub>O<sub>2</sub> 30% (Sigma-Aldrich®) diluted 1/100 for 20 min to inhibit endogenous peroxidases. Blocking of non-specific antigenic sites was achieved over 1 hour using a 0.2% Triton X-100/0.1M PBS (Sigma-Aldrich®) (PBST) solution containing 4.5% normal goat serum or 5% bovine serum albumin. Sections were then incubated at +4°C with the 4G8 (Biolegend 800706, 1/500), Iba1 (Wako 1919741, 1/1000), CD68 (Serotec – Biorad MCA 1957, 1/800) or GFAP (Dako Z0334, 1/10000) antibody diluted in a 3%NGS/PBST solution for 48h, or with the AT8 (Thermo MN1020B, 1/500) or AT100 (Thermo MN1060, 1/500) antibody diluted in a 3%NGS/PBST solution for 96h. After rinsing, an incubation with the appropriate biotinylated secondary antibody diluted to 1/1000 in PBST was performed for 1h at RT, followed by a 1h incubation at room temperature with a 1:250 dilution of an avidin-biotin complex solution (ABC Vectastain kit, Vector Laboratories®). Revelation was performed using the DAB Peroxidase Substrate Kit (DAB SK4100 kit, Vector Laboratories®). Sections were mounted on Superfrost Plus slides (Thermo-Scientific®). For the AT8 and AT100 labellings, a cresyl violet counterstain was performed. All sections were then dehydrated in successive baths of ethanol at 50°, 70°, 96° and 100° and in xylene. Slides were mounted with the Eukitt® mounting medium (Chem-Lab®).

Stained sections were scanned using an Axio Scan.Z1 (Zeiss® - Z-stack images acquired at 20× (z-stacks with 16 planes, 1µm steps with extended depth of focus)). Each slice was extracted individually in the .czi format using the Zen 2.0 (Zeiss®) software. Image processing and analysis were performed with the ImageJ software. Macros were developed for each staining in order to achieve a reproducible semi-automated quantification. Images were imported with a 50% reduction in resolution (0.44 µm/pixel), converted to the RGB format and compressed in .Tif format. For the 4G8, Iba1 and CD68 immunostainings, segmentation was performed through an automatic local thresholding using the Phansalkar method (radius=15). Amyloid load was evaluated after quantification of the 4G8-labelled particles between 8 and 2,000

$\mu\text{m}^2$ , and normalization to the surface area of each ROI. Microglial activity was evaluated as a percentage of Iba1- or CD68-positive surface area in each ROI. For the AT8 and AT100 stainings, the blue component of each image was extracted in order to remove the cresyl violet counter-staining from the analysis. An automatic local thresholding of the staining was carried out with the Phansalkar method and the severity of tau pathology was evaluated as a percentage of AT8-positive or AT100-positive surface area in each ROI. In addition for the AT8 immunostaining, a quantification of neuritic plaques and AD-like neurofibrillary tangles was performed by manual counting. The AT8-positive area stained within neuritic plaques was evaluated by drawing circular regions of interest (with a constant area of  $6\mu\text{m}^2$ ), and by quantifying the percentage of tau-positive regions within each ROI, using the same thresholding method as previously described. A semi-quantitative analysis of neuropil threads was also performed by assigning a severity score based on the intensity and extent of AT8-positive staining in each ROI. All quantifications were performed on adjacent slices between -0.34 mm and -4.36 mm from bregma. Ten adjacent slices were analyzed for the 4G8 staining, and 5 for Iba1, CD68, AT8, and AT100 stainings. All ROIs were manually segmented using the Paxinos and Franklin Neuro-Anatomical Atlas of Mouse Brain (Paxinos and Franklin, 2001).

## **6. Gallyas silver staining**

Free-floating sections were mounted on Superfrost Plus (Thermo-Scientific®) slides and dried overnight prior to Gallyas staining. Sections were permeabilized by successive incubations in toluene (2x5min) followed by ethanol at 100°, 90° and 70° (2 min per solution). Slides were then incubated in a 0.25% potassium permanganate solution for 15 min, in 2% oxalic acid for 2 min then in a lanthanum nitrate solution (0.04g/l lanthanum nitrate, 0.2g/l sodium acetate, 10% H<sub>2</sub>O<sub>2</sub> 30%) for 1h to reduce non-specific background. Several rinses with distilled water were performed followed by an incubation in an alkaline silver iodide solution (3.5% AgNO<sub>3</sub> 1%, 40g/l NaOH, 100g/l KI) for 2 min. The reaction was neutralized with 0.5% glacial acetic acid baths (3x1min) and sections were incubated for 20 min in a developing solution (2g/l NH<sub>4</sub>NO<sub>3</sub>, 2g/l AgNO<sub>3</sub>, 10g/l tungstosilicic acid, 0.76% formaldehyde 37%, 50g/l anhydrous Na<sub>2</sub>CO<sub>3</sub>). Several rinses with 0.5% acetic acid (3x1min) followed by an incubation in 1% gold chloride solution for 5min were then carried out. Sections were rinsed with distilled water and the staining was fixed with a 1% sodium thiosulfate solution. All sections were then rinsed with distilled water and dehydrated for 1 to 5 min in successive baths of ethanol at 50°, 70°, 96°

and 100° and in xylene. Slides were mounted with the Eukitt® mounting medium (Chem-Lab®). All steps were performed between 20 and 25°C.

## 7. Co-staining of microglia and amyloid plaques

In order to evaluate microglial load surrounding amyloid plaques, the co-staining of microglia and amyloid plaques was performed. Free-floating sections were permeabilized in a 0.2% Triton X-100/0.1M PBS (Sigma-Aldrich®) solution for 3x10min. Slices were stained by MXO4 dye (Tocris #4920, 1/300) for 30 min at RT, and then washed in a 0.1M PBS solution. Sections were blocked in a 4.5%NGS/PBST solution for 1h at RT before being incubated with the Iba1 antibody (Wako 1919741, 1/1000). On the next day, sections were rinsed in 0.1M PBS and incubated for 1h at RT with the appropriate secondary antibody diluted to 1/1000 in PBST (anti-rabbit AlexaFluor 633). Sections were rinsed and mounted on Superfrost Plus (Thermo-Scientific®) slides with the Vectashield® mounting medium with a refractive index of 1.45. Images of stained sections were acquired using a Leica DMI6000 confocal optical microscope (TCS SPE) with a 40x oil-immersion objective (refractive index 1.518) and the Leica Las X software. A confocal zoom of 3 and a pinhole aperture fixed at 1 Airy were applied. Acquisition was performed in sequential mode with a sampling rate of 1024x1024 and a scanning speed of 700 Hz. Image resolution was 60 nm/pixel and the optical section was 0.896 µm. 12 separate planes with a 0.1 µm step were acquired. The excitation wavelengths were 633 nm (for Iba1) or 350 nm (for Aβ). Image acquisition was performed on 2 slices located between -3.28 mm and -4.24 mm from the bregma, with 3 images per slice for the CA1 region and for the perirhinal/entorhinal cortex. 3D deconvolution of the images was performed using the AutoQuant X3 software. The deconvoluted 8-bit images were analyzed using the ImageJ software. Quantification of microglial load around plaques was based on a thresholding procedure applied across all images to segment microglial cells. MXO4-positive surfaces were dilated as circular regions of interest (with a diameter of 40 µm) were drawn around the amyloid plaque to define a dilated plaque area. Microglial staining within the dilated surface, *e.g.* within the plaque area, was included in the analysis.

## REFERENCES

Gary C, Lam S, Herard AS, Koch JE, Petit F, Gipchtein P, *et al.* Encephalopathy induced by Alzheimer brain inoculation in a non-human primate. *Acta Neuropathol Commun* 2019; 7(126).

Paxinos G, Franklin KBJ. The mouse brain in stereotaxic coordinates. second ed. San Diego: Academic Press; 2001.



## SUPPLEMENTARY TABLES

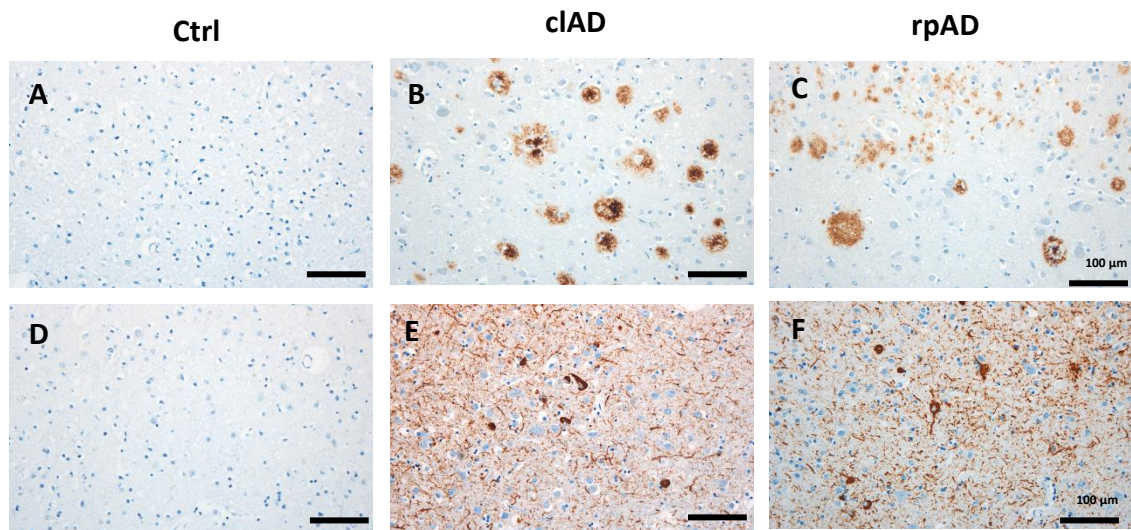
Patient					Neuropathology						
ID	Age	Gender	Disease progression (months)	Post mortem delay (hours)	Braak stage	Thal stage	CAA	$\alpha$ -synuclein	TDP43	Hippocampal sclerosis	PrPSc
Ctrl1	66	M	-	26	II	0	0	0	0	0	0
Ctrl2	76	M	-	?	II	0	0	0	0	0	0
clAD1	79	F	78	48.6	V	5	Type2+	0	0	0	0
clAD2	87	F	72	29	V-VI	4	Type1+++	0	0	0	0
clAD3	89	F	96	30.6	V	5	Type1	0	0	0	0
clAD4	71	M	66	54	VI	4	Type2+ Amygdala	0	0	0	0
rpAD1	84	F	6	79	V	4	Type2	0	0	0	0
rpAD2	81	F	36	?	V	5	Type1	0	0	0	0
rpAD3	81	F	36	26	VI	4	0	0	0	0	0
rpAD4	86	F	36	20.5	V	4	Type2	0	0	0	0

**Supplementary Table 1. Patient characteristics.** Age-matched classical (clAD) and rapidly evolving (rpAD) AD patients were selected based on disease duration (over or under 36 months) and neuropathological evaluation, including similar Braak and Thal stages. Brains were negative for  $\alpha$ -synuclein, TAR DNA-binding protein 43 (TDP43), hippocampal sclerosis and pathological prion PrPSc. Two non-AD control individuals (Ctrl) were also included in this study.

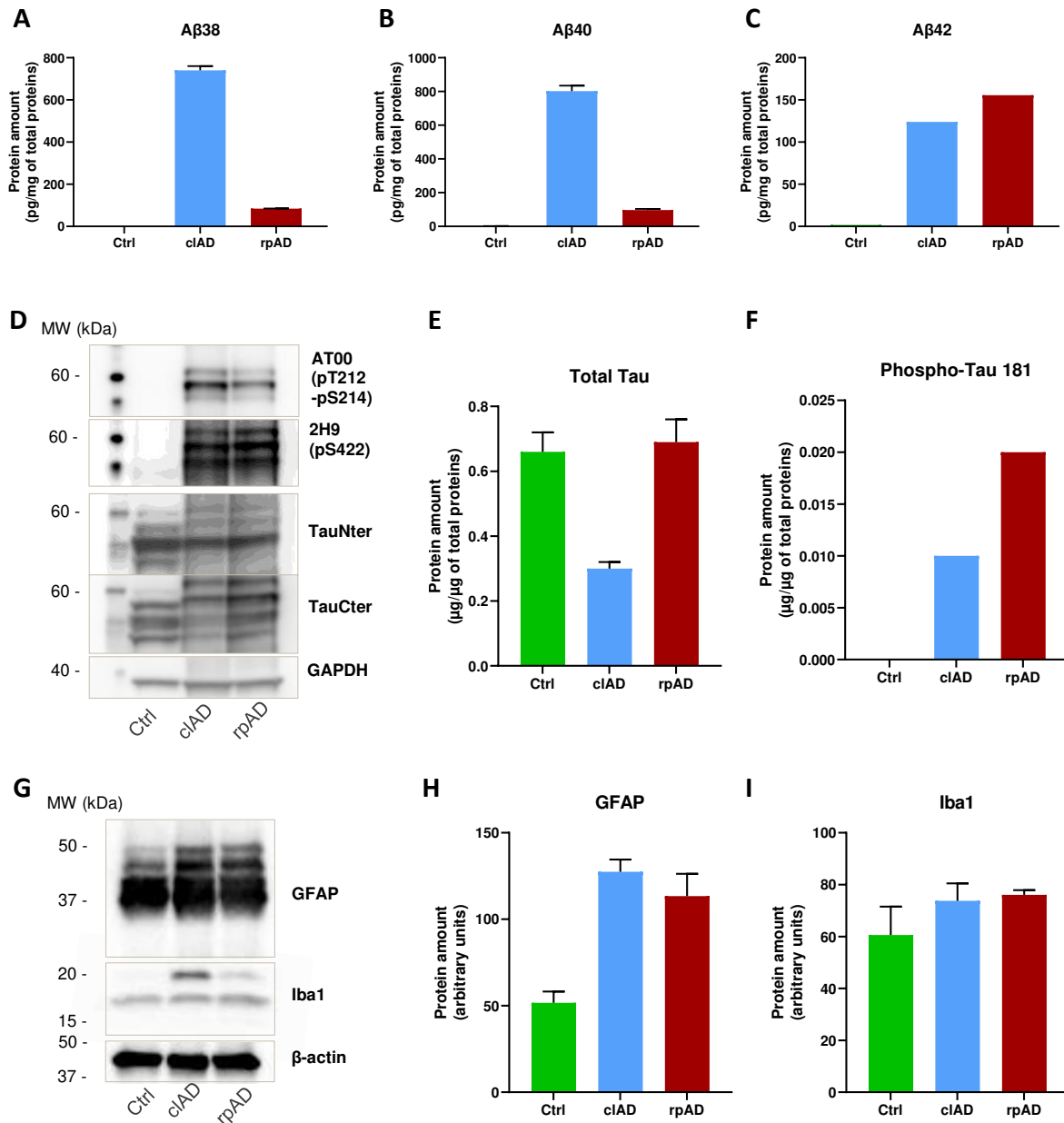
	old APP <sub>swe</sub> /PS1 <sub>de9</sub>	Ctrl-Inoculated	ciAD-inoculated	rpAD-Inoculated
(1) Amyloid plaques	+	+	++	++
(2) Neuritic plaques (plaque count)	Detected (not quantified)	+	+	+
(3) Neuritic plaques (Tau positivity within plaques)		+	++	++
(4) Neuropil threads and NFTs		0	+	+
(5) Tau spreading			+	+
(6) Synaptic loss compared to Ctrl inoculated			0	++
(6-1) Factors associated with synaptic loss			- Tau pathology - Reduction of microglial load	
(7) Cognitive impairments compared to Ctrl inoculated			0	++
(7-1) Factors associated with cognitive impairments			- Synaptic loss - Amyloid load - Tau pathology - Reduction of microglial load	

**Supplementary Table 2. Overview of the results of this study.** The study focused on A $\beta$  plaque-bearing APP<sub>swe</sub>/PS1<sub>dE9</sub> mice (1). Old mice and mice inoculated with Ctrl-human brain extract presented with tau-positive neuritic plaques (2). Inoculation of AD-brain extracts increased tau positivity within neuritic plaques (3) and induced neuropil threads and NFTs in inoculated mice (4). Tau lesions spread in regions connected to the inoculation site (5). Synaptic (6) and cognitive impairments (7) were detected in animals inoculated with brains from patients with a rapidly evolving form of AD (rpAD). Synaptic loss was associated with tau pathologies and a reduction of activated microglial load (6-1). Cognitive impairments were associated with synaptic loss, with amyloid and tau loads, and to a lesser extent with a reduction of activated microglial load (7-1).

## SUPPLEMENTARY FIGURES

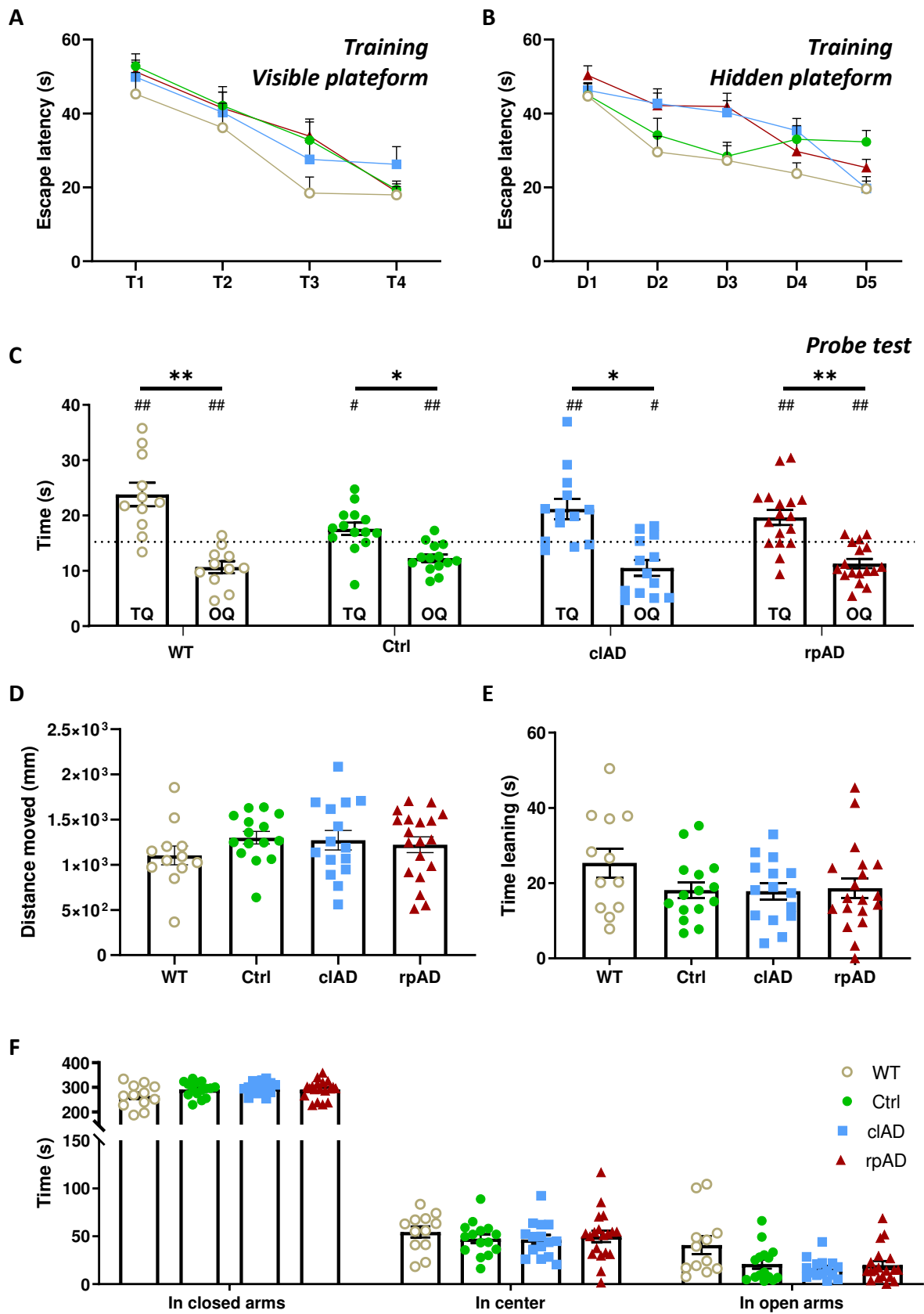


**Supplementary Figure 1. Amyloid and tau pathological evaluations in human brain samples.** Representative images of Ctrl, cIAD and rpAD brain samples stained for amyloid (A-C, 6F3D anti-A $\beta$  antibody) and tau (D-F, polyclonal anti-tau antibody) pathologies. Scale bars = 100  $\mu$ m.



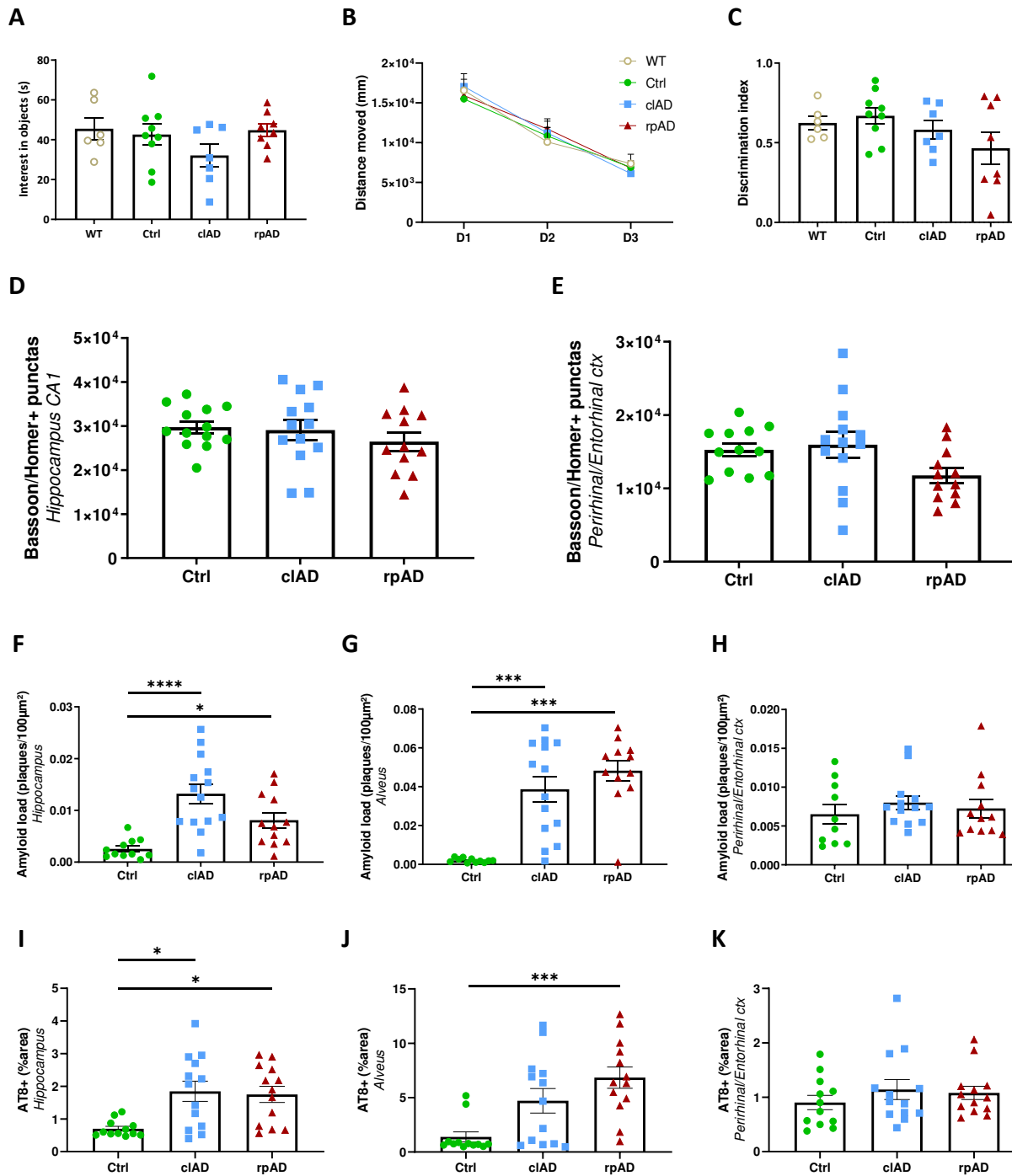
**Supplementary Figure 2. Biological characteristics of brain homogenates inoculated to animals.** Three brain homogenates were prepared from the 2 Ctrl, 4 ciAD and 4 rpAD cases (Ctrl, ciAD and rpAD homogenates respectively). All quantifications of the inoculated brain homogenates (Ctrl, ciAD or rpAD) were performed in duplicate and data are shown as mean  $\pm$  standard deviation of the replicates. (A-C) Quantifications of total A $\beta_{38}$ , A $\beta_{40}$  and A $\beta_{42}$  of the inoculated brain extracts (MSD technology). Both AD inocula had more A $\beta$  proteins compared to the Ctrl one. The ciAD inoculum showed more A $\beta_{38}$  and A $\beta_{40}$  than the rpAD one. (D-F) Tau profile evaluation revealed a pathological hyperphosphorylated

tau triplet at 60, 64 and 69 kDa observed in AD and a typical shift in the molecular weight of the Alzheimer Tau-Cter triplet in western blots (D). Total tau (E) and pathological phospho-tau 181 levels (F) were assessed using ELISA quantifications. (G-I) Neuroinflammatory profile evaluation by western blots revealed higher astrocytic presence (GFAP-positive) in cAD and rpAD inocula compared to the Ctrl extract (G-H). Microglial (Iba1-positive) levels were similar in the Ctrl, cAD and rpAD groups (G, I).



**Supplementary Figure 3. Inoculated mice showed similar spatial memory performances and anxiety levels at 8 mpi.**

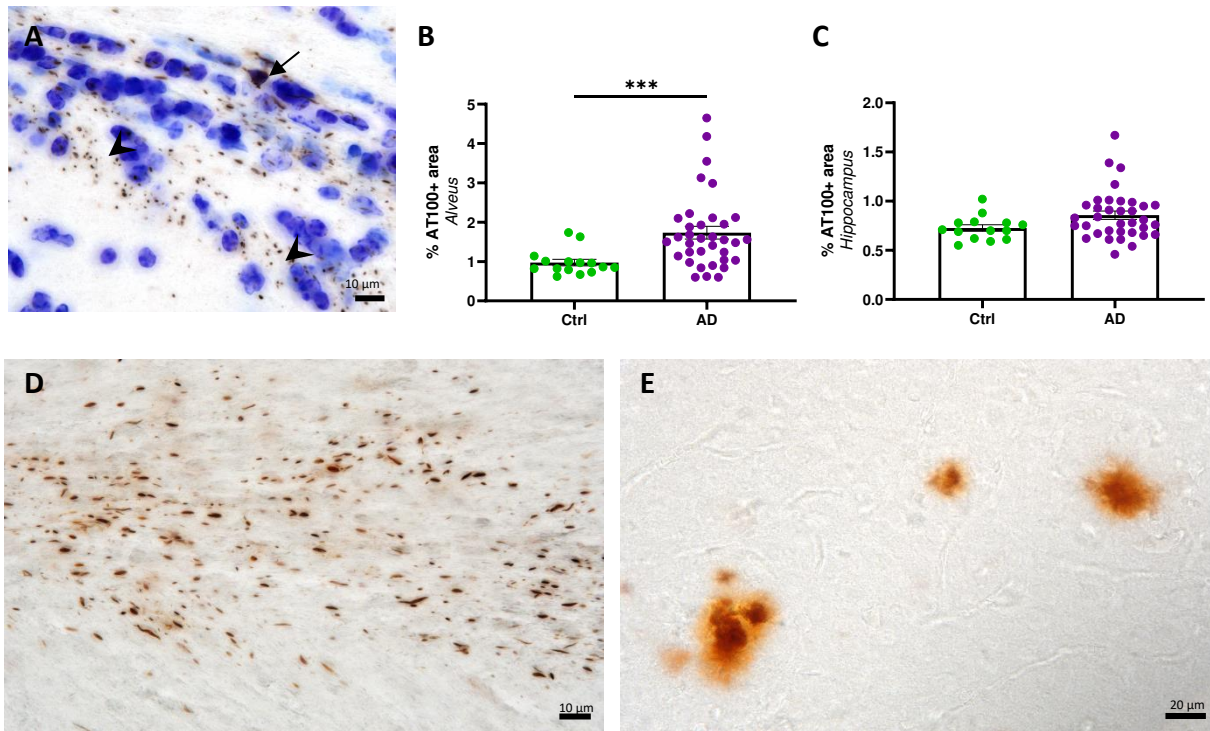
(A-C) Spatial memory was assessed using the Morris water maze test. During the visible platform phase (A), escape latencies steadily decreased across the four trials ( $F_{(2,649, 135.1)} = 36.67$ ,  $p < 0.0001$ ; two-way repeated measures ANOVA with the Geisser-Greenhouse correction and Dunnett's multiple comparisons). No difference was observed between the groups ( $F_{(3, 51)} = 1.87$ ,  $p = 0.15$ ; two-way repeated measures ANOVA with the Geisser-Greenhouse correction and Dunnett's multiple comparisons). For the hidden platform training phase (B), escape latencies were averaged across three trials per day and slowly decreased across the trials and days suggesting that mice had successfully learnt the platform position ( $F_{(3,575, 182.3)} = 36.09$ ,  $p < 0.0001$ ; two-way repeated measures ANOVA with the Geisser-Greenhouse correction and Dunnett's multiple comparisons). No difference was observed between the groups suggesting that Ctrl, cIAD and rpAD brain inoculations do not differentially impact spatial learning abilities in APP<sub>swe</sub>/PS1<sub>dE9</sub> mice after an eight-month incubation period ( $F_{(2, 41)} = 0.85$ ,  $p = 0.88$ ; two-way repeated measures ANOVA with the Geisser-Greenhouse correction and Dunnett's multiple comparisons). During the probe test evaluating spatial memory (C), the time spent in the target quadrant (TQ) was significantly higher than the time spent in the opposite one (OQ) (\* $p < 0.05$  for Ctrl and cIAD-inoculated APP<sub>swe</sub>/PS1<sub>dE9</sub> mice or \*\* $p < 0.01$  for WT mice and rpAD-inoculated APP<sub>swe</sub>/PS1<sub>dE9</sub> mice; two-way repeated measures ANOVA with the Geisser-Greenhouse correction and Dunnett's multiple comparisons). Moreover, the time spent both in the TQ and OQ was significantly different from 15 seconds, which corresponds to 25% of the trial duration (#  $p < 0.05$ ; one-sample Wilcoxon's signed-rank test). Spatial memory retention was evaluated after 72 hours. All groups performed as well as the WT group by spending more time in the target quadrant than in the opposite one, suggesting that memory is not impaired in APP<sub>swe</sub>/PS1<sub>dE9</sub> Ctrl or AD-inoculated mice (for the groups:  $F_{(3, 51)} = 0.83$ ,  $p > 0.05$ ; for TQ versus OQ:  $p = 0.0028$ ,  $0.0217$ ,  $0.0117$  and  $0.0013$ , respectively for Wt, Ctrl, cIAD and rpAD groups; two-way ANOVA with the Geisser-Greenhouse correction and Dunnett's multiple comparisons). (D-F) Anxiety levels were assessed using the elevated plus maze. Comparable travelled distance (D), time spent leaning over the maze (E) and time spent in the different areas of the maze (open/closed arms and center of the maze) (F) were reported between the groups ( $p > 0.05$ ; Kruskal-Wallis' test with Dunn's multiple comparisons). Data are shown as mean  $\pm$  s.e.m.



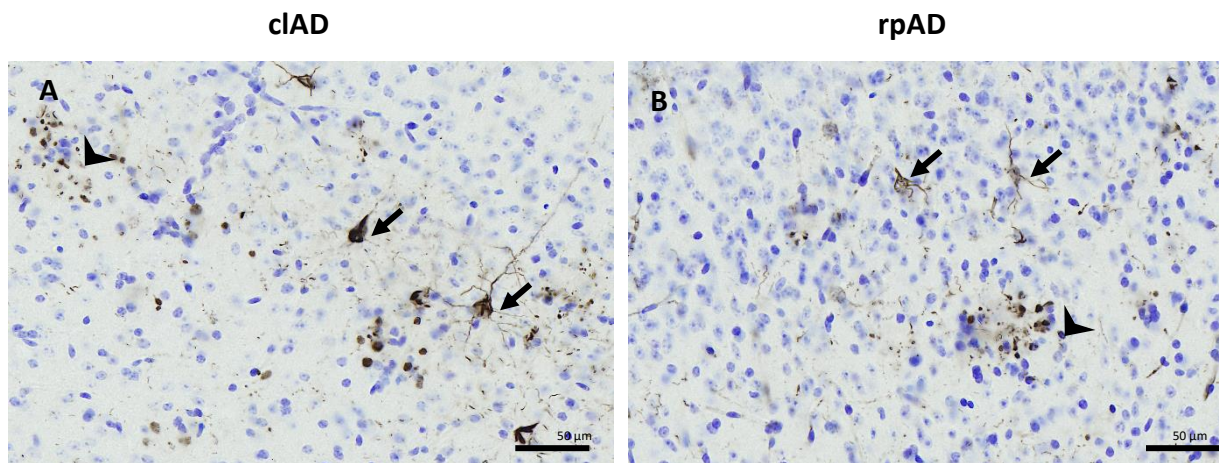
**Supplementary Figure 4. Cognitive performance, synaptic density, amyloid and tau loads evaluations at 4 mpi.** (A-C) Object recognition performances were evaluated at 4 mpi using a V-maze test. WT mice and APP<sub>SWE</sub>/PS1<sub>dE9</sub> mice inoculated with Ctrl, cIAD or rpAD brain extracts had comparable exploratory activity, as suggested by the time spent on exploring the objects (A) ( $p > 0.05$ ; Kruskal-Wallis with Dunn's multiple comparisons) and the distance



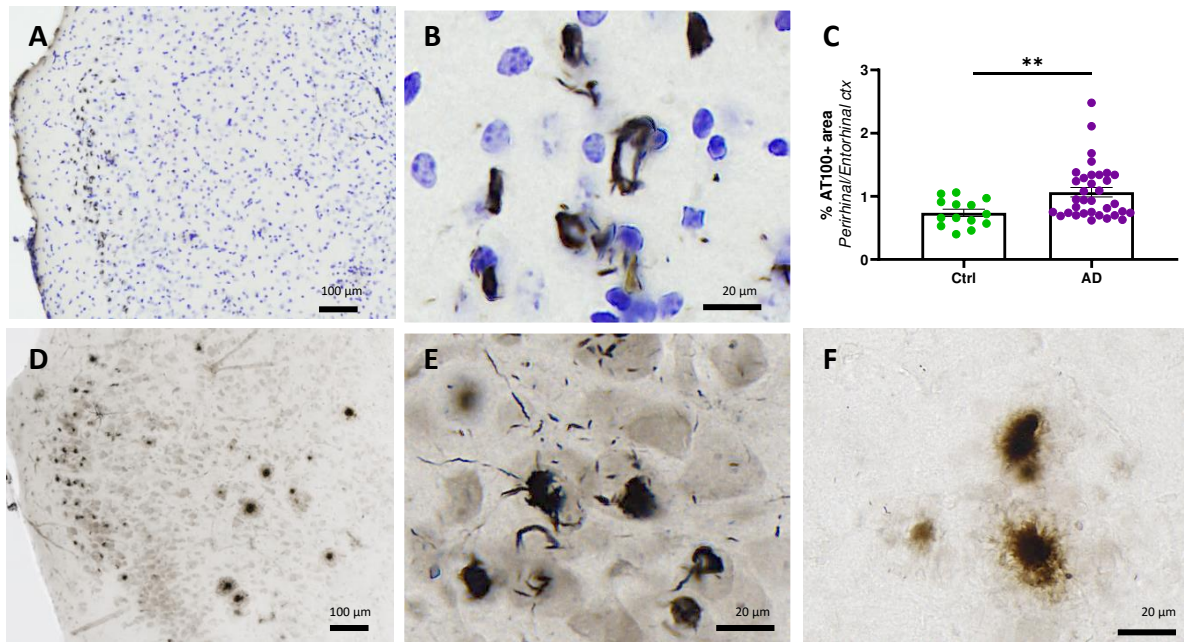
moved throughout the 3-day test (B) (for the days:  $F_{(1.89, 49.15)} = 152.6$ ,  $p < 0.0001$ ; for the groups:  $F_{(3, 26)} = 0.041$ ,  $p = 0.99$ ; two-way repeated measures ANOVA with the Geisser-Greenhouse correction and Dunnett's multiple comparisons). No difference in the novel object recognition test was reported between the groups, as similar discrimination indexes were observed (C) ( $p > 0.05$ ; Kruskal-Wallis with Dunn's multiple comparisons). (D-E) Quantification of Bassoon and Homer colocalization at 4 mpi did not show any differences in the CA1 (D) and in the perirhinal/entorhinal cortex (E) between the groups ( $p > 0.05$ ; Kruskal-Wallis with Dunn's multiple comparisons). (F-H) Amyloid load quantification at 4 mpi revealed that AD (cIAD and rpAD) brain inoculation accelerates amyloid deposition in the alveus (F) and hippocampus (G), but not the perirhinal/entorhinal cortex (H) (respectively for cIAD and rpAD mice, in the alveus  $p = 0.0008$  and  $0.0003$ , in the hippocampus  $p < 0.0001$  and  $p = 0.041$ , in the perirhinal/entorhinal cortex  $p > 0.05$ ; Kruskal-Wallis with Dunn's multiple comparisons). (I-K) AT8-positive tau overall quantification at 4 mpi revealed that AD (cIAD and rpAD) brain inoculation induces tau lesions in the alveus (I) and hippocampus (J), but not the perirhinal/entorhinal cortex (K) (respectively for cIAD and rpAD mice, in the alveus  $p = 0.080$  and  $0.0006$ , in the hippocampus  $p = 0.016$  and  $0.011$ , in the perirhinal/entorhinal cortex  $p > 0.05$ ; Kruskal-Wallis with Dunn's multiple comparisons). \* $p < 0.05$ ; \*\*\* $p < 0.001$ ; \*\*\*\* $p < 0.0001$ .  $n_{\text{Ctrl}} = 11$ ,  $n_{\text{cIAD}} = 14$ ,  $n_{\text{rpAD}} = 12$  mice. Data are shown as mean  $\pm$  s.e.m.



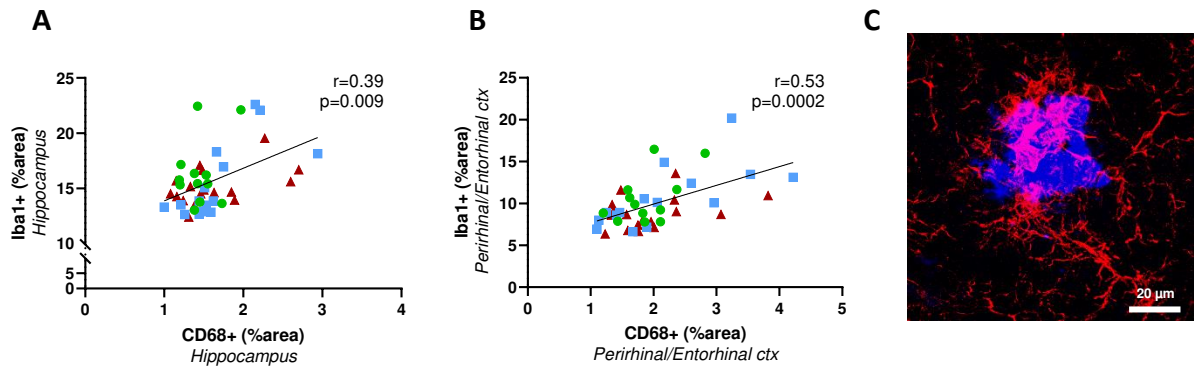
**Supplementary Figure 5. AT100 and Gallyas-positive lesions next to the inoculation site of *APP<sub>swe</sub>/PS1<sub>dE9</sub>* mice 8 months after AD brain extracts injection.** (A) AT100 staining revealed NTs (arrowheads) and NFTs (arrow). (B-C) Overall quantification of AT100 labeling showed increased labeling in the alveus (B) and a trend for increased labeling in the hippocampus (C) of AD inoculated mice ( $p=0.0007$  and  $0.092$  respectively, Mann-Whitney test). Gallyas silver staining revealed neuropil threads (D) as well as amyloid plaques (E) in AD-inoculated mice.  $n_{Ctrl}=15$ ,  $n_{AD}=35$ . Data are shown as mean  $\pm$  s.e.m. Scale bars =  $10\ \mu\text{m}$  (A, D) and  $20\ \mu\text{m}$  (E).



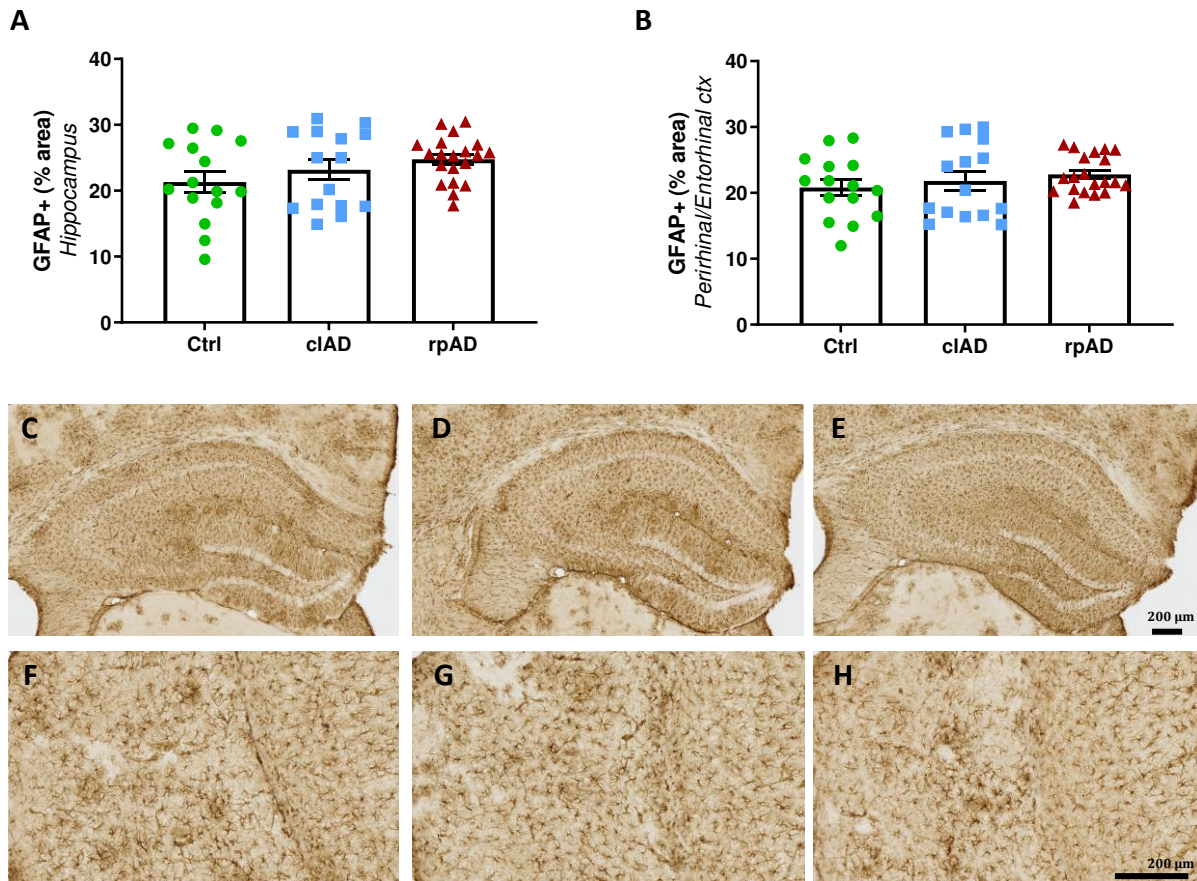
**Supplementary Figure 6. AT8-positive lesions in the visual cortex of  $APP_{Swe}/PS1_{dE9}$  mice 8 months after AD brain extract inoculation.** AT8 staining revealed NFTs (arrows) surrounded by neuropil threads, as well as neuritic plaques (arrowheads), in the visual cortex of cIAD (A) and rpAD (B) brain-inoculated mice. Scale bars = 50  $\mu$ m.



**Supplementary Figure 7. AT100- and Gallyas-positive lesions spreading to the perirhinal/entorhinal cortex of *APP<sub>swe</sub>/PS1<sub>dE9</sub>* mice 8 months after AD brain extract injection.** (A-B) AT100 staining revealed NFTs in the perirhinal/entorhinal cortex. (C) Overall quantification of AT100 labelling showed increased labelling in the perirhinal/entorhinal cortex of AD-inoculated mice compared to Ctrl-inoculated ones ( $p=0.005$ , Mann-Whitney test). (D-F) Gallyas silver staining revealed labelled neurons evoking NFTs (E) as well as amyloid plaques (F).  $n_{Ctrl}=15$ ,  $n_{AD}=35$ . Data are shown as mean  $\pm$  s.e.m. Scale bars = 100  $\mu$ m (A, D) and 20  $\mu$ m (B, E, F).



**Supplementary Figure 8. Iba1 and CD68 staining.** Iba1 staining level was correlated with CD68 labelling in the hippocampus (A) and in the perirhinal/entorhinal cortex (B). Confocal microscopy of Iba1-positive microglia surrounding amyloid deposition stained by MXO4 (C). Scale bar = 20 $\mu\text{m}$ .



**Supplementary Figure 9. Astrocytic coverage was similar in the hippocampus and perirhinal/entorhinal cortex of AD- and Ctrl-inoculated  $APP_{swe}/PS1_{dE9}$  mice at 8 mpi.** GFAP staining revealed similar astrocytic loads in the hippocampus (A, C-E) and perirhinal/entorhinal cortex (B, F-H) of Ctrl, cIAD and rpAD-inoculated  $APP_{swe}/PS1_{dE9}$  mice at 8 mpi.  $n_{Ctrl}=15$ ,  $n_{cIAD}=15$ ,  $n_{rpAD}=20$  mice. Data are shown as mean  $\pm$  s.e.m. Scale bars = 200  $\mu$ m.

### 1.3. Complementary data

#### 1.3.1. Distinct neuroanatomical pathways are affected by tau pathology following AD brain extracts inoculation

In our study, rpAD brain-inoculated mice displayed novel object recognition deficits but preserved spatial memory functions, compared with control and cIAD-inoculated mice. To further apprehend these differential alterations of cognitive functions, tau pathology was evaluated in areas of the CA1, dentate gyrus and entorhinal cortex either involved in context-free memory (*e.g.* novel object recognition) or in context-rich memory (*e.g.* spatial memory). Indeed, entorhinal projections to the hippocampus exhibit a striking organization pattern as:

- The context-free memory pathway is associated with the perirhinal cortex and lateral entorhinal axons that project to the distal part of CA1 and to the septal part of the dentate gyrus (**Figure 44A**);
- The context-rich memory pathway is associated with the postrhinal cortex and medial entorhinal axons that terminate in the proximal part of CA1 and in the temporal part of the dentate gyrus (Bekiari et al., 2015; Groen et al., 2003; van Strien et al., 2009) (**Figure 44B**).

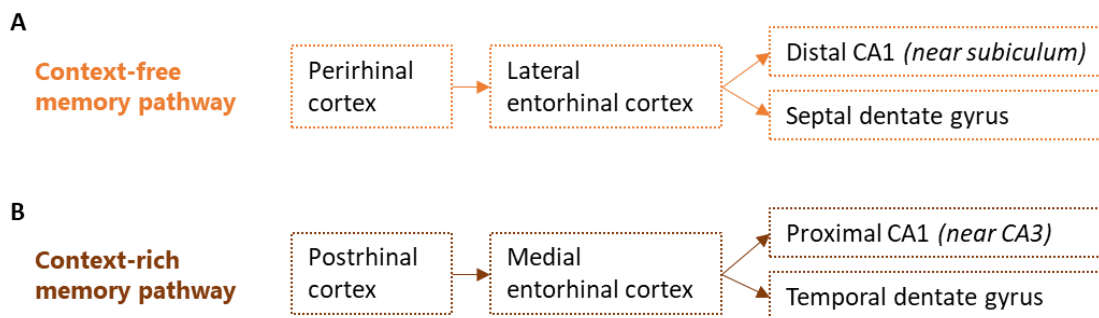


**Figure 44: Context-free and context-rich memory pathways**

(A) The context-free memory involves the perirhinal cortex and lateral entorhinal axons projecting to the distal part of CA1 next to the subiculum and to the septal part of the dentate gyrus. (B) The context-rich memory pathway involves the postrhinal cortex and medial entorhinal axons projecting to the proximal part of CA1 near CA3 and to the temporal part of the dentate gyrus (Bekiari et al., 2015; Groen et al., 2003; van Strien et al., 2009).

Evaluation of AT8-positive stained areas in context-free and context-rich memory pathways was performed on four adjacent slices between -2.06 mm and -4.36 mm from bregma. All regions of interest (ROI) were manually segmented using the Paxinos and Franklin Neuro-Anatomical Atlas of Mouse Brain (Paxinos and Franklin, 2012).

Quantification revealed that hippocampal areas (CA1 and dentate gyrus) associated with both context-free and context-rich memory pathways showed increased tau deposition in AD-inoculated mice compared with Ctrl-inoculated ones (**Figure 45A-B**) ( $p < 0.05$  in all regions for both AD groups). However, only the perirhinal/lateral entorhinal cortex associated with context-free memory, and not the medial entorhinal cortex associated with context rich memory, displayed significantly more tau in AD-inoculated mice compared to Ctrl-inoculated animals (**Figure 45C**) (for context-free memory  $p < 0.001$  and for context-rich memory  $p > 0.05$ , in both AD groups).

Moreover, in AD-inoculated animals, context-free memory-associated areas displayed more tau than the ones associated with context-rich memory ( $p < 0.001$  in the CA1,  $p < 0.0001$  in the dentate gyrus and  $p < 0.05$  in the entorhinal cortex, for both AD groups). No difference in tau load was however reported between cIAD and rpAD-inoculated mice in any region ( $p > 0.05$ ). For Ctrl-inoculated animals, no difference was found between the studied regions and we hypothesize that AT8-positive staining only reflected neuritic plaques endogenously produced in this model ( $p > 0.05$ ) (**Figure 45**).

Taken together, these data suggest that the context-free memory pathway was more affected by tau pathology than the context-rich memory pathway in AD-inoculated mice. As the severity of tau pathology correlates with cognitive alterations in our model, this provides a possible explanation regarding the occurrence of novel object recognition deficits and the absence of spatial memory alterations in rpAD-inoculated mice. However, no difference in tau pathology was observed in the context-free memory pathway between rpAD- and cIAD-inoculated animals, suggesting the involvement of other factors, possibly interacting with one another and associated with small differences below the significance threshold, in the occurrence of such contrasting cognitive profiles.



# 1. Relationships between cognitive, synaptic and neuropathological changes in AD brain-inoculated mice

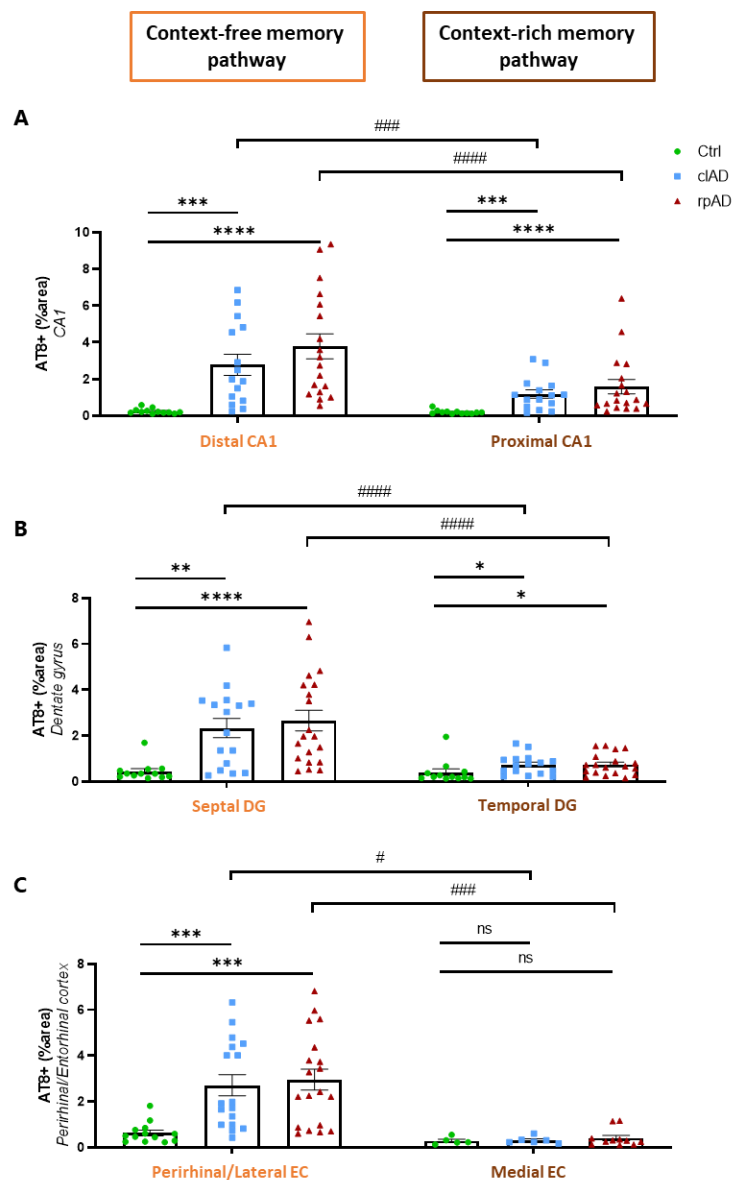


**Figure 45: Quantification of tau pathology in context-free and context-rich memory pathways**

Both context-free and context-rich memory pathways were associated with an increase in tau deposition in the CA1 region (A) and in the dentate gyrus (B) of AD-inoculated mice compared with Ctrl-inoculated mice (respectively for context-free and context-rich memory pathways, for cIAD:  $p=0.0004$  and  $0.0002$  in the CA1,  $p=0.0024$  and  $0.014$  in the dentate gyrus; for rpAD:  $p<0.0001$  for both pathways in the CA1,  $p<0.0001$  and  $0.02$  in the dentate gyrus). However, only the lateral entorhinal cortex displayed significantly more tau in AD mice than in Ctrl mice, as opposed to the medial entorhinal cortex (C) (for context-free memory,  $p=0.0007$  and  $0.0002$  respectively for cIAD and rpAD groups; for context-rich memory,  $p>0.05$  for both groups). \* $p<0.05$ ; \*\* $p<0.01$ ; \*\*\* $p<0.001$ ; \*\*\*\* $p<0.0001$ ; Kruskal-Wallis with Dunn's multiple comparisons test. Additionally, context-free memory-associated areas (on the left of each

graph) displayed more tau than the ones associated with context-rich memory (on the right of each graph) in the CA1, dentate gyrus and entorhinal cortex of AD-inoculated animals (respectively for cIAD and rpAD-inoculated mice,  $p=0.0004$  and  $<0.0001$  in the CA1,  $p<0.0001$  for both groups in the dentate gyrus,  $p=0.031$  and  $0.001$  in the entorhinal cortex). # $p<0.05$ ; ### $p<0.001$ ; #### $p<0.0001$ ; Wilcoxon matched-pairs signed rank test.  $n_{Ctrl}=15$ ,  $n_{cIAD}=15$ ,  $n_{rpAD}=20$ ,  $n_{WT}=12$  mice. Data are shown as mean  $\pm$  s.e.m. DG: dentate gyrus, EC: entorhinal cortex.

### 1.3.2. Cognitive alterations cannot solely be explained by a dose effect

Among the potential explanations for heterogeneous performances in the novel object recognition task following rpAD or cIAD brain extracts inoculations, the impact of tau inoculated doses was investigated.

Indeed, in our study, rpAD and cIAD patients did not display the exact same amounts of A $\beta$  and tau levels in their brains. Globally, rpAD and cIAD inoculated brain extracts showed similar levels of A $\beta_{42}$ , but A $\beta_{38}$  and A $\beta_{40}$  levels were greater in the cIAD extract and phospho-tau181 levels were greater in the rpAD extract. Thus, using the same hippocampal coordinates as with the previous cohort, we inoculated a new cohort of APP/PS1dE9 mice ( $n=8$ /group) with cIAD or rpAD brain extracts displaying normalized levels of phospho-tau181. As in the previous study, APP/PS1dE9 mice and wild-type littermates inoculated with the control brain extract were used as controls ( $n=4$  and  $n=9$ , respectively). At 8 mpi, novel object discrimination performances revealed the same trend as with the previously inoculated cohort. Indeed, despite similar exploratory activities (**Figure 46A**), rpAD mice showed lower cognitive scores compared with Ctrl and cIAD-inoculated mice, although no statistical difference was reported (**Figure 46B**). Altogether, these data suggest that differences between rpAD-, cIAD- and Ctrl-inoculated animals may not solely be explained by a dose effect.

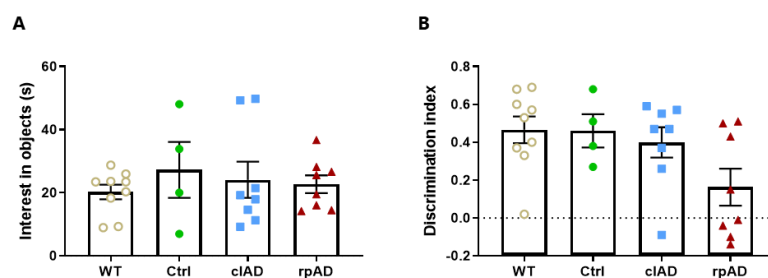


**Figure 46: Novel object recognition performances following the inoculation of Ctrl or AD brain extracts with normalized phospho-tau181 levels.**

Object recognition performances were evaluated in a V-maze, 8 months after human brain extracts inoculations. (A) Similar exploratory activities were reported between the groups as suggested by the time spent on exploring the objects. (B) The discrimination index reflects the ability to discriminate a novel object from a familiar, previously explored one. Despite the absence of statistical difference between the groups, mice inoculated with the phospho-tau181-normalized rpAD brain extract tended to perform worse than the other groups, suggesting the occurrence of a slight cognitive deficit.  $p > 0.05$ , Kruskal-Wallis with Dunn's multiple comparisons.  $n_{\text{Ctrl}}=4$ ,  $n_{\text{clAD}}=8$ ,  $n_{\text{rpAD}}=8$ ,  $n_{\text{WT}}=9$  mice. Data are shown as mean  $\pm$  s.e.m.

### **1.3.3. Characterization of A $\beta$ pathology in rpAD and clAD patients**

In collaboration with the Brain institute (ICM, Paris), further characterization of human rpAD and clAD brain samples, including those involved in this study, has been initiated. Neuropathological evaluation performed by Susana Boluda (MD, PhD) revealed that heterogeneity in A $\beta$  plaque morphology was particularly prominent in rpAD cases compared with clAD cases for whom plaques showed more homogeneous morphologies (**Figure 47A-C**). Furthermore, A $\beta$  plaques were segmented using a linear Bayesian algorithm and morphometric analysis was performed with the Visiopharm software by Lev Stimmer (PhD). The results showed that despite the absence of differences in A $\beta$  plaque load, overall, rpAD cases displayed smaller, denser and less convoluted plaques than clAD cases ( $p=0.23$  for A $\beta$  load,  $p=0.04$  for perimeter,  $p=0.02$  for integrated density,  $p=0.04$  for convexity; Visiopharm software) (**Figure 47D-G**).

Altogether, these data suggest that rpAD and clAD patients are characterized by different A $\beta$  pathology profiles. Further evaluation of rpAD and clAD brain samples, in particular of tau pathology and microglial activity, is ongoing to complete these results.

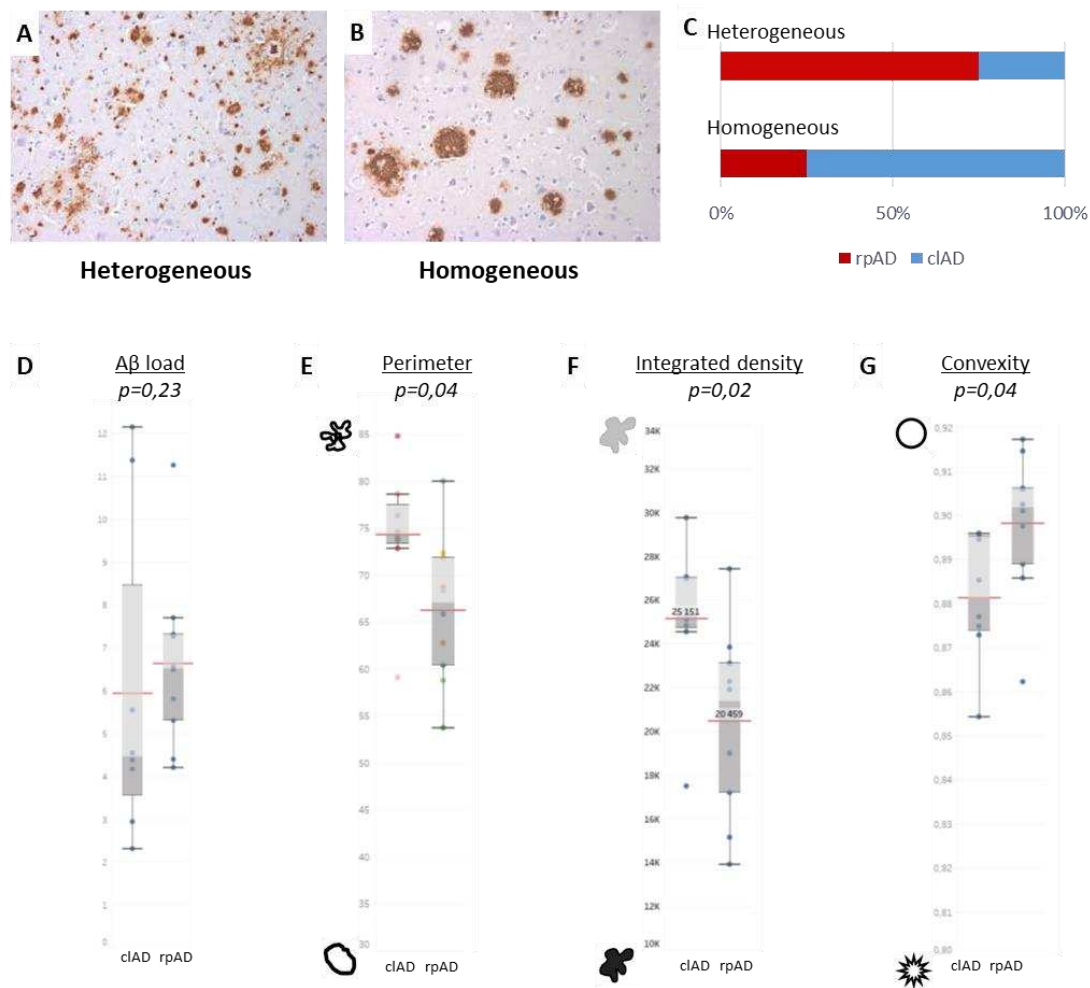


**Figure 47: Characterization of A $\beta$  deposition in rpAD and clAD patients**

(A-C) Neuropathological evaluation of rpAD and clAD brains revealing more heterogeneous plaque morphology (A) in rpAD cases than in clAD for whom plaques showed more homogeneous morphologies (B) (6F3D antibody). (C) Percentage of rpAD ( $n_{rpAD}=10$ ) and clAD ( $n_{clAD}=11$ ) cases predominantly showing heterogeneous or homogeneous plaque morphology in their brain. (D-G) Evaluation of A $\beta$  load (D), plaque perimeter (E), integrated density (F) and convexity (G) using the Visiopharm software in clAD and rpAD patients. Morphometry analysis revealed that rpAD cases display similar A $\beta$  loads but smaller, denser and less convoluted plaques than clAD cases ( $n_{rpAD}=10$ ,  $n_{clAD}=8$ ). Courtesy from Susana Boluda and Lev Stimmer from the Brain Institute (ICM, Paris).



---

## 2. Encephalopathy induced by AD brain inoculation in a non-human primate

---

### 2.1. Context, objectives & abstract

The host in which the proteopathic seeds are inoculated provides the biochemical and physiological environment that modulates lesion emergence and functional impacts (Jucker and Walker, 2013). Non-human primates (NHPs) are phylogenetically close to humans and show many similarities with them in terms of physiology, neuroanatomy and behavioral complexity. In addition, A $\beta$  and tau proteins are highly homologous in NHPs and humans. However, few studies have been conducted on NHPs because of practical and ethical concerns, including limited availability, their long lifespan and elevated costs. A long-term study conducted on marmosets (*Callithrix jacchus*) showed that AD brain inoculations can induce sparse A $\beta$  lesions but no evidence of tau, cognitive decline, neurodegeneration or functional AD hallmarks was found (Baker et al., 1994, 1993a, 1993b; Ridley et al., 2006).

In this second article, we evaluated the impacts of human AD brain homogenates inoculation on both brain function and brain integrity in mouse lemur primates (n=6/group). The gray mouse lemur (*Microcebus murinus*) is a prosimian primate that presents many advantages including being the smallest and fastest developing primate with a relatively short life expectancy of approximately twelve years in captivity. Interestingly, aged mouse lemurs (over the age of 6) can replicate some aspects of the human aging process and develop AD-like pathological features that better resemble alterations found in sporadic AD compared to transgenic mouse models. These features include A $\beta$  and tau deposits, brain atrophy and cognitive decline (Bons et al., 2006; Languille et al., 2012).

Here, we used a multimodal approach involving longitudinal cognitive assessments, electroencephalography and morphological MRI studies for up to 18 months following the inoculations. These data were further completed by the immunohistopathological examination of brain tissues. We showed that AD brain extracts inoculations into the hippocampus and overlying parietal cortex of mouse lemurs lead to an encephalopathy associated with a progressive alteration of long-term memory and learning abilities, neuronal activity modifications, cerebral atrophy and neuronal loss. In some animals, sparse A $\beta$  and tau

depositions close to the inoculated regions were also detected and no sign of pronounced glial reactivity was reported. Overall, our study is timely and important, as it is the first one to highlight neuronal and clinical alterations in a primate following AD brain extracts inoculations.

### **2.2. Article**

*Published in Acta Neuropathologica Communications (<https://doi.org/10.1186/s40478-019-0771-x>).*


Gary, C., **Lam, S.**, Hérard, A.-S., Koch, J.E., Petit, F., Gipchtein, P., Sawiak, S.J., Caillierez, R., Eddarkaoui, S., Colin, M., Aujard, F., Deslys, J.-P., Brouillet, E., Buée, L., Comoy, E.E., Pifferi, F., Picq, J.-L., Dhenain, M. Encephalopathy induced by Alzheimer brain inoculation in a non-human primate. *Acta Neuropathol. Commun.* 7(1):126. 2019.

RESEARCH

Open Access

# Encephalopathy induced by Alzheimer brain inoculation in a non-human primate



Charlotte Gary<sup>1,2</sup>, Suzanne Lam<sup>1,2†</sup>, Anne-Sophie Hérard<sup>1,2†</sup>, James E. Koch<sup>1,2,3</sup>, Fanny Petit<sup>1,2</sup>, Pauline Gipchtein<sup>1,2</sup>, Stephen J. Sawiak<sup>4,5</sup>, Raphaëlle Caillierez<sup>6</sup>, Sabiha Eddarkaoui<sup>6</sup>, Morvane Colin<sup>6</sup>, Fabienne Aujard<sup>7</sup>, Jean-Philippe Deslys<sup>8</sup>, French Neuropathology Network<sup>9</sup>, Emmanuel Brouillet<sup>1,2</sup>, Luc Buée<sup>6</sup>, Emmanuel E. Comoy<sup>8</sup>, Fabien Pifferi<sup>7†</sup>, Jean-Luc Picq<sup>1,2,10†</sup> and Marc Dhenain<sup>1,2\*</sup> 

## Abstract

Alzheimer's disease is characterized by cognitive alterations, cerebral atrophy and neuropathological lesions including neuronal loss, accumulation of misfolded and aggregated  $\beta$ -amyloid peptides (A $\beta$ ) and tau proteins. Iatrogenic induction of A $\beta$  is suspected in patients exposed to pituitary-derived hormones, dural grafts, or surgical instruments, presumably contaminated with A $\beta$ . Induction of A $\beta$  and tau lesions has been demonstrated in transgenic mice after contamination with Alzheimer's disease brain homogenates, with very limited functional consequences. Unlike rodents, primates naturally express A $\beta$  or tau under normal conditions and attempts to transmit Alzheimer pathology to primates have been made for decades. However, none of earlier studies performed any detailed functional assessments. For the first time we demonstrate long term memory and learning impairments in a non-human primate (*Microcebus murinus*) following intracerebral injections with Alzheimer human brain extracts. Animals inoculated with Alzheimer brain homogenates displayed progressive cognitive impairments (clinical tests assessing cognitive and motor functions), modifications of neuronal activity (detected by electroencephalography), widespread and progressive cerebral atrophy (in vivo MRI assessing cerebral volume loss using automated voxel-based analysis), neuronal loss in the hippocampus and entorhinal cortex (post mortem stereology). They displayed parenchymal and vascular A $\beta$  depositions and tau lesions for some of them, in regions close to the inoculation sites. Although these lesions were sparse, they were never detected in control animals. Tau-positive animals had the lowest performances in a memory task and displayed the greatest neuronal loss. Our study is timely and important as it is the first one to highlight neuronal and clinical dysfunction following inoculation of Alzheimer's disease brain homogenates in a primate. Clinical signs in a chronic disease such as Alzheimer take a long time to be detectable. Documentation of clinical deterioration and/or dysfunction following intracerebral inoculations with Alzheimer human brain extracts could lead to important new insights about Alzheimer initiation processes.

**Keywords:** Alzheimer's disease,  $\beta$ -Amyloid pathology, Cerebral atrophy, Cognitive impairment, *Microcebus murinus*, Mouse, Neurodegenerative disease, Neuronal function, Prion, Tau pathology

\* Correspondence: [marc.dhenain@cea.fr](mailto:marc.dhenain@cea.fr)

<sup>†</sup>Suzanne Lam, Anne-Sophie Hérard, Fabien Pifferi and Jean-Luc Picq contributed equally to this work.

<sup>1</sup>Centre National de la Recherche Scientifique (CNRS), Université Paris-Sud, Université Paris-Saclay UMR 9199, Laboratoire des Maladies Neurodégénératives, 18 Route du Panorama, F-92265 Fontenay-aux-Roses, France

<sup>2</sup>Commissariat à l'Energie Atomique et aux Energies Alternatives (CEA), Direction de la Recherche Fondamentale (DRF), Institut François Jacob, MIRCen, 18 Route du Panorama, F-92265 Fontenay-aux-Roses, France

Full list of author information is available at the end of the article





## Introduction

Alzheimer's disease is a neurodegenerative disease characterized by cognitive alterations, cerebral atrophy [1] and neuropathological lesions including neuronal loss [2], accumulation of misfolded and aggregated  $\beta$ -amyloid peptide and tau proteins [3]. Patients exposed to cadaver-derived hormones, dural grafts or to surgical instruments, presumably contaminated with  $\beta$ -amyloid peptide (A $\beta$ ), have a higher risk of developing early-onset A $\beta$  pathology than non-exposed subjects [4–6]. Experimental induction (or acceleration) of  $\beta$ -amyloidosis or tauopathy has been described in rodents after intracerebral and even peripheral contamination with pathological A $\beta$  or tau-bearing brain homogenates [7, 8]. However, none of the long-term transmission studies with A $\beta$  or tau-positive inocula provided evidence for pronounced cognitive decline or neurodegeneration [9]. Aged non-human primates can naturally develop  $\beta$ -amyloid lesions [10] and a long-term study in marmosets demonstrated induction of sparse  $\beta$ -amyloidosis 3.5 to 7 years post-inoculation, but there was no evidence of cognitive decline, neurodegeneration, functional Alzheimer's disease hallmarks, or other clinical signs [11]. This calls for additional clinical analysis in primates after inoculation with Alzheimer's disease brain homogenates.

Here, we used a multimodal approach, including non-invasive methods, to evaluate the impact of inoculation of human Alzheimer's disease-brain homogenates on both brain function and integrity in mouse lemur primates (*Microcebus murinus*). These small primates (body length: 12 cm; weight: 60–120 g) have a maximal lifespan of 12 years in our colony [12], although longer lifespans have been reported in some breeding colonies [13, 14], and are considered to be “old” after 6 years [12]. Mouse lemurs are widely used models to study human aging [15] since they display age-related alterations of their sensorial system, motor functions, biological rhythms, and immune and endocrine systems [12]. Their cerebral aging profile is similar to that of humans, as some can display age-related cognitive alterations associated with cerebral atrophy [16]. Like humans and other non-human primates, they are genetically heterogeneous, providing a natural diversity of aging profiles. In addition, genes associated with  $\beta$ -amyloidosis, such as amyloid precursor protein (APP), are similar in humans and mouse lemurs [17]. They can develop intracellular deposits of APP/A $\beta$  [18, 19], as well as  $\beta$ -amyloid plaques which can be detected in 25% of the animals over 8 years of age [20, 21], as well as tauopathy [21, 22]. Finally, their small size and reduced lifespan (compared to macaques) facilitates the creation of experimental cohorts to evaluate factors that modulate cerebral aging.

Human brain homogenates from Alzheimer's disease or control patients were inoculated in the brain of 12

adult mouse lemurs. We performed longitudinal cognitive assessments, electroencephalography (EEG), and morphological magnetic resonance imaging (MRI) studies up to 18 months post-inoculation (mpi), followed by immunohistopathological examination of brain tissues. In parallel, transgenic mice were also inoculated to assess the pathological potential of our homogenates. The inoculation of Alzheimer's disease-brain homogenates in primates induced an encephalopathy characterized by pronounced cognitive, functional, and morphological alterations, as well as neuronal loss. Most alterations were not seen 6 mpi but became evident at 12 mpi, ruling out immediate pathogenicity of the homogenates. Sparse  $\beta$ -amyloid and tau lesions were also detected in the brains of Alzheimer's disease-inoculated mouse lemurs at the inoculation sites and spreading from the inoculation sites could be highlighted in some animals, but these lesions were never detected in control animals. These results show that inoculation of Alzheimer's disease brain homogenates induces a pathology leading to cognitive impairments, clinical signs, neuronal loss and alteration of neuronal activity in a primate.

## Materials and methods

### Human brain samples

Frozen brain tissue samples (parietal cortex) from two Alzheimer's disease patients (Braak and Braak stage VI, Thal stages 5 and 4, respectively) and one control individual (Braak and Braak/Thal stages 0) were obtained from brains collected in a brain donation program of the GIE NeuroCEB Brain Bank run by a consortium of Patient Associations: ARSEP (French association for research on multiple sclerosis), CSC (cerebellar ataxias), France Alzheimer, and France Parkinson, with the support of the Fondation Plan Alzheimer and IHU A-ICM (Additional file 1: Table S1). The consent forms were signed by either the patients themselves or their next of kin in their name, in accordance with French bioethics laws. The GIE NeuroCEB Brain Bank has been declared at the Ministry of Higher Education and Research and has received approval to distribute samples (agreement AC-2013-1887).

These brain tissues were first assessed by immunohistochemistry. They were cut into 4- $\mu$ m-thick paraffin sections. Sections were deparaffinized in xylene, successively rehydrated through ethanol (100, 90, and 70%), and finally rinsed under running tap water for 10 min. They were then incubated in 99% formic acid for 5 min, washed again under running tap water, quenched for endogenous peroxidase with 3% hydrogen peroxide and 20% methanol, and finally washed in water. Sections were then blocked by incubating the sections at room temperature for 30 min in 4% bovine serum albumin (BSA) in 0.05 M tris-buffered saline, with 0.05% Tween

20, pH 8 (TBS-Tween, Sigma). They were then incubated overnight at +4 °C with the 6F3D anti-A $\beta$  antibody (Dako, Glostrup, Denmark, 1/200), polyclonal anti-tau antibody (Dako, Glostrup, Denmark, 1/500), and monoclonal anti-alpha-synuclein (LB509, Zymed, USA, 1/250) routinely used for the detection of  $\beta$ -amyloid, tau and alpha-synuclein deposits, respectively. The sections were further incubated with a biotinylated secondary antibody (25 min at room temperature), and the presence of the secondary antibody revealed by streptavidin–horseradish peroxidase conjugate using diaminobenzidine as chromogen (Dako, Glostrup, Denmark), after which they were counterstained with Harris hematoxylin.

#### Preparation of human brain homogenates and biochemical analysis

Parietal cortex samples were individually homogenized at 20% weight/volume (w/v) in a sterile 5% glucose solution (Virbac, Boulogne, France) in a ribolyser sample homogenizer (Hybaid, FastPrep FP120, Bio 101, Thermo Savant). Brain homogenates were then aliquoted into sterile polypropylene tubes and stored at –80 °C until use.

Brain homogenates were further characterized by biochemistry. For A $\beta$ , brain 20% homogenates were diluted in 6.8 M guanidine and 68 mM TrisHCl to obtain a final concentration of 5 M guanidine, protease inhibitor (Complete Mini, Sigma Aldrich, MO, USA) added, and vortexed for 3 h at room temperature. A $\beta$  immunoquantification was performed in duplicate with human A $\beta$ <sub>1–42</sub> ELISA kits (Invitrogen, Carlsbad, CA, USA) and A $\beta$ <sub>1–40</sub> ELISA kits (Invitrogen) according to the manufacturer's instructions. For tau characterization, brain homogenates were sonicated on ice for 5 min, centrifuged for 5 min at 3000  $\times$  g at +4 °C, diluted in 20 mM Tris/2% SDS and sonicated on ice for 5 min. Samples were diluted to 1  $\mu$ g/ $\mu$ L, diluted in 2X lithium dodecyl sulfate (LDS, Thermo Fisher Scientific, Villebon sur Yvette, France) buffer with reducers, and heated at +100 °C for 10 min. Ten  $\mu$ g of samples were loaded on Criterion gels (Biorad, Hercules, CA, USA) and migrated in MOPS buffer for 90 min at 165 V on ice. After protein transfer on nitrocellulose sheets, either pS396 (Life technologies, Carlsbad, CA, USA) or tau-Cter antibodies [23] were incubated overnight at +4 °C. A peroxidase coupled secondary anti-rabbit antibody (ref-23817-2, Biovalley, Nanterre, France) was then applied for 45 min at room temperature. Immunoblotting (or western blotting) was revealed by ECL. GAPDH (ref sc-25778, Santacruz, Nanterre, France) was used as a loading control. Operators were blinded to the status of the patients. Brain homogenates were also characterized for the presence of prion proteins by western blotting. Fragments from frontal cortex and

cerebellum were homogenized in an isotonic glucose solution. Scrapie-associated fibrils were purified after digestion by proteinase K. Polyacrylamide gel electrophoresis was performed and PrPres was evaluated with 3F4 (Signet, 0.04  $\mu$ g/ml) antibodies and revealed by electrochemoluminescence. Tau was characterized by western blotting using pS396 (Life technologies, Carlsbad, CA, USA) or tau-Cter antibodies [23]. Brain homogenates were also characterized for the presence of Prion proteins by western blotting according to protocols routinely used in the GIE NeuroCEB Brain Bank.

#### Ethical statement for animal experiments

All animal experiments were conducted in accordance with the European Community Council Directive 2010/63/UE. Animal care was in accordance with institutional guidelines and experimental procedures were approved by local ethical committees (authorizations 12–089; ethics committees CETEA-CEA DSV IdF N°44, France, and agreement APAFIS#2264–2015101320441671 from CEEA75, Lille, France).

#### Animals and overall experimental plan

Experiments were conducted on 12 middle-aged mouse lemurs (age = 3.5  $\pm$  0.2 years; males were used in the study as, in our colony, females are reserved for breeding). They were all born and bred in a laboratory breeding colony (UMR 7179 CNRS/MNHN, France; European Institutions Agreement #962773). Mouse lemurs were maintained at a constant temperature of 24–26 °C and relative humidity of 55% and were housed in individual cages with an enriched environment (jumping and hiding). Seasonal lighting (summer: 14 h of light/10 h of dark; winter: 10 h of light/14 h of dark) was applied to coincide with the seasonal rhythm of the animals. Their diet consisted of fresh apples and a homemade mixture of banana, cereals, eggs, and milk and animals had free access to tap water. Before entering the study, all animals were examined for health and given an ophthalmological examination. None of them were previously involved in pharmacological trials or invasive studies. The experiment was based on the inoculation of human brain homogenates from Alzheimer's disease patients (AD-inoculated group) or a control subject (CTRL-inoculated group) into the brains of mouse lemurs ( $n$  = 6 animals per group). Group assignments of the animals were performed to obtain two homogeneous groups based on pre-inoculation learning abilities. Longitudinal behavioral, EEG, and morphological MRI studies were performed up to 18 mpi, followed by immunohistopathological examinations of brain tissues (age at death = 5.0  $\pm$  0.2 years, Additional file 1: Table S2), with investigators blind to the group assignment when assessing these

outcomes. Five year-old mouse lemurs are considered middle-aged and they usually do not display cerebral atrophy,  $\beta$ -amyloid or tau lesions. We chose to inoculate young adults ( $3.5 \pm 0.2$  years) and to follow them during 18 months when they reached a middle-aged stage (age at euthanasia around 5 years) in order to avoid any drawback linked to aging that could affect cerebral atrophy and/or neuropathological status. Two control-inoculated animals were euthanized for ethical reasons at 12 mpi due to an abdominal infection following self-removal of abdominal sutures after wireless telemetry transmitter explantation. These animals were thus not evaluated by MRI at 12, 15, or 18 mpi or for behavioral studies at 18 mpi.

Mouse experiments were performed in eight-week-old APP/PS1<sub>ΔE9</sub> mouse model of  $\beta$ -amyloidosis ( $n = 21$ ) [24] and five-week-old Tau30<sup>+/+</sup> mouse model of tauopathy ( $n = 15$ ) [25]. The same brain homogenates as those used in lemurs were inoculated in the mice. APP/PS1<sub>ΔE9</sub> mice were followed-up for 4 months, while Tau30<sup>+/+</sup> mice were followed-up for 1 month before immunohistochemical examinations of their brains.

#### Stereotaxic injections in mouse lemurs

In mouse lemurs, brain homogenates were injected using stereotaxic surgery in four different sites surrounding the parietal cortex in order to spread the homogenates in wide brain regions. The 20% aliquoted homogenates were diluted to 10% (w/v) in sterile Dulbecco's phosphate-buffered saline (PBS, Gibco, ThermoFisher Scientific, France) extemporaneously. Six animals received brain extract from the control patient (CTRL-inoculated group) and six received brain extract from Alzheimer's disease patients ( $n = 3$  per patient, AD-inoculated group). Animals were fasted the day before surgery. Pre-anesthesia (atropine, 0.025 mg/kg, subcutaneous injection) was performed 30 min before anesthesia (Isoflurane, Vetflurane, 4.5% for induction and 1–2% for maintenance) as described previously [26]. Animals were then placed in a stereotaxic frame (Phymep, France). Burr holes were drilled 1.25 mm in front of the interaural axis. Using 26-gauge needles, 6.5  $\mu$ L of 10% w/v brain homogenates were injected bilaterally (L +/- 2.5 mm) 3 mm below the brain surface. Homogenates were inoculated at 1  $\mu$ L/min. Needles were kept in place for additional 2 min before they were slowly moved 2 mm above where bilateral injections were also performed (same volume and injection speed as described above). Needles were kept in place for additional 5 min before being slowly removed. Respiration rate was monitored during the entire procedure and body temperature was maintained at  $37 \pm 0.5$  °C with a heating blanket or air-heating system. The surgical area was cleaned before and after surgery (iodinate povidone, Vetedine, Vetoquinol, France), the incision sutured, and the animals were placed in an incubator at 25 °C and monitored until

recovery from anesthesia. Mouse lemurs were followed up to 18 months after inoculation (Additional file 1: Table S2).

#### Stereotaxic injections in mice

Control- or Alzheimer's disease-brain homogenates (prepared identically to those injected into the mouse lemurs) were injected bilaterally in the dorsal hippocampus (AP -2 mm, DV -2 mm, L +/- 1 mm [27]) of eight-week-old female APP/PS1<sub>ΔE9</sub> mice ( $n = 21$ ) and five-week-old Tau30<sup>+/+</sup> mice ( $n = 15$ ) of both sexes. Mice were randomly assigned to control- (APP/PS1<sub>ΔE9</sub>:  $n = 6$  and Tau30<sup>+/+</sup>:  $n = 5$ ) or Alzheimer's disease-inoculated groups (APP/PS1<sub>ΔE9</sub>:  $n = 6$  and 9 per patient, Tau30<sup>+/+</sup>:  $n = 5$  per patient). They were anaesthetized by intraperitoneal ketamine-xylazine injection (Imalgène 1000, Merial, France (1 mg/10 g); 2% Rompun, Bayer Healthcare, Leverkusen, Germany (0.1 mg/10 g)) and placed in a stereotaxic frame (Phymep, France). Respiration rate was monitored and body temperature was maintained at  $37 \pm 0.5$  °C with a heating blanket during surgery. After making a midline incision of the scalp, burr holes were drilled in the appropriate location. Bilateral intrahippocampal injections of 2  $\mu$ L 10% brain homogenates were performed with a 26-gauge needle. The surgical area was cleaned before and after surgery (iodinate povidone, Vetedine, Vetoquinol, France), the incision sutured, and the animals placed in an incubator (temperature 25 °C) and monitored until recovery from anesthesia.

#### Behavioral evaluations

##### Accelerating rotarod task

Mouse lemurs were evaluated with the accelerating rotarod task (model 7750, Ugo Basile, Italy) before inoculation and every 6 mpi. Animals were placed on a 5-cm-diameter rotating cylinder turning at 20 rotations per minute (rpm). The rod then accelerated steadily up to 40 rpm until the end of the test, which was reached when the animal fell or gripped onto the rod during at least three consecutive turns without stabilizing its balance. Latency to fall off or grip the rod was recorded for each trial. Animals underwent five consecutive trials and the best result was recorded with values expressed in seconds. The apparatus was cleaned with ethanol between each trial and each animal.

##### Visual discrimination test

The cognition of mouse lemurs was evaluated in an apparatus (Additional file 2: Figure S1a) adapted from the Lashley jumping stand apparatus [28], which is a vertical cage made of plywood walls, except for the front panel, which is a one-way mirror allowing observation. Two discrimination tasks were performed: a learning task and a long-term memory task. These tests involved a succession

of visual discrimination tasks during which the mouse lemur had to jump from a heightened central platform to one of two lateral boards, one of which allowed access to a reinforcing chamber containing a positive reward (the possibility of reaching a safe nestbox for a 2-min rest). As mouse lemurs prefer confined spaces, reaching a nest when placed in an open space is a strong motivator for behavioral testing. If no jump is performed within 1 min, the central station can be progressively and gently tilted downwards creating a slippery slope, encouraging the mouse lemur to jump. Boards can be covered with removable and easily-discriminable patches of varied shape, texture, and pattern (i.e. visual discrimination clues). Each board can be locked in a stable position or unlocked to become unstable and fall if a lemur jumps on it. For a pair of patches, one is always associated with the stable board, giving access to the nest (positive result), and the other with the unstable board that falls when the lemur jumps on it (negative result). During a discrimination task, the mouse lemur had to identify the positive stimulus which signaled access to the nest. Left/right locations of the stimuli were randomly alternated during the attempts with the restriction of no more than three consecutive trials in the same configuration. Testing continued until a success criterion - defined as eight correct choices out of 10 successive attempts - was achieved. Before the first test, lemurs underwent a habituation session composed of seven trials. For the first four trials, only one fixed central board was attached just below the nestbox opening. In trial 1, a cylindrical rod connected the central station to the board so that no jump was required to reach the nestbox. In trial 2, the rod was removed so that the mouse lemur had to jump onto the central board to access the nestbox. In trials 3 and 4, an opaque vertical screen was added above the middle of the board masking the nestbox opening. The mouse lemur had to jump onto the board and then walk under the screen to access the nestbox. For the final three trials, the fixed landing platform was placed alternately to the left or right of the nestbox opening which was masked by the opaque screen. After the habituation session, mouse lemurs underwent the first discrimination learning task - distinguishing between a pair of patches - to test their learning abilities. This task was performed before inoculation and then at 6, 12, and 18 mpi with a new set of discrimination task stimuli each time (i.e. a new pair of patches). Long-time retention was also evaluated at the three post-inoculation time points through recall of the discrimination task from 6 months prior (Additional file 2: Figure S1b).

#### **Electroencephalography (EEG)**

EEG studies were conducted in mouse lemurs using telemetric devices as described before [29, 30]. Animals received pre-anesthesia (5 mg/mL Diazepam, Roche, France,

intramuscular injection of 200  $\mu$ L/100 g) and were then anesthetized with isoflurane. A wireless telemetry transmitter (2.5 g, PhysioTel F20-EET, Data Science, St Paul, MN, USA), equipped with simultaneous recording for one EEG and one electromyogram (EMG) channel (1–500 Hz sampling rate), was implanted in the abdominal cavity. The electrode leads were threaded subcutaneously from the abdomen to the skull. Electrodes were placed on the dura mater of the anterior frontal cortex according to a stereotaxic atlas of the mouse lemur brain and secured using dental cement [31]. The frontal cortex, and not the parietal cortex in which brains homogenates were inoculated, was chosen for this evaluation to focus on the impact of the brain homogenate inoculation on cerebral networks, including those distant from the inoculation site. For EMG recording, bipolar electrodes were sutured into the neck muscles using non-absorbable polyamide sutures. Animals were monitored for respiration rate and body temperature during surgery, observed until anesthesia recovery, and allowed to recover from surgery for 1 week before recording. EEG and EMG data were continuously collected using PC running Dataquest software (Data Science International, St Paul, MN, USA) linked to a receiver base (RPC-1, Data Science, St Paul, MN, USA), placed on the floor of the home cage inhabited by the implanted animals. Electrodes and the telemetry transmitter were removed after 1 week of recording under the same surgical conditions as for implantation. The EEG data were analyzed with Neuroscore v2.1.0 (Data Science International, St Paul, MN, USA). Analysis focused on the active state, determined by locomotor activity recording (included in the telemetry data of EMG recordings). EEGs were performed before inoculation and 6 and 12 mpi. We focused on delta (0.5–4 Hz), theta (4–8 Hz), alpha (8–12 Hz), sigma (12–16 Hz), and beta (16–24 Hz) frequency waves. At each time point, each wave was normalized according to mean values of the control-inoculated animals. The operator was blinded to the group attribution during EEG signal processing.

#### **Morphological MRI**

Brain images were recorded on a 7.0 Tesla spectrometer (Agilent, USA) using a four-channel phase surface coil (RapidBiomedical, Rimpar, Germany) actively decoupled from the transmitting birdcage probe (RapidBiomedical, Rimpar, Germany). Two-dimensional fast spin-echo images were recorded with an isotropic nominal resolution of 230  $\mu$ m (128 slices, TR/TE = 10000/17.4 ms, rare factor = 4; field of view = 29.4  $\times$  29.4 mm<sup>2</sup>, matrix = 128  $\times$  128, slice thickness = 230  $\mu$ m, acquisition time = 32 min). MR images were zero-filled to reach an apparent isotropic resolution of 115  $\mu$ m. Animals were anesthetized and monitored as described for stereotaxic injections. MR images were recorded for each animal before

inoculation, 15 days after inoculation and then every 3 months until 18 mpi.

Images were analyzed using voxel-based morphometry by applying SPM8 (Wellcome Trust Institute of Neurology, University College London, UK, [www.fil.ion.ucl.ac.uk/spm](http://www.fil.ion.ucl.ac.uk/spm)) with the SPMouse toolbox (<http://spmmouse.org>) for animal brain morphometry [32]. Fifteen-day post-inoculation images were not included in this analysis, as they were only used to ensure accurate injection cannula placement and the lack of acute lesions following surgery.

The brain images were segmented into gray (GM) and white matter (WM) tissue probability maps using locally developed priors, then spatially transformed to the standard space, defined by Sawiak et al., using a GM mouse-lemur template [32]. Affine regularization was set for an average-sized template, with a bias non-uniformity FWHM cut off of 10 mm and a 5 mm basis-function cut off and sampling distance of 0.3 mm. The resulting GM and WM portions were output in rigid template space, and DARTEL [33] was used to create non-linearly registered maps for each subject and common templates for the cohort of animals. The warped GM portions for each subject were adjusted using the Jacobian determinant from the DARTEL registration fields to preserve tissue amounts (“optimized VBM” [34]) and smoothed with a Gaussian kernel of 600 μm to produce maps for analysis.

A general linear model was designed to evaluate relative changes in GM values as a function of time between the control- and Alzheimer’s disease-inoculated groups. Longitudinal follow-up of each animal was considered in the design matrix, and total intracranial volumes were treated as covariates of no interest. This type of analysis produces t-statistic and color-coded maps that are the product of a statistical analysis performed at every voxel in the brain. Contiguous groups of voxels that attain statistical significance, called clusters, are displayed on brain images.

With the general linear model, if the brain of one animal is defined by the number “j”, and the location of a pixel is defined as “k”. The signal within a pixel ( $Y_j^k$ ) can be explained by the following equation

$$Y_j^k = x_{j,1}\beta_1^k + x_{j,2}\beta_2^k + T_j^1\beta_3^k + T_j^2\beta_4^k + \dots + T_j^6\beta_8^k + T_j^7\beta_9^k + \dots + T_j^{12}\beta_{14}^k + TIV_j\beta_{15}^k + \epsilon_j^k$$

With  $\beta_1^k$  = Alzheimer’s disease brain inoculation effect ( $n = 42$  images);  $\beta_2^k$  = control brain inoculation effect ( $n = 36$  images);  $\beta_3^k$  = Longitudinal follow-up for Alzheimer’s disease-brain inoculated animal #1 ( $n = 7$  values, i.e. at 0, 3, 6, 9, 12, 15, and 18 mpi);  $\beta_4^k$  = Longitudinal follow-up for Alzheimer’s disease-

brain inoculated animal #2 ( $n = 7$  values, i.e. at 0, 3, 6, 9, 12, 15, and 18 mpi);...;  $\beta_8^k$  = Longitudinal follow-up for Alzheimer’s disease-brain inoculated animal #6;  $\beta_9^k$  = Longitudinal follow-up for control animal #1;...;  $\beta_{14}^k$  = Longitudinal follow-up for control animal #6; ...;  $\beta_{15}^k$  = total intracranial volume (TIV) for each animal. The Alzheimer’s disease-brain inoculation effect is defined by  $x_{j,1}\beta_1^k$  and the control-brain inoculation effect is defined by  $x_{j,2}\beta_2^k$ . Thus, if the image corresponds to an Alzheimer’s disease-inoculated animal,  $x_{j,1} = 1$  and  $x_{j,2} = 0$ , if the image corresponds to a control-inoculated animal,  $x_{j,1} = 0$  and  $x_{j,2} = 1$ .  $T_j^x$  is the time post-inoculation for each animal  $x$ . Otherwise,  $T_j^x = 0$ . TIV corresponds to the total intracranial volume value for each animal. It was similar for the different images from the same animal followed-up longitudinally. The term  $\epsilon_j^k$  corresponds to the “error” of the measure for each animal.

As an example, on the basis of this model, for image 1 of animal 1 (Alzheimer’s disease group, image before inoculation ( $T_1^1 = 1$ )):  $Y_1^k = \beta_1^k + 1\beta_3^k + TIV_1\beta_{15}^k + \epsilon_1^k$ ; for image 2 of animal 1 (Alzheimer’s disease group, image at 3 mpi ( $T_2^1 = 3\text{ months} = 92$  days)):  $Y_2^k = \beta_1^k + 92\beta_3^k + TIV_2\beta_{15}^k + \epsilon_2^k$ ; for image 3 of animal 1 (Alzheimer’s disease group, image at 6 mpi ( $T_3^1 = 6\text{ months} = 183$  days)):  $Y_3^k = \beta_1^k + 183\beta_3^k + TIV_3\beta_{15}^k + \epsilon_3^k$  ... for image 1 from animal 7 (control group image before inoculation ( $T_{43}^7 = 1$ )):  $Y_{43}^k = \beta_2^k + 1\beta_9^k + TIV_{43}\beta_{15}^k + \epsilon_{43}^k$ ; for image 2 of animal 7 (control group image at 3 mpi ( $T_{44}^7 = 3\text{ months} = 92$  days)):  $Y_{44}^k = \beta_2^k + 92\beta_9^k + TIV_{44}\beta_{15}^k + \epsilon_{44}^k$ .

A contrast defines a linear combination of  $\beta$  as  $c^T\beta$ . For example, the test evaluating whether the probability of pixels from animals inoculated with Alzheimer’s disease-brains to be GM is lower than that for control-brain inoculated animals is defined using a contrast  $c^T\beta = \{-1\ 1\ 0\ \dots\}^T$ . The Null hypothesis is  $H_0 : c^T\beta = 0$ , whereas the alternative hypotheses is  $H_1 : c^T\beta > 0$ . This hypothesis is tested with:

$$T = \frac{c^T\beta}{\sqrt{\sigma^2 c^T (X^T X)^{-1} c}} = \frac{\text{contrast}}{\sqrt{\text{estimated variance}}}$$

This analysis allows the removal of confounding effects, such as repetition of the measures during longitudinal evaluation of the same animal (i.e.  $\beta_3^k, \beta_4^k, \dots, \beta_8^k, \beta_9^k, \dots, \beta_{14}^k$ ) or TIV ( $\beta_{15}^k$ ) from the raw data. In other words, volumetric scans were entered as the dependent variable. The treatment groups of the animals (Alzheimer’s

disease or control-brain inoculation) were the independent variables. Longitudinal follow-up effect and TIV were covariates.

One-tailed t-test contrasts were set up to find areas in which probability values from GM maps were different in Alzheimer's disease and control-brain inoculated animals (i.e.  $c^T\beta = \{-1\ 1\ 0\dots\}^T$  or  $\{1\ -1\ 0\dots\}^T$  contrasts). To control for multiple comparisons, an adjusted  $p$ -value was calculated using the voxel-wise false discovery rate (FDR-corrected  $p < 0.05$ ), with extent threshold values of 10 voxels, meaning that clusters required 10 contiguous voxels to be selected as relevant [35]. Voxels with a modulated GM value below 0.2 were not considered for statistical analysis. The operator was blinded to the group attribution during image processing.

The rate of atrophy evolution over time was then further evaluated based on changes of the Jacobian determinant. More specifically, the change in the Jacobian determinant was calculated for each subject relative to baseline and averaged groups, yielding mean volume changes from baseline to time  $t$  post-inoculation of  $\Delta\bar{J}^{AD}(t)$  and  $\Delta\bar{J}^{CTRL}(t)$  for Alzheimer's disease- and control-inoculated groups, respectively. Subtracting these highlighted voxels showing differential atrophy between groups at each stage. We evaluated differences in atrophy over the first 6 months, further atrophy that occurred from six to 12 months, and later atrophy occurring from 12 to 18 months: i.e.  $\Delta\bar{J}^{AD}(6) - \Delta\bar{J}^{CTRL}(6)$ ,  $(\Delta\bar{J}^{AD}(12) - \Delta\bar{J}^{CTRL}(12)) - (\Delta\bar{J}^{AD}(6) - \Delta\bar{J}^{CTRL}(6))$  and  $(\Delta\bar{J}^{AD}(18) - \Delta\bar{J}^{CTRL}(18)) - (\Delta\bar{J}^{AD}(12) - \Delta\bar{J}^{CTRL}(12))$ .

### **Immunohistochemistry and biochemistry**

Five mouse lemurs from each group were studied by immunohistochemistry. The last animal from each group was not evaluated by immunohistochemistry as its brain was sampled for future inoculations in new cohorts of animals (second passages). All mice were included in immunohistochemical analyses. Each animal studied by immunohistochemistry was euthanized with an overdose of sodium pentobarbital (100 mg/kg intraperitoneally) followed by intracardiac perfusion with 4% paraformaldehyde in PBS. After overnight post-fixation, brains were cryoprotected using 15 and 30% sucrose solutions. Brain coronal sections (40- $\mu$ m-thick) were cut on a sliding freezing microtome (SM2400, Leica Microsystems). Twenty series of sections were performed. The floating histological serial sections were preserved in a storage solution (30% glycerol, 30% ethylene glycol, 30% distilled water, and 10% phosphate buffer) at  $-20^\circ\text{C}$  until use.

Serial sections of the entire brains of mouse lemurs were used for A $\beta$  (4G8), tau (AT8, MC1, and AT100), glial fibrillary acidic protein (GFAP), and neuronal

nuclei (NeuN) using immunohistochemistry. One series of sections (i.e. one section every 20th sections, which represents approximately 12 sections) was used for each staining, except for NeuN that used 4 series (i.e. one section every 5th sections). Monoclonal antibody AT8 (Thermo Scientific MN1020B, USA) recognizes phosphorylated residues serine 202 and threonine 205 of Tau. The monoclonal antibody AT100 (Thermo Scientific MN1060, USA) recognizes phosphorylated residues threonine 212 and serine 214 of Tau. The monoclonal antibody MC1 was a generous gift from Peter Davies and recognizes conformational changes in residues seven to nine and 313–322. Human sections were used as positive controls. Free-floating sections were rinsed in 0.1 M PBS and incubated in 0.3% hydrogen peroxide for 20 min. For 4G8 staining, sections were pre-treated with 80% formic for 2 min. Pre-treatment with PBS - Triton 0.5% (Triton X-100, Sigma Aldrich, MO, USA) and 3% bovine serum albumin (BSA) blocking was performed at  $+4^\circ\text{C}$  for 30 min before a 2 day-incubation with either biotinylated 4G8 (Covance, NJ, USA, 1/250), GFAP (Dako, Denmark, 1/5000), or NeuN (Abcam, Cambridge, UK, 1/2000) antibodies. Sections stained for tau lesions were pre-treated with 1x Citrate Buffer, in a  $100^\circ\text{C}$  water bath for 30 min for antigen unmasking. Then they were processed with PBS - Triton 0.2% (Triton X-100, Sigma Aldrich, MO, USA) and 10% normal goat serum (NGS) 10% blocking at  $+4^\circ\text{C}$  for 1 h before a 3 day-incubation at  $4^\circ\text{C}$  with AT8 (1/500 in PBS - Triton 0.2% and NGS 5%), MC1 (1/500 in PBS - Triton 0.2% and NGS 5%) or AT100 (1/200 in PBS - Triton 0.2% and NGS 5%). Sections were incubated in biotinylated anti-mouse or anti-rabbit secondary antibodies (IgG, Vector Laboratories, Burlingame, CA, USA) in PBS - Triton 0.2% for 1 h before revelation. The ABC Vectastain kit (Vector Laboratories, Burlingame, CA, USA) was used to amplify DAB revelation (DAB SK4100 kit, Vector Laboratories, Burlingame, CA, USA). Sections stained for Tau were also counterstained with cresyl violet for 45 s or counterstained with Olig2 (Millipore AB9610, USA, 1/500) to detect oligodendrocytes. Images of stained serial sections were digitized with an Axio ScanZ.1 slide scanner (Zeiss, Jena, Germany) at X20 (0.22  $\mu$ m in plane resolution). The scanned files were exported as jpeg RGB images with a 30% compression (0.73  $\mu$ m in plane resolution) using Zen 2.0 (Zeiss, Jena, Germany).

Quantification of intracellular APP/A $\beta$  deposits was performed blind using 4G8 stained-sections and ImageJ 1.52b (<https://imagej.nih.gov/ij/>). Briefly, 4G8-positive objects were segmented using the same threshold for each animal. Then masks were created to exclude brain

vessels from parenchyma. Overlap between 4G8-positive objects and these masks was used to evaluate 4G8-positive staining either in brain parenchyma (ImageJ ROI manager and analyze particles function). Three brain regions (caudate nucleus, putamen, and hippocampus) were studied. Quantification of GFAP-stained sections was blindly performed using ImageJ 1.52b. Each structure (frontal cortex, entorhinal cortex, amygdala, hippocampus, posterior cingulate, and retrosplenial cortices) was manually defined for both hemispheres. GFAP staining density was evaluated as relative optical density ( $\log(255/(255-\text{GFAP gray level}))$ ) in each structure.

Microglial reaction was further evaluated in mouse lemurs by Western blot analysis. Proteins were extracted from two floating brain sections from each mouse lemur, taken at the level of the inoculation site (Qproteome FFPE – Tissue Extraction Buffer, Qiagen). Extracted total proteins were detected by immunoblotting using SDS-PAGE (Criterion TGX Stain-Free Precast Gel 4–20%, Bio-Rad), UV activation, nitrocellulose membrane transfer (Trans-Blot Turbo RTA Transfer Kit, Bio-Rad) and by blotting with anti-Iba1 rabbit polyclonal antibody (Wako, 1:1000) followed by anti-rabbit secondary antibody (Invitrogen, 1:5000) and by Clarity Western ECL chemiluminescence revelation (Bio-Rad). Proteins were migrated together with a molecular weight marker (Precision Plus Protein Standards Unstained, Bio-Rad) ranging from 10 to 250 kD. Images of the blots were digitized with a ChemiDoc Imaging System (Bio-Rad) and quantified with the Image Lab Software 5.2.1 (Bio-Rad).

Serial sections of the entire brain of APP/PS1 $_{\Delta E9}$  mice were stained for the evaluation of A $\beta$  pathology, as well as inflammation (Iba1 and GFAP). Brain sections were rinsed with PBS, and then incubated in 0.3% hydrogen peroxide for 20 min. Sections were then blocked with PBS-0.5% Triton (Triton X-100, Sigma, St Louis, MO, USA) and 4.5% normal goat serum (NGS) for 30 min before overnight incubation with BAM10 (Sigma, A3981, 1/10,000), Iba1 (Wako, VA, USA, /1000), or GFAP (Dako, Denmark, 1/10000) antibodies at 4 °C. Sections were rinsed with PBS and then successively incubated with 1/1000 anti-mouse IgG secondary antibody (BA-9200; Vector Labs) at room temperature for 1 h and ABC Vectastain (Vector Labs) before DAB revelation (DAB SK4100 kit, Vector Labs). Images of stained sections were digitized with a Zeiss Axio Scan.Z1 (Zeiss, Jena, Germany) whole slide imaging microscope at X20 (0.22  $\mu\text{m}$  in plane resolution). The scanned files were exported as jpeg RGB images with a 30% compression (0.73  $\mu\text{m}$  in plane resolution) using Zen 2.0 (Zeiss, Jena, Germany). Sections stained for A $\beta$  were blindly analyzed and A $\beta$  in the hippocampus quantified using ImageJ software [36]. Segmentation of

$\beta$ -amyloid deposits was performed in two sections corresponding to AP -1.70/– 2.30 mm [27]. It was based on the determination of a threshold defined as  $T = M_{\text{signal}} + 10 \times SD_{\text{signal}}$ , where  $M_{\text{signal}}$  and  $SD_{\text{signal}}$  represent the mean and standard deviation of the signal within a CA1 region of interest in which  $\beta$ -amyloid deposits were not visible.

Neuroinflammation was blindly evaluated after manual adjustment of a threshold adjusted to select the stained microglial and astroglial cells. Their load was quantified by densitometry in the inoculated brain region (CA1) using Explora Nova Mercator.

Brains sections from tau30 $^{+/+}$  mice were stained with anti-AT8 antibodies. Serial sections from the entire brain were washed in PBS-0.2% Triton and treated for 30 min with H $_2$ O $_2$  (0.3%). Non-specific binding was then blocked using the MOM kit (Vector MKB2213) (1/100 in PBS, Vector) for 60 min. Incubation with AT8 (Thermo Scientific MN1020, 1/500) in PBS-0.2% Triton was performed overnight at 4 °C. After several washes, labelling was amplified by incubation with an anti-mouse biotinylated IgG (1/400 in PBS-0.2% Triton, Vector) for 60 min followed by the application of the ABC kit (1:400 in PBS, Vector) prior to visualization with 0.5 mg/ml DAB (Vector) in 50 mmol/L Tris-HCl, pH 7.6, containing 0.075% H $_2$ O $_2$ . Brain sections were mounted onto gelatin-coated slides, stained for 1 min in a cresyl violet solution (0.5%), washed in water containing 2% acetic acid, dehydrated by passage through a graded series of alcohol and toluene solutions and mounted with Vectamount (Vector) for microscopic analysis. Images were digitized with a Zeiss Axio Scan.Z1 (Zeiss, Jena, Germany) whole slide imaging microscope at X20 (0.22  $\mu\text{m}$  in plane resolution). The density of AT8-positive cell-soma profiles in the hippocampus was evaluated in two sections corresponding to AP -1.70/– 2.30 mm [27]. AT8-positive cell soma were manually counted (“PointPicker” tool from ImageJ [36]) and expressed as the total number of AT8-positive cell soma profiles visible in the dorsal hippocampus.

#### **Stereological counting of NeuN-positive neurons**

The optical fractionator method [37, 38] was used to obtain an unbiased stereological estimate of the total number of NeuN-positive cells in the CA1/2 and CA3 layers of the hippocampus, layers I, II, and III-VI of the entorhinal cortex, and the cingulate/retrosplenial cortex. Measurements were performed on the left hemisphere of the brain. Cells were counted using a Leica DM6000 microscope equipped with a digital color camera (MicroFireTM, Optronics, Goleta, CA, USA), an x-y motorized stage controller, a motorized z-axis, and Mercator stereology software (Explora Nova, La Rochelle, France). The regions were

delineated using a 4X objective in accordance with the mouse lemur brain atlas [31]. Section thickness (from 11 to 13  $\mu\text{m}$ ) was measured at three locations for each section analyzed. Sampling was performed unilaterally within the delineated areas with a 40X oil-immersion objective. Counting frames were adapted for each brain region, and areas of the counting frames (a/f) were  $30 \times 30 \mu\text{m}^2$  to  $100 \times 100 \mu\text{m}^2$ , depending on the brain region, while sampling areas were separated by x-y steps of 50–50  $\mu\text{m}$  to 150–150  $\mu\text{m}$ , depending on the brain region. The fraction of the section plane sampled (ASF) was calculated as the ratio (a/f)/(x\*y) (Additional file 1: Table S3). Disector height was 10  $\mu\text{m}$  with a guard zone of 1  $\mu\text{m}$  from the surface of the section generating counts of 90–2500 sampled cells per animal, depending on the structure, and the mean coefficient of error (CE) of the estimates was 0.06 (Additional file 1: Table S3). The total number of NeuN-positive cells within each region was calculated according to the following formula:  $N_{\text{tot}} = \Sigma Q^- \times 1/SSF \times 1/ASF \times 1/TSF$ , in which  $\Sigma Q^-$  is the number of sampled cells and SSF is the section sampling fraction. One out of ten sections was sampled, leaving 200  $\mu\text{m}$  intervals between two sampled sections. ASF is the area of the sampling fraction and TSF the thickness of the sampling fraction. Values of SSF, ASF, and TSF for each region are given in Additional file 1: Table S3. All histological data (surface, volume measurements, and cell counts) were performed by an investigator (SL) blind to the group assignment of the animals.

### Statistical analysis

Statistical analyses were performed using GraphPad Prism software (San Diego, CA, USA). In most graphics, data are shown as scatter plots with median and interquartile interval. Control-inoculated animals, as well as animals inoculated with each Alzheimer brain homogenates are displayed with different color codes. Behavioral studies are not displayed as scatter plots but as mean  $\pm$  standard deviation (SD) to represent cognition evolution over time. Cognitive and motor experiments were evaluated by two-way repeated measures ANOVA (post-inoculation delay, group) followed by Bonferroni's multiple comparisons post-hoc tests. Data normality and variance homogeneity were evaluated using Shapiro-Wilk and Cochran C tests, respectively, and data from behavioral experiments were reciprocally transformed to obtain normality and variance homogeneity. The values within control-inoculated animals were highly homogeneous for each post-inoculation time. We thus replaced missing data for 18 mpi from the two control-inoculated mouse lemurs that died with the worst values in the control-inoculated group at 18 mpi. EEG, neuronal counts and intracellular  $\beta$ -amyloid load in mouse lemurs, and  $\beta$ -amyloid, tau and inflammation in

mice were evaluated by Mann-Whitney tests. Spearman's rank correlations were performed to examine relationships between EEG and behavioral data. The proportion of mouse lemurs with  $\beta$ -amyloid lesions in the control- and Alzheimer-inoculated groups was compared using the Chi-square test. No statistical methods were used to pre-determine sample size. Sample size to compare control and Alzheimer-inoculated mice and mouse lemurs in future studies was estimated on the basis of the experimental results obtained during the current experiments assuming a significance level of 5%, a power of 80% and two-sided tests. Estimations for quantitative values used a two-sample t-test on the basis of the mean and standard deviation obtained for the different measures in this study (BiostaTGV module, <https://biostatgv.sentiweb.fr/?module=etudes/sujets#>). The standard deviation used for this estimation was the square root of the pooled variance from each group. Estimations for proportional values (proportion of lemurs with A $\beta$ , CAA or Tau in the brain) were based on a chi-squared test (BiostaTGV module based on epiR package 0.9–9.6, <https://biostatgv.sentiweb.fr/?module=etudes/sujets#>).

## Results

### Characterization of human brain samples and homogenates

Frozen brain tissue samples (parietal cortex) from two Alzheimer's disease patients (Braak and Braak stage VI, Thal stages 5 and 4, respectively) and one control individual (Braak and Braak/Thal stages 0) were used in the current study. The brains of the Alzheimer's disease patients displayed typical lesions ( $\beta$ -amyloid plaques and tau tangles) while no lesions were found in the control subject (Additional file 3: Figure S2a-h). One Alzheimer case (AD1) displayed  $\beta$ -amyloid angiopathy in addition to  $\beta$ -amyloid plaques while the second Alzheimer patient (AD2) did not display angiopathy (Additional file 3: Figure S2a-d). Immunohistochemical staining for alpha-synuclein was negative for all brain samples. Biochemical analysis revealed high A $\beta_{1-42}$  and A $\beta_{1-40}$  levels only in Alzheimer's disease-brain homogenates (Additional file 3: Figure S2i-j). AD1 displayed higher A $\beta_{1-40}$  and lower A $\beta_{1-42}$  levels than AD2 (Additional file 3: Figure S2i-j). Western blotting showed a typical shift in the molecular weight of the Alzheimer tau-Cter triplet [23] and the presence of pathological pS396 tau only in Alzheimer samples (Additional file 3: Figure S2k-l). All brain samples were negative for presence of Prion proteins assessed by western blotting (Additional file 4: Figure S3).

### Alzheimer's disease brain inoculation effectively induces $\beta$ -amyloid and tau lesions in transgenic mice

Prior to being used in mouse lemurs, the Alzheimer's disease and control brains were inoculated in the



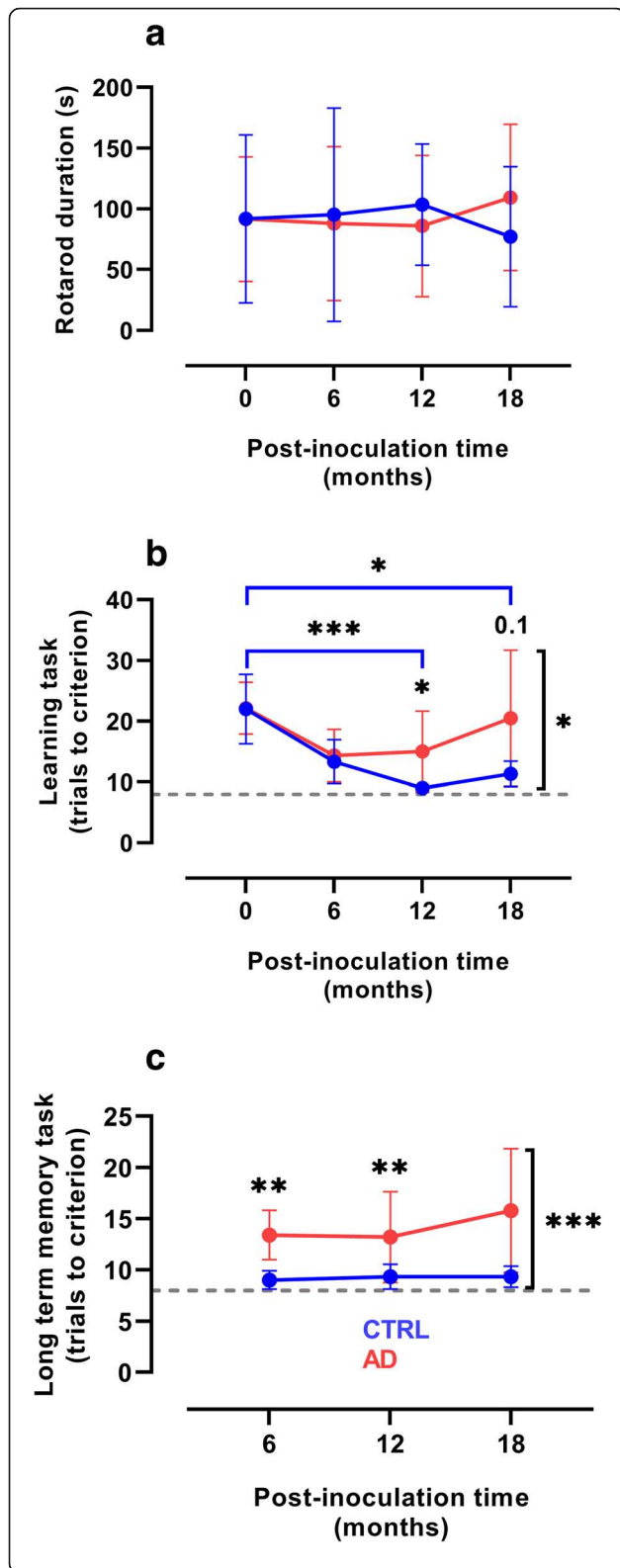


**Fig. 1** Cognitive dysfunction in Alzheimer-inoculated mouse lemurs. **a** The rotarod test did not reveal any motor dysfunction in either Alzheimer- (AD) or control- (CTRL) inoculated group. **b** Progressive learning impairment in the animals of the Alzheimer-inoculated group. Animals allocated to Alzheimer- and control- inoculated groups performed similarly before inoculation and improved similarly up to 6 mpi. Only the control-inoculated group continued to improve at 12 and 18 mpi ( $p < 0.0001$  and  $p = 0.01$ , respectively). Learning abilities were also lower in the Alzheimer-inoculated group than in the control-inoculated group at 12 mpi ( $p = 0.03$ ) and tended to be lower at 18 mpi ( $p = 0.10$ ). The overall performance of the Alzheimer-inoculated group was significantly worse than that of the control-inoculated group ( $p = 0.02$ ). **c** The overall performance of the Alzheimer-inoculated group in the long-term memory task at 6 and 18 mpi was significantly worse than that of control animals ( $p = 0.0002$ ,  $0.0036$ , and  $0.0024$ , respectively). \* $p < 0.05$ ; \*\* $p < 0.01$ ; \*\*\* $p < 0.001$  ( $n = 6$  per group, two-way repeated measures ANOVA with Bonferroni's post-hoc tests). Plots presents mean  $\pm$  standard deviation. Dashed lines in **(b, c)** indicate the best possible scores

deposition in APP/PS1<sub>DE9</sub> and Tau30<sup>+/+</sup> mice ( $p = 0.009$  and  $p = 0.0007$ , respectively, Additional file 5: Figure S4a-f). Within the Alzheimer group, the  $\beta$ -amyloid load was higher in the mice inoculated with the brain presenting with  $\beta$ -amyloid angiopathy as compared to the mice inoculated with the brain without angiopathy ( $p = 0.01$ ). No difference was detected for tau lesions. This experiment confirmed the ability of the Alzheimer's disease brain homogenates to induce transmission of Alzheimer's disease-related lesions in mice.

#### Alzheimer's disease brain inoculation induces cognitive alterations in mouse lemurs

Following the mouse studies, 12 adult mouse lemurs were inoculated with the same Alzheimer's disease and control human brain homogenates. Motor functions, assessed with a rotarod test were similar in both groups (Fig. 1a). Cognitive evaluation was performed every 6 months in a jumping-stand apparatus [28] (Additional file 2: Figure S1a) and consisted of two tasks (Additional file 2: Figure S1b). The first was a learning task that rated visual discrimination acquisition abilities, whereas the second was a long-term memory task that assessed retention of the discrimination problem learned 6 months before. Before brain homogenate inoculation, animals assigned to Alzheimer- and control-inoculated groups performed similarly in the learning task (Fig. 1b). Animals from both groups showed similar improvement in their learning abilities 6 months after inoculation (Fig. 1b). However, performance then diverged with control-inoculated animals further improving at 12 mpi, until reaching the best possible scores (thus demonstrating learning set acquisition), whereas the Alzheimer-inoculated group progressively worsened at both 12 and 18 mpi, with overall performance significantly

hippocampus of APP/PS1<sub>DE9</sub> and Tau30<sup>+/+</sup> mouse models of  $\beta$ -amyloid and tau lesions. Alzheimer's disease brain homogenates led to increased A $\beta$  and tau

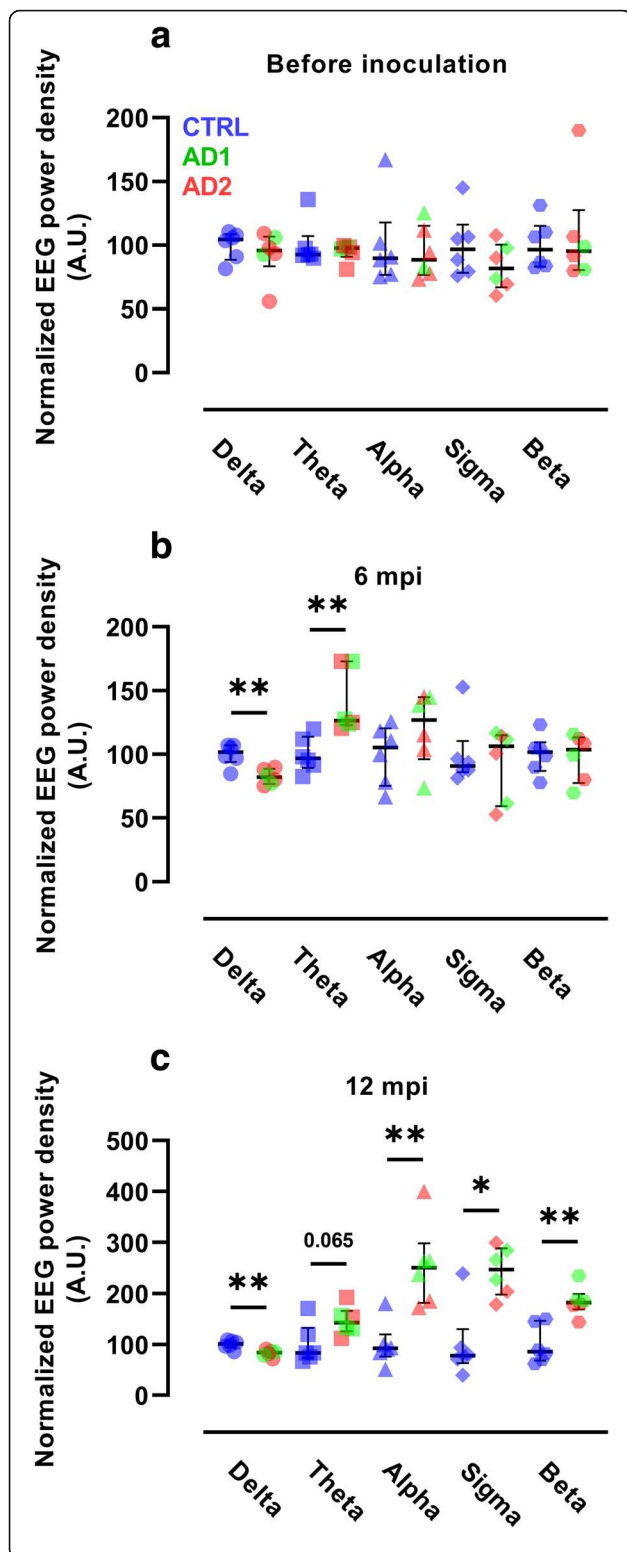


**Fig. 2** Neuronal activity alterations in Alzheimer-inoculated mouse lemurs. Evolution of EEG frequency power densities in the Alzheimer- (AD) and control- (CTRL) inoculated groups before inoculation (**a**), and 6 (**b**) and 12 (**c**) mpi ( $n = 6$  per group). **a** EEG frequency power densities were similar in the two groups before inoculation. **b** At 6 mpi, the Alzheimer-inoculated group showed a lower delta frequency (0.5–4 Hz) and a higher theta frequency (4–8 Hz) than the control-inoculated group ( $p = 0.009$  and  $p = 0.002$ , respectively, Mann-Whitney tests). **c** At 12 mpi, the alterations in delta frequency were maintained ( $p = 0.009$ , Mann-Whitney test). In addition, alpha (8–12 Hz), sigma (12–16 Hz), and beta (16–24 Hz) frequencies were higher in the Alzheimer-inoculated group than in the control-inoculated group ( $p = 0.004$ ,  $p = 0.015$ , and  $p = 0.009$ , respectively, Mann-Whitney tests). \* $p < 0.05$ ; \*\* $p < 0.01$ . Scatter plots display median and interquartile interval. CTRL-inoculated animals are in blue, AD1-inoculated in green and AD2-inoculated in red

than those of control-inoculated group (Fig. 1c). We did not detect any difference between the scores obtained by the animals inoculated with tissue homogenates from the two Alzheimer brains.

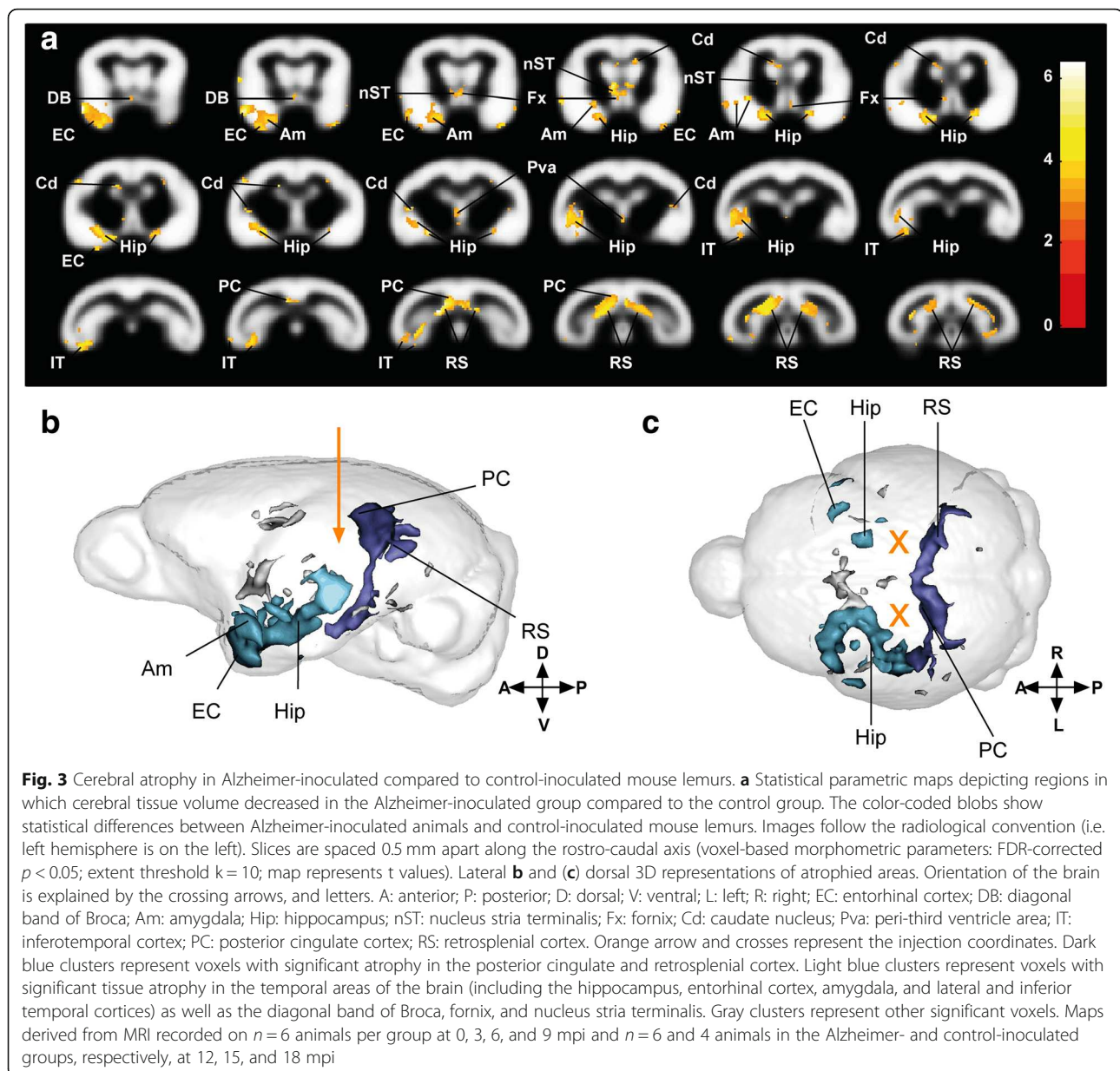
**Alzheimer’s disease brain inoculation alter EEG measures**

Longitudinal EEG studies were performed in mouse lemurs in order to further evaluate neuronal activity in the Alzheimer- and control-inoculated groups. EEG measures were recorded in the frontal cortex during the active state before the inoculation (Fig. 2a). At 6 mpi, slow wave EEG frequencies were altered, with a lower delta frequency and a higher theta frequency in the Alzheimer- than in the control-inoculated group (Fig. 2b). In addition, the decrease in delta frequency correlated significantly with impairment of long-term memory ( $p = 0.009$ , Additional file 6: Figure S5). Lemurs from the Alzheimer-inoculated group still displayed a significantly lower delta frequency and a significantly higher fast wave (alpha, sigma, and beta) frequency (Fig. 2c) at 12 mpi than lemurs from the control-inoculated group. We did not detect any difference between the scores obtained by the animals inoculated with tissue homogenates from the two Alzheimer brains.

**Alzheimer’s disease brain inoculation induces a progressive cerebral atrophy**

Alzheimer’s disease is morphologically characterized by progressive cerebral atrophy affecting the hippocampus and the cortex. We recorded MR images of the brains of lemurs from Alzheimer- and control-inoculated groups every 3 months. Automated voxel-based analysis was performed to evaluate cerebral atrophy. The Alzheimer-inoculated group displayed strong bilateral atrophy of the retrosplenial and posterior cingulate cortices (two areas close to the inoculation sites) relative to the control-inoculated group (Fig. 3a-c, dark blue clusters in b-c; Additional file 1: Table S4). Atrophy also involved temporal

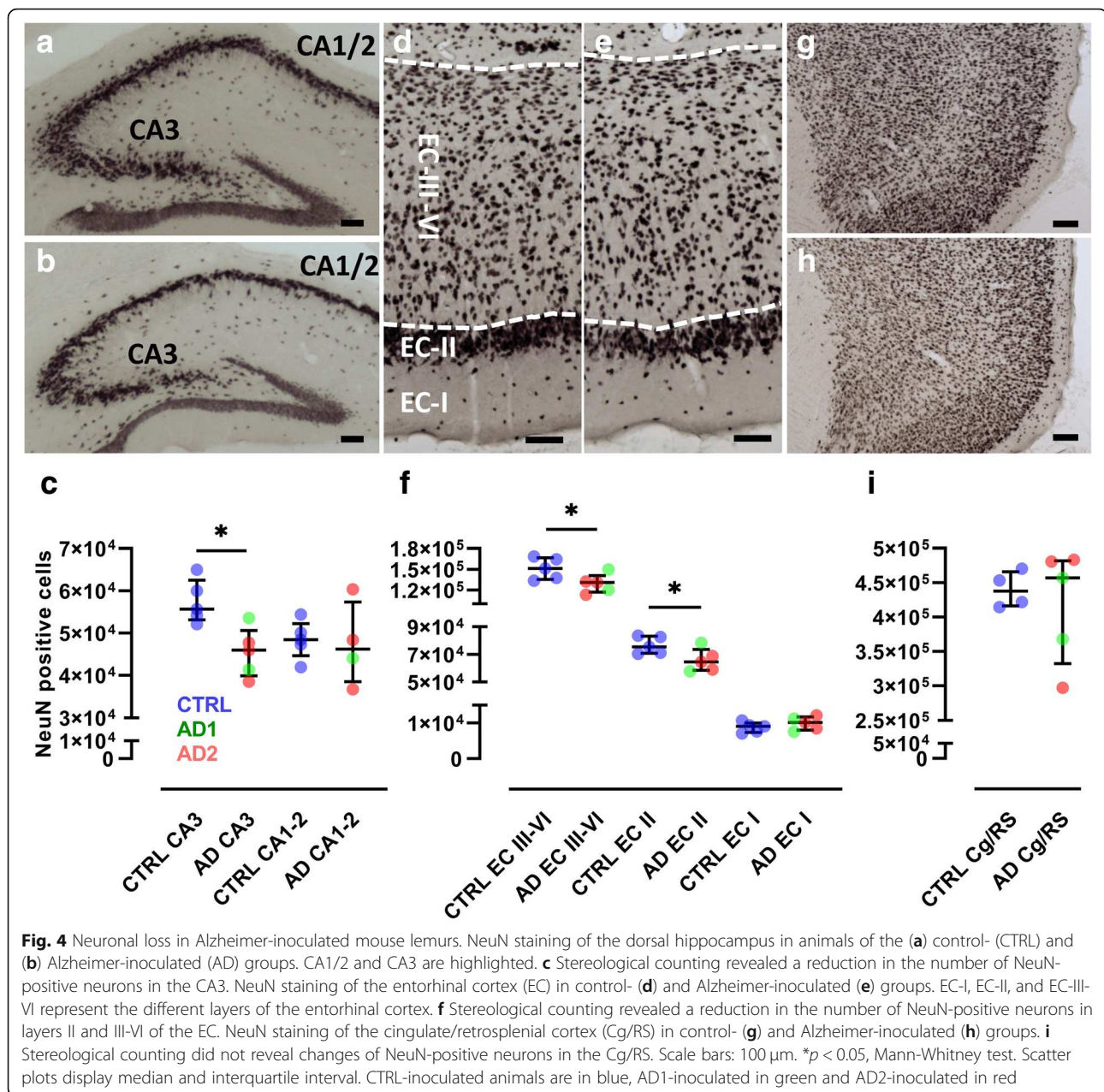
lower than that of control-inoculated group (Fig. 1c). The overall performance of the Alzheimer-inoculated group in the long-term memory task and their performance at 6 and 18 mpi were significantly worse



regions, including the hippocampus, entorhinal cortex, amygdala, and inferior temporal cortex (Fig. 3a-c, light blue clusters in b-c) with greater atrophy in the left hemisphere as compared to the right hemisphere. We also detected atrophy in the diagonal band of Broca, fornix, stria terminalis, parietal cortex, and caudate nucleus (Fig. 3a-c, gray clusters in b-c; Additional file 1: Table S4). Follow-up of the atrophied regions showed that the process was mild at 6 mpi and mainly developed from 6 to 12 mpi. Thus, atrophy was not associated with an acute effect of the inoculation and continued to spread from 12 to 18 mpi, although to a lesser extent (Additional file 7: Figure S6).

### Alzheimer’s disease brain inoculation induces neuronal loss

Mouse lemurs were euthanized at 18 mpi, at  $5.0 \pm 0.2$  years of age. Serial sections of the entire brains were stained with NeuN antibody and neurons counted in the hippocampus, entorhinal and cingulate/retrosplenial (RS) cortices by unbiased stereology (Fig. 4a-c). There was significant neuronal loss in the CA3 pyramidal layer of the hippocampus ( $p = 0.02$ ) and in layers II ( $p = 0.03$ ) and III to VI (III-VI,  $p = 0.03$ ) of the entorhinal cortex (Fig. 4d-f). Neuronal counts in these three structures positively correlated with each other (all  $p < 0.02$ ). Neuronal counts in the CA1/2 region of the hippocampus, layer I of the entorhinal



cortex, and cingulate/retrosplenial cortex were not significantly affected by inoculation with Alzheimer’s disease brain homogenates (Fig. 4g-i). We did not detect any difference in neuronal counts in the animals inoculated with tissue homogenates from the two Alzheimer brains.

**Alzheimer’s disease brain inoculation induces  $\beta$ -amyloid and tau lesions**

We then evaluated mouse lemur brain sections for A $\beta$  and tau pathologies (Table 1). In two out of five Alzheimer-inoculated mouse lemurs A $\beta$  and tau deposits were detected close to the inoculation sites (Figs. 5 and 6). In the

three other Alzheimer-inoculated animals A $\beta$  deposits were also detected, but tau was not detected. Neither type of deposit was detected in the control-inoculated animals.  $\beta$ -amyloid deposits were found as  $\beta$ -amyloid plaques (Figs. 5a-b, 6) as well as bands of parenchymal  $\beta$ -amyloid deposits surrounding white matter tracts (Figs. 5f-g and 6) in animals inoculated with tissue homogenates from the two Alzheimer brains (AD1 and AD2).  $\beta$ -amyloid angiopathy was detected only in one animal inoculated with the tissue homogenate from the Alzheimer brain displaying  $\beta$ -amyloid angiopathy (Fig. 5c-e). Tau lesions were detected using different antibodies including AT8, MC1 and AT100 (Fig. 5h-q), and were mainly in the form of neuropil threads

**Table 1**  $\beta$ -amyloid and tau lesions in mouse lemurs of the Alzheimer- (AD) and control-inoculated (CTRL) groups.  $\beta$ -amyloid plaques or  $\beta$ -amyloid angiopathy (CAA) were detected only in Alzheimer-inoculated animals. Tau lesions detected in two Alzheimer-inoculated animals (AT8, MC1 and AT100 antibodies). \* correspond to two animals that were euthanized at 12 months post inoculation. AD1 displayed  $\beta$ -amyloid angiopathy, high  $A\beta_{1-40}$  and low  $A\beta_{1-42}$  levels. AD2 did not display angiopathy and had low  $A\beta_{1-40}$  and high  $A\beta_{1-42}$  levels

Group	Animal	$\beta$ -Amyloid	Tau - AT8	Tau - MC1	Tau - AT100
AD2	265B	+ (plaques)	++	++	++
AD2	260B	+ (plaques)	++	++	++
AD1	169ABC	$\pm$ (plaques)	0	0	0
AD2	190IAB	$\pm$ (plaques)	0	0	0
AD1	211DBA	$\pm$ (CAA)	0	0	0
CTRL	189CBD	0	0	0	0
CTRL	190IC	0	0	0	0
CTRL	169ABB	0	0	0	0
CTRL	259BB*	0	0	0	0
CTRL	213ABA*	0	0	0	0

(Fig. 5j-n). Intracellular tau positive structures were also detected in the form of globular tau positive cells, horse-shoe and punctiform tau accumulation (Fig. 5o). We also found rare somatodendritic inclusions (Fig. 5k, p) as well as immunoreactive neurites with varicosities or “strings of beads” labeling (Fig. 5k), a pattern that is considered indicative of early changes in the process of tau-related neurofibrillary degeneration [39, 40]. Tau lesions were not colocalized with oligodendrocytes (Fig. 5q), but they were always seen in regions in which  $\beta$ -amyloid could be detected (Fig. 5h-i and 6). The two animals displaying tau lesions were inoculated with different Alzheimer brain samples (one animal inoculated with AD1 and one animal inoculated with AD2). To further evaluate the impact of the induced tau pathology on the clinical/neuropathological outcomes, we split the Alzheimer-inoculated animals into two subgroups of tau-positive and tau-negative animals (Additional file 8: Figure S7). The two animals displaying tau lesions had the worst memory scores at 18 mpi as well as the lowest neuronal counts in the CA3 region of the hippocampus.

Interestingly,  $\beta$ -amyloid depositions and tau inclusions could be visualized in several coronal brain sections encompassing the injection sites and the levels up to 1 mm anterior and 1 mm posterior to the injection site, and up to  $\sim$ 2 mm away from the injection site in the section plane, suggesting the spreading of the lesion (Figs. 5 and 6).

We also focused on 4G8-positive intracellular staining that reflects APP/ $A\beta$  deposition in mouse lemurs [18, 19]. Intracellular staining was measured in both groups (Additional file 9: Figure S8), but

there were no statistically significant differences between Alzheimer- and control-inoculated groups either in particular structures like the hippocampus (Additional file 9: Figure S8d), the caudate and putamen (not shown) or in the whole brain (Additional file 9: Figure S8h).

We did not detect obvious signs of astrocytic reactivity in any mouse lemur (Fig. 7a-b, e), and the evaluation of microglial reactivity did not reveal any difference between the Alzheimer- and control-inoculated groups (Fig. 7c-d, f). These results are consistent with the lack of differences in inflammation detected in APP/PS1<sub>dE9</sub> mice between both groups (Additional file 5: Figure S4g-j).

## Discussion

This study demonstrated that inoculation of Alzheimer’s disease brain homogenates in middle-aged mouse lemurs induces alterations of long term memory and progressive loss of learning ability, modifications of neuronal activity detected by EEG, widespread and progressive cerebral atrophy, and neuronal loss in the hippocampus and entorhinal cortex. The Alzheimer’s disease brain homogenates that induced these alterations accelerated the occurrence of  $\beta$ -amyloid and tau lesions in transgenic mouse models of  $\beta$ -amyloid or tau. This result in mice is consistent with the literature [7, 8].  $\beta$ -amyloid and tau lesions were also induced in mouse lemurs by inoculation with Alzheimer’s disease brain homogenates but not with the control brain homogenates. These lesions were localized close to the inoculation sites, which supports the role of the Alzheimer’s disease brain homogenates in inducing them. This is the first direct evidence of transmission of both  $\beta$ -amyloid and tau lesions in a non-transgenic animal. Interestingly, the lesions observed in mouse lemurs were sparse while they were more severe in transgenic mice. Thus, experimental transmission using the same Alzheimer’s disease brain homogenates leads to differential effects in different species.

Alzheimer’s disease is characterized by the presence of substantial amount of  $\beta$ -amyloid plaques [41, 42] in association with tau pathology [3]. In humans, the absence of these lesions precludes the diagnosis of Alzheimer’s disease. Brains of Alzheimer patients are also characterized by neuronal loss that exceeds tau pathology [2] and cerebral atrophy. Studies of the impact of experimental inoculation of Alzheimer brain homogenates in mice usually focus only on  $\beta$ -amyloid and tau lesions, but do not reveal consequences of inoculations on clinical signs, neuronal alterations or cerebral atrophy, despite the importance of these signs for Alzheimer’s disease. In the mouse lemurs of this study while the sparsity of the induced amyloid and tau lesions do not directly support a diagnosis for an “Alzheimer-like” pathology,

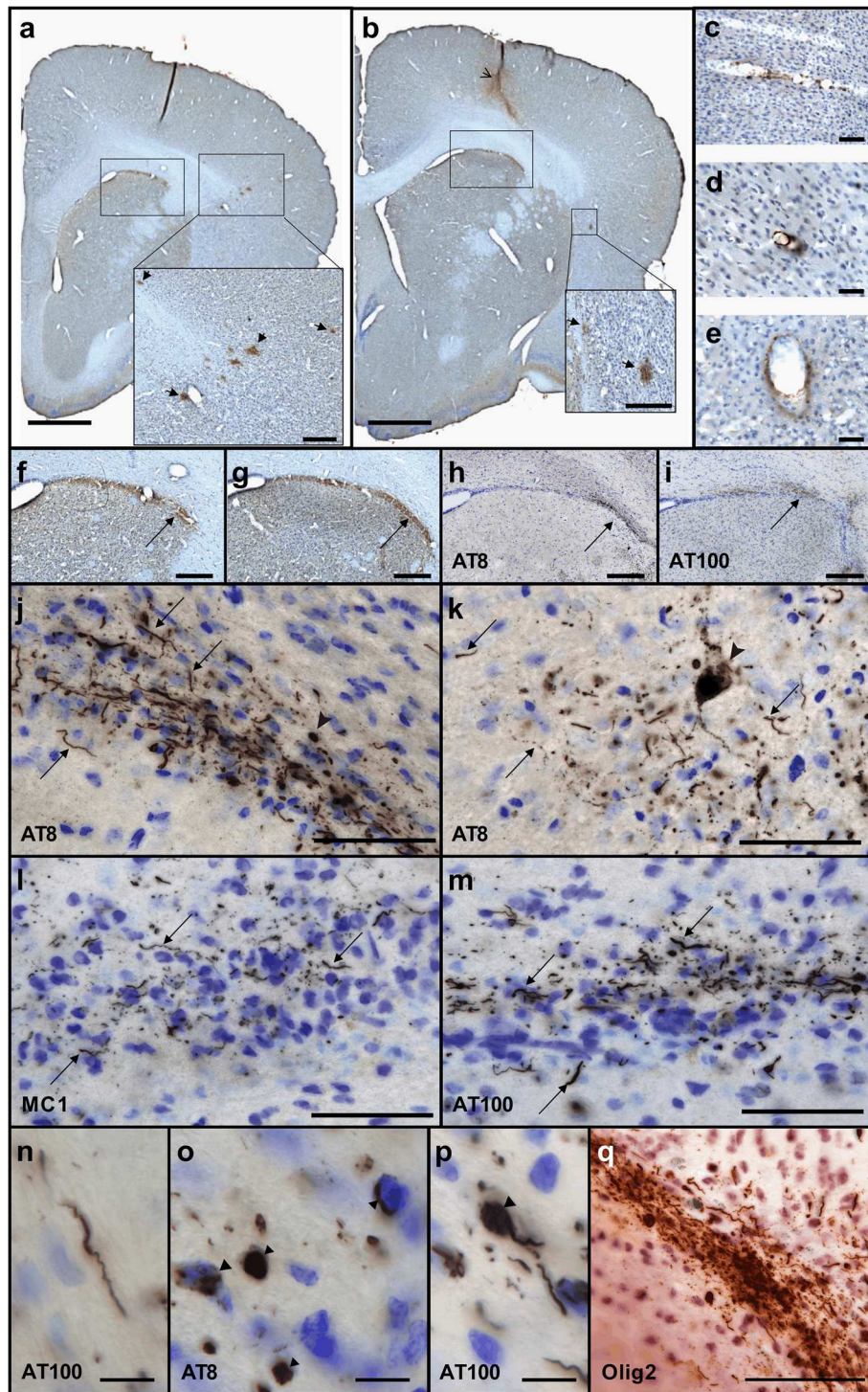


**Fig. 5** (See legend on next page.)

the encephalopathy developed by the inoculated lemurs is clinically relevant as it was associated with cognitive alterations, widespread cerebral atrophy, modifications of neuronal activity, and neuronal loss. Further, this encephalopathy is likely related to

Alzheimer pathology as it was induced by inoculation of Alzheimer brain homogenates (and not control homogenates) and because the inoculated animals presented with  $\beta$ -amyloid and tau lesions even if they were sparse.

(See figure on previous page.)

**Fig. 5** Amyloid depositions and tau inclusions in Alzheimer-inoculated mouse lemurs. **a, b**  $\beta$ -amyloid plaques (insets, arrows) revealed in two brain sections, immunostained for A $\beta$  (4G8), separated from 1 mm in an animal from the Alzheimer-inoculated group. The inoculation site is shown with an open arrow (**b**).  $\beta$ -amyloid could also be detected in blood vessels (**c-e**) as well as in the parenchyma (**f-g**) close to the corpus callosum (arrows, images in **f-g** correspond to frames in **a-b**). Immunostaining for tau lesions using AT8 (**h, j, k, o**), MC1 (**l**) and AT100 (**i, m-n, p**). **h-i** frames display the same regions as the ones shown in (**f-g**): tau lesions (arrows) were detected in the same regions as A $\beta$ . **j-n** are magnified images showing tau in neuropil threads (arrows). Intracellular tau positive structures were also detected in the form of globular positive cells (arrow), horseshoe intracellular accumulation (dotted arrow) and punctiform intracellular accumulation (arrowhead) (**o**). Rare somatodendritic inclusions (arrowhead **k, p**) as well as immunoreactive neurites with varicosities or "strings of beads" labeling (**k**: dotted arrow) were also detected. Tau stainings were counterstained with cresyl violet to identify neurons in (**h-p**). **q** displays AT8 sections double-stained for oligodendrocytes. Tau-positive lesions were not colocalized with oligodendrocytes (AT8 (brown) and Olig2 (red)). Scale bars: 1 mm (**a-b**), 200  $\mu$ m (insets in **a-b, e-i**), 50  $\mu$ m (**c-e, j-m, q**), 10 $\mu$ m (**n-p**)

The neuronal loss reported in the mouse lemurs inoculated with Alzheimer's disease brain homogenates involved the CA3 region of the hippocampus as well as the layers II and III to VI of the entorhinal cortex. These alterations are consistent with the macroscopic atrophy detected in the hippocampus and entorhinal cortex by MRI. The Alzheimer-inoculated animals also displayed a macroscopic atrophy of the retrosplenial and posterior cingulate cortices. The CA3 region is connected with layers II and III of the entorhinal cortex by the perforant path [43], and layer II of the entorhinal cortex is connected to the retrosplenial and

the posterior cingulate cortices [44]. Thus, the atrophy occurred within an organized network rather than randomly in the brain. This network connecting CA3, layer II of the entorhinal, retrosplenial and posterior cingulate cortices is strongly involved in memory for contextual information that is important for the long-term retention of a simple visual discrimination task [45, 46]. Its alteration in Alzheimer-inoculated mouse lemurs is thus consistent with their memory impairments. In addition to the neuronal loss, we found progressive impairments of neuronal activity detected first at a lower delta frequency and then at a

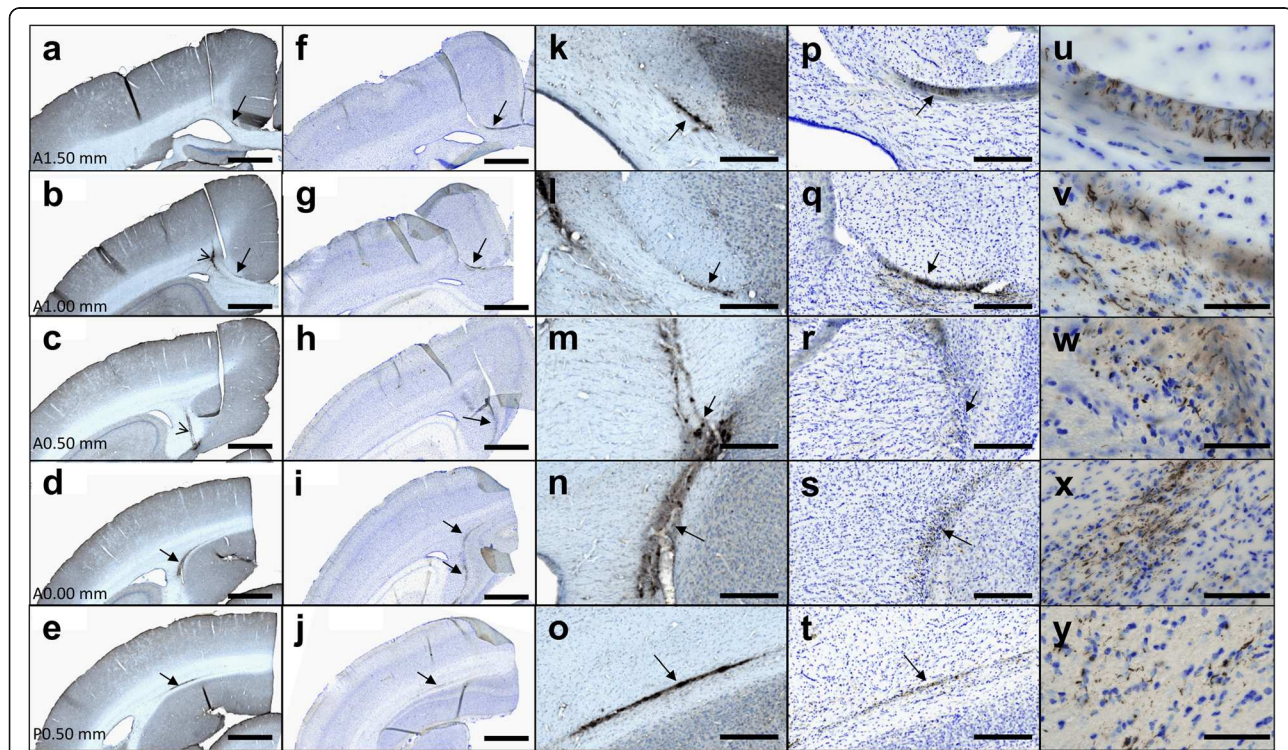


**Fig. 6** Diffusion of  $\beta$ -amyloid deposits and tau inclusions in Alzheimer-inoculated mouse lemurs. Immunostaining of A $\beta$  (4G8, **a-e, k-o** (magnified views)) and tau (AT8, **f-j, p-y** (magnified views)) in 5 successive brain sections. **u-y** displays magnification of the tau-positive lesions from (**f-j**) or (**p-t**).  $\beta$ -amyloid and tau deposits (**a-t**) were seen exactly at the same locations (arrows). They spread from the inoculation site (open arrow in **b, c**) to regions localized one millimeter ahead and behind the inoculation site (A1.50 mm to P0.50 mm correspond to spatial references in the Bons atlas [31]). Scale bars: 1 mm (**a-j**), 200  $\mu$ m (**k-t**), 50  $\mu$ m (**u-y**)

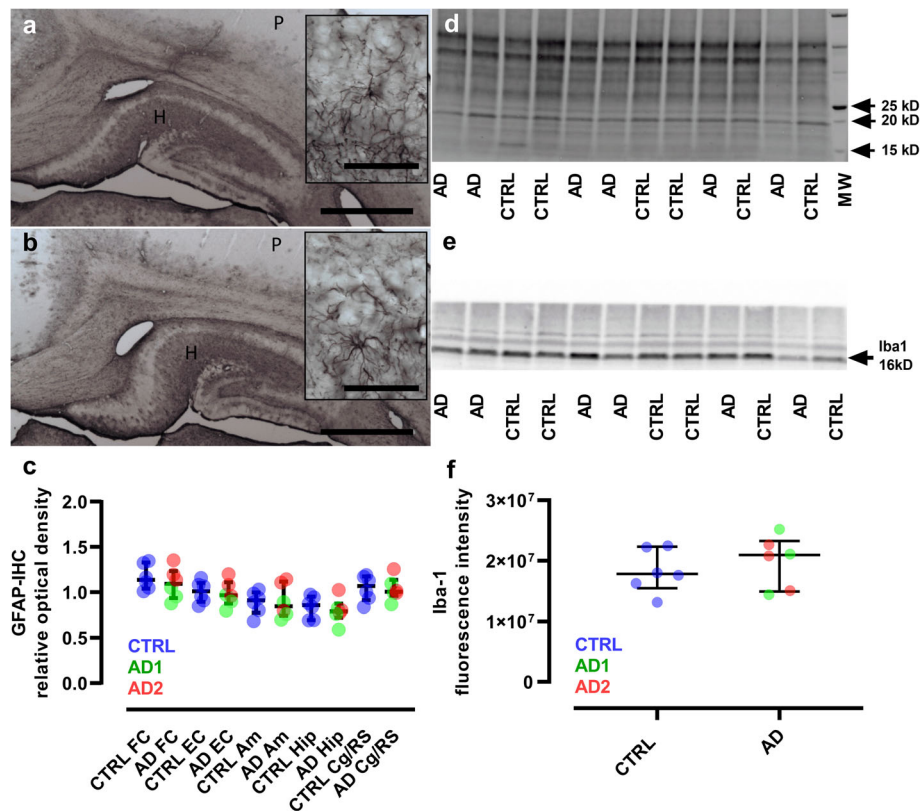


**Fig. 7** Lack of glial reactivity in inoculated lemurs. **a-b**, Immunostaining of astrocytes (GFAP) in the hippocampus (H) and parietal cortex (P) of control (**a**) and Alzheimer-inoculated (**b**) animals. Regional differences are seen including lower GFAP-immunoreactivity in the cortices which is generally found in lemurs. No qualitative difference in astrocyte morphology was detected between control- and Alzheimer-inoculated animals. Scale bars: main frame: 1 mm; inserts: 50  $\mu$ m. **(c)** Quantitative evaluations of astrocyte reactivity did not provide evidence of changes in GFAP-immunoreactivity or astrocyte morphology between control- and Alzheimer-inoculated animals (Mann-Whitney tests). **d-f** Microglia reactivity was evaluated by western blot analysis (Iba1). The unstained -UV activated- blot used for total protein amount normalization is presented in **(d)**, while the blot probed with Iba-1 antibody showing a specific 16kD band is displayed in **(e)**. **f** Quantitative evaluations of the blots did not show any difference between Iba-1 expression in control- and Alzheimer-inoculated animals (Mann-Whitney test). Scatter plots display median and interquartile interval. CTRL-inoculated animals are in blue, AD1-inoculated in green and AD2-inoculated in red.  $N = 6$  animals per group. FC: frontal cortex; EC: entorhinal cortex; Am: amygdala; Hip: hippocampus; Cg/RS: cingulate cortex/retrosplenial cortex

higher theta frequency in EEG measures. This suggests a long-distance functional impact of the pathological brain homogenate on neuronal network activity.

Mouse lemurs were euthanized 18 months after inoculation of brain homogenates as they displayed clinical signs including cognitive alterations, modifications of neuronal activity detected by EEG, and cerebral atrophy. The lack of severe  $\beta$ -amyloidosis, tau lesions or neuroinflammation in their brains despite their clinical signs is intriguing.  $\beta$ -amyloid and tau lesions were detected 4 and 1 mpi in mouse models of amyloidosis and tauopathy, respectively. Thus the Alzheimer brain homogenates that we used are able to induce  $\beta$ -amyloid and tau lesions relatively quickly in mice. We made the choice to follow up the mouse lemurs up to 18 months after inoculation, where they reach around 5 years and are considered as middle-aged, in order to avoid age-related cognitive or neuropathological impairments. Thus, we cannot rule out the possibility that

they would have developed stronger neuropathological lesions if they had lived longer. Indeed,  $\beta$ -amyloid and/or tau accumulation in non-human primates has been reported to take many years [11]. However, since in humans with Alzheimer’s disease the amyloid or tau lesions occur before cognitive alterations, cerebral atrophy or neuronal loss [47], we expected to detect stronger  $\beta$ -amyloid and/or tau lesions in lemurs that displayed clinical signs. These expectations were based on the facts that primates: i. naturally express  $\beta$ -amyloid or tau under normal conditions; ii. are genetically more similar to humans than transgenic mouse models of Alzheimer’s disease [48]; and iii. Can naturally display age-related cerebral atrophy associated with cognitive changes [16], all resulting in primates being relevant models to explore impact of experimental inoculation of Alzheimer brain homogenates that cannot be evaluated in mouse models. With this in mind, one interpretation of the observed presence of encephalopathy not



associated with a strong inflammatory process,  $\beta$ -amyloid or tau deposition following Alzheimer brain homogenate intracerebral inoculation lies in research on prion diseases. Indeed, the induction of clinical signs and neuronal death in the absence of detectable pathological protein accumulation after inoculation of brain homogenates was previously reported for classical prion diseases [49]. In prion diseases, this is explained by the presence of soluble agents that are thought to be neurotoxic [50]. Further, as soluble, oligomeric, forms of  $\beta$ -amyloid [51] and tau [52] are known to be toxic for the brain, one possible explanation for our results is that inoculation of human Alzheimer brain homogenates led to the production of such oligomers that were toxic for neurons. The two animals presenting with aggregated tau lesions had the worst memory scores and the lowest neuronal density in CA3. Given the low density of these tau lesions, we rule out that they directly induced neuronal loss. However, they could be associated with soluble forms of tau, an entity that induces more neuronal loss than aggregated tau proteins [53]. One can however not exclude the influence of other as yet unidentified factors leading to the reported encephalopathy.

Although the evidence for cognitive and pathological alterations in Alzheimer's brain-inoculated middle-aged animals emphasizes our findings, one limitation of the current study is that it was designed to focus on neuropathological alterations and brains were perfused with paraformaldehyde, which limited our ability to perform biochemical analysis. Future studies should include more in-depth examination of biochemical changes following Alzheimer brain inoculation. Thioflavin-T binding affinity should be used to assess the fibrillary nature of the  $\beta$ -amyloid and tau compounds present in animal brains [54].  $\beta$ -amyloid and tau oligomers should then be evaluated by mass spectrometry [55], RT-QuIC analysis [55], immunoprecipitation experiments, and fast protein liquid chromatography [54]. Atomic force microscopy as well as a newly developed ELISA-like technique called sFIDA (Surface-Based Fluorescence Intensity Distribution Analysis Assay) should also be used to further describe the oligomers and their size [54, 56].

Another potential limitation of the study may be the small size of the animal groups that can be reached while working with primates. Using results from our studies (mean/standard deviation obtained for the different measures, proportion of animals displaying with amyloid or tau pathologies in our experimental groups) we could estimate the sample size to compare groups of control- and Alzheimer-inoculated animals assuming a significance level of 5%, a power of 80%, and two-sided tests (Additional file 1: Table S5, [57]). In mouse lemurs, small number of animals ( $n < 5$ ) per arm are required to detect memory

alterations or EEG changes after 6 mpi as well as cerebral A $\beta$  deposition at 18 mpi. Detection of neuronal loss in the CA3 as well as in layers II and III to VI of the entorhinal cortex requires from 5 to 8 animals. These values should be compared to estimations of sample sizes in mice that require from 1 to 8 mice to assess tau or amyloid deposition. They show that the number of mouse lemurs required to obtain scientific results is in the same range as the one required for transgenic rodents. Mouse lemurs however provide new types of information as they can spontaneously display amyloid or tau lesions on a wild-type/primate genetic background as well as neuronal loss associated to clinical outcomes. They can be ideal models to assess the impact of various amyloid/tau strains on disease occurrence or the role of oligomers on clinical outcomes in primates.

In conclusion, our results indicate that Alzheimer's disease brain homogenate inoculation induces an encephalopathy characterized by neuronal loss, progressive atrophy, neuronal activity alterations and cognitive impairments as well as sparse  $\beta$ -amyloid and tau depositions. The clinical signs can be explained by the neuronal loss, cerebral atrophy and neuronal networks dysfunction. Tau lesions may be a strong determinant, but not the only one, in the induction of the neuronal loss and clinical outcome. Further studies are necessary to evaluate the nature of relationships between the different lesions induced by Alzheimer's disease brain homogenate inoculation and to assess the mechanisms leading to encephalopathy induced by these inoculations.

## Additional files

**Additional file 1: Table S1** Human brain sample characteristics and staging. **Table S2** Schedule of the experimental protocol. **Table S3** Sampling parameters for stereological counting of NeuN-positive neurons. **Table S4** Brain regions with gray matter loss in the Alzheimer's disease-inoculated group relative to the control-inoculated group. **Table S5** Estimated sample size to compare control and Alzheimer-inoculated mice and mouse lemurs assuming a significance level of 5%, a power of 80%, and two-sided tests. (DOCX 46 kb)

**Additional file 2: Figure S1** Cognitive test in mouse lemurs. (TIF 5572 kb)

**Additional file 3: Figure S2** Characterization of human brain samples and homogenates. (TIF 19464 kb)

**Additional file 4: Figure S3** Prion protein examination in human brain samples. (TIF 9854 kb)

**Additional file 5: Figure S4** A $\beta$  and Tau pathology in mice after inoculation with human brain homogenates. (TIF 26552 kb)

**Additional file 6: Figure S5** Correlation between cognitive abilities and EEG delta frequency. (TIF 4153 kb)

**Additional file 7: Figure S6** Time-dependent evolution of cerebral atrophy in inoculated lemurs. (TIF 19870 kb)

**Additional file 8: Figure S7** Impact of tau pathology on memory and neuronal loss. (TIF 8800 kb)

**Additional file 9: Figure S8** Similar level of intracellular 4G8-positive structures in Alzheimer's disease and control-inoculated lemurs. (TIF 21279 kb)

### Acknowledgements

We thank V. Buee-Scherrer for biochemical evaluation of tau. We also thank the donors and the Brain Donation Program of the "GIE NeuroCEB" Brain Bank run by a consortium of Patient Associations: ARSEP (association for research on multiple sclerosis), CSC (cerebellar ataxias), France Alzheimer and France Parkinson, with the support of Fondation Plan Alzheimer and IHU A-ICM for providing the brain samples used in this study.

GIE Neuro-CEB: Charles Duyckaerts, Véronique Sazdovitch, Sabrina Leclère-Turbant and Marie-Claire Artaud-Botté; The national network includes the following neuropathologists: Anne Vital (Bordeaux), Françoise Chapon (Caen), Jean-Louis Kemeny (Clermont-Ferrand), Claude-Alain Maurage & Vincent Deramecourt (Lille), David Meyronet & Nathalie Streichenberger (Lyon), André Maues de Paula (Marseille), Valérie Rigau (Montpellier), Fanny Vandenbos-Burel (Nice), Charles Duyckaerts (Paris), Danielle Seilhean (Paris), Véronique Sazdovitch (Paris), Serge Milin (Poitiers), Dan Christian Chiforeanu (Rennes), Annie Laquerrière (Rouen), Béatrice Lannes (Strasbourg), Marie-Bernadette Delisle & Emmanuelle Uro-Coste (Toulouse).

### Authors' contributions

CG, JK, EEC, JLP, FPI, and MD designed the study. MD coordinated the study. FNN provided the human brain samples. LB, SE, FNN, ASH, and CG characterized the brain samples. CG, MD, and JK performed the inoculations and the MRI study. CG, SJS, JLP, and MD, designed the MRI analysis. FA and FPI raised the mouse lemurs and conducted the EEG evaluations. JLP performed cognitive evaluation. FPI performed rotarod test. FPe, PG, ASH and CG performed the immunohistological studies of the mouse lemur brains. SL performed the stereology of the mouse lemur brains. CG and SL conducted the experiments and measurements in APP/PS1<sub>JEF</sub> mice. RC, MC and LB performed the experiments in Tau30+/+ mice. CG, ASH and MD were responsible for statistical analysis and wrote the manuscript. JK, LB, CD, ASH, JPD, EEC, JLP, and FPI revised the manuscript. All authors read and approved the final manuscript.

### Funding

This study was funded by the France-Alzheimer Association, the Fondation Plan Alzheimer, and the CEA Bottom-Up program.

### Availability of data and materials

The datasets during and/or analysed during the current study available from the corresponding author on reasonable request.

### Competing interests

The authors declare that they have no competing interests.

### Author details

<sup>1</sup>Centre National de la Recherche Scientifique (CNRS), Université Paris-Sud, Université Paris-Saclay UMR 9199, Laboratoire des Maladies Neurodégénératives, 18 Route du Panorama, F-92265 Fontenay-aux-Roses, France. <sup>2</sup>Commissariat à l'Energie Atomique et aux Energies Alternatives (CEA), Direction de la Recherche Fondamentale (DRF), Institut François Jacob, MIRcen, 18 Route du Panorama, F-92265 Fontenay-aux-Roses, France. <sup>3</sup>University of Wisconsin Oshkosh, 800 Algoma Boulevard, Oshkosh, WI 54901, USA. <sup>4</sup>Wolfson Brain Imaging Centre, University of Cambridge, Addenbrooke's Hospital, Cambridge Biomedical Campus, Cambridge CB2 0QQ, UK. <sup>5</sup>Behavioural and Clinical Neuroscience Institute, University of Cambridge, Cambridge Biomedical Campus, Cambridge CB2 0QQ, UK. <sup>6</sup>LabEx DISTALZ (Development of Innovative Strategies for a Transdisciplinary approach to Alzheimer's disease), Université de Lille, Inserm, CHU-Lille, UMR-S1172, Alzheimer & Tauopathies, Rue Polonovski, 59045 Lille, France. <sup>7</sup>UMR7179 CNRS-MNHN, MECADEV (Adaptive Mechanisms and Evolution), 1 Avenue du Petit Château, 91800 Brunoy, France. <sup>8</sup>Commissariat à l'Energie Atomique et aux Energies Alternatives (CEA), Direction de la Recherche Fondamentale (DRF), Institut François Jacob, SEPIA, Université Paris-Saclay, 18 Route du Panorama, F-92265 Fontenay-aux-Roses, France. <sup>9</sup>GIE Neuro-CEB/Neuropathologist Network: Plate-Forme de Ressources Biologiques, Bâtiment Roger Baillet, Hôpital de la Pitié-Salpêtrière, 47-83 Boulevard de l'Hôpital, Cedex 13, 75651 Paris, France. <sup>10</sup>Laboratoire de Psychopathologie et de Neuropsychologie, EA, 2027, Université Paris 8, St-Denis, France.

Received: 15 July 2019 Accepted: 15 July 2019

Published online: 04 September 2019

### References

- Frisoni GB, Fox NC, Jack CR Jr, Scheltens P, Thompson PM (2010) The clinical use of structural MRI in Alzheimer disease. *Nat Rev Neurol* 6:67–77. <https://doi.org/10.1038/nrneuro.2009.215>
- Gomez-Isla T, Hollister R, West H, Mui S, Growdon JH, Petersen RC, Parisi JE, Hyman BT (1997) Neuronal loss correlates with but exceeds neurofibrillary tangles in Alzheimer's disease. *Ann Neurol* 41:17–24. <https://doi.org/10.1002/ana.410410106>
- Duyckaerts C, Delatour B, Potier MC (2009) Classification and basic pathology of Alzheimer disease. *Acta Neuropathol* 118:5–36. <https://doi.org/10.1007/s00401-009-0532-1>
- Jaunmuktane Z, Mead S, Ellis M, Wadsworth JD, Nicoll AJ, Kenny J, Launchbury F, Linehan J, Richard-Loendt A, Walker AS, Rudge P, Collinge J, Brandner S (2015) Evidence for human transmission of amyloid-beta pathology and cerebral amyloid angiopathy. *Nature* 525:247–250. <https://doi.org/10.1038/nature15369>
- Jaunmuktane Z, Quaegebeur A, Taipa R, Viana-Baptista M, Barbosa R, Koriath C, Sciot R, Mead S, Brandner S (2018) Evidence of amyloid-beta cerebral amyloid angiopathy transmission through neurosurgery. *Acta Neuropathol* 135:671–679. <https://doi.org/10.1007/s00401-018-1822-2>
- Kovacs GG, Lutz MI, Ricken G, Strobel T, Hoftberger R, Preusser M, Regelsberger G, Honigschnabl S, Reiner A, Fischer P, Budka H, Hainfellner JA (2016) Dura mater is a potential source of Abeta seeds. *Acta Neuropathol* 131:911–923. <https://doi.org/10.1007/s00401-016-1565-x>
- Clavaguera F, Hench J, Lavenir I, Schweighauser G, Frank S, Goedert M, Tolnay M (2014) Peripheral administration of tau aggregates triggers intracerebral tauopathy in transgenic mice. *Acta Neuropathol* 127:299–301. <https://doi.org/10.1007/s00401-013-1231-5>
- Eisele YS, Fritschi SK, Hamaguchi T, Obermuller U, Fuger P, Skodras A, Schafer C, Odenthal J, Heikenwalder M, Staufenbiel M, Jucker M (2014) Multiple factors contribute to the peripheral induction of cerebral beta-amyloidosis. *J Neurosci* 34:10264–10273. <https://doi.org/10.1523/JNEUROSCI.1608-14.2014>
- Beekes M, Thomzig A, Schulz-Schaeffer WJ, Burger R (2014) Is there a risk of prion-like disease transmission by Alzheimer- or Parkinson-associated protein particles? *Acta Neuropathol* 128:463–476. <https://doi.org/10.1007/s00401-014-1324-9>
- Heuer E, Rosen RF, Cintron A, Walker LC (2012) Nonhuman primate models of Alzheimer-like cerebral proteopathy. *Curr Pharm Des* 18:1159–1169. <https://doi.org/10.2174/138161212799315885>
- Ridley RM, Baker HF, Windle CP, Cummings RM (2006) Very long term studies of the seeding of beta-amyloidosis in primates. *J Neural Transm* 113:1243–1251. <https://doi.org/10.1007/s00702-005-0385-2>
- Langui S, Blanc S, Blin O, Canale C, Dal-Pan A, Devau G, Dhenain M, Dorieux O, Epelbaum J, Gomez D, Hardy I, Henry PY, Irving EA, Marchal J, Mestre-Frances N, Perret M, Picq JL, Pifferi F, Rahman A, Schenker EI, Terrien J, They M, Verdier JM, Aujard F (2012) The grey mouse lemur: a non-human primate model for ageing studies. *Ageing Res Rev* 11:150–162. <https://doi.org/10.1016/j.arr.2011.07.001>
- Blanco MB, Zehr SM (2015) Striking longevity in a hibernating lemur. *J Zool* 296:177–188. <https://doi.org/10.1111/jzo.12230>
- Fischer KE, Austad SN (2011) The development of small primate models for aging research. *ILAR J* 52:78–88. <https://doi.org/10.1093/ilar.52.1.78>
- Pifferi F, Terrien J, Marchal J, Dal-Pan A, Djelti F, Hardy I, Chahory S, Cordonnier N, Desquilbet L, Hurion M, Zahariev A, Chery I, Zizzari P, Perret M, Epelbaum J, Blanc S, Picq J-L, Dhenain M, Aujard F (2018) Caloric restriction increases lifespan but affects brain integrity in grey mouse lemur primates. *Comm Biol* 1:30. <https://doi.org/10.1038/s42003-018-0024-8>
- Picq JL, Aujard F, Volk A, Dhenain M (2012) Age-related cerebral atrophy in nonhuman primates predicts cognitive impairments. *Neurobiol Aging* 33:1096–1109. <https://doi.org/10.1016/j.neurobiolaging.2010.09.009>
- Silhol S, Calenda A, Jallageas V, Mestre-Frances N, Bellis M, Bons N (1996)  $\beta$ -amyloid protein precursor in *Microcebus murinus*: genotyping and brain localization. *Neurobiol Dis* 3:169–182. <https://doi.org/10.1006/nbdi.1996.0017>
- Mestre-Frances N, Keller E, Calenda A, Barelli H, Checler F, Bons N (2000) Immunohistochemical analysis of cerebral cortical and vascular lesions in the primate *Microcebus murinus* reveal distinct amyloid beta

- 1–42 and beta 1–40 immunoreactivity profiles. *Neurobiol Dis* 7:1–8. <https://doi.org/10.1006/nbdi.1999.0270>
19. Roy M, Cardoso C, Dorieux O, Malmgren C, Epelbaum S, Petit F, Kraska A, Brouillet E, Delatour B, Perret M, Aujard F, Dhenain M (2015) Age-associated evolution of plasmatic amyloid in mouse lemur primates: relationship with intracellular amyloid deposition. *Neurobiol Aging* 36:149–156. <https://doi.org/10.1016/j.neurobiolaging.2014.07.017>
  20. Bons N, Mestre N, Pette A (1991) Senile plaques and neurofibrillary changes in the brain of an aged lemurian primate, *Microcebus murinus*. *Neurobiol Aging* 13:99–105. [https://doi.org/10.1016/0197-4580\(92\)90016-Q](https://doi.org/10.1016/0197-4580(92)90016-Q)
  21. Giannakopoulos P, Silhol S, Jallageas V, Mallet J, Bons N, Bouras C, Delaere P (1997) Quantitative analysis of tau protein-immunoreactive accumulations and beta amyloid protein deposits in the cerebral cortex of the mouse lemur, *Microcebus murinus*. *Acta Neuropathol* 94:131–139. <https://doi.org/10.1007/s004010050684>
  22. Kraska A, Dorieux O, Picq J-L, Petit F, Bourrin E, Chenu E, Volk A, Perret M, Hantraye P, Mestre-Frances N, Aujard F, Dhenain M (2011) Age associated cerebral atrophy in mouse lemur Primates. *Neurobiol Aging* 32:894–906. <https://doi.org/10.1016/j.neurobiolaging.2009.05.018>
  23. Papegaey A, Eddarkaoui S, Deramecourt V, Fernandez-Gomez FJ, Pantano P, Obriot H, Machala C, Anquetil V, Camuzat A, Brice A, Maurage CA, Le Ber I, Duyckaerts C, Buee L, Sergeant N, Buee-Scherrer V (2016) Reduced tau protein expression is associated with frontotemporal degeneration with progranulin mutation. *Acta Neuropathol Commun* 4:74. <https://doi.org/10.1186/s40478-016-0345-0>
  24. Garcia-Alloza M, Robbins EM, Zhang-Nunes SX, Purcell SM, Betensky RA, Raju S, Prada C, Greenberg SM, Bacskai BJ, Frosch MP (2006) Characterization of amyloid deposition in the APP<sup>swe</sup>/PS1<sup>ΔE9</sup> mouse model of Alzheimer disease. *Neurobiol Dis* 24:516–524. <https://doi.org/10.1016/j.nbd.2006.08.017>
  25. Schindowski K, Bretteville A, Leroy K, Begard S, Brion JP, Hamdane M, Buee L (2006) Alzheimer's disease-like tau neuropathology leads to memory deficits and loss of functional synapses in a novel mutated tau transgenic mouse without any motor deficits. *Am J Pathol* 169:599–616. <https://doi.org/10.2353/ajpath.2006.060002>
  26. Dhenain M, Chenu E, Hisley CK, Aujard F, Volk A (2003) Regional atrophy in the brain of lissencephalic mouse lemur primates: measurement by automatic histogram-based segmentation of MR images. *Magn Reson Med* 50:984–992. <https://doi.org/10.1002/mrm.10612>
  27. Paxinos G, Franklin KBJ (2001) *The Mouse Brain in Stereotaxic Coordinates*. Second Edition, Academic Press, San Diego
  28. Picq JL, Villain N, Gary C, Pifferi F, Dhenain M (2015) Jumping stand apparatus reveals rapidly specific age-related cognitive impairments in mouse lemur primates. *PLoS One* 10:e0146238. <https://doi.org/10.1371/journal.pone.0146238>
  29. Infarinato F, Rahman A, Del Percio C, Lamberty Y, Bordet R, Richardson JC, Forloni G, Drinkenburg W, Lopez S, Aujard F, Babiloni C, Pifferi F, Consortium IMIP (2015) On-going frontal alpha rhythms are dominant in passive state and desynchronize in active state in adult gray mouse lemurs. *PLoS One* 10:e0143719. <https://doi.org/10.1371/journal.pone.0143719>
  30. Rahman A, Languille S, Lamberty Y, Babiloni C, Perret M, Bordet R, Blin OJ, Jacob T, Auffret A, Schenker E, Richardson J, Pifferi F, Aujard F (2013) Sleep deprivation impairs spatial retrieval but not spatial learning in the non-human primate grey mouse lemur. *PLoS One* 8:e64493. <https://doi.org/10.1371/journal.pone.0064493>
  31. Bons N, Sihol S, Barbier V, Mestre-Frances N, Albe-Fessard D (1998) A stereotaxic atlas of the grey lesser mouse lemur brain (*Microcebus murinus*). *Brain Res Bull* 46:1–173. [https://doi.org/10.1016/S0361-9230\(97\)00458-9](https://doi.org/10.1016/S0361-9230(97)00458-9)
  32. Sawiak SJ, Picq JL, Dhenain M (2014) Voxel-based morphometry analyses of in vivo MRI in the aging mouse lemur primate. *Front Aging Neurosci* 6:82. <https://doi.org/10.3389/fnagi.2014.00082>
  33. Ashburner J (2007) A fast diffeomorphic image registration algorithm. *Neuroimage* 38:95–113. <https://doi.org/10.1016/j.neuroimage.2007.07.007>
  34. Good CD, Johnsrude IS, Ashburner J, Henson RN, Friston KJ, Frackowiak RS (2001) A voxel-based morphometric study of ageing in 465 normal adult human brains. *Neuroimage* 14:21–36. <https://doi.org/10.1006/nimg.2001.0786>
  35. Genovese CR, Lazar NA, Nichols T (2002) Thresholding of statistical maps in functional neuroimaging using the false discovery rate. *Neuroimage* 15:870–878. <https://doi.org/10.1006/nimg.2001.1037>
  36. Rasband WS (1997–2011) ImageJ, U. S. National Institutes of Health, Bethesda. <http://imagej.nih.gov/ij/>
  37. Diguët E, Petit F, Escartin C, Cambon K, Bizat N, Dufour N, Hantraye P, Deglon N, Brouillet E (2009) Normal aging modulates the neurotoxicity of mutant huntingtin. *PLoS One* 4:e4637. <https://doi.org/10.1371/journal.pone.0004637>
  38. West MJ, Slomianka L, Gundersen HJG (1991) Unbiased stereological estimation of the total number of neurons in the subdivisions of the rat hippocampus using the optical fractionator. *Anat Rec* 231:482–497. <https://doi.org/10.1002/ar.1092310411>
  39. Braak H, Del Tredici K (2011) The pathological process underlying Alzheimer's disease in individuals under thirty. *Acta Neuropathol* 121:171–181. <https://doi.org/10.1007/s00401-010-0789-4>
  40. Caillierez R, Begard S, Lecolle K, Deramecourt V, Zommer N, Dujardin S, Loyens A, Dufour N, Auregan G, Winderickx J, Hantraye P, Deglon N, Buee L, Colin M (2013) Lentiviral delivery of the human wild-type tau protein mediates a slow and progressive neurodegenerative tau pathology in the rat brain. *Mol Ther* 21:1358–1368. <https://doi.org/10.1038/mt.2013.66>
  41. Jack CR Jr, Knopman DS, Chetelat G, Dickson D, Fagan AM, Frisoni GB, Jagust W, Mormino EC, Petersen RC, Sperling RA, van der Flier WM, Villemagne VL, Visser PJ, Vos SJ (2016) Suspected non-Alzheimer disease pathophysiology - concept and controversy. *Nat Rev Neurol* 12:117–124. <https://doi.org/10.1038/nrneurol.2015.251>
  42. Monsell SE, Kukull WA, Roher AE, Maarouf CL, Serrano G, Beach TG, Caselli RJ, Montine TJ, Reiman EM (2015) Characterizing apolipoprotein E epsilon 4 carriers and noncarriers with the clinical diagnosis of mild to moderate Alzheimer dementia and minimal beta-amyloid peptide plaques. *Jama Neurol* 72:1124–1131. <https://doi.org/10.1001/jama.2015.1721>
  43. Deng W, Aimone JB, Gage FH (2010) New neurons and new memories: how does adult hippocampal neurogenesis affect learning and memory? *Nat Rev Neurosci* 11:339–350. <https://doi.org/10.1038/nrn2822>
  44. Bird CM, Burgess N (2008) The hippocampus and memory: insights from spatial processing. *Nat Rev Neurosci* 9:182–194. <https://doi.org/10.1038/nrn2335>
  45. McDonald RJ, King AL, Wasiaik TD, Zelinski EL, Hong NS (2007) A complex associative structure formed in the mammalian brain during acquisition of a simple visual discrimination task: dorsolateral striatum, amygdala, and hippocampus. *Hippocampus* 17:759–774. <https://doi.org/10.1002/hipo.20333>
  46. Ranganath C, Ritchey M (2012) Two cortical systems for memory-guided behaviour. *Nat Rev Neurosci* 13:713–726. <https://doi.org/10.1038/nrn3338>
  47. Jack CR Jr, Knopman DS, Jagust WJ, Petersen RC, Weiner MW, Aisen PS, Shaw LM, Vemuri P, Wiste HJ, Weigand SD, Lesnick TG, Pankratz VS, Donohue MC, Trojanowski JQ (2013) Tracking pathophysiological processes in Alzheimer's disease: an updated hypothetical model of dynamic biomarkers. *Lancet Neurol* 12:207–216. [https://doi.org/10.1016/S1474-4422\(12\)70291-0](https://doi.org/10.1016/S1474-4422(12)70291-0)
  48. Rosen RF, Tomidokoro Y, Farberg AS, Dooyema J, Ciliax B, Preuss TM, Neubert TA, Ghiso JA, LeVine H 3rd, Walker LC (2016) Comparative pathobiology of beta-amyloid and the unique susceptibility of humans to Alzheimer's disease. *Neurobiol Aging* 44:185–196. <https://doi.org/10.1016/j.neurobiolaging.2016.04.019>
  49. Lasmezas CI, Deslys JP, Robain O, Jaegly A, Beringue V, Peyrin JM, Fournier JG, Hauw JJ, Rossier J, Dormont D (1997) Transmission of the BSE agent to mice in the absence of detectable abnormal prion protein. *Science* 275:402–405. <https://doi.org/10.1126/science.275.5298.402>
  50. Caughey B, Baron GS, Chesebro B, Jeffrey M (2009) Getting a grip on prions: oligomers, amyloids, and pathological membrane interactions. *Annu Rev Biochem* 78:177–204. <https://doi.org/10.1146/annurev.biochem.78.082907.145410>
  51. Haass C, Selkoe DJ (2007) Soluble protein oligomers in neurodegeneration: lessons from the Alzheimer's amyloid beta-peptide. *Nat Rev Mol Cell Biol* 8:101–112. <https://doi.org/10.1038/nrn2101>
  52. Lasagna-Reeves CA, Castillo-Carranza DL, Sengupta U, Clos AL, Jackson GR, Kaye R (2011) Tau oligomers impair memory and induce synaptic and mitochondrial dysfunction in wild-type mice. *Mol Neurodegener* 6:39. <https://doi.org/10.1186/1750-1326-6-39>
  53. d'Orange M, Auregan G, Cheramy D, Gaudin-Guerif M, Lieger S, Guillermin M, Stimmer L, Josephine C, Herard AS, Gaillard MC, Petit F, Kiessling MC, Schmitz C, Colin M, Buee L, Panayi F, Diguët E, Brouillet E, Hantraye P, Bemelmans AP, Cambon K (2018) Potentiating tangle formation reduces acute toxicity of soluble tau species in the rat. *Brain* 141:535–549. <https://doi.org/10.1093/brain/awx342>

54. Lasagna-Reeves CA, Castillo-Carranza DL, Sengupta U, Guerrero-Munoz MJ, Kiritoshi T, Neugebauer V, Jackson GR, Kaye R (2012) Alzheimer brain-derived tau oligomers propagate pathology from endogenous tau. *Sci Rep* 2:700
55. Di Fede G, Catania M, Maderna E, Ghidoni R, Benussi L, Tonoli E, Giaccone G, Moda F, Paterlini A, Campagnani I, Sorrentino S, Colombo L, Kubis A, Bistaffa E, Ghetti B, Tagliavini F (2018) Molecular subtypes of Alzheimer's disease. *Sci Rep* 8. <https://doi.org/10.1038/S41598-018-21641-1>
56. Schemmert S, Schartmann E, Zafiu C, Kass B, Hartwig S, Lehr S, Bannach O, Langen KJ, Shah NJ, Kutzsche J, Willuweit A, Willbold D (2019) A oligomer elimination restores cognition in transgenic Alzheimer's mice with full-blown pathology. *Mol Neurobiol* 56:2211–2223. <https://doi.org/10.1007/s12035-018-1209-3>
57. Festing M, Altman D (2002) Guidelines for the design and statistical analysis of experiments using laboratory animals. (erratum in *ILAR J*. 2005;46(3):320). *ILAR J* 43:244–258. <https://doi.org/10.1093/ilar.43.4.244>

### Publisher's Note

Springer Nature remains neutral with regard to jurisdictional claims in published maps and institutional affiliations.

**Ready to submit your research? Choose BMC and benefit from:**

- fast, convenient online submission
- thorough peer review by experienced researchers in your field
- rapid publication on acceptance
- support for research data, including large and complex data types
- gold Open Access which fosters wider collaboration and increased citations
- maximum visibility for your research: over 100M website views per year

**At BMC, research is always in progress.**

Learn more [biomedcentral.com/submissions](https://biomedcentral.com/submissions)



## Encephalopathy induced by Alzheimer brain inoculation in a non-human primate

Charlotte Gary, Suzanne Lam, Anne-Sophie Hérard, James E. Koch, Fanny Petit, Pauline Gipchtein, Stephen J. Sawiak, Raphaëlle Caillierez, Sabiha Eddarkaoui, Morvane Colin, Fabienne Aujard, Jean-Philippe Deslys, French Neuropathology Network, Emmanuel Brouillet, Luc Buée, Emmanuel E. Comoy, Fabien Pifferi, Jean-Luc Picq, Marc Dhenain

### Supplementary data

#### Supplementary Tables

Patient	Braak and Braak stage	Thal phase	Age (years)	Post-mortem delay (hours)	Immunohistochemistry
AD1	VI	5	76	10	Tau-positive (AT8, Innogenetic, 1/500) A $\beta$ -positive, including amyloid angiopathy (6F3D, Dako, 1/200) Alpha-synuclein-negative (LB509, Zymed, 1/250)
AD2	VI	4	83	21	Tau-positive (AT8, Innogenetic, 1/500) A $\beta$ -positive, without amyloid angiopathy (6F3D, Dako, 1/200) Alpha-synuclein negative (LB509, Zymed, 1/250)
CTRL	0	0	69	6	Tau-negative (AT8, Innogenetic, 1/500) A $\beta$ -negative (6F3D, Dako, 1/200) Alpha-synuclein-negative (LB509, Zymed, 1/250)

**Suppl. Table 1** Human brain sample characteristics and staging. Human parietal cortex

samples were obtained from two Alzheimer's patients (AD1 and AD2) and one control (CTRL) individual. They were tested for several pathologies by the French reference laboratory (C. Duyckaerts, Pitié-Salpêtrière hospital, Paris, France). Only the Alzheimer brains presented Alzheimer lesions. No other pathologies were detected in the brains.

Experimental protocol	Before inoculation	3 mpi	6 mpi	9 mpi	12 mpi	15 mpi	18 mpi
Rotarod test	X		X		X		X
Learning tasks	X		X		X		X
Long-term memory tasks			X		X		X
Electroencephalography	X		X		X		
MRI and atrophy evaluation	X	X	X	X	X	X	X
Immunohistochemistry							X
Stereological evaluation of neuronal loss (NeuN)							X
Evaluation of amyloid (4G8) and tau (AT8, MC1, AT100) lesions							X

**Suppl. Table 2** Schedule of the experimental protocol. mpi: months post-inoculation. MRI: magnetic resonance imaging.

Brain regions	SSF	NES	ACF ( $\mu\text{m}^2$ )	x-y steps ( $\mu\text{m}$ )	ASF	TSF- $\mu\text{m}$ mean $\pm$ SEM	CE mean $\pm$ SEM	Sampled cells per animal
CA1/2	1/10	7-10	30*30	50-50	0.36	11.63 $\pm$ 0.03	0.037 $\pm$ 0.002	430-700
CA3	1/10	5-7	30*30	50-50	0.36	11.63 $\pm$ 0.03	0.064 $\pm$ 0.002	485-760
EC-I	1/10	6	100*100	150-150	0.44	12.21 $\pm$ 0.10	0.067 $\pm$ 0.001	90-170
EC-II	1/10	6	30*30	75-75	0.16	12.21 $\pm$ 0.10	0.073 $\pm$ 0.000	400-530
EC-III-VI	1/10	6	50*50	150-150	0.11	12.21 $\pm$ 0.10	0.064 $\pm$ 0.000	650-800
Cing/RS	1/10	5-8	50*50	150-150	0.11	11.59 $\pm$ 0.07	0.056 $\pm$ 0.001	1600-2500

**Suppl. Table 3** Sampling parameters for stereological counting of NeuN-positive neurons. SSF: Section sampling fraction; NES: Number of evaluated sections; ACF: Area of counting frames; x-y steps: x-y steps between each counting frame; ASF: Area of the sampling fractions; TSF: Thickness of the sampling fraction; CE: Coefficient of error; CA1/2: CA1/2 region of the hippocampus; CA3: CA3 region of the hippocampus; EC-1, EC-2, EC-III-VI: Layers I, II, III-VI of the entorhinal cortex; Cing/RS: Cingulate cortex/retrosplenial cortex.



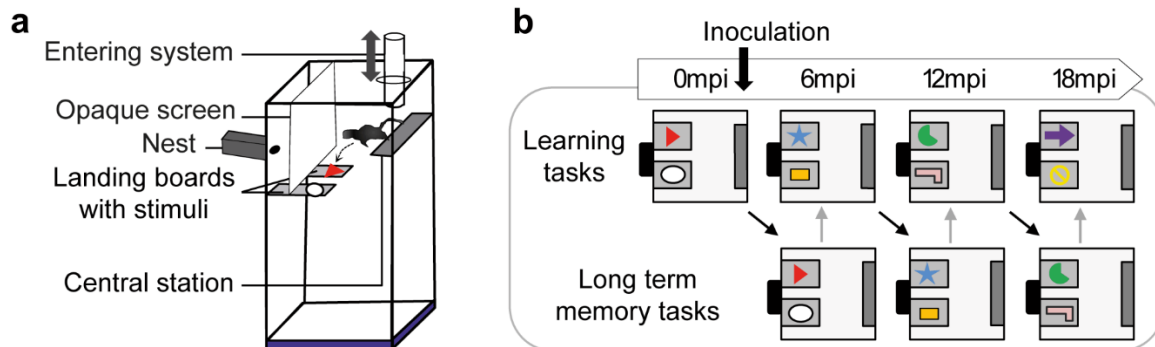
Brain regions	Cluster size (voxels)	Peak FDR-corrected	p-value	Peak T value
Entorhinal cortex, amygdala, hippocampus and inferior temporal cortex	1562	***	0.0004	6.3952
Cingulate and retrosplenial cortices	1342	***	0.0004	6.3777
Diagonal band of Broca, fornix and nucleus and stria terminalis	184	**	0.0013	5.7422
Ventral hippocampus	103	*	0.0109	4.2790
Caudate nucleus	70	**	0.0059	4.8479
Entorhinal cortex	59	*	0.0117	4.2231
Lateral temporal cortex	55	**	0.0062	4.7998
Peri-third ventricle area	52	*	0.0112	4.2488
Inferior temporal cortex	47	*	0.0175	3.8968
Fornix and stria terminalis	33	**	0.0061	4.8140
Parietal cortex	31	**	0.0045	5.0162
Amygdala	30	*	0.0102	4.4005
Lateral temporal cortex	23	*	0.0221	3.6795
Amygdala	22	*	0.0267	3.4984
Parietal cortex	18	*	0.0227	3.6538
Amygdala	18	*	0.0255	3.5305
Inferior temporal cortex	17	*	0.0221	3.6785
Caudate nucleus	16	**	0.0067	4.7113
Fornix	15	*	0.0172	3.9105
Inferior temporal cortex	15	*	0.0193	3.7971
Caudate nucleus	14	*	0.0233	3.6270
Inferior temporal cortex	13	*	0.0234	3.6142
Inferior temporal cortex	13	*	0.0140	4.0705
Entorhinal cortex	11	*	0.0135	4.1200
Parietal cortex	10	*	0.0108	4.3009
Amygdala	10	*	0.0255	3.5285

**Suppl. Table 4** Brain regions with gray matter loss in the Alzheimer's disease-inoculated group relative to the control-inoculated group. N = 6 animals per group at 0, 3, 6, 9 mpi and n = 6 and 4 in the Alzheimer- and control-inoculated groups, respectively at 12, 15, and 18 mpi. \*p < 0.05; \*\*p < 0.01; \*\*\*p < 0.001.

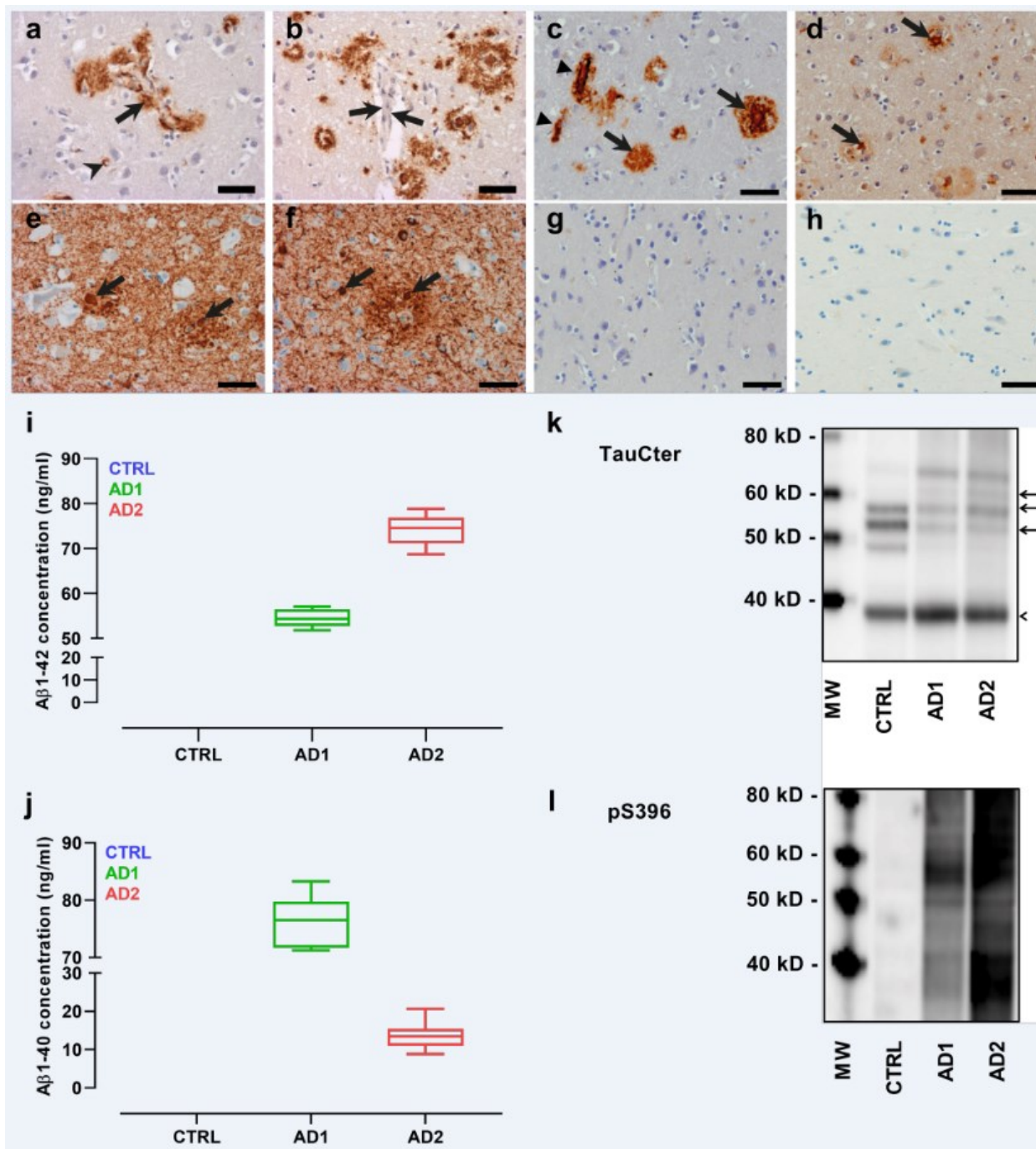
Species	Measure	mpi	Sample size
Tau30 <sup>+/+</sup> mice	Tau deposition in the soma of hippocampal neurons	1	1
APP/PS1dE9 mice	A $\beta$ deposition in the hippocampus	4	8
Mouse lemurs	Learning task D2	6	249
Mouse lemurs	Learning task D3	12	10
Mouse lemurs	Learning task D4	18	13
Mouse lemurs	Memory Task D1r	6	1
Mouse lemurs	Memory task D2r	12	3
Mouse lemurs	Memory task D3r	18	2
Mouse lemurs	EEG Delta 6 mpi	6	3
Mouse lemurs	EEG Theta 6 mpi	6	4
Mouse lemurs	EEG Delta 12 mpi	12	4
Mouse lemurs	EEG Theta 12 mpi	12	9
Mouse lemurs	EEG Alpha 12 mpi	12	3
Mouse lemurs	EEG Sigma 12 mpi	12	3
Mouse lemurs	EEG Beta 12 mpi	12	3
Mouse lemurs	NeuN-CA3	18	5
Mouse lemurs	NeuN-CA1-2	18	1067
Mouse lemurs	NeuN-EC-III-VI	18	8
Mouse lemurs	NeuN-EC-II	18	7
Mouse lemurs	NeuN-EC-I	18	52
Mouse lemurs	NeuN-Cg/RS	18	46
Mouse lemurs	A $\beta$ deposition in the brain	18	3
Mouse lemurs	CAA in the brain	18	35
Mouse lemurs	Tau deposition in the brain	18	15

**Suppl. Table 5** Estimated sample size to compare control and Alzheimer-inoculated mice and mouse lemurs assuming a significance level of 5%, a power of 80%, and two-sided tests. The different effects were classified according to species (Tau30<sup>+/+</sup> mice, APP/PS1dE9 mice or mouse lemurs). mpi represents the time post inoculation for the measure. Sample size represents the number of animal per experimental arm.

## Supplementary Figures



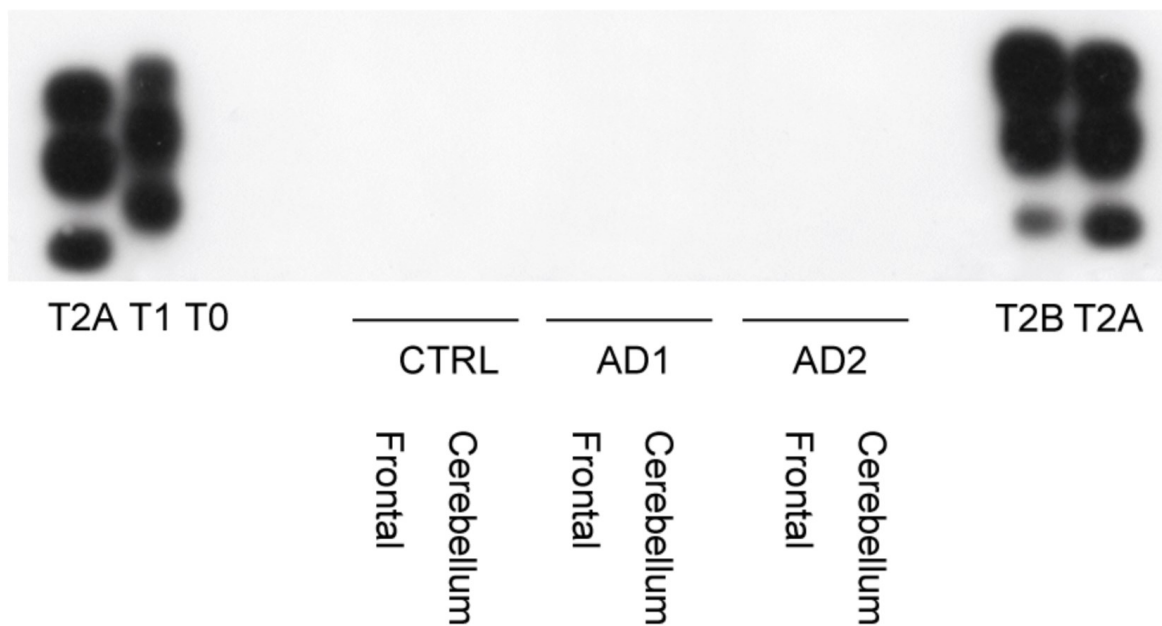
**Suppl. Fig. 1** Cognitive test in mouse lemurs. **a** Pairwise visual discrimination task jumping-stand apparatus. Lemurs had to jump from a central platform to one of two boards that displayed different visual stimuli. One board gave access to a positive outcome (nest containing a reward) and the other led to a negative (and non-rewarding) outcome (fall). An increasing number of trials required to achieve the criterion indicates a performance decline. **b** Schematic overview of the cognitive tasks. A learning task was performed before inoculation (0 months post-inoculation (mpi)). Long-term memory tasks consisted of the repetition of the discrimination task learned six months before. New learning tasks involving novel pairs of stimuli were performed every six months, after long-term memory tasks (black arrows: six months after; gray arrows: one day after).



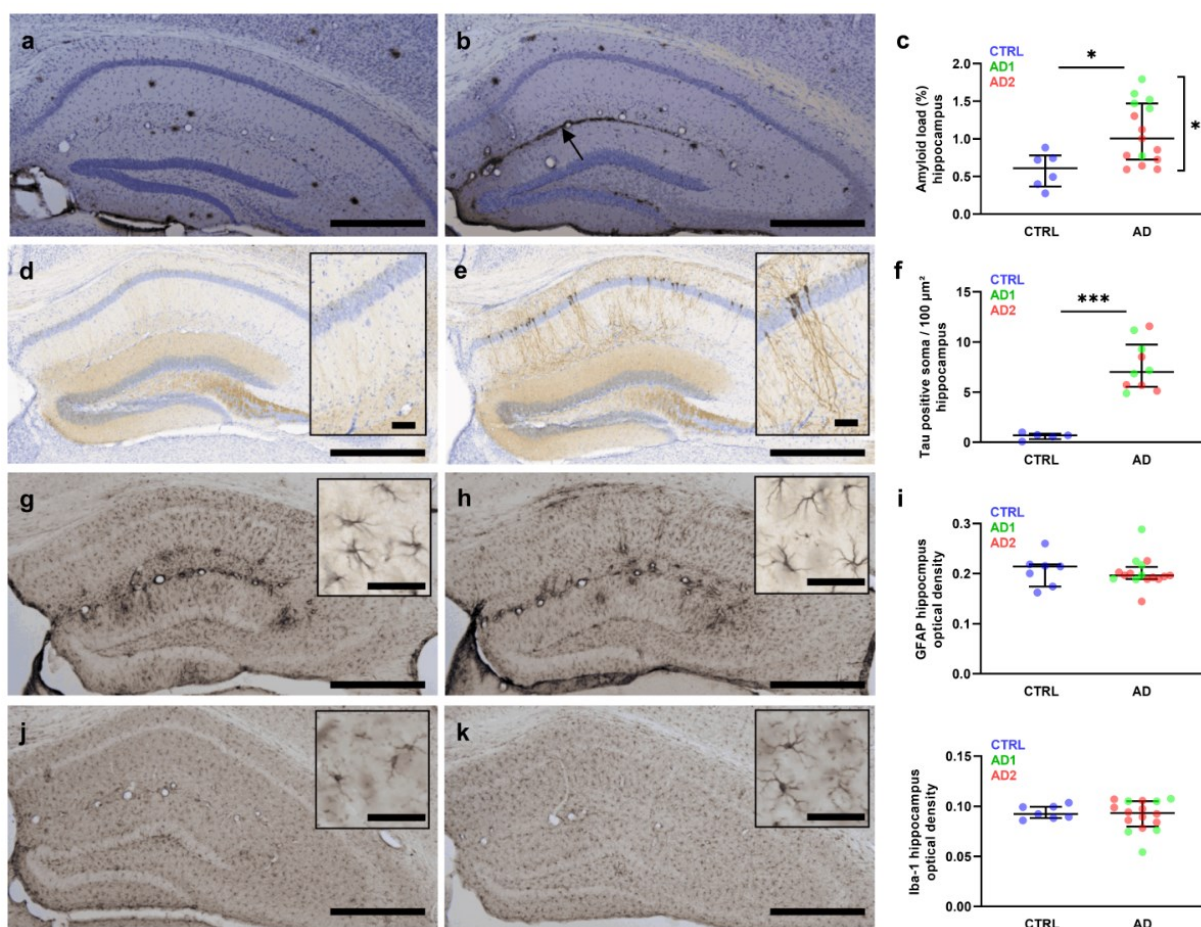
(Aβ1-42 values updated 2019-12-03)

**Suppl. Fig. 2** Characterization of human brain samples and homogenates. **a-e** Immunohistochemical staining (6F3D antibody) for Aβ in the two Alzheimer samples (**a-d**) and the control sample (**e**). **a** One subject (AD1) displayed amyloid angiopathy. The arrowhead points to a capillary, wall of which is immunoreactive for Aβ. The black arrow points to a small artery with severe amyloid angiopathy, sometimes forming parenchymal deposits. **b** The second patient (AD2) displayed numerous senile plaques, diffuse and stellate deposits. A vessel without amyloid deposition is seen in the middle of the field (black

arrows). No amyloid angiopathy was detected in that case. **c-d** Other sections from AD1 (**c**) and AD2 (**d**) showing amyloid plaques (black arrows). Arrow heads (in **c**) correspond to amyloid angiopathy. **e-f, h** Immunohistochemical staining (polyclonal anti-tau antibody) for tau lesions of the same samples. Tau positive NFTs are indicated with arrows in the two Alzheimer samples (**e-f**). Most of the brown labelling corresponds to neuropil threads. Amyloid or tau lesions were not detected in the control subject (**g, h**). **i-l** Biochemical characterization of human brain homogenates.  $A\beta_{1-42}$  (**i**)  $A\beta_{1-40}$  (**j**) were only detected in Alzheimer brain homogenates (20% weight/volume, ELISA). The AD1 patient that displayed more amyloid angiopathy also had more  $A\beta_{1-40}$  than AD2. **k** Typical shift of tau-Cter triplets in the Alzheimer samples relative to control sample (western blot, black arrows) (Papegaey *et al.*, *Acta Neuropathol Commun* 2016, 4: 74. <https://doi.org/10.1186/s40478-016-0345-0>). Arrow head corresponds to GAPDH loading reference. **l** Pathological pS396-positive tau smears were only detected in Alzheimer samples (western blot). Graphs display median and interquartile interval. Scale bars: 50  $\mu\text{m}$ .



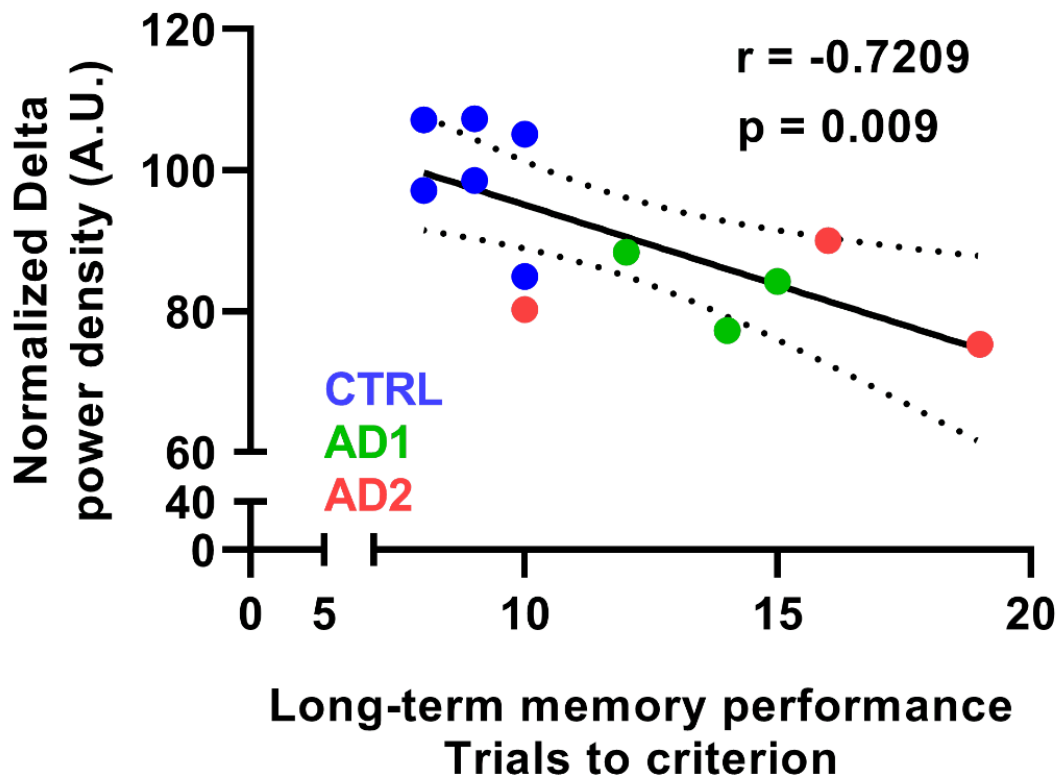
**Suppl. Fig. 3** Prion protein examination in human brain samples. Western blot patterns of PrPres from control (CTRL) and Alzheimer (AD) brain samples displayed no signs of PrPres pathology. T2A, PrPres type 2A control from a patient with sporadic CJD; T1, PrPres type 1 control from a patient with sporadic CJD; T2B, PrPres type 2B control from a patient with variant CJD (Parchi P *et al.*, *Ann Neurol* 1999, 46: 224-233.1999, [https://doi.org/10.1002/1531-8249\(199908\)46:2<224::AID-ANA12>3.0.CO;2-W](https://doi.org/10.1002/1531-8249(199908)46:2<224::AID-ANA12>3.0.CO;2-W)).



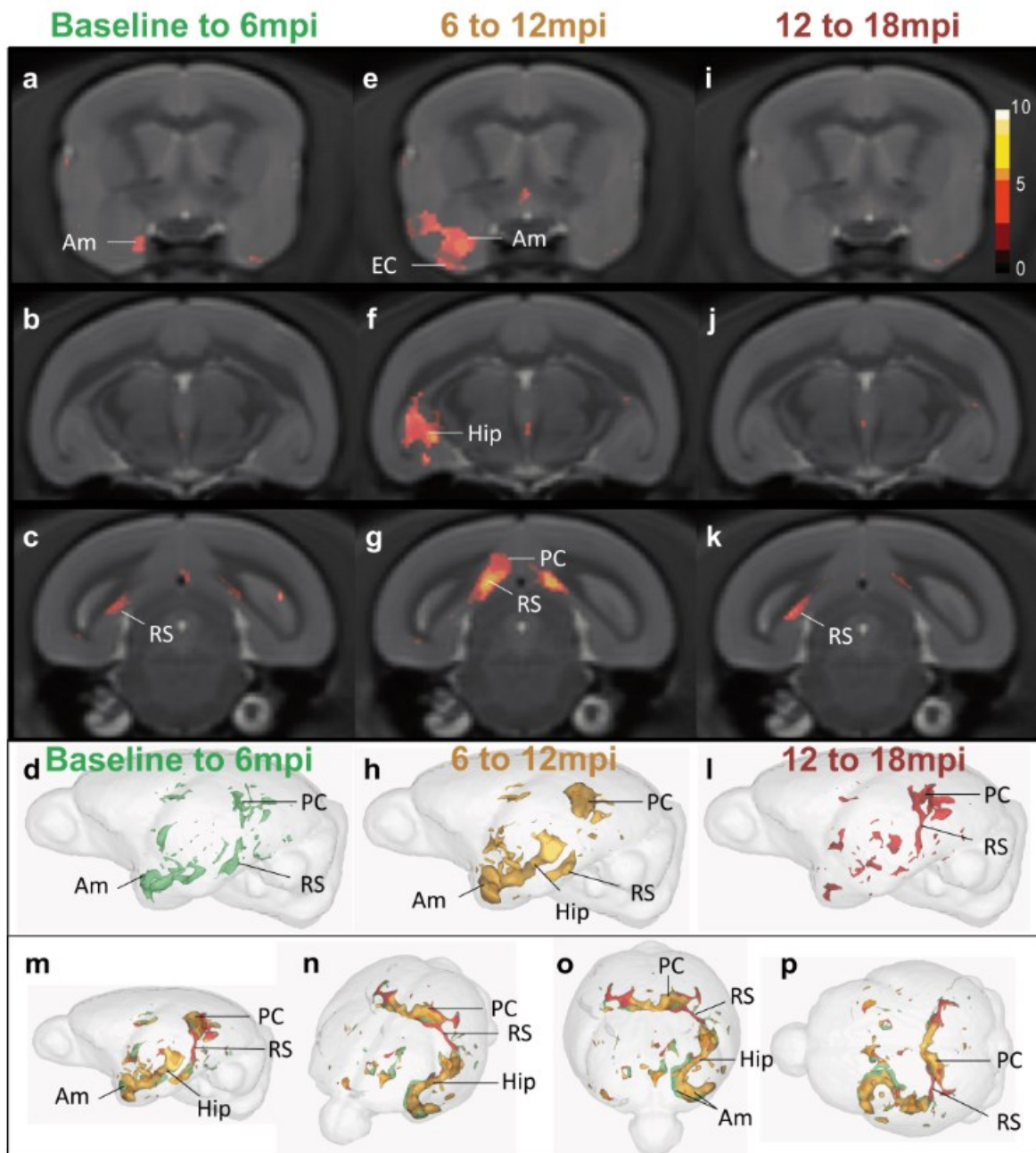
**Suppl. Fig. 4** A $\beta$  and Tau pathology in mice after inoculation with human brain homogenates. **a-c** Acceleration of A $\beta$  deposition (arrow) in the hippocampus of an Alzheimer-inoculated APP/PS1 $\Delta$ E9 mouse (**b**) four months after inoculation compared to a control-inoculated mouse (**a**) (Bam10 staining, n = 6 and 16 control- and Alzheimer-inoculated mice, respectively). **c** Quantification of the A $\beta$  load, showing greater amyloid load in the Alzheimer-inoculated group than in control-inoculated mice. Animals inoculated with the brain presenting with amyloid angiopathy (AD1) had a higher amyloid load than the mice inoculated with the brain without angiopathy (AD2) (p = 0.01). **d-f** Acceleration of tau deposition in the hippocampus of an Alzheimer-inoculated Tau30<sup>+/+</sup> mouse (**e**) one month after inoculation compared to a control-inoculated mouse (**d**) (AT8 staining, n = 5 and 10 control- and Alzheimer-inoculated animals, respectively). **f** Quantification of the density of Tau-positive somas showed more tau deposition in the Alzheimer-inoculated Tau30<sup>+/+</sup> mice than control-inoculated mice. **g-i** Similar GFAP staining in control- (**g**) and Alzheimer-inoculated (**h**) APP/PS1 $\Delta$ E9 mice four months after inoculation (n = 6 and 16 control- and Alzheimer-inoculated animals, respectively). **j-l** Similar Iba-1 staining in control- (**j**) and Alzheimer-inoculated (**k**)

APP/PS1<sub>ΔE9</sub> mice four months after inoculation (n = 6 and 16 control- and Alzheimer-inoculated animals, respectively). \*p < 0.05, \*\*\*p < 0.001, Mann-Whitney tests. Scale bars: main images: 500 μm; insets: 50 μm. Scatter plots display median and interquartile interval. CTRL-inoculated animals are in blue, AD1-inoculated in green and AD2-inoculated in red.





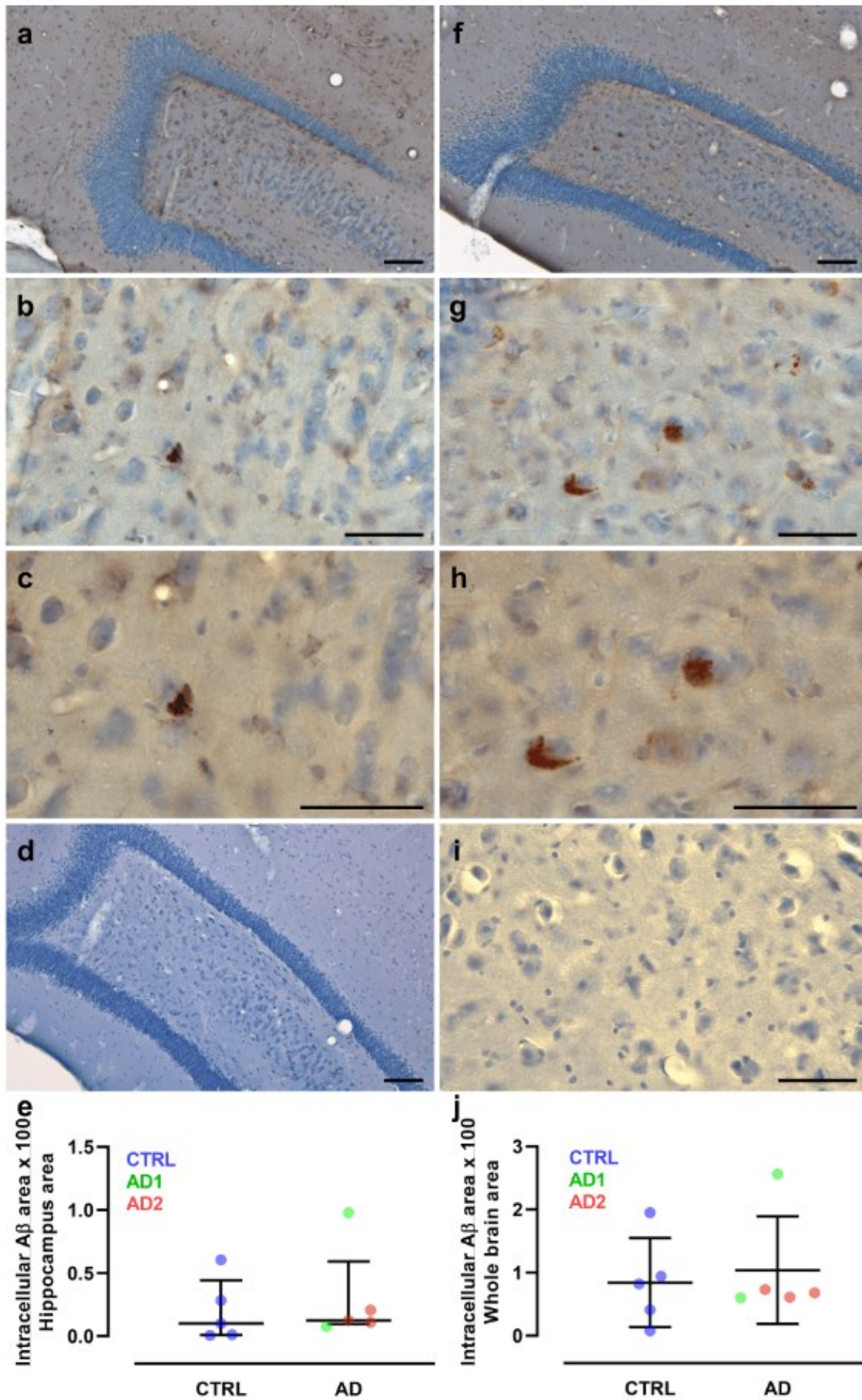
**Suppl. Fig. 5** Correlation between cognitive abilities and EEG delta frequency. Delta frequency measured by EEG at 6 mpi inversely correlated with long-term memory performance (Spearman's rank correlation test).  $n = 6$  animals per group. CTRL-inoculated animals are in blue, AD1-inoculated in green and AD2-inoculated in red.



**Suppl. Fig. 6** Time-dependent evolution of cerebral atrophy in inoculated lemurs. Rate of atrophy evolution in Alzheimer- relative to control-inoculated animals between baseline and 6 mpi (**a-d**), 6 mpi and 12 mpi (**e-h**), and 12 mpi and 18 mpi (**i-l**). 3D representations of atrophy rates between each time slot are presented in **d** (baseline to 6 mpi, green), **h** (6 to 12 mpi, orange), **i** (12 to 18 mpi, red). **m-p** show all the time slots on the same 3D views. **a-d** The atrophy process was low from baseline to 6 mpi, suggesting a limited acute effect induced by Alzheimer-brain inoculation. It involved mostly the amygdala and the ventral portion of the retrosplenial cortex. Rate of atrophy was low in the posterior cingulate cortex

at this stage. **e-h** The atrophy rate was maximal from 6 to 12 mpi. At this stage, it continued to involve the amygdala, the retrosplenial cortex in a more dorsal area and also reached the hippocampus, and the posterior cingulate cortex. **i-l** Evolution of the atrophy process was more limited from 12 to 18 mpi and involved mainly the retrosplenial cortex and the posterior cingulate cortex. EC: entorhinal cortex; Am: amygdala; Hip: hippocampus; PC: posterior cingulate cortex; RS: retrosplenial cortex. The colored scale represents group-wise differences in percentage local volume loss relative to baseline, calculated from the Jacobian determinants of the image registration parameters.





**Suppl. Fig. 8** Similar level of intracellular 4G8-positive structures in Alzheimer’s disease and control-inoculated lemurs. Immunostaining with 4G8 in the hippocampus of Alzheimer’s

disease- (**a-c**) and control-inoculated animals (**f-h**) showing intracellular labelling in both groups. Quantification of intracellular labelling did not show any difference in the hippocampus (**e**) or in the whole brain (**j**). **d-i** shows the same staining in an Alzheimer's disease-inoculated animal in the absence of primary antibody. Intracellular structures were not detected when the primary antibody was omitted. Scale bars: 100  $\mu\text{m}$  (**a, f, d**); 50  $\mu\text{m}$  (**b-c, g-i**). Scatter plots display median and interquartile interval. CTRL-inoculated animals are in blue, AD1-inoculated in green and AD2-inoculated in red.



---

## 3. Transmission of A $\beta$ and tau pathologies is associated with cognitive impairments in a primate

---

### 3.1. Context, objectives & abstract

AD definite diagnosis relies on the occurrence and spreading of both A $\beta$  and tau depositions in the brain, along with characteristic clinical manifestations (McKhann et al., 2011). Neuropathological observational studies in humans have suggested the iatrogenic transmission of A $\beta$  pathology in patients exposed to compounds (cadaver-sourced human growth hormone, dura mater) or neurosurgical tools contaminated with A $\beta$  (Duyckaerts et al., 2018; Hervé et al., 2018; Jaunmuktane et al., 2015b). Evidence of tau iatrogenic transmission is not as widely reported as for A $\beta$  and is still debated (Jaunmuktane et al., 2021). In addition, there is little information regarding the cognitive and clinical impacts of A $\beta$  and tau iatrogenic transmissions.

In this third study, we aimed to characterize the transmission of A $\beta$  and tau pathologies as well as downstream clinical manifestations in mouse lemurs, using AD brain extracts inoculations and following an inoculation paradigm different from the one used in the previous article (see **Results chapter – § 2. Encephalopathy induced by AD brain inoculation in a non-human primate**). Thus, I developed and validated a new stereotactic injection procedure to promote the seeding and spreading of A $\beta$  and tau seeds throughout the brain and improve surgical accuracy. In this study, AD brain extracts were inoculated in the posterior cingulate cortex and underlying corpus callosum of young 1.5-year-old mouse lemurs (n=6/group).

We showed that, using our new methodology, the intracerebral inoculation of AD brain extracts into mouse lemur primates systematically leads to A $\beta$  and tau depositions in several brain regions, both close to and distant from the inoculation sites, following a 21-month-long incubation period. Progressive cognitive impairments and widespread cerebral atrophy were also induced in comparison with control brain-inoculated lemurs, and limited neuroinflammation was detected. These results were replicated using two different batches of AD brain extracts. This is the first study demonstrating the transmission of an AD-like phenotype in a primate that includes both AD neuropathological lesions, *e.g.* widespread A $\beta$



### 3. Transmission of A $\beta$ and tau pathologies is associated with cognitive impairments in a primate

---

and tau deposits and AD clinical hallmarks, *e.g.* cognitive decline and brain atrophy. Taken together, this suggests that AD brain extract-inoculated primates, expressing physiological levels of endogenous A $\beta$  and tau, could be used as relevant models of Alzheimer pathology. Additionally, our experimental data support recent studies suggesting that both A $\beta$  and tau pathologies can be iatrogenically transmitted in humans. They also outline that such transmission could be associated with cognitive impairments and cerebral atrophy, therefore emphasizing the need for a systematic monitoring of morphological and functional alterations in individuals at risk of developing iatrogenic A $\beta$  and tau pathologies.

#### **3.2. Article**

*Published in Acta Neuropathologica Communications (<https://doi.org/10.1186/s40478-021-01266-8>).*


**Lam S.**, Petit F., Hérard AS., Boluda S., Eddarkaoui S., Guillermier M., The Brain Bank Neuro-CEB Neuropathology Network, Buée L., Duyckaerts C., Haïk S., Picq J.L., Dhenain M. Transmission of amyloid-beta and tau pathologies is associated with cognitive impairments in a primate. *Acta Neuropathol. Commun.* 9, 165. 2021.

RESEARCH

Open Access



# Transmission of amyloid-beta and tau pathologies is associated with cognitive impairments in a primate

Suzanne Lam<sup>1,2</sup>, Fanny Petit<sup>1,2</sup>, Anne-Sophie Hérard<sup>1,2</sup>, Susana Boluda<sup>3,4</sup>, Sabiha Eddarkaoui<sup>5</sup>, Martine Guillermier<sup>1,2</sup>, The Brain Bank Neuro-C. E. B. Neuropathology Network, Luc Buée<sup>5</sup>, Charles Duyckaerts<sup>3,4</sup>, Stéphane Haïk<sup>3,4</sup>, Jean-Luc Picq<sup>1,2,6</sup> and Marc Dhenain<sup>1,2\*</sup> 

## Abstract

Amyloid- $\beta$  (A $\beta$ ) pathology transmission has been described in patients following iatrogenic exposure to compounds contaminated with A $\beta$  proteins. It can induce cerebral A $\beta$  angiopathy resulting in brain hemorrhages and devastating clinical impacts. Iatrogenic transmission of tau pathology is also suspected but not experimentally proven. In both scenarios, lesions were detected several decades after the putatively triggering medico-surgical act. There is however little information regarding the cognitive repercussions in individuals who do not develop cerebral hemorrhages. In the current study, we inoculated the posterior cingulate cortex and underlying corpus callosum of young adult primates (*Microcebus murinus*) with either Alzheimer's disease or control brain extracts. This led to widespread A $\beta$  and tau pathologies in all of the Alzheimer-inoculated animals following a 21-month-long incubation period ( $n = 12$ ) whereas none of the control brain extract-inoculated animals developed such lesions ( $n = 6$ ). A $\beta$  deposition affected almost all cortical regions. Tau pathology was also detected in A $\beta$ -deposit-free regions distant from the inoculation sites (e.g. in the entorhinal cortex), while some regions adjacent, but not connected, to the inoculation sites were spared (e.g. the occipital cortex). Alzheimer-inoculated animals developed cognitive deficits and cerebral atrophy compared to controls. These pathologies were induced using two different batches of Alzheimer brain extracts. This is the first experimental demonstration that tau can be transmitted by human brain extracts inoculations in a primate. We also showed for the first time that the transmission of widespread A $\beta$  and tau pathologies can be associated with cognitive decline. Our results thus reinforce the need to organize a systematic monitoring of individuals who underwent procedures associated with a risk of A $\beta$  and tau iatrogenic transmission. They also provide support for Alzheimer brain-inoculated primates as relevant models of Alzheimer pathology.

**Keywords:** Amyloid- $\beta$  pathology, Alzheimer's disease, Cerebral atrophy, Prion, Tau pathology, Transmission

## Introduction

Prion diseases can occur after iatrogenic transmission of misfolded prion proteins. The aberrant proteins propagate by imposing their abnormal conformation on the

homologous normal host cell proteins which are continually produced in the natural course of cellular metabolism. Neuropathological observational studies in humans have suggested that amyloid- $\beta$  (A $\beta$ ) pathology is transmissible through a similar mechanism to that of acquired prion diseases [17]. To date, 76 cases of A $\beta$  pathology have been reported following exposure to cadaver-sourced human growth hormones [9, 17], dura mater grafts [14] or after cerebral surgeries with instruments

\*Correspondence: marc.dhenain@cea.fr

<sup>1</sup> Laboratoire des Maladies Neurodégénératives, Université Paris-Saclay, CEA, CNRS, 18 Route du Panorama, 92265 Fontenay-aux-Roses, France  
Full list of author information is available at the end of the article



© The Author(s) 2021. **Open Access** This article is licensed under a Creative Commons Attribution 4.0 International License, which permits use, sharing, adaptation, distribution and reproduction in any medium or format, as long as you give appropriate credit to the original author(s) and the source, provide a link to the Creative Commons licence, and indicate if changes were made. The images or other third party material in this article are included in the article's Creative Commons licence, unless indicated otherwise in a credit line to the material. If material is not included in the article's Creative Commons licence and your intended use is not permitted by statutory regulation or exceeds the permitted use, you will need to obtain permission directly from the copyright holder. To view a copy of this licence, visit <http://creativecommons.org/licenses/by/4.0/>. The Creative Commons Public Domain Dedication waiver (<http://creativecommons.org/publicdomain/zero/1.0/>) applies to the data made available in this article, unless otherwise stated in a credit line to the data.

contaminated with A $\beta$  [9, 21]. The pathology occurred as A $\beta$  plaques in the brain as well as vascular A $\beta$  pathology that could be associated with fatal cerebral hemorrhages. Observational evidence of tau iatrogenic transmission is not as widely reported as for A $\beta$ . A recent article detected tau lesions after incubation periods exceeding three decades in patients with iatrogenic A $\beta$  pathology [16]. However, because of the long incubation time in humans, it remains difficult to determine whether the A $\beta$  and tau pathologies were really transmitted. Another critical question is whether, in the absence of severe cerebral hemorrhages, A $\beta$  and/or tau transmissions can lead to cognitive impairments.

Experimental studies in transgenic mice overexpressing A $\beta$  precursor protein (APP) have shown transmissibility of A $\beta$  pathology after the intracerebral inoculation of Alzheimer's disease (AD) brain extracts [26]. Transmission of tau pathology is also described in mice overexpressing mutated tau proteins [6]. The host in which the proteopathic seeds are inoculated provides the biochemical and physiological environment that modulates lesion emergence and functional impact [18]. Transgenic mouse models of A $\beta$  or tau pathology rely on high A $\beta$  production or mutated tau protein expression, respectively. Thus, one key limitation of these models is that they provide a very different brain environment from the one found in human brains. Because of their phylogenetic proximity, primates have a brain environment closer to the human brain. A long-term study on marmosets (*Callithrix jacchus*) revealed the induction of sparse amyloidosis 3.5 years after intracerebral inoculations of AD brain homogenates [2, 23, 34]. However, tau pathologies or other AD-like features were not reported, even seven years later.

Mouse lemurs (*Microcebus murinus*) are small primates with an A $\beta$ <sub>1-42</sub> sequence that is homologous to that of humans [37], while mice differ by three amino acids [8]. Protein sequence issued from gene for Microtubule Associated Protein Tau (MAPT) has 94.3% identity with human gene, while murine MAPT gene has 88.8% identity (Additional File 1: Fig. S1a). Recently, our group showed that following an 18-month-incubation period, AD brain inoculations in the hippocampus and overlying cortex of mouse lemurs can lead to cognitive decline, functional alterations and cerebral atrophy associated with neuronal loss, but very sparse A $\beta$  and tau deposits [11]. In the present study, we inoculated the posterior cingulate cortex and underlying corpus callosum of young adult mouse lemurs with either AD or control brain extracts. The posterior cingulate cortex was chosen as it is a functional cerebral hub in mouse lemurs [10]. The corpus callosum was chosen based on the assumption that migration of seeds could follow white matter

tracts. As fragmentation of A $\beta$  seeds by extended sonication was shown to increase seeding capacity of brain extracts [20], we carefully sonicated the inoculated samples. Following a 21-month incubation period, all of AD-inoculated mouse lemurs (n = 12) developed extensive A $\beta$  and tau pathologies in several brain regions, providing evidence for the spreading of these pathologies in the brain. Animals inoculated with control-brain extracts did not develop any A $\beta$  plaques or tau deposits. Similar results were replicated using two different types of AD-brain extracts. AD-inoculated animals also developed progressive cognitive impairments and cerebral atrophy.

## Results

### Tau isoforms in mouse lemurs

In humans, MAPT gene can produce a variety of isoforms by alternative splicing. In normal adult human brain there are six isoforms that differ by sequences from exons 2 and 3 that encode N-terminal sequences, and exon 10 that encodes a microtubule binding repeat sequence. When this latter exon is present there are four microtubule binding repeats (4R-tau) and when absent there are three microtubule-binding repeats (3R-tau) [24]. In adult humans, all six brain isoforms are present leading to the presence of both 4R and 3R tau [15]. In adult wild-type mice, the 4R tau is the only isoform [24]. Analysis of tau isoforms in mouse lemurs by immunoblots showed that mouse lemurs present with both the 4R and 3R isoforms, while the isoforms corresponding to exon 2 were not detected due to either their absence or differences in the protein sequence (Additional File 1: Fig. S1b).

### Characterization and inoculation of human brain homogenates

We prepared two brain homogenates from sporadic AD patients, with each homogenate consisting of a combination of four brain extracts from patients with either a slowly evolving form of AD (defined by a disease duration of 5 to 8 years (AD1)) or a rapidly evolving form of AD (defined by a disease duration of 6 months to 3 years (AD2)). A third "control" homogenate, was prepared from the brains of two non-demented individuals (Ctrl). The characteristics of the selected subjects are presented in Additional File 1: Table S1 and Additional File 1: Fig. S2. The amount of A $\beta$ , tau and neuroinflammatory proteins differed slightly between the brain homogenates, as the AD2 brain extract displayed more total tau and phospho-tau181, but less A $\beta$ <sub>38</sub> and A $\beta$ <sub>40</sub> than the AD1 one (Additional File 1: Fig. S2g-l). Iba1 and GFAP levels were similar in the two AD homogenates (Additional File 1: Fig. S2m-o). Brain homogenates were bilaterally inoculated into the posterior cingulate cortex and

underlying corpus callosum of young-adult 1.5-year-old mouse lemurs (6.25  $\mu\text{l}/\text{site}$ ,  $n=6/\text{group}$ ). This corresponded to 33.75, 34.56 and 34.37  $\mu\text{g}$  of total proteins per site, respectively for the Ctrl, AD1 and AD2 groups. This corresponds to 0, 0.75 and 1 pg of A $\beta$ 42 and 0, 0.063 and 0.125  $\mu\text{g}$  of phospho-tau181. As depicted in Additional File 1: Fig. S3 showing regions connected to the posterior cingulate, the needle tract passed through the medial part of the parietal cortex (Brodmann area 7) [27].

### A $\beta$ pathology induction and spreading after AD brain inoculation

Mouse lemurs were euthanized at 21 months post-inoculation (mpi) and their brains were studied by histology. All of AD-inoculated animals ( $n=12$ ) developed A $\beta$  deposits (Figs. 1, 2, 3 and 4), whereas none of the Ctrl-inoculated animals displayed any A $\beta$  pathology ( $n=6$ , Fig. 5a–b). These deposits were detected using 4G8 (Fig. 1a, c, g–h) or A $\beta$ 42 (Fig. 1b, d) antibodies as well as a Thioflavin S staining (Fig. 1e–f). They occurred in the forms of diffuse (Fig. 1a–b) and dense (Fig. 1c–f) parenchymal A $\beta$  plaques or A $\beta$  angiopathy affecting cortical and hippocampal vessels (Fig. 1g–h), although angiopathy was less prominent than parenchymal deposits. A $\beta$  pathology spread widely throughout the brain and was detected in most cortical regions (Figs. 2, 3, 4a, c–f). Indeed, animals from both AD-inoculated groups showed A $\beta$  deposition in the inoculated posterior cingulate cortex (Figs. 2i, 3a) and/or around the needle tract in the parietal cortex (area 7) (Figs. 2l–n, r, 3b). Adjacent regions including the retrosplenial cortex (Figs. 2q, 3c), anterior cingulate cortex (Figs. 2a, e, 3d) and parietal area 5 (Figs. 2j–k, 3e) also displayed A $\beta$  pathology. Additionally, A $\beta$  plaques were detected in the hippocampus (Figs. 2p, t, 3f) and other regions more distant from the inoculation sites including the superior temporal cortex (areas 22, 21 and 20) (Figs. 2g, o, s, 3g), the parietal cortex involving the primary somatosensory cortex (areas 1–3, Fig. 2c, f) and the frontal cortex, including the primary motor cortex (area 4, Figs. 2b, 3h). Occipital areas also displayed A $\beta$  deposits (area 17, Fig. 2u–v; area 18, Fig. 2w–x). A $\beta$  pathology was not detected in the entorhinal cortex (Fig. 3i) or in deep grey nuclei, brainstem or cerebellum. Quantitative analysis did not reveal any difference between the two AD-inoculated groups (Fig. 3).

### Tau pathology induction and spreading after AD brain inoculation

All AD-inoculated lemurs developed intraneuronal tau accumulations resembling neurofibrillary tangles (NFTs, Fig. 6a–d) and neuropil threads (NTs, Fig. 6e–h), at the inoculation sites and in several other regions (Figs. 4b, g–j, Figs. 7, 8 and 9). Conversely, Ctrl-inoculated animals

did not display any tau pathology (Fig. 5c–d). In AD-inoculated animals, tau pathology was detected using AT8 that detects phosphorylation of S202 and T205 [38] (Figs. 6, 7), AT100 that detects phosphorylation at T212 and at S214 that is phosphorylated in AD brains but not in normal brains [38] (Fig. 6d, g), an anti-pS422 antibody (phosphorylation at S422 occurs in AD but not in normal brains [38], Fig. 6c, f), and Gallyas silver staining (Fig. 6h). Neuritic plaques were not detected in any animal. AT8-positive NFTs were localized at the level of the inoculation site (posterior cingulate cortex (Figs. 7i, 8a), parietal area 7 (Figs. 7m, 8b) as well as in juxtaposing regions (retrosplenial cortex (Figs. 7n, q, s, 8c), anterior cingulate cortex (Figs. 7a, c, 8d), parietal area 5 (Figs. 7e, 8e)). They were also detected within the hippocampus (Figs. 7k, o, r, 8f) and temporal area 22 (Fig. 7g). Although temporal regions such as area 21 was never involved, some regions more distant from the inoculation sites displayed NFTs (temporal area 20 (Figs. 7l, p, t, 8g), area 13–16, parietal areas 1–3, frontal area 4 (Fig. 8h) and entorhinal cortex (Figs. 7h, 8i)). Occipital regions (areas 18–17) as well as the most frontal regions did not display tau-positive NFTs, despite the presence of A $\beta$  deposits (Fig. 4). AT8-positive neuropil threads were mainly localized at the inoculation sites (posterior cingulate cortex (Figs. 7i, 8a), corpus callosum (Figs. 7f, j, Fig. 9b), but were barely present around the needle tract (area 7, Figs. 7m, 9c). They were also induced to a lesser degree in juxtaposing regions (retrosplenial cortex (Figs. 7n, 9d), anterior cingulate cortex (Fig. 9e), parietal area 5 (Figs. 7e, 9f)) and in distant regions (temporal area 20 (Figs. 7p, 9g), entorhinal cortex (Fig. 9h) and amygdala (Fig. 7b, d). Except for one or two animals, neuropil threads were not detected in the hippocampus (Fig. 9i) nor in the frontal cortex (area 4, Fig. 9j). As was the case for A $\beta$ , quantitative analysis did not reveal any difference in tau pathologies between the two AD-inoculated groups (Figs. 8 and 9).

### Similar microglial response in AD- and Ctrl-inoculated animals

Neuroinflammation was assessed using a histological marker for activated microglia (HLA-DR). Reactive microglia were observed both in the parenchyma (Fig. 10a) and around the vasculature (Fig. 10b) of AD- and Ctrl- inoculated animals. Microglial response mainly involved the inoculation sites (Fig. 10c–e) and was not detected in other regions, even in the presence of A $\beta$  plaques. We did not detect any differences between the groups, suggesting that the inoculation of AD-brain extracts does not induce an exacerbated neuroinflammatory response in comparison with human Ctrl-brain extract.

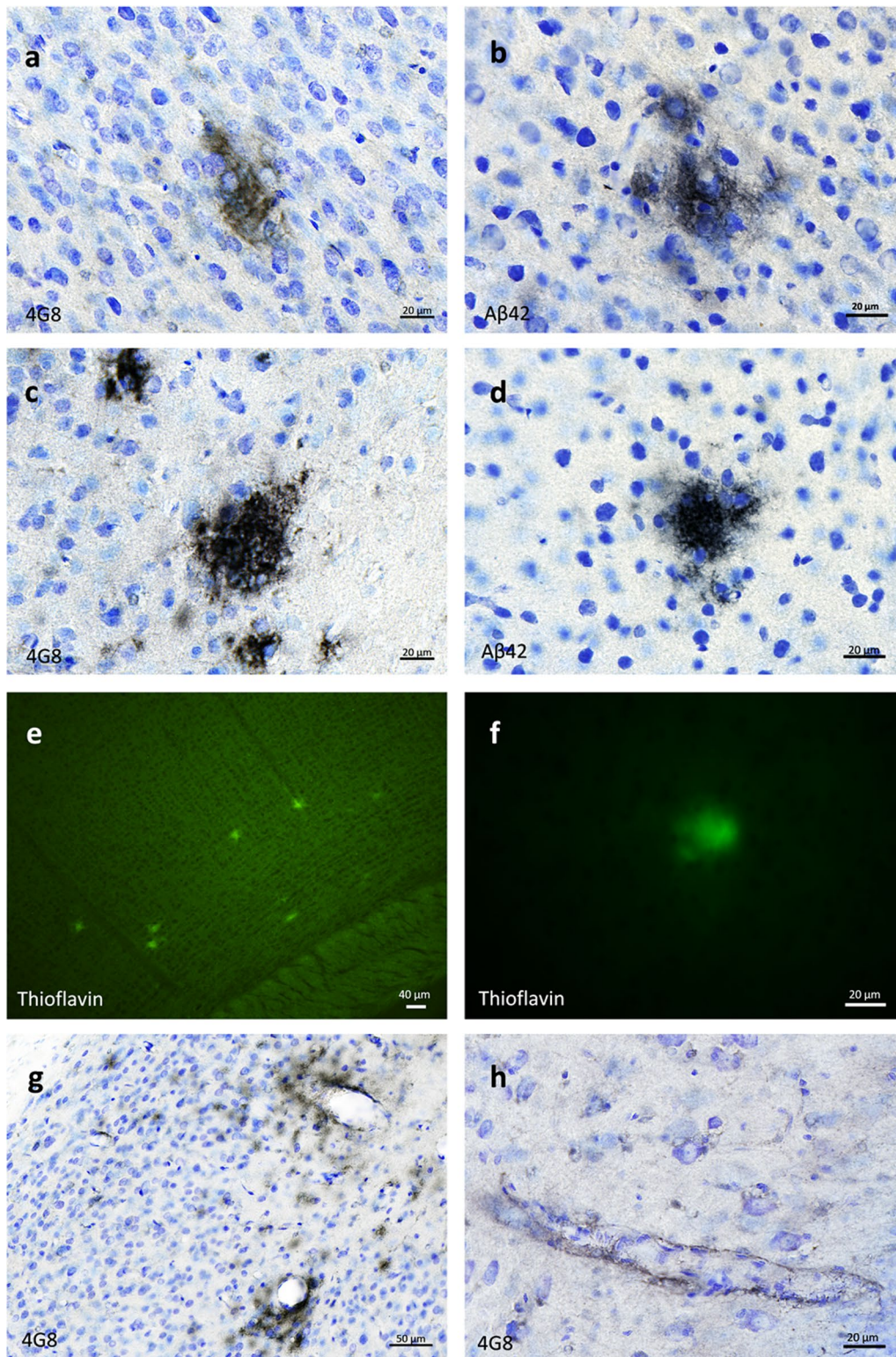


**Fig. 1** Aβ plaques and vascular deposits in AD-inoculated mouse lemurs. Parenchymal diffuse **a-b** and dense **c-d** plaques stained by 4G8 or Aβ42 antibodies in AD-brain inoculated mouse lemurs. Plaques were also Thioflavin S-positive **e-f**. Cerebral Aβ angiopathy was also observed in cortical regions **g** and in the hippocampus **h** (4G8 antibody). Scale bars: 20 μm in a-d, f, h; 40 μm in e; 50 μm in g

### Cognitive deficits induced by AD brain inoculation

Learning and long-term memory capabilities were evaluated using discrimination tasks in a jumping stand apparatus [31] before inoculation and at 4, 9, 15 and 21 mpi. The jumping stand apparatus was designed to test the cognition of mouse lemurs using discrimination tasks while taking into account their arboreal lifestyle as well as their sensorial and behavioral skills. At each time-point, a new pair of visual stimuli was introduced to the animals, and learning abilities were evaluated as the lemur had to identify the positive stimulus to reach its nesting box (Additional File 2). Long-term memory was evaluated through the recall of the discrimination task learned during the previous session, 4 to 6 months earlier. At the final timepoint, *i.e.* at 21 mpi, and following a successful discrimination learning session, a reversal learning test was performed to evaluate cognitive flexibility.

AD-inoculated animals showed lower learning abilities in comparison with Ctrl animals (Fig. 11a). Indeed, for the first discrimination task, before the inoculation of the brain extracts (M0), all groups required a similar number of trials to learn the rewarded stimulus ( $15.3 \pm 5.8$ ,  $16.8 \pm 8.6$  and  $14.5 \pm 7.4$  trials for Ctrl, AD1 and AD2 inoculated animals, respectively). Learning performances improved in the Ctrl-inoculated group, reaching the best possible score (at least 8 correct choices out of the first 10 consecutive trials) as early as during the second learning session at 4 mpi (M4), thus demonstrating highly effective acquisition of the learning set. Conversely, learning abilities in the two AD groups declined markedly over time, and performances were significantly worse compared to the Ctrl group throughout the follow-up (Fig. 11a,  $p = 0.0002$  and  $p = 0.004$ , respectively for AD1 and AD2). Long-term memory performance also differed between the groups throughout the study, but no post-hoc differences were detected between AD-inoculated animals and controls (Fig. 11b). A reversal learning test was performed only at 21 mpi and Ctrl animals performed better than AD1 or AD2-inoculated lemurs (Fig. 11c,  $p = 0.024$  and  $p = 0.0045$ , respectively). For all of the evaluated cognitive functions, no statistical difference was observed between AD1- and AD2-inoculated lemurs (Fig. 11a–c). Altogether, these data suggest that inoculation with AD brain extracts impairs learning abilities as well as

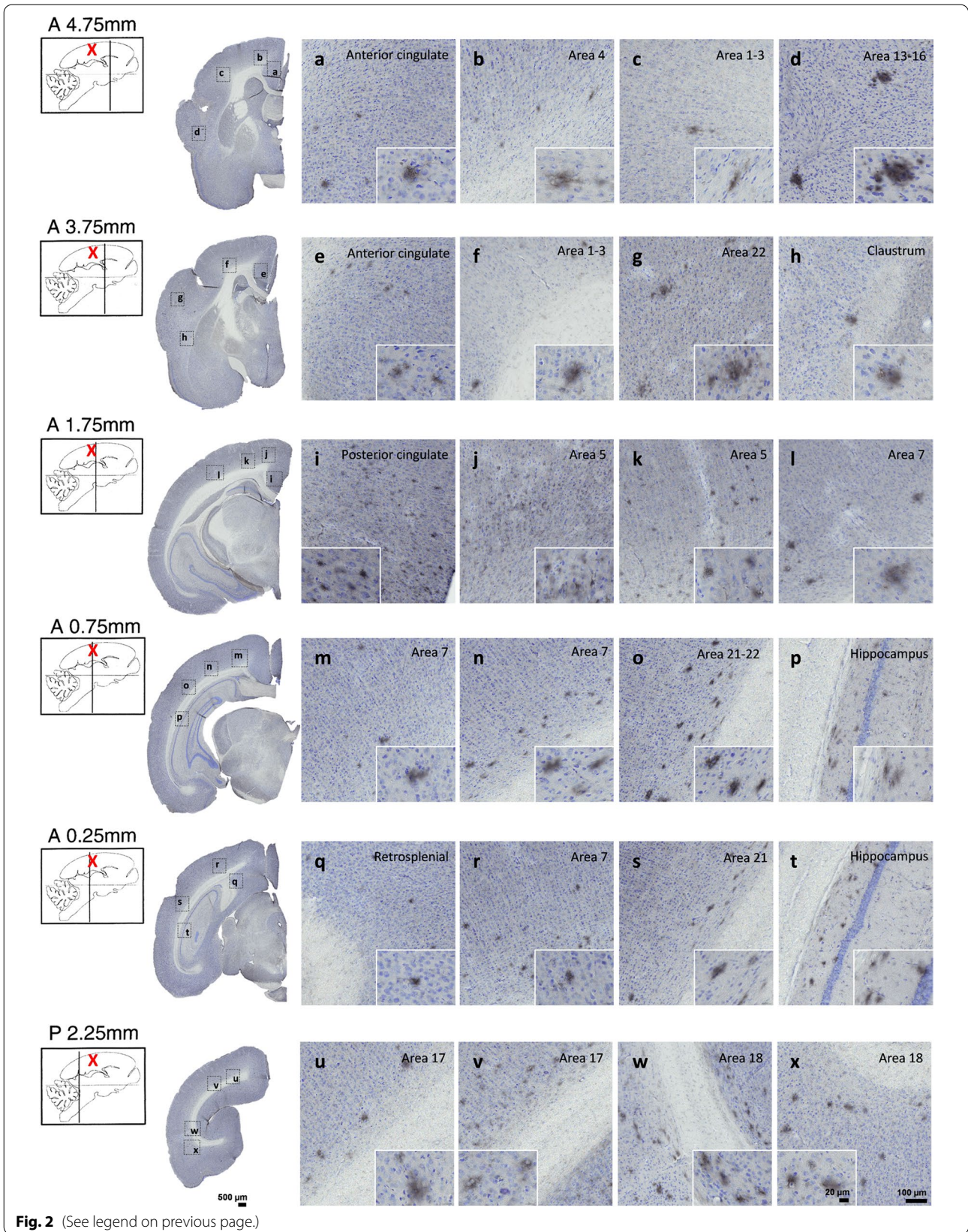
cognitive flexibility, while long-term memory is globally preserved. Additionally, motor function was evaluated and showed that, as expected, all animals displayed similar motor skills all throughout the follow-up (Fig. 11d). These data suggest that cognitive deficits observed in AD-inoculated animals in the jumping stand apparatus were not related to motor impairments.

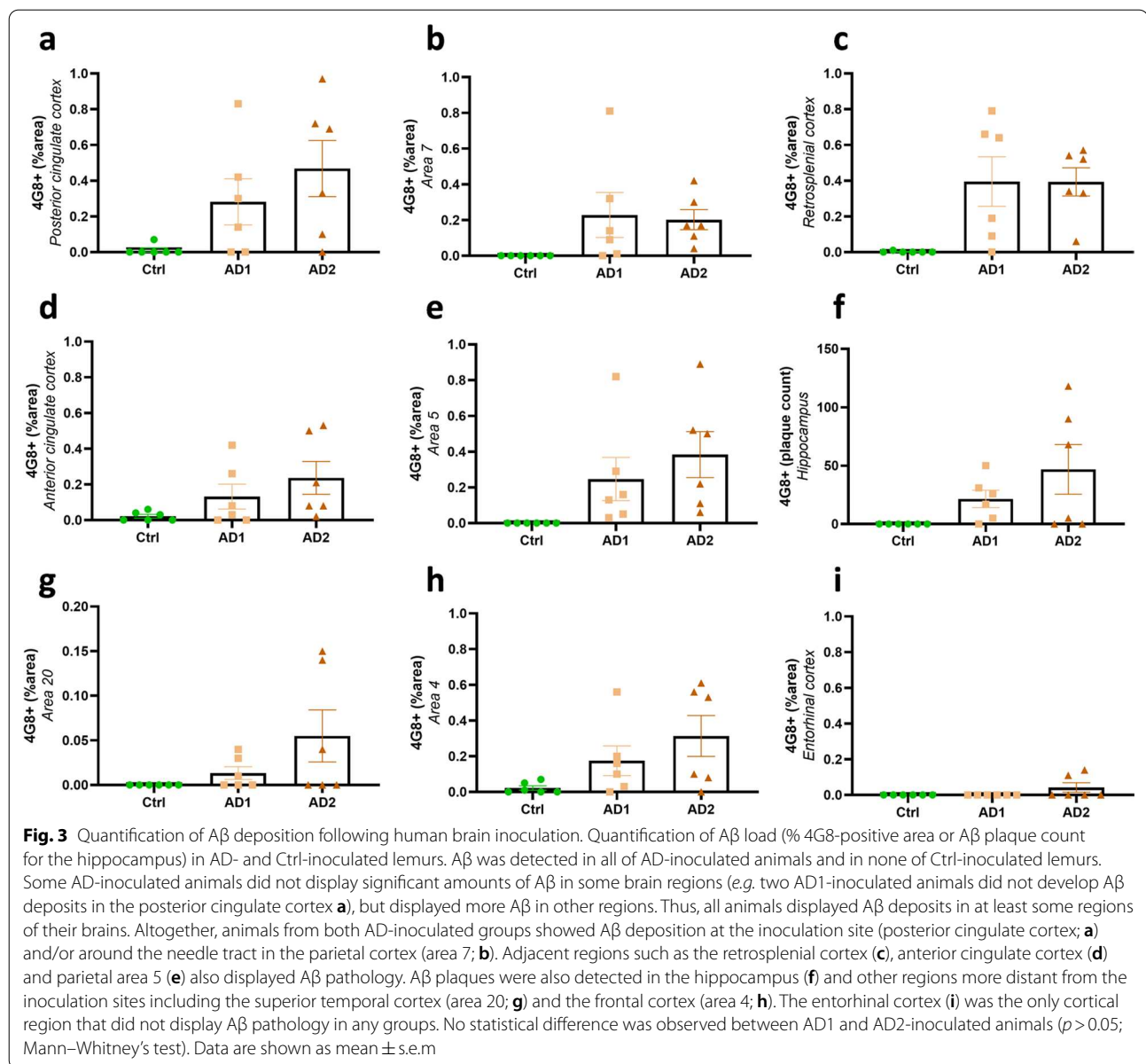
### Progressive cerebral atrophy induced by AD brain inoculation

Brain MRI acquisitions were performed before inoculation and at 4, 9, 15 and 21 mpi. To increase statistical power, AD1 and AD2-inoculated animals were grouped within a unique AD group to be compared with Ctrl-inoculated lemurs. Cerebral atrophy was evaluated using an automated voxel-based morphometry analysis [36]. To control for multiple comparisons, an adjusted p-value was calculated using the voxel-wise false discovery rate (FDR-corrected  $p < 0.05$ ), with extent threshold values of 10 voxels. At 4 mpi, only a slight atrophy was detected in the inoculated posterior cingulate cortex of AD animals, compared to the Ctrl group (Fig. 12a). This atrophy did not progress between 4 and 9 mpi (Fig. 12b), but between 9 and 15 mpi significant bilateral atrophy occurred in several other brain regions (Fig. 12c). It involved the inoculation site, *i.e.* the posterior cingulate cortex, and the parietal cortex (area 7, site with the needle tract) of AD brain-inoculated lemurs (Fig. 12c). Grey matter loss was also observed close to the inoculation sites in the retrosplenial, parietal area 5 and anterior cingulate cortices (Fig. 12c). In addition, cerebral atrophy was reported in several other cortical areas including the prefrontal cortex (antero-medial area), frontal cortex (superior frontal cortex, areas 4 and 6), parietal areas 1–3, temporal cortex (entorhinal and periamygdalar cortices), insular cortex (areas 13–16), and occipital visual cortex (areas 18 and 17) (Fig. 12c). Atrophy was also detected in some sub-cortical regions such as the hippocampus, the basal forebrain (including the diagonal band of Broca and nucleus accumbens), claustrum, septum, basal ganglia (including the caudate nucleus and putamen) and medial thalamus (Fig. 12c). Atrophy did not further increase from 15 to 21 months post-inoculation (Fig. 12d).

(See figure on next page.)

**Fig. 2** A $\beta$  pathology throughout the brains of mouse lemurs inoculated with AD brain extracts. Representative images of 4G8 immunolabelling showing A $\beta$  pathology throughout the brains of mouse lemurs following AD brain extracts inoculations. A $\beta$  deposition was observed in the inoculated posterior cingulate cortex (i) and around the needle tract in the parietal cortex (area 7; **l-n, r**). Adjacent regions including the retrosplenial cortex (**q**), parietal area 5 (**j-k**) and anterior cingulate cortex (**a, e**) also displayed A $\beta$  pathology. Additionally, A $\beta$  plaques were detected in the hippocampus (**p, t**) and other regions more distant from the inoculation sites including the superior temporal cortex (areas 22 and 21; **g, o, s**), the parietal areas 1–3 (**c, f**) and the frontal cortex (area 4; **b**). Occipital areas also displayed A $\beta$  deposits (areas 17 and 18; **u-x**). The red crosses indicate the inoculated region. Scale bars: 500  $\mu$ m in whole slice images, 100  $\mu$ m in zooms and 20  $\mu$ m in inserts





## Discussion

For the first time in a primate, we induced widespread A $\beta$  and tau pathologies along with cognitive impairments and cerebral atrophy following the focal inoculation of AD brain extracts in the cingulate cortex and underlying corpus callosum. These results were replicated using two different batches of AD brain extracts.

A $\beta$  deposits were detected using specific antibodies as well as Thioflavin S staining. They were observed close to the inoculation site and in almost all cortical regions (except for the entorhinal cortex) as well as in the hippocampus, suggesting their efficient spreading within the whole brain. Tau-positive pathology occurred in the

forms of neurofibrillary tangles and neuropil threads while neuritic plaques were not detected. They were detected using several antibodies (AT8, AT100, ps422) and Gallyas staining. Tau pathology was evident at the inoculation site and throughout the brain. However some brain regions that were relatively close to the inoculation sites were spared, such as temporal (area 21) and occipital regions (areas 18 and 17). This suggests that the spatial progression of tau did not occur solely via a systematic isotropic diffusion from the injection site to proximal regions. Interestingly, regions such as the entorhinal cortex, that are connected to the cingulate cortex [29] and are distant from the inoculation site were tau-positive but



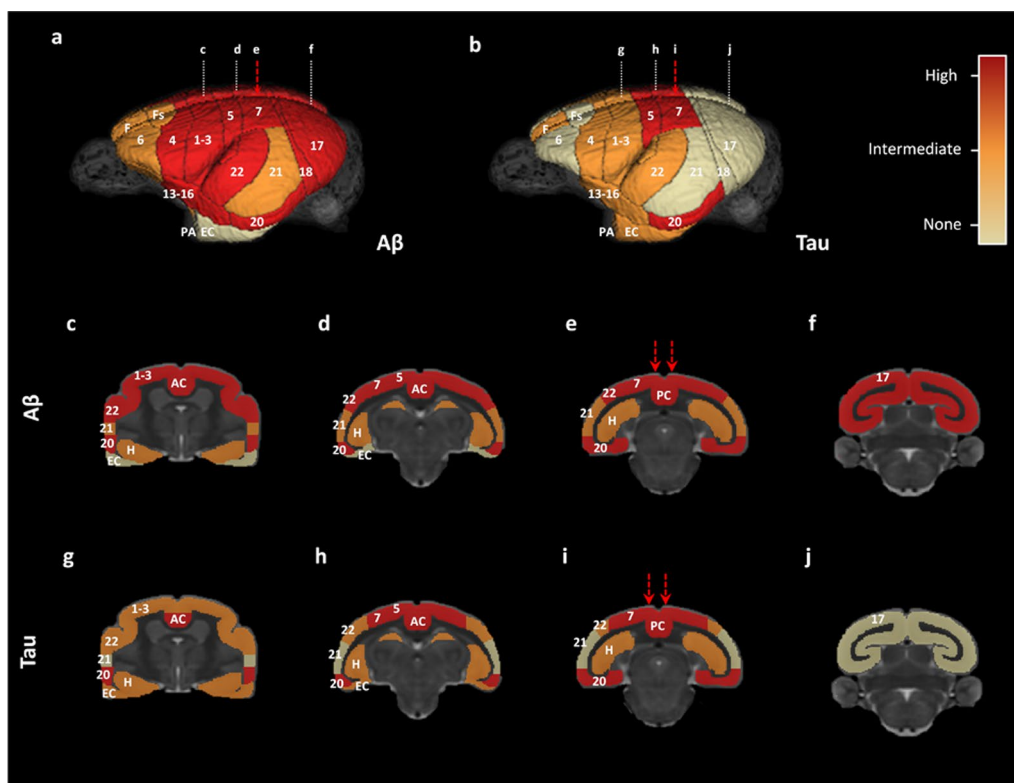


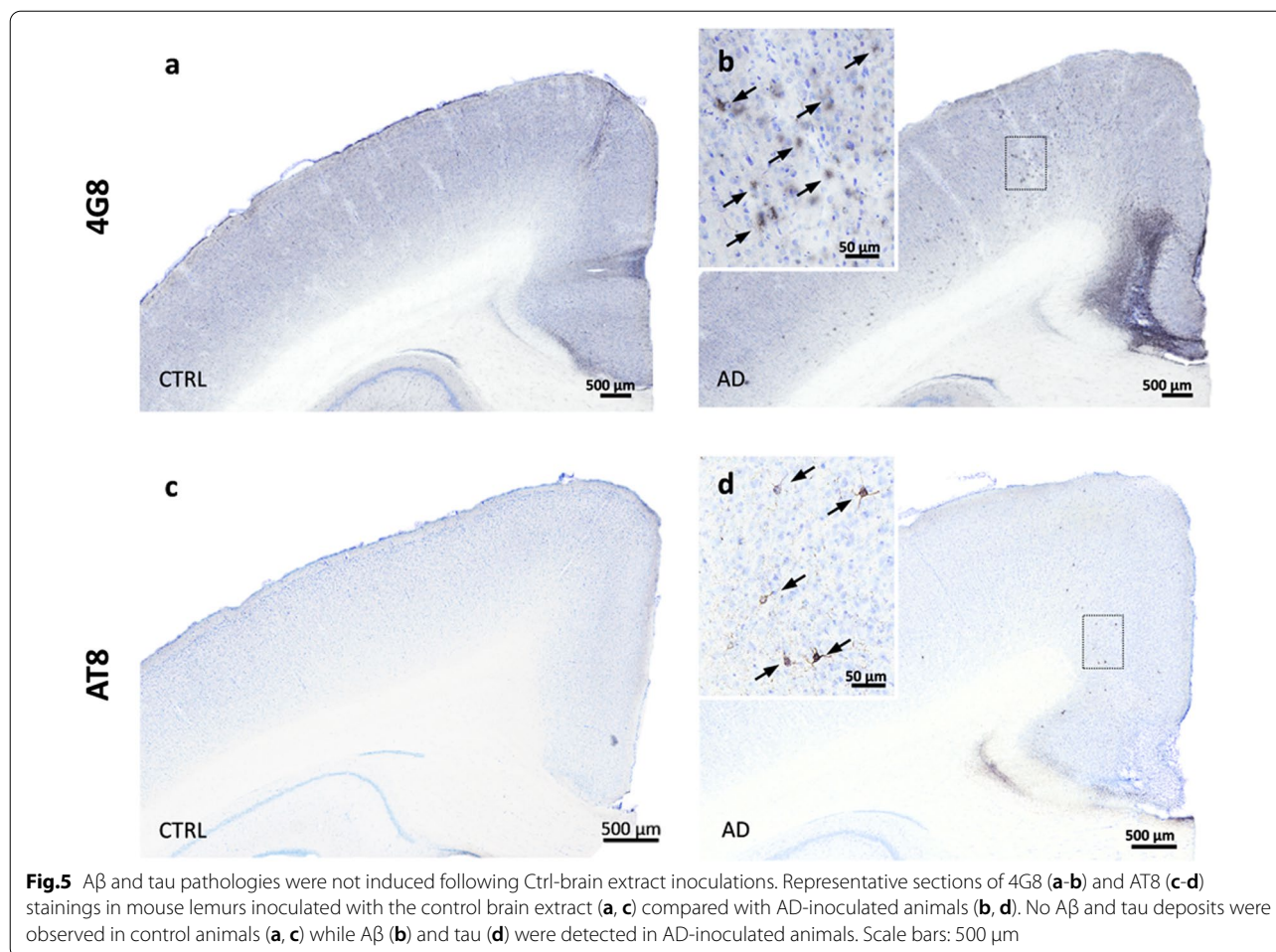
**Fig. 4** Overview of A $\beta$  and tau pathology spreading throughout the brains of mouse lemurs inoculated with AD brain extracts. Three-dimensional rendering of A $\beta$  and tau pathologies in mouse lemur brains using a three-level semi-quantitative scale (no lesions/intermediate/high lesion load). **(a, c-f)** A $\beta$  pathology involved almost all cortical regions, except for the entorhinal cortex. The hippocampus was also A $\beta$ -positive. **(b, g-j)** High levels of tau lesions were reported at the inoculated sites (posterior cingulate cortex, area 7) as well as in juxtaposing regions such as the area 5. Distant regions such as the area 20 also displayed high tau pathology. The hippocampus, entorhinal cortex, and other cortical areas displayed intermediate tau lesion loads. The red arrows indicate the needle tracts. Numbers represent Brodmann areas as reported in the mouse lemur brain by (Le Gros Clark, 1931). AC: anterior cingulate cortex, EC: entorhinal cortex, F: antero-medial frontal cortex, Fs: superior frontal cortex, H: hippocampus, PA: peri-amygdalar cortex, PC: posterior cingulate cortex

A $\beta$ -negative. This suggests that tau pathology occurred, at least in part, through a transit along neuroanatomical pathways and following different routes as compared to A $\beta$ . Importantly, both A $\beta$  and tau pathologies were detected after a relatively short incubation period of 21 months in young-adult 1.5-year-old primates that are typically devoid of any lesions at this age. We speculate that aggregate deposition might have started even earlier since cerebral atrophy was detected between 9 and 15 mpi.

A chronic neuroinflammatory response, evaluated by HLA-DR staining, was detected at the inoculation sites after human brain extracts inoculation. Such inflammation was not observed in non-inoculated animals (data not shown). Here, inflammation was restricted to the cingulate cortex and underlying corpus callosum, while A $\beta$  and tau pathologies were widespread in the brains of AD-inoculated animals. Also, no difference in microglial activation was observed between the groups of AD- or

Ctrl-inoculated animals. This suggests that neuroinflammation cannot explain most of the differences between AD- and Ctrl-inoculated animals. However, one cannot exclude that subtle changes in cell morphology or differences in secreted mediators reflecting different stages of activation could have occurred in AD- and Ctrl-inoculated animals.

Many questions remain following the several neuropathological observational studies in humans showing that A $\beta$  pathology is transmissible [17]. In particular, it is critical to assess whether tau pathology can also be iatrogenically transmitted. Only one recent article suggested that tau could also be detected in patients with iatrogenic A $\beta$  pathology [16]. However this study could not answer if the tauopathy was transmitted or was a consequence of A $\beta$  pathology. Experimental studies in transgenic mouse models have suggested that tau can be transmitted [6], but these models mainly rely on tau protein overexpression. Here, we show definitively that tau pathologies can



be transmitted in a primate expressing physiological levels of endogenous tau proteins. Staining for tau pathology was well marked and not necessarily in the direct vicinity of Aβ pathology nor in the same regions. At least three different hypothesis could explain this tau transmission. First, tau seeds from the inoculated brain extracts were responsible for the induction of the tau pathology. This hypothesis is consistent with the fact that brain extracts can induce tau pathologies in mice [7, 11] and that immunodepletion for tau suppresses tau pathology induction [7]. The second hypothesis is that Aβ contained in the human brain extracts (possibly oligomeric forms of Aβ) induced tau pathology in mouse lemur's brain in addition to the induction of Aβ pathology. Thus, tau pathology would not occur through a direct seeding effect of the inoculated human-tau pathology. The lack of co-localization of Aβ plaques (that are known to be also a reservoir for Aβ oligomers) and tau lesions does not support this hypothesis. The third hypothesis is that the inoculated brain extracts contained an undetected compound other than Aβ or tau that induced tau pathology. While we can

not rule out this hypothesis, it seems less likely than the first one.

Previous studies have evaluated Aβ and tau pathology induction in primates following the inoculation of AD brain extracts. A 3.5 to 7-year-long study conducted on marmosets intracerebrally inoculated with large volumes of AD brain extracts (300 μl of 10% homogenates distributed within 6 inoculation sites) led to moderate Aβ deposition in most animals but not to tau pathology nor to other AD-like pathological features [2, 23, 34]. In a previous study, our group inoculated AD brain extracts in the hippocampus and overlying cortex of mouse lemurs, leading to sparse Aβ and tau deposits close to the inoculation site [11]. The more severe Aβ and tau pathological inductions observed in the present study, after inoculation of a relatively small volume of brain extracts (25 μl), could in part be explained by variations in brain extract preparations and injection protocols. Here, we sonicated each sample prior to the inoculation as this procedure was shown to enhance the seeding and spreading capacities of brain extracts, supposedly by increasing the level

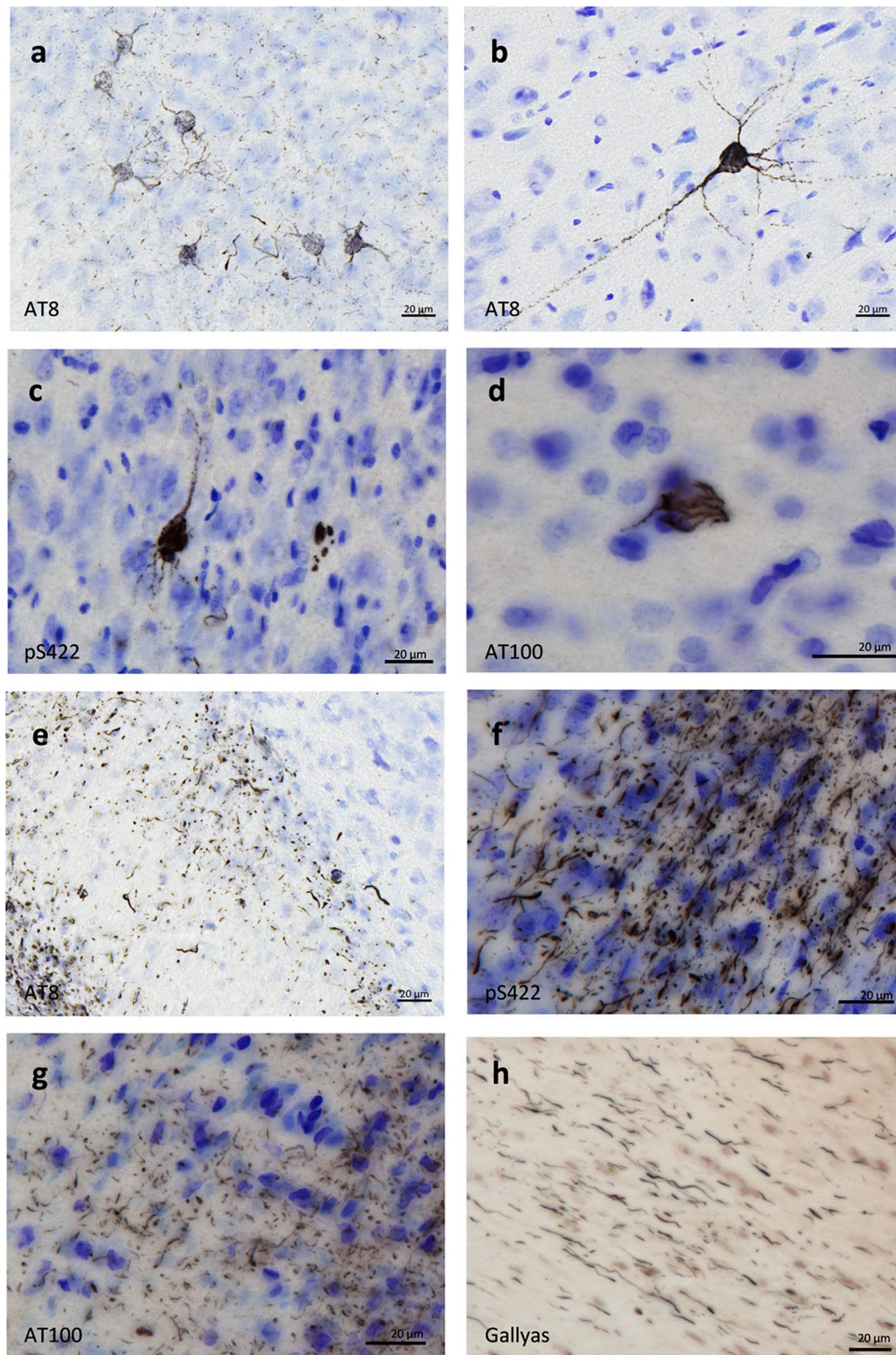


**Fig. 6** Intraneuronal neurofibrillary tangle and neuropil threads in AD-inoculated animals. AT8-positive neurofibrillary tangle in AD brain inoculated in mouse lemurs were detected after staining with AT8 (**a-b**), an antibody detecting phosphorylation of S422 (**c**), and another one targeting phosphorylation of T212 and S214 (AT100) (**d**). Neuropil threads were revealed after staining with AT8 (**e**), anti-pS422 antibody (**f**), AT100 (**g**), and Gallyas staining (**h**). Scale bars: 20 µm

of molecular interfaces for templated misfolding and generating smaller A $\beta$  and tau assemblies that can more readily propagate through the brain than large fibrils [20]. Obviously, A $\beta$ /tau-positive samples that contaminated humans (e.g. cadaver-sourced human growth hormones or dura matter) were not sonicated, which could explain much longer incubation times in iatrogenic transmission cases. In addition, in the present study, the injections were performed into highly connected brain areas, such as the corpus callosum and the posterior cingulate cortex. The former is indeed the major commissural tract connecting both hemispheres and the latter is a functional connectivity hub in mouse lemurs [10]. Moreover, the cingulate cortex is involved in the default-mode network, which is disrupted and highly vulnerable to A $\beta$  deposition in AD [5]. Additionally, it is one of the first regions to display atrophy in the course of AD [3].

Whether A $\beta$  and tau iatrogenic transmissions can be associated with clinical impacts in humans remains to be elucidated. Here, along with neuropathological lesions in their brains, AD-inoculated animals displayed cognitive impairments and bilateral brain atrophy. In humans, NFT deposition has been associated with clinical decline [28]. Here, even if we cannot conclude that there is a direct link between A $\beta$  and tau pathologies and cognitive deficits, the occurrence of cognitive alterations suggests that exogenous exposure to misfolded A $\beta$  and tau seeds can translate into clinical manifestations. This is in line with our previous study showing that AD brain extract inoculation in mouse lemurs leads to cognitive impairments despite sparse A $\beta$  and tau deposition [11]. Altogether, this raises concerns about the potential cognitive consequences in patients exposed to contaminated compounds, including vials of human cadaver-derived growth hormones that were shown to contain both A $\beta$  and tau seeds [9, 32].

Cerebral atrophy was prominent close to the inoculation site, *i.e.* the posterior cingulate, where it was first detected at 4 months post-inoculation. Atrophy worsened mainly from 9 to 15 months post-inoculation. This course of atrophy evolution suggests that grey matter loss was not related to an acute toxic effect of the inoculation. Atrophy also gradually spread to several other

regions in AD-inoculated animals. Atrophy of the posterior cingulate cortex and connected prefrontal regions [39] and basal ganglia [19] is consistent with deficits in object discrimination learning and cognitive flexibility in AD brain extract-inoculated lemurs, as these structures are thought to play a critical role in instrumental learning and shifting abilities [30, 33, 35].

In conclusion, we provided the first experimental evidence of the transmission of an AD-like phenotype in a non-human primate that includes A $\beta$  and tau pathologies as well as cognitive impairments and cerebral atrophy. This first demonstration of the transmission of tau pathology in a primate calls for further studies in humans to assess the transmission of tau in subjects exposed to contaminated cadaver-derived compounds and surgical material. Our experimental study also outlined the possible consequences of A $\beta$  and tau transmissions in terms of cognitive impairments and cerebral atrophy. Evaluating these aspects of the pathology in patients at risk for A $\beta$  and tau iatrogenic transmission through a systematic monitoring of AD biomarkers is thus urgently needed. Finally, our study also suggests that AD brain-inoculated mouse lemurs are highly relevant models to explore AD pathophysiology and ensure a greater translation of pre-clinical studies to patients.

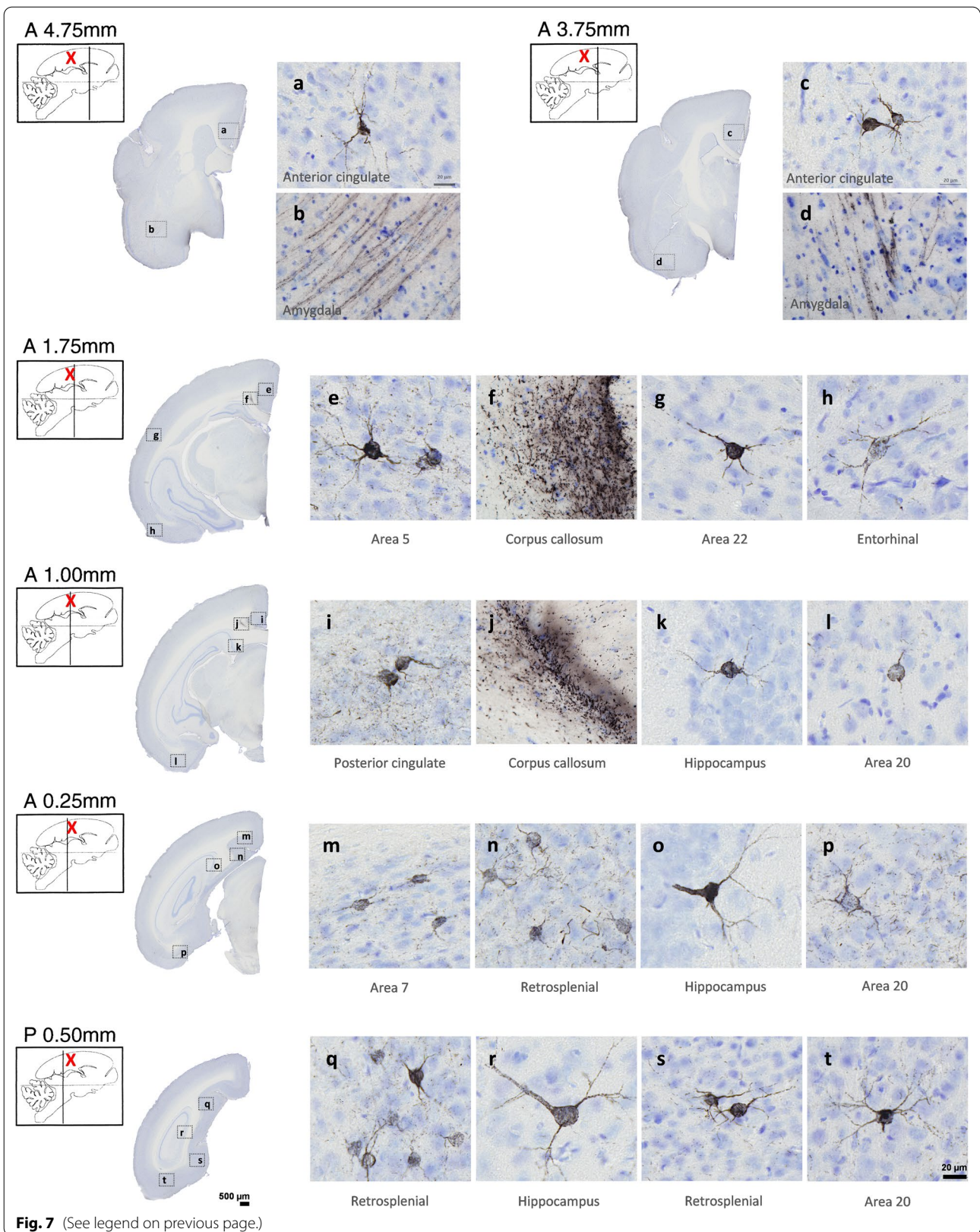
## Materials and methods

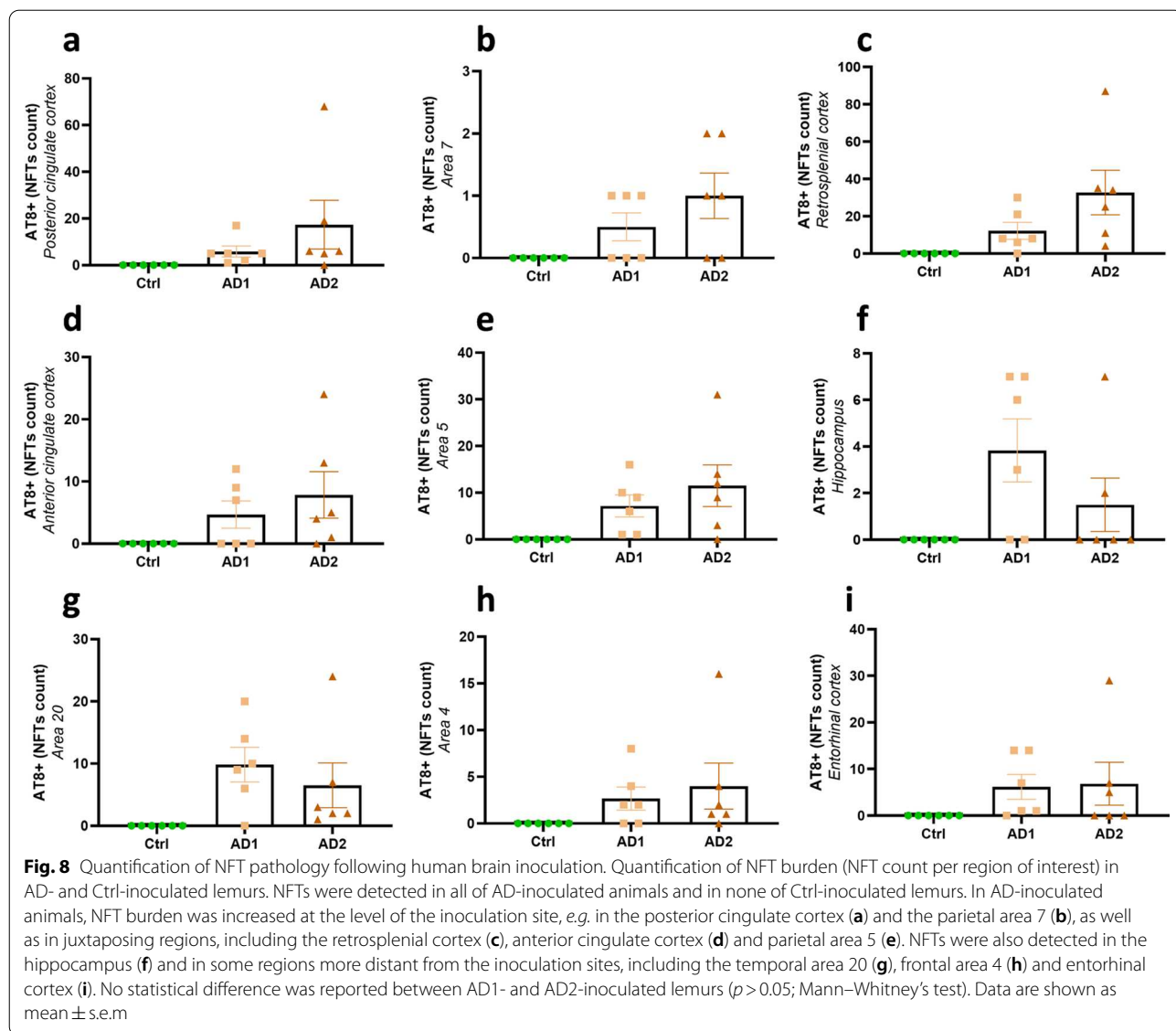
### Mouse lemurs

Mouse lemurs were reproduced in an approved breeding center (UMR 7179 CNRS/MNHN, France; European Institutions Agreement #962,773) and housed in our laboratory (Commissariat à l'Energie Atomique, Fontenay-aux-Roses center; European Institutions Agreement #B92-032-02). Animals were housed individually in enriched cages containing a wooden nesting box and equipment allowing them to climb and jump freely. The environment was maintained at a constant temperature of 24–26 °C with a relative humidity of 55%. The photoperiodic regime was based on a biannual alternation of long and short days (14 h of light at 250–350 lx/10 h of darkness in the summer period, 10 h of light at 250–350 lx/14 h of darkness in the winter period) in order to artificially reproduce the seasonal rhythm of the animals.

(See figure on next page.)

**Fig. 7** Tau pathology throughout the brains of mouse lemurs inoculated with AD brain extracts. Representative images of AT8 immunolabelling showing tau pathology following AD brain extract inoculations in mouse lemurs. NFTs were observed at the level of the inoculation sites, e.g. in the posterior cingulate cortex (**i**) and the parietal area 7 (**m**), as well as in juxtaposing regions such as the retrosplenial cortex (**n, q, s**), anterior cingulate cortex (**a, c**), parietal area 5 (**e**). They were also detected within the hippocampus (**k, o, r**) and temporal area 22 (**g**). Additionally, some regions more distant from the inoculation sites also displayed NFTs, e.g. the temporal area 20 (**l, p, t**) and the entorhinal cortex (**h**). Neuropil threads were mainly observed at the inoculation sites, e.g. in the corpus callosum (**f, j**) and posterior cingulate cortex (**i**). They were slightly induced around the needle tract (area 7; **m**), in juxtaposing regions such as the retrosplenial cortex (**n**), parietal area 5 (**e**) and in distant regions such as the temporal area 20 (**p**) and the amygdala (**b, d**). The red crosses indicate the inoculated region. Scale bars: 500  $\mu$ m in whole slice images, 20  $\mu$ m in zoomed images





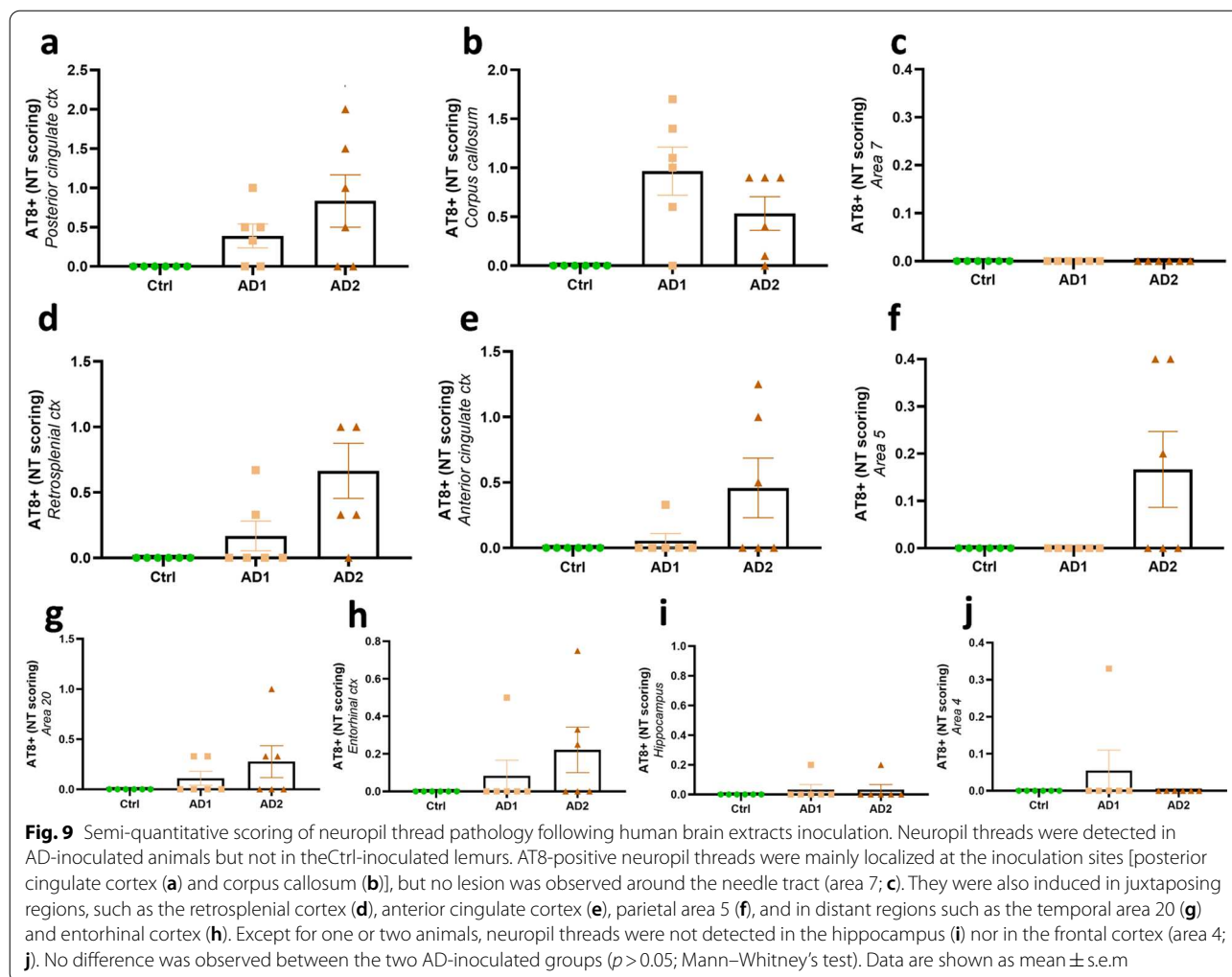
Diet consisted of fresh fruits and a preparation based on cottage cheese, eggs, cereals and bananas. Water and food were available ad libitum.

Eighteen males were studied. In order to limit any age-related modifications during the longitudinal follow-up, only young-adults (1.5-year-old) were included. Mouse lemurs were assigned to an experimental group in order to obtain cognitively comparable groups before the inoculations. After human brain inoculation, a 21-month-long follow-up was conducted on the animals. Five other mouse lemurs were evaluated for characterization of tau isoforms by immunoblots. They were sacrificed due to various non-cerebral, non-experimental pathologies (age 9.7 to 10.5 years). All experimental procedures were performed in compliance with the European Union directive

on the protection of animals used for scientific purposes (2010/63/EU). They were approved by a local ethics committee (CETEA-CEA DSV IdF) as well as by the French Ministry of Education and Research (authorization A17\_083).

**Protein extraction and western blots for mouse lemur brains**

Hippocampi and cortices from five non-inoculated mouse lemurs were dissected and snap frozen in 1.5 mL tubes (Eppendorf). Tissues were homogenized in 10 volumes of ice-cooled Tris-sucrose buffer (Tris–HCl 10 mM, pH 7.4 10% sucrose added with protease inhibitor (Complete mini EDTA-free, Roche)) and were sonicated (20 pulses of 1 s, amplitude 40%, 60 kHz) on ice. After 1 h



at 4 °C, protein concentrations were determined using the BCA Protein Dosage Kit (BioRad, France). Samples were diluted with lithium dodecyl sulphate buffer supplemented with reducing agents (Invitrogen) and then separated on 12% NuPAGE Novex (Invitrogen). Proteins were transferred to nitrocellulose (20  $\mu$ g for mouse lemurs, 10  $\mu$ g for control human brains), which were then saturated with 5% non-fat dried milk or 5% bovine serum albumin in TNT (Tris 15 mM pH 8, NaCl 140 mM, 0.05% Tween) and incubated at 4 °C for 24 h with the primary antibodies (TauCter (clone 9F6, LB lab-made), TauNter (12–21, LB lab-made), Tau3R (Millipore ref 05,803), Tau4R (Millipore ref 05,804), TauE2 (Lot1, LB lab-made)). Appropriate HRP-conjugated secondary antibodies (anti-mouse PI-2000 and anti-rabbit PI-1000, Vector Laboratories) were incubated for 45 min at room temperature and signal was visualized using a chemoluminescence kit (ECL, Amersham Bioscience) and a LAS4000 imaging system (Fujifilm).

### Human brain samples

Frozen brain samples (parietal cortex) from clinically different AD patients (four patients with classical slowly evolving forms of AD and four with a rapidly evolving form of AD) and two age-matched control individuals were collected from a brain donation program of the GIE NeuroCEB and the National Reference Center (CNR)-prion brain banks. Consent forms were signed by either the patients themselves or their next of kin in their name, in accordance with French bioethics laws. The classical slowly evolving AD cases (AD1) were characterized by a disease duration of 5 to 8 years. The rapidly evolving AD cases (AD2) were characterized by a disease duration of 6 months to 3 years. No case of hippocampal sclerosis was reported and all brain samples (Ctrl, AD1, AD2) were PrP<sup>Sc</sup> negative. AD1 and AD2 brain samples were also negative for  $\alpha$ -synuclein and TDP-43.

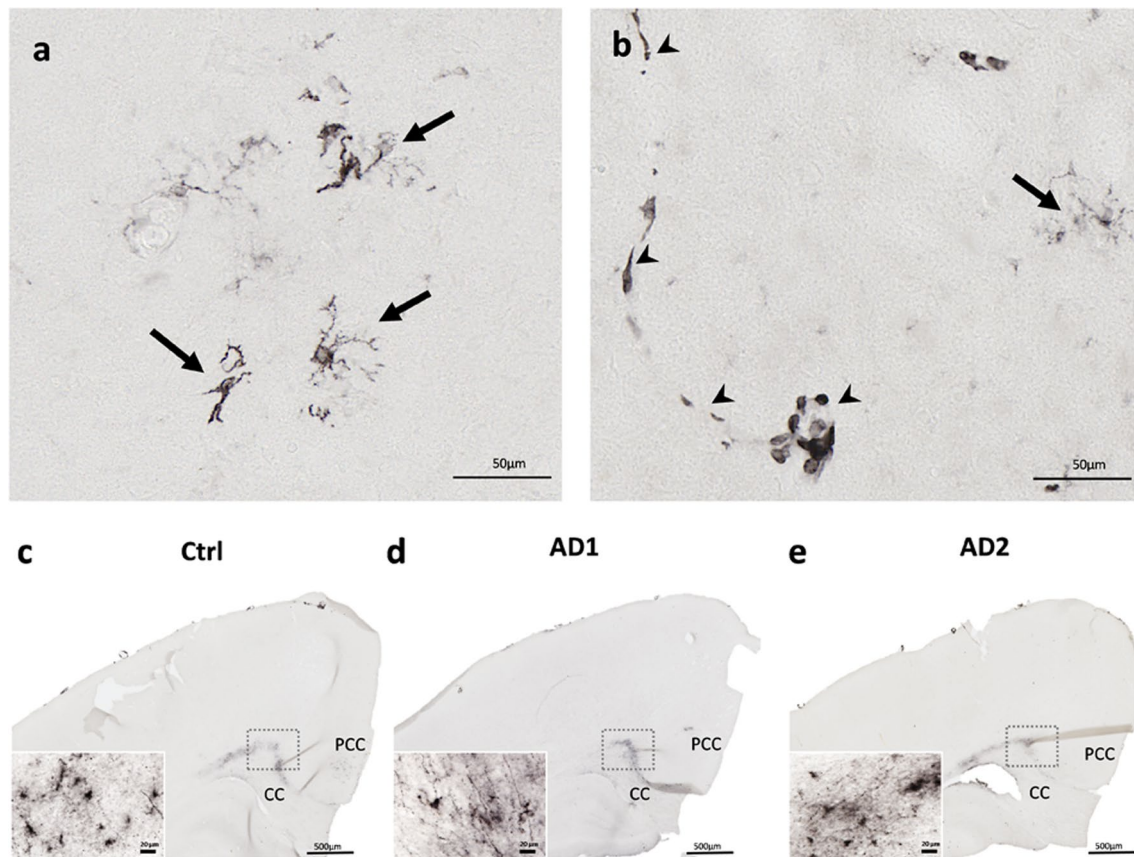


**Fig. 10** Similar microglial response after the inoculation of Ctrl or AD brain extracts. Representative stainings of microgliosis (HLA-DR antibody) in the parenchyma (**a-b**, arrows) and in the vasculature (**b**, arrowheads). Staining was observed at the inoculation sites, *i.e.* the posterior cingulate cortex (PCC) and the corpus callosum (CC) (**c-e**) but not at distance of these regions. No difference was observed between the groups. Scale bars: 50  $\mu$ m in **a-b**, 500  $\mu$ m in **c-e** and 20  $\mu$ m in inserts

### Neuropathological characterization

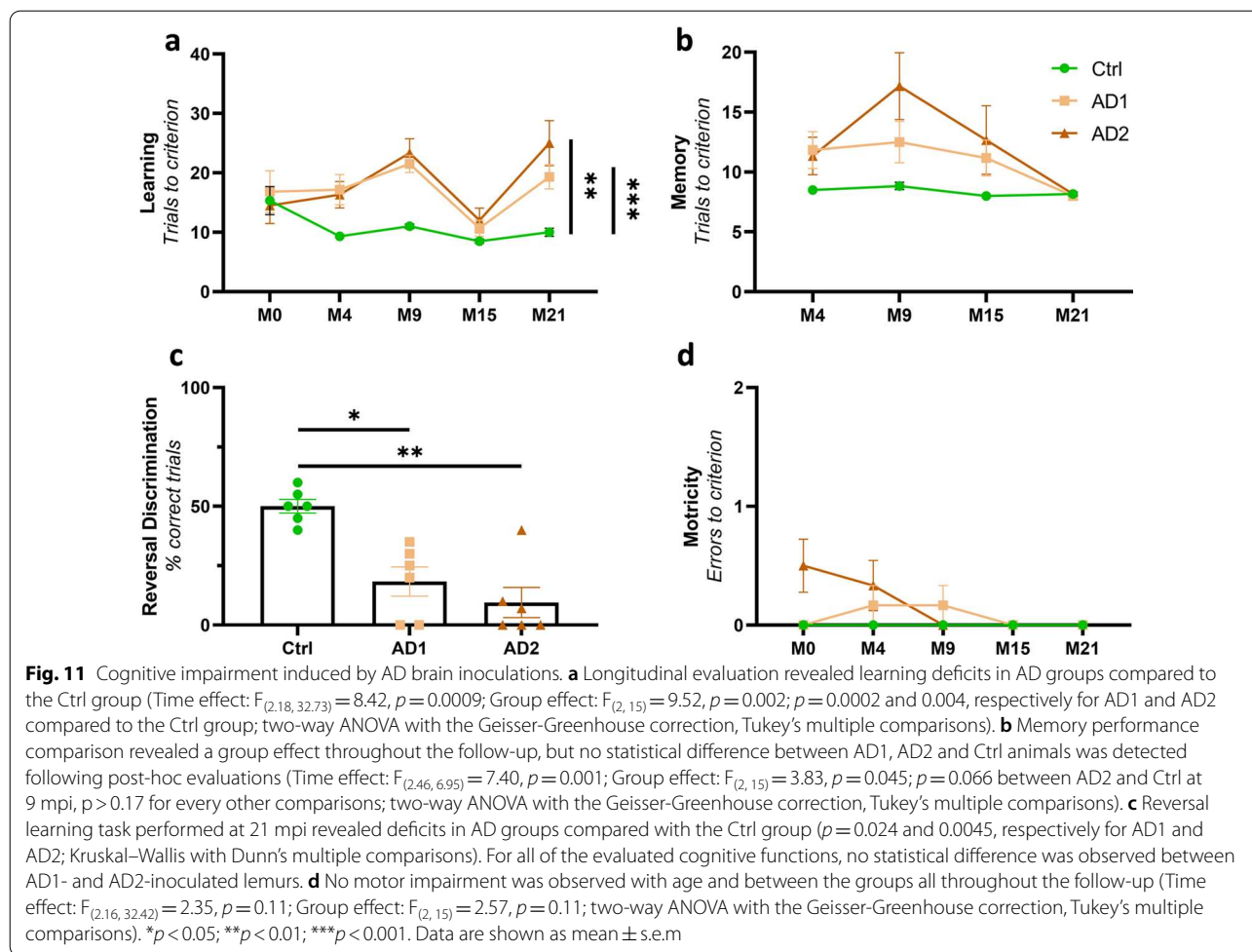
All brain tissues were assessed by immunohistochemistry, as previously described in Gary et al. 2019 [11]. Briefly, 4- $\mu$ m-thick paraffin sections were cut, deparaffinized in xylene, successively rehydrated in ethanol (100, 90, and 70%) and rinsed under running tap water for 10 min before immunohistological staining. They were then incubated in 99% formic acid for 5 min, quenched for endogenous peroxidase with 3% hydrogen peroxide and 20% methanol, and washed in water. Sections were blocked at room temperature for 30 min in 4% bovine serum albumin (BSA) in 0.05 M tris-buffered saline, with 0.05% Tween 20, pH 8 (TBS-Tween, Sigma). They were then incubated overnight at +4 °C with the 6F3D anti-A $\beta$  antibody (Dako, 1/200), polyclonal anti-tau antibody (Dako, 1/500), monoclonal anti-alpha-synuclein (LB509, Zymed, 1/250), polyclonal anti-TDP43 (Protein Tech Group, 1/1000) routinely used for A $\beta$ , tau, alpha-synuclein and TDP43 detection, respectively. Sections were further incubated with a biotinylated secondary

antibody for 25 min at room temperature, and the presence of the secondary antibody was revealed by a streptavidin–horseradish peroxidase conjugate using diaminobenzidine (Dako, Glostrup, Denmark). Sliced were counterstained with Harris hematoxylin.

### Protein extraction for human brains

For tau protein extraction, brain homogenates were sonicated on ice for 5 min, centrifuged for 5 min at 3,000  $\times$  g at +4 °C, diluted in 20 mM Tris/2% SDS and sonicated on ice for 5 min. For A $\beta$ , Iba1 and GFAP protein extractions, brain homogenates were sonicated (6 strokes, cycle 0.5, 30% amplitude) in a lysis buffer at a final concentration of 50 mM Tris–HCl pH 7.4, 150 mM NaCl, 1% Triton-X-100 supplemented with 1X protease inhibitors (cOmplete™ Mini, EDTA-free Protease Inhibitor Cocktail, Roche) and 1/100 diluted phosphatase inhibitors (Phosphatase Inhibitor Cocktail 2, Sigma-Aldrich). Samples were centrifuged at 20,000  $\times$  g for 20 min at +4 °C and the supernatant was collected for further use. Extracted





samples were stored at  $-80\text{ }^{\circ}\text{C}$  after evaluation of total protein concentration by a BCA assay (Pierce™). The obtained concentration was used for the normalization of proteins. Total protein concentration was 5.40, 5.53 and  $5.50\text{ }\mu\text{g}/\mu\text{L}$  respectively for the Ctrl, AD1 and AD2 homogenates.

#### Western blots for human brain extracts

For tau characterization, samples were diluted to  $1\text{ }\mu\text{g}/\mu\text{L}$ , diluted in 2X lithium dodecyl sulfate (LDS, Thermo

Fisher Scientific) buffer with reducers and heated at  $+100\text{ }^{\circ}\text{C}$  for 10 min.  $15\text{ }\mu\text{g}$  of samples were loaded on a 12% Bis-Tris Criterion™ gel (Bio-Rad) and migrated in MOPS buffer for 1 h at 165 V on ice. After protein transfer on nitrocellulose sheets, migration and quality of the transfer were checked with a ponceau S staining. The membrane was saturated for 1 h at room temperature, and was then incubated with the AT100 (pT212-pS214, Life technologies MN1060), 2H9 (pS422, 4BioDx 4BDX-1501), tau-Nter (12–21, LB lab-made) or

(See figure on next page.)

**Fig. 12** Progressive cerebral atrophy induced by AD brain inoculation. Statistical heatmaps of t-values depicting regions in which grey matter volume decreased in AD-inoculated animals compared with Ctrl-inoculated ones (voxel-based morphometry, FDR-corrected  $p < 0.05$ ; voxel threshold extent  $k = 10$ ). To increase statistical power, AD1 and AD2-inoculated animals were grouped within a unique AD group. Longitudinal follow-up revealed a slight atrophy in the inoculated posterior cingulate region at 4 mpi (**a**). No intergroup difference in brain volume was observed between 4 and 9 mpi (**b**). Grey matter loss however extended to several other regions by 15 mpi (**c**), without further progressing afterwards until 21 mpi (**d**). Lateral (**e**) and dorsal (**f**) three-dimensional representations showing clusters of atrophied areas. The red arrow and crosses indicate the injection needle tract. 1–3: cerebral cortex areas 1–3, 4: cerebral cortex area 4, 5: cerebral cortex area 5, 6: cerebral cortex area 6, 7: cerebral cortex area 7, 17–18: cerebral cortex areas 17–18, AC: anterior cingulate cortex, BF: basal forebrain, Cd: caudate nucleus, Cl: claustrum, EC: entorhinal cortex, F: antero-medial frontal cortex, Fs: superior frontal cortex, H: hippocampus, Ins: insular cortex (areas 13–16), P: putamen, PA: peri-amygdalar cortex, PC: posterior cingulate cortex, RS: retrosplenial cortex, S: septum, Th: median thalamus [22]

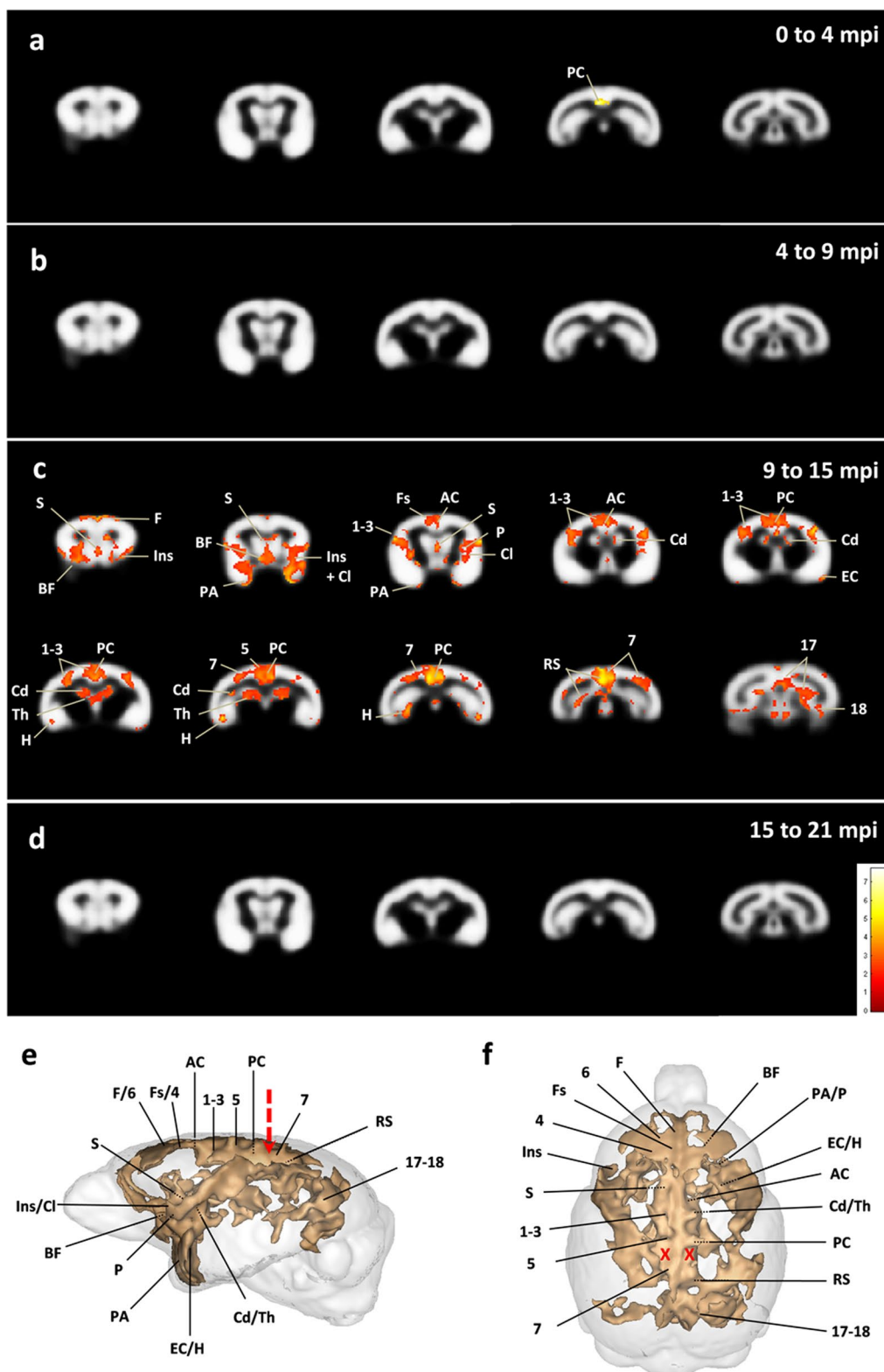


**Fig. 12** (See legend on previous page.)

tau-Cter (clone 9F6, LB lab-made) antibodies overnight at +4 °C. A peroxidase coupled secondary anti-rabbit or anti-mouse antibody was then applied for 45 min at room temperature. Immunoblotting was revealed by ECL. GAPDH (Sigma 9545) was used as a loading control. For Iba1 and GFAP evaluations, extracted samples were denatured at +90 °C for 5 min in a buffer containing 1X LDS (NuPAGE<sup>®</sup> LDS sample buffer, Invitrogen) and DTT 1X (NuPAGE<sup>®</sup> sample reducing agent, Invitrogen). 10 µg of denatured protein were loaded per well. Samples and molecular weight marker (Bio-Rad Precision Plus Protein<sup>™</sup> Dual Color standards) were loaded on 4–20% Criterion<sup>™</sup> TGX<sup>™</sup> gels (Bio-Rad) and migration was performed in a 1X tris–glycine buffer (Bio-Rad) at 120 V for 1 h. Proteins were then transferred to a nitrocellulose membrane using the Trans-Blot<sup>®</sup> Turbo<sup>™</sup> (Biorad) system. Migration and quality of the transfer were checked with a ponceau S staining. The membrane was then blocked with a TBS/0.1%Tween, 5% milk solution for 1 h at RT, and incubated with the primary antibody Iba1 (Wako 1,919,741, 1/2000), GFAP (Dako Z0334, 1/5000) or actin (Sigma A2066, 1/5000) diluted in saturation buffer overnight at +4 °C. After washing in TBS/0.1%Tween solution, the membrane was incubated with the appropriate secondary HRP-conjugate antibody diluted to 1/5000 in TBS/0.1%Tween for 1 h at RT. The chemiluminescent signal was revealed using the Clarity western ECL (Bio-Rad) kit and the Chemidoc<sup>™</sup> MP (Bio-Rad) imaging system. Protein band intensities were quantified on the ImageJ software and normalized by the actin expression level.

#### ELISA quantifications

For A $\beta$  protein quantification, all assay-specific material (pre-coated microtiter plate, buffers, antibodies, standard solutions) was provided in the V-PLEX kit A $\beta$  Peptide Panel 1 (6E10) (MSD<sup>®</sup>). Human brain homogenates were diluted to 1/5 (Ctrl samples) or 1/10 (AD1 and AD2 samples) in the dilution buffer. As described in the manufacturer's protocol, the microtiter plate was blocked for 1 h at RT with the appropriate buffer. After washing, 25 µl of detection antibody and 25 µl of diluted sample or standard were added in duplicate to the wells and incubated under continuous agitation for 2 h at RT. Wells were washed and 150 µl of reading buffer was added. Plate reading was performed with the MSD Sector Imager 2400 (model 1200) multiplex assay system. A $\beta$ <sub>1-38</sub>, A $\beta$ <sub>1-40</sub> and A $\beta$ <sub>1-42</sub> quantifications were performed with the Discovery Workbench 4.0 MSD<sup>®</sup> software. Tau protein quantifications (total tau and phospho-tau181) were performed according to the manufacturer's protocol. Briefly, brain homogenates were diluted to 1/100 and 1/200 in the provided dilution buffer. 50 µl of standards

or samples, as well as 50 µl of detection antibody solution were added to wells and incubated for 14 h at +4 °C. After washing, 100 µl of 1X anti-rabbit IgG HRP solution was added for a 30 min incubation period at RT. 100 µl of stabilized chromogen were then added to each well for 30 min at RT, in the dark. The reaction was stopped by adding 100 µl of Stop solution and the plate was read at 450 nm within the hour. Data were analyzed with GraphPad Prism 7 using the 4PL method. All samples were tested in duplicates.

#### Human brain extracts preparation

Parietal cortex samples were individually homogenized at 10% weight/volume (w/v) in a sterile 1X Dulbecco's phosphate buffer solution in CK14 soft tissue homogenizing tubes at 5000 rpm for 20 s (Precellys<sup>®</sup>, Bertin technologies). Brain extracts were then sonicated on ice for 5 s at 40% amplitude and centrifuged at 3000 g for 5 min at +4 °C. The supernatant was aliquoted in sterile polypropylene tubes and stored at –80 °C until use.

Before the stereotaxic injection, 10% Ctrl, AD1 or AD2 individual brain extracts were thawed on ice and combined together according to their group. The three resulting combined samples (Ctrl, AD1 and AD2 brain extracts) were sonicated (70% amplitude, 10 s on/off; Branson SFX 150 cell disruptor sonicator, 3.17 mm microtip probe Emerson, Bron) on ice in a sterile environment.

#### Stereotaxic surgery

Stereotaxic surgery was performed to infuse the brain extracts, bilaterally in the posterior cingulate cortex and the underlying corpus callosum. Mouse lemurs have a brain structure that can show significant interindividual variation. The stereotaxic injection protocol developed during this study ensures that this variability is taken into account and therefore improves the accuracy of the injections. This protocol is based on a magnetic resonance imaging (MRI) acquisition followed by a surgical procedure. Mouse lemurs were maintained in a stable position on a non-magnetic bed, compatible with the MRI and stereotaxic equipment, and for which the positions of the anesthetic mask, muzzle bar and ear bars were adjustable to fit the morphology of each animal. An intra-laboratory validation was performed prior to this study. Animals were fasted the day before the intervention. Water was available ad libitum up to 1 h before anesthesia.

Injection coordinates for the inoculated structures were calculated in reference to a landmark that crossed the middle of the ear bar for the antero-posterior axis, interhemispheric fissure for the left–right axis, and the skull surface for the dorso-ventral axis. We chose this landmark as it could be visualized both in MRI and under

the surgeon's binocular magnifying glass. The coordinates of the targeted regions were defined on the MRI and were transposed into stereotaxic coordinates for the surgery.

The MR exams were performed using the following procedure. Mouse lemurs were pre-anesthetized by a subcutaneous injection of glycopyrronium bromide (0.05 ml/kg; Robinul-V<sup>®</sup>) 30 min before isoflurane anesthesia (induction at 4.5%, maintenance at 1.5%; Vetflurane<sup>®</sup>). Throughout the procedure, their respiratory rhythm was monitored and body temperature was maintained at  $37 \pm 0.5$  °C using a heated blanket. The MRI system was an 11.7 Tesla Bruker BioSpec (Bruker, Ettlingen, Germany) running ParaVision 6.0.1. Images were acquired using a T2-weighted multi-slice multi-echo sequence with the following parameters: TR=7100 ms; TE=24.20 ms; echo spacing=4.40 ms; echo average=10; slice thickness=0.23 mm; number of slices=128; Axial-AP; Read/Phase/Slice: Y/X/Z; resolution=0.156 × 0.156 after zero-filling-interpolation (2.5 × 2.5); matrix=104 × 104; field of view=40 × 40 mm<sup>2</sup>; bandwidth=100,000 Hz; acquisition duration: 12min18s.

Just after the MRI, animals were placed in a stereotaxic frame (Phymep). Local anesthesia was performed with a subcutaneous injection of lidocaine (5 mg/kg; 0.5% Xylovet, Ceva), after cleaning the incision site with povidone iodine (Vétédine<sup>®</sup>). Injections were performed bilaterally into the corpus callosum followed by the overlying posterior cingulate cortex, at the previously defined coordinates. Using 1 ml-Hamilton syringes and 34-gauge needles, 6.25 µl of human brain homogenates were administered per injection site, at a 0.5 µl/min rate. At the end of each injection, needles were held in place for five additional minutes before removal. The incised area was cleaned with 10% povidone iodine (Vétédine<sup>®</sup>) and sutured. Animals then received a subcutaneous injection of a 0.9% sodium chloride solution (1 ml/100 g) for rehydration, after which they were placed in a ventilated heating box (25 °C) and monitored until full recovery from anesthesia. Two weeks after the injection, an MRI was performed to evaluate potential post-operative complications (increased inflammation, cerebral hemorrhage). No imaging abnormalities were detected in any animals.

### **Behavioral tests**

Learning, long term memory performance and reversal learning abilities were evaluated using discrimination tests in a jumping stand apparatus [31]. Motor skills were evaluated using a tower test [25]. All tests were conducted using devices adapted to lemurs developed by our team or other mouse lemur specialists.

*Visual discrimination test in a jumping stand apparatus* The jumping stand apparatus evaluates lemurs' learning and long-term memory performances using discrimination tests [11, 31] (Additional File 2). The device is a vertical cage made of plywood walls, except for the front panel which consists in a one-way mirror allowing observation. During the test, the animal is placed on an elevated central platform and must jump from this starting platform to one of the two landing platforms. If no spontaneous jump is performed within a minute, the central platform can be tilted slightly downwards, creating a slippery slope, to encourage the animal to jump. Each landing platform is associated with a different visual stimulus, characterized by a specific shape, texture and pattern. For each pair of visual stimuli, one is associated with a positive reinforcement (*i.e.* a stable platform giving access to a 2-min rest in a wooden nesting box), whereas the other one is associated with a negative reinforcement (*i.e.* an unstable platform leading to a fall to the bottom of the cage). After a fall, the mouse lemur is left at the bottom of the cage for 20 s before the next trial. As mouse lemurs prefer confined spaces, reaching their nesting box when placed in an open space is a strong motivator for behavioral testing. During a discrimination task, the mouse lemur had to identify the positive stimulus, the location of which was randomly alternated between the two landing platforms over the course of the test and changed at least every three trials. The test ended when the success criterion (*i.e.* at least 8 correct choices out of 10 consecutive attempts) was reached. The score given to an animal during learning and memory tasks was the number of trials required to reach this criterion.

Before the first test, an habituation session consisting of 7 trials was carried out. During the first four trials, only one stable central landing platform was available in front of the nesting box opening. Trial 1 was characterized by the presence of a board directly connecting the departure platform to the landing platform, so that jumping was not required to access the nesting box. This board was removed for trial 2, during which the lemur needed to jump to reach the stable landing platform. During trial 3 and 4, an opaque screen was placed above the landing platform in order to hide the opening of the nesting box. The animal therefore needed to jump onto the stable landing platform and go under the screen to reach the reward. During trial 5 to 7, an unstable platform was introduced, and alternately placed either on the right or on left of the nesting box entrance.

Learning abilities were evaluated as the lemur had to identify the positive stimulus out of the two stimuli to reach its nesting box. Long-term memory performance reflected the ability of mouse lemurs to remember the positive stimulus presented 4 or 6 months earlier. In

order to create experimental groups with comparable learning capacities, the learning test was carried out before the inoculation with human brain homogenates (M0). Memory performance was evaluated 4 months later, followed (one day later) by a new learning task. Longitudinal evaluation was performed by a succession of learning and memory tasks at 4, 9, 15 and 21 months post-inoculation. At each timepoint, a new pair of visual stimuli was introduced to the animals for the new learning task. The third cognitive task was a reversal learning task conducted at 21 mpi. After a successful discrimination learning session, the outcomes associated with the two stimuli were reversed. Twenty consecutive trials were performed for each animal and the percentage of correct choices was compared between the groups.

**Motricity test** The tower test was designed to evaluate motor performances of the lemurs through the achievement of successive high jumps [25]. Similarly to the jumping stand apparatus, it is based on the strong motivation of mouse lemurs to reach their nesting box in order to escape the discomfort felt in open spaces. The device is a  $180 \times 35 \times 35$  cm tower with three opaque sides and one transparent Plexiglas side. It is crossed horizontally by seven metal rods with a diameter of 5 mm and gradually spaced from one another by 10 cm (at the bottom) to 30 cm (at the top). Jumps with increasing difficulty need to be completed in order to reach the reward. A nesting box can be positioned at three different levels, making it accessible after reaching rod 5 (low position), 6 (intermediate position) or 7 (high position). The test was monitored by a camera placed in front of the tower.

During the test, the lemur was placed on the floor of the tower and had to jump from rod to rod in order to reach the nesting box made accessible after jumping on rod 7. Jumps were either performed spontaneously or after a stimulus in case of immobility (>3 min). This stimulus could be visual (introduction of a visual stimulus at the bottom of the tower), or mechanical in case of a more prolonged inactivity when on a rod (rotation of the rod on which the lemur was located). When the animal reached the nesting box, it was rewarded with a 5-min rest inside.

When the animal was introduced to the device for the first time, an habituation session consisting of six trials was carried out. Throughout the trials, the nesting box was gradually moved upwards, from the lower position during trial 1 and 2, to the intermediate position during trial 3 and 4, and finally to the upper position during trial 5 and 6.

The motricity test phase consisted of three consecutive trials during which the nesting box was placed at the upper position. The number of falls between the

last two rods, spaced by 30 cm, was used as a criterion reflecting motor performances. Motricity tests were performed following the visual discrimination test before human brain inoculation and at 4, 9, 15 and 21 months post-inoculation.

#### **Morphological MRI**

Brain volume evolution was evaluated throughout the study, starting before inoculation and then at 4, 9, 15 and 21 months post-inoculation. All images were acquired on a 11.7 Tesla MRI (Bruker Corporation), using the following parameters: TR=8000 ms; TE=28.05 ms; echo spacing=5.10 ms; echo average=10; slice thickness=0.23 mm; number of slices=128, Axial-AP; Read/Phase/Slice: Y/X/Z; resolution=0.115 × 0.115 after zero-filling interpolation (1.34 × 1.34); matrix=192 × 192; field of view=29.44 × 29.44 mm<sup>2</sup>; bandwidth=100,000 Hz; acquisition duration: 25min36s. Animals were anesthetized and monitored as previously described for stereotaxic injections.

Images were analyzed using voxel-based morphometry by applying SPM8 (Wellcome Trust Institute of Neurology, University College London, UK, [www.fil.ion.ucl.ac.uk/spm](http://www.fil.ion.ucl.ac.uk/spm)) with the SPMouse toolbox (<http://spmmouse.org>) for animal brain morphometry using a procedure already implemented for mouse lemurs [11, 36]. The brain images were segmented into grey (GM) and white matter (WM) tissue probability maps using locally developed priors, then spatially transformed to the standard space, defined by Sawiak et al., using a GM mouse lemur template [36]. Affine regularization was set for an average-sized template, with a bias non-uniformity FWHM cut-off of 10 mm and a 5 mm basis-function cut off and sampling distance of 0.3 mm. The resulting GM and WM portions were output in rigid template space, and DARTEL [1] was used to create non-linearly registered maps for each subject and common templates for the cohort of animals. The warped GM portions for each subject were adjusted using the Jacobian determinant from the DARTEL registration fields to preserve tissue amounts ("optimized VBM" [13]) and smoothed with a Gaussian kernel of 600 μm to produce maps for analysis.

A general linear model was designed to evaluate relative changes in GM values as a function of time between the control- and Alzheimer's disease-inoculated groups. This type of analysis produces t-statistics and color-coded maps that are the product of a statistical analysis performed at every voxel in the brain. Contiguous groups of voxels that attain statistical significance, called clusters, are displayed on brain images. To control for multiple comparisons, an adjusted p-value was calculated using the voxel-wise false discovery rate (FDR-corrected  $p < 0.05$ ), with extent threshold values of 10 voxels,

meaning that clusters required 10 contiguous voxels to be selected as relevant [12]. Voxels with a modulated GM value below 0.2 were not considered for statistical analysis. The operator was blinded to the group attribution during image processing.

### Histology

Mouse lemurs were sacrificed at 21 mpi with an intraperitoneal injection of pentobarbital sodium (0.1 ml/100 g; Exagon, Axience). Twenty minutes before sacrifice, a subcutaneous administration of buprenorphine (0.1 mg/100 g; Vétergésic<sup>®</sup>) was performed for analgesia. Animals were perfused intracardially with cold sterile 0.1 M PBS for 4 min, at a rate of 8 ml/min. The brain was post-fixed in 4% paraformaldehyde for 48 h at +4 °C, transferred in a 15% sucrose solution for 24 h and in a 30% sucrose solution for 48 h at +4 °C for cryoprotection. Serial coronal sections of 40 µm were performed with a microtome (SM2400, Leica Microsystem) and stored at -20 °C in a storing solution (glycerol 30%, ethylene glycol 30%, distilled water 30%, phosphate buffer 10%). Free-floating sections were rinsed in a 0.1 M PBS solution (10% Sigma-Aldrich<sup>®</sup> phosphate buffer, 0.9% Sigma-Aldrich<sup>®</sup> NaCl, distilled water) before use.

**Immunohistology, Thioflavin S and Gallyas silver staining** Mouse lemur brain sections were stained for amyloid-β (4G8 and Aβ42 antibodies, Thioflavin S), tau (AT8, AT100, pS422 antibodies and Gallyas silver staining) and microglia (HLA-DR antibody). A pretreatment with 70% formic acid (VWR<sup>®</sup>) for 20 min at room temperature (RT) was performed for the 4G8 labelling. For the HLA-DR and AT100 stainings, the pretreatment consisted in a 30 min-long incubation in EDTA 1X citrate (Diagnostic BioSystems<sup>®</sup>) at 95 °C followed by rinsings in 0.5% Triton X-100/0.05 M Tris-HCl Buffered Saline solution (TBS) or a PBS solution respectively, for 2 × 10 min. For the 4G8, Aβ42, AT8, AT100, pS422 and HLA-DR stainings, tissues were then incubated in hydrogen peroxide H<sub>2</sub>O<sub>2</sub> 30% (Sigma-Aldrich<sup>®</sup>) diluted 1/100 for 20 min to inhibit endogenous peroxidases. Blocking of non-specific antigenic sites was achieved over 1 h using a 0.2% Triton X-100/0.1 M PBS (Sigma-Aldrich<sup>®</sup>) (PBST) or 0.5% Triton X-100/0.05 M TBS (TBST) solution containing 3% bovine serum albumin or 4.5% normal goat serum, depending on the staining. Sections were then incubated at +4 °C with the 4G8 (Biolegend 800,706, 1/350), Aβ42 (Invitrogen 44,344, 1/500) or pS422 (Abcam 79,415, 1/1000) antibody diluted in a 3%BSA/PBST solution for 48 h or for 96 h with the AT8 antibody (Thermo MN1020B, 1/500), in a 3%BSA/TBST solution with the HLA-DR antibody (Dako M0746) for 48 h or in a 5%NGS/TBST solution with the AT100 antibody (Thermo MN1060, 1/250) for 96 h. After rinsing,

an incubation with the appropriate biotinylated secondary antibody diluted to 1/1000 in PBST or TBST was performed for 1 h at RT, followed by a 1 h incubation at RT with a 1:250 dilution of an avidin-biotin complex solution (ABC Vectastain kit, Vector Laboratories<sup>®</sup>). Revelation was performed using the DAB Peroxidase Substrate Kit (DAB SK4100 kit, Vector Laboratories<sup>®</sup>). Sections were mounted on Superfrost Plus slides (Thermo-Scientific<sup>®</sup>). For the 4G8, Aβ42, AT8, AT100 and pS422 labellings, a cresyl violet counterstain was performed. All sections were then dehydrated in successive baths of ethanol at 50°, 70°, 96° and 100° and in xylene. Slides were mounted with the Eukitt<sup>®</sup> mounting medium (Chem-Lab<sup>®</sup>).

For the Thioflavin S staining, free-floating sections were first mounted on Superfrost Plus (Thermo-Scientific<sup>®</sup>) slides and dried overnight. Sections were then incubated with a Thioflavin S (Sigma T1892) solution for 20 min at RT. They were then incubated in ethanol 100° and mounted with the FluorSave medium.

Free-floating sections were mounted on Superfrost Plus (Thermo-Scientific<sup>®</sup>) slides and dried overnight prior to Gallyas staining. All steps of the Gallyas staining were performed between 20 and 25 °C. Section were permeabilized by successive incubations in toluene (2 × 5 min) followed by ethanol at 100°, 90° and 70° (2 min per solution). Slides were then incubated in a 0.25% potassium permanganate solution for 15 min, in 2% oxalic acid for 2 min then in a lanthanum nitrate solution (0.04 g/l lanthanum nitrate, 0.2 g/l sodium acetate, 10% H<sub>2</sub>O<sub>2</sub> 30%) for 1 h to reduce non-specific background. Several rinses with distilled water were performed followed by an incubation in an alkaline silver iodide solution (3.5% AgNO<sub>3</sub> 1%, 40 g/l NaOH, 100 g/l KI) for 2 min. The reaction was neutralized with 0.5% glacial acetic acid baths (3 × 1 min) and sections were incubated for 20 min in a developing solution (2 g/l NH<sub>4</sub>NO<sub>3</sub>, 2 g/l AgNO<sub>3</sub>, 10 g/l tungstosilicic acid, 0.76% formaldehyde 37%, 50 g/l anhydrous Na<sub>2</sub>CO<sub>3</sub>). Several rinses with 0.5% acetic acid (3 × 1 min) followed by an incubation in 1% gold chloride solution for 5 min were then carried out. Sections were rinsed with distilled water and the staining was fixed with a 1% sodium thiosulfate solution. All sections were then rinsed with distilled water and dehydrated for 1 to 5 min in successive baths of ethanol at 50°, 70°, 96° and 100° and in xylene. Slides were mounted with Eukitt<sup>®</sup> mounting medium (Chem-Lab<sup>®</sup>).

### Image analysis

Z-stack images were acquired at 20 × (z-stacks with 16 planes, 1 µm steps with extended depth of focus) using an Axio Scan.Z1 (Zeiss<sup>®</sup>). Each slice was extracted individually in the.czi format using the Zen 2.0 (Zeiss<sup>®</sup>) software. Image processing and analysis were performed with the

ImageJ software (<https://imagej.nih.gov/ij/>). Images were imported with a 50% reduction in resolution (0.44  $\mu\text{m}/\text{pixel}$ ), converted to the RGB format and compressed in.tif format.

For the 4G8 immunostaining, the blue component of each image was extracted along with the background in order to remove the cresyl violet counter-staining from the analysis. Segmentation was performed with a manual threshold set at 202/255. Clusters of pixels with a radius below 15  $\mu\text{m}$  were removed. A $\beta$  load was evaluated as a percentage of 4G8-positive surface area in each ROI, except for the hippocampus. In the hippocampus, the number of plaques was manually counted as A $\beta$  deposition was mainly concentrated in some areas and the evaluation of an overall staining was not appropriate. For the AT8 staining, AD-like neurofibrillary tangles quantification was performed by manually counting the lesions and neuropil threads were evaluated by using a semi-quantitative scoring system based on the intensity and extent of the lesions (0 = absent, 1 = slight to moderate, 2 = moderate to severe). For the HLA-DR staining, a semi-quantitative analysis was performed by assigning a severity score based on the intensity and extent of the staining at the inoculation sites (0 = absent, 1 = slight, 2 = moderate, 3 = severe). All quantifications were performed on adjacent slices between A4.50 mm and P1.50 mm from bregma. 4G8 and AT8 were analyzed on 10 slices, HLA-DR on 3 slices adjacent to the inoculation site. ROIs were manually segmented using a mouse lemur atlas previously presented by our group [27], which was based on the reference atlases by Le Gros Clark [22] and Bons [4].

The three-dimensional rendering of A $\beta$  and tau pathologies in mouse lemur brains was based on regions of interests defined in a digital atlas of mouse lemurs [27]. A $\beta$  or tau lesions were reported within regions of interests using a three-level semi-quantitative scale (no lesions/intermediate/high lesion load). The ITK-SNAP software (<http://www.itksnap.org>) was used to create the surface/2D renderings of lesion loads.

### Statistical analysis

Statistical analysis was performed using the GraphPad Prism software 9. For human brain characterization, data are shown as mean  $\pm$  standard deviation of the replicates. Mouse lemur histological data are shown on scattered dot plots with mean  $\pm$  standard error of the mean (s.e.m.) and Mann–Whitney's test was carried out to compare results between the AD1 and AD2 groups. Behavioral studies data are shown as mean  $\pm$  standard error of the mean (s.e.m.) to represent performance evolution over time. Cognitive and motor performances which included repeated measures were evaluated using a two-way repeated measures

ANOVA with the Geisser-Greenhouse correction and Tukey's multiple comparisons. The significance level was set at  $p < 0.05$ .

### Supplementary Information

The online version contains supplementary material available at <https://doi.org/10.1186/s40478-021-01266-8>.

**Additional file 1.** Supplementary table and figures.

**Additional file 2.** Movie showing three consecutive trials in a jumping stand apparatus.

### Acknowledgements

The project was funded by the Association France-Alzheimer-2016. S.L. was founded by the Ministère de l'Enseignement Supérieur, de la Recherche et de l'Innovation, and by the Fondation pour la Recherche Médicale-2020. The project was performed in a core facility supported by/member of NeurAT-RIS—ANR-11-INBS-0011. It was also supported by internal funds from the Laboratory of Neurodegenerative Diseases UMR9199 CEA/CNRS and MIRCen. We thank the donors and the Brain Donation Program of the "The Brainbank Neuro-CEB Neuropathology Network" run by a consortium of Patient Associations: ARSLA (association for research on amyotrophic lateral sclerosis), CSC (cerebellar ataxias), Fondation ARSEP (association for research on multiple sclerosis), France DFT (fronto-temporal dementia), Fondation Vaincre Alzheimer, France Parkinson, with the support of Fondation Plan Alzheimer and IHU A-ICM for providing the brain samples used in this study. We thank James Koch (University of Wisconsin Oshkosh, USA) for critical review of this article.

### Authors' contributions

S.L., F.P., A.S.H., J.L.P., and M.D. contributed to the study conception and design. N.N.N., S.H., C.D. provided the human brain samples. N.N.N., S.L., S.B., C.D. and S.H. characterized the human brain samples. S.L. and M.G. performed the inoculations in mouse lemurs. J.L.P. designed and performed cognitive evaluations. F.P., S.L., A.S.H. designed and performed the immunohistological analysis in animals. S.E., L.B., A.S.H., and S.L. performed biochemical analysis. S.L., J.L.P. and M.D. wrote the manuscript. All authors commented on previous versions of the manuscript. All authors read and approved the final manuscript.

### Declarations

#### Competing interests

The authors declare no competing financial interests.

#### Author details

<sup>1</sup>Laboratoire des Maladies Neurodégénératives, Université Paris-Saclay, CEA, CNRS, 18 Route du Panorama, 92265 Fontenay-aux-Roses, France. <sup>2</sup>Commissariat à l'Energie Atomique et aux Energies Alternatives (CEA), Direction de la Recherche Fondamentale (DRF), Institut François Jacob, MIRCen, 18 Route du Panorama, 92265 Fontenay-aux-Roses, France. <sup>3</sup>Institut du Cerveau, UMR 7225, Sorbonne Université, Paris Brain Institute-ICM, CNRS, AP-HP, Hôpital de la Pitié Salpêtrière, Inserm U1127 DMU Neurosciences, Paris, France. <sup>4</sup>Brainbank NeuroCEB Neuropathology Network : Plateforme de Ressources Biologiques, Hôpital de La Pitié-Salpêtrière, Bâtiment Roger Baillet, 47-83 boulevard de l'Hôpital, 75651 Paris Cedex 13, France. <sup>5</sup>Université de Lille, CHU-Lille, LabEx DISTALZ, Alzheimer & Tauopathies, Rue Polonovski, 59045 Lille, France. <sup>6</sup>Laboratory of Cognitive Functioning and Dysfunctioning (DysCo), University of Paris 8, 93526 cedex Saint-Denis, France. <sup>7</sup>Angers, France. <sup>8</sup>Bordeaux, France. <sup>9</sup>Caen, France. <sup>10</sup>Clermont-Ferrand, France. <sup>11</sup>Grenoble, France. <sup>12</sup>Lille, France. <sup>13</sup>Limoges, France. <sup>14</sup>Lyon, France. <sup>15</sup>Marseille, France. <sup>16</sup>Montpellier, France. <sup>17</sup>Nice, France. <sup>18</sup>Paris, France. <sup>19</sup>Rennes, France. <sup>20</sup>Rouen, France. <sup>21</sup>Strasbourg, France.

Received: 28 July 2021 Accepted: 22 September 2021

Published online: 12 October 2021

## References

- Ashburner J (2007) A fast diffeomorphic image registration algorithm. *Neuroimage* 38:95–113. <https://doi.org/10.1016/j.neuroimage.2007.07.007>
- Baker HF, Ridley RM, Duchon LW, Crow TJ, Bruton CJ (1993) Evidence for the experimental transmission of cerebral beta-amyloidosis to primates. *Int J Exp Pathol* 74:441–454
- Baron JC, Chetelat G, Desgranges B, Percey G, Landeau B, de la Sayette V, Eustache F (2001) In vivo mapping of gray matter loss with voxel-based morphometry in mild Alzheimer's disease. *Neuroimage* 14:298–309
- Bons N, Sihol S, Barbier V, Mestre-Frances N, Albe-Fessard D (1998) A stereotaxic atlas of the grey lesser mouse lemur brain (*Microcebus murinus*). *Brain Res Bull* 46:1–173. [https://doi.org/10.1016/S0361-9230\(97\)00458-9](https://doi.org/10.1016/S0361-9230(97)00458-9)
- Buckner RL, Sepulcre J, Talukdar T, Krienen FM, Liu H, Hedden T, Andrews-Hanna JR, Sperling RA, Johnson KA (2009) Cortical hubs revealed by intrinsic functional connectivity: mapping, assessment of stability, and relation to Alzheimer's disease. *J Neurosci* 29:1860–1873. <https://doi.org/10.1523/JNEUROSCI.5062-08.2009>
- Clavaguera F, Akatsu H, Fraser G, Crowther RA, Frank S, Hench J, Probst A, Winkler DT, Reichwald J, Staufenbiel M, Ghetti B, Goedert M, Tolnay M (2013) Brain homogenates from human tauopathies induce tau inclusions in mouse brain. *Proc Natl Acad Sci USA* 110:9535–9540. <https://doi.org/10.1073/pnas.1301175110>
- Clavaguera F, Bolmont T, Crowther RA, Abramowski D, Frank S, Probst A, Fraser G, Stalder AK, Beibel M, Staufenbiel M, Jucker M, Goedert M, Tolnay M (2009) Transmission and spreading of tauopathy in transgenic mouse brain. *Nat Cell Biol* 11:909–913
- Dhenain M (2001) Age-related cognitive and neurobiological alterations in animals. In: Boller F, Cappa S (eds) *Handbook of neuropsychology*, 2nd edn. Elsevier, Amsterdam, pp 1–21
- Duyckaerts C, Sazdovitch V, Ando K, Seilhean D, Privat N, Yilmaz Z, Peckeu L, Amar E, Comoy E, Maceski A, Lehmann S, Brion JP, Brandel JP, Haik S (2018) Neuropathology of iatrogenic Creutzfeldt-Jakob disease and immunoassay of French cadaver-sourced growth hormone batches suggest possible transmission of tauopathy and long incubation periods for the transmission of Abeta pathology. *Acta Neuropathol* 135:201–212. <https://doi.org/10.1007/s00401-017-1791-x>
- Garin CM, Nadkarni NA, Landeau B, Chetelat G, Picq J-L, Bougacha S, Dhenain M (2021) Resting state functional atlas and cerebral networks in mouse lemur primates at 117 Tesla. *NeuroImage* 226:117589. <https://doi.org/10.1016/j.neuroimage.2020.117589>
- Gary C, Lam S, Herard AS, Koch JE, Petit F, Gipchtein P, Sawiak SJ, Caillierez R, Eddarkaooui S, Colin M, Aujard J, Deslys JP, Network FN, Brouillet E, Buée L, Comoy EE, Pifferi F, Picq J-L, Dhenain M (2019) Encephalopathy induced by Alzheimer brain inoculation in a non-human primate. *Acta Neuropathol Commun*. <https://doi.org/10.1186/s40478-019-0771-x>
- Genovese CR, Lazar NA, Nichols T (2002) Thresholding of statistical maps in functional neuroimaging using the false discovery rate. *Neuroimage* 15:870–878. <https://doi.org/10.1006/nimg.2001.1037>
- Good CD, Johnsrude IS, Ashburner J, Henson RN, Friston KJ, Frackowiak RS (2001) A voxel-based morphometric study of ageing in 465 normal adult human brains. *Neuroimage* 14:21–36. <https://doi.org/10.1006/nimg.2001.0786>
- Herve D, Porche M, Cabrejo L, Guidoux C, Tournier-Lasserre E, Nicolas G, Adle-Biasette H, Plu I, Chabriat H, Duyckaerts C (2018) Fatal Abeta cerebral amyloid angiopathy 4 decades after a dural graft at the age of 2 years. *Acta Neuropathol* 135:801–803. <https://doi.org/10.1007/s00401-018-1828-9>
- Hong M, Zhukareva V, Vogelsberg-Ragaglia V, Wszolek Z, Reed L, Miller BI, Geschwind DH, Bird TD, McKeel D, Goate A, Morris JC, Wilhelmsen KC, Schellenberg GD, Trojanowski JQ, Lee VMY (1998) Mutation-specific functional impairments in distinct Tau isoforms of hereditary FTDP-17. *Science* 282:1914–1917. <https://doi.org/10.1126/science.282.5395.1914>
- Jaunmuktane Z, Banerjee G, Paine S, Parry-Jones A, Rudge P, Grieve J, Toma AK, Farmer SF, Mead S, Houlden H, Werring DJ, Brandner S (2021) Alzheimer's disease neuropathological change three decades after iatrogenic amyloid-beta transmission. *Acta Neuropathol* 142:211–215. <https://doi.org/10.1007/s00401-021-02326-y>
- Jaunmuktane Z, Mead S, Ellis M, Wadsworth JD, Nicoll AJ, Kenny J, Launchbury F, Linehan J, Richard-Loendt A, Walker AS, Rudge P, Collinge J, Brandner S (2015) Evidence for human transmission of amyloid-beta pathology and cerebral amyloid angiopathy. *Nature* 525:247–250. <https://doi.org/10.1038/nature15369>
- Jucker M, Walker LC (2018) Propagation and spread of pathogenic protein assemblies in neurodegenerative diseases. *Nat Neurosci* 21:1341–1349. <https://doi.org/10.1038/s41593-018-0238-6>
- Kunishio K, Haber SN (1994) Primate cingulo-striatal projection - limbic striatal versus sensorimotor striatal input. *J Comp Neurol* 350:337–356. <https://doi.org/10.1002/cne.903500302>
- Langer F, Eisele YS, Fritsch SK, Staufenbiel M, Walker LC, Jucker M (2011) Soluble Abeta seeds are potent inducers of cerebral beta-amyloid deposition. *J Neurosci* 31:14488–14495. <https://doi.org/10.1523/JNEUROSCI.3088-11.2011>
- Lauwers E, Lalli G, Brandner S, Collinge J, Compennolle V, Duyckaerts C, Edgren G, Haik S, Hardy J, Helmy A, Ivins AJ, Jaunmuktane Z, Jucker M, Knight R, Lemmens R, Lin IC, Love S, Mead S, Perry VH, Pickett J, Poppy G, Radford SE, Rousseau F, Routledge C, Schiavo G, Schymkowitz J, Selkoe DJ, Smith C, Thal DR, Theys T, Tiberghien P, van den Burg P, Vandekerckhove P, Walton C, Zaaijer HL, Zetterberg H, De Strooper B (2020) Potential human transmission of amyloid beta pathology: surveillance and risks. *Lancet Neurol* 19:872–878. [https://doi.org/10.1016/S1474-4422\(20\)30238-6](https://doi.org/10.1016/S1474-4422(20)30238-6)
- Le Gros Clark WE (1931) The brain of *Microcebus murinus*. *Proc Zool Soc London* 101:463–486
- Macleod CJ, Baker HF, Ridley RM, Mori H (2000) Naturally occurring and experimentally induced beta-amyloid deposits in the brains of marmosets (*Callithrix jacchus*). *J Neural Transm* 107:799–814. <https://doi.org/10.1007/s007020070060>
- McMillan P, Korvatska E, Poorkaj P, Evstafjeva Z, Robinson L, Greenup L, Leverenz J, Schellenberg GD, D'Souza I (2008) Tau isoform regulation is region- and cell-specific in mouse brain. *J Comp Neurol* 511:788–803. <https://doi.org/10.1002/cne.21867>
- Mestre-Frances N, Serratrice N, Gennetier A, Devau G, Cobo S, Trouche SG, Fontès P, Zussy C, De Deurwaerdere P, Salinas S, Mennechet FJD, Dusonchet J, Schneider BL, Saggio I, Kalatzis V, Luquin-Piudo MR, Verdier J-M, Kremer EJ (2018) Exogenous LRRK2G2019S induces parkinsonian-like pathology in a nonhuman primate. *JCI Insight* 3:e98202. <https://doi.org/10.1172/jci.insight.98202>
- Meyer-Luehmann M, Coomaraswamy J, Bolmont T, Kaeser S, Schaefer C, Kilger E, Neuenschwander A, Abramowski D, Frey P, Jaton AL, Vigouret JM, Paganetti P, Walsh DM, Mathews PM, Ghiso J, Staufenbiel M, Walker LC, Jucker M (2006) Exogenous induction of cerebral beta-amyloidogenesis is governed by agent and host. *Science* 313:1781–1784. <https://doi.org/10.1126/science.1131864>
- Nadkarni NA, Bougacha S, Garin C, Dhenain M, Picq JL (2019) A 3D population-based brain atlas of the mouse lemur primate with examples of applications in aging studies and comparative anatomy. *Neuroimage* 185:85–95. <https://doi.org/10.1016/j.neuroimage.2018.10.010>
- Nelson PT, Alafuzoff I, Bigio EH, Bouras C, Braak H, Cairns NJ, Castellani RJ, Crain BJ, Davies P, Del Tredici K, Duyckaerts C, Frosch MP, Haroutunian V, Hof PR, Hulette CM, Hyman BT, Iwatsubo T, Jellinger KA, Jicha GA, Kovari E, Kukull WA, Leverenz JB, Love S, Mackenzie IR, Mann DM, Masliah E, McKeel AC, Montine TJ, Morris JC, Schneider JA, Sonnen JA, Thal DR, Trojanowski JQ, Troncoso JC, Wisniewski T, Woltjer RL, Beach TG (2012) Correlation of Alzheimer disease neuropathologic changes with cognitive status: a review of the literature. *J Neuropathol Exp Neurol* 71:362–381. <https://doi.org/10.1097/NEN.0b013e31825018f7>
- Parvizi J, Van Hoesen GW, Buckwalter J, Damasio A (2006) Neural connections of the posteromedial cortex in the macaque. *Proc Natl Acad Sci USA* 103:1563–1568. <https://doi.org/10.1073/pnas.0507729103>
- Pearson JM, Heilbronner SR, Barack DL, Hayden BY, Platt ML (2011) Posterior cingulate cortex: adapting behavior to a changing world. *Trends Cogn Sci* 15:143–151. <https://doi.org/10.1016/j.tics.2011.02.002>
- Picq JL, Villain N, Gary C, Pifferi F, Dhenain M (2015) Jumping stand apparatus reveals rapidly specific age-related cognitive impairments in mouse lemur primates. *PLoS ONE* 10:e0146238. <https://doi.org/10.1371/journal.pone.0146238>
- Purro SA, Farrow MA, Linehan J, Nazari T, Thomas DX, Chen ZC, Mengel D, Saito T, Saito T, Rudge P, Brandner S, Walsh DM, Collinge J (2018) Transmission of amyloid-beta protein pathology from cadaveric



- pituitary growth hormone. *Nature* 564:415. <https://doi.org/10.1038/s41586-018-0790-y>
33. Ragozzino ME, Ragozzino KE, Mizumori SJY, Kesner RP (2002) Role of the dorsomedial striatum in behavioral flexibility for response and visual cue discrimination learning. *Behav Neurosci* 116:105–115. <https://doi.org/10.1037/0735-7044.116.1.105>
34. Ridley RM, Baker HF, Windle CP, Cummings RM (2006) Very long term studies of the seeding of beta-amyloidosis in primates. *J Neural Transm* 113:1243–1251. <https://doi.org/10.1007/s00702-005-0385-2>
35. Rolls ET (2000) The orbitofrontal cortex and reward. *Cereb Cortex* 10:284–294. <https://doi.org/10.1093/cercor/10.3.284>
36. Sawiak SJ, Picq JL, Dhenain M (2014) Voxel-based morphometry analyses of in vivo MRI in the aging mouse lemur primate. *Front Aging Neurosci* 6:82. <https://doi.org/10.3389/fnagi.2014.00082>
37. Silhol S, Calenda A, Jallageas V, MestreFrances N, Bellis M, Bons N (1996)  $\beta$ -Amyloid protein precursor in *Microcebus murinus*: genotyping and brain localization. *Neurobiol Dis* 3:169–182. <https://doi.org/10.1006/nbdi.1996.0017>
38. Simic G, Leko MB, Wray S, Harrington C, Delalle I, Jovanov-Milosevic N, Bazadona D, Buee L, de Silva R, Di Giovanni G, Wischik C, Hof PR (2016) Tau protein hyperphosphorylation and aggregation in Alzheimer's disease and other tauopathies, and possible neuroprotective strategies. *Biomolecules*. <https://doi.org/10.3390/biom6010006>
39. Vogt BA, Pandya DN (1987) Cingulate cortex of the Rhesus-monkey.2. Cortical afferents *J Comp Neurol* 262:271–289. <https://doi.org/10.1002/cne.902620208>

### Publisher's Note

Springer Nature remains neutral with regard to jurisdictional claims in published maps and institutional affiliations.

Ready to submit your research? Choose BMC and benefit from:

- fast, convenient online submission
- thorough peer review by experienced researchers in your field
- rapid publication on acceptance
- support for research data, including large and complex data types
- gold Open Access which fosters wider collaboration and increased citations
- maximum visibility for your research: over 100M website views per year

At BMC, research is always in progress.

Learn more [biomedcentral.com/submissions](https://biomedcentral.com/submissions)



# Transmission of amyloid-beta and tau pathologies is associated with cognitive impairments in a primate

Suzanne Lam, Fanny Petit, Anne-Sophie Hérard, Susana Boluda, Sabiha Eddarkaoui,

Martine Guillermier, The Brain Bank Neuro-CEB Neuropathology Network, Luc Buée,

Charles Duyckaerts, Stéphane Haïk, Jean-Luc Picq, Marc Dhenain

## Supplementary material

### Additional file 1

#### SUPPLEMENTARY TABLES

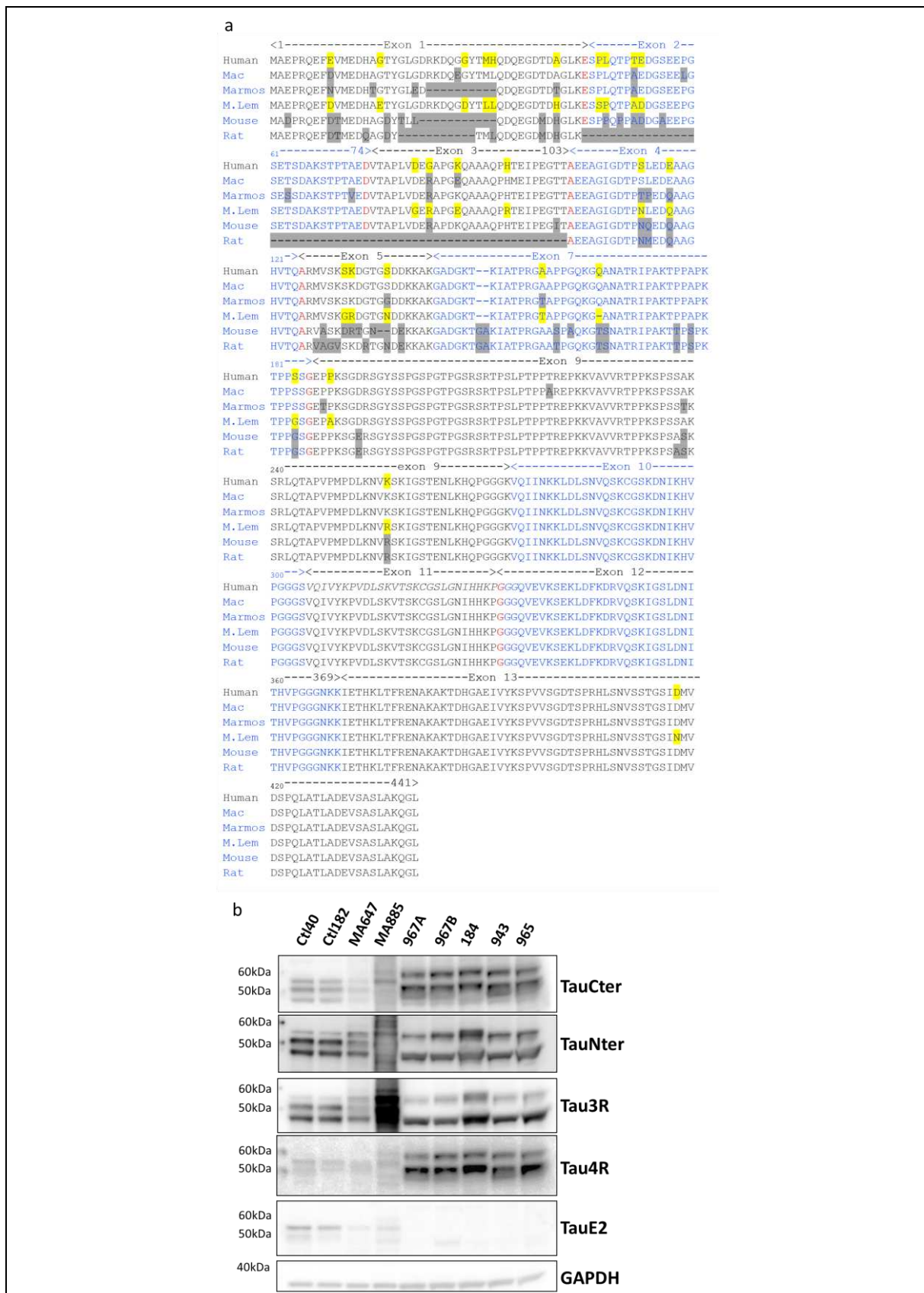
##### Supplementary Table 1

Patient				Neuropathology							
ID	Age	Gender	Disease progression (months)	Post mortem delay (hours)	Braak and Braak stage	Thal phase	CAA	$\alpha$ -synuclein	TDP43	Hippocampal sclerosis	PrPSc
1-Ctrl	66	M	-	26	II	0	0	0	0	0	0
2-Ctrl	76	M	-	NA	II	0	0	0	0	0	0
1-AD1	79	F	78	49	V	5	Type2	0	0	0	0
2-AD1	87	F	72	29	V-VI	4	Type1	0	0	0	0
3-AD1	89	F	96	31	V	5	Type1	0	0	0	0
4-AD1	71	M	66	54	VI	4	Type2	Amygdala	0	0	0
1-AD2	84	F	6	79	V	4	Type2	0	0	0	0
2-AD2	81	F	36	NA	V	5	Type1	0	0	0	0
3-AD2	81	F	36	26	VI	4	0	0	0	0	0
4-AD2	86	F	36	21	V	4	Type2	0	0	0	0

**Supplementary Table 1: Patient characteristics.** Age-matched slowly (AD1) and rapidly (AD2) evolving AD patients were selected based on disease duration (over or under 36 months) and neuropathological evaluation, including similar Braak and Thal stages. Brains were negative for  $\alpha$ -synuclein, TDP43, hippocampal sclerosis and pathological prion PrPSc. Two non-AD control individuals were also included in this study. NA: not available.

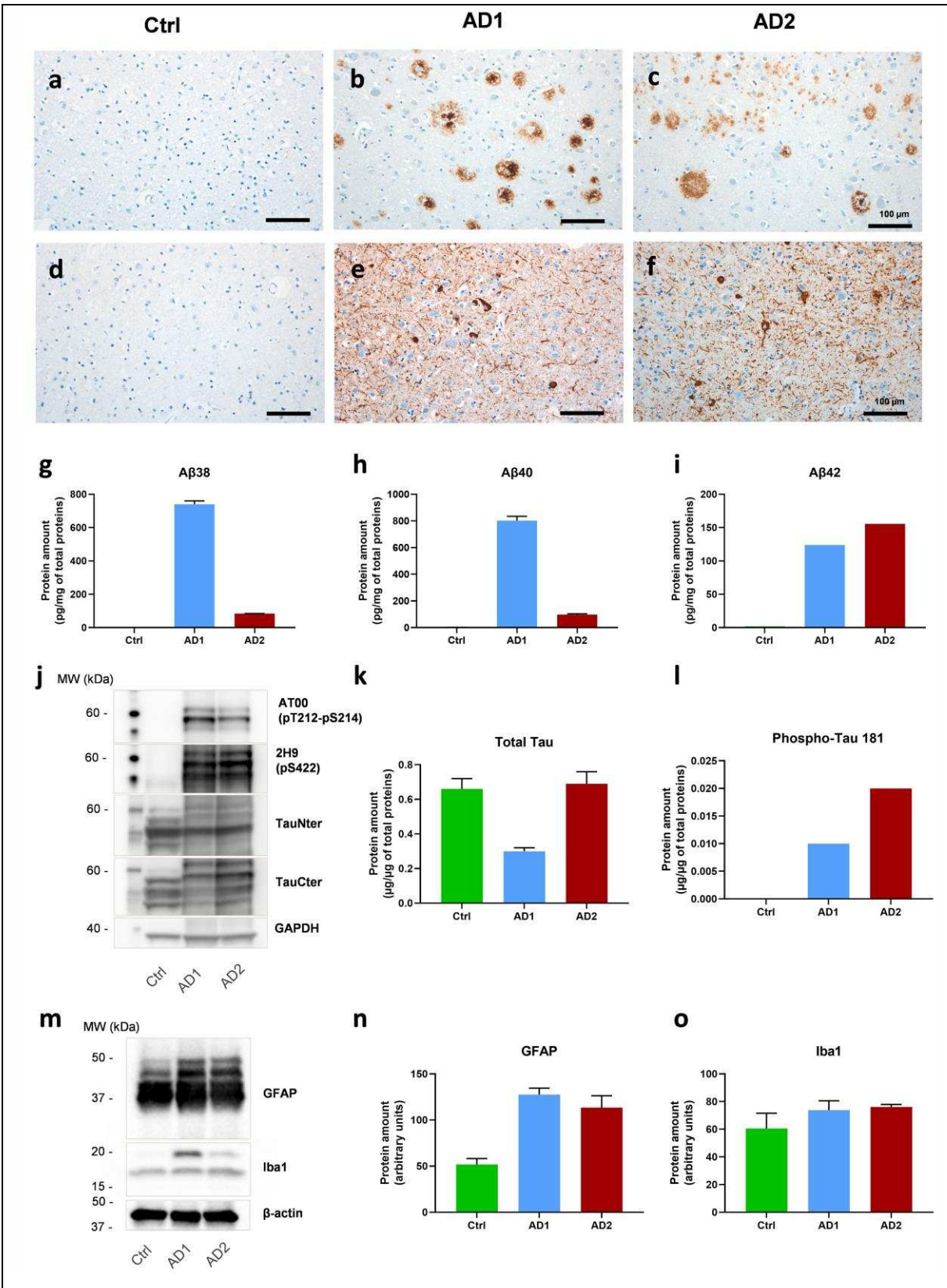
# SUPPLEMENTARY FIGURES

## Supplementary Figure 1



**Supplementary Figure 1: Protein sequence issued from MAPT gene in mouse lemurs and tau protein isoforms.** (a) Comparison of proteins sequences for MAPT genes (issued from <http://www.ensembl.org/>) in humans (MAPT-204 ENST00000351559.10), macaques (Mac: MAPT-204 ENSMMUT00000005855.4), marmosets (Marmos: MAPT-202 ENSCJAT00000039192.4), mouse lemurs (M. Lem: MAPT-201 ENSMICT00000067450.1), mice (Mapt-201 ENSMUST00000100347.11), and rats (Mapt-201 ENSRNOT00000006947.8). Different exons are colored black and blue. Residue overlaps splice sites are labelled in red. Differences between humans and mouse lemurs are displayed in yellow. Differences between humans and other species are displayed in gray. (b) Tau isoform expression was examined by immunoblots using antibodies specific for tauCter, tauNter, tau3R, tau4R, and tauE2. TauCter, tauNter, tau3R, and tau4R were detected in the five (non-inoculated) mouse lemurs evaluated in this study (967A, 967B, 184, 943, 965). Isoforms corresponding to exon 2 were not detected.

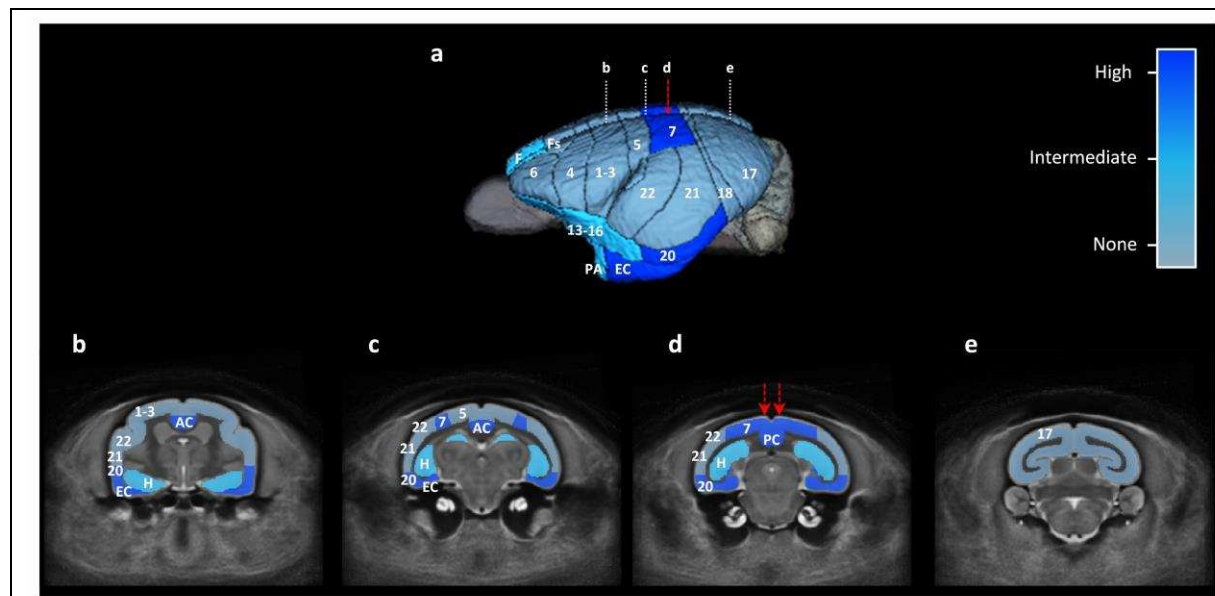
Supplementary Figure 2



Supplementary Figure 2: Characteristics of human brain samples and brain extracts inoculated to animals. Representative images of Ctrl, AD1 and AD2 brain samples stained

for A $\beta$  (a-c) and tau (d-f) pathologies. Scale bars = 100  $\mu$ m. Three brain extracts were prepared from 2 control individuals, 4 cases with a slowly evolving form of AD and 4 cases with a rapidly evolving form of AD (Ctrl, AD1 and AD2 brain extracts, respectively). All quantifications of the brain extracts (Ctrl, AD1 or AD2) were performed in duplicate and data are shown as mean  $\pm$  standard deviation of the replicates. (g-i) Quantifications of total A $\beta_{38}$ , A $\beta_{40}$  and A $\beta_{42}$  of the brain extracts (MSD technology). Both AD brain extracts had more A $\beta$  proteins compared to the Ctrl one. The AD1 extract showed more A $\beta_{38}$  and A $\beta_{40}$  than the AD2 one. (j-l) Tau profile evaluation by western blot revealed a pathological hyperphosphorylated tau triplet at 60, 64 and 69 kDa observed in AD and a typical shift in the molecular weight of the Alzheimer Tau-Cter triplet in AD1 and AD2 brain extracts (j). Total tau (k) and pathological phospho-tau 181 levels (l) were assessed using ELISA quantification. Neuroinflammatory profile evaluation by western blots revealed higher astrocytic presence (GFAP-positive) in AD1 and AD2 brain extracts compared to the Ctrl extract (m-n). Microglial (Iba1-positive) levels were similar in the Ctrl, AD1 and AD2 groups (m, o).

### Supplementary Figure 3



**Supplementary Figure 3: Connectivity of the cingulate cortex in mouse lemurs.** Three-dimensional rendering of regions connected to the cingulate cortex. Regions are classified according to three levels of connectivity (not connected/intermediate/high connectivity). Connectivity was determined based on literature in primates (Vogt, 1987; Parvizi, 2006). Three-dimensional rendering relied on a digital atlas of mouse lemurs (Nadkarni, 2019) and on the use of the ITK-SNAP software (<http://www.itksnap.org>). The red arrows indicate the needle tracts. Numbers represent Brodmann areas as reported in the mouse lemur brain by (Le Gros Clark, 1931). AC: anterior cingulate cortex, EC: entorhinal cortex, F: antero-medial frontal cortex, Fs: superior frontal cortex, H: hippocampus, PA: peri-amygdalar cortex, PC: posterior cingulate cortex.

#### References

- Vogt BA, Pandya DN (1987) Cingulate cortex of the Rhesus-monkey .2. Cortical afferents. *J Comp Neurol* 262: 271-289. <https://doi.org/DOI 10.1002/cne.902620208>
- Parvizi J, Van Hoesen GW, Buckwalter J, Damasio A (2006) Neural connections of the posteromedial cortex in the macaque. *Proc Natl Acad Sci USA* 103: 1563-1568. <https://doi.org/10.1073/pnas.0507729103>
- Nadkarni NA, Bougacha S, Garin C, Dhenain M, Picq JL (2019) A 3D population-based brain atlas of the mouse lemur primate with examples of applications in aging studies and comparative anatomy. *Neuroimage* 185: 85-95. <https://doi.org/10.1016/j.neuroimage.2018.10.010>
- Le Gros Clark WE (1931) The brain of *Microcebus murinus*. *Proc Zool Soc London* 101: 463-486.

## Additional file 2 (movie to download)



### **Additional File 2: Movie showing three consecutive trials in a jumping stand apparatus.**

The jumping stand apparatus evaluates learning and long-term memory performances of lemurs using discrimination tests. The device is a vertical cage made of plywood walls, except for the front panel which consists in a one-way mirror allowing observation. During the test, the animal is placed on a elevated central platform (10 first seconds of the movie) and must jump from this starting platform to one of the two landing platforms. Each landing platform is associated with a different visual stimulus, characterized by a specific shape, texture and pattern (circular object versus rectangular straw-mat in this example). For each pair of visual stimuli, one is associated with a positive reinforcement (*i.e.* a stable landing platform giving access to a 2-min rest in a wooden nesting box), whereas the other one is associated with a negative reinforcement (*i.e.* an unstable landing platform leading to a fall to the bottom of the cage). The mouse lemurs has to learn the rule by trial and error. In this movie, during the first trial, the mouse lemur makes the wrong choice by jumping towards



the straw-mat and falls. During the second trial, it changes its strategy and jump towards the circular object. It keep the same strategy during the third trial. In this movie, one can see how the lemur observes the different objects before its jump.

# **DISCUSSION**



AD diagnosis relies on the occurrence of both clinical signs and typical A $\beta$  and tau neuropathological lesions. These lesions spread in a highly stereotyped pattern throughout the brain and are associated with a progressive neurodegenerative process including synaptic loss. Neuropathological observational studies in humans have suggested the iatrogenic transmission of A $\beta$  and tau pathologies in patients exposed to compounds or neurosurgical tools contaminated with A $\beta$  and tau (Duyckaerts et al., 2018; Hervé et al., 2018; Jaunmuktane et al., 2021, 2015b). Experimentally, the transmission of such pathologies has been widely demonstrated in transgenic rodent models, through the intracerebral inoculation of either synthetic or brain-derived proteopathic seeds (Clavaguera et al., 2013; Iba et al., 2013; Meyer-Luehmann et al., 2006; Stöhr et al., 2012). These models are valuable tools to better understand AD pathophysiology and characterize the mechanisms involved in the development and progression of AD cardinal features. However, few studies have evaluated the functional and neuronal impacts of such transmission, especially in non-human primates. Here, we recapitulated A $\beta$  and tau pathologies, neuronal alterations and cognitive deficits in two different models (APP/PS1dE9 mice and mouse lemur primates) through the intracerebral inoculation of AD brain extracts. Furthermore, we explored the relationships between these lesions and discussed the implications of such transmission for human pathology.

---

## 1. The APP/PS1dE9 mouse model

---

Brain homogenates (rpAD, cIAD, Ctrl) were inoculated bilaterally (2  $\mu$ l/site) in the dorsal hippocampus (CA1) of 2-month-old APP/PS1dE9 mice. At this age, mice produce high levels of A $\beta$  leading to amyloid plaque deposition at around 4 months of age (Garcia-Alloza et al., 2006b). This model expresses the endogenous murine tau protein isoforms and is not transgenic for any human tau. Mice were euthanized 4 or 8 months after the inoculations (mpi).

## **1.1. Transmission of AD-like neuropathological lesions after AD brain extract inoculation**

### **1.1.1. A $\beta$ and tau pathologies**

In accordance with several studies, AD brain extract intrahippocampal inoculation progressively increased A $\beta$  deposition in the hippocampus and surrounding areas of APP/PS1dE9 mice, as opposed to A $\beta$ -negative control brain inoculation (Kane et al., 2000; Meyer-Luehmann et al., 2006). Additionally, substantial amounts of plaques were also detected in other regions such as the perirhinal/entorhinal cortex. However, since no significant difference was reported between the groups, we hypothesize that plaques detected in this region may have mostly resulted from the model's intrinsic expression of A $\beta$  pathology at 6 and 10 months of age (respectively for the 4 and 8 mpi cohorts).

Tau pathologies in the forms of neuritic plaques, neuropil threads and neurofibrillary tangles, were also severely induced by AD brain extracts inoculation. Additionally, these lesions progressively spread from the hippocampus to connected brain regions such as the perirhinal/entorhinal cortex. Interestingly in this region, neuropil threads and neurofibrillary tangles were mainly induced in the external layers (II-III) of the cortex that project to the dentate gyrus via the perforant pathway and to the CA1 region via the temporo-ammonic pathway, respectively. Conversely, internal layers (V-VI) of the cortex that receive projections from the CA1 region were not labeled. This suggests that tau spreading might have followed a retrograde pathway. However, as many reciprocal and bidirectional connections occur between these structures, additional experiments are needed to further support this hypothesis.

Interestingly, some neuritic plaques were also observed in control-inoculated mice but these lesions resembled those that spontaneously occur with age in our model (Metaxas et al., 2019) and were associated with a lower AT8-stained area compared with the ones induced by AD brain extract inoculation. Our results therefore highlight that, in accordance with a previous study (He et al., 2018), A $\beta$  plaques create a microenvironment that facilitates the occurrence of tau lesions within neuritic plaques, and that such lesions are further amplified by the exogenous exposure to human AD brains, presumably because of the presence of pathological tau seeds. No difference in either A $\beta$  or tau pathologies was reported between rpAD and cIAD-

inoculated mice. Altogether, this model appears as a valuable tool to better understand AD pathophysiology since it allows to evaluate the development of both A $\beta$  and tau pathologies in a context that does not rely on the artificial genetic manipulation of tau.

### 1.1.2. Neuroinflammation

Activated microglia and reactive astrocytes around A $\beta$  and tau lesions are prominent features of AD and growing evidence suggests that they play a crucial role in regulating AD pathology (Serrano-Pozo et al., 2011b). In our model, microglial activity was assessed in various regions including the hippocampus and perirhinal/entorhinal cortex. No difference in overall microglial activation nor in microglial recruitment around amyloid plaques was reported between the groups. Similarly, no difference in astrocytic reactivity was detected between the inoculated groups.

Increased microglial activation has been associated with synaptic loss in experimental models of amyloidosis and tauopathy (Dejanovic et al., 2018; Spangenberg et al., 2016). However, experimental data and human genetic evidence, exemplified by the large effect of the loss-of-function TREM2 mutations on AD risk and on microglial function, argues that microglia have a protective function that lowers the incidence of AD (Hansen et al., 2018). In addition, imaging studies in humans suggest that high microglial activity is associated with lower rates of decline in early cases of AD (Hamelin et al., 2016). Despite the absence of inter-group differences, and as discussed below (see **Discussion chapter – § 1.3. Relationships between neuropathological lesions**), our model appears to support this hypothesis since reduced microglial activation was linked to increased synaptic loss. Exploring the brain inflammatory status through the measurement of pro- and anti-inflammatory factors could however further uphold this hypothesis. In addition, the comparison of microglial morphology and transcriptomic analysis of microglial populations around A $\beta$  deposits or in lesion-free areas should provide valuable information regarding the multiple states of microglial activation and their implication in the pathology observed in our model (Hansen et al., 2018).

## **1.2. Transmission of heterogeneous cognitive and synaptic profiles after the inoculation of different AD brain extracts**

Despite the fact that rpAD and clAD-inoculated mice did not display any differences in A $\beta$  deposition, tau pathology or neuroinflammation, differences in the levels of cognitive and synaptic impairments were reported.

### **1.2.1. Alteration of specific cognitive functions**

Two tasks evaluating memory function were performed on inoculated mice: an object recognition task (V-maze) and a spatial memory task (Morris water maze). Interestingly at 8 mpi, novel object recognition, but not spatial learning and memory, deficits were detected in mice inoculated with the rpAD brain extract compared to clAD- and Ctrl-inoculated animals. This suggests the selective alteration of some networks involved in memory function and the relative sparing of others in the rpAD group.

To evaluate this hypothesis, we further characterized tau pathology in areas of the hippocampus and entorhinal cortex involved either in context-free memory (*e.g.* novel object recognition) or in context-rich memory (*e.g.* spatial memory) (see **Results chapter – § 1.3. Complementary data**). In both the hippocampus and the entorhinal cortex, areas associated with context-free memory displayed more tau than the ones associated with context-rich memory in AD-inoculated mice. As the severity of tau pathology correlates with cognitive alterations in our model, this provides a possible explanation regarding the occurrence of novel object recognition deficits and the absence of spatial memory alterations in rpAD-inoculated mice. The context-free memory pathway directly implicated the inoculated area (distal CA1) which could explain the more abundant tau load in this region and associated projections (Bekiari et al., 2015; Groen et al., 2003; van Strien et al., 2009). No difference in tau pathology was however reported in the context-free and in the context-rich memory pathways between clAD and rpAD-inoculated mice. We hypothesize that synergistic interactions between several factors (*e.g.* tau, microgliosis, A $\beta$ ), possibly associated with small differences below the significance threshold, might have entailed dramatic changes in cognitive performances. In addition, other factors, including soluble assemblies or various strains of A $\beta$  and tau, may have been implicated in the induction of such contrasting cognitive

profiles (see **Discussion chapter – § 1.4. Mechanistic hypothesis for heterogeneous phenotypes**).

As no difference in cognitive performance was observed at 4 mpi, our study suggests that alterations occurred progressively and did not result from an acute process following human brain inoculations.

It is however worth mentioning that mice cognitive functions can hardly be put in parallel with human cognition, as the mouse brain shows major differences in terms of cortical architecture and functional organization compared with the human brain. Additionally, the high attrition rates in AD drug development following preclinical validation in rodents further underlies the limited predictive validity of pharmacological effects on rodent cognition (Stephan et al., 2019). Given their close evolutionary relationship to humans, resorting to non-human primate models to confirm cognitive impacts of drug candidates appears essential.

### **1.2.2. Synaptic alterations**

A decrease in synaptic density was observed in the hippocampus and perirhinal/entorhinal cortex of rpAD-inoculated mice compared with Ctrl- and cIAD-inoculated animals. Interestingly, in our model, the severity of cognitive alterations correlated with synaptic defects in the hippocampus. In humans, synaptic alterations lead to the collapse of neural networks and are the best correlate to cognitive decline (Terry et al., 1991). Taken together, these data further suggest that specific neuronal networks were disrupted following rpAD brain extracts inoculation.

Further investigation would however be interesting to clearly identify the origins of the synaptic impairments that were induced in our model. Here, we evaluated the colocalization of pre- and postsynaptic markers as an index of synaptic density. More specifically, we quantified the colocalization between Bassoon, a component of the presynaptic active zone involved in its structural maintenance and a regulator of presynaptic ubiquitination and proteostasis (Waites et al., 2013), and Homer1, a postsynaptic density scaffold protein that regulates glutamatergic synapses and is involved in synaptic plasticity, calcium signaling and spine morphogenesis (Yoon et al., 2021). In AD, the mechanisms associated with synaptic damage are thought to involve axonal transport impairments, as suggested by the altered



expression of genes associated with synaptic structural elements, vesicle trafficking and release, neurotransmitter receptors and receptor trafficking (Overk and Masliah, 2014). Aside from synaptic loss, changes in LTP and LTD involved in synaptic plasticity are also crucial in AD-associated cognitive alterations. Thus, exploring the integrity of each of these functions using other synaptic markers and through transcriptomic and electrophysiological experiments could help to further characterize the origins of synaptic and cognitive changes resulting from the exposure to rpAD brain extracts.

### **1.3. Relationships between neuropathological lesions**

Synaptic alterations have been associated with both A $\beta$  and tau in various experimental models (Pooler et al., 2014; Selkoe, 2002; Spires-Jones and Hyman, 2014). In our model, synaptic deficits were associated with the severity of tau pathology in the hippocampus and the perirhinal/entorhinal cortex, therefore supporting the contribution of tau to synaptic alterations. Tau-positive synapses can be engulfed by microglia through the complement pathway therefore arguing that synaptic loss may result from inadequate pruning (Dejanovic et al., 2018). Additionally, it has been suggested that tau may induce local apoptotic mechanisms leading to phosphatidylserine exposure on synapses, to which C1q complement proteins can bind (Païdassi et al., 2008) and act as a “eat-me” signal to microglia (Brelstaff et al., 2018). Further investigation on the complement pathway activation in our model may provide mechanistic explanations regarding the induced synaptic loss. Neuroinflammatory factors such as C1q, C3 or IL-33 were shown to modulate synaptic density by altering their formation and elimination (Dejanovic et al., 2018; Litvinchuk et al., 2018; Wang et al., 2021). As we did not characterize the cytokinic profiles of our inocula, we cannot rule out that they might have contained distinct concentrations or panels of pro- and anti-inflammatory cytokines that could have influenced synaptic integrity.

Unexpectedly, A $\beta$  pathology was weakly linked to synaptic changes in our model, which contrasts with many studies (Selkoe, 2002; Spires-Jones and Hyman, 2014). It is however important to underline that since our model spontaneously develops high A $\beta$  pathology, A $\beta$ -related synaptic changes might have similarly occurred in all of the experimental groups. Indeed, the APP/PS1dE9 mouse model was shown to display a decrease in pre- and

postsynaptic markers colocalization by the age of three months (Hong et al., 2016), as well as LTP deficits by the age of 6 months (Viana da Silva et al., 2016).

Several studies have also suggested that microglia can engulf amyloid deposits and prevent their toxicity by shielding them off from neurons (Condello et al., 2015). This protective activity has been shown to depend on TREM2 and involves microglial activation into a disease-associated state characterized by a decrease in “homeostatic” genes (*e.g.* CX3CR1, P2RY12, TMEM119) and an increase in “neurodegeneration-related” genes (*e.g.* APOE, AXL, CSF1, CLEC7a and some major histocompatibility complex class II genes) (Hansen et al., 2018). In our study, reduced synaptic density was associated with a decrease in microglial load and activation. We hypothesized that a decrease in microglia-mediated amyloid shielding could lead to increased synaptotoxicity. Preliminary studies do not support this hypothesis but further investigation on the microenvironment surrounding lesions, more particularly on microglia transcriptomic profile around plaques and tau deposits, is ongoing. In addition, the presence of A $\beta$  and tau accumulations at the synapse and the assessment of microglial phagocytic function around synapses should provide more insight into the role of microglia in synaptic loss. Interestingly, it has been suggested that through the elimination of A $\beta$ -affected synapses, microglia might prevent A $\beta$  spreading and A $\beta$ -mediated tau hyperphosphorylation, and therefore protect neuronal networks from excessive damage (Edwards, 2019). In our study, it is however important to underline that no intergroup difference was observed in microglial activation between Ctrl and AD-inoculated animals and no difference in A $\beta$  and tau loads was reported between cIAD and rpAD brain-injected mice. This suggests that AD heterogeneity might result from a cumulative effect of all these factors but, as discussed in the next paragraph, does not rule out the involvement of other key players that have not been captured in our study.

#### **1.4. Mechanistic hypothesis for heterogeneous phenotypes**

In our study, we provided the first experimental evidence that the intracerebral inoculation of different sporadic AD brain extracts can have different impacts on synaptic density and cognitive performances. However, despite these differences in rpAD and cIAD-inoculated mice, similar A $\beta$  plaque burden, tau deposition levels and neuroinflammation were reported. Multiple causes could be involved in the development of such contrasting pathologies,

including differences in A $\beta$  and tau inoculated doses. Indeed, inoculated AD brain extracts showed similar levels of A $\beta_{42}$ , but the rpAD brain extract displayed more phospho-tau181. A complementary cohort of mice inoculated with normalized levels of phospho-tau181 showed novel object discrimination performances that followed the same trend as the one previously observed with the first cohort (see **Results chapter – § 1.3. Complementary data**). Indeed, following phospho-tau181 level normalization, mice inoculated with the rpAD brain extract still showed lower cognitive scores compared with the other groups, although no statistical difference was reported possibly due to smaller group sizes and marked interindividual variability. Altogether, these data suggest that differences between rpAD, cAD and Ctrl-inoculated animals may not solely be explained by a dose effect.

In addition, differences in A $\beta$  and tau oligomeric species associated with each form of AD could also be involved. Indeed, many studies in humans and animal models have highlighted the impact of soluble species in neuronal and glial alterations that underlie synaptic failure and cognitive impairment in AD (Ferreira et al., 2015). In humans, A $\beta$  oligomer cerebral and plasmatic levels have been correlated with cognitive status (Meng et al., 2019; Tomic et al., 2009), and increased levels of A $\beta$  oligomers have been observed in synapses in early AD, prior to plaque deposition (Bilousova et al., 2016). In addition, although NFT pathology correlates with clinical decline and disease severity, neurodegeneration far exceeds NFT burden in AD (Gómez-Isla et al., 1997; Nelson et al., 2012). Tau oligomers have also been detected in AD brains (Lasagna-Reeves et al., 2012b), including in cortical synapses (Henkins et al., 2012), and were correlated with memory loss in mice (Berger et al., 2007). Thus, it has been suggested that insoluble fibrils, evaluated in our study, may not be toxic *per se* but rather act as reservoirs of soluble bioactive oligomers (Shankar et al., 2008; Spires-Jones et al., 2009). The implication of A $\beta$  and tau oligomers and more particularly their presence at the synapse and their interactions with microglia should be further investigated in our model.

In the context of AD, evidence for the existence of A $\beta$  and tau strains has been suggested, mainly in studies exploring the characteristics of genetic AD (Watts et al., 2014). The origin of AD heterogeneity in sporadic forms of the disease is less studied. However, it has been suggested that typical/classical AD and rapidly evolving AD phenotypes could be linked to different A $\beta$  and tau strains exhibiting distinct properties (Dujardin et al., 2020; Qiang et al.,

2017; Rasmussen et al., 2017). Thus, it would be interesting to further characterize our human brain samples and evaluate if each type of samples, *i.e.* cIAD or rpAD, shows distinct strain-like properties. Furthermore, the serial transmission of such properties in inoculated animals should be evaluated. This study has been initiated in collaboration with the Brain Institute (ICM, Paris), and promising preliminary results have already emerged (see **Results chapter – § 1.3. Complementary data**). Indeed, in consistency with previous studies as well as with our mouse and lemur seeding experiments, we did not detect any differences in A $\beta$  plaque load between rpAD and cIAD patients (Cohen et al., 2015; Drummond et al., 2017). Additionally, heterogeneity in plaque morphology was particularly prominent in rpAD cases. This is consistent with a recent study showing that A $\beta$  assemblies molecular heterogeneity, associated with distinct aggregation kinetics, can be linked to different subgroups of sporadic AD (Di Fede et al., 2018). Moreover, structural diversity in A $\beta_{42}$  and/or A $\beta_{40}$ , as well as increased levels of A $\beta_{42}$  oligomers were found to be associated with a rapid cognitive decline, suggesting that A $\beta$  fibril thermodynamics are different in cIAD and rpAD patients (Cohen et al., 2015; Qiang et al., 2017). Globally, morphometric analysis of A $\beta$  deposits in our patients reported that rpAD cases displayed smaller, denser and less convoluted plaques than cIAD cases. This is in line with a previous study showing that smaller particles of A $\beta_{42}$  are found in the hippocampus and posterior cingulate cortex of rpAD patients, compared to cIAD patients (Cohen et al., 2015). Further characterization of A $\beta$  and tau assemblies at the biochemical, biophysical and ultrastructural levels will be performed using mass spectrometry (Di Fede et al., 2018), Forster Resonance Energy Transfer (FRET)-based biosensor (Sanders et al., 2014) and real-time Quaking induced conversion (RT-QuIC) (Kraus et al., 2019) experiments to better characterize our brain samples and assess the potential occurrence of a strain effect in our models.

---

## 2. The mouse lemur primate model

---

The host in which the proteopathic seeds are inoculated provides the biochemical and physiological environment that modulates lesion emergence and functional impacts (Jucker and Walker, 2013). Because of their phylogenetic proximity, NHPs have a brain environment closer to the human brain than that of transgenic mice. In particular, the mouse lemur primate appears as an emerging model of AD as many aspects of its pathological ageing process resemble sporadic AD pathology. Indeed, it naturally models biological heterogeneity and spontaneously develops AD-like lesions, including A $\beta$  and tau deposits, impaired cognitive function and brain atrophy, starting at 6 years of age. As in sporadic AD, these lesions are not associated with specific mutations in APP or presenilin genes (Bons et al., 2006).

Brain homogenates were bilaterally inoculated in two independent cohorts of mouse lemur primates (6.25 $\mu$ l/site, n=6/group). In the first cohort (see **Results chapter – § 2. Encephalopathy induced by AD brain inoculation in a non-human primate**), AD and Ctrl brain extracts were injected in the hippocampus and overlying cortex of 3.5-year-old mouse lemurs. The longitudinal follow-up lasted 18 months. In the second cohort (see **Results chapter - § 3. Transmission of A $\beta$  and tau pathologies is associated with cognitive impairments in a primate**), two types of AD brains (AD1 and AD2) and a Ctrl brain extract were injected in the posterior cingulate cortex and underlying corpus callosum of 1.5-year-old mouse lemurs. The longitudinal follow-up lasted 21 months.

### 2.1. First transmission of an AD-like phenotype in a primate

#### 2.1.1. A $\beta$ and tau pathologies

Approximately 20% of mouse lemurs above the age of 6 can spontaneously develop A $\beta$  and tau lesions. Parenchymal A $\beta$  plaques are predominantly observed in occipital and parietal cortical regions (Languille et al., 2012). Tau lesions appear early in the neocortex and affect the subiculum, entorhinal cortex and amygdala of animals over 8 years old (Bons et al., 2006; Giannakopoulos et al., 1997). To limit the occurrence of spontaneous lesions in our models, mouse lemurs were euthanized before the age of 6, *i.e.* at 5 $\pm$ 0.2 years old for the first cohort, and at 3.6 $\pm$ 0.6 years old for the second cohort.

For the first time in a NHP, we showed that AD brain extracts intracerebral inoculations can induced both A $\beta$  and tau pathologies. All of AD brain extracts-inoculated animals of the second cohort indeed showed A $\beta$  and tau lesions whereas no pathology was detected in any of the Ctrl-inoculated lemurs. As in humans, diffuse and focal amyloid plaques were detected in the parenchyma and vascular amyloidosis affected both small and large vessels. Tau pathology was observed in the forms of neuropil threads and intracellular neurofibrillary tangle-like lesions. A $\beta$  and tau deposits were detected close to the inoculation sites and in several other brain regions suggesting the effective seeding and spreading of both pathologies. A $\beta$  and tau deposition patterns in our study involved regions that are typically affected by A $\beta$  or tau pathologies in old lemurs (Bons et al., 2006; Giannakopoulos et al., 1997; Languille et al., 2012). However, here, the fact A $\beta$  and tau deposits were also reported in several other brain regions, involved young animals that are typically devoid of any lesions, and were induced only and systematically after AD brain extracts inoculations, suggests that they did not occur spontaneously but were rather induced by our experimental procedure.

Regions affected by A $\beta$  and tau lesions were similar but did not completely overlap suggesting that both pathologies might have occurred independently from each other. This is supported by the fact that no correlation has been reported between A $\beta$  and tau lesions in aged mouse lemurs (Giannakopoulos et al., 1997). Interestingly, tau pathology did not affect some temporal and occipital brain regions that were relatively close to the inoculation sites. This suggests that the spatial progression of tau did not solely occur via a systematic isotropic diffusion from the injection site to proximal regions. Finally, and as highlighted by studies conducted on mice and old lemurs, variations in regional susceptibility to A $\beta$  and tau pathologies may also explain differences in their spatiotemporal depositions (Bons et al., 2006; Eisele et al., 2009; Giannakopoulos et al., 1997; Iba et al., 2013; Languille et al., 2012).

Previous studies have evaluated A $\beta$  and tau pathology induction in primates following the inoculation of AD brain extracts or synthetic aggregates. In particular, a 3.5 to 7-year-long study conducted on marmosets (*Callithrix jacchus*) intracerebrally inoculated with large volumes of AD brain extracts (300  $\mu$ l of 10% homogenates distributed within 6 inoculation sites) induced moderate amyloid deposition in most animals but did not lead to tau lesions nor to other AD-like pathological features (Baker et al., 1994, 1993a, 1993b; Ridley et al.,

## 2. The mouse lemur primate model

---

2006). Interestingly, intracerebroventricular injections of synthetic A $\beta$  oligomers in adult cynomolgus macaques were shown to promote tau pathology, neuroinflammation and synaptic loss. However, this study required a heavy procedure involving repeated injections of high doses of oligomers and failed to induce fibrillary amyloid deposits (Forny-Germano et al., 2014). Given the complex interactions between A $\beta$  and tau pathologies in AD (Busche and Hyman, 2020 & see **Introduction chapter - § 1.7. AD pathophysiology**), the occurrence of both lesions in the same model appears to be critical in order to replicate AD pathogenesis. In particular, the absence of both A $\beta$  and tau neuropathological lesions could contribute to poor translation between preclinical and clinical trials. Comparatively, our experimental design therefore seems more advantageous, as it induces both A $\beta$  and tau pathologies and only requires a single surgery involving small volumes of injected material.

In our first cohort of lemurs, the sparsity of A $\beta$  and tau lesions was striking. The seeding ability of the AD brain extracts was confirmed in transgenic mouse models of amyloidosis and tauopathy, thus underlining the influence of the host in the occurrence of neuropathological lesions. Discrepancies in neuropathological findings between our two cohorts of lemurs could result from specific properties of the seeding agents and the impact of local environment, *i.e.* the inoculated brain regions. Indeed, for the second cohort, we sonicated each sample before inoculation as this procedure was shown to increase the seeding and spreading capacities of brain extracts, by generating smaller and more bioactive A $\beta$  and tau aggregates that can more readily propagate through the brain than large fibrils (Langer et al., 2011). In addition, our surgical procedure was refined and allowed more precise injections into highly connected brain areas, *i.e.* the corpus callosum and overlying posterior cingulate cortex. The former is indeed the major commissural tract connecting both hemispheres and the latter is a functional connectivity hub in mouse lemurs (Garin et al., 2021) and humans (Buckner et al., 2009). The posterior cingulate is moreover involved in the default-mode network which is disrupted and highly vulnerable to A $\beta$  deposition in AD (Buckner et al., 2009). Therefore, we hypothesize that introducing misfolded seeds into these particular regions might have further promoted the spreading of AD neuropathological lesions throughout the brain.

### **2.1.2. Neuroinflammation**

A localized neuroinflammatory response was detected in Ctrl and AD brain extracts-inoculated lemurs, but not in non-injected animals. This suggests that the inoculation of human brain extracts can lead to a chronic neuroinflammatory response. No difference in microglial and/or astrocytic activations was however reported between the groups of AD- or Ctrl-inoculated mouse lemurs, in both cohorts. This suggests neuroinflammation cannot explain most of the differences observed between AD- and Ctrl-inoculated animals. However, one cannot exclude that subtle changes in cell morphology or differences in secreted mediators reflecting different stages of glial activation could have occurred. In marmosets, the co-injection of A $\beta$  fibrils and lipopolysaccharide showed that animals suffering from chronic inflammation developed plaques after 5 months as opposed to the ones that only received A $\beta$  fibrils (Philippens et al., 2017). This highlights the role of immune modulation on the development of amyloidosis in NHPs and the need for further investigation in our model.

### **2.1.3. Cognitive impairments**

Longitudinal evaluation of cognitive performances was performed periodically in a jumping stand apparatus, designed to take into account the mouse lemur's arboreal lifestyle as well as its sensorial and behavioral skills. Learning and long-term memory were evaluated using discrimination tasks. For the second cohort only, a reversal learning test was also performed to evaluate cognitive flexibility at the final timepoint. Learning abilities were similar in all groups before the inoculation. As expected, human brain inoculations did not affect motricity in mouse lemurs. This suggests that performances in the jumping stand apparatus were not impacted by motor dysfunction.

Interestingly, each cohort of mouse lemurs displayed different profiles of cognitive alterations in accordance with the inoculated regions and induced neuronal alterations. In the first cohort, mouse lemurs were inoculated in the hippocampus and showed a global decrease in learning performances but mostly, memory function was impacted compared to Ctrl animals. In the second cohort, inoculated in the posterior cingulate cortex, learning and reversal discrimination performances were altered in AD-inoculated mouse lemurs whereas memory was preserved. Surprisingly in this cohort, ADs and Ctrl groups all passed the learning task with a perfect score at 15 mpi, although AD-inoculated lemurs performed significantly worse than



## 2. The mouse lemur primate model

---

Ctrl-inoculated animals both at the previous and at the next timepoints of the follow-up (*i.e.* at 9 and 21 mpi). Possible explanations include that animals exhibited a positive transfer of learning resulting from successive trainings at previous timepoints and the fact that the pair of visual cues used at 15 mpi for the learning task was unexpectedly easier to discriminate than the other ones.

In the reversal discrimination task, Ctrl-inoculated animals performed two and five times better than AD1 (*i.e.* cIAD) and AD2 (*i.e.* rpAD) animals respectively, and although no statistical difference was observed, the AD1 group performed two times better than the AD2 group. This is reminiscent of our behavioral data collected in large cohorts of mice in which the rpAD group performed worse than Ctrl and cIAD-inoculated animals. Here, a similar trend was observed despite the small size of mouse lemur groups and might suggest the transmission of heterogeneous cognitive profiles in primates, although further investigation is required to support this hypothesis.

Altogether, mouse lemurs inoculated with AD brain extracts in specific brain regions can therefore develop cognitive alterations that are clinically relevant in AD patients for whom memory and learning abilities are typically disrupted at early stages of the disease (Jahn, 2013).

### **2.1.4. Morphological and neuronal alterations**

Strong bilateral atrophy affecting several brain regions was observed using voxel-based morphometric analysis of anatomical MRIs performed on AD-inoculated mouse lemurs. The course of atrophy evolution in both cohorts suggests that gray matter loss was not related to an acute toxic reaction following human brain extracts inoculations. In both of our studies, the limbic system was involved but each sub-region was more or less impacted according to the inoculation sites. For instance, a marked widespread atrophy of the hippocampus was reported in the first cohort whereas in the second one, hippocampal atrophy remained very localized. Conversely, the posterior cingulate cortex, its surroundings and projection areas were more impacted in the second cohort. Taken together, gray matter loss was reported to start close to the inoculation sites and gradually spread to several other brain regions in both cohorts.

Neuronal loss in the hippocampus (CA3) and entorhinal cortex (layers II-VI) accompanied brain macroscopic atrophy in the first cohort. These regions are connected by the perforant path (Deng et al., 2010), and layer II of the entorhinal cortex is connected to the posterior cingulate and retrosplenial cortices (Bird and Burgess, 2008), suggesting that neuronal loss occurred within an organized network rather than randomly. In addition, neuronal activity evaluated by EEG measures in the frontal cortex was progressively impaired suggesting a long-distance functional impact of AD brain extracts inoculations.

Stereology analysis and synaptic loss evaluation in macroscopically atrophied regions observed in the second cohort would also allow a better characterization of neuronal alterations occurring in our model. In addition, resting-state functional MRIs based on blood-oxygen level dependent signals were performed during the follow-up of this second cohort and are currently processed to evaluate potential disruptions of functional connectivity. Indeed, A $\beta$  and tau are known to alter brain connectivity in mice (Bero et al., 2012; Degiorgis et al., 2020), and in our study, both pathologies were severely observed in atrophied regions associated to the default-mode network, including the posterior cingulate cortex, which is disrupted in AD (Buckner et al., 2009). Importantly however, although closer to the human brain than rodents, one limitation of the mouse lemur brain lies in its small size (approximately 23 mm long, 18 mm wide and 1.7g weight) and its distinct macroscopic organization showing reduced cortical surface in comparison with humans (Bons et al., 1998; Le Gros Clark, 1931). Nonetheless, the evaluation of relationships between connectivity impairments and neuropathological lesions in a primate would have a strong translational value.

## **2.2. Relationships between induced pathological hallmarks**

In mouse lemurs, the first cohort was inoculated in the hippocampus and overlying parietal cortex. This led to cerebral atrophy in these regions along with memory dysfunction. Brain regions showing neuronal loss (*e.g.* the hippocampus and entorhinal cortex) are involved in memory function for contextual information that is important for the long-term retention of a simple visual discrimination task (McDonald et al., 2007; Ranganath and Ritchey, 2012). Neuronal loss affecting this network could therefore participate in the occurrence of spatial memory deficits observed in this cohort. In contrast, our second cohort was inoculated in the posterior cingulate cortex and underlying corpus callosum. The atrophy of the posterior

## 2. The mouse lemur primate model

---

cingulate cortex along with prefrontal regions and basal ganglia was consistent with the decline in object discrimination learning and cognitive flexibility in AD-inoculated animals. Indeed, alterations of these regions can lead to impairments of the executive system function involving response inhibition, resulting in difficulties in learning new associations and perseverative tendencies (Izquierdo et al., 2004; Ridley et al., 1981; Wilson and Gaffan, 2008). In addition, alterations in the perceptual analysis of the stimuli or a dysfunction of attentional or reinforcement mechanisms could also contribute to visual discrimination learning and reversal learning deficits (Ridley et al., 1981). Altogether, these data suggest that, as in humans, macroscopic alterations targeting specific brain regions can result in the impairment of distinct AD-relevant cognitive functions in the mouse lemur.

NFT deposition has been associated with clinical decline and neurodegeneration in humans (Nelson et al., 2012). In our model, mouse lemurs displayed severe amounts of A $\beta$  and tau lesions in the posterior cingulate cortex and surrounding areas, which is consistent with the pattern of brain atrophy. However, atrophy was also observed in some regions, *e.g.* the basal forebrain and basal ganglia, devoid of such lesions. Tangles were shown to form after cognitive decline and neurodegeneration onset in different models (Mroczko et al., 2019). Neurodegeneration occurring in these A $\beta$ - and tau-negative regions may therefore result from the presence of soluble aggregates since such species have been associated with neuronal and cognitive alterations in humans and animal models, as previously discussed (see **Discussion chapter – § 1.4. Mechanistic hypothesis for heterogeneous phenotypes**). In the first cohort, the absence of lesions despite the occurrence of cognitive, morphological and functional alterations also suggests the involvement of soluble species and is reminiscent of suspected non-Alzheimer's pathophysiology (SNAP) cases showing neurodegeneration and functional impairments but no evidence of A $\beta$  and tau pathologies (Chételat et al., 2016; Jack et al., 2018). Investigating the role of soluble oligomeric species in the induced phenotypes and establishing the relationships between soluble species, insoluble aggregates, morphological and functional alterations thus appear critical to further characterize our model.

### **2.3. Implications for human pathology**

Although no evidence suggests the transmission of AD in humans, many questions remain following the several observational studies showing that A $\beta$  pathology is indeed transmissible

(Jaunmuktane et al., 2015b). In particular, whether tau pathology can also be transmitted in humans remains unclear. Only one recent article suggested that widespread tau deposition could be detected in patients with iatrogenic A $\beta$  pathology, but whether tau pathology was directly transmitted or a consequence of A $\beta$  deposition remains uncertain (Jaunmuktane et al., 2021). Experimental studies conducted on transgenic mouse models have suggested that both A $\beta$  and tau lesions can be transmitted, but these models are mostly based on the overexpression of mutated human genes (Clavaguera et al., 2013; Meyer-Luehmann et al., 2006). Here, we clearly showed that both A $\beta$  and tau lesions can be transmitted in a primate expressing physiological levels of endogenous APP and tau proteins. In our second cohort, this transmission was observed in all of AD brain extracts-inoculated animals and was replicated using two different batches of AD brain extracts. As tau was detected at high levels and not necessarily in the direct vicinity of A $\beta$  lesions nor in the same regions, we hypothesize that tau pathology was directly transmitted, as opposed to only being a consequence of A $\beta$  deposition. Thus, our results provide strong arguments for the reinforcement of preventive procedures involving non-standard decontamination methods to ensure the complete removal of misfolded seeds from compounds and surgical instruments and prevent the potential transmission of both A $\beta$  and tau pathologies. Indeed, archival vials of human cadaver-derived growth hormones have been shown to contain both A $\beta$  and tau seeds (Duyckaerts et al., 2018; Purro et al., 2018), therefore potentially exposing receiving patients to A $\beta$  and tau iatrogenic transmissions.

In humans, iatrogenic A $\beta$ , and potentially tau, pathologies were detected several decades following the putatively triggering medico-surgical act. In our study, they were observed after a relatively short incubation period of 21 months in young (1.5-year-old) primates that are typically devoid of any lesions at this age. We hypothesize that this might, at least in part, be due to the extensive sonication of brain extracts prior to inoculation. To our knowledge, samples suspected to be responsible for the iatrogenic transmission of A $\beta$  and tau pathologies in humans did not undergo such procedure, thus potentially explaining much longer incubation times.

Whether A $\beta$  and tau iatrogenic transmissions can be associated with clinical impacts in humans remains to be elucidated. Here, our experimental study outlines that A $\beta$  and tau

## 2. The mouse lemur primate model

---

transmissions in a primate can be associated with cognitive impairments and cerebral atrophy. Even if we cannot conclude on a causal link between A $\beta$  and tau depositions and clinical manifestations, this suggests that the exposure to misfolded A $\beta$  and tau seeds contained in AD brains might lead to clinical alterations. Although extremely challenging, our data thus emphasize the need for a systematic monitoring of morphological and functional alterations in individuals at risk of developing iatrogenic A $\beta$  and tau pathologies.

# **CONCLUSION & PERSPECTIVES**



Observational studies in humans have suggested that A $\beta$  and tau pathologies are transmissible through a mechanism similar to that of acquired prion diseases (Duyckaerts et al., 2018; Jaunmuktane et al., 2021, 2015b). Experimentally, the demonstration of such transmission has been widely performed in mice overexpressing mutated human genes, and following the inoculation of synthetic or brain-derived proteopathic seeds (Clavaguera et al., 2013; Iba et al., 2013; Meyer-Luehmann et al., 2006; Stöhr et al., 2012). These models are valuable tools to better understand AD pathophysiology and characterize the mechanisms involved in the development and progression of AD cardinal features.

Here, we showed that the intracerebral inoculation of human AD brain extracts can modulate both A $\beta$  and tau lesions, in A $\beta$  plaque-bearing mice expressing physiological levels of endogenous murine tau. The inoculation of various AD brain extracts led to different levels of cognitive impairments associated with synaptic loss. Synaptic and cognitive alterations were associated with multiple factors, including the severity of tau pathologies and lower microglial activity, as well as A $\beta$  deposition for cognitive changes. Taken together, our study highlights the major contribution of tau to AD-related neurodegenerative processes and suggests that microglial activity may protect against synaptic loss. Ongoing investigation on the microenvironment surrounding A $\beta$  and tau lesions, with a particular focus on microglial activation profiles, as well as on the involvement of soluble aggregates and distinct strains could further provide mechanistic explanations about the heterogeneous phenotypes induced by various AD brain extracts.

Several questions remain unanswered regarding the consequences of A $\beta$  and tau iatrogenic transmissions. Here, we provided the first experimental evidence of an AD-like phenotype transmission in a primate that includes A $\beta$  and tau pathologies, cognitive deficits and cerebral atrophy. Our work has many implications since it supports recent evidence suggesting that A $\beta$  and tau can be transmitted in humans and outlines that such transmission can be associated with morphological and cognitive alterations. Reinforcing surgical tool decontamination procedures and implementing a systematic monitoring of individuals at risk for A $\beta$  and tau iatrogenic transmission thus appear critical. Furthermore, our results also suggest that AD brain-inoculated mouse lemurs are highly relevant models to explore AD pathophysiology and could ensure a greater translation of preclinical studies to clinical trials.





# REFERENCES



- 2021 Alzheimer's disease facts and figures, 2021. . *Alzheimers Dement. J. Alzheimers Assoc.* 17, 327–406. <https://doi.org/10.1002/alz.12328>
- Abdel Rassoul, R., Alves, S., Pantesco, V., De Vos, J., Michel, B., Perret, M., Mestre-Francés, N., Verdier, J.-M., Devau, G., 2010. Distinct transcriptome expression of the temporal cortex of the primate *Microcebus murinus* during brain aging versus Alzheimer's disease-like pathology. *PLoS One* 5. <https://doi.org/10.1371/journal.pone.0012770>
- Abiega, O., Beccari, S., Diaz-Aparicio, I., Nadjar, A., Layé, S., Leyrolle, Q., Gómez-Nicola, D., Domercq, M., Pérez-Samartín, A., Sánchez-Zafra, V., Paris, I., Valero, J., Savage, J.C., Hui, C.-W., Tremblay, M.-È., Deudero, J.J.P., Brewster, A.L., Anderson, A.E., Zaldumbide, L., Galbarriatu, L., Marinas, A., Vivanco, M. dM, Matute, C., Maletic-Savatic, M., Encinas, J.M., Sierra, A., 2016. Neuronal Hyperactivity Disturbs ATP Microgradients, Impairs Microglial Motility, and Reduces Phagocytic Receptor Expression Triggering Apoptosis/Microglial Phagocytosis Uncoupling. *PLoS Biol.* 14, e1002466. <https://doi.org/10.1371/journal.pbio.1002466>
- Abu-Rumeileh, S., Capellari, S., Parchi, P., 2018. Rapidly Progressive Alzheimer's Disease: Contributions to Clinical-Pathological Definition and Diagnosis. *J. Alzheimers Dis. JAD* 63, 887–897. <https://doi.org/10.3233/JAD-171181>
- Adle-Biassette, H., Verney, C., Peoc'h, K., Dauge, M.-C., Razavi, F., Choudat, L., Gressens, P., Budka, H., Henin, D., 2006. Immunohistochemical Expression of Prion Protein (PrPC) in the Human Forebrain During Development. *J. Neuropathol. Exp. Neurol.* 65, 698–706. <https://doi.org/10.1097/01.jnen.0000228137.10531.72>
- Agostinho, P., Pliássova, A., Oliveira, C.R., Cunha, R.A., 2015. Localization and Trafficking of Amyloid- $\beta$  Protein Precursor and Secretases: Impact on Alzheimer's Disease. *J. Alzheimers Dis.* 45, 329–347. <https://doi.org/10.3233/JAD-142730>
- Agrawal, N., Skelton, A.A., 2019. Structure and Function of Alzheimer's Amyloid  $\beta$  Proteins from Monomer to Fibrils: A Mini Review. *Protein J.* 38, 425–434. <https://doi.org/10.1007/s10930-019-09854-3>
- Aizenstein, H.J., Nebes, R.D., Saxton, J.A., Price, J.C., Mathis, C.A., Tsopelas, N.D., Ziolkowski, S.K., James, J.A., Snitz, B.E., Houck, P.R., Bi, W., Cohen, A.D., Lopresti, B.J., DeKosky, S.T., Halligan, E.M., Klunk, W.E., 2008. Frequent amyloid deposition without significant cognitive impairment among the elderly. *Arch. Neurol.* 65, 1509–1517. <https://doi.org/10.1001/archneur.65.11.1509>
- Allred, M.J., Duff, K.E., Ginsberg, S.D., 2012. Microarray analysis of CA1 pyramidal neurons in a mouse model of tauopathy reveals progressive synaptic dysfunction. *Neurobiol. Dis.* 45, 751–762. <https://doi.org/10.1016/j.nbd.2011.10.022>
- Alonso, A.C., Zaidi, T., Grundke-Iqbal, I., Iqbal, K., 1994. Role of abnormally phosphorylated tau in the breakdown of microtubules in Alzheimer disease. *Proc. Natl. Acad. Sci. U. S. A.* 91, 5562–5566.
- American Psychiatric Association, 2013. *Diagnostic and Statistical Manual of Mental Disorders, Fifth Edition.* ed. American Psychiatric Association. <https://doi.org/10.1176/appi.books.9780890425596>
- Anchisi, D., Borroni, B., Franceschi, M., Kerrouche, N., Kalbe, E., Beuthien-Beumann, B., Cappa, S., Lenz, O., Ludecke, S., Marcone, A., Mielke, R., Ortelli, P., Padovani, A., Pelati, O., Pupi, A., Scarpini, E., Weisenbach, S., Herholz, K., Salmon, E., Holthoff, V., Sorbi, S., Fazio, F., Perani, D., 2005. Heterogeneity of Brain Glucose Metabolism in Mild Cognitive Impairment and Clinical Progression to Alzheimer Disease. *Arch. Neurol.* 62, 1728. <https://doi.org/10.1001/archneur.62.11.1728>
- Andorfer, C., Acker, C.M., Kress, Y., Hof, P.R., Duff, K., Davies, P., 2005. Cell-cycle reentry and cell death in transgenic mice expressing nonmutant human tau isoforms. *J. Neurosci. Off. J. Soc. Neurosci.* 25, 5446–5454. <https://doi.org/10.1523/JNEUROSCI.4637-04.2005>
- Andorfer, C., Kress, Y., Espinoza, M., de Silva, R., Tucker, K.L., Barde, Y.-A., Duff, K., Davies, P., 2003. Hyperphosphorylation and aggregation of tau in mice expressing normal human tau isoforms. *J. Neurochem.* 86, 582–590. <https://doi.org/10.1046/j.1471-4159.2003.01879.x>

- Ardiles, Á.O., Tapia-Rojas, C.C., Mandal, M., Alexandre, F., Kirkwood, A., Inestrosa, N.C., Palacios, A.G., 2012. Postsynaptic dysfunction is associated with spatial and object recognition memory loss in a natural model of Alzheimer's disease. *Proc. Natl. Acad. Sci.* <https://doi.org/10.1073/pnas.1201209109>
- Armstrong, R.A., Nochlin, D., Bird, T.D., 2000. Neuropathological heterogeneity in Alzheimer's disease: a study of 80 cases using principal components analysis. *Neuropathol. Off. J. Jpn. Soc. Neuropathol.* 20, 31–37. <https://doi.org/10.1046/j.1440-1789.2000.00284.x>
- Arndt, J.W., Qian, F., Smith, B.A., Quan, C., Kilambi, K.P., Bush, M.W., Walz, T., Pepinsky, R.B., Bussi ere, T., Hamann, S., Cameron, T.O., Weinreb, P.H., 2018. Structural and kinetic basis for the selectivity of aducanumab for aggregated forms of amyloid- $\beta$ . *Sci. Rep.* 8, 6412. <https://doi.org/10.1038/s41598-018-24501-0>
- Arnsten, A.F.T., Datta, D., Tredici, K.D., Braak, H., 2021. Hypothesis: Tau pathology is an initiating factor in sporadic Alzheimer's disease. *Alzheimers Dement.* 17, 115–124. <https://doi.org/10.1002/alz.12192>
- Arranz, A.M., De Strooper, B., 2019. The role of astroglia in Alzheimer's disease: pathophysiology and clinical implications. *Lancet Neurol.* 18, 406–414. [https://doi.org/10.1016/S1474-4422\(18\)30490-3](https://doi.org/10.1016/S1474-4422(18)30490-3)
- Asai, H., Ikezu, S., Tsunoda, S., Medalla, M., Luebke, J., Haydar, T., Wolozin, B., Butovsky, O., K ugler, S., Ikezu, T., 2015. Depletion of microglia and inhibition of exosome synthesis halt tau propagation. *Nat. Neurosci.* 18, 1584–1593. <https://doi.org/10.1038/nn.4132>
- Ba, M., Li, X., Ng, K.P., Pascoal, T.A., Mathotaarachchi, S., Rosa-Neto, P., Gauthier, S., Alzheimer's Disease Neuroimaging Initiative, 2017. The prevalence and biomarkers' characteristic of rapidly progressive Alzheimer's disease from the Alzheimer's Disease Neuroimaging Initiative database. *Alzheimers Dement. N. Y. N* 3, 107–113. <https://doi.org/10.1016/j.trci.2016.12.005>
- Baker, H.F., Ridley, R.M., Duchen, L.W., Crow, T.J., Bruton, C.J., 1994. Induction of beta (A4)-amyloid in primates by injection of Alzheimer's disease brain homogenate. Comparison with transmission of spongiform encephalopathy. *Mol. Neurobiol.* 8, 25–39. <https://doi.org/10.1007/BF02778005>
- Baker, H.F., Ridley, R.M., Duchen, L.W., Crow, T.J., Bruton, C.J., 1993a. Evidence for the experimental transmission of cerebral beta-amyloidosis to primates. *Int. J. Exp. Pathol.* 74, 441–454.
- Baker, H.F., Ridley, R.M., Duchen, L.W., Crow, T.J., Bruton, C.J., 1993b. Experimental induction of beta-amyloid plaques and cerebral angiopathy in primates. *Ann. N. Y. Acad. Sci.* 695, 228–231. <https://doi.org/10.1111/j.1749-6632.1993.tb23057.x>
- Banerjee, G., Adams, M.E., Jaunmuktane, Z., Alistair Lammie, G., Turner, B., Wani, M., Sawhney, I.M.S., Houlden, H., Mead, S., Brandner, S., Werring, D.J., 2019. Early onset cerebral amyloid angiopathy following childhood exposure to cadaveric dura. *Ann. Neurol.* 85, 284–290. <https://doi.org/10.1002/ana.25407>
- Barth elemy, N.R., Bateman, R.J., Hirtz, C., Marin, P., Becher, F., Sato, C., Gabelle, A., Lehmann, S., 2020. Cerebrospinal fluid phospho-tau T217 outperforms T181 as a biomarker for the differential diagnosis of Alzheimer's disease and PET amyloid-positive patient identification. *Alzheimers Res. Ther.* 12, 26. <https://doi.org/10.1186/s13195-020-00596-4>
- Bekiari, C., Grivas, I., Giannakopoulou, A., Michaloudi-Pavlou, H., Kostopoulos, G., Papadopoulos, G., 2015. Dentate Gyrus Variation along Its Septo-Temporal Axis: Structure and Function in Health and Disease. pp. 137–198. <https://doi.org/10.13140/2.1.1628.3205>
- Bemiller, S.M., McCray, T.J., Allan, K., Formica, S.V., Xu, G., Wilson, G., Kokiko-Cochran, O.N., Crish, S.D., Lasagna-Reeves, C.A., Ransohoff, R.M., Landreth, G.E., Lamb, B.T., 2017. TREM2 deficiency exacerbates tau pathology through dysregulated kinase signaling in a mouse model of tauopathy. *Mol. Neurodegener.* 12, 74. <https://doi.org/10.1186/s13024-017-0216-6>
- Bennett, R.E., DeVos, S.L., Dujardin, S., Corjuc, B., Gor, R., Gonzalez, J., Roe, A.D., Frosch, M.P., Pitstick, R., Carlson, G.A., Hyman, B.T., 2017. Enhanced Tau Aggregation in the Presence of Amyloid  $\beta$ . *Am. J. Pathol.* 187, 1601–1612. <https://doi.org/10.1016/j.ajpath.2017.03.011>

- Benzinger, T.L., Gregory, D.M., Burkoth, T.S., Miller-Auer, H., Lynn, D.G., Botto, R.E., Meredith, S.C., 1998. Propagating structure of Alzheimer's beta-amyloid(10-35) is parallel beta-sheet with residues in exact register. *Proc. Natl. Acad. Sci. U. S. A.* 95, 13407–13412. <https://doi.org/10.1073/pnas.95.23.13407>
- Berger, Z., Roder, H., Hanna, A., Carlson, A., Rangachari, V., Yue, M., Wszolek, Z., Ashe, K., Knight, J., Dickson, D., Andorfer, C., Rosenberry, T.L., Lewis, J., Hutton, M., Janus, C., 2007. Accumulation of pathological tau species and memory loss in a conditional model of tauopathy. *J. Neurosci. Off. J. Soc. Neurosci.* 27, 3650–3662. <https://doi.org/10.1523/JNEUROSCI.0587-07.2007>
- Bernales, S., Soto, M.M., McCullagh, E., 2012. Unfolded protein stress in the endoplasmic reticulum and mitochondria: a role in neurodegeneration. *Front. Aging Neurosci.* 4. <https://doi.org/10.3389/fnagi.2012.00005>
- Bero, A.W., Bauer, A.Q., Stewart, F.R., White, B.R., Cirrito, J.R., Raichle, M.E., Culver, J.P., Holtzman, D.M., 2012. Bidirectional relationship between functional connectivity and amyloid- $\beta$  deposition in mouse brain. *J. Neurosci. Off. J. Soc. Neurosci.* 32, 4334–4340. <https://doi.org/10.1523/JNEUROSCI.5845-11.2012>
- Besser, L.M., Mock, C., Teylan, M.A., Hassenstab, J., Kukull, W.A., Cray, J.F., 2019. Differences in Cognitive Impairment in Primary Age-Related Tauopathy Versus Alzheimer Disease. *J. Neuropathol. Exp. Neurol.* 78, 219–228. <https://doi.org/10.1093/jnen/nly132>
- Betthausen, T.J., Cody, K.A., Zammit, M.D., Murali, D., Converse, A.K., Barnhart, T.E., Stone, C.K., Rowley, H.A., Johnson, S.C., Christian, B.T., 2019. In Vivo Characterization and Quantification of Neurofibrillary Tau PET Radioligand 18F-MK-6240 in Humans from Alzheimer Disease Dementia to Young Controls. *J. Nucl. Med.* 60, 93–99. <https://doi.org/10.2967/jnumed.118.209650>
- Billings, L.M., Oddo, S., Green, K.N., McGaugh, J.L., LaFerla, F.M., 2005. Intraneuronal A $\beta$  causes the onset of early Alzheimer's disease-related cognitive deficits in transgenic mice. *Neuron* 45, 675–688. <https://doi.org/10.1016/j.neuron.2005.01.040>
- Bilousova, T., Miller, C.A., Poon, W.W., Vinters, H.V., Corrada, M., Kawas, C., Hayden, E.Y., Teplow, D.B., Glabe, C., Albay, R., Cole, G.M., Teng, E., Gylys, K.H., 2016. Synaptic Amyloid- $\beta$  Oligomers Precede p-Tau and Differentiate High Pathology Control Cases. *Am. J. Pathol.* 186, 185–198. <https://doi.org/10.1016/j.ajpath.2015.09.018>
- Bird, C.M., Burgess, N., 2008. The hippocampus and memory: insights from spatial processing. *Nat. Rev. Neurosci.* 9, 182–194. <https://doi.org/10.1038/nrn2335>
- Biscetti, L., Salvadori, N., Farotti, L., Cataldi, S., Eusebi, P., Paciotti, S., Parnetti, L., 2019. The added value of A $\beta$ 42/A $\beta$ 40 in the CSF signature for routine diagnostics of Alzheimer's disease. *Clin. Chim. Acta* 494, 71–73. <https://doi.org/10.1016/j.cca.2019.03.001>
- Bitan, G., Kirkitadze, M.D., Lomakin, A., Vollers, S.S., Benedek, G.B., Teplow, D.B., 2003. Amyloid beta-protein (A $\beta$ ) assembly: A $\beta$ 40 and A $\beta$ 42 oligomerize through distinct pathways. *Proc. Natl. Acad. Sci. U. S. A.* 100, 330–335. <https://doi.org/10.1073/pnas.222681699>
- Blennow, K., de Leon, M.J., Zetterberg, H., 2006. Alzheimer's disease. *Lancet Lond. Engl.* 368, 387–403. [https://doi.org/10.1016/S0140-6736\(06\)69113-7](https://doi.org/10.1016/S0140-6736(06)69113-7)
- Blennow, K., Zetterberg, H., 2018. Biomarkers for Alzheimer's disease: current status and prospects for the future. *J. Intern. Med.* 284, 643–663. <https://doi.org/10.1111/joim.12816>
- Bloom, G.S., 2014. Amyloid- $\beta$  and Tau: The Trigger and Bullet in Alzheimer Disease Pathogenesis. *JAMA Neurol.* 71, 505. <https://doi.org/10.1001/jamaneurol.2013.5847>
- Bloudek, L.M., Spackman, D.E., Blankenburg, M., Sullivan, S.D., 2011. Review and Meta-Analysis of Biomarkers and Diagnostic Imaging in Alzheimer's Disease. *J. Alzheimers Dis.* 26, 627–645. <https://doi.org/10.3233/JAD-2011-110458>
- Bobba, A., Amadoro, G., Valenti, D., Corsetti, V., Lassandro, R., Atlante, A., 2013. Mitochondrial respiratory chain Complexes I and IV are impaired by  $\beta$ -amyloid via direct interaction and through Complex I-dependent ROS production, respectively. *Mitochondrion* 13, 298–311. <https://doi.org/10.1016/j.mito.2013.03.008>

- Bolmont, T., Clavaguera, F., Meyer-Luehmann, M., Herzig, M.C., Radde, R., Staufenbiel, M., Lewis, J., Hutton, M., Tolnay, M., Jucker, M., 2007. Induction of tau pathology by intracerebral infusion of amyloid-beta -containing brain extract and by amyloid-beta deposition in APP x Tau transgenic mice. *Am. J. Pathol.* 171, 2012–2020. <https://doi.org/10.2353/ajpath.2007.070403>
- Boluda, S., Iba, M., Zhang, B., Raible, K.M., Lee, V.M.-Y., Trojanowski, J.Q., 2015. Differential induction and spread of tau pathology in young PS19 tau transgenic mice following intracerebral injections of pathological tau from Alzheimer’s disease or corticobasal degeneration brains. *Acta Neuropathol. (Berl.)* 129, 221–237. <https://doi.org/10.1007/s00401-014-1373-0>
- Bons, N., Jallageas, V., Silhol, S., Mestre-Frances, N., Petter, A., Delacourte, A., 1995. Immunocytochemical characterization of Tau proteins during cerebral aging of the lemurian primate *Microcebus murinus*. *C. R. Acad. Sci. III* 318, 77–83.
- Bons, N., Mestre, N., Petter, A., 1992. Senile plaques and neurofibrillary changes in the brain of an aged lemurian primate, *Microcebus murinus*. *Neurobiol. Aging* 13, 99–105.
- Bons, N., Rieger, F., Prudhomme, D., Fisher, A., Krause, K.-H., 2006. *Microcebus murinus*: a useful primate model for human cerebral aging and Alzheimer’s disease? *Genes Brain Behav.* 5, 120–130. <https://doi.org/10.1111/j.1601-183X.2005.00149.x>
- Bons, N., Silhol, S., Barbié, V., Mestre-Francis, N., Albe-Fessard, D., 1998. A stereotaxic atlas of the grey lesser mouse lemur brain (*Microcebus murinus*). *Brain Res. Bull.* 46, 1–173. [https://doi.org/10.1016/s0361-9230\(97\)00458-9](https://doi.org/10.1016/s0361-9230(97)00458-9)
- Bowler, J.V., Munoz, D.G., Merskey, H., Hachinski, V., 1998. Factors affecting the age of onset and rate of progression of Alzheimer’s disease. *J. Neurol. Neurosurg. Psychiatry* 65, 184–190. <https://doi.org/10.1136/jnnp.65.2.184>
- Braak, H., Alafuzoff, I., Arzberger, T., Kretschmar, H., Del Tredici, K., 2006. Staging of Alzheimer disease-associated neurofibrillary pathology using paraffin sections and immunocytochemistry. *Acta Neuropathol. (Berl.)* 112, 389–404. <https://doi.org/10.1007/s00401-006-0127-z>
- Braak, H., Braak, E., 1991. Neuropathological stageing of Alzheimer-related changes. *Acta Neuropathol. (Berl.)* 82, 239–259. <https://doi.org/10.1007/BF00308809>
- Braak, H., Braak, E., Grundke-Iqbal, I., Iqbal, K., 1986. Occurrence of neuropil threads in the senile human brain and in Alzheimer’s disease: a third location of paired helical filaments outside of neurofibrillary tangles and neuritic plaques. *Neurosci. Lett.* 65, 351–355.
- Braak, H., Del Tredici, K., 2015. Neuroanatomy and pathology of sporadic Alzheimer’s disease. *Adv. Anat. Embryol. Cell Biol.* 215, 1–162.
- Braak, H., Del Tredici, K., 2015. The preclinical phase of the pathological process underlying sporadic Alzheimer’s disease. *Brain J. Neurol.* 138, 2814–2833. <https://doi.org/10.1093/brain/awv236>
- Braak, H., Del Tredici, K., 2011. Alzheimer’s pathogenesis: is there neuron-to-neuron propagation? *Acta Neuropathol. (Berl.)* 121, 589–595. <https://doi.org/10.1007/s00401-011-0825-z>
- Braak, H., Zetterberg, H., Del Tredici, K., Blennow, K., 2013. Intraneuronal tau aggregation precedes diffuse plaque deposition, but amyloid- $\beta$  changes occur before increases of tau in cerebrospinal fluid. *Acta Neuropathol. (Berl.)* 126, 631–641. <https://doi.org/10.1007/s00401-013-1139-0>
- Braidy, N., Poljak, A., Jayasena, T., Mansour, H., Inestrosa, N.C., Sachdev, P.S., 2015. Accelerating Alzheimer’s research through “natural” animal models. *Curr. Opin. Psychiatry* 28, 155–164. <https://doi.org/10.1097/YCO.0000000000000137>
- Breijyeh, Z., Karaman, R., 2020. Comprehensive Review on Alzheimer’s Disease: Causes and Treatment. *Molecules* 25. <https://doi.org/10.3390/molecules25245789>
- Brelstaff, J., Tolkovsky, A.M., Ghetti, B., Goedert, M., Spillantini, M.G., 2018. Living Neurons with Tau Filaments Aberrantly Expose Phosphatidylserine and Are Phagocytosed by Microglia. *Cell Rep.* 24, 1939–1948.e4. <https://doi.org/10.1016/j.celrep.2018.07.072>
- Bribián, A., Fontana, X., Llorens, F., Gavín, R., Reina, M., García-Verdugo, J.M., Torres, J.M., Castro, F. de, Río, J.A. del, 2012. Role of the Cellular Prion Protein in Oligodendrocyte Precursor Cell

- Proliferation and Differentiation in the Developing and Adult Mouse CNS. *PLOS ONE* 7, e33872. <https://doi.org/10.1371/journal.pone.0033872>
- Briggs, R., Kennelly, S.P., O'Neill, D., 2016. Drug treatments in Alzheimer's disease. *Clin. Med.* 16, 247–253. <https://doi.org/10.7861/clinmedicine.16-3-247>
- Brown, G.C., Neher, J.J., 2014. Microglial phagocytosis of live neurons. *Nat. Rev. Neurosci.* 15, 209–216. <https://doi.org/10.1038/nrn3710>
- Brown, P., Brandel, J.-P., Sato, T., Nakamura, Y., MacKenzie, J., Will, R.G., Ladogana, A., Pocchiari, M., Leschek, E.W., Schonberger, L.B., 2012. Iatrogenic Creutzfeldt-Jakob Disease, Final Assessment. *Emerg. Infect. Dis.* 18, 901–907. <https://doi.org/10.3201/eid1806.120116>
- Brun, A., Englund, E., 1981. Regional pattern of degeneration in Alzheimer's disease: neuronal loss and histopathological grading. *Histopathology* 5, 549–564.
- Buccione, I., Perri, R., Carlesimo, G.A., Fadda, L., Serra, L., Scalmana, S., Caltagirone, C., 2007. Cognitive and behavioural predictors of progression rates in Alzheimer's disease. *Eur. J. Neurol.* 14, 440–446. <https://doi.org/10.1111/j.1468-1331.2007.01693.x>
- Buckner, R.L., Andrews-Hanna, J.R., Schacter, D.L., 2008. The brain's default network: anatomy, function, and relevance to disease. *Ann. N. Y. Acad. Sci.* 1124, 1–38. <https://doi.org/10.1196/annals.1440.011>
- Buckner, R.L., Sepulcre, J., Talukdar, T., Krienen, F.M., Liu, H., Hedden, T., Andrews-Hanna, J.R., Sperling, R.A., Johnson, K.A., 2009. Cortical Hubs Revealed by Intrinsic Functional Connectivity: Mapping, Assessment of Stability, and Relation to Alzheimer's Disease. *J. Neurosci.* 29, 1860–1873. <https://doi.org/10.1523/JNEUROSCI.5062-08.2009>
- Buée, L., Bussi re, T., Bu e-Scherrer, V., Delacourte, A., Hof, P.R., 2000. Tau protein isoforms, phosphorylation and role in neurodegenerative disorders. *Brain Res. Brain Res. Rev.* 33, 95–130. [https://doi.org/10.1016/s0165-0173\(00\)00019-9](https://doi.org/10.1016/s0165-0173(00)00019-9)
- Burwinkel, M., Lutzenberger, M., Heppner, F.L., Schulz-Schaeffer, W., Baier, M., 2018. Intravenous injection of beta-amyloid seeds promotes cerebral amyloid angiopathy (CAA). *Acta Neuropathol. Commun.* 6, 23. <https://doi.org/10.1186/s40478-018-0511-7>
- Busche, M.A., Hyman, B.T., 2020. Synergy between amyloid- $\beta$  and tau in Alzheimer's disease. *Nat. Neurosci.* 23, 1183–1193. <https://doi.org/10.1038/s41593-020-0687-6>
- Bussian, T.J., Aziz, A., Meyer, C.F., Swenson, B.L., van Deursen, J.M., Baker, D.J., 2018. Clearance of senescent glial cells prevents tau-dependent pathology and cognitive decline. *Nature* 562, 578–582. <https://doi.org/10.1038/s41586-018-0543-y>
- Butters, M.A., Lopez, O.L., Becker, J.T., 1996. Focal temporal lobe dysfunction in probable Alzheimer's disease predicts a slow rate of cognitive decline. *Neurology* 46, 687–692. <https://doi.org/10.1212/wnl.46.3.687>
- Calenda, A., Jallageas, V., Silhol, S., Bellis, M., Bons, N., 1995. Identification of a unique apolipoprotein E allele in *Microcebus murinus*; ApoE brain distribution and co-localization with beta-amyloid and tau proteins. *Neurobiol. Dis.* 2, 169–176. <https://doi.org/10.1006/nbdi.1995.0018>
- Calenda, A., Mestre-Franc s, N., Czech, C., Pradier, L., Petter, A., Bons, N., Bellis, M., 1996. Molecular cloning, sequencing, and brain expression of the presenilin 1 gene in *Microcebus murinus*. *Biochem. Biophys. Res. Commun.* 228, 430–439. <https://doi.org/10.1006/bbrc.1996.1678>
- Calenda, A., Mestre-Franc s, N., Czech, C., Pradier, L., Petter, A., Perret, M., Bons, N., Bellis, M., 1998. Cloning of the Presenilin 2 cDNA and Its Distribution in Brain of the Primate, *Microcebus murinus*: Coexpression with  $\beta$ APP and Tau Proteins. *Neurobiol. Dis.* 5, 323–333. <https://doi.org/10.1006/nbdi.1998.0205>
- Cali, I., Cohen, M.L., Haik, S., Parchi, P., Giaccone, G., Collins, S.J., Kofskey, D., Wang, H., McLean, C.A., Brandel, J.-P., Privat, N., Sazdovitch, V., Duyckaerts, C., Kitamoto, T., Belay, E.D., Maddox, R.A., Tagliavini, F., Pocchiari, M., Leschek, E., Appleby, B.S., Safar, J.G., Schonberger, L.B., Gambetti, P., 2018. Iatrogenic Creutzfeldt-Jakob disease with Amyloid- $\beta$  pathology: an international study. *Acta Neuropathol. Commun.* 6. <https://doi.org/10.1186/s40478-017-0503-z>
- Califf, R.M., 2018. Biomarker definitions and their applications. *Exp. Biol. Med.* 243, 213–221. <https://doi.org/10.1177/1535370217750088>



- Canevari, L., Abramov, A.Y., Duchon, M.R., 2004. Toxicity of amyloid beta peptide: tales of calcium, mitochondria, and oxidative stress. *Neurochem. Res.* 29, 637–650. <https://doi.org/10.1023/b:nere.0000014834.06405.af>
- Cappa, A., Calcagni, M.L., Villa, G., Giordano, A., Marra, C., De Rossi, G., Puopolo, M., Gainotti, G., 2001. Brain perfusion abnormalities in Alzheimer's disease: comparison between patients with focal temporal lobe dysfunction and patients with diffuse cognitive impairment. *J. Neurol. Neurosurg. Psychiatry* 70, 22–27. <https://doi.org/10.1136/jnnp.70.1.22>
- Caruso, D., Barron, A.M., Brown, M.A., Abbiati, F., Carrero, P., Pike, C.J., Garcia-Segura, L.M., Melcangi, R.C., 2013. Age-related changes in neuroactive steroid levels in 3xTg-AD mice. *Neurobiol. Aging* 34, 1080–1089. <https://doi.org/10.1016/j.neurobiolaging.2012.10.007>
- Castle, A.R., Gill, A.C., 2017. Physiological Functions of the Cellular Prion Protein. *Front. Mol. Biosci.* 4. <https://doi.org/10.3389/fmolb.2017.00019>
- Cavazzoni, P., 2021. FDA's Decision to Approve New Treatment for Alzheimer's Disease. FDA.
- Centonze, D., Muzio, L., Rossi, S., Cavanini, F., De Chiara, V., Bergami, A., Musella, A., D'Amelio, M., Cavallucci, V., Martorana, A., Bergamaschi, A., Cencioni, M.T., Diamantini, A., Butti, E., Comi, G., Bernardi, G., Cecconi, F., Battistini, L., Furlan, R., Martino, G., 2009. Inflammation triggers synaptic alteration and degeneration in experimental autoimmune encephalomyelitis. *J. Neurosci. Off. J. Soc. Neurosci.* 29, 3442–3452. <https://doi.org/10.1523/JNEUROSCI.5804-08.2009>
- Chandra, A., Dervenoulas, G., Politis, M., for the Alzheimer's Disease Neuroimaging Initiative, 2019. Magnetic resonance imaging in Alzheimer's disease and mild cognitive impairment. *J. Neurol.* 266, 1293–1302. <https://doi.org/10.1007/s00415-018-9016-3>
- Charidimou, A., Gang, Q., Werring, D.J., 2012. Sporadic cerebral amyloid angiopathy revisited: recent insights into pathophysiology and clinical spectrum. *J. Neurol. Neurosurg. Psychiatry* 83, 124–137. <https://doi.org/10.1136/jnnp-2011-301308>
- Chávez-Gutiérrez, L., Bammens, L., Benilova, I., Vandersteen, A., Benurwar, M., Borgers, M., Lismont, S., Zhou, L., Van Cleynenbreugel, S., Esselmann, H., Wiltfang, J., Serneels, L., Karran, E., Gijzen, H., Schymkowitz, J., Rousseau, F., Broersen, K., De Strooper, B., 2012. The mechanism of  $\gamma$ -Secretase dysfunction in familial Alzheimer disease. *EMBO J.* 31, 2261–2274. <https://doi.org/10.1038/emboj.2012.79>
- Chen, G., Xu, T., Yan, Y., Zhou, Y., Jiang, Y., Melcher, K., Xu, H.E., 2017. Amyloid beta: structure, biology and structure-based therapeutic development. *Acta Pharmacol. Sin.* 38, 1205–1235. <https://doi.org/10.1038/aps.2017.28>
- Chen, Q., Zhou, Z., Zhang, L., Wang, Y., Zhang, Y., Zhong, M., Xu, S., Chen, C., Li, L., Yu, Z., 2012. Tau protein is involved in morphological plasticity in hippocampal neurons in response to BDNF. *Neurochem. Int.* 60, 233–242. <https://doi.org/10.1016/j.neuint.2011.12.013>
- Chen, Y., Fu, A.K.Y., Ip, N.Y., 2019. Synaptic dysfunction in Alzheimer's disease: Mechanisms and therapeutic strategies. *Pharmacol. Ther.* 195, 186–198. <https://doi.org/10.1016/j.pharmthera.2018.11.006>
- Chételat, G., Ossenkoppele, R., Villemagne, V.L., Perrotin, A., Landeau, B., Mézenge, F., Jagust, W.J., Dore, V., Miller, B.L., Egret, S., Seeley, W.W., van der Flier, W.M., La Joie, R., Ames, D., van Berckel, B.N.M., Scheltens, P., Barkhof, F., Rowe, C.C., Masters, C.L., de La Sayette, V., Bouwman, F., Rabinovici, G.D., 2016. Atrophy, hypometabolism and clinical trajectories in patients with amyloid-negative Alzheimer's disease. *Brain J. Neurol.* 139, 2528–2539. <https://doi.org/10.1093/brain/aww159>
- Chitravas, N., Jung, R.S., Kofskey, D.M., Blevins, J.E., Gambetti, P., Leigh, R.J., Cohen, M.L., 2011. Treatable neurological disorders misdiagnosed as Creutzfeldt-Jakob disease. *Ann. Neurol.* 70, 437–444. <https://doi.org/10.1002/ana.22454>
- Cho, D.-H., Nakamura, T., Fang, J., Cieplak, P., Godzik, A., Gu, Z., Lipton, S.A., 2009. S-nitrosylation of Drp1 mediates beta-amyloid-related mitochondrial fission and neuronal injury. *Science* 324, 102–105. <https://doi.org/10.1126/science.1171091>

- Chong, F.P., Ng, K.Y., Koh, R.Y., Chye, S.M., 2018. Tau Proteins and Tauopathies in Alzheimer's Disease. *Cell. Mol. Neurobiol.* 38, 965–980. <https://doi.org/10.1007/s10571-017-0574-1>
- Chun, H., Im, H., Kang, Y.J., Kim, Y., Shin, J.H., Won, W., Lim, J., Ju, Y., Park, Y.M., Kim, S., Lee, S.E., Lee, J., Woo, J., Hwang, Y., Cho, Hyesun, Jo, S., Park, J.-H., Kim, D., Kim, D.Y., Seo, J.-S., Gwag, B.J., Kim, Y.S., Park, K.D., Kaang, B.-K., Cho, Hansang, Ryu, H., Lee, C.J., 2020. Severe reactive astrocytes precipitate pathological hallmarks of Alzheimer's disease via H<sub>2</sub>O<sub>2</sub> – production. *Nat. Neurosci.* 23, 1555–1566. <https://doi.org/10.1038/s41593-020-00735-y>
- Chung, W.-S., Verghese, P.B., Chakraborty, C., Joung, J., Hyman, B.T., Ulrich, J.D., Holtzman, D.M., Barres, B.A., 2016. Novel allele-dependent role for APOE in controlling the rate of synapse pruning by astrocytes. *Proc. Natl. Acad. Sci.* 113, 10186–10191. <https://doi.org/10.1073/pnas.1609896113>
- Cintron, A.F., Dalal, N.V., Dooyema, J., Betarbet, R., Walker, L.C., 2015. Transport of cargo from periphery to brain by circulating monocytes. *Brain Res.* 1622, 328–338. <https://doi.org/10.1016/j.brainres.2015.06.047>
- Cirrito, J.R., Yamada, K.A., Finn, M.B., Sloviter, R.S., Bales, K.R., May, P.C., Schoepp, D.D., Paul, S.M., Mennerick, S., Holtzman, D.M., 2005. Synaptic activity regulates interstitial fluid amyloid-beta levels in vivo. *Neuron* 48, 913–922. <https://doi.org/10.1016/j.neuron.2005.10.028>
- Clavaguera, F., Akatsu, H., Fraser, G., Crowther, R.A., Frank, S., Hench, J., Probst, A., Winkler, D.T., Reichwald, J., Staufenbiel, M., Ghetti, B., Goedert, M., Tolnay, M., 2013. Brain homogenates from human tauopathies induce tau inclusions in mouse brain. *Proc. Natl. Acad. Sci. U. S. A.* 110, 9535–9540. <https://doi.org/10.1073/pnas.1301175110>
- Clavaguera, F., Bolmont, T., Crowther, R.A., Abramowski, D., Frank, S., Probst, A., Fraser, G., Stalder, A.K., Beibel, M., Staufenbiel, M., Jucker, M., Goedert, M., Tolnay, M., 2009. Transmission and spreading of tauopathy in transgenic mouse brain. *Nat. Cell Biol.* 11, 909–913. <https://doi.org/10.1038/ncb1901>
- Clavaguera, F., Hench, J., Lavenir, I., Schweighauser, G., Frank, S., Goedert, M., Tolnay, M., 2014. Peripheral administration of tau aggregates triggers intracerebral tauopathy in transgenic mice. *Acta Neuropathol. (Berl.)* 127, 299–301. <https://doi.org/10.1007/s00401-013-1231-5>
- Clayton, K., Delpech, J.C., Herron, S., Iwahara, N., Ericsson, M., Saito, T., Saido, T.C., Ikezu, S., Ikezu, T., 2021. Plaque associated microglia hyper-secrete extracellular vesicles and accelerate tau propagation in a humanized APP mouse model. *Mol. Neurodegener.* 16, 18. <https://doi.org/10.1186/s13024-021-00440-9>
- Cohen, M., Appleby, B., Safar, J.G., 2016. Distinct prion-like strains of amyloid beta implicated in phenotypic diversity of Alzheimer's disease. *Prion* 10, 9–17. <https://doi.org/10.1080/19336896.2015.1123371>
- Cohen, M.L., Kim, C., Haldiman, T., ElHag, M., Mehndiratta, P., Pichet, T., Lissemore, F., Shea, M., Cohen, Y., Chen, W., Blevins, J., Appleby, B.S., Surewicz, K., Surewicz, W.K., Sajatovic, M., Tatsuoka, C., Zhang, S., Mayo, P., Butkiewicz, M., Haines, J.L., Lerner, A.J., Safar, J.G., 2015. Rapidly progressive Alzheimer's disease features distinct structures of amyloid-β. *Brain J. Neurol.* 138, 1009–1022. <https://doi.org/10.1093/brain/awv006>
- Cohen, R.M., Rezai-Zadeh, K., Weitz, T.M., Rentsendorj, A., Gate, D., Spivak, I., Bholat, Y., Vasilevko, V., Glabe, C.G., Breunig, J.J., Rakic, P., Davtayan, H., Agadjanyan, M.G., Kepe, V., Barrio, J.R., Bannykh, S., Szekely, C.A., Pechnick, R.N., Town, T., 2013. A transgenic Alzheimer rat with plaques, tau pathology, behavioral impairment, oligomeric aβ, and frank neuronal loss. *J. Neurosci. Off. J. Soc. Neurosci.* 33, 6245–6256. <https://doi.org/10.1523/JNEUROSCI.3672-12.2013>
- Collinge, J., 2005. Molecular neurology of prion disease. *J. Neurol. Neurosurg. Psychiatry* 76, 906–919. <https://doi.org/10.1136/jnnp.2004.048660>
- Collinge, J., Palmer, M.S., Dryden, A.J., 1991. Genetic predisposition to iatrogenic Creutzfeldt-Jakob disease. *Lancet Lond. Engl.* 337, 1441–1442. [https://doi.org/10.1016/0140-6736\(91\)93128-v](https://doi.org/10.1016/0140-6736(91)93128-v)

- Collinge, J., Sidle, K.C., Meads, J., Ironside, J., Hill, A.F., 1996. Molecular analysis of prion strain variation and the aetiology of “new variant” CJD. *Nature* 383, 685–690. <https://doi.org/10.1038/383685a0>
- Collinge, J., Whitfield, J., McKintosh, E., Beck, J., Mead, S., Thomas, D.J., Alpers, M.P., 2006. Kuru in the 21st century—an acquired human prion disease with very long incubation periods. *The Lancet* 367, 2068–2074. [https://doi.org/10.1016/S0140-6736\(06\)68930-7](https://doi.org/10.1016/S0140-6736(06)68930-7)
- Collingridge, G.L., Peineau, S., Howland, J.G., Wang, Y.T., 2010. Long-term depression in the CNS. *Nat. Rev. Neurosci.* 11, 459–473. <https://doi.org/10.1038/nrn2867>
- Colonna, M., Butovsky, O., 2017. Microglia Function in the Central Nervous System During Health and Neurodegeneration. *Annu. Rev. Immunol.* 35, 441–468. <https://doi.org/10.1146/annurev-immunol-051116-052358>
- Condello, C., Lemmin, T., Stöhr, J., Nick, M., Wu, Y., Maxwell, A.M., Watts, J.C., Caro, C.D., Oehler, A., Keene, C.D., Bird, T.D., van Duinen, S.G., Lannfelt, L., Ingelsson, M., Graff, C., Giles, K., DeGrado, W.F., Prusiner, S.B., 2018. Structural heterogeneity and intersubject variability of A $\beta$  in familial and sporadic Alzheimer’s disease. *Proc. Natl. Acad. Sci. U. S. A.* 115, E782–E791. <https://doi.org/10.1073/pnas.1714966115>
- Condello, C., Yuan, P., Schain, A., Grutzendler, J., 2015. Microglia constitute a barrier that prevents neurotoxic protofibrillar A $\beta$ 42 hotspots around plaques. *Nat. Commun.* 6, 6176. <https://doi.org/10.1038/ncomms7176>
- Corder, E.H., Saunders, A.M., Strittmatter, W.J., Schmechel, D.E., Gaskell, P.C., Small, G.W., Roses, A.D., Haines, J.L., Pericak-Vance, M.A., 1993. Gene dose of apolipoprotein E type 4 allele and the risk of Alzheimer’s disease in late onset families. *Science* 261, 921–923. <https://doi.org/10.1126/science.8346443>
- Crary, J.F., Trojanowski, J.Q., Schneider, J.A., Abisambra, J.F., Abner, E.L., Alafuzoff, I., Arnold, S.E., Attems, J., Beach, T.G., Bigio, E.H., Cairns, N.J., Dickson, D.W., Gearing, M., Grinberg, L.T., Hof, P.R., Hyman, B.T., Jellinger, K., Jicha, G.A., Kovacs, G.G., Knopman, D.S., Kofler, J., Kukull, W.A., Mackenzie, I.R., Masliah, E., McKee, A., Montine, T.J., Murray, M.E., Neltner, J.H., Santa-Maria, I., Seeley, W.W., Serrano-Pozo, A., Shelanski, M.L., Stein, T., Takao, M., Thal, D.R., Toledo, J.B., Troncoso, J.C., Vonsattel, J.P., White, C.L., Wisniewski, T., Woltjer, R.L., Yamada, M., Nelson, P.T., 2014. Primary age-related tauopathy (PART): a common pathology associated with human aging. *Acta Neuropathol. (Berl.)* 128, 755–766. <https://doi.org/10.1007/s00401-014-1349-0>
- Crowther, R.A., 1991. Straight and paired helical filaments in Alzheimer disease have a common structural unit. *Proc. Natl. Acad. Sci. U. S. A.* 88, 2288–2292. <https://doi.org/10.1073/pnas.88.6.2288>
- Cruz Hernández, J.C., Bracko, O., Kersbergen, C.J., Muse, V., Haft-Javaherian, M., Berg, M., Park, L., Vinarscik, L.K., Ivasyk, I., Rivera, D.A., Kang, Y., Cortes-Canteli, M., Peyrounette, M., Doyeux, V., Smith, A., Zhou, J., Otte, G., Beverly, J.D., Davenport, E., Davit, Y., Lin, C.P., Strickland, S., Iadecola, C., Lorthois, S., Nishimura, N., Schaffer, C.B., 2019. Neutrophil adhesion in brain capillaries reduces cortical blood flow and impairs memory function in Alzheimer’s disease mouse models. *Nat. Neurosci.* 22, 413–420. <https://doi.org/10.1038/s41593-018-0329-4>
- Cummings, J., 2018. Lessons Learned from Alzheimer Disease: Clinical Trials with Negative Outcomes. *Clin. Transl. Sci.* 11, 147–152. <https://doi.org/10.1111/cts.12491>
- Cummings, J., Aisen, P., Lemere, C., Atri, A., Sabbagh, M., Salloway, S., 2021. Aducanumab produced a clinically meaningful benefit in association with amyloid lowering. *Alzheimers Res. Ther.* 13, 98. <https://doi.org/10.1186/s13195-021-00838-z>
- Cummings, J.L., Morstorf, T., Zhong, K., 2014. Alzheimer’s disease drug-development pipeline: few candidates, frequent failures. *Alzheimers Res. Ther.* 6, 37. <https://doi.org/10.1186/alzrt269>
- Cummings, J.L., Tong, G., Ballard, C., 2019. Treatment Combinations for Alzheimer’s Disease: Current and Future Pharmacotherapy Options. *J. Alzheimers Dis. JAD* 67, 779–794. <https://doi.org/10.3233/JAD-180766>

- Dai, C.-L., Tung, Y.C., Liu, F., Gong, C.-X., Iqbal, K., 2017. Tau passive immunization inhibits not only tau but also A $\beta$  pathology. *Alzheimers Res. Ther.* 9, 1. <https://doi.org/10.1186/s13195-016-0227-5>
- Davies, D.S., Ma, J., Jegathees, T., Goldsbury, C., 2017. Microglia show altered morphology and reduced arborization in human brain during aging and Alzheimer's disease. *Brain Pathol. Zurich Switz.* 27, 795–808. <https://doi.org/10.1111/bpa.12456>
- de Calignon, A., Polydoro, M., Suárez-Calvet, M., William, C., Adamowicz, D.H., Kopeikina, K.J., Pitstick, R., Sahara, N., Ashe, K.H., Carlson, G.A., Spires-Jones, T.L., Hyman, B.T., 2012. Propagation of tau pathology in a model of early Alzheimer's disease. *Neuron* 73, 685–697. <https://doi.org/10.1016/j.neuron.2011.11.033>
- Deane, R., Du Yan, S., Subramanian, R.K., LaRue, B., Jovanovic, S., Hogg, E., Welch, D., Manness, L., Lin, C., Yu, J., Zhu, H., Ghiso, J., Frangione, B., Stern, A., Schmidt, A.M., Armstrong, D.L., Arnold, B., Liliensiek, B., Nawroth, P., Hofman, F., Kindy, M., Stern, D., Zlokovic, B., 2003. RAGE mediates amyloid-beta peptide transport across the blood-brain barrier and accumulation in brain. *Nat. Med.* 9, 907–913. <https://doi.org/10.1038/nm890>
- Degiorgis, L., Karatas, M., Sourty, M., Faivre, E., Lamy, J., Noblet, V., Bienert, T., Reiser, M., von Elverfeldt, D., Buée, L., Blum, D., Boutillier, A.-L., Armspach, J.-P., Blanc, F., Harsan, L.-A., 2020. Brain network remodelling reflects tau-related pathology prior to memory deficits in Thy-Tau22 mice. *Brain* 143, 3748–3762. <https://doi.org/10.1093/brain/awaa312>
- Dejanovic, B., Huntley, M.A., De Mazière, A., Meilandt, W.J., Wu, T., Srinivasan, K., Jiang, Z., Gandham, V., Friedman, B.A., Ngu, H., Foreman, O., Carano, R.A.D., Chih, B., Klumperman, J., Bakalarski, C., Hanson, J.E., Sheng, M., 2018. Changes in the Synaptic Proteome in Tauopathy and Rescue of Tau-Induced Synapse Loss by C1q Antibodies. *Neuron* 100, 1322-1336.e7. <https://doi.org/10.1016/j.neuron.2018.10.014>
- Dekhtyar, S., Marseglia, A., Xu, W., Darin-Mattsson, A., Wang, H.-X., Fratiglioni, L., 2019. Genetic risk of dementia mitigated by cognitive reserve: A cohort study. *Ann. Neurol.* 86, 68–78. <https://doi.org/10.1002/ana.25501>
- Delacourte, A., Sautière, P.E., Watzet, A., Mourton-Gilles, C., Petter, A., Bons, N., 1995. Biochemical characterization of Tau proteins during cerebral aging of the lemurian primate *Microcebus murinus*. *C. R. Acad. Sci. III* 318, 85–89.
- Deng, W., Aimone, J.B., Gage, F.H., 2010. New neurons and new memories: how does adult hippocampal neurogenesis affect learning and memory? *Nat. Rev. Neurosci.* 11, 339–350. <https://doi.org/10.1038/nrn2822>
- Deslys, J.P., Marcé, D., Dormont, D., 1994. Similar genetic susceptibility in iatrogenic and sporadic Creutzfeldt-Jakob disease. *J. Gen. Virol.* 75 ( Pt 1), 23–27. <https://doi.org/10.1099/0022-1317-75-1-23>
- DeTure, M.A., Dickson, D.W., 2019. The neuropathological diagnosis of Alzheimer's disease. *Mol. Neurodegener.* 14, 32. <https://doi.org/10.1186/s13024-019-0333-5>
- DeVos, S.L., Corjuc, B.T., Oakley, D.H., Nobuhara, C.K., Bannan, R.N., Chase, A., Commins, C., Gonzalez, J.A., Dooley, P.M., Frosch, M.P., Hyman, B.T., 2018. Synaptic Tau Seeding Precedes Tau Pathology in Human Alzheimer's Disease Brain. *Front. Neurosci.* 12, 267. <https://doi.org/10.3389/fnins.2018.00267>
- Di Fede, G., Catania, M., Maderna, E., Ghidoni, R., Benussi, L., Tonoli, E., Giaccone, G., Moda, F., Paterlini, A., Campagnani, I., Sorrentino, S., Colombo, L., Kubis, A., Bistaffa, E., Ghetti, B., Tagliavini, F., 2018. Molecular subtypes of Alzheimer's disease. *Sci. Rep.* 8, 3269. <https://doi.org/10.1038/s41598-018-21641-1>
- Di Scala, C., Yahji, N., Boutemour, S., Flores, A., Rodriguez, L., Chahinian, H., Fantini, J., 2016. Common molecular mechanism of amyloid pore formation by Alzheimer's  $\beta$ -amyloid peptide and  $\alpha$ -synuclein. *Sci. Rep.* 6, 28781. <https://doi.org/10.1038/srep28781>
- Dickey, C.A., Kamal, A., Lundgren, K., Klosak, N., Bailey, R.M., Dunmore, J., Ash, P., Shoraka, S., Zlatkovic, J., Eckman, C.B., Patterson, C., Dickson, D.W., Nahman, N.S., Hutton, M., Burrows, F., Petrucelli, L., 2007. The high-affinity HSP90-CHIP complex recognizes and selectively

- degrades phosphorylated tau client proteins. *J. Clin. Invest.* 117, 648–658. <https://doi.org/10.1172/JCI29715>
- Dickson, D.W., 1997. The pathogenesis of senile plaques. *J. Neuropathol. Exp. Neurol.* 56, 321–339. <https://doi.org/10.1097/00005072-199704000-00001>
- Dickstein, D.L., Brautigam, H., Stockton, S.D., Schmeidler, J., Hof, P.R., 2010. Changes in dendritic complexity and spine morphology in transgenic mice expressing human wild-type tau. *Brain Struct. Funct.* 214, 161–179. <https://doi.org/10.1007/s00429-010-0245-1>
- Dixit, R., Ross, J.L., Goldman, Y.E., Holzbaur, E.L.F., 2008. Differential regulation of dynein and kinesin motor proteins by tau. *Science* 319, 1086–1089. <https://doi.org/10.1126/science.1152993>
- Djelti, F., Dhenain, M., Terrien, J., Picq, J.-L., Hardy, I., Champeval, D., Perret, M., Schenker, E., Epelbaum, J., Aujard, F., 2016. Impaired fasting blood glucose is associated to cognitive impairment and cerebral atrophy in middle-aged non-human primates. *Aging* 9, 173–186. <https://doi.org/10.18632/aging.101148>
- Doens, D., Fernández, P.L., 2014. Microglia receptors and their implications in the response to amyloid  $\beta$  for Alzheimer's disease pathogenesis. *J. Neuroinflammation* 11, 48. <https://doi.org/10.1186/1742-2094-11-48>
- Dorieux, O., 2012. Vieillesse cérébrale chez un primate non humain, le Microcèbe : approches fonctionnelles et anatomiques (These de doctorat). Paris 5.
- Dorostkar, M.M., Zou, C., Blazquez-Llorca, L., Herms, J., 2015. Analyzing dendritic spine pathology in Alzheimer's disease: problems and opportunities. *Acta Neuropathol. (Berl.)* 130, 1–19. <https://doi.org/10.1007/s00401-015-1449-5>
- Dourlen, P., Kilinc, D., Malmanche, N., Chapuis, J., Lambert, J.-C., 2019. The new genetic landscape of Alzheimer's disease: from amyloid cascade to genetically driven synaptic failure hypothesis? *Acta Neuropathol. (Berl.)* 138, 221–236. <https://doi.org/10.1007/s00401-019-02004-0>
- Drummond, E., Nayak, S., Faustin, A., Pires, G., Hickman, R.A., Askenazi, M., Cohen, M., Haldiman, T., Kim, C., Han, X., Shao, Y., Safar, J.G., Ueberheide, B., Wisniewski, T., 2017. Proteomic differences in amyloid plaques in rapidly progressive and sporadic Alzheimer's disease. *Acta Neuropathol. (Berl.)* 133, 933–954. <https://doi.org/10.1007/s00401-017-1691-0>
- Drummond, E., Wisniewski, T., 2017. Alzheimer's disease: experimental models and reality. *Acta Neuropathol. (Berl.)* 133, 155–175. <https://doi.org/10.1007/s00401-016-1662-x>
- Du, H., Guo, L., Yan, S., Sosunov, A.A., McKhann, G.M., Yan, S.S., 2010. Early deficits in synaptic mitochondria in an Alzheimer's disease mouse model. *Proc. Natl. Acad. Sci. U. S. A.* 107, 18670–18675. <https://doi.org/10.1073/pnas.1006586107>
- Duff, K., Knight, H., Refolo, L.M., Sanders, S., Yu, X., Picciano, M., Malester, B., Hutton, M., Adamson, J., Goedert, M., Burki, K., Davies, P., 2000. Characterization of pathology in transgenic mice over-expressing human genomic and cDNA tau transgenes. *Neurobiol. Dis.* 7, 87–98. <https://doi.org/10.1006/nbdi.1999.0279>
- Dujardin, S., Bégard, S., Caillierez, R., Lachaud, C., Delattre, L., Carrier, S., Loyens, A., Galas, M.-C., Bousset, L., Melki, R., Aurégan, G., Hantraye, P., Brouillet, E., Buée, L., Colin, M., 2014. Ectosomes: a new mechanism for non-exosomal secretion of tau protein. *PloS One* 9, e100760. <https://doi.org/10.1371/journal.pone.0100760>
- Dujardin, S., Commins, C., Lathuiliere, A., Beerepoot, P., Fernandes, A.R., Kamath, T.V., De Los Santos, M.B., Klickstein, N., Corjuc, D.L., Corjuc, B.T., Dooley, P.M., Viode, A., Oakley, D.H., Moore, B.D., Mullin, K., Jean-Gilles, D., Clark, R., Atchison, K., Moore, R., Chibnik, L.B., Tanzi, R.E., Frosch, M.P., Serrano-Pozo, A., Elwood, F., Steen, J.A., Kennedy, M.E., Hyman, B.T., 2020. Tau molecular diversity contributes to clinical heterogeneity in Alzheimer's disease. *Nat. Med.* <https://doi.org/10.1038/s41591-020-0938-9>
- Dumurgier, J., Sabia, S., 2020. [Epidemiology of Alzheimer's disease: latest trends]. *Rev. Prat.* 70, 149–151.
- Duran-Aniotz, C., Morales, R., Moreno-Gonzalez, I., Hu, P.P., Fedynyshyn, J., Soto, C., 2014. Aggregate-Depleted Brain Fails to Induce A $\beta$  Deposition in a Mouse Model of Alzheimer's Disease. *PLOS ONE* 9, e89014. <https://doi.org/10.1371/journal.pone.0089014>

- Duran-Aniotz, C., Morales, R., Moreno-Gonzalez, I., Hu, P.P., Soto, C., 2013. Brains from non-Alzheimer's individuals containing amyloid deposits accelerate A $\beta$  deposition in vivo. *Acta Neuropathol. Commun.* 1. <https://doi.org/10.1186/2051-5960-1-76>
- Duyckaerts, C., Bannicub, M., Grignon, Y., Uchihara, T., He, Y., Piette, F., Hauw, J.J., 1997a. Modeling the relation between neurofibrillary tangles and intellectual status. *Neurobiol. Aging* 18, 267–273.
- Duyckaerts, C., Braak, H., Brion, J.-P., Buée, L., Del Tredici, K., Goedert, M., Halliday, G., Neumann, M., Spillantini, M.G., Tolnay, M., Uchihara, T., 2015. PART is part of Alzheimer disease. *Acta Neuropathol. (Berl.)* 129, 749–756. <https://doi.org/10.1007/s00401-015-1390-7>
- Duyckaerts, C., Delatour, B., Potier, M.-C., 2009. Classification and basic pathology of Alzheimer disease. *Acta Neuropathol. (Berl.)* 118, 5–36. <https://doi.org/10.1007/s00401-009-0532-1>
- Duyckaerts, C., Sazdovitch, V., Ando, K., Seilhean, D., Privat, N., Yilmaz, Z., Peckeu, L., Amar, E., Comoy, E., Maceski, A., Lehmann, S., Brion, J.-P., Brandel, J.-P., Haïk, S., 2018. Neuropathology of iatrogenic Creutzfeldt-Jakob disease and immunoassay of French cadaver-sourced growth hormone batches suggest possible transmission of tauopathy and long incubation periods for the transmission of Abeta pathology. *Acta Neuropathol. (Berl.)* 135, 201–212. <https://doi.org/10.1007/s00401-017-1791-x>
- Duyckaerts, C., Uchihara, T., Seilhean, D., He, Y., Hauw, J.J., 1997b. Dissociation of Alzheimer type pathology in a disconnected piece of cortex. *Acta Neuropathol. (Berl.)* 93, 501–507. <https://doi.org/10.1007/s004010050645>
- Eberle, M., Kappeler, P.M., 2004. Selected polyandry: Female choice and inter-sexual conflict in a small nocturnal solitary primate (*Microcebus murinus*). *Behav. Ecol. Sociobiol.* 57, 91–100. <https://doi.org/10.1007/s00265-004-0823-4>
- Edwards, F.A., 2019. A Unifying Hypothesis for Alzheimer's Disease: From Plaques to Neurodegeneration. *Trends Neurosci.* 42, 310–322. <https://doi.org/10.1016/j.tins.2019.03.003>
- Eisele, Y.S., Bolmont, T., Heikenwalder, M., Langer, F., Jacobson, L.H., Yan, Z.-X., Roth, K., Aguzzi, A., Staufenbiel, M., Walker, L.C., Jucker, M., 2009. Induction of cerebral beta-amyloidosis: intracerebral versus systemic Abeta inoculation. *Proc. Natl. Acad. Sci. U. S. A.* 106, 12926–12931. <https://doi.org/10.1073/pnas.0903200106>
- Eisele, Y.S., Duyckaerts, C., 2016. Propagation of A $\beta$  pathology: hypotheses, discoveries, and yet unresolved questions from experimental and human brain studies. *Acta Neuropathol. (Berl.)* 131, 5–25. <https://doi.org/10.1007/s00401-015-1516-y>
- Eisele, Y.S., Fritschi, S.K., Hamaguchi, T., Obermüller, U., Föger, P., Skodras, A., Schäfer, C., Odenthal, J., Heikenwalder, M., Staufenbiel, M., Jucker, M., 2014. Multiple factors contribute to the peripheral induction of cerebral  $\beta$ -amyloidosis. *J. Neurosci. Off. J. Soc. Neurosci.* 34, 10264–10273. <https://doi.org/10.1523/JNEUROSCI.1608-14.2014>
- Eisele, Y.S., Obermüller, U., Heilbronner, G., Baumann, F., Kaeser, S.A., Wolburg, H., Walker, L.C., Staufenbiel, M., Heikenwalder, M., Jucker, M., 2010. Peripherally applied Abeta-containing inoculates induce cerebral beta-amyloidosis. *Science* 330, 980–982. <https://doi.org/10.1126/science.1194516>
- Elfenbein, H.A., Rosen, R.F., Stephens, S.L., Switzer, R.C., Smith, Y., Pare, J., Mehta, P.D., Warzok, R., Walker, L.C., 2007. Cerebral beta-amyloid angiopathy in aged squirrel monkeys. *Histol. Histopathol.* 22, 155–167. <https://doi.org/10.14670/HH-22.155>
- Elmaleh, D.R., Farlow, M.R., Conti, P.S., Tompkins, R.G., Kundakovic, L., Tanzi, R.E., 2019. Developing Effective Alzheimer's Disease Therapies: Clinical Experience and Future Directions. *J. Alzheimers Dis. JAD* 71, 715–732. <https://doi.org/10.3233/JAD-190507>
- Engmann, O., Giese, K.P., 2009. Crosstalk between Cdk5 and GSK3 $\beta$ : Implications for Alzheimer's Disease. *Front. Mol. Neurosci.* 2. <https://doi.org/10.3389/neuro.02.002.2009>
- Evans, L.D., Wassmer, T., Fraser, G., Smith, J., Perkinson, M., Billinton, A., Livesey, F.J., 2018. Extracellular Monomeric and Aggregated Tau Efficiently Enter Human Neurons through

- Overlapping but Distinct Pathways. *Cell Rep.* 22, 3612–3624. <https://doi.org/10.1016/j.celrep.2018.03.021>
- Fá, M., Puzzo, D., Piacentini, R., Staniszewski, A., Zhang, H., Baltrons, M.A., Li Puma, D.D., Chatterjee, I., Li, J., Saeed, F., Berman, H.L., Ripoli, C., Gulisano, W., Gonzalez, J., Tian, H., Costa, J.A., Lopez, P., Davidowitz, E., Yu, W.H., Haroutunian, V., Brown, L.M., Palmeri, A., Sigurdsson, E.M., Duff, K.E., Teich, A.F., Honig, L.S., Sierks, M., Moe, J.G., D’Adamio, L., Grassi, C., Kanaan, N.M., Fraser, P.E., Arancio, O., 2016. Extracellular Tau Oligomers Produce An Immediate Impairment of LTP and Memory. *Sci. Rep.* 6, 19393. <https://doi.org/10.1038/srep19393>
- Fagiani, F., Lanni, C., Racchi, M., Pascale, A., Govoni, S., 2019. Amyloid- $\beta$  and Synaptic Vesicle Dynamics: A Cacophonous Orchestra. *J. Alzheimers Dis. JAD* 72, 1–14. <https://doi.org/10.3233/JAD-190771>
- Falcon, B., Cavallini, A., Angers, R., Glover, S., Murray, T.K., Barnham, L., Jackson, S., O’Neill, M.J., Isaacs, A.M., Hutton, M.L., Szekeres, P.G., Goedert, M., Bose, S., 2015. Conformation determines the seeding potencies of native and recombinant Tau aggregates. *J. Biol. Chem.* 290, 1049–1065. <https://doi.org/10.1074/jbc.M114.589309>
- Fan, Z., Brooks, D.J., Okello, A., Edison, P., 2017. An early and late peak in microglial activation in Alzheimer’s disease trajectory. *Brain J. Neurol.* 140, 792–803. <https://doi.org/10.1093/brain/aww349>
- Ferreira, D., Nordberg, A., Westman, E., 2020. Biological subtypes of Alzheimer disease: A systematic review and meta-analysis. *Neurology* 94, 436–448. <https://doi.org/10.1212/WNL.0000000000009058>
- Ferreira, D., Pereira, J.B., Volpe, G., Westman, E., 2019. Subtypes of Alzheimer’s Disease Display Distinct Network Abnormalities Extending Beyond Their Pattern of Brain Atrophy. *Front. Neurol.* 10, 524. <https://doi.org/10.3389/fneur.2019.00524>
- Ferreira, D., Shams, S., Cavallin, L., Viitanen, M., Martola, J., Granberg, T., Shams, M., Aspelin, P., Kristoffersen-Wiberg, M., Nordberg, A., Wahlund, L.-O., Westman, E., 2018a. The contribution of small vessel disease to subtypes of Alzheimer’s disease: a study on cerebrospinal fluid and imaging biomarkers. *Neurobiol. Aging* 70, 18–29. <https://doi.org/10.1016/j.neurobiolaging.2018.05.028>
- Ferreira, D., Verhagen, C., Hernández-Cabrera, J.A., Cavallin, L., Guo, C.-J., Ekman, U., Muehlboeck, J.-S., Simmons, A., Barroso, J., Wahlund, L.-O., Westman, E., 2017. Distinct subtypes of Alzheimer’s disease based on patterns of brain atrophy: longitudinal trajectories and clinical applications. *Sci. Rep.* 7. <https://doi.org/10.1038/srep46263>
- Ferreira, D., Wahlund, L.-O., Westman, E., 2018b. The heterogeneity within Alzheimer’s disease. *Aging* 10, 3058–3060. <https://doi.org/10.18632/aging.101638>
- Ferreira, S.T., Lourenco, M.V., Oliveira, M.M., De Felice, F.G., 2015. Soluble amyloid- $\beta$  oligomers as synaptotoxins leading to cognitive impairment in Alzheimer’s disease. *Front. Cell. Neurosci.* 9. <https://doi.org/10.3389/fncel.2015.00191>
- Figueiredo, C.P., Clarke, J.R., Ledo, J.H., Ribeiro, F.C., Costa, C.V., Melo, H.M., Mota-Sales, A.P., Saraiva, L.M., Klein, W.L., Sebollela, A., Felice, F.G.D., Ferreira, S.T., 2013. Memantine Rescues Transient Cognitive Impairment Caused by High-Molecular-Weight A $\beta$  Oligomers But Not the Persistent Impairment Induced by Low-Molecular-Weight Oligomers. *J. Neurosci.* 33, 9626–9634. <https://doi.org/10.1523/JNEUROSCI.0482-13.2013>
- Fitzpatrick, A.W.P., Falcon, B., He, S., Murzin, A.G., Murshudov, G., Garringer, H.J., Crowther, R.A., Ghetti, B., Goedert, M., Scheres, S.H.W., 2017. Cryo-EM structures of tau filaments from Alzheimer’s disease. *Nature* 547, 185–190. <https://doi.org/10.1038/nature23002>
- Folstein, M.F., Folstein, S.E., McHugh, P.R., 1975. “Mini-mental state”. A practical method for grading the cognitive state of patients for the clinician. *J. Psychiatr. Res.* 12, 189–198. [https://doi.org/10.1016/0022-3956\(75\)90026-6](https://doi.org/10.1016/0022-3956(75)90026-6)
- Fonseca, M.I., Zhou, J., Botto, M., Tenner, A.J., 2004. Absence of C1q Leads to Less Neuropathology in Transgenic Mouse Models of Alzheimer’s Disease. *J. Neurosci.* 24, 6457–6465. <https://doi.org/10.1523/JNEUROSCI.0901-04.2004>

- Forlenza, O.V., Radanovic, M., Talib, L.L., Aprahamian, I., Diniz, B.S., Zetterberg, H., Gattaz, W.F., 2015. Cerebrospinal fluid biomarkers in Alzheimer's disease: Diagnostic accuracy and prediction of dementia. *Alzheimers Dement. Diagn. Assess. Dis. Monit.* 1, 455–463. <https://doi.org/10.1016/j.dadm.2015.09.003>
- Forner, S., Baglietto-Vargas, D., Martini, A.C., Trujillo-Estrada, L., LaFerla, F.M., 2017. Synaptic Impairment in Alzheimer's Disease: A Dysregulated Symphony. *Trends Neurosci.* 40, 347–357. <https://doi.org/10.1016/j.tins.2017.04.002>
- Forny-Germano, L., Silva, N.M.L. e, Batista, A.F., Brito-Moreira, J., Gralle, M., Boehnke, S.E., Coe, B.C., Lablans, A., Marques, S.A., Martinez, A.M.B., Klein, W.L., Houzel, J.-C., Ferreira, S.T., Munoz, D.P., Felice, F.G.D., 2014. Alzheimer's Disease-Like Pathology Induced by Amyloid- $\beta$  Oligomers in Nonhuman Primates. *J. Neurosci.* 34, 13629–13643. <https://doi.org/10.1523/JNEUROSCI.1353-14.2014>
- Fransdemiche, M.L., De Seranno, S., Rush, T., Borel, E., Elie, A., Arnal, I., Lanté, F., Buisson, A., 2014. Activity-dependent tau protein translocation to excitatory synapse is disrupted by exposure to amyloid-beta oligomers. *J. Neurosci. Off. J. Soc. Neurosci.* 34, 6084–6097. <https://doi.org/10.1523/JNEUROSCI.4261-13.2014>
- Fratiglioni, L., Paillard-Borg, S., Winblad, B., 2004. An active and socially integrated lifestyle in late life might protect against dementia. *Lancet Neurol.* 3, 343–353. [https://doi.org/10.1016/S1474-4422\(04\)00767-7](https://doi.org/10.1016/S1474-4422(04)00767-7)
- Fritschi, S.K., Cintron, A., Ye, L., Mahler, J., Bühler, A., Baumann, F., Neumann, M., Nilsson, K.P.R., Hammarström, P., Walker, L.C., Jucker, M., 2014a. A $\beta$  seeds resist inactivation by formaldehyde. *Acta Neuropathol. (Berl.)* 128, 477–484. <https://doi.org/10.1007/s00401-014-1339-2>
- Fritschi, S.K., Langer, F., Kaeser, S.A., Maia, L.F., Portelius, E., Pinotsi, D., Kaminski, C.F., Winkler, D.T., Maetzler, W., Keyvani, K., Spitzer, P., Wiltfang, J., Kaminski Schierle, G.S., Zetterberg, H., Staufenbiel, M., Jucker, M., 2014b. Highly potent soluble amyloid- $\beta$  seeds in human Alzheimer brain but not cerebrospinal fluid. *Brain J. Neurol.* 137, 2909–2915. <https://doi.org/10.1093/brain/awu255>
- Frontzek, K., Lutz, M.I., Aguzzi, A., Kovacs, G.G., Budka, H., 2016. Amyloid- $\beta$  pathology and cerebral amyloid angiopathy are frequent in iatrogenic Creutzfeldt-Jakob disease after dural grafting. *Swiss Med. Wkly.* 146, w14287. <https://doi.org/10.4414/smw.2016.14287>
- Frost, B., Jacks, R.L., Diamond, M.I., 2009. Propagation of tau misfolding from the outside to the inside of a cell. *J. Biol. Chem.* 284, 12845–12852. <https://doi.org/10.1074/jbc.M808759200>
- Frost, G.R., Li, Y.-M., 2017. The role of astrocytes in amyloid production and Alzheimer's disease. *Open Biol.* 7. <https://doi.org/10.1098/rsob.170228>
- Frost, J.L., Schafer, D.P., 2016. Microglia: Architects of the Developing Nervous System. *Trends Cell Biol.* 26, 587–597. <https://doi.org/10.1016/j.tcb.2016.02.006>
- Fu, H., Hussaini, S.A., Wegmann, S., Profaci, C., Daniels, J.D., Herman, M., Emrani, S., Figueroa, H.Y., Hyman, B.T., Davies, P., Duff, K.E., 2016. 3D Visualization of the Temporal and Spatial Spread of Tau Pathology Reveals Extensive Sites of Tau Accumulation Associated with Neuronal Loss and Recognition Memory Deficit in Aged Tau Transgenic Mice. *PLoS One* 11, e0159463. <https://doi.org/10.1371/journal.pone.0159463>
- Fuster-Matanzo, A., Barreda, E.G. de, Dawson, H.N., Vitek, M.P., Avila, J., Hernández, F., 2009. Function of tau protein in adult newborn neurons. *FEBS Lett.* 583, 3063–3068. <https://doi.org/10.1016/j.febslet.2009.08.017>
- Gajdusek, D.C., Gibbs, C.J., Alpers, M., 1966. Experimental transmission of a Kuru-like syndrome to chimpanzees. *Nature* 209, 794–796.
- Galton, C.J., Patterson, K., Xuereb, J.H., Hodges, J.R., 2000. Atypical and typical presentations of Alzheimer's disease: a clinical, neuropsychological, neuroimaging and pathological study of 13 cases. *Brain J. Neurol.* 123 Pt 3, 484–498. <https://doi.org/10.1093/brain/123.3.484>
- Games, D., Adams, D., Alessandrini, R., Barbour, R., Berthelette, P., Blackwell, C., Carr, T., Clemens, J., Donaldson, T., Gillespie, F., 1995. Alzheimer-type neuropathology in transgenic mice



- overexpressing V717F beta-amyloid precursor protein. *Nature* 373, 523–527. <https://doi.org/10.1038/373523a0>
- Garcia-Alloza, M., Robbins, E.M., Zhang-Nunes, S.X., Purcell, S.M., Betensky, R.A., Raju, S., Prada, C., Greenberg, S.M., Bacskai, B.J., Frosch, M.P., 2006a. Characterization of amyloid deposition in the APP<sup>swE</sup>/PS1<sup>dE9</sup> mouse model of Alzheimer disease. *Neurobiol. Dis.* 24, 516–524. <https://doi.org/10.1016/j.nbd.2006.08.017>
- Garcia-Alloza, M., Robbins, E.M., Zhang-Nunes, S.X., Purcell, S.M., Betensky, R.A., Raju, S., Prada, C., Greenberg, S.M., Bacskai, B.J., Frosch, M.P., 2006b. Characterization of amyloid deposition in the APP<sup>swE</sup>/PS1<sup>dE9</sup> mouse model of Alzheimer disease. *Neurobiol. Dis.* 24, 516–524. <https://doi.org/10.1016/j.nbd.2006.08.017>
- Gardner, L.E., White, J.D., Eimerbrink, M.J., Boehm, G.W., Chumley, M.J., 2016. Imatinib methanesulfonate reduces hyperphosphorylation of tau following repeated peripheral exposure to lipopolysaccharide. *Neuroscience* 331, 72–77. <https://doi.org/10.1016/j.neuroscience.2016.06.007>
- Garin, C.M., Nadkarni, N.A., Landeau, B., Chételat, G., Picq, J.-L., Bougacha, S., Dhenain, M., 2021. Resting state functional atlas and cerebral networks in mouse lemur primates at 11.7 Tesla. *NeuroImage* 226, 117589. <https://doi.org/10.1016/j.neuroimage.2020.117589>
- Gary, C., Hérard, A.-S., Hanss, Z., Dhenain, M., 2018. Plasma Amyloid Is Associated with White Matter and Subcortical Alterations and Is Modulated by Age and Seasonal Rhythms in Mouse Lemur Primates. *Front. Aging Neurosci.* 10, 35. <https://doi.org/10.3389/fnagi.2018.00035>
- Gary, C., Lam, S., Hérard, A.-S., Koch, J.E., Petit, F., Gipchtein, P., Sawiak, S.J., Caillierez, R., Eddarkaoui, S., Colin, M., Aujard, F., Deslys, J.-P., Brouillet, E., Buée, L., Comoy, E.E., Pifferi, F., Picq, J.-L., Dhenain, M., 2019. Encephalopathy induced by Alzheimer brain inoculation in a non-human primate. *Acta Neuropathol. Commun.* 7. <https://doi.org/10.1186/s40478-019-0771-x>
- Gatz, M., Reynolds, C.A., Fratiglioni, L., Johansson, B., Mortimer, J.A., Berg, S., Fiske, A., Pedersen, N.L., 2006. Role of genes and environments for explaining Alzheimer disease. *Arch. Gen. Psychiatry* 63, 168–174. <https://doi.org/10.1001/archpsyc.63.2.168>
- Gearing, M., Rebeck, G.W., Hyman, B.T., Tigges, J., Mirra, S.S., 1994. Neuropathology and apolipoprotein E profile of aged chimpanzees: implications for Alzheimer disease. *Proc. Natl. Acad. Sci. U. S. A.* 91, 9382–9386. <https://doi.org/10.1073/pnas.91.20.9382>
- Gearing, M., Tigges, J., Mori, H., Mirra, S.S., 1997. beta-Amyloid (A beta) deposition in the brains of aged orangutans. *Neurobiol. Aging* 18, 139–146. [https://doi.org/10.1016/s0197-4580\(97\)00012-2](https://doi.org/10.1016/s0197-4580(97)00012-2)
- Gearing, M., Tigges, J., Mori, H., Mirra, S.S., 1996. A beta40 is a major form of beta-amyloid in nonhuman primates. *Neurobiol. Aging* 17, 903–908. [https://doi.org/10.1016/s0197-4580\(96\)00164-9](https://doi.org/10.1016/s0197-4580(96)00164-9)
- Gefen, T., Gasho, K., Rademaker, A., Lalehzari, M., Weintraub, S., Rogalski, E., Wieneke, C., Bigio, E., Geula, C., Mesulam, M.-M., 2012. Clinically concordant variations of Alzheimer pathology in aphasic versus amnesic dementia. *Brain J. Neurol.* 135, 1554–1565. <https://doi.org/10.1093/brain/aws076>
- Geijselaers, S.L.C., Sep, S.J.S., Stehouwer, C.D.A., Biessels, G.J., 2015. Glucose regulation, cognition, and brain MRI in type 2 diabetes: a systematic review. *Lancet Diabetes Endocrinol.* 3, 75–89. [https://doi.org/10.1016/S2213-8587\(14\)70148-2](https://doi.org/10.1016/S2213-8587(14)70148-2)
- Gemma, C., Bachstetter, A.D., 2013. The role of microglia in adult hippocampal neurogenesis. *Front. Cell. Neurosci.* 7, 229. <https://doi.org/10.3389/fncel.2013.00229>
- Geula, C., Nagykerly, N., Wu, C.-K., 2002. Amyloid-beta deposits in the cerebral cortex of the aged common marmoset (*Callithrix jacchus*): incidence and chemical composition. *Acta Neuropathol. (Berl.)* 103, 48–58. <https://doi.org/10.1007/s004010100429>
- Ghetti, B., Oblak, A.L., Boeve, B.F., Johnson, K.A., Dickerson, B.C., Goedert, M., 2015. Invited review: Frontotemporal dementia caused by microtubule-associated protein tau gene (MAPT) mutations: a chameleon for neuropathology and neuroimaging. *Neuropathol. Appl. Neurobiol.* 41, 24–46. <https://doi.org/10.1111/nan.12213>

- Giaccone, G., Maderna, E., Marucci, G., Catania, M., Erbetta, A., Chiapparini, L., Indaco, A., Caroppo, P., Bersano, A., Parati, E., Di Fede, G., Caputi, L., 2019. Iatrogenic early onset cerebral amyloid angiopathy 30 years after cerebral trauma with neurosurgery: vascular amyloid deposits are made up of both A $\beta$ 40 and A $\beta$ 42. *Acta Neuropathol. Commun.* 7, 70. <https://doi.org/10.1186/s40478-019-0719-1>
- Giannakopoulos, P., Silhol, S., Jallageas, V., Mallet, J., Bons, N., Bouras, C., Delaère, P., 1997. Quantitative analysis of tau protein-immunoreactive accumulations and beta amyloid protein deposits in the cerebral cortex of the mouse lemur, *Microcebus murinus*. *Acta Neuropathol. (Berl.)* 94, 131–139. <https://doi.org/10.1007/s004010050684>
- Gibbons, G.S., Banks, R.A., Kim, B., Xu, H., Changolkar, L., Leight, S.N., Riddle, D.M., Li, C., Gathagan, R.J., Brown, H.J., Zhang, B., Trojanowski, J.Q., Lee, V.M.-Y., 2017. GFP-Mutant Human Tau Transgenic Mice Develop Tauopathy Following CNS Injections of Alzheimer’s Brain-Derived Pathological Tau or Synthetic Mutant Human Tau Fibrils. *J. Neurosci.* 37, 11485–11494. <https://doi.org/10.1523/JNEUROSCI.2393-17.2017>
- Gibbs, C.J., Gajdusek, D.C., Asher, D.M., Alpers, M.P., Beck, E., Daniel, P.M., Matthews, W.B., 1968. Creutzfeldt-Jakob disease (spongiform encephalopathy): transmission to the chimpanzee. *Science* 161, 388–389.
- Goedert, M., Falcon, B., Clavaguera, F., Tolnay, M., 2014. Prion-like mechanisms in the pathogenesis of tauopathies and synucleinopathies. *Curr. Neurol. Neurosci. Rep.* 14, 495. <https://doi.org/10.1007/s11910-014-0495-z>
- Goedert, M., Spillantini, M.G., Jakes, R., Rutherford, D., Crowther, R.A., 1989. Multiple isoforms of human microtubule-associated protein tau: sequences and localization in neurofibrillary tangles of Alzheimer’s disease. *Neuron* 3, 519–526. [https://doi.org/10.1016/0896-6273\(89\)90210-9](https://doi.org/10.1016/0896-6273(89)90210-9)
- Gomes, L.A., Hipp, S.A., Rijal Upadhaya, A., Balakrishnan, K., Ospitalieri, S., Koper, M.J., Largo-Barrientos, P., Uytterhoeven, V., Reichwald, J., Rabe, S., Vandenberghe, R., von Arnim, C.A.F., Tousseyn, T., Feederle, R., Giudici, C., Willem, M., Staufenbiel, M., Thal, D.R., 2019. A $\beta$ -induced acceleration of Alzheimer-related  $\tau$ -pathology spreading and its association with prion protein. *Acta Neuropathol. (Berl.)*. <https://doi.org/10.1007/s00401-019-02053-5>
- Gomez-Arboledas, A., Davila, J.C., Sanchez-Mejias, E., Navarro, V., Nuñez-Díaz, C., Sanchez-Varo, R., Sanchez-Mico, M.V., Trujillo-Estrada, L., Fernandez-Valenzuela, J.J., Vizuete, M., Comella, J.X., Galea, E., Vitorica, J., Gutierrez, A., 2018. Phagocytic clearance of presynaptic dystrophies by reactive astrocytes in Alzheimer’s disease. *Glia* 66, 637–653. <https://doi.org/10.1002/glia.23270>
- Gómez-Isla, T., Hollister, R., West, H., Mui, S., Growdon, J.H., Petersen, R.C., Parisi, J.E., Hyman, B.T., 1997. Neuronal loss correlates with but exceeds neurofibrillary tangles in Alzheimer’s disease. *Ann. Neurol.* 41, 17–24. <https://doi.org/10.1002/ana.410410106>
- Gómez-Isla, T., Price, J.L., McKeel, D.W., Morris, J.C., Growdon, J.H., Hyman, B.T., 1996. Profound loss of layer II entorhinal cortex neurons occurs in very mild Alzheimer’s disease. *J. Neurosci. Off. J. Soc. Neurosci.* 16, 4491–4500.
- Gong, C.X., Singh, T.J., Grundke-Iqbal, I., Iqbal, K., 1993. Phosphoprotein phosphatase activities in Alzheimer disease brain. *J. Neurochem.* 61, 921–927. <https://doi.org/10.1111/j.1471-4159.1993.tb03603.x>
- González-Reyes, R.E., Nava-Mesa, M.O., Vargas-Sánchez, K., Ariza-Salamanca, D., Mora-Muñoz, L., 2017. Involvement of Astrocytes in Alzheimer’s Disease from a Neuroinflammatory and Oxidative Stress Perspective. *Front. Mol. Neurosci.* 10. <https://doi.org/10.3389/fnmol.2017.00427>
- Gorlovoy, P., Larionov, S., Pham, T.T.H., Neumann, H., 2009. Accumulation of tau induced in neurites by microglial proinflammatory mediators. *FASEB J.* 23, 2502–2513. <https://doi.org/10.1096/fj.08-123877>
- Gorno-Tempini, M.L., Brambati, S.M., Ginex, V., Ogar, J., Dronkers, N.F., Marcone, A., Perani, D., Garibotto, V., Cappa, S.F., Miller, B.L., 2008. The logopenic/phonological variant of primary

- progressive aphasia. *Neurology* 71, 1227–1234.  
<https://doi.org/10.1212/01.wnl.0000320506.79811.da>
- Götz, J., Chen, F., van Dorpe, J., Nitsch, R.M., 2001. Formation of neurofibrillary tangles in P301L tau transgenic mice induced by Aβ<sub>42</sub> fibrils. *Science* 293, 1491–1495.  
<https://doi.org/10.1126/science.1062097>
- Gouras, G.K., Tsai, J., Naslund, J., Vincent, B., Edgar, M., Checler, F., Greenfield, J.P., Haroutunian, V., Buxbaum, J.D., Xu, H., Greengard, P., Relkin, N.R., 2000. Intraneuronal Aβ<sub>42</sub> accumulation in human brain. *Am. J. Pathol.* 156, 15–20. [https://doi.org/10.1016/s0002-9440\(10\)64700-1](https://doi.org/10.1016/s0002-9440(10)64700-1)
- Greenberg, S.G., Davies, P., 1990. A preparation of Alzheimer paired helical filaments that displays distinct tau proteins by polyacrylamide gel electrophoresis. *Proc. Natl. Acad. Sci.* 87, 5827–5831. <https://doi.org/10.1073/pnas.87.15.5827>
- Greicius, M.D., Srivastava, G., Reiss, A.L., Menon, V., 2004. Default-mode network activity distinguishes Alzheimer’s disease from healthy aging: Evidence from functional MRI. *Proc. Natl. Acad. Sci. U. S. A.* 101, 4637–4642. <https://doi.org/10.1073/pnas.0308627101>
- Groen, T., Miettinen, P., Kadish, I., 2003. The entorhinal cortex of the mouse: Organization of the projection to the hippocampal formation. *Hippocampus* 13, 133–49.  
<https://doi.org/10.1002/hipo.10037>
- Guerreiro, R., Brás, J., Hardy, J., 2013. SnapShot: Genetics of Alzheimer’s Disease. *Cell* 155, 968–968.e1.  
<https://doi.org/10.1016/j.cell.2013.10.037>
- Guo, J.L., Narasimhan, S., Changolkar, L., He, Z., Stieber, A., Zhang, B., Gathagan, R.J., Iba, M., McBride, J.D., Trojanowski, J.Q., Lee, V.M.Y., 2016. Unique pathological tau conformers from Alzheimer’s brains transmit tau pathology in nontransgenic mice. *J. Exp. Med.* 213, 2635–2654.  
<https://doi.org/10.1084/jem.20160833>
- Guo, T., Noble, W., Hanger, D.P., 2017. Roles of tau protein in health and disease. *Acta Neuropathol. (Berl.)* 133, 665–704. <https://doi.org/10.1007/s00401-017-1707-9>
- Haass, C., Mandelkow, E., 2010. Fyn-Tau-Amyloid: A Toxic Triad. *Cell* 142, 356–358.  
<https://doi.org/10.1016/j.cell.2010.07.032>
- Habib, N., McCabe, C., Medina, S., Varshavsky, M., Kitsberg, D., Dvir-Szternfeld, R., Green, G., Dionne, D., Nguyen, L., Marshall, J.L., Chen, F., Zhang, F., Kaplan, T., Regev, A., Schwartz, M., 2020. Disease-associated astrocytes in Alzheimer’s disease and aging. *Nat. Neurosci.* 23, 701–706.  
<https://doi.org/10.1038/s41593-020-0624-8>
- Halle, A., Hornung, V., Petzold, G.C., Stewart, C.R., Monks, B.G., Reinheckel, T., Fitzgerald, K.A., Latz, E., Moore, K.J., Golenbock, D.T., 2008. The NALP3 inflammasome is involved in the innate immune response to amyloid-β. *Nat. Immunol.* 9, 857–865. <https://doi.org/10.1038/ni.1636>
- Hamaguchi, T., Eisele, Y.S., Varvel, N.H., Lamb, B.T., Walker, L.C., Jucker, M., 2012. The presence of Aβ seeds, and not age per se, is critical to the initiation of Aβ deposition in the brain. *Acta Neuropathol. (Berl.)* 123, 31–37. <https://doi.org/10.1007/s00401-011-0912-1>
- Hamaguchi, T., Komatsu, J., Sakai, K., Noguchi-Shinohara, M., Aoki, S., Ikeuchi, T., Yamada, M., 2019. Cerebral hemorrhagic stroke associated with cerebral amyloid angiopathy in young adults about 3 decades after neurosurgeries in their infancy. *J. Neurol. Sci.* 399, 3–5.  
<https://doi.org/10.1016/j.jns.2019.01.051>
- Hamaguchi, T., Taniguchi, Y., Sakai, K., Kitamoto, T., Takao, M., Murayama, S., Iwasaki, Y., Yoshida, M., Shimizu, H., Kakita, A., Takahashi, H., Suzuki, H., Naiki, H., Sanjo, N., Mizusawa, H., Yamada, M., 2016. Significant association of cadaveric dura mater grafting with subpial Aβ deposition and meningeal amyloid angiopathy. *Acta Neuropathol. (Berl.)* 132, 313–315.  
<https://doi.org/10.1007/s00401-016-1588-3>
- Hamelin, L., Lagarde, J., Dorothée, G., Leroy, C., Labit, M., Comley, R.A., de Souza, L.C., Corne, H., Dauphinot, L., Bertoux, M., Dubois, B., Gervais, P., Colliot, O., Potier, M.C., Bottlaender, M., Sarazin, M., Clinical IMABio3 team, 2016. Early and protective microglial activation in Alzheimer’s disease: a prospective study using 18F-DPA-714 PET imaging. *Brain J. Neurol.* 139, 1252–1264. <https://doi.org/10.1093/brain/aww017>

- Hamilton, R.L., 2000. Lewy bodies in Alzheimer's disease: a neuropathological review of 145 cases using alpha-synuclein immunohistochemistry. *Brain Pathol. Zurich Switz.* 10, 378–384. <https://doi.org/10.1111/j.1750-3639.2000.tb00269.x>
- Hampel, H., Buerger, K., Zinkowski, R., Teipel, S.J., Goernitz, A., Andreasen, N., Sjoegren, M., DeBernardis, J., Kerkman, D., Ishiguro, K., Ohno, H., Vanmechelen, E., Vanderstichele, H., McCulloch, C., Moller, H.-J., Davies, P., Blennow, K., 2004. Measurement of phosphorylated tau epitopes in the differential diagnosis of Alzheimer disease: a comparative cerebrospinal fluid study. *Arch. Gen. Psychiatry* 61, 95–102. <https://doi.org/10.1001/archpsyc.61.1.95>
- Hanseeuw, B.J., Betensky, R.A., Jacobs, H.I.L., Schultz, A.P., Sepulcre, J., Becker, J.A., Cosio, D.M.O., Farrell, M., Quiroz, Y.T., Mormino, E.C., Buckley, R.F., Papp, K.V., Amariglio, R.A., Dewachter, I., Ivanoiu, A., Huijbers, W., Hedden, T., Marshall, G.A., Chhatwal, J.P., Rentz, D.M., Sperling, R.A., Johnson, K., 2019. Association of Amyloid and Tau With Cognition in Preclinical Alzheimer Disease. *JAMA Neurol.* 76, 915–924. <https://doi.org/10.1001/jamaneurol.2019.1424>
- Hansen, D.V., Hanson, J.E., Sheng, M., 2018. Microglia in Alzheimer's disease. *J. Cell Biol.* 217, 459–472. <https://doi.org/10.1083/jcb.201709069>
- Hansson, O., Lehmann, S., Otto, M., Zetterberg, H., Lewczuk, P., 2019. Advantages and disadvantages of the use of the CSF Amyloid  $\beta$  (A $\beta$ ) 42/40 ratio in the diagnosis of Alzheimer's Disease. *Alzheimers Res. Ther.* 11, 34. <https://doi.org/10.1186/s13195-019-0485-0>
- Hardy, J., Selkoe, D.J., 2002. The amyloid hypothesis of Alzheimer's disease: progress and problems on the road to therapeutics. *Science* 297, 353–356. <https://doi.org/10.1126/science.1072994>
- Harper, J.D., Wong, S.S., Lieber, C.M., Lansbury, P.T., 1997. Observation of metastable Abeta amyloid protofibrils by atomic force microscopy. *Chem. Biol.* 4, 119–125. [https://doi.org/10.1016/s1074-5521\(97\)90255-6](https://doi.org/10.1016/s1074-5521(97)90255-6)
- Härtig, W., Klein, C., Brauer, K., Schüppel, K.F., Arendt, T., Brückner, G., Bigl, V., 2000. Abnormally phosphorylated protein tau in the cortex of aged individuals of various mammalian orders. *Acta Neuropathol. (Berl.)* 100, 305–312. <https://doi.org/10.1007/s004010000183>
- Hartmann, C.A., Martins, V.R., Lima, F.R.S., 2013. High levels of Cellular Prion Protein improve astrocyte development. *FEBS Lett.* 587, 238–244. <https://doi.org/10.1016/j.febslet.2012.11.032>
- HAS, 2016. Haute Autorité de Santé - Médicaments de la maladie d'Alzheimer : un intérêt médical insuffisant pour justifier leur prise en charge par la solidarité nationale [WWW Document]. URL [http://www.has-sante.fr/portail/jcms/c\\_2679466/fr/medicaments-de-la-maladie-d-alzheimer-un-interet-medical-insuffisant-pour-justifier-leur-prise-en-charge-par-la-solidarite-nationale](http://www.has-sante.fr/portail/jcms/c_2679466/fr/medicaments-de-la-maladie-d-alzheimer-un-interet-medical-insuffisant-pour-justifier-leur-prise-en-charge-par-la-solidarite-nationale) (accessed 5.6.17).
- He, Y., Zheng, M.-M., Ma, Y., Han, X.-J., Ma, X.-Q., Qu, C.-Q., Du, Y.-F., 2012. Soluble oligomers and fibrillar species of amyloid  $\beta$ -peptide differentially affect cognitive functions and hippocampal inflammatory response. *Biochem. Biophys. Res. Commun.* 429, 125–130. <https://doi.org/10.1016/j.bbrc.2012.10.129>
- He, Z., Guo, J.L., McBride, J.D., Narasimhan, S., Kim, H., Changolkar, L., Zhang, B., Gathagan, R.J., Yue, C., Dengler, C., Stieber, A., Nitla, M., Coulter, D.A., Abel, T., Brunden, K.R., Trojanowski, J.Q., Lee, V.M.-Y., 2018. Amyloid- $\beta$  plaques enhance Alzheimer's brain tau-seeded pathologies by facilitating neuritic plaque tau aggregation. *Nat. Med.* 24, 29–38. <https://doi.org/10.1038/nm.4443>
- Head, E., McCleary, R., Hahn, F.F., Milgram, N.W., Cotman, C.W., 2000. Region-specific age at onset of beta-amyloid in dogs. *Neurobiol. Aging* 21, 89–96. [https://doi.org/10.1016/s0197-4580\(00\)00093-2](https://doi.org/10.1016/s0197-4580(00)00093-2)
- Head, E., Pop, V., Sarsoza, F., Kaye, R., Beckett, T.L., Studzinski, C.M., Tomic, J.L., Glabe, C.G., Murphy, M.P., 2010. Amyloid-beta peptide and oligomers in the brain and cerebrospinal fluid of aged canines. *J. Alzheimers Dis. JAD* 20, 637–646. <https://doi.org/10.3233/JAD-2010-1397>
- Hebert, L.E., Beckett, L.A., Scherr, P.A., Evans, D.A., 2001. Annual Incidence of Alzheimer Disease in the United States Projected to the Years 2000 Through 2050. *Alzheimer Dis. Assoc. Disord.* 15, 169–173.

- Heilbronner, G., Eisele, Y.S., Langer, F., Kaeser, S.A., Novotny, R., Nagarathinam, A., Aslund, A., Hammarström, P., Nilsson, K.P.R., Jucker, M., 2013. Seeded strain-like transmission of  $\beta$ -amyloid morphotypes in APP transgenic mice. *EMBO Rep.* 14, 1017–1022. <https://doi.org/10.1038/embor.2013.137>
- Hellwig, S., Masuch, A., Nestel, S., Katzmarski, N., Meyer-Luehmann, M., Biber, K., 2015. Forebrain microglia from wild-type but not adult 5xFAD mice prevent amyloid- $\beta$  plaque formation in organotypic hippocampal slice cultures. *Sci. Rep.* 5. <https://doi.org/10.1038/srep14624>
- Heneka, M.T., Kummer, M.P., Stutz, A., Delekate, A., Schwartz, S., Vieira-Saecker, A., Griep, A., Axt, D., Remus, A., Tzeng, T.-C., Gelpi, E., Halle, A., Korte, M., Latz, E., Golenbock, D.T., 2013. NLRP3 is activated in Alzheimer's disease and contributes to pathology in APP/PS1 mice. *Nature* 493, 674–678. <https://doi.org/10.1038/nature11729>
- Heneka, M.T., McManus, R.M., Latz, E., 2018. Inflammasome signalling in brain function and neurodegenerative disease. *Nat. Rev. Neurosci.* 19, 610–621. <https://doi.org/10.1038/s41583-018-0055-7>
- Henkins, K.M., Sokolow, S., Miller, C.A., Vinters, H.V., Poon, W.W., Cornwell, L.B., Saing, T., Gyls, K.H., 2012. Extensive p-Tau Pathology and SDS-Stable p-Tau Oligomers in Alzheimer's Cortical Synapses. *Brain Pathol.* 22, 826–833. <https://doi.org/10.1111/j.1750-3639.2012.00598.x>
- Hérard, A.-S., Petit, F., Gary, C., Guillermier, M., Boluda, S., Garin, C.M., Lam, S., Dhenain, M., 2020. Induction of amyloid- $\beta$  deposits from serially transmitted, histologically silent, A $\beta$  seeds issued from human brains. *Acta Neuropathol. Commun.* 8. <https://doi.org/10.1186/s40478-020-01081-7>
- Herndon, J.G., Moss, M.B., Rosene, D.L., Killiany, R.J., 1997. Patterns of cognitive decline in aged rhesus monkeys. *Behav. Brain Res.* 87, 25–34. [https://doi.org/10.1016/S0166-4328\(96\)02256-5](https://doi.org/10.1016/S0166-4328(96)02256-5)
- Herskovits, A.Z., Locascio, J.J., Peskind, E.R., Li, G., Hyman, B.T., 2013. A Luminex Assay Detects Amyloid  $\beta$  Oligomers in Alzheimer's Disease Cerebrospinal Fluid. *PLOS ONE* 8, e67898. <https://doi.org/10.1371/journal.pone.0067898>
- Hervé, D., Porché, M., Cabrejo, L., Guidoux, C., Tournier-Lasserre, E., Nicolas, G., Adle-Biassette, H., Plu, I., Chabriat, H., Duyckaerts, C., 2018. Fatal A $\beta$  cerebral amyloid angiopathy 4 decades after a dural graft at the age of 2 years. *Acta Neuropathol. (Berl.)* 135, 801–803. <https://doi.org/10.1007/s00401-018-1828-9>
- Hesse, C., Rosengren, L., Andreasen, N., Davidsson, P., Vanderstichele, H., Vanmechelen, E., Blennow, K., 2001. Transient increase in total tau but not phospho-tau in human cerebrospinal fluid after acute stroke. *Neurosci. Lett.* 297, 187–190. [https://doi.org/10.1016/S0304-3940\(00\)01697-9](https://doi.org/10.1016/S0304-3940(00)01697-9)
- Holmes, B.B., DeVos, S.L., Kfoury, N., Li, M., Jacks, R., Yanamandra, K., Ouidja, M.O., Brodsky, F.M., Marasa, J., Bagchi, D.P., Kotzbauer, P.T., Miller, T.M., Papy-Garcia, D., Diamond, M.I., 2013. Heparan sulfate proteoglycans mediate internalization and propagation of specific proteopathic seeds. *Proc. Natl. Acad. Sci. U. S. A.* 110, E3138–E3147. <https://doi.org/10.1073/pnas.1301440110>
- Holmes, B.B., Furman, J.L., Mahan, T.E., Yamasaki, T.R., Mirbaha, H., Eades, W.C., Belaygorod, L., Cairns, N.J., Holtzman, D.M., Diamond, M.I., 2014. Proteopathic tau seeding predicts tauopathy in vivo. *Proc. Natl. Acad. Sci. U. S. A.* 111, E4376–E4385. <https://doi.org/10.1073/pnas.1411649111>
- Holtzman, D.M., 2001. Role of apoe/A $\beta$  interactions in the pathogenesis of Alzheimer's disease and cerebral amyloid angiopathy. *J. Mol. Neurosci.* MN 17, 147–155. <https://doi.org/10.1385/JMN:17:2:147>
- Holtzman, D.M., Herz, J., Bu, G., 2012. Apolipoprotein E and apolipoprotein E receptors: normal biology and roles in Alzheimer disease. *Cold Spring Harb. Perspect. Med.* 2, a006312. <https://doi.org/10.1101/cshperspect.a006312>
- Hong, S., Beja-Glasser, V.F., Nfonoyim, B.M., Frouin, A., Li, S., Ramakrishnan, S., Merry, K.M., Shi, Q., Rosenthal, A., Barres, B.A., Lemere, C.A., Selkoe, D.J., Stevens, B., 2016. Complement and microglia mediate early synapse loss in Alzheimer mouse models. *Science* 352, 712–716. <https://doi.org/10.1126/science.aad8373>

- Honig, L.S., Tang, M.-X., Albert, S., Costa, R., Luchsinger, J., Manly, J., Stern, Y., Mayeux, R., 2003. Stroke and the risk of Alzheimer disease. *Arch. Neurol.* 60, 1707–1712. <https://doi.org/10.1001/archneur.60.12.1707>
- Hoover, B.R., Reed, M.N., Su, J., Penrod, R.D., Kotilinek, L.A., Grant, M.K., Pitstick, R., Carlson, G.A., Lanier, L.M., Yuan, L.-L., Ashe, K.H., Liao, D., 2010. Tau mislocalization to dendritic spines mediates synaptic dysfunction independently of neurodegeneration. *Neuron* 68, 1067–1081. <https://doi.org/10.1016/j.neuron.2010.11.030>
- Hopp, S.C., Lin, Y., Oakley, D., Roe, A.D., DeVos, S.L., Hanlon, D., Hyman, B.T., 2018. The role of microglia in processing and spreading of bioactive tau seeds in Alzheimer’s disease. *J. Neuroinflammation* 15, 269. <https://doi.org/10.1186/s12974-018-1309-z>
- Hughes, C.P., Berg, L., Danziger, W.L., Coben, L.A., Martin, R.L., 1982. A new clinical scale for the staging of dementia. *Br. J. Psychiatry J. Ment. Sci.* 140, 566–572. <https://doi.org/10.1192/bjp.140.6.566>
- Hwang, J., Kim, C.M., Jeon, S., Lee, J.M., Hong, Y.J., Roh, J.H., Lee, J.-H., Koh, J.-Y., Na, D.L., 2015. Prediction of Alzheimer’s disease pathophysiology based on cortical thickness patterns. *Alzheimers Dement. Diagn. Assess. Dis. Monit.* 2, 58–67. <https://doi.org/10.1016/j.dadm.2015.11.008>
- Hyman, B.T., 2011. Amyloid-dependent and amyloid-independent stages of Alzheimer disease. *Arch. Neurol.* 68, 1062–1064. <https://doi.org/10.1001/archneurol.2011.70>
- Iadanza, M.G., Jackson, M.P., Hewitt, E.W., Ranson, N.A., Radford, S.E., 2018. A new era for understanding amyloid structures and disease. *Nat. Rev. Mol. Cell Biol.* <https://doi.org/10.1038/s41580-018-0060-8>
- Iba, M., Guo, J.L., McBride, J.D., Zhang, B., Trojanowski, J.Q., Lee, V.M.-Y., 2013. Synthetic tau fibrils mediate transmission of neurofibrillary tangles in a transgenic mouse model of Alzheimer’s-like tauopathy. *J. Neurosci. Off. J. Soc. Neurosci.* 33, 1024–1037. <https://doi.org/10.1523/JNEUROSCI.2642-12.2013>
- Ironside, J.W., Ritchie, D.L., Head, M.W., 2017. Prion diseases. *Handb. Clin. Neurol.* 145, 393–403. <https://doi.org/10.1016/B978-0-12-802395-2.00028-6>
- Irwin, D.J., Cohen, T.J., Grossman, M., Arnold, S.E., Xie, S.X., Lee, V.M.-Y., Trojanowski, J.Q., 2012. Acetylated tau, a novel pathological signature in Alzheimer’s disease and other tauopathies. *Brain J. Neurol.* 135, 807–818. <https://doi.org/10.1093/brain/aws013>
- Ising, C., Venegas, C., Zhang, S., Scheiblich, H., Schmidt, S.V., Vieira-Saecker, A., Schwartz, S., Albaset, S., McManus, R.M., Tejera, D., Griep, A., Santarelli, F., Brosseron, F., Opitz, S., Stunden, J., Merten, M., Kaye, R., Golenbock, D.T., Blum, D., Latz, E., Buée, L., Heneka, M.T., 2019. NLRP3 inflammasome activation drives tau pathology. *Nature* 575, 669–673. <https://doi.org/10.1038/s41586-019-1769-z>
- Ito, K., Corrigan, B., Zhao, Q., French, J., Miller, R., Soares, H., Katz, E., Nicholas, T., Billing, B., Anziano, R., Fullerton, T., Alzheimer’s Disease Neuroimaging Initiative, 2011. Disease progression model for cognitive deterioration from Alzheimer’s Disease Neuroimaging Initiative database. *Alzheimers Dement. J. Alzheimers Assoc.* 7, 151–160. <https://doi.org/10.1016/j.jalz.2010.03.018>
- Ittner, L.M., Ke, Y.D., Delerue, F., Bi, M., Gladbach, A., van Eersel, J., Wölfing, H., Chieng, B.C., Christie, M.J., Napier, I.A., Eckert, A., Staufenbiel, M., Hardeman, E., Götz, J., 2010. Dendritic function of tau mediates amyloid-beta toxicity in Alzheimer’s disease mouse models. *Cell* 142, 387–397. <https://doi.org/10.1016/j.cell.2010.06.036>
- Iturria-Medina, Y., Sotero, R.C., Toussaint, P.J., Evans, A.C., Initiative, and the A.D.N., 2014. Epidemic Spreading Model to Characterize Misfolded Proteins Propagation in Aging and Associated Neurodegenerative Disorders. *PLOS Comput. Biol.* 10, e1003956. <https://doi.org/10.1371/journal.pcbi.1003956>
- Iwasaki, Y., Imamura, K., Iwai, K., Kobayashi, Y., Akagi, A., Mimuro, M., Miyahara, H., Kitamoto, T., Yoshida, M., 2018. Autopsied case of non-plaque-type dura mater graft-associated

- Creutzfeldt-Jakob disease presenting with extensive amyloid- $\beta$  deposition. *Neuropathology* 38, 549–556. <https://doi.org/10.1111/neup.12503>
- Izquierdo, A., Suda, R.K., Murray, E.A., 2004. Bilateral Orbital Prefrontal Cortex Lesions in Rhesus Monkeys Disrupt Choices Guided by Both Reward Value and Reward Contingency. *J. Neurosci.* 24, 7540–7548. <https://doi.org/10.1523/JNEUROSCI.1921-04.2004>
- Jack, C.R., Bennett, D.A., Blennow, K., Carrillo, M.C., Dunn, B., Haeberlein, S.B., Holtzman, D.M., Jagust, W., Jessen, F., Karlawish, J., Liu, E., Molinuevo, J.L., Montine, T., Phelps, C., Rankin, K.P., Rowe, C.C., Scheltens, P., Siemers, E., Snyder, H.M., Sperling, R., Contributors, 2018. NIA-AA Research Framework: Toward a biological definition of Alzheimer's disease. *Alzheimers Dement. J. Alzheimers Assoc.* 14, 535–562. <https://doi.org/10.1016/j.jalz.2018.02.018>
- Jack, C.R., Holtzman, D.M., 2013. Biomarker Modeling of Alzheimer's Disease. *Neuron* 80, 1347–1358. <https://doi.org/10.1016/j.neuron.2013.12.003>
- Jagust, W., 2018. Imaging the evolution and pathophysiology of Alzheimer disease. *Nat. Rev. Neurosci.* 19, 687–700. <https://doi.org/10.1038/s41583-018-0067-3>
- Jahn, H., 2013. Memory loss in Alzheimer's disease. *Dialogues Clin. Neurosci.* 15, 445–454.
- Janelidze, S., Mattsson, N., Palmqvist, S., Smith, R., Beach, T.G., Serrano, G.E., Chai, X., Proctor, N.K., Eichenlaub, U., Zetterberg, H., Blennow, K., Reiman, E.M., Stomrud, E., Dage, J.L., Hansson, O., 2020a. Plasma P-tau181 in Alzheimer's disease: relationship to other biomarkers, differential diagnosis, neuropathology and longitudinal progression to Alzheimer's dementia. *Nat. Med.* 26, 379–386. <https://doi.org/10.1038/s41591-020-0755-1>
- Janelidze, S., Stomrud, E., Smith, R., Palmqvist, S., Mattsson, N., Airey, D.C., Proctor, N.K., Chai, X., Shcherbinin, S., Sims, J.R., Triana-Baltzer, G., Theunis, C., Slemmon, R., Mercken, M., Kolb, H., Dage, J.L., Hansson, O., 2020b. Cerebrospinal fluid p-tau217 performs better than p-tau181 as a biomarker of Alzheimer's disease. *Nat. Commun.* 11, 1683. <https://doi.org/10.1038/s41467-020-15436-0>
- Janelins, M.C., Mastrangelo, M.A., Park, K.M., Sudol, K.L., Narrow, W.C., Oddo, S., LaFerla, F.M., Callahan, L.M., Federoff, H.J., Bowers, W.J., 2008. Chronic Neuron-Specific Tumor Necrosis Factor-Alpha Expression Enhances the Local Inflammatory Environment Ultimately Leading to Neuronal Death in 3xTg-AD Mice. *Am. J. Pathol.* 173, 1768–1782. <https://doi.org/10.2353/ajpath.2008.080528>
- Jankowsky, J.L., Fadale, D.J., Anderson, J., Xu, G.M., Gonzales, V., Jenkins, N.A., Copeland, N.G., Lee, M.K., Younkin, L.H., Wagner, S.L., Younkin, S.G., Borchelt, D.R., 2004. Mutant presenilins specifically elevate the levels of the 42 residue beta-amyloid peptide in vivo: evidence for augmentation of a 42-specific gamma secretase. *Hum. Mol. Genet.* 13, 159–170. <https://doi.org/10.1093/hmg/ddh019>
- Janus, C., Flores, A.Y., Xu, G., Borchelt, D.R., 2015. Behavioral abnormalities in APPSwe/PS1dE9 mouse model of AD-like pathology: comparative analysis across multiple behavioral domains. *Neurobiol. Aging* 36, 2519–2532. <https://doi.org/10.1016/j.neurobiolaging.2015.05.010>
- Jaunmuktane, Z., Banerjee, G., Paine, S., Parry-Jones, A., Rudge, P., Grieve, J., Toma, A.K., Farmer, S.F., Mead, S., Houlden, H., Werring, D.J., Brandner, S., 2021. Alzheimer's disease neuropathological change three decades after iatrogenic amyloid- $\beta$  transmission. *Acta Neuropathol. (Berl.)* 142, 211–215. <https://doi.org/10.1007/s00401-021-02326-y>
- Jaunmuktane, Z., Brandner, S., 2020. Invited Review: The role of prion-like mechanisms in neurodegenerative diseases. *Neuropathol. Appl. Neurobiol.* 46, 522–545. <https://doi.org/10.1111/nan.12592>
- Jaunmuktane, Z., Mead, S., Ellis, M., Wadsworth, J.D.F., Nicoll, A.J., Kenny, J., Launchbury, F., Linehan, J., Richard-Loendt, A., Walker, A.S., Rudge, P., Collinge, J., Brandner, S., 2015a. Evidence for human transmission of amyloid- $\beta$  pathology and cerebral amyloid angiopathy. *Nature* 525, 247–250. <https://doi.org/10.1038/nature15369>
- Jaunmuktane, Z., Mead, S., Ellis, M., Wadsworth, J.D.F., Nicoll, A.J., Kenny, J., Launchbury, F., Linehan, J., Richard-Loendt, A., Walker, A.S., Rudge, P., Collinge, J., Brandner, S., 2015b. Evidence for

- human transmission of amyloid- $\beta$  pathology and cerebral amyloid angiopathy. *Nature* 525, 247–250. <https://doi.org/10.1038/nature15369>
- Jaunmuktane, Z., Quaegebeur, A., Taipa, R., Viana-Baptista, M., Barbosa, R., Koriath, C., Scot, R., Mead, S., Brandner, S., 2018. Evidence of amyloid- $\beta$  cerebral amyloid angiopathy transmission through neurosurgery. *Acta Neuropathol. (Berl.)* 135, 671–679. <https://doi.org/10.1007/s00401-018-1822-2>
- Jeganathan, S., von Bergen, M., Brutlach, H., Steinhoff, H.-J., Mandelkow, E., 2006. Global Hairpin Folding of Tau in Solution. *Biochemistry* 45, 2283–2293. <https://doi.org/10.1021/bi0521543>
- Jiang, Q., Lee, C.Y.D., Mandrekar, S., Wilkinson, B., Cramer, P., Zelcer, N., Mann, K., Lamb, B., Willson, T.M., Collins, J.L., Richardson, J.C., Smith, J.D., Comery, T.A., Riddell, D., Holtzman, D.M., Tontonoz, P., Landreth, G.E., 2008. ApoE promotes the proteolytic degradation of A $\beta$ . *Neuron* 58, 681–693. <https://doi.org/10.1016/j.neuron.2008.04.010>
- Jin, M., Shepardson, N., Yang, T., Chen, G., Walsh, D., Selkoe, D.J., 2011. Soluble amyloid beta-protein dimers isolated from Alzheimer cortex directly induce Tau hyperphosphorylation and neuritic degeneration. *Proc. Natl. Acad. Sci. U. S. A.* 108, 5819–5824. <https://doi.org/10.1073/pnas.1017033108>
- Johnson, J.K., Head, E., Kim, R., Starr, A., Cotman, C.W., 1999. Clinical and pathological evidence for a frontal variant of Alzheimer disease. *Arch. Neurol.* 56, 1233–1239. <https://doi.org/10.1001/archneur.56.10.1233>
- Jones, E., Mead, S., 2020. Genetic risk factors for Creutzfeldt-Jakob disease. *Neurobiol. Dis.* 142, 104973. <https://doi.org/10.1016/j.nbd.2020.104973>
- Jonsson, T., Stefansson, H., Steinberg, S., Jonsdottir, I., Jonsson, P.V., Snaedal, J., Bjornsson, S., Huttenlocher, J., Levey, A.I., Lah, J.J., Rujescu, D., Hampel, H., Giegling, I., Andreassen, O.A., Engedal, K., Ulstein, I., Djurovic, S., Ibrahim-Verbaas, C., Hofman, A., Ikram, M.A., van Duijn, C.M., Thorsteinsdottir, U., Kong, A., Stefansson, K., 2013. Variant of TREM2 Associated with the Risk of Alzheimer's Disease [WWW Document]. <http://dx.doi.org/10.1056/NEJMoa1211103>. <https://doi.org/10.1056/NEJMoa1211103>
- Jucker, M., Walker, L.C., 2013. Self-propagation of pathogenic protein aggregates in neurodegenerative diseases. *Nature* 501, 45–51. <https://doi.org/10.1038/nature12481>
- Jucker, M., Walker, L.C., 2011. Pathogenic protein seeding in Alzheimer disease and other neurodegenerative disorders. *Ann. Neurol.* 70, 532–540. <https://doi.org/10.1002/ana.22615>
- Juottonen, K., Laakso, M.P., Partanen, K., Soininen, H., 1999. Comparative MR analysis of the entorhinal cortex and hippocampus in diagnosing Alzheimer disease. *Am. J. Neuroradiol.* 20, 139–144.
- Kabaso, D., Coskren, P.J., Henry, B.I., Hof, P.R., Wearne, S.L., 2009. The Electrotonic Structure of Pyramidal Neurons Contributing to Prefrontal Cortical Circuits in Macaque Monkeys Is Significantly Altered in Aging. *Cereb. Cortex N. Y. NY* 19, 2248–2268. <https://doi.org/10.1093/cercor/bhn242>
- Kamphuis, W., Mamber, C., Moeton, M., Kooijman, L., Sluijs, J.A., Jansen, A.H.P., Verveer, M., de Groot, L.R., Smith, V.D., Rangarajan, S., Rodríguez, J.J., Orre, M., Hol, E.M., 2012. GFAP isoforms in adult mouse brain with a focus on neurogenic astrocytes and reactive astrogliosis in mouse models of Alzheimer disease. *PloS One* 7, e42823. <https://doi.org/10.1371/journal.pone.0042823>
- Kane, M.D., Lipinski, W.J., Callahan, M.J., Bian, F., Durham, R.A., Schwarz, R.D., Roher, A.E., Walker, L.C., 2000. Evidence for Seeding of  $\beta$ -Amyloid by Intracerebral Infusion of Alzheimer Brain Extracts in  $\beta$ -Amyloid Precursor Protein-Transgenic Mice. *J. Neurosci.* 20, 3606–3611.
- Karantzoulis, S., Galvin, J.E., 2011. Distinguishing Alzheimer's disease from other major forms of dementia. *Expert Rev. Neurother.* 11, 1579–1591. <https://doi.org/10.1586/ern.11.155>
- Kaufman, S.K., Sanders, D.W., Thomas, T.L., Ruchinkas, A.J., Vaquer-Alicea, J., Sharma, A.M., Miller, T.M., Diamond, M.I., 2016. Tau Prion Strains Dictate Patterns of Cell Pathology, Progression Rate, and Regional Vulnerability In Vivo. *Neuron* 92, 796–812. <https://doi.org/10.1016/j.neuron.2016.09.055>



- Kaufman, S.K., Thomas, T.L., Del Tredici, K., Braak, H., Diamond, M.I., 2017. Characterization of tau prion seeding activity and strains from formaldehyde-fixed tissue. *Acta Neuropathol. Commun.* 5. <https://doi.org/10.1186/s40478-017-0442-8>
- Khoury, R., Ghossoub, E., 2019. Diagnostic biomarkers of Alzheimer's disease: A state-of-the-art review. *Biomark. Neuropsychiatry* 1, 100005. <https://doi.org/10.1016/j.bionps.2019.100005>
- Kilgore, M., Miller, C.A., Fass, D.M., Hennig, K.M., Haggarty, S.J., Sweatt, J.D., Rumbaugh, G., 2010. Inhibitors of class 1 histone deacetylases reverse contextual memory deficits in a mouse model of Alzheimer's disease. *Neuropsychopharmacol. Off. Publ. Am. Coll. Neuropsychopharmacol.* 35, 870–880. <https://doi.org/10.1038/npp.2009.197>
- Kimura, N., Nakamura, S., Goto, N., Narushima, E., Hara, I., Shichiri, S., Saitou, K., Nose, M., Hayashi, T., Kawamura, S., Yoshikawa, Y., 2001. Senile plaques in an aged western lowland gorilla. *Exp. Anim.* 50, 77–81. <https://doi.org/10.1538/expanim.50.77>
- Kimura, T., Whitcomb, D.J., Jo, J., Regan, P., Piers, T., Heo, S., Brown, C., Hashikawa, T., Murayama, M., Seok, H., Sotiropoulos, I., Kim, E., Collingridge, G.L., Takashima, A., Cho, K., 2014. Microtubule-associated protein tau is essential for long-term depression in the hippocampus. *Philos. Trans. R. Soc. B Biol. Sci.* 369, 20130144. <https://doi.org/10.1098/rstb.2013.0144>
- Kitazawa, M., Cheng, D., Tsukamoto, M.R., Koike, M.A., Wes, P.D., Vasilevko, V., Cribbs, D.H., LaFerla, F.M., 2011. Blocking IL-1 Signaling Rescues Cognition, Attenuates Tau Pathology, and Restores Neuronal  $\beta$ -Catenin Pathway Function in an Alzheimer's Disease Model. *J. Immunol.* 187, 6539–6549. <https://doi.org/10.4049/jimmunol.1100620>
- Kitazawa, M., Oddo, S., Yamasaki, T.R., Green, K.N., LaFerla, F.M., 2005. Lipopolysaccharide-Induced Inflammation Exacerbates Tau Pathology by a Cyclin-Dependent Kinase 5-Mediated Pathway in a Transgenic Model of Alzheimer's Disease. *J. Neurosci.* 25, 8843–8853. <https://doi.org/10.1523/JNEUROSCI.2868-05.2005>
- Kivipelto, M., Helkala, E.L., Laakso, M.P., Hänninen, T., Hallikainen, M., Alhainen, K., Soininen, H., Tuomilehto, J., Nissinen, A., 2001. Midlife vascular risk factors and Alzheimer's disease in later life: longitudinal, population based study. *BMJ* 322, 1447–1451.
- Knowles, R.B., Wyart, C., Buldyrev, S.V., Cruz, L., Urbanc, B., Hasselmo, M.E., Stanley, H.E., Hyman, B.T., 1999. Plaque-induced neurite abnormalities: implications for disruption of neural networks in Alzheimer's disease. *Proc. Natl. Acad. Sci. U. S. A.* 96, 5274–5279. <https://doi.org/10.1073/pnas.96.9.5274>
- Koffie, R.M., Meyer-Luehmann, M., Hashimoto, T., Adams, K.W., Mielke, M.L., Garcia-Alloza, M., Micheva, K.D., Smith, S.J., Kim, M.L., Lee, V.M., Hyman, B.T., Spire-Jones, T.L., 2009. Oligomeric amyloid beta associates with postsynaptic densities and correlates with excitatory synapse loss near senile plaques. *Proc. Natl. Acad. Sci. U. S. A.* 106, 4012–4017. <https://doi.org/10.1073/pnas.0811698106>
- Kollmer, M., Close, W., Funk, L., Rasmussen, J., Bsoul, A., Schierhorn, A., Schmidt, M., Sigurdson, C.J., Jucker, M., Fändrich, M., 2019. Cryo-EM structure and polymorphism of A $\beta$  amyloid fibrils purified from Alzheimer's brain tissue. *Nat. Commun.* 10, 4760. <https://doi.org/10.1038/s41467-019-12683-8>
- Kovacs, G.G., Lutz, M.I., Ricken, G., Ströbel, T., Höftberger, R., Preusser, M., Regelsberger, G., Hönigschnabl, S., Reiner, A., Fischer, P., Budka, H., Hainfellner, J.A., 2016. Dura mater is a potential source of A $\beta$  seeds. *Acta Neuropathol. (Berl.)* 131, 911–923. <https://doi.org/10.1007/s00401-016-1565-x>
- Krabbe, G., Halle, A., Matyash, V., Rinnenthal, J.L., Eom, G.D., Bernhardt, U., Miller, K.R., Prokop, S., Kettenmann, H., Heppner, F.L., 2013. Functional Impairment of Microglia Coincides with Beta-Amyloid Deposition in Mice with Alzheimer-Like Pathology. *PLoS ONE* 8. <https://doi.org/10.1371/journal.pone.0060921>
- Kraska, A., Dorieux, O., Picq, J.-L., Petit, F., Bourrin, E., Chenu, E., Volk, A., Perret, M., Hantraye, P., Mestre-Frances, N., Aujard, F., Dhenain, M., 2011. Age-associated cerebral atrophy in mouse lemur primates. *Neurobiol. Aging* 32, 894–906. <https://doi.org/10.1016/j.neurobiolaging.2009.05.018>

- Kraus, A., Saijo, E., Metrick, M.A., Newell, K., Sigurdson, C.J., Zanusso, G., Ghetti, B., Caughey, B., 2019. Seeding selectivity and ultrasensitive detection of tau aggregate conformers of Alzheimer disease. *Acta Neuropathol. (Berl.)* 137, 585–598. <https://doi.org/10.1007/s00401-018-1947-3>
- Ksiazak-Reding, H., Liu, W.K., Yen, S.H., 1992. Phosphate analysis and dephosphorylation of modified tau associated with paired helical filaments. *Brain Res.* 597, 209–219. [https://doi.org/10.1016/0006-8993\(92\)91476-u](https://doi.org/10.1016/0006-8993(92)91476-u)
- Kulikova, A., Makarov, A., Kozin, S., 2015. Roles of zinc ions and structural polymorphism of  $\beta$ -amyloid in the development of Alzheimer's disease. *Mol. Biol.* 49, 217–230. <https://doi.org/10.1134/S0026893315020065>
- Kunkle, B.W., Grenier-Boley, B., Sims, R., Bis, J.C., Damotte, V., Naj, A.C., Boland, A., Vronskaya, M., van der Lee, S.J., Amlie-Wolf, A., Bellenguez, C., Frizatti, A., Chouraki, V., Martin, E.R., Sleegers, K., Badarinarayan, N., Jakobsdottir, J., Hamilton-Nelson, K.L., Moreno-Grau, S., Olasso, R., Raybould, R., Chen, Y., Kuzma, A.B., Hiltunen, M., Morgan, T., Ahmad, S., Vardarajan, B.N., Epelbaum, J., Hoffmann, P., Boada, M., Beecham, G.W., Garnier, J.-G., Harold, D., Fitzpatrick, A.L., Valladares, O., Moutet, M.-L., Gerrish, A., Smith, A.V., Qu, L., Bacq, D., Denning, N., Jian, X., Zhao, Y., Del Zompo, M., Fox, N.C., Choi, S.-H., Mateo, I., Hughes, J.T., Adams, H.H., Malamon, J., Sanchez-Garcia, F., Patel, Y., Brody, J.A., Dombroski, B.A., Naranjo, M.C.D., Daniilidou, M., Eiriksdottir, G., Mukherjee, S., Wallon, D., Uphill, J., Aspelund, T., Cantwell, L.B., Garzia, F., Galimberti, D., Hofer, E., Butkiewicz, M., Fin, B., Scarpini, E., Sarnowski, C., Bush, W.S., Meslage, S., Kornhuber, J., White, C.C., Song, Y., Barber, R.C., Engelborghs, S., Sordon, S., Vojnovic, D., Adams, P.M., Vandenberghe, R., Mayhaus, M., Cupples, L.A., Albert, M.S., De Deyn, P.P., Gu, W., Himali, J.J., Beekly, D., Squassina, A., Hartmann, A.M., Orellana, A., Blacker, D., Rodriguez-Rodriguez, E., Lovestone, S., Garcia, M.E., Doody, R.S., Munoz-Fernandez, C., Sussams, R., Lin, H., Fairchild, T.J., Benito, Y.A., Holmes, C., Karamujic-Comic, H., Frosch, M.P., Thonberg, H., Maier, W., Roshchupkin, G., Ghetti, B., Giedraitis, V., Kawalia, A., Li, S., Huebinger, R.M., Kilander, L., Moebus, S., Hernández, I., Kamboh, M.I., Brundin, R., Turton, J., Yang, Q., Katz, M.J., Concari, L., Lord, J., Beiser, A.S., Keene, C.D., Helisalmi, S., Kloszewska, I., Kukull, W.A., Koivisto, A.M., Lynch, A., Tarraga, L., Larson, E.B., Haapasalo, A., Lawlor, B., Mosley, T.H., Lipton, R.B., Solfrizzi, V., Gill, M., Longstreth, W.T., Montine, T.J., Frisardi, V., Diez-Fairen, M., Rivadeneira, F., Petersen, R.C., Deramecourt, V., Alvarez, I., Salani, F., Ciaramella, A., Boerwinkle, E., Reiman, E.M., Fievet, N., Rotter, J.I., Reisch, J.S., Hanon, O., Cupidi, C., Andre Uitterlinden, A.G., Royall, D.R., Dufouil, C., Maletta, R.G., de Rojas, I., Sano, M., Brice, A., Cecchetti, R., George-Hyslop, P.S., Ritchie, K., Tsolaki, M., Tsuang, D.W., Dubois, B., Craig, D., Wu, C.-K., Soininen, H., Avramidou, D., Albin, R.L., Fratiglioni, L., Germanou, A., Apostolova, L.G., Keller, L., Koutroumani, M., Arnold, S.E., Panza, F., Gkatzima, O., Asthana, S., Hannequin, D., Whitehead, P., Atwood, C.S., Caffarra, P., Hampel, H., Quintela, I., Carracedo, Á., Lannfelt, L., Rubinsztein, D.C., Barnes, L.L., Pasquier, F., Frölich, L., Barral, S., McGuinness, B., Beach, T.G., Johnston, J.A., Becker, J.T., Passmore, P., Bigio, E.H., Schott, J.M., Bird, T.D., Warren, J.D., Boeve, B.F., Lupton, M.K., Bowen, J.D., Proitsi, P., Boxer, A., Powell, J.F., Burke, J.R., Kauwe, J.S.K., Burns, J.M., Mancuso, M., Buxbaum, J.D., Bonuccelli, U., Cairns, N.J., McQuillin, A., Cao, C., Livingston, G., Carlson, C.S., Bass, N.J., Carlsson, C.M., Hardy, J., Carney, R.M., Bras, J., Carrasquillo, M.M., Guerreiro, R., Allen, M., Chui, H.C., Fisher, E., Masullo, C., Crocco, E.A., DeCarli, C., Bisceglia, G., Dick, M., Ma, L., Duara, R., Graff-Radford, N.R., Evans, D.A., Hodges, A., Faber, K.M., Scherer, M., Fallon, K.B., Riemenschneider, M., Fardo, D.W., Heun, R., Farlow, M.R., Kölsch, H., Ferris, S., Leber, M., Foroud, T.M., Heuser, I., Galasko, D.R., Giegling, I., Gearing, M., Hüll, M., Geschwind, D.H., Gilbert, J.R., Morris, J., Green, R.C., Mayo, K., Growdon, J.H., Feulner, T., Hamilton, R.L., Harrell, L.E., Drichel, D., Honig, L.S., Cushion, T.D., Huentelman, M.J., Hollingworth, P., Hulette, C.M., Hyman, B.T., Marshall, R., Jarvik, G.P., Meggy, A., Abner, E., Menzies, G.E., Jin, L.-W., Leonenko, G., Real, L.M., Jun, G.R., Baldwin, C.T., Grozeva, D., Karydas, A., Russo, G., Kaye, J.A., Kim, R., Jessen, F., Kowall, N.W., Vellas, B., Kramer, J.H., Vardy, E., LaFerla, F.M., Jöckel, K.-H., Lah, J.J., Dichgans, M., Leverenz, J.B., Mann, D., Levey, A.I., Pickering-Brown, S., Lieberman, A.P., Klopp, N., Lunetta, K.L., Wichmann, H.-E., Lyketsos,

- C.G., Morgan, K., Marson, D.C., Brown, K., Martiniuk, F., Medway, C., Mash, D.C., Nöthen, M.M., Masliah, E., Hooper, N.M., McCormick, W.C., Daniele, A., McCurry, S.M., Bayer, A., McDavid, A.N., Gallacher, J., McKee, A.C., Bussche, H. van den, Mesulam, M., Brayne, C., Miller, B.L., Riedel-Heller, S., Miller, C.A., Miller, J.W., Al-Chalabi, A., Morris, J.C., Shaw, C.E., Myers, A.J., Wiltfang, J., O'Bryant, S., Olichney, J.M., Alvarez, V., Parisi, J.E., Singleton, A.B., Paulson, H.L., Collinge, J., Perry, W.R., Mead, S., Peskind, E., Cribbs, D.H., Rossor, M., Pierce, A., Ryan, N.S., Poon, W.W., Nacmias, B., Potter, H., Sorbi, S., Quinn, J.F., Sacchinelli, E., Raj, A., Spalletta, G., Raskind, M., Caltagirone, C., Bossù, P., Orfei, M.D., Reisberg, B., Clarke, R., Reitz, C., Smith, A.D., Ringman, J.M., Warden, D., Roberson, E.D., Wilcock, G., Rogaeve, E., Bruni, A.C., Rosen, H.J., Gallo, M., Rosenberg, R.N., Ben-Shlomo, Y., Sager, M.A., Mecocci, P., Saykin, A.J., Pastor, P., Cuccaro, M.L., Vance, J.M., Schneider, J.A., Schneider, L.S., Slifer, S., Seeley, W.W., Smith, A.G., Sonnen, J.A., Spina, S., Stern, R.A., Swerdlow, R.H., Tang, M., Tanzi, R.E., Trojanowski, J.Q., Troncoso, J.C., Deerlin, V.M.V., Eldik, L.J.V., Vinters, H.V., Vonsattel, J.P., Weintraub, S., Welsh-Bohmer, K.A., Wilhelmsen, K.C., Williamson, J., Wingo, T.S., Woltjer, R.L., Wright, C.B., Yu, C.-E., Yu, L., Saba, Y., Pilotto, A., Bullido, M.J., Peters, O., Crane, P.K., Bennett, D., Bosco, P., Coto, E., Boccardi, V., Jager, P.L.D., Lleo, A., Warner, N., Lopez, O.L., Ingelsson, M., Deloukas, P., Cruchaga, C., Graff, C., Gwilliam, R., Fornage, M., Goate, A.M., Sanchez-Juan, P., Kehoe, P.G., Amin, N., Ertekin-Taner, N., Berr, C., Debette, S., Love, S., Launer, L.J., Younkin, S.G., Dartigues, J.-F., Corcoran, C., Ikram, M.A., Dickson, D.W., Nicolas, G., Campion, D., Tschanz, J., Schmidt, H., Hakonarson, H., Clarimon, J., Munger, R., Schmidt, R., Farrer, L.A., Broeckhoven, C.V., O'Donovan, M.C., DeStefano, A.L., Jones, L., Haines, J.L., Deleuze, J.-F., Owen, M.J., Gudnason, V., Mayeux, R., Escott-Price, V., Psaty, B.M., Ramirez, A., Wang, L.-S., Ruiz, A., Duijn, C.M. van, Holmans, P.A., Seshadri, S., Williams, J., Amouyel, P., Schellenberg, G.D., Lambert, J.-C., Pericak-Vance, M.A., 2019. Genetic meta-analysis of diagnosed Alzheimer's disease identifies new risk loci and implicates A $\beta$ , tau, immunity and lipid processing. *Nat. Genet.* 51, 414–430. <https://doi.org/10.1038/s41588-019-0358-2>
- Lacor, P.N., Buniel, M.C., Furlow, P.W., Clemente, A.S., Velasco, P.T., Wood, M., Viola, K.L., Klein, W.L., 2007. Abeta oligomer-induced aberrations in synapse composition, shape, and density provide a molecular basis for loss of connectivity in Alzheimer's disease. *J. Neurosci. Off. J. Soc. Neurosci.* 27, 796–807. <https://doi.org/10.1523/JNEUROSCI.3501-06.2007>
- Lacreuse, A., Russell, J.L., Hopkins, W.D., Herndon, J.G., 2014. Cognitive and motor aging in female chimpanzees. *Neurobiol. Aging* 35, 623–632. <https://doi.org/10.1016/j.neurobiolaging.2013.08.036>
- Lai, Z.C., Moss, M.B., Killiany, R.J., Rosene, D.L., Herndon, J.G., 1995. Executive system dysfunction in the aged monkey: spatial and object reversal learning. *Neurobiol. Aging* 16, 947–954. [https://doi.org/10.1016/0197-4580\(95\)02014-4](https://doi.org/10.1016/0197-4580(95)02014-4)
- Lam, B., Masellis, M., Freedman, M., Stuss, D.T., Black, S.E., 2013. Clinical, imaging, and pathological heterogeneity of the Alzheimer's disease syndrome. *Alzheimers Res. Ther.* 5, 1. <https://doi.org/10.1186/alzrt155>
- Landau, S.M., Marks, S.M., Mormino, E.C., Rabinovici, G.D., Oh, H., O'Neil, J.P., Wilson, R.S., Jagust, W.J., 2012. Association of lifetime cognitive engagement and low  $\beta$ -amyloid deposition. *Arch. Neurol.* 69, 623–629. <https://doi.org/10.1001/archneurol.2011.2748>
- Lane, C.A., Hardy, J., Schott, J.M., 2018. Alzheimer's disease. *Eur. J. Neurol.* 25, 59–70. <https://doi.org/10.1111/ene.13439>
- Langer, F., Eisele, Y.S., Fritschi, S.K., Staufenbiel, M., Walker, L.C., Jucker, M., 2011. Soluble A $\beta$  seeds are potent inducers of cerebral  $\beta$ -amyloid deposition. *J. Neurosci. Off. J. Soc. Neurosci.* 31, 14488–14495. <https://doi.org/10.1523/JNEUROSCI.3088-11.2011>
- Languille, S., Blanc, S., Blin, O., Canale, C.I., Dal-Pan, A., Devau, G., Dhenain, M., Dorieux, O., Epelbaum, J., Gomez, D., Hardy, I., Henry, P.-Y., Irving, E.A., Marchal, J., Mestre-Francés, N., Perret, M., Picq, J.-L., Pifferi, F., Rahman, A., Schenker, E., Terrien, J., Théry, M., Verdier, J.-M., Aujard, F., 2012. The grey mouse lemur: A non-human primate model for ageing studies. *Ageing Res. Rev.* 11, 150–162. <https://doi.org/10.1016/j.arr.2011.07.001>

- Larson, M., Sherman, M.A., Amar, F., Nuvolone, M., Schneider, J.A., Bennett, D.A., Aguzzi, A., Lesné, S.E., 2012. The complex PrP(c)-Fyn couples human oligomeric A $\beta$  with pathological tau changes in Alzheimer's disease. *J. Neurosci. Off. J. Soc. Neurosci.* 32, 16857–16871a. <https://doi.org/10.1523/JNEUROSCI.1858-12.2012>
- Lasagna-Reeves, C.A., Castillo-Carranza, D.L., Sengupta, U., Clos, A.L., Jackson, G.R., Kaye, R., 2011. Tau oligomers impair memory and induce synaptic and mitochondrial dysfunction in wild-type mice. *Mol. Neurodegener.* 6, 39. <https://doi.org/10.1186/1750-1326-6-39>
- Lasagna-Reeves, C.A., Castillo-Carranza, D.L., Sengupta, U., Guerrero-Munoz, M.J., Kiritoshi, T., Neugebauer, V., Jackson, G.R., Kaye, R., 2012a. Alzheimer brain-derived tau oligomers propagate pathology from endogenous tau. *Sci. Rep.* 2, 700. <https://doi.org/10.1038/srep00700>
- Lasagna-Reeves, C.A., Castillo-Carranza, D.L., Sengupta, U., Sarmiento, J., Troncoso, J., Jackson, G.R., Kaye, R., 2012b. Identification of oligomers at early stages of tau aggregation in Alzheimer's disease. *FASEB J. Off. Publ. Fed. Am. Soc. Exp. Biol.* 26, 1946–1959. <https://doi.org/10.1096/fj.11-199851>
- Laurén, J., Gimbel, D.A., Nygaard, H.B., Gilbert, J.W., Strittmatter, S.M., 2009. Cellular Prion Protein Mediates Impairment of Synaptic Plasticity by Amyloid- $\beta$  Oligomers. *Nature* 457, 1128–1132. <https://doi.org/10.1038/nature07761>
- Le Gros Clark, W.E., 1931. 23. The Brain of *Microcebus murinus*. *Proc. Zool. Soc. Lond.* 101, 463–486. <https://doi.org/10.1111/j.1096-3642.1931.tb01023.x>
- Lee, S.-H., Meilandt, W.J., Xie, L., Gandham, V.D., Ngu, H., Barck, K.H., Rezzonico, M.G., Imperio, J., Lalehzadeh, G., Huntley, M.A., Stark, K.L., Foreman, O., Carano, R.A.D., Friedman, B.A., Sheng, M., Easton, A., Bohlen, C.J., Hansen, D.V., 2021. Trem2 restrains the enhancement of tau accumulation and neurodegeneration by  $\beta$ -amyloid pathology. *Neuron*. <https://doi.org/10.1016/j.neuron.2021.02.010>
- Legreneur, P., Thévenet, F.-R., Libourel, P.-A., Monteil, K.M., Montuelle, S., Pouydebat, E., Bels, V., 2010. Hindlimb interarticular coordinations in *Microcebus murinus* in maximal leaping. *J. Exp. Biol.* 213, 1320–1327. <https://doi.org/10.1242/jeb.041079>
- Lehmann, M., Ghosh, P.M., Madison, C., Laforce, R., Corbetta-Rastelli, C., Weiner, M.W., Greicius, M.D., Seeley, W.W., Gorno-Tempini, M.L., Rosen, H.J., Miller, B.L., Jagust, W.J., Rabinovici, G.D., 2013. Diverging patterns of amyloid deposition and hypometabolism in clinical variants of probable Alzheimer's disease. *Brain J. Neurol.* 136, 844–858. <https://doi.org/10.1093/brain/aws327>
- Leissring, M.A., Farris, W., Chang, A.Y., Walsh, D.M., Wu, X., Sun, X., Frosch, M.P., Selkoe, D.J., 2003. Enhanced Proteolysis of  $\beta$ -Amyloid in APP Transgenic Mice Prevents Plaque Formation, Secondary Pathology, and Premature Death. *Neuron* 40, 1087–1093. [https://doi.org/10.1016/S0896-6273\(03\)00787-6](https://doi.org/10.1016/S0896-6273(03)00787-6)
- Leroy, K., Ando, K., Laporte, V., Dedecker, R., Suain, V., Authélet, M., Héraud, C., Pierrot, N., Yilmaz, Z., Octave, J.-N., Brion, J.-P., 2012. Lack of tau proteins rescues neuronal cell death and decreases amyloidogenic processing of APP in APP/PS1 mice. *Am. J. Pathol.* 181, 1928–1940. <https://doi.org/10.1016/j.ajpath.2012.08.012>
- Lesné, S., Koh, M.T., Kotilinek, L., Kaye, R., Glabe, C.G., Yang, A., Gallagher, M., Ashe, K.H., 2006. A specific amyloid-beta protein assembly in the brain impairs memory. *Nature* 440, 352–357. <https://doi.org/10.1038/nature04533>
- Lesné, S.E., Sherman, M.A., Grant, M., Kuskowski, M., Schneider, J.A., Bennett, D.A., Ashe, K.H., 2013. Brain amyloid- $\beta$  oligomers in ageing and Alzheimer's disease. *Brain J. Neurol.* 136, 1383–1398. <https://doi.org/10.1093/brain/awt062>
- Leverenz, J.B., Fishel, M.A., Peskind, E.R., Montine, T.J., Nochlin, D., Steinbart, E., Raskind, M.A., Schellenberg, G.D., Bird, T.D., Tsuang, D., 2006. Lewy body pathology in familial Alzheimer disease: evidence for disease- and mutation-specific pathologic phenotype. *Arch. Neurol.* 63, 370–376. <https://doi.org/10.1001/archneur.63.3.370>

- Leyns, C.E.G., Gratuze, M., Narasimhan, S., Jain, N., Koscal, L.J., Jiang, H., Manis, M., Colonna, M., Lee, V.M.Y., Ulrich, J.D., Holtzman, D.M., 2019. TREM2 function impedes tau seeding in neuritic plaques. *Nat. Neurosci.* 22, 1217–1222. <https://doi.org/10.1038/s41593-019-0433-0>
- Leyns, C.E.G., Holtzman, D.M., 2017. Glial contributions to neurodegeneration in tauopathies. *Mol. Neurodegener.* 12, 50. <https://doi.org/10.1186/s13024-017-0192-x>
- Leyns, C.E.G., Ulrich, J.D., Finn, M.B., Stewart, F.R., Koscal, L.J., Serrano, J.R., Robinson, G.O., Anderson, E., Colonna, M., Holtzman, D.M., 2017. TREM2 deficiency attenuates neuroinflammation and protects against neurodegeneration in a mouse model of tauopathy. *Proc. Natl. Acad. Sci.* 114, 11524–11529. <https://doi.org/10.1073/pnas.1710311114>
- Leyton, C.E., Villemagne, V.L., Savage, S., Pike, K.E., Ballard, K.J., Piguet, O., Burrell, J.R., Rowe, C.C., Hodges, J.R., 2011. Subtypes of progressive aphasia: application of the International Consensus Criteria and validation using  $\beta$ -amyloid imaging. *Brain J. Neurol.* 134, 3030–3043. <https://doi.org/10.1093/brain/awr216>
- Li, L., Shi, R., Gu, J., Tung, Y.C., Zhou, Y., Zhou, D., Wu, R., Chu, D., Jin, N., Deng, K., Xu, J., Gong, C.-X., Iqbal, K., Liu, F., 2021. Alzheimer’s disease brain contains tau fractions with differential prion-like activities. *Acta Neuropathol. Commun.* 9. <https://doi.org/10.1186/s40478-021-01127-4>
- Li, X.-L., Hu, N., Tan, M.-S., Yu, J.-T., Tan, L., 2014. Behavioral and Psychological Symptoms in Alzheimer’s Disease. *BioMed Res. Int.* 2014, e927804. <https://doi.org/10.1155/2014/927804>
- Li, Y., Liu, L., Barger, S.W., Griffin, W.S.T., 2003. Interleukin-1 mediates pathological effects of microglia on tau phosphorylation and on synaptophysin synthesis in cortical neurons through a p38-MAPK pathway. *J. Neurosci. Off. J. Soc. Neurosci.* 23, 1605–1611.
- Lian, H., Litvinchuk, A., Chiang, A.C.-A., Aithmitti, N., Jankowsky, J.L., Zheng, H., 2016. Astrocyte-Microglia Cross Talk through Complement Activation Modulates Amyloid Pathology in Mouse Models of Alzheimer’s Disease. *J. Neurosci. Off. J. Soc. Neurosci.* 36, 577–589. <https://doi.org/10.1523/JNEUROSCI.2117-15.2016>
- Liddel, S.A., Guttenplan, K.A., Clarke, L.E., Bennett, F.C., Bohlen, C.J., Schirmer, L., Bennett, M.L., Münch, A.E., Chung, W.-S., Peterson, T.C., Wilton, D.K., Frouin, A., Napier, B.A., Panicker, N., Kumar, M., Buckwalter, M.S., Rowitch, D.H., Dawson, V.L., Dawson, T.M., Stevens, B., Barres, B.A., 2017. Neurotoxic reactive astrocytes are induced by activated microglia. *Nature* 541, 481–487. <https://doi.org/10.1038/nature21029>
- Lim, A., Tsuang, D., Kukull, W., Nochlin, D., Leverenz, J., McCormick, W., Bowen, J., Teri, L., Thompson, J., Peskind, E.R., Raskind, M., Larson, E.B., 1999. Clinico-neuropathological correlation of Alzheimer’s disease in a community-based case series. *J. Am. Geriatr. Soc.* 47, 564–569. <https://doi.org/10.1111/j.1532-5415.1999.tb02571.x>
- Litvinchuk, A., Wan, Y.-W., Swartzlander, D.B., Chen, F., Cole, A., Propson, N.E., Wang, Q., Zhang, B., Liu, Z., Zheng, H., 2018. Complement C3aR Inactivation Attenuates Tau Pathology and Reverses an Immune Network Deregulated in Tauopathy Models and Alzheimer’s Disease. *Neuron* 100, 1337–1353.e5. <https://doi.org/10.1016/j.neuron.2018.10.031>
- Liu, C.-C., Zhao, N., Fu, Y., Wang, N., Linares, C., Tsai, C.-W., Bu, G., 2017. ApoE4 Accelerates Early Seeding of Amyloid Pathology. *Neuron* 96, 1024–1032.e3. <https://doi.org/10.1016/j.neuron.2017.11.013>
- Liu, F., Li, B., Tung, E.-J., Grundke-Iqbal, I., Iqbal, K., Gong, C.-X., 2007. Site-specific effects of tau phosphorylation on its microtubule assembly activity and self-aggregation. *Eur. J. Neurosci.* 26, 3429–3436. <https://doi.org/10.1111/j.1460-9568.2007.05955.x>
- Liu, L., Drouet, V., Wu, J.W., Witter, M.P., Small, S.A., Clelland, C., Duff, K., 2012. Trans-synaptic spread of tau pathology in vivo. *PLoS One* 7, e31302. <https://doi.org/10.1371/journal.pone.0031302>
- Long, J.M., Holtzman, D.M., 2019. Alzheimer Disease: An Update on Pathobiology and Treatment Strategies. *Cell* 179, 312–339. <https://doi.org/10.1016/j.cell.2019.09.001>
- Lu, J.-X., Qiang, W., Yau, W.-M., Schwieters, C.D., Meredith, S.C., Tycko, R., 2013. Molecular structure of  $\beta$ -amyloid fibrils in Alzheimer’s disease brain tissue. *Cell* 154. <https://doi.org/10.1016/j.cell.2013.08.035>

- Lučiūnaitė, A., McManus, R.M., Jankunec, M., Rácz, I., Dansokho, C., Dalgėdienė, I., Schwartz, S., Brosseron, F., Heneka, M.T., 2019. Soluble A $\beta$  oligomers and protofibrils induce NLRP3 inflammasome activation in microglia. *J. Neurochem.* e14945. <https://doi.org/10.1111/jnc.14945>
- Lue, L.-F., Schmitz, C.T., Serrano, G., Sue, L.I., Beach, T.G., Walker, D.G., 2015. TREM2 Protein Expression Changes Correlate with Alzheimer's Disease Neurodegenerative Pathologies in Post-Mortem Temporal Cortices. *Brain Pathol. Zurich Switz.* 25, 469–480. <https://doi.org/10.1111/bpa.12190>
- Luo, W., Liu, W., Hu, X., Hanna, M., Caravaca, A., Paul, S.M., 2015. Microglial internalization and degradation of pathological tau is enhanced by an anti-tau monoclonal antibody. *Sci. Rep.* 5, 11161. <https://doi.org/10.1038/srep11161>
- Lutermann, H., Schmelting, B., Radespiel, U., Ehresmann, P., Zimmermann, E., 2006. The role of survival for the evolution of female philopatry in a solitary forager, the grey mouse lemur (*Microcebus murinus*). *Proc. Biol. Sci.* 273, 2527–2533. <https://doi.org/10.1098/rspb.2006.3603>
- Lyons, D.M., Yang, C., Eliez, S., Reiss, A.L., Schatzberg, A.F., 2004. Cognitive Correlates of White Matter Growth and Stress Hormones in Female Squirrel Monkey Adults. *J. Neurosci.* 24, 3655–3662. <https://doi.org/10.1523/JNEUROSCI.0324-04.2004>
- Maclean, C.J., Baker, H.F., Ridley, R.M., Mori, H., 2000. Naturally occurring and experimentally induced beta-amyloid deposits in the brains of marmosets (*Callithrix jacchus*). *J. Neural Transm. Vienna Austria* 1996 107, 799–814. <https://doi.org/10.1007/s007020070060>
- Magaki, S., Tang, Z., Tung, S., Williams, C.K., Lo, D., Yong, W.H., Khanlou, N., Vinters, H.V., 2018. The effects of cerebral amyloid angiopathy on integrity of the blood-brain barrier. *Neurobiol. Aging* 70, 70–77. <https://doi.org/10.1016/j.neurobiolaging.2018.06.004>
- Mairet-Coello, G., Courchet, J., Pieraut, S., Courchet, V., Maximov, A., Polleux, F., 2013. The CAMKK2-AMPK Kinase Pathway Mediates the Synaptotoxic Effects of A $\beta$  Oligomers through Tau Phosphorylation. *Neuron* 78, 94–108. <https://doi.org/10.1016/j.neuron.2013.02.003>
- Malcolm, J.C., Breuillaud, L., Do Carmo, S., Hall, H., Welikovitsh, L.A., Macdonald, J.A., Goedert, M., Cuelllo, A.C., 2019. Neuropathological changes and cognitive deficits in rats transgenic for human mutant tau recapitulate human tauopathy. *Neurobiol. Dis.* 127, 323–338. <https://doi.org/10.1016/j.nbd.2019.03.018>
- Maloney, J.A., Bainbridge, T., Gustafson, A., Zhang, S., Kyauk, R., Steiner, P., van der Brug, M., Liu, Y., Ernst, J.A., Watts, R.J., Atwal, J.K., 2014. Molecular mechanisms of Alzheimer disease protection by the A673T allele of amyloid precursor protein. *J. Biol. Chem.* 289, 30990–31000. <https://doi.org/10.1074/jbc.M114.589069>
- Manczak, M., Anekonda, T.S., Henson, E., Park, B.S., Quinn, J., Reddy, P.H., 2006. Mitochondria are a direct site of A beta accumulation in Alzheimer's disease neurons: implications for free radical generation and oxidative damage in disease progression. *Hum. Mol. Genet.* 15, 1437–1449. <https://doi.org/10.1093/hmg/ddl066>
- Mann, U.M., Mohr, E., Gearing, M., Chase, T.N., 1992. Heterogeneity in Alzheimer's disease: progression rate segregated by distinct neuropsychological and cerebral metabolic profiles. *J. Neurol. Neurosurg. Psychiatry* 55, 956–959. <https://doi.org/10.1136/jnnp.55.10.956>
- Marcus, C., Mena, E., Subramaniam, R.M., 2014. Brain PET in the diagnosis of Alzheimer's disease. *Clin. Nucl. Med.* 39, e413–e426. <https://doi.org/10.1097/RLU.0000000000000547>
- Márquez, M., Serafin, A., Fernández-Bellon, H., Serrat, S., Ferrer-Admetlla, A., Bertranpetit, J., Ferrer, I., Pumarola, M., 2008. Neuropathologic findings in an aged albino gorilla. *Vet. Pathol.* 45, 531–537. <https://doi.org/10.1354/vp.45-4-531>
- Marra, C., Silveri, M.C., Gainotti, G., 2000. Predictors of Cognitive Decline in the Early Stage of Probable Alzheimer's Disease. *Dement. Geriatr. Cogn. Disord.* 11, 212–218. <https://doi.org/10.1159/000017239>
- Martínez, G., Vernooij, R.W., Padilla, P.F., Zamora, J., Flicker, L., Cosp, X.B., 2017a. 18F PET with florbetaben for the early diagnosis of Alzheimer's disease dementia and other dementias in

- people with mild cognitive impairment (MCI). *Cochrane Database Syst. Rev.* <https://doi.org/10.1002/14651858.CD012883>
- Martínez, G., Vernooij, R.W., Padilla, P.F., Zamora, J., Flicker, L., Cosp, X.B., 2017b. 18F PET with flutemetamol for the early diagnosis of Alzheimer's disease dementia and other dementias in people with mild cognitive impairment (MCI). *Cochrane Database Syst. Rev.* <https://doi.org/10.1002/14651858.CD012884>
- Masliah, E., Sisk, A., Mallory, M., Mucke, L., Schenk, D., Games, D., 1996. Comparison of neurodegenerative pathology in transgenic mice overexpressing V717F beta-amyloid precursor protein and Alzheimer's disease. *J. Neurosci. Off. J. Soc. Neurosci.* 16, 5795–5811.
- Masters, C.L., Selkoe, D.J., 2012. Biochemistry of Amyloid  $\beta$ -Protein and Amyloid Deposits in Alzheimer Disease. *Cold Spring Harb. Perspect. Med.* 2. <https://doi.org/10.1101/cshperspect.a006262>
- Matias, I., Morgado, J., Gomes, F.C.A., 2019. Astrocyte Heterogeneity: Impact to Brain Aging and Disease. *Front. Aging Neurosci.* 11. <https://doi.org/10.3389/fnagi.2019.00059>
- Matsuda, H., 2012. Voxel-based Morphometry of Brain MRI in Normal Aging and Alzheimer's Disease. *Aging Dis.* 4, 29–37.
- Mattsson, N., Cullen, N.C., Andreasson, U., Zetterberg, H., Blennow, K., 2019. Association Between Longitudinal Plasma Neurofilament Light and Neurodegeneration in Patients With Alzheimer Disease. *JAMA Neurol.* 76, 791–799. <https://doi.org/10.1001/jamaneurol.2019.0765>
- Mattsson, N., Zetterberg, H., Janelidze, S., Insel, P.S., Andreasson, U., Stomrud, E., Palmqvist, S., Baker, D., Tan Hehir, C.A., Jeromin, A., Hanlon, D., Song, L., Shaw, L.M., Trojanowski, J.Q., Weiner, M.W., Hansson, O., Blennow, K., ADNI Investigators, 2016. Plasma tau in Alzheimer disease. *Neurology* 87, 1827–1835. <https://doi.org/10.1212/WNL.0000000000003246>
- Mayeux, R., 2003. Epidemiology of neurodegeneration. *Annu. Rev. Neurosci.* 26, 81–104. <https://doi.org/10.1146/annurev.neuro.26.043002.094919>
- Mayeux, R., Stern, Y., 2012. Epidemiology of Alzheimer Disease. *Cold Spring Harb. Perspect. Med.* 2. <https://doi.org/10.1101/cshperspect.a006239>
- McDonald, R.J., King, A.L., Wasiak, T.D., Zelinski, E.L., Hong, N.S., 2007. A complex associative structure formed in the mammalian brain during acquisition of a simple visual discrimination task: dorsolateral striatum, amygdala, and hippocampus. *Hippocampus* 17, 759–774. <https://doi.org/10.1002/hipo.20333>
- McInnes, J., Wierda, K., Snellinx, A., Bounti, L., Wang, Y.-C., Stancu, I.-C., Apóstolo, N., Gevaert, K., Dewachter, I., Spires-Jones, T.L., De Strooper, B., De Wit, J., Zhou, L., Verstreken, P., 2018. Synaptogyrin-3 Mediates Presynaptic Dysfunction Induced by Tau. *Neuron* 97, 823–835.e8. <https://doi.org/10.1016/j.neuron.2018.01.022>
- McKhann, G.M., Knopman, D.S., Chertkow, H., Hyman, B.T., Jack, C.R., Kawas, C.H., Klunk, W.E., Koroshetz, W.J., Manly, J.J., Mayeux, R., Mohs, R.C., Morris, J.C., Rossor, M.N., Scheltens, P., Carrillo, M.C., Thies, B., Weintraub, S., Phelps, C.H., 2011. The diagnosis of dementia due to Alzheimer's disease: recommendations from the National Institute on Aging-Alzheimer's Association workgroups on diagnostic guidelines for Alzheimer's disease. *Alzheimers Dement. J. Alzheimers Assoc.* 7, 263–269. <https://doi.org/10.1016/j.jalz.2011.03.005>
- McLean, C.A., Cherny, R.A., Fraser, F.W., Fuller, S.J., Smith, M.J., Beyreuther, K., Bush, A.I., Masters, C.L., 1999. Soluble pool of Abeta amyloid as a determinant of severity of neurodegeneration in Alzheimer's disease. *Ann. Neurol.* 46, 860–866.
- Meng, X., Li, T., Wang, X., Lv, X., Sun, Z., Zhang, J., Su, F., Kang, S., Kim, S., An, S.S.A., Yu, X., Zhang, C., Wang, H., 2019. Association between increased levels of amyloid- $\beta$  oligomers in plasma and episodic memory loss in Alzheimer's disease. *Alzheimers Res. Ther.* 11, 89. <https://doi.org/10.1186/s13195-019-0535-7>
- Merezhko, M., Brunello, C.A., Yan, X., Vihinen, H., Jokitalo, E., Uronen, R.-L., Huttunen, H.J., 2018. Secretion of Tau via an Unconventional Non-vesicular Mechanism. *Cell Rep.* 25, 2027–2035.e4. <https://doi.org/10.1016/j.celrep.2018.10.078>
- Mestre-Francés, N., Keller, E., Calenda, A., Barelli, H., Checler, F., Bons, N., 2000. Immunohistochemical analysis of cerebral cortical and vascular lesions in the primate *Microcebus murinus* reveal

- distinct amyloid beta1-42 and beta1-40 immunoreactivity profiles. *Neurobiol. Dis.* 7, 1–8. <https://doi.org/10.1006/nbdi.1999.0270>
- Metaxas, A., Thygesen, C., Kempf, S.J., Anzalone, M., Vaitheeswaran, R., Petersen, S., Landau, A.M., Audrain, H., Teeling, J.L., Darvesh, S., Brooks, D.J., Larsen, M.R., Finsen, B., 2019. Ageing and amyloidosis underlie the molecular and pathological alterations of tau in a mouse model of familial Alzheimer’s disease. *Sci. Rep.* 9, 15758. <https://doi.org/10.1038/s41598-019-52357-5>
- Meyer-Luehmann, M., Coomaraswamy, J., Bolmont, T., Kaeser, S., Schaefer, C., Kilger, E., Neuenschwander, A., Abramowski, D., Frey, P., Jaton, A.L., Vigouret, J.-M., Paganetti, P., Walsh, D.M., Mathews, P.M., Ghiso, J., Staufenbiel, M., Walker, L.C., Jucker, M., 2006. Exogenous induction of cerebral beta-amyloidogenesis is governed by agent and host. *Science* 313, 1781–1784. <https://doi.org/10.1126/science.1131864>
- Mielke, M.M., Hagen, C.E., Xu, J., Chai, X., Vemuri, P., Lowe, V.J., Airey, D.C., Knopman, D.S., Roberts, R.O., Machulda, M.M., Jack, C.R., Petersen, R.C., Dage, J.L., 2018. Plasma phospho-tau181 increases with Alzheimer’s disease clinical severity and is associated with tau- and amyloid-positron emission tomography. *Alzheimers Dement. J. Alzheimers Assoc.* 14, 989–997. <https://doi.org/10.1016/j.jalz.2018.02.013>
- Min, S.-W., Cho, S.-H., Zhou, Y., Schroeder, S., Haroutunian, V., Seeley, W.W., Huang, E.J., Shen, Y., Masliah, E., Mukherjee, C., Meyers, D., Cole, P.A., Ott, M., Gan, L., 2010. Acetylation of tau inhibits its degradation and contributes to tauopathy. *Neuron* 67, 953–966. <https://doi.org/10.1016/j.neuron.2010.08.044>
- Mirra, S.S., Heyman, A., McKeel, D., Sumi, S.M., Crain, B.J., Brownlee, L.M., Vogel, F.S., Hughes, J.P., van Belle, G., Berg, L., 1991. The Consortium to Establish a Registry for Alzheimer’s Disease (CERAD). Part II. Standardization of the neuropathologic assessment of Alzheimer’s disease. *Neurology* 41, 479–486. <https://doi.org/10.1212/wnl.41.4.479>
- Mirza, Z., Pillai, V.G., Kamal, M.A., 2014. Protein interactions between the C-terminus of A $\beta$ -peptide and phospholipase A2—a structure biology based approach to identify novel Alzheimer’s therapeutics. *CNS Neurol. Disord. Drug Targets* 13, 1224–1231. <https://doi.org/10.2174/1871527313666140917112248>
- Mitchell, T.W., Nissanov, J., Han, L.Y., Mufson, E.J., Schneider, J.A., Cochran, E.J., Bennett, D.A., Lee, V.M., Trojanowski, J.Q., Arnold, S.E., 2000. Novel method to quantify neurofibrillary threads in brains from elders with or without cognitive impairment. *J. Histochem. Cytochem. Off. J. Histochem. Soc.* 48, 1627–1638. <https://doi.org/10.1177/002215540004801206>
- Montine, T.J., Phelps, C.H., Beach, T.G., Bigio, E.H., Cairns, N.J., Dickson, D.W., Duyckaerts, C., Frosch, M.P., Masliah, E., Mirra, S.S., Nelson, P.T., Schneider, J.A., Thal, D.R., Trojanowski, J.Q., Vinters, H.V., Hyman, B.T., National Institute on Aging, Alzheimer’s Association, 2012. National Institute on Aging-Alzheimer’s Association guidelines for the neuropathologic assessment of Alzheimer’s disease: a practical approach. *Acta Neuropathol. (Berl.)* 123, 1–11. <https://doi.org/10.1007/s00401-011-0910-3>
- Moore, T.L., Killiany, R.J., Herndon, J.G., Rosene, D.L., Moss, M.B., 2006. Executive system dysfunction occurs as early as middle-age in the rhesus monkey. *Neurobiol. Aging* 27, 1484–1493. <https://doi.org/10.1016/j.neurobiolaging.2005.08.004>
- Morales, R., Bravo-Alegria, J., Duran-Aniotz, C., Soto, C., 2015. Titration of biologically active amyloid- $\beta$  seeds in a transgenic mouse model of Alzheimer’s disease. *Sci. Rep.* 5, 9349. <https://doi.org/10.1038/srep09349>
- Morales, R., Duran-Aniotz, C., Castilla, J., Estrada, L.D., Soto, C., 2012. De novo induction of amyloid- $\beta$  deposition in vivo. *Mol. Psychiatry* 17, 1347–1353. <https://doi.org/10.1038/mp.2011.120>
- Morales, R., Moreno-Gonzalez, I., Soto, C., 2013. Cross-seeding of misfolded proteins: implications for etiology and pathogenesis of protein misfolding diseases. *PLoS Pathog.* 9, e1003537. <https://doi.org/10.1371/journal.ppat.1003537>
- Moreno, H., Morfini, G., Buitrago, L., Ujlaki, G., Choi, S., Yu, E., Moreira, J.E., Avila, J., Brady, S.T., Pant, H., Sugimori, M., Llinás, R.R., 2016. Tau pathology-mediated presynaptic dysfunction. *Neuroscience* 325, 30–38. <https://doi.org/10.1016/j.neuroscience.2016.03.044>



- Mosher, K.I., Wyss-Coray, T., 2014. Microglial Dysfunction in Brain Aging and Alzheimer's Disease. *Biochem. Pharmacol.* 88, 594–604. <https://doi.org/10.1016/j.bcp.2014.01.008>
- Mroczo, B., Groblewska, M., Litman-Zawadzka, A., 2019. The Role of Protein Misfolding and Tau Oligomers (TauOs) in Alzheimer's Disease (AD). *Int. J. Mol. Sci.* 20. <https://doi.org/10.3390/ijms20194661>
- Mucke, L., Masliah, E., Yu, G.-Q., Mallory, M., Rockenstein, E.M., Tatsuno, G., Hu, K., Kholodenko, D., Johnson-Wood, K., McConlogue, L., 2000. High-Level Neuronal Expression of A $\beta$ 1–42 in Wild-Type Human Amyloid Protein Precursor Transgenic Mice: Synaptotoxicity without Plaque Formation. *J. Neurosci.* 20, 4050–4058. <https://doi.org/10.1523/JNEUROSCI.20-11-04050.2000>
- Mucke, L., Selkoe, D.J., 2012. Neurotoxicity of Amyloid  $\beta$ -Protein: Synaptic and Network Dysfunction. *Cold Spring Harb. Perspect. Med.* 2, a006338. <https://doi.org/10.1101/cshperspect.a006338>
- Mudher, A., Colin, M., Dujardin, S., Medina, M., Dewachter, I., Alavi Naini, S.M., Mandelkow, E.-M., Mandelkow, E., Buée, L., Goedert, M., Brion, J.-P., 2017. What is the evidence that tau pathology spreads through prion-like propagation? *Acta Neuropathol. Commun.* 5, 99. <https://doi.org/10.1186/s40478-017-0488-7>
- Mufson, E.J., Ward, S., Binder, L., 2014. Prefibrillar Tau Oligomers in MCI and Alzheimer Disease. *Neurodegener. Dis.* 13, 151–153. <https://doi.org/10.1159/000353687>
- Mukhin, V.N., Pavlov, K.I., Klimentko, V.M., 2017. Mechanisms of Neuron Loss in Alzheimer's Disease. *Neurosci. Behav. Physiol.* 47, 508–516. <https://doi.org/10.1007/s11055-017-0427-x>
- Mukrasch, M.D., Bibow, S., Korukottu, J., Jeganathan, S., Biernat, J., Griesinger, C., Mandelkow, E., Zweckstetter, M., 2009. Structural Polymorphism of 441-Residue Tau at Single Residue Resolution. *PLoS Biol.* 7. <https://doi.org/10.1371/journal.pbio.1000034>
- Muralidar, S., Ambi, S.V., Sekaran, S., Thirumalai, D., Palaniappan, B., 2020. Role of tau protein in Alzheimer's disease: The prime pathological player. *Int. J. Biol. Macromol.* 163, 1599–1617. <https://doi.org/10.1016/j.ijbiomac.2020.07.327>
- Murray, M., Lowe, V., Graff-Radford, N., Liesinger, A.M., Cannon, A., Przybelski, S., Rawal, B., Parisi, J., Petersen, R., Kantarci, K., Ross, O., Duara, R., Knopman, D., Jack, C., Dickson, D., 2015. Clinicopathologic and 11C-Pittsburgh compound B implications of Thal amyloid phase across the Alzheimer's disease spectrum. *undefined.*
- Murray, M.E., Graff-Radford, N.R., Ross, O.A., Petersen, R.C., Duara, R., Dickson, D.W., 2011. Neuropathologically defined subtypes of Alzheimer's disease with distinct clinical characteristics: A retrospective study. *Lancet Neurol.* 10, 785–796. [https://doi.org/10.1016/S1474-4422\(11\)70156-9](https://doi.org/10.1016/S1474-4422(11)70156-9)
- Na, H.K., Kang, D.R., Kim, S., Seo, S.W., Heilman, K.M., Noh, Y., Na, D.L., 2016. Malignant progression in parietal-dominant atrophy subtype of Alzheimer's disease occurs independent of onset age. *Neurobiol. Aging* 47, 149–156. <https://doi.org/10.1016/j.neurobiolaging.2016.08.001>
- Nakagawa, T., Zhu, H., Morishima, N., Li, E., Xu, J., Yankner, B.A., Yuan, J., 2000. Caspase-12 mediates endoplasmic-reticulum-specific apoptosis and cytotoxicity by amyloid- $\beta$ . *Nature* 403, 98–103. <https://doi.org/10.1038/47513>
- Nakamura, S., Nakayama, H., Goto, N., Ono, F., Sakakibara, I., Yoshikawa, Y., 1998. Histopathological studies of senile plaques and cerebral amyloidosis in cynomolgus monkeys. *J. Med. Primatol.* 27, 244–252. <https://doi.org/10.1111/j.1600-0684.1998.tb00244.x>
- Narasimhan, S., Guo, J.L., Changolkar, L., Stieber, A., McBride, J.D., Silva, L.V., He, Z., Zhang, B., Gathagan, R.J., Trojanowski, J.Q., Lee, V.M.Y., 2017. Pathological Tau Strains from Human Brains Recapitulate the Diversity of Tauopathies in Nontransgenic Mouse Brain. *J. Neurosci. Off. J. Soc. Neurosci.* 37, 11406–11423. <https://doi.org/10.1523/JNEUROSCI.1230-17.2017>
- Nath, S., Agholme, L., Kurudenkandy, F.R., Granseth, B., Marcusson, J., Hallbeck, M., 2012. Spreading of neurodegenerative pathology via neuron-to-neuron transmission of  $\beta$ -amyloid. *J. Neurosci. Off. J. Soc. Neurosci.* 32, 8767–8777. <https://doi.org/10.1523/JNEUROSCI.0615-12.2012>
- Nelson, P.T., Alafuzoff, I., Bigio, E.H., Bouras, C., Braak, H., Cairns, N.J., Castellani, R.J., Crain, B.J., Davies, P., Del Tredici, K., Duyckaerts, C., Frosch, M.P., Haroutunian, V., Hof, P.R., Hulette, C.M.,

- Hyman, B.T., Iwatsubo, T., Jellinger, K.A., Jicha, G.A., Kövari, E., Kukull, W.A., Leverenz, J.B., Love, S., Mackenzie, I.R., Mann, D.M., Masliah, E., McKee, A.C., Montine, T.J., Morris, J.C., Schneider, J.A., Sonnen, J.A., Thal, D.R., Trojanowski, J.Q., Troncoso, J.C., Wisniewski, T., Woltjer, R.L., Beach, T.G., 2012. Correlation of Alzheimer disease neuropathologic changes with cognitive status: a review of the literature. *J. Neuropathol. Exp. Neurol.* 71, 362–381. <https://doi.org/10.1097/NEN.0b013e31825018f7>
- Nortley, R., Korte, N., Izquierdo, P., Hirunpattarasilp, C., Mishra, A., Jaunmuktane, Z., Kyrargyri, V., Pfeiffer, T., Khennouf, L., Madry, C., Gong, H., Richard-Loendt, A., Huang, W., Saito, T., Saido, T.C., Brandner, S., Sethi, H., Attwell, D., 2019. Amyloid  $\beta$  oligomers constrict human capillaries in Alzheimer's disease via signaling to pericytes. *Science* 365. <https://doi.org/10.1126/science.aav9518>
- Oddo, S., Caccamo, A., Shepherd, J.D., Murphy, M.P., Golde, T.E., Kaye, R., Metherate, R., Mattson, M.P., Akbari, Y., LaFerla, F.M., 2003. Triple-transgenic model of Alzheimer's disease with plaques and tangles: intracellular Abeta and synaptic dysfunction. *Neuron* 39, 409–421. [https://doi.org/10.1016/s0896-6273\(03\)00434-3](https://doi.org/10.1016/s0896-6273(03)00434-3)
- Oikawa, N., Kimura, N., Yanagisawa, K., 2010. Alzheimer-type tau pathology in advanced aged nonhuman primate brains harboring substantial amyloid deposition. *Brain Res.* 1315, 137–149. <https://doi.org/10.1016/j.brainres.2009.12.005>
- Ollinger, K., Kagedal, K., Nath, S., 2019. Amyloid- $\beta$  induced membrane damage instigates tunnelling nanotubes and direct cell-to-cell transfer. *bioRxiv* 655340. <https://doi.org/10.1101/655340>
- Olsson, B., Lautner, R., Andreasson, U., Öhrfelt, A., Portelius, E., Bjerke, M., Hölttä, M., Rosén, C., Olsson, C., Strobel, G., Wu, E., Dakin, K., Petzold, M., Blennow, K., Zetterberg, H., 2016. CSF and blood biomarkers for the diagnosis of Alzheimer's disease: a systematic review and meta-analysis. *Lancet Neurol.* 15, 673–684. [https://doi.org/10.1016/S1474-4422\(16\)00070-3](https://doi.org/10.1016/S1474-4422(16)00070-3)
- Origlia, N., Bonadonna, C., Rosellini, A., Leznik, E., Arancio, O., Yan, S.S., Domenici, L., 2010. Microglial receptor for advanced glycation end product-dependent signal pathway drives beta-amyloid-induced synaptic depression and long-term depression impairment in entorhinal cortex. *J. Neurosci. Off. J. Soc. Neurosci.* 30, 11414–11425. <https://doi.org/10.1523/JNEUROSCI.2127-10.2010>
- Orre, M., Kamphuis, W., Osborn, L.M., Jansen, A.H.P., Kooijman, L., Bossers, K., Hol, E.M., 2014. Isolation of glia from Alzheimer's mice reveals inflammation and dysfunction. *Neurobiol. Aging* 35, 2746–2760. <https://doi.org/10.1016/j.neurobiolaging.2014.06.004>
- Ossenkoppele, R., Pijnenburg, Y.A.L., Perry, D.C., Cohn-Sheehy, B.I., Scheltens, N.M.E., Vogel, J.W., Kramer, J.H., van der Vlies, A.E., La Joie, R., Rosen, H.J., van der Flier, W.M., Grinberg, L.T., Rozemuller, A.J., Huang, E.J., van Berckel, B.N.M., Miller, B.L., Barkhof, F., Jagust, W.J., Scheltens, P., Seeley, W.W., Rabinovici, G.D., 2015. The behavioural/dysexecutive variant of Alzheimer's disease: clinical, neuroimaging and pathological features. *Brain J. Neurol.* 138, 2732–2749. <https://doi.org/10.1093/brain/awv191>
- Ossenkoppele, R., Schonhaut, D.R., Schöll, M., Lockhart, S.N., Ayakta, N., Baker, S.L., O'Neil, J.P., Janabi, M., Lazaris, A., Cantwell, A., Vogel, J., Santos, M., Miller, Z.A., Bettcher, B.M., Vessel, K.A., Kramer, J.H., Gorno-Tempini, M.L., Miller, B.L., Jagust, W.J., Rabinovici, G.D., 2016. Tau PET patterns mirror clinical and neuroanatomical variability in Alzheimer's disease. *Brain J. Neurol.* 139, 1551–1567. <https://doi.org/10.1093/brain/aww027>
- Ost, M., Nylén, K., Csajbok, L., Öhrfelt, A.O., Tullberg, M., Wikkelsö, C., Nellgård, P., Rosengren, L., Blennow, K., Nellgård, B., 2006. Initial CSF total tau correlates with 1-year outcome in patients with traumatic brain injury. *Neurology* 67, 1600–1604. <https://doi.org/10.1212/01.wnl.0000242732.06714.0f>
- Overk, C.R., Masliah, E., 2014. Pathogenesis of synaptic degeneration in Alzheimer's disease and Lewy body disease. *Biochem. Pharmacol.* 88, 508–516. <https://doi.org/10.1016/j.bcp.2014.01.015>
- Ovod, V., Ramsey, K.N., Mawuenyega, K.G., Bollinger, J.G., Hicks, T., Schneider, T., Sullivan, M., Paumier, K., Holtzman, D.M., Morris, J.C., Benzinger, T., Fagan, A.M., Patterson, B.W., Bateman, R.J., 2017. Amyloid  $\beta$  concentrations and stable isotope labeling kinetics of human

- plasma specific to central nervous system amyloidosis. *Alzheimers Dement.* 13, 841–849. <https://doi.org/10.1016/j.jalz.2017.06.2266>
- Païdassi, H., Tacnet-Delorme, P., Garlatti, V., Darnault, C., Ghebrehiwet, B., Gaboriaud, C., Arlaud, G.J., Frchet, P., 2008. C1q Binds Phosphatidylserine and Likely Acts as a Multiligand-Bridging Molecule in Apoptotic Cell Recognition. *J. Immunol.* 180, 2329–2338. <https://doi.org/10.4049/jimmunol.180.4.2329>
- Pallas-Bazarra, N., Jurado-Arjona, J., Navarrete, M., Esteban, J.A., Hernández, F., Ávila, J., Llorens-Martin, M., 2016. Novel function of Tau in regulating the effects of external stimuli on adult hippocampal neurogenesis. *EMBO J.* 35, 1417–1436. <https://doi.org/10.15252/embj.201593518>
- Palmer, M.S., Dryden, A.J., Hughes, J.T., Collinge, J., 1991. Homozygous prion protein genotype predisposes to sporadic Creutzfeldt-Jakob disease. *Nature* 352, 340–342. <https://doi.org/10.1038/352340a0>
- Palmqvist, S., Insel, P.S., Stomrud, E., Janelidze, S., Zetterberg, H., Brix, B., Eichenlaub, U., Dage, J.L., Chai, X., Blennow, K., Mattsson, N., Hansson, O., 2019. Cerebrospinal fluid and plasma biomarker trajectories with increasing amyloid deposition in Alzheimer’s disease. *EMBO Mol. Med.* 11. <https://doi.org/10.15252/emmm.201911170>
- Palmqvist, S., Schöll, M., Strandberg, O., Mattsson, N., Stomrud, E., Zetterberg, H., Blennow, K., Landau, S., Jagust, W., Hansson, O., 2017. Earliest accumulation of  $\beta$ -amyloid occurs within the default-mode network and concurrently affects brain connectivity. *Nat. Commun.* 8, 1214. <https://doi.org/10.1038/s41467-017-01150-x>
- Pan, K.M., Baldwin, M., Nguyen, J., Gasset, M., Serban, A., Groth, D., Mehlhorn, I., Huang, Z., Fletterick, R.J., Cohen, F.E., 1993. Conversion of alpha-helices into beta-sheets features in the formation of the scrapie prion proteins. *Proc. Natl. Acad. Sci. U. S. A.* 90, 10962–10966.
- Park, J., Jang, M., Chang, S., 2013. Deleterious effects of soluble amyloid- $\beta$  oligomers on multiple steps of synaptic vesicle trafficking. *Neurobiol. Dis.* 55, 129–139. <https://doi.org/10.1016/j.nbd.2013.03.004>
- Parkhurst, C.N., Yang, G., Ninan, I., Savas, J.N., Yates, J.R., Lafaille, J.J., Hempstead, B.L., Littman, D.R., Gan, W.-B., 2013. Microglia promote learning-dependent synapse formation through brain-derived neurotrophic factor. *Cell* 155, 1596–1609. <https://doi.org/10.1016/j.cell.2013.11.030>
- Pastor, P., Roe, C.M., Villegas, A., Bedoya, G., Chakraverty, S., García, G., Tirado, V., Norton, J., Ríos, S., Martínez, M., Kosik, K.S., Lopera, F., Goate, A.M., 2003. Apolipoprotein Epsilon4 modifies Alzheimer’s disease onset in an E280A PS1 kindred. *Ann. Neurol.* 54, 163–169. <https://doi.org/10.1002/ana.10636>
- Paxinos, G., Franklin, K., 2012. Paxinos and Franklin’s the Mouse Brain in Stereotaxic Coordinates - 4th Edition. Academic Press.
- Pérez, M., Avila, J., Hernández, F., 2019. Propagation of Tau via Extracellular Vesicles. *Front. Neurosci.* 13, 698. <https://doi.org/10.3389/fnins.2019.00698>
- Perez-Nievas, B.G., Stein, T.D., Tai, H.-C., Dols-Icardo, O., Scotton, T.C., Barroeta-Espar, I., Fernandez-Carballo, L., de Munain, E.L., Perez, J., Marquie, M., Serrano-Pozo, A., Frosch, M.P., Lowe, V., Parisi, J.E., Petersen, R.C., Ikonomic, M.D., López, O.L., Klunk, W., Hyman, B.T., Gómez-Isla, T., 2013. Dissecting phenotypic traits linked to human resilience to Alzheimer’s pathology. *Brain* 136, 2510–2526. <https://doi.org/10.1093/brain/awt171>
- Perret, M., 2005. Relationship between urinary estrogen levels before conception and sex ratio at birth in a primate, the gray mouse lemur. *Hum. Reprod. Oxf. Engl.* 20, 1504–1510. <https://doi.org/10.1093/humrep/deh802>
- Perret, M., 1997. Change in photoperiodic cycle affects life span in a prosimian primate (*Microcebus murinus*). *J. Biol. Rhythms* 12, 136–145. <https://doi.org/10.1177/074873049701200205>
- Persson, K., Eldholm, R.S., Barca, M.L., Cavallin, L., Ferreira, D., Knapkog, A.-B., Selbæk, G., Brækhus, A., Saltvedt, I., Westman, E., Engedal, K., 2017. MRI-assessed atrophy subtypes in Alzheimer’s disease and the cognitive reserve hypothesis. *PloS One* 12, e0186595. <https://doi.org/10.1371/journal.pone.0186595>

- Peters, A., Kemper, T., 2012. A review of the structural alterations in the cerebral hemispheres of the aging rhesus monkey. *Neurobiol. Aging* 33, 2357–2372. <https://doi.org/10.1016/j.neurobiolaging.2011.11.015>
- Peters, A., Sethares, C., Luebke, J.I., 2008. Synapses are lost during aging in the primate prefrontal cortex. *Neuroscience* 152, 970–981. <https://doi.org/10.1016/j.neuroscience.2007.07.014>
- Petkova, A.T., Buntkowsky, G., Dyda, F., Leapman, R.D., Yau, W.-M., Tycko, R., 2004. Solid state NMR reveals a pH-dependent antiparallel beta-sheet registry in fibrils formed by a beta-amyloid peptide. *J. Mol. Biol.* 335, 247–260. <https://doi.org/10.1016/j.jmb.2003.10.044>
- Petkova, A.T., Leapman, R.D., Guo, Z., Yau, W.-M., Mark P. Mattson, Tycko, R., 2005. Self-Propagating, Molecular-Level Polymorphism in Alzheimer's  $\beta$ -Amyloid Fibrils. *Science* 307, 262–265. <https://doi.org/10.1126/science.1105850>
- Philippens, I.H., Ormel, P.R., Baarends, G., Johansson, M., Remarque, E.J., Doverskog, M., 2017. Acceleration of Amyloidosis by Inflammation in the Amyloid-Beta Marmoset Monkey Model of Alzheimer's Disease. *J. Alzheimers Dis.* 55, 101–113. <https://doi.org/10.3233/JAD-160673>
- Piacentini, R., Puma, D.D.L., Mainardi, M., Lazzarino, G., Tavazzi, B., Arancio, O., Grassi, C., 2017. Reduced gliotransmitter release from astrocytes mediates tau-induced synaptic dysfunction in cultured hippocampal neurons. *Glia* 65, 1302–1316. <https://doi.org/10.1002/glia.23163>
- Pickett, E.K., Koffie, R.M., Wegmann, S., Henstridge, C.M., Herrmann, A.G., Colom-Cadena, M., Lleo, A., Kay, K.R., Vaught, M., Soberman, R., Walsh, D.M., Hyman, B.T., Spires-Jones, T.L., 2016. Non-Fibrillar Oligomeric Amyloid- $\beta$  within Synapses. *J. Alzheimers Dis.* 53, 787–800. <https://doi.org/10.3233/JAD-160007>
- Picq, J.-L., Aujard, F., Volk, A., Dhenain, M., 2012. Age-related cerebral atrophy in nonhuman primates predicts cognitive impairments. *Neurobiol. Aging* 33, 1096–1109. <https://doi.org/10.1016/j.neurobiolaging.2010.09.009>
- Pifferi, F., Epelbaum, J., Aujard, F., 2019. Strengths and Weaknesses of the Gray Mouse Lemur (*Microcebus murinus*) as a Model for the Behavioral and Psychological Symptoms and Neuropsychiatric Symptoms of Dementia. *Front. Pharmacol.* 10, 1291. <https://doi.org/10.3389/fphar.2019.01291>
- Pillai, J.A., Appleby, B.S., Safar, J., Leverenz, J.B., 2018. Rapidly Progressive Alzheimer's Disease in Two Distinct Autopsy Cohorts. *J. Alzheimers Dis. JAD* 64, 973–980. <https://doi.org/10.3233/JAD-180155>
- Pini, L., Pievani, M., Bocchetta, M., Altomare, D., Bosco, P., Cavedo, E., Galluzzi, S., Marizzoni, M., Frisoni, G.B., 2016. Brain atrophy in Alzheimer's Disease and aging. *Ageing Res. Rev., Brain Imaging and Aging* 30, 25–48. <https://doi.org/10.1016/j.arr.2016.01.002>
- Pittman, A.M., Fung, H.-C., de Silva, R., 2006. Untangling the tau gene association with neurodegenerative disorders. *Hum. Mol. Genet.* 15, R188–R195. <https://doi.org/10.1093/hmg/ddl190>
- Poduri, A., Gearing, M., Rebeck, G.W., Mirra, S.S., Tigges, J., Hyman, B.T., 1994. Apolipoprotein E4 and beta amyloid in senile plaques and cerebral blood vessels of aged rhesus monkeys. *Am. J. Pathol.* 144, 1183–1187.
- Polydoro, M., Acker, C.M., Duff, K., Castillo, P.E., Davies, P., 2009. Age-dependent impairment of cognitive and synaptic function in the htau mouse model of tau pathology. *J. Neurosci. Off. J. Soc. Neurosci.* 29, 10741–10749. <https://doi.org/10.1523/JNEUROSCI.1065-09.2009>
- Pontecorvo, M.J., Devous, M.D., Kennedy, I., Navitsky, M., Lu, M., Galante, N., Salloway, S., Doraiswamy, P.M., Southeikal, S., Arora, A.K., McGeehan, A., Lim, N.C., Xiong, H., Trucchio, S.P., Joshi, A.D., Shcherbinin, S., Teske, B., Fleisher, A.S., Mintun, M.A., 2019. A multicentre longitudinal study of flortaucipir (18F) in normal ageing, mild cognitive impairment and Alzheimer's disease dementia. *Brain* 142, 1723–1735. <https://doi.org/10.1093/brain/awz090>
- Pooler, A.M., Noble, W., Hanger, D.P., 2014. A role for tau at the synapse in Alzheimer's disease pathogenesis. *Neuropharmacology* 76 Pt A, 1–8. <https://doi.org/10.1016/j.neuropharm.2013.09.018>

- Pooler, A.M., Phillips, E.C., Lau, D.H.W., Noble, W., Hanger, D.P., 2013. Physiological release of endogenous tau is stimulated by neuronal activity. *EMBO Rep.* 14, 389–394. <https://doi.org/10.1038/embor.2013.15>
- Pooler, A.M., Polydoro, M., Maury, E.A., Nicholls, S.B., Reddy, S.M., Wegmann, S., William, C., Saqran, L., Cagsal-Getkin, O., Pitstick, R., Beier, D.R., Carlson, G.A., Spires-Jones, T.L., Hyman, B.T., 2015. Amyloid accelerates tau propagation and toxicity in a model of early Alzheimer's disease. *Acta Neuropathol. Commun.* 3, 14. <https://doi.org/10.1186/s40478-015-0199-x>
- Portet, F., Scarmeas, N., Cosentino, S., Helzner, E.P., Stern, Y., 2009. Extrapyramidal signs before and after diagnosis of incident Alzheimer disease in a prospective population study. *Arch. Neurol.* 66, 1120–1126. <https://doi.org/10.1001/archneurol.2009.196>
- Posner, H., Curiel, R., Edgar, C., Hendrix, S., Liu, E., Loewenstein, D.A., Morrison, G., Shinobu, L., Wesnes, K., Harvey, P.D., 2017. Outcomes Assessment in Clinical Trials of Alzheimer's Disease and its Precursors: Readying for Short-term and Long-term Clinical Trial Needs. *Innov. Clin. Neurosci.* 14, 22–29.
- Pozueta, J., Lefort, R., Shelanski, M.L., 2013. Synaptic changes in Alzheimer's disease and its models. *Neuroscience, Dendritic Spine Plasticity in Brain Disorders* 251, 51–65. <https://doi.org/10.1016/j.neuroscience.2012.05.050>
- Preisiche, O., Schultz, S.A., Apel, A., Kuhle, J., Kaeser, S.A., Barro, C., Gräber, S., Kuder-Buletta, E., LaFougere, C., Laske, C., Vöglein, J., Levin, J., Masters, C.L., Martins, R., Schofield, P.R., Rossor, M.N., Graff-Radford, N.R., Salloway, S., Ghetti, B., Ringman, J.M., Noble, J.M., Chhatwal, J., Goate, A.M., Benzinger, T.L.S., Morris, J.C., Bateman, R.J., Wang, G., Fagan, A.M., McDade, E.M., Gordon, B.A., Jucker, M., Dominantly Inherited Alzheimer Network, 2019. Serum neurofilament dynamics predicts neurodegeneration and clinical progression in presymptomatic Alzheimer's disease. *Nat. Med.* 25, 277–283. <https://doi.org/10.1038/s41591-018-0304-3>
- Preusser, M., Ströbel, T., Gelpi, E., Eiler, M., Broessner, G., Schmutzhard, E., Budka, H., 2006. Alzheimer-type neuropathology in a 28 year old patient with iatrogenic Creutzfeldt-Jakob disease after dural grafting. *J. Neurol. Neurosurg. Psychiatry* 77, 413–416. <https://doi.org/10.1136/jnnp.2005.070805>
- Price, J.L., McKeel, D.W., Buckles, V.D., Roe, C.M., Xiong, C., Grundman, M., Hansen, L.A., Petersen, R.C., Parisi, J.E., Dickson, D.W., Smith, C.D., Davis, D.G., Schmitt, F.A., Markesbery, W.R., Kaye, J., Kurlan, R., Hulette, C., Kurland, B.F., Higdon, R., Kukull, W., Morris, J.C., 2009. Neuropathology of Nondemented Aging: Presumptive Evidence for Preclinical Alzheimer Disease. *Neurobiol. Aging* 30, 1026–1036. <https://doi.org/10.1016/j.neurobiolaging.2009.04.002>
- Price, J.L., Morris, J.C., 1999. Tangles and plaques in nondemented aging and “preclinical” Alzheimer's disease. *Ann. Neurol.* 45, 358–368.
- Prusiner, S.B., 1982. Novel proteinaceous infectious particles cause scrapie. *Science* 216, 136–144.
- Purro, S.A., Farrow, M.A., Linehan, J., Nazari, T., Thomas, D.X., Chen, Z., Mengel, D., Saito, T., Saido, T., Rudge, P., Brandner, S., Walsh, D.M., Collinge, J., 2018. Transmission of amyloid- $\beta$  protein pathology from cadaveric pituitary growth hormone. *Nature* 564, 415–419. <https://doi.org/10.1038/s41586-018-0790-y>
- Puzzo, D., Lee, L., Palmeri, A., Calabrese, G., Arancio, O., 2014. Behavioral assays with mouse models of Alzheimer's disease: practical considerations and guidelines. *Biochem. Pharmacol.* 88, 450–467. <https://doi.org/10.1016/j.bcp.2014.01.011>
- Qiang, W., Yau, W.-M., Lu, J.-X., Collinge, J., Tycko, R., 2017. Structural variation in amyloid- $\beta$  fibrils from Alzheimer's disease clinical subtypes. *Nature* 541, 217–221. <https://doi.org/10.1038/nature20814>
- Qiu, C., Kivipelto, M., Agüero-Torres, H., Winblad, B., Fratiglioni, L., 2004. Risk and protective effects of the APOE gene towards Alzheimer's disease in the Kungsholmen project: variation by age and sex. *J. Neurol. Neurosurg. Psychiatry* 75, 828–833. <https://doi.org/10.1136/jnnp.2003.021493>

- Rahimi, J., Kovacs, G.G., 2014. Prevalence of mixed pathologies in the aging brain. *Alzheimer's Res. Ther.* 6, 82. <https://doi.org/10.1186/s13195-014-0082-1>
- Rahman, A., Lamberty, Y., Schenker, E., Cella, M., Languille, S., Bordet, R., Richardson, J., Pifferi, F., Aujard, F., 2017. Effects of acute administration of donepezil or memantine on sleep-deprivation-induced spatial memory deficit in young and aged non-human primate grey mouse lemurs (*Microcebus murinus*). *PloS One* 12, e0184822. <https://doi.org/10.1371/journal.pone.0184822>
- Rajendran, L., Honsho, M., Zahn, T.R., Keller, P., Geiger, K.D., Verkade, P., Simons, K., 2006. Alzheimer's disease beta-amyloid peptides are released in association with exosomes. *Proc. Natl. Acad. Sci. U. S. A.* 103, 11172–11177. <https://doi.org/10.1073/pnas.0603838103>
- Rajendran, L., Paolicelli, R.C., 2018. Microglia-Mediated Synapse Loss in Alzheimer's Disease. *J. Neurosci. Off. J. Soc. Neurosci.* 38, 2911–2919. <https://doi.org/10.1523/JNEUROSCI.1136-17.2017>
- Ranganath, C., Ritchey, M., 2012. Two cortical systems for memory-guided behaviour. *Nat. Rev. Neurosci.* 13, 713–726. <https://doi.org/10.1038/nrn3338>
- Raposo, N., Planton, M., Siegfried, A., Calviere, L., Payoux, P., Albucher, J.-F., Viguier, A., Delisle, M.-B., Uro-Coste, E., Chollet, F., Bonneville, F., Olivot, J.-M., Pariente, J., 2020. Amyloid- $\beta$  transmission through cardiac surgery using cadaveric dura mater patch. *J. Neurol. Neurosurg. Psychiatry* 91, 440–441. <https://doi.org/10.1136/jnnp-2019-321927>
- Rasero, J., Alonso-Montes, C., Diez, I., Olabarrieta-Landa, L., Remaki, L., Escudero, I., Mateos, B., Bonifazi, P., Fernandez, M., Arango-Lasprilla, J.C., Stramaglia, S., Cortes, J.M., Alzheimer's Disease Neuroimaging Initiative, 2017. Group-Level Progressive Alterations in Brain Connectivity Patterns Revealed by Diffusion-Tensor Brain Networks across Severity Stages in Alzheimer's Disease. *Front. Aging Neurosci.* 9, 215. <https://doi.org/10.3389/fnagi.2017.00215>
- Rasmussen, J., Mahler, J., Beschoner, N., Kaeser, S.A., Häslner, L.M., Baumann, F., Nyström, S., Portelius, E., Blennow, K., Lashley, T., Fox, N.C., Sepulveda-Falla, D., Glatzel, M., Oblak, A.L., Ghetti, B., Nilsson, K.P.R., Hammarström, P., Staufenbiel, M., Walker, L.C., Jucker, M., 2017. Amyloid polymorphisms constitute distinct clouds of conformational variants in different etiological subtypes of Alzheimer's disease. *Proc. Natl. Acad. Sci. U. S. A.* 114, 13018–13023. <https://doi.org/10.1073/pnas.1713215114>
- Rasmussen, M.K., Mestre, H., Nedergaard, M., 2018. The glymphatic pathway in neurological disorders. *Lancet Neurol.* 17, 1016–1024. [https://doi.org/10.1016/S1474-4422\(18\)30318-1](https://doi.org/10.1016/S1474-4422(18)30318-1)
- Rf, R., As, F., M, G., J, D., Pm, L., Dc, A., J, D.-T., G, C., Dh, G., Jf, P., Tq, D., Wd, H., Tm, P., Lc, W., 2008. Tauopathy with paired helical filaments in an aged chimpanzee. *J. Comp. Neurol.* 509, 259–270. <https://doi.org/10.1002/cne.21744>
- Ridley, R.M., Baker, H.F., Windle, C.P., Cummings, R.M., 2006. Very long term studies of the seeding of beta-amyloidosis in primates. *J. Neural Transm. Vienna Austria* 1996 113, 1243–1251. <https://doi.org/10.1007/s00702-005-0385-2>
- Ridley, R.M., Haystead, T.A., Baker, H.F., 1981. An analysis of visual object reversal learning in the marmoset after amphetamine and haloperidol. *Pharmacol. Biochem. Behav.* 14, 345–351. [https://doi.org/10.1016/0091-3057\(81\)90401-9](https://doi.org/10.1016/0091-3057(81)90401-9)
- Riek, R., Eisenberg, D.S., 2016. The activities of amyloids from a structural perspective. *Nature* 539, 227–235. <https://doi.org/10.1038/nature20416>
- Ries, M., Sastre, M., 2016. Mechanisms of A $\beta$  Clearance and Degradation by Glial Cells. *Front. Aging Neurosci.* 8, 160. <https://doi.org/10.3389/fnagi.2016.00160>
- Ritchie, D.L., Adlard, P., Peden, A.H., Lowrie, S., Le Grice, M., Burns, K., Jackson, R.J., Yull, H., Keogh, M.J., Wei, W., Chinnery, P.F., Head, M.W., Ironside, J.W., 2017. Amyloid- $\beta$  accumulation in the CNS in human growth hormone recipients in the UK. *Acta Neuropathol. (Berl.)* 134, 221–240. <https://doi.org/10.1007/s00401-017-1703-0>
- Rodríguez-Arellano, J.J., Parpura, V., Zorec, R., Verkhratsky, A., 2016. Astrocytes in physiological aging and Alzheimer's disease. *Neuroscience, Dynamic and metabolic astrocyte-neuron interactions*

- in healthy and diseased brain 323, 170–182.  
<https://doi.org/10.1016/j.neuroscience.2015.01.007>
- Rodriguez-Callejas, J.D., Fuchs, E., Perez-Cruz, C., 2016. Evidence of Tau Hyperphosphorylation and Dystrophic Microglia in the Common Marmoset. *Front. Aging Neurosci.* 8. <https://doi.org/10.3389/fnagi.2016.00315>
- Rosen, R.F., Fritz, J.J., Dooyema, J., Cintron, A.F., Hamaguchi, T., Lah, J.J., LeVine, H., Jucker, M., Walker, L.C., 2012. Exogenous seeding of cerebral  $\beta$ -amyloid deposition in  $\beta$ APP-transgenic rats. *J. Neurochem.* 120, 660–666. <https://doi.org/10.1111/j.1471-4159.2011.07551.x>
- Rosen, R.F., Walker, L.C., Levine, H., 2011. PIB binding in aged primate brain: enrichment of high-affinity sites in humans with Alzheimer’s disease. *Neurobiol. Aging* 32, 223–234. <https://doi.org/10.1016/j.neurobiolaging.2009.02.011>
- Roy, M., Cardoso, C., Dorieux, O., Malgorn, C., Epelbaum, S., Petit, F., Kraska, A., Brouillet, E., Delatour, B., Perret, M., Aujard, F., Dhenain, M., 2015. Age-associated evolution of plasmatic amyloid in mouse lemur primates: relationship with intracellular amyloid deposition. *Neurobiol. Aging* 36, 149–156. <https://doi.org/10.1016/j.neurobiolaging.2014.07.017>
- Ruiz-Riquelme, A., Lau, H.H.C., Stuart, E., Goczi, A.N., Wang, Z., Schmitt-Ulms, G., Watts, J.C., 2018. Prion-like propagation of  $\beta$ -amyloid aggregates in the absence of APP overexpression. *Acta Neuropathol. Commun.* 6, 26. <https://doi.org/10.1186/s40478-018-0529-x>
- Saito, T., Mihira, N., Matsuba, Y., Sasaguri, H., Hashimoto, S., Narasimhan, S., Zhang, B., Murayama, S., Higuchi, M., Lee, V.M.Y., Trojanowski, J.Q., Saido, T.C., 2019. Humanization of the entire murine Mapt gene provides a murine model of pathological human tau propagation. *J. Biol. Chem.* 294, 12754–12765. <https://doi.org/10.1074/jbc.RA119.009487>
- Saman, S., Kim, W., Raya, M., Visnick, Y., Miro, S., Saman, S., Jackson, B., McKee, A.C., Alvarez, V.E., Lee, N.C.Y., Hall, G.F., 2012. Exosome-associated tau is secreted in tauopathy models and is selectively phosphorylated in cerebrospinal fluid in early Alzheimer disease. *J. Biol. Chem.* 287, 3842–3849. <https://doi.org/10.1074/jbc.M111.277061>
- Sanchez-Mejias, E., Navarro, V., Jimenez, S., Sanchez-Mico, M., Sanchez-Varo, R., Nuñez-Díaz, C., Trujillo-Estrada, L., Davila, J.C., Vizueté, M., Gutierrez, A., Vitorica, J., 2016. Soluble phospho-tau from Alzheimer’s disease hippocampus drives microglial degeneration. *Acta Neuropathol. (Berl.)* 132, 897–916. <https://doi.org/10.1007/s00401-016-1630-5>
- Sanders, D.W., Kaufman, S.K., DeVos, S.L., Sharma, A.M., Mirbaha, H., Li, A., Barker, S.J., Foley, A., Thorpe, J.R., Serpell, L.C., Miller, T.M., Grinberg, L.T., Seeley, W.W., Diamond, M.I., 2014. Distinct tau prion strains propagate in cells and mice and define different tauopathies. *Neuron* 82, 1271–1288. <https://doi.org/10.1016/j.neuron.2014.04.047>
- Sani, S., Traul, D., Klink, A., Niaraki, N., Gonzalo-Ruiz, A., Wu, C.-K., Geula, C., 2003. Distribution, progression and chemical composition of cortical amyloid-beta deposits in aged rhesus monkeys: similarities to the human. *Acta Neuropathol. (Berl.)* 105, 145–156. <https://doi.org/10.1007/s00401-002-0626-5>
- SantaCruz, K., Lewis, J., Spires, T., Paulson, J., Kotilinek, L., Ingelsson, M., Guimaraes, A., DeTure, M., Ramsden, M., McGowan, E., Forster, C., Yue, M., Orne, J., Janus, C., Mariash, A., Kuskowski, M., Hyman, B., Hutton, M., Ashe, K.H., 2005. Tau Suppression in a Neurodegenerative Mouse Model Improves Memory Function. *Science* 309, 476–481. <https://doi.org/10.1126/science.1113694>
- Scarmeas, N., Albert, M., Brandt, J., Blacker, D., Hadjigeorgiou, G., Papadimitriou, A., Dubois, B., Sarazin, M., Wegesin, D., Marder, K., Bell, K., Honig, L., Stern, Y., 2005. Motor signs predict poor outcomes in Alzheimer disease. *Neurology* 64, 1696–1703. <https://doi.org/10.1212/01.WNL.0000162054.15428.E9>
- Schafer, D.P., Lehrman, E.K., Kautzman, A.G., Koyama, R., Mardinly, A.R., Yamasaki, R., Ransohoff, R.M., Greenberg, M.E., Barres, B.A., Stevens, B., 2012. Microglia Sculpt Postnatal Neural Circuits in an Activity and Complement-Dependent Manner. *Neuron* 74, 691–705. <https://doi.org/10.1016/j.neuron.2012.03.026>

- Schafer, D.P., Lehrman, E.K., Stevens, B., 2013. The “quad-partite” synapse: microglia-synapse interactions in the developing and mature CNS. *Glia* 61, 24–36. <https://doi.org/10.1002/glia.22389>
- Scheff, S.W., Price, D.A., Schmitt, F.A., Mufson, E.J., 2006. Hippocampal synaptic loss in early Alzheimer’s disease and mild cognitive impairment. *Neurobiol. Aging* 27, 1372–1384. <https://doi.org/10.1016/j.neurobiolaging.2005.09.012>
- Scheltens, N.M.E., Galindo-Garre, F., Pijnenburg, Y.A.L., van der Vlies, A.E., Smits, L.L., Koene, T., Teunissen, C.E., Barkhof, F., Wattjes, M.P., Scheltens, P., van der Flier, W.M., 2016. The identification of cognitive subtypes in Alzheimer’s disease dementia using latent class analysis. *J. Neurol. Neurosurg. Psychiatry* 87, 235–243. <https://doi.org/10.1136/jnnp-2014-309582>
- Scheltens, N.M.E., Tijms, B.M., Koene, T., Barkhof, F., Teunissen, C.E., Wolfsgruber, S., Wagner, M., Kornhuber, J., Peters, O., Cohn-Sheehy, B.I., Rabinovici, G.D., Miller, B.L., Kramer, J.H., Scheltens, P., van der Flier, W.M., Alzheimer’s Disease Neuroimaging Initiative, German Dementia Competence Network, University of California San Francisco Memory and Aging Center, Amsterdam Dementia Cohort, 2017. Cognitive subtypes of probable Alzheimer’s disease robustly identified in four cohorts. *Alzheimers Dement. J. Alzheimers Assoc.* 13, 1226–1236. <https://doi.org/10.1016/j.jalz.2017.03.002>
- Schindler, S.E., Bollinger, J.G., Ovod, V., Mawuenyega, K.G., Li, Y., Gordon, B.A., Holtzman, D.M., Morris, J.C., Benzinger, T.L.S., Xiong, C., Fagan, A.M., Bateman, R.J., 2019. High-precision plasma  $\beta$ -amyloid 42/40 predicts current and future brain amyloidosis. *Neurology* 93, e1647–e1659. <https://doi.org/10.1212/WNL.00000000000008081>
- Schmidt, C., Haïk, S., Satoh, K., Rábano, A., Martínez-Martin, P., Roeber, S., Brandel, J.-P., Calero-Lara, M., de Pedro-Cuesta, J., Laplanche, J.-L., Hauw, J.-J., Kretschmar, H., Zerr, I., 2012. Rapidly progressive Alzheimer’s disease: a multicenter update. *J. Alzheimers Dis. JAD* 30, 751–756. <https://doi.org/10.3233/JAD-2012-120007>
- Schmidt, C., Redyk, K., Meissner, B., Krack, L., Ahsen, N. von, Roeber, S., Kretschmar, H., Zerr, I., 2010. Clinical Features of Rapidly Progressive Alzheimer’s Disease. *Dement. Geriatr. Cogn. Disord.* 29, 371–378. <https://doi.org/10.1159/000278692>
- Schmidt, C., Wolff, M., Weitz, M., Bartlau, T., Korth, C., Zerr, I., 2011. Rapidly progressive Alzheimer disease. *Arch. Neurol.* 68, 1124–1130. <https://doi.org/10.1001/archneurol.2011.189>
- Schmidtke, D., Zimmermann, E., Trouche, S.G., Fontès, P., Verdier, J.-M., Mestre-Francés, N., 2020. Linking cognition to age and amyloid- $\beta$  burden in the brain of a nonhuman primate (*Microcebus murinus*). *Neurobiol. Aging* 94, 207–216. <https://doi.org/10.1016/j.neurobiolaging.2020.03.025>
- Schultz, C., Hubbard, G.B., Del Tredici, K., Braak, E., Braak, H., 2001. Tau pathology in neurons and glial cells of aged baboons. *Adv. Exp. Med. Biol.* 487, 59–69. [https://doi.org/10.1007/978-1-4615-1249-3\\_5](https://doi.org/10.1007/978-1-4615-1249-3_5)
- Schultz, C., Hubbard, G.B., Rüb, U., Braak, E., Braak, H., 2000. Age-related progression of tau pathology in brains of baboons. *Neurobiol. Aging* 21, 905–912. [https://doi.org/10.1016/s0197-4580\(00\)00176-7](https://doi.org/10.1016/s0197-4580(00)00176-7)
- Schütt, T., Helboe, L., Pedersen, L.Ø., Waldemar, G., Berendt, M., Pedersen, J.T., 2016. Dogs with Cognitive Dysfunction as a Spontaneous Model for Early Alzheimer’s Disease: A Translational Study of Neuropathological and Inflammatory Markers. *J. Alzheimers Dis. JAD* 52, 433–449. <https://doi.org/10.3233/JAD-151085>
- Scialò, C., De Cecco, E., Manganotti, P., Legname, G., 2019. Prion and Prion-Like Protein Strains: Deciphering the Molecular Basis of Heterogeneity in Neurodegeneration. *Viruses* 11. <https://doi.org/10.3390/v11030261>
- Seidl, J.N.T., Massman, P.J., 2016. Rapidly Versus Slowly Progressing Patients With Alzheimer’s Disease: Differences in Baseline Cognition. *Am. J. Alzheimers Dis. Other Dement.* 31, 318–325. <https://doi.org/10.1177/1533317515617720>
- Selkoe, D.J., 2002. Alzheimer’s disease is a synaptic failure. *Science* 298, 789–791. <https://doi.org/10.1126/science.1074069>



- Selkoe, D.J., Hardy, J., 2016. The amyloid hypothesis of Alzheimer's disease at 25 years. *EMBO Mol. Med.* 8, 595–608. <https://doi.org/10.15252/emmm.201606210>
- Seo, J., Kritskiy, O., Watson, L.A., Barker, S.J., Dey, D., Raja, W.K., Lin, Y.-T., Ko, T., Cho, S., Penney, J., Silva, M.C., Sheridan, S.D., Lucente, D., Gusella, J.F., Dickerson, B.C., Haggarty, S.J., Tsai, L.-H., 2017. Inhibition of p25/Cdk5 Attenuates Tauopathy in Mouse and iPSC Models of Frontotemporal Dementia. *J. Neurosci. Off. J. Soc. Neurosci.* 37, 9917–9924. <https://doi.org/10.1523/JNEUROSCI.0621-17.2017>
- Serrano-Pozo, A., Frosch, M.P., Masliah, E., Hyman, B.T., 2011a. Neuropathological alterations in Alzheimer disease. *Cold Spring Harb. Perspect. Med.* 1, a006189. <https://doi.org/10.1101/cshperspect.a006189>
- Serrano-Pozo, A., Mielke, M.L., Gómez-Isla, T., Betensky, R.A., Growdon, J.H., Frosch, M.P., Hyman, B.T., 2011b. Reactive glia not only associates with plaques but also parallels tangles in Alzheimer's disease. *Am. J. Pathol.* 179, 1373–1384. <https://doi.org/10.1016/j.ajpath.2011.05.047>
- Shankar, G.M., Li, S., Mehta, T.H., Garcia-Munoz, A., Shepardson, N.E., Smith, I., Brett, F.M., Farrell, M.A., Rowan, M.J., Lemere, C.A., Regan, C.M., Walsh, D.M., Sabatini, B.L., Selkoe, D.J., 2008. Amyloid-beta protein dimers isolated directly from Alzheimer's brains impair synaptic plasticity and memory. *Nat. Med.* 14, 837–842. <https://doi.org/10.1038/nm1782>
- Sheline, Y.I., Raichle, M.E., Snyder, A.Z., Morris, J.C., Head, D., Wang, S., Mintun, M.A., 2010. Amyloid Plaques Disrupt Resting State Default Mode Network Connectivity in Cognitively Normal Elderly. *Biol. Psychiatry* 67, 584–587. <https://doi.org/10.1016/j.biopsych.2009.08.024>
- Shi, Y., Holtzman, D.M., 2018. Interplay between innate immunity and Alzheimer's disease: APOE and TREM2 in the spotlight. *Nat. Rev. Immunol.* 18, 759–772. <https://doi.org/10.1038/s41577-018-0051-1>
- Shibata, M., Yamada, S., Kumar, S.R., Calero, M., Bading, J., Frangione, B., Holtzman, D.M., Miller, C.A., Strickland, D.K., Ghiso, J., Zlokovic, B.V., 2000. Clearance of Alzheimer's amyloid-ss(1-40) peptide from brain by LDL receptor-related protein-1 at the blood-brain barrier. *J. Clin. Invest.* 106, 1489–1499. <https://doi.org/10.1172/JCI10498>
- Shin, W.S., Di, J., Murray, K.A., Sun, C., Li, B., Bitan, G., Jiang, L., 2019. Different Amyloid- $\beta$  Self-Assemblies Have Distinct Effects on Intracellular Tau Aggregation. *Front. Mol. Neurosci.* 12, 268. <https://doi.org/10.3389/fnmol.2019.00268>
- Sidoryk-Wegrzynowicz, M., Gerber, Y.N., Ries, M., Sastre, M., Tolkovsky, A.M., Spillantini, M.G., 2017. Astrocytes in mouse models of tauopathies acquire early deficits and lose neurosupportive functions. *Acta Neuropathol. Commun.* 5, 89. <https://doi.org/10.1186/s40478-017-0478-9>
- Silhol, S., Calenda, A., Jallageas, V., Mestre-Frances, N., Bellis, M., Bons, N., 1996. beta-Amyloid protein precursor in *Microcebus murinus*: genotyping and brain localization. *Neurobiol. Dis.* 3, 169–182. <https://doi.org/10.1006/nbdi.1996.0017>
- Simoneau, S., Rezaei, H., Salès, N., Kaiser-Schulz, G., Lefebvre-Roque, M., Vidal, C., Fournier, J.-G., Comte, J., Wopfner, F., Grosclaude, J., Schätzl, H., Lasmézas, C.I., 2007. In Vitro and In Vivo Neurotoxicity of Prion Protein Oligomers. *PLOS Pathog.* 3, e125. <https://doi.org/10.1371/journal.ppat.0030125>
- Simpson, D.A., Masters, C.L., Ohlrich, G., Purdie, G., Stuart, G., Tannenberg, A.E.G., 1996. Iatrogenic Creutzfeldt-Jakob disease and its neurosurgical implications. *J. Clin. Neurosci.* 3, 118–123. [https://doi.org/10.1016/S0967-5868\(96\)90003-X](https://doi.org/10.1016/S0967-5868(96)90003-X)
- Sivanesan, S., Tan, A., Rajadas, J., 2013. Pathogenesis of Abeta oligomers in synaptic failure. *Curr. Alzheimer Res.* 10, 316–323. <https://doi.org/10.2174/1567205011310030011>
- Skachokova, Z., Martinisi, A., Flach, M., Sprenger, F., Naegelin, Y., Steiner-Monard, V., Sollberger, M., Monsch, A.U., Goedert, M., Tolnay, M., Winkler, D.T., 2019. Cerebrospinal fluid from Alzheimer's disease patients promotes tau aggregation in transgenic mice. *Acta Neuropathol. Commun.* 7, 72. <https://doi.org/10.1186/s40478-019-0725-3>
- Skillbäck, T., Rosén, C., Asztely, F., Mattsson, N., Blennow, K., Zetterberg, H., 2014. Diagnostic performance of cerebrospinal fluid total tau and phosphorylated tau in Creutzfeldt-Jakob

- disease: results from the Swedish Mortality Registry. *JAMA Neurol.* 71, 476–483. <https://doi.org/10.1001/jamaneurol.2013.6455>
- Sloane, J.A., Pietropaolo, M.F., Rosene, D.L., Moss, M.B., Peters, A., Kemper, T., Abraham, C.R., 1997. Lack of correlation between plaque burden and cognition in the aged monkey. *Acta Neuropathol. (Berl.)* 94, 471–478. <https://doi.org/10.1007/s004010050735>
- Smolek, T., Madari, A., Farbakova, J., Kandrac, O., Jadhav, S., Cente, M., Brezovakova, V., Novak, M., Zilka, N., 2016. Tau hyperphosphorylation in synaptosomes and neuroinflammation are associated with canine cognitive impairment. *J. Comp. Neurol.* 524, 874–895. <https://doi.org/10.1002/cne.23877>
- Snider, B.J., Norton, J., Coats, M.A., Chakraverty, S., Hou, C.E., Jervis, R., Lendon, C.L., Goate, A.M., McKeel, D.W., Morris, J.C., 2005. Novel presenilin 1 mutation (S170F) causing Alzheimer disease with Lewy bodies in the third decade of life. *Arch. Neurol.* 62, 1821–1830. <https://doi.org/10.1001/archneur.62.12.1821>
- Sofroniew, M.V., Vinters, H.V., 2010. Astrocytes: biology and pathology. *Acta Neuropathol. (Berl.)* 119, 7–35. <https://doi.org/10.1007/s00401-009-0619-8>
- Sokol, D.K., Maloney, B., Long, J.M., Ray, B., Lahiri, D.K., 2011. Autism, Alzheimer disease, and fragile X: APP, FMRP, and mGluR5 are molecular links. *Neurology* 76, 1344–1352. <https://doi.org/10.1212/WNL.0b013e3182166dc7>
- Sondag, C.M., Dhawan, G., Combs, C.K., 2009. Beta amyloid oligomers and fibrils stimulate differential activation of primary microglia. *J. Neuroinflammation* 6, 1. <https://doi.org/10.1186/1742-2094-6-1>
- Song, H.-L., Shim, S., Kim, D.-H., Won, S.-H., Joo, S., Kim, S., Jeon, N.L., Yoon, S.-Y., 2014.  $\beta$ -Amyloid is transmitted via neuronal connections along axonal membranes. *Ann. Neurol.* 75, 88–97. <https://doi.org/10.1002/ana.24029>
- Soto, C., Pritzkow, S., 2018. Protein misfolding, aggregation, and conformational strains in neurodegenerative diseases. *Nat. Neurosci.* 21, 1332–1340. <https://doi.org/10.1038/s41593-018-0235-9>
- Spangenberg, E.E., Lee, R.J., Najafi, A.R., Rice, R.A., Elmore, M.R.P., Blurton-Jones, M., West, B.L., Green, K.N., 2016. Eliminating microglia in Alzheimer’s mice prevents neuronal loss without modulating amyloid- $\beta$  pathology. *Brain* 139, 1265–1281. <https://doi.org/10.1093/brain/aww016>
- Sperling, R.A., LaViolette, P.S., O’Keefe, K., O’Brien, J., Rentz, D.M., Pihlajamaki, M., Marshall, G., Hyman, B.T., Selkoe, D.J., Hedden, T., Buckner, R.L., Becker, J.A., Johnson, K.A., 2009. Amyloid deposition is associated with impaired default network function in older persons without dementia. *Neuron* 63, 178–188. <https://doi.org/10.1016/j.neuron.2009.07.003>
- Spires-Jones, T.L., Hyman, B.T., 2014. The intersection of amyloid beta and tau at synapses in Alzheimer’s disease. *Neuron* 82, 756–771. <https://doi.org/10.1016/j.neuron.2014.05.004>
- Spires-Jones, T.L., Stoothoff, W.H., de Calignon, A., Jones, P.B., Hyman, B.T., 2009. Tau pathophysiology in neurodegeneration: a tangled issue. *Trends Neurosci.* 32, 150–159. <https://doi.org/10.1016/j.tins.2008.11.007>
- Stancu, I.-C., Cremers, N., Vanrusselt, H., Couturier, J., Vanoosthuyse, A., Kessels, S., Lodder, C., Brône, B., Huaux, F., Octave, J.-N., Terwel, D., Dewachter, I., 2019. Aggregated Tau activates NLRP3-ASC inflammasome exacerbating exogenously seeded and non-exogenously seeded Tau pathology in vivo. *Acta Neuropathol. (Berl.)* 137, 599–617. <https://doi.org/10.1007/s00401-018-01957-y>
- Stancu, I.-C., Vasconcelos, B., Ris, L., Wang, P., Villers, A., Peeraer, E., Buist, A., Terwel, D., Baatsen, P., Oyelami, T., Pierrot, N., Casteels, C., Bormans, G., Kienlen-Campard, P., Octave, J.-N., Moechars, D., Dewachter, I., 2015. Templated misfolding of Tau by prion-like seeding along neuronal connections impairs neuronal network function and associated behavioral outcomes in Tau transgenic mice. *Acta Neuropathol. (Berl.)* 129, 875–894. <https://doi.org/10.1007/s00401-015-1413-4>

- Steenland, K., Goldstein, F.C., Levey, A., Wharton, W., 2016. A Meta-Analysis of Alzheimer's Disease Incidence and Prevalence Comparing African-Americans and Caucasians. *J. Alzheimers Dis. JAD* 50, 71–76. <https://doi.org/10.3233/JAD-150778>
- Steffen, J., Krohn, M., Paarmann, K., Schwitlick, C., Brüning, T., Marreiros, R., Müller-Schiffmann, A., Korth, C., Braun, K., Pahnke, J., 2016. Revisiting rodent models: Octodon degus as Alzheimer's disease model? *Acta Neuropathol. Commun.* 4, 91. <https://doi.org/10.1186/s40478-016-0363-y>
- Stephan, M., Volkman, P., Rossner, M.J., 2019. Assessing behavior and cognition in rodents, nonhuman primates, and humans: where are the limits of translation? *Dialogues Clin. Neurosci.* 21, 249–259. <https://doi.org/10.31887/DCNS.2019.21.3/mrossner>
- Stern, Y., 2012. Cognitive reserve in ageing and Alzheimer's disease. *Lancet Neurol.* 11, 1006–1012. [https://doi.org/10.1016/S1474-4422\(12\)70191-6](https://doi.org/10.1016/S1474-4422(12)70191-6)
- Stern, Y., 2009. Cognitive reserve. *Neuropsychologia* 47, 2015–2028. <https://doi.org/10.1016/j.neuropsychologia.2009.03.004>
- Stern, Y., 2006. Cognitive reserve and Alzheimer disease. *Alzheimer Dis. Assoc. Disord.* 20, S69-74. <https://doi.org/10.1097/00002093-200607001-00010>
- Stern, Y., 2002. What is cognitive reserve? Theory and research application of the reserve concept. *J. Int. Neuropsychol. Soc. JINS* 8, 448–460.
- Stern, Y., Albert, S., Tang, M.X., Tsai, W.Y., 1999. Rate of memory decline in AD is related to education and occupation: cognitive reserve? *Neurology* 53, 1942–1947. <https://doi.org/10.1212/wnl.53.9.1942>
- Stoeck, K., Schmitz, M., Ebert, E., Schmidt, C., Zerr, I., 2014. Immune responses in rapidly progressive dementia: a comparative study of neuroinflammatory markers in Creutzfeldt-Jakob disease, Alzheimer's disease and multiple sclerosis. *J. Neuroinflammation* 11, 170. <https://doi.org/10.1186/s12974-014-0170-y>
- Stöhr, J., Condello, C., Watts, J.C., Bloch, L., Oehler, A., Nick, M., DeArmond, S.J., Giles, K., DeGrado, W.F., Prusiner, S.B., 2014. Distinct synthetic A $\beta$  prion strains producing different amyloid deposits in bigenic mice. *Proc. Natl. Acad. Sci. U. S. A.* 111, 10329–10334. <https://doi.org/10.1073/pnas.1408968111>
- Stöhr, J., Watts, J.C., Mensinger, Z.L., Oehler, A., Grillo, S.K., DeArmond, S.J., Prusiner, S.B., Giles, K., 2012. Purified and synthetic Alzheimer's amyloid beta (A $\beta$ ) prions. *Proc. Natl. Acad. Sci. U. S. A.* 109, 11025–11030. <https://doi.org/10.1073/pnas.1206555109>
- Streit, W.J., Braak, H., Xue, Q.-S., Bechmann, I., 2009. Dystrophic (senescent) rather than activated microglial cells are associated with tau pathology and likely precede neurodegeneration in Alzheimer's disease. *Acta Neuropathol. (Berl.)* 118, 475–485. <https://doi.org/10.1007/s00401-009-0556-6>
- Suárez-Calvet, M., Karikari, T.K., Ashton, N.J., Lantero Rodríguez, J., Milà-Alomà, M., Gispert, J.D., Salvadó, G., Minguillon, C., Fauria, K., Shekari, M., Grau-Rivera, O., Arenaza-Urquijo, E.M., Sala-Vila, A., Sánchez-Benavides, G., González-de-Echávarri, J.M., Kollmorgen, G., Stoops, E., Vanmechelen, E., Zetterberg, H., Blennow, K., Molinuevo, J.L., 2020. Novel tau biomarkers phosphorylated at T181, T217 or T231 rise in the initial stages of the preclinical Alzheimer's continuum when only subtle changes in A $\beta$  pathology are detected. *EMBO Mol. Med.* 12. <https://doi.org/10.15252/emmm.202012921>
- Sunde, M., Serpell, L.C., Bartlam, M., Fraser, P.E., Pepys, M.B., Blake, C.C., 1997. Common core structure of amyloid fibrils by synchrotron X-ray diffraction. *J. Mol. Biol.* 273, 729–739. <https://doi.org/10.1006/jmbi.1997.1348>
- Suo, Z., Tan, J., Placzek, A., Crawford, F., Fang, C., Mullan, M., 1998. Alzheimer's  $\beta$ -amyloid peptides induce inflammatory cascade in human vascular cells: the roles of cytokines and CD40. *Brain Res.* 807, 110–117. [https://doi.org/10.1016/S0006-8993\(98\)00780-X](https://doi.org/10.1016/S0006-8993(98)00780-X)
- Tadenev, A.L.D., Burgess, R.W., 2019. Model validity for preclinical studies in precision medicine: precisely how precise do we need to be? *Mamm. Genome* 30, 111–122. <https://doi.org/10.1007/s00335-019-09798-0>

- Tai, H.-C., Serrano-Pozo, A., Hashimoto, T., Frosch, M.P., Spiess-Jones, T.L., Hyman, B.T., 2012. The synaptic accumulation of hyperphosphorylated tau oligomers in Alzheimer disease is associated with dysfunction of the ubiquitin-proteasome system. *Am. J. Pathol.* 181, 1426–1435. <https://doi.org/10.1016/j.ajpath.2012.06.033>
- Takahashi, M., Miyata, H., Kametani, F., Nonaka, T., Akiyama, H., Hisanaga, S., Hasegawa, M., 2015. Extracellular association of APP and tau fibrils induces intracellular aggregate formation of tau. *Acta Neuropathol. (Berl.)* 129, 895–907. <https://doi.org/10.1007/s00401-015-1415-2>
- Takahashi, R.H., Milner, T.A., Li, F., Nam, E.E., Edgar, M.A., Yamaguchi, H., Beal, M.F., Xu, H., Greengard, P., Gouras, G.K., 2002. Intraneuronal Alzheimer abeta42 accumulates in multivesicular bodies and is associated with synaptic pathology. *Am. J. Pathol.* 161, 1869–1879. [https://doi.org/10.1016/s0002-9440\(10\)64463-x](https://doi.org/10.1016/s0002-9440(10)64463-x)
- Tampellini, D., Capetillo-Zarate, E., Dumont, M., Huang, Z., Yu, F., Lin, M.T., Gouras, G.K., 2010. Effects of synaptic modulation on beta-amyloid, synaptophysin, and memory performance in Alzheimer's disease transgenic mice. *J. Neurosci. Off. J. Soc. Neurosci.* 30, 14299–14304. <https://doi.org/10.1523/JNEUROSCI.3383-10.2010>
- Tampellini, D., Rahman, N., Gallo, E.F., Huang, Z., Dumont, M., Capetillo-Zarate, E., Ma, T., Zheng, R., Lu, B., Nanus, D.M., Lin, M.T., Gouras, G.K., 2009. Synaptic Activity Reduces Intraneuronal A $\beta$ , Promotes APP Transport to Synapses, and Protects against A $\beta$ -Related Synaptic Alterations. *J. Neurosci.* 29, 9704–9713. <https://doi.org/10.1523/JNEUROSCI.2292-09.2009>
- Tampellini, D., Rahman, N., Lin, M.T., Capetillo-Zarate, E., Gouras, G.K., 2011. Impaired  $\beta$ -amyloid secretion in Alzheimer's disease pathogenesis. *J. Neurosci. Off. J. Soc. Neurosci.* 31, 15384–15390. <https://doi.org/10.1523/JNEUROSCI.2986-11.2011>
- Tapp, P.D., Siwak, C.T., Gao, F.Q., Chiou, J.-Y., Black, S.E., Head, E., Muggenburg, B.A., Cotman, C.W., Milgram, N.W., Su, M.-Y., 2004. Frontal Lobe Volume, Function, and  $\beta$ -Amyloid Pathology in a Canine Model of Aging. *J. Neurosci.* 24, 8205–8213. <https://doi.org/10.1523/JNEUROSCI.1339-04.2004>
- Terry, R.D., Masliah, E., Salmon, D.P., Butters, N., DeTeresa, R., Hill, R., Hansen, L.A., Katzman, R., 1991. Physical basis of cognitive alterations in Alzheimer's disease: synapse loss is the major correlate of cognitive impairment. *Ann. Neurol.* 30, 572–580. <https://doi.org/10.1002/ana.410300410>
- Thal, D.R., Capetillo-Zarate, E., Del Tredici, K., Braak, H., 2006a. The Development of Amyloid beta Protein Deposits in the Aged Brain. *Sci. Aging Knowl. Environ.* 2006, re1. <https://doi.org/10.1126/sageke.2006.6.re1>
- Thal, D.R., Capetillo-Zarate, E., Del Tredici, K., Braak, H., 2006b. The development of amyloid beta protein deposits in the aged brain. *Sci. Aging Knowl. Environ.* SAGE KE 2006, re1. <https://doi.org/10.1126/sageke.2006.6.re1>
- Thal, D.R., Larionov, S., Abramowski, D., Wiederhold, K.-H., Van Dooren, T., Yamaguchi, H., Haass, C., Van Leuven, F., Staufenbiel, M., Capetillo-Zarate, E., 2007. Occurrence and co-localization of amyloid  $\beta$ -protein and apolipoprotein E in perivascular drainage channels of wild-type and APP-transgenic mice. *Neurobiol. Aging* 28, 1221–1230. <https://doi.org/10.1016/j.neurobiolaging.2006.05.029>
- Thal, D.R., Rüb, U., Orantes, M., Braak, H., 2002. Phases of A beta-deposition in the human brain and its relevance for the development of AD. *Neurology* 58, 1791–1800. <https://doi.org/10.1212/wnl.58.12.1791>
- Thal, D.R., Walter, J., Saido, T.C., Fändrich, M., 2015. Neuropathology and biochemistry of A $\beta$  and its aggregates in Alzheimer's disease. *Acta Neuropathol. (Berl.)* 129, 167–182. <https://doi.org/10.1007/s00401-014-1375-y>
- Thies, E., Mandelkow, E.-M., 2007. Missorting of tau in neurons causes degeneration of synapses that can be rescued by the kinase MARK2/Par-1. *J. Neurosci. Off. J. Soc. Neurosci.* 27, 2896–2907. <https://doi.org/10.1523/JNEUROSCI.4674-06.2007>

- Thomé, A., Gray, D.T., Erickson, C.A., Lipa, P., Barnes, C.A., 2016. Memory impairment in aged primates is associated with region-specific network dysfunction. *Mol. Psychiatry* 21, 1257–1262. <https://doi.org/10.1038/mp.2015.160>
- Thored, P., Heldmann, U., Gomes-Leal, W., Gisler, R., Darsalia, V., Taneera, J., Nygren, J.M., Jacobsen, S.-E.W., Ekdahl, C.T., Kokaia, Z., Lindvall, O., 2009. Long-term accumulation of microglia with proneurogenic phenotype concomitant with persistent neurogenesis in adult subventricular zone after stroke. *Glia* 57, 835–849. <https://doi.org/10.1002/glia.20810>
- Tian, H., Davidowitz, E., Lopez, P., Emadi, S., Moe, J., Sierks, M., 2013. Trimeric Tau Is Toxic to Human Neuronal Cells at Low Nanomolar Concentrations. *Int. J. Cell Biol.* 2013, e260787. <https://doi.org/10.1155/2013/260787>
- Tomic, J.L., Pensalfini, A., Head, E., Glabe, C.G., 2009. Soluble fibrillar oligomer levels are elevated in Alzheimer's disease brain and correlate with cognitive dysfunction. *Neurobiol. Dis.* 35, 352–358. <https://doi.org/10.1016/j.nbd.2009.05.024>
- Tondo, G., Iaccarino, L., Caminiti, S.P., Presotto, L., Santangelo, R., Iannaccone, S., Magnani, G., Perani, D., 2020. The combined effects of microglia activation and brain glucose hypometabolism in early-onset Alzheimer's disease. *Alzheimers Res. Ther.* 12, 50. <https://doi.org/10.1186/s13195-020-00619-0>
- Tosto, G., Gasparini, M., Brickman, A.M., Letteri, F., Renie', R., Piscopo, P., Talarico, G., Canevelli, M., Confalonni, A., Bruno, G., 2015. Neuropsychological predictors of rapidly progressive Alzheimer's disease. *Acta Neurol. Scand.* 132, 417–422. <https://doi.org/10.1111/ane.12415>
- Trzeciakiewicz, H., Tseng, J.-H., Wander, C.M., Madden, V., Tripathy, A., Yuan, C.-X., Cohen, T.J., 2017. A Dual Pathogenic Mechanism Links Tau Acetylation to Sporadic Tauopathy. *Sci. Rep.* 7, 44102. <https://doi.org/10.1038/srep44102>
- Tsay, H.-J., Huang, Y.-C., Huang, F.-L., Chen, C.-P., Tsai, Y.-C., Wang, Y.-H., Wu, M.-F., Chiang, F.-Y., Shiao, Y.-J., 2013. Amyloid  $\beta$  peptide-mediated neurotoxicity is attenuated by the proliferating microglia more potently than by the quiescent phenotype. *J. Biomed. Sci.* 20, 78. <https://doi.org/10.1186/1423-0127-20-78>
- Uchida, K., Nakayama, H., Goto, N., 1991. Pathological studies on cerebral amyloid angiopathy, senile plaques and amyloid deposition in visceral organs in aged dogs. *J. Vet. Med. Sci.* 53, 1037–1042. <https://doi.org/10.1292/jvms.53.1037>
- Uno, H., Alsum, P.B., Dong, S., Richardson, R., Zimbric, M.L., Thieme, C.S., Houser†, W.D., 1996. Cerebral amyloid angiopathy and plaques, and visceral amyloidosis in aged macaques. *Neurobiol. Aging, Development of Animal Models of Alzheimer's Disease: Status of the Field* 17, 275–281. [https://doi.org/10.1016/0197-4580\(95\)02063-2](https://doi.org/10.1016/0197-4580(95)02063-2)
- Valenzuela, M.J., Sachdev, P., Wen, W., Chen, X., Brodaty, H., 2008. Lifespan mental activity predicts diminished rate of hippocampal atrophy. *PloS One* 3, e2598. <https://doi.org/10.1371/journal.pone.0002598>
- van Strien, N.M., Cappaert, N.L.M., Witter, M.P., 2009. The anatomy of memory: an interactive overview of the parahippocampal–hippocampal network. *Nat. Rev. Neurosci.* 10, 272–282. <https://doi.org/10.1038/nrn2614>
- Vasconcelos, B., Stancu, I.-C., Buist, A., Bird, M., Wang, P., Vanoosthuysse, A., Van Kolen, K., Verheyen, A., Kienlen-Campard, P., Octave, J.-N., Baatsen, P., Moechars, D., Dewachter, I., 2016. Heterotypic seeding of Tau fibrillization by pre-aggregated A $\beta$  provides potent seeds for prion-like seeding and propagation of Tau-pathology in vivo. *Acta Neuropathol. (Berl.)* 131, 549–569. <https://doi.org/10.1007/s00401-015-1525-x>
- Vasile, F., Dossi, E., Rouach, N., 2017. Human astrocytes: structure and functions in the healthy brain. *Brain Struct. Funct.* 222, 2017–2029. <https://doi.org/10.1007/s00429-017-1383-5>
- Vautheny, A., Duwat, C., Aurégan, G., Joséphine, C., Hérard, A.-S., Jan, C., Mitja, J., Gipchtein, P., Gaillard, M.-C., Buée, L., Blum, D., Hantraye, P., Bonvento, G., Brouillet, E., Cambon, K., Bemelmans, A.-P., 2021. THY-Tau22 mouse model accumulates more tauopathy at late stage of the disease in response to microglia deactivation through TREM2 deficiency. *Neurobiol. Dis.* 155, 105398. <https://doi.org/10.1016/j.nbd.2021.105398>

- Vaz, M., Silvestre, S., 2020. Alzheimer's disease: Recent treatment strategies. *Eur. J. Pharmacol.* 887, 173554. <https://doi.org/10.1016/j.ejphar.2020.173554>
- Venegas, C., Kumar, S., Franklin, B.S., Dierkes, T., Brinkschulte, R., Tejera, D., Vieira-Saecker, A., Schwartz, S., Santarelli, F., Kummer, M.P., Griep, A., Gelpi, E., Beilharz, M., Riedel, D., Golenbock, D.T., Geyer, M., Walter, J., Latz, E., Heneka, M.T., 2017. Microglia-derived ASC specks cross-seed amyloid- $\beta$  in Alzheimer's disease. *Nature* 552, 355–361. <https://doi.org/10.1038/nature25158>
- Verges, D.K., Restivo, J.L., Goebel, W.D., Holtzman, D.M., Cirrito, J.R., 2011. Opposing synaptic regulation of amyloid- $\beta$  metabolism by NMDA receptors in vivo. *J. Neurosci. Off. J. Soc. Neurosci.* 31, 11328–11337. <https://doi.org/10.1523/JNEUROSCI.0607-11.2011>
- Vergheze, P.B., Castellano, J.M., Holtzman, D.M., 2011. Apolipoprotein E in Alzheimer's disease and other neurological disorders. *Lancet Neurol.* 10, 241–252. [https://doi.org/10.1016/S1474-4422\(10\)70325-2](https://doi.org/10.1016/S1474-4422(10)70325-2)
- Verkhatsky, A., Olabarria, M., Noristani, H.N., Yeh, C.-Y., Rodriguez, J.J., 2010. Astrocytes in Alzheimer's disease. *Neurotherapeutics* 7, 399–412. <https://doi.org/10.1016/j.nurt.2010.05.017>
- Verkhatsky, A., Zorec, R., Rodríguez, J.J., Parpura, V., 2016. Astroglia dynamics in ageing and Alzheimer's disease. *Curr. Opin. Pharmacol.* 26, 74–79. <https://doi.org/10.1016/j.coph.2015.09.011>
- Viana da Silva, S., Haberl, M.G., Zhang, P., Bethge, P., Lemos, C., Gonçalves, N., Gorlewicz, A., Malezieux, M., Gonçalves, F.Q., Grosjean, N., Blanchet, C., Frick, A., Nägerl, U.V., Cunha, R.A., Mülle, C., 2016. Early synaptic deficits in the APP/PS1 mouse model of Alzheimer's disease involve neuronal adenosine A2A receptors. *Nat. Commun.* 7, 11915. <https://doi.org/10.1038/ncomms11915>
- Violet, M., Delattre, L., Tardivel, M., Sultan, A., Chauderlier, A., Caillierez, R., Talahari, S., Nessler, F., Lefebvre, B., Bonnefoy, E., Buee, L., Galas, M.-C., 2014. A major role for Tau in neuronal DNA and RNA protection in vivo under physiological and hyperthermic conditions. *Front. Cell. Neurosci.* 8. <https://doi.org/10.3389/fncel.2014.00084>
- Vogel, J.W., Iturria-Medina, Y., Strandberg, O.T., Smith, R., Levitis, E., Evans, A.C., Hansson, O., 2020. Spread of pathological tau proteins through communicating neurons in human Alzheimer's disease. *Nat. Commun.* 11, 2612. <https://doi.org/10.1038/s41467-020-15701-2>
- Volianskis, A., Køstner, R., Mølgaard, M., Hass, S., Jensen, M.S., 2010. Episodic memory deficits are not related to altered glutamatergic synaptic transmission and plasticity in the CA1 hippocampus of the APP<sup>swe</sup>/PS1 $\Delta$ E9-deleted transgenic mice model of  $\beta$ -amyloidosis. *Neurobiol. Aging* 31, 1173–1187. <https://doi.org/10.1016/j.neurobiolaging.2008.08.005>
- Wadsworth, J.D., Hill, A.F., Beck, J.A., Collinge, J., 2003. Molecular and clinical classification of human prion disease. *Br. Med. Bull.* 66, 241–254. <https://doi.org/10.1093/bmb/66.1.241>
- Waites, C.L., Leal-Ortiz, S.A., Okerlund, N., Dalke, H., Fejtova, A., Altmann, W.D., Gundelfinger, E.D., Garner, C.C., 2013. Bassoon and Piccolo maintain synapse integrity by regulating protein ubiquitination and degradation. *EMBO J.* 32, 954–969. <https://doi.org/10.1038/emboj.2013.27>
- Walker, D.G., Lue, L.-F., Beach, T.G., 2002. Increased expression of the urokinase plasminogen-activator receptor in amyloid  $\beta$  peptide-treated human brain microglia and in AD brains. *Brain Res.* 926, 69–79. [https://doi.org/10.1016/S0006-8993\(01\)03298-X](https://doi.org/10.1016/S0006-8993(01)03298-X)
- Walker, L.C., 2020. A $\beta$  Plaques. *Free Neuropathol.* 1. <https://doi.org/10.17879/freeneuropathology-2020-3025>
- Walker, L.C., Callahan, M.J., Bian, F., Durham, R.A., Roher, A.E., Lipinski, W.J., 2002. Exogenous induction of cerebral beta-amyloidosis in betaAPP-transgenic mice. *Peptides* 23, 1241–1247. [https://doi.org/10.1016/s0196-9781\(02\)00059-1](https://doi.org/10.1016/s0196-9781(02)00059-1)
- Walker, L.C., Schelle, J., Jucker, M., 2016. The Prion-Like Properties of Amyloid- $\beta$  Assemblies: Implications for Alzheimer's Disease. *Cold Spring Harb. Perspect. Med.* 6. <https://doi.org/10.1101/cshperspect.a024398>

- Wallin, A.K., Blennow, K., Zetterberg, H., Londos, E., Minthon, L., Hansson, O., 2010. CSF biomarkers predict a more malignant outcome in Alzheimer disease. *Neurology* 74, 1531–1537. <https://doi.org/10.1212/WNL.0b013e3181dd4dd8>
- Walsh, D.M., Klyubin, I., Fadeeva, J.V., Cullen, W.K., Anwyl, R., Wolfe, M.S., Rowan, M.J., Selkoe, D.J., 2002. Naturally secreted oligomers of amyloid beta protein potently inhibit hippocampal long-term potentiation in vivo. *Nature* 416, 535–539. <https://doi.org/10.1038/416535a>
- Wang, W.-Y., Tan, M.-S., Yu, J.-T., Tan, L., 2015. Role of pro-inflammatory cytokines released from microglia in Alzheimer's disease. *Ann. Transl. Med.* 3, 136. <https://doi.org/10.3978/j.issn.2305-5839.2015.03.49>
- Wang, Y., Balaji, V., Kaniyappan, S., Krüger, L., Irsen, S., Tepper, K., Chandupatla, R., Maetzler, W., Schneider, A., Mandelkow, E., Mandelkow, E.-M., 2017. The release and trans-synaptic transmission of Tau via exosomes. *Mol. Neurodegener.* 12, 5. <https://doi.org/10.1186/s13024-016-0143-y>
- Wang, Y., Fu, W.-Y., Cheung, K., Hung, K.-W., Chen, C., Geng, H., Yung, W.-H., Qu, J.Y., Fu, A.K.Y., Ip, N.Y., 2021. Astrocyte-secreted IL-33 mediates homeostatic synaptic plasticity in the adult hippocampus. *Proc. Natl. Acad. Sci.* 118. <https://doi.org/10.1073/pnas.2020810118>
- Wang, Y., Ulland, T.K., Ulrich, J.D., Song, W., Tzaferis, J.A., Hole, J.T., Yuan, P., Mahan, T.E., Shi, Y., Gilfillan, S., Cella, M., Grutzendler, J., DeMattos, R.B., Cirrito, J.R., Holtzman, D.M., Colonna, M., 2016. TREM2-mediated early microglial response limits diffusion and toxicity of amyloid plaques. *J. Exp. Med.* 213, 667–675. <https://doi.org/10.1084/jem.20151948>
- Watts, J.C., Condello, C., Stöhr, J., Oehler, A., Lee, J., DeArmond, S.J., Lannfelt, L., Ingelsson, M., Giles, K., Prusiner, S.B., 2014. Serial propagation of distinct strains of A $\beta$  prions from Alzheimer's disease patients. *Proc. Natl. Acad. Sci. U. S. A.* 111, 10323–10328. <https://doi.org/10.1073/pnas.1408900111>
- Wang, X., Sun, G., Feng, T., Zhang, J., Huang, X., Wang, T., Xie, Z., Chu, X., Yang, J., Wang, H., Chang, S., Gong, Y., Ruan, L., Zhang, G., Yan, S., Lian, W., Du, C., Yang, D., Zhang, Q., Lin, F., Liu, J., Zhang, H., Ge, C., Xiao, S., Ding, J., Geng, M., 2019. Sodium oligomannate therapeutically remodels gut microbiota and suppresses gut bacterial amino acids-shaped neuroinflammation to inhibit Alzheimer's disease progression. *Cell Res.* 29, 787–803. <https://doi.org/10.1038/s41422-019-0216-x>
- Weickenmeier, J., Jucker, M., Goriely, A., Kuhl, E., 2019. A physics-based model explains the prion-like features of neurodegeneration in Alzheimer's disease, Parkinson's disease, and amyotrophic lateral sclerosis. *J. Mech. Phys. Solids* 124, 264–281. <https://doi.org/10.1016/j.jmps.2018.10.013>
- Weller, R.O., Boche, D., Nicoll, J.A.R., 2009. Microvasculature changes and cerebral amyloid angiopathy in Alzheimer's disease and their potential impact on therapy. *Acta Neuropathol. (Berl.)* 118, 87–102. <https://doi.org/10.1007/s00401-009-0498-z>
- West, M.J., Coleman, P.D., Flood, D.G., Troncoso, J.C., 1994. Differences in the pattern of hippocampal neuronal loss in normal ageing and Alzheimer's disease. *Lancet Lond. Engl.* 344, 769–772.
- Whitmer, R.A., Sidney, S., Selby, J., Johnston, S.C., Yaffe, K., 2005. Midlife cardiovascular risk factors and risk of dementia in late life. *Neurology* 64, 277–281. <https://doi.org/10.1212/01.WNL.0000149519.47454.F2>
- Whitwell, J.L., Graff-Radford, J., Tosakulwong, N., Weigand, S.D., Machulda, M., Senjem, M.L., Schwarz, C.G., Spychalla, A.J., Jones, D.T., Drubach, D.A., Knopman, D.S., Boeve, B.F., Ertekin-Taner, N., Petersen, R.C., Lowe, V.J., Jack, C.R., Josephs, K.A., 2018. [18F]AV-1451 clustering of entorhinal and cortical uptake in Alzheimer's disease. *Ann. Neurol.* 83, 248–257. <https://doi.org/10.1002/ana.25142>
- Wilson, C.R.E., Gaffan, D., 2008. Prefrontal-inferotemporal interaction is not always necessary for reversal learning. *J. Neurosci.* 28, 5529–5538. <https://doi.org/10.1523/JNEUROSCI.0952-08.2008>
- Wu, J.W., Herman, M., Liu, L., Simoes, S., Acker, C.M., Figueroa, H., Steinberg, J.I., Margittai, M., Kaye, R., Zurzolo, C., Di Paolo, G., Duff, K.E., 2013. Small misfolded Tau species are internalized via

- bulk endocytosis and anterogradely and retrogradely transported in neurons. *J. Biol. Chem.* 288, 1856–1870. <https://doi.org/10.1074/jbc.M112.394528>
- Wu, J.W., Hussaini, S.A., Bastille, I.M., Rodriguez, G.A., Mrejeru, A., Rilett, K., Sanders, D.W., Cook, C., Fu, H., Boonen, R.A.C.M., Herman, M., Nahmani, E., Emrani, S., Figueroa, Y.H., Diamond, M.I., Clelland, C.L., Wray, S., Duff, K.E., 2016. Neuronal activity enhances tau propagation and tau pathology in vivo. *Nat. Neurosci.* 19, 1085–1092. <https://doi.org/10.1038/nn.4328>
- Yamada, K., Holth, J.K., Liao, F., Stewart, F.R., Mahan, T.E., Jiang, H., Cirrito, J.R., Patel, T.K., Hochgräfe, K., Mandelkow, E.-M., Holtzman, D.M., 2014. Neuronal activity regulates extracellular tau in vivo. *J. Exp. Med.* 211, 387–393. <https://doi.org/10.1084/jem.20131685>
- Yamamoto, K., Tanei, Z.-I., Hashimoto, T., Wakabayashi, T., Okuno, H., Naka, Y., Yizhar, O., Fenno, L.E., Fukayama, M., Bito, H., Cirrito, J.R., Holtzman, D.M., Deisseroth, K., Iwatsubo, T., 2015. Chronic optogenetic activation augments a $\beta$  pathology in a mouse model of Alzheimer disease. *Cell Rep.* 11, 859–865. <https://doi.org/10.1016/j.celrep.2015.04.017>
- Yan, P., Hu, X., Song, H., Yin, K., Bateman, R.J., Cirrito, J.R., Xiao, Q., Hsu, F.F., Turk, J.W., Xu, J., Hsu, C.Y., Holtzman, D.M., Lee, J.-M., 2006. Matrix metalloproteinase-9 degrades amyloid-beta fibrils in vitro and compact plaques in situ. *J. Biol. Chem.* 281, 24566–24574. <https://doi.org/10.1074/jbc.M602440200>
- Yan, S.D., Chen, X., Fu, J., Chen, M., Zhu, H., Roher, A., Slattery, T., Zhao, L., Nagashima, M., Morser, J., Migheli, A., Nawroth, P., Stern, D., Schmidt, A.M., 1996. RAGE and amyloid-beta peptide neurotoxicity in Alzheimer's disease. *Nature* 382, 685–691. <https://doi.org/10.1038/382685a0>
- Yang, T., Li, S., Xu, H., Walsh, D.M., Selkoe, D.J., 2017. Large Soluble Oligomers of Amyloid  $\beta$ -Protein from Alzheimer Brain Are Far Less Neuroactive Than the Smaller Oligomers to Which They Dissociate. *J. Neurosci.* 37, 152–163. <https://doi.org/10.1523/JNEUROSCI.1698-16.2016>
- Yao, Z., Gao, M., Huang, Y., 2018. Acetylation of Lysine Residues within the MT-binding Repeats Specifically Modulates the Structure Ensemble of Tau. *FASEB J.* 32, lb34–lb34. [https://doi.org/10.1096/fasebj.2018.32.1\\_supplement.lb34](https://doi.org/10.1096/fasebj.2018.32.1_supplement.lb34)
- Ye, L., Fritsch, S.K., Schelle, J., Obermüller, U., Degenhardt, K., Kaeser, S.A., Eisele, Y.S., Walker, L.C., Baumann, F., Staufenbiel, M., Jucker, M., 2015a. Persistence of A $\beta$  seeds in APP null mouse brain. *Nat. Neurosci.* 18, 1559–1561. <https://doi.org/10.1038/nn.4117>
- Ye, L., Hamaguchi, T., Fritsch, S.K., Eisele, Y.S., Obermüller, U., Jucker, M., Walker, L.C., 2015b. Progression of Seed-Induced A $\beta$  Deposition within the Limbic Connectome. *Brain Pathol. Zurich Switz.* 25, 743–752. <https://doi.org/10.1111/bpa.12252>
- Yoon, S., Piguel, N.H., Khalatyan, N., Dionisio, L.E., Savas, J.N., Penzes, P., 2021. Homer1 promotes dendritic spine growth through ankyrin-G and its loss reshapes the synaptic proteome. *Mol. Psychiatry* 1–15. <https://doi.org/10.1038/s41380-020-00991-1>
- Yoshiike, Y., Chui, D.-H., Akagi, T., Tanaka, N., Takashima, A., 2003. Specific compositions of amyloid-beta peptides as the determinant of toxic beta-aggregation. *J. Biol. Chem.* 278, 23648–23655. <https://doi.org/10.1074/jbc.M212785200>
- Yoshiyama, Y., Higuchi, M., Zhang, B., Huang, S.-M., Iwata, N., Saido, T.C., Maeda, J., Suhara, T., Trojanowski, J.Q., Lee, V.M.-Y., 2007. Synapse loss and microglial activation precede tangles in a P301S tauopathy mouse model. *Neuron* 53, 337–351. <https://doi.org/10.1016/j.neuron.2007.01.010>
- Yu, L., Edalji, R., Harlan, J.E., Holzman, T.F., Lopez, A.P., Labkovsky, B., Hillen, H., Barghorn, S., Ebert, U., Richardson, P.L., Miesbauer, L., Solomon, L., Bartley, D., Walter, K., Johnson, R.W., Hajduk, P.J., Olejniczak, E.T., 2009. Structural characterization of a soluble amyloid beta-peptide oligomer. *Biochemistry* 48, 1870–1877. <https://doi.org/10.1021/bi802046n>
- Yuan, P., Condello, C., Keene, C.D., Wang, Y., Bird, T.D., Paul, S.M., Luo, W., Colonna, M., Baddeley, D., Grutzendler, J., 2016. TREM2 Haplodeficiency in Mice and Humans Impairs the Microglia Barrier Function Leading to Decreased Amyloid Compaction and Severe Axonal Dystrophy. *Neuron* 90, 724–739. <https://doi.org/10.1016/j.neuron.2016.05.003>



- Zafar, S., Shafiq, M., Younas, N., Schmitz, M., Ferrer, I., Zerr, I., 2017. Prion Protein Interactome: Identifying Novel Targets in Slowly and Rapidly Progressive Forms of Alzheimer's Disease. *J. Alzheimers Dis.* JAD 59, 265–275. <https://doi.org/10.3233/JAD-170237>
- Zamanian, J.L., Xu, L., Foo, L.C., Nouri, N., Zhou, L., Giffard, R.G., Barres, B.A., 2012. Genomic Analysis of Reactive Astroglia. *J. Neurosci.* 32, 6391–6410. <https://doi.org/10.1523/JNEUROSCI.6221-11.2012>
- Zanjani, H., Finch, C.E., Kemper, C., Atkinson, J., McKeel, D., Morris, J.C., Price, J.L., 2005. Complement Activation in Very Early Alzheimer Disease. *Alzheimer Dis. Assoc. Disord.* 19, 55–66. <https://doi.org/10.1097/01.wad.0000165506.60370.94>
- Zempel, H., Thies, E., Mandelkow, E., Mandelkow, E.-M., 2010. A $\beta$  Oligomers Cause Localized Ca<sup>2+</sup> Elevation, Missorting of Endogenous Tau into Dendrites, Tau Phosphorylation, and Destruction of Microtubules and Spines. *J. Neurosci.* 30, 11938–11950. <https://doi.org/10.1523/JNEUROSCI.2357-10.2010>
- Zhao, R., Hu, W., Tsai, J., Li, W., Gan, W.-B., 2017. Microglia limit the expansion of  $\beta$ -amyloid plaques in a mouse model of Alzheimer's disease. *Mol. Neurodegener.* 12, 47. <https://doi.org/10.1186/s13024-017-0188-6>
- Zhou, L., McInnes, J., Wierda, K., Holt, M., Herrmann, A.G., Jackson, R.J., Wang, Y.-C., Swerts, J., Beyens, J., Miskiewicz, K., Vilain, S., Dewachter, I., Moechars, D., De Strooper, B., Spires-Jones, T.L., De Wit, J., Verstreken, P., 2017. Tau association with synaptic vesicles causes presynaptic dysfunction. *Nat. Commun.* 8, 15295. <https://doi.org/10.1038/ncomms15295>
- Ziegler-Waldkirch, S., d'Errico, P., Sauer, J.-F., Erny, D., Savanthrapadian, S., Loreth, D., Katzmarski, N., Blank, T., Bartos, M., Prinz, M., Meyer-Luehmann, M., 2018. Seed-induced A $\beta$  deposition is modulated by microglia under environmental enrichment in a mouse model of Alzheimer's disease. *EMBO J.* 37, 167–182. <https://doi.org/10.15252/embj.201797021>

# **ANNEXES**



## ANNEX I – ADDITIONAL PUBLICATION

---

Hérard AS., Petit F., Gary C., Guillermier M., Boluda S., Garin C., **Lam S.**, Dhenain M. Induction of amyloid- $\beta$  deposits from serially transmitted, histologically silent, A $\beta$  seeds issued from human brains. *Acta Neuropathologica Communications*. 30;8(1):205. 2020. <https://doi.org/10.1186/s40478-020-01081-7>.

RESEARCH

Open Access



# Induction of amyloid- $\beta$ deposits from serially transmitted, histologically silent, A $\beta$ seeds issued from human brains

Anne-Sophie Hérard<sup>1,2†</sup>, Fanny Petit<sup>1,2†</sup>, Charlotte Gary<sup>1,2</sup>, Martine Guillermier<sup>1,2</sup>, Susana Boluda<sup>3,4</sup>, Clément M. Garin<sup>1,2</sup>, The Brainbank Neuro-CEB Neuropathology Network<sup>5</sup>, Suzanne Lam<sup>1,2</sup> and Marc Dhenain<sup>1,2\*</sup> 

## Abstract

In humans, iatrogenic transmission of cerebral amyloid- $\beta$  (A $\beta$ )-amyloidosis is suspected following inoculation of pituitary-derived hormones or dural grafts presumably contaminated with A $\beta$  proteins as well as after cerebral surgeries. Experimentally, intracerebral inoculation of brain homogenate extracts containing misfolded A $\beta$  can seed A $\beta$  deposition in transgenic mouse models of amyloidosis or in non-human primates. The transmission of cerebral A $\beta$  is governed by the host and by the inoculated samples. It is critical to better characterize the propensities of different hosts to develop A $\beta$  deposition after contamination by an A $\beta$ -positive sample as well as to better assess which biological samples can transmit this lesion. A $\beta$  precursor protein (huAPP<sub>wt</sub>) mice express humanized non-mutated forms of A $\beta$  precursor protein and do not spontaneously develop A $\beta$  or amyloid deposits. We found that inoculation of A $\beta$ -positive brain extracts from Alzheimer patients in these mice leads to a sparse A $\beta$  deposition close to the alveus 18 months post-inoculation. However, it does not induce cortical or hippocampal A $\beta$  deposition. Secondary inoculation of apparently amyloid deposit-free hippocampal extracts from these huAPP<sub>wt</sub> mice to APP<sub>swe</sub>/PS1<sub>dE9</sub> mouse models of amyloidosis enhanced A $\beta$  deposition in the alveus 9 months post-inoculation. This suggests that A $\beta$  seeds issued from human brain samples can persist in furtive forms in brain tissues while maintaining their ability to foster A $\beta$  deposition in receptive hosts that overexpress endogenous A $\beta$ . This work emphasizes the need for high-level preventive measures, especially in the context of neurosurgery, to prevent the risk of iatrogenic transmission of A $\beta$  lesions from samples with sparse amyloid markers.

**Keywords:**  $\beta$ -amyloid pathology, Alzheimer's disease, A $\beta$  transmission

## Introduction

Epidemiological data suggest that, in humans, iatrogenic cerebral A $\beta$ -amyloidosis can be induced following administration of cadaver-sourced human growth hormone [3, 9] or dura mater graft [8] containing amyloid- $\beta$  (A $\beta$ ) proteins as well as after cerebral surgeries potentially involving tools contaminated with A $\beta$  [10]. In addition to their occurrence in parenchymal tissue, these iatrogenic induced lesions can affect cerebral vasculature leading to amyloid angiopathy sometimes associated to cerebral hemorrhages inducing dramatic clinical signs and fatality

\*Correspondence: marc.dhenain@cea.fr

<sup>†</sup>Anne-Sophie Hérard and Fanny Petit equally contributed to this work  
<sup>1</sup>Laboratoire des Maladies Neurodégénératives, Université Paris-Saclay, CEA, CNRS, 18 Route du Panorama, 92265 Fontenay-aux-Roses, France  
Full list of author information is available at the end of the article



© The Author(s) 2020. **Open Access** This article is licensed under a Creative Commons Attribution 4.0 International License, which permits use, sharing, adaptation, distribution and reproduction in any medium or format, as long as you give appropriate credit to the original author(s) and the source, provide a link to the Creative Commons licence, and indicate if changes were made. The images or other third party material in this article are included in the article's Creative Commons licence, unless indicated otherwise in a credit line to the material. If material is not included in the article's Creative Commons licence and your intended use is not permitted by statutory regulation or exceeds the permitted use, you will need to obtain permission directly from the copyright holder. To view a copy of this licence, visit <http://creativecommons.org/licenses/by/4.0/>. The Creative Commons Public Domain Dedication waiver (<http://creativecommons.org/publicdomain/zero/1.0/>) applies to the data made available in this article, unless otherwise stated in a credit line to the data.

[1, 8, 10]. A $\beta$  deposition can be induced experimentally in mouse models that overexpress mutated forms of A $\beta$  protein precursor (A $\beta$ PP) after intracerebral inoculation of A $\beta$ -containing brain extracts issued from transgenic mouse models of amyloidosis or from Alzheimer's disease patients [5, 14]. The experimental transmission of A $\beta$ -amyloidosis is considered to be related to A $\beta$  seeds that act as self-propagating agents responsible for its initiation, progression and spreading in the brain. It has been observed that there is variability in the development of A $\beta$  deposition between different hosts, e.g. different mouse models, which implies that host factors are critical for in vivo seeding [14]. The ability to induce A $\beta$  deposition is also governed by the inoculated samples [14]. In order to assess the risk of iatrogenic contamination, it is critical: (1) to extensively characterize the hosts in which A $\beta$  deposition can be induced, especially in animals with low propensities to develop amyloidosis; (2) to evaluate the potential of different brain samples to induce A $\beta$  deposition. Our group recently showed that inoculation of human AD brain extracts to non-human primates that have a cerebral environment close to the human one can induce cerebral A $\beta$  deposition [5]. Here, we found that intra-hippocampal inoculation of human AD brain extracts to huAPP<sub>wt</sub> mice, a model that expresses humanized non-mutated forms of A $\beta$ PP and does not spontaneously develop amyloid deposits, induces slight A $\beta$  deposition in regions surrounding the alveus but not in other parts of the hippocampus or brain regions. This suggests that induction of cerebral A $\beta$  deposition is low in models that have a low propensity to develop amyloid pathology. We then showed that apparently A $\beta$ -deposit-free hippocampal samples from AD-inoculated huAPP<sub>wt</sub> mice enhance A $\beta$  deposition in the APP<sub>swe</sub>/PS1<sub>ΔE9</sub> mouse model 9 months after their intrahippocampal inoculation. Thus, A $\beta$  seeds can be transmitted from apparently A $\beta$ -deposit-negative samples and induce A $\beta$  deposition in hosts that have a high propensity to develop amyloid pathology. This suggests that the prevention of iatrogenic amyloid transmission from one patient to another does not rely solely on the amyloid status of the donors since samples with sparse A $\beta$  lesions can induce pathology in a receptive host.

## Materials and methods

### Human brain samples

Frozen brain tissue samples (parietal cortex) from two Alzheimer's disease patients (Braak stage VI, Thal phases 5 and 4, respectively) and one control individual that did not show clinical or histological signs of neurological disease (Braak stage/Thal phase 0) were obtained through a brain donation program of the Brainbank Neuro-CEB Neuropathology Network. The consent forms were

signed by either the patients themselves or their next of kin in their name, in accordance with French bioethics laws. The Brainbank Neuro-CEB Neuropathology Network has been declared at the Ministry of Higher Education and Research and has received approval to distribute samples (agreement AC-2013-1887).

Detailed histological and biochemical characterization of these brains were previously published, as well as the preparation and assessment of human brain homogenates [5]. Operators were blinded to the status of the patients. The routine detection of A $\beta$  and tau deposits was performed with the 6F3D anti-A $\beta$  antibody (Dako, Glostrup, Denmark, 1/200) and polyclonal anti-tau antibody (Dako, Glostrup, Denmark, 1/500). Parietal cortex homogenates (20% weight/volume in a sterile 5% glucose solution) were aliquoted into sterile polypropylene tubes and stored at  $-80^{\circ}\text{C}$  until use. The 20% aliquoted homogenates were diluted to 10% (w/v) in sterile Dulbecco's phosphate-buffered saline (PBS, Gibco, ThermoFisher Scientific, France) extemporaneously prior to inoculation in mice. The extracts from the two Alzheimer brain samples were shown to be able to induce amyloid deposition four months after inoculation in two-month-old female APP<sub>swe</sub>/PS1<sub>ΔE9</sub> mice [5].

### Ethical statement for animal experiments

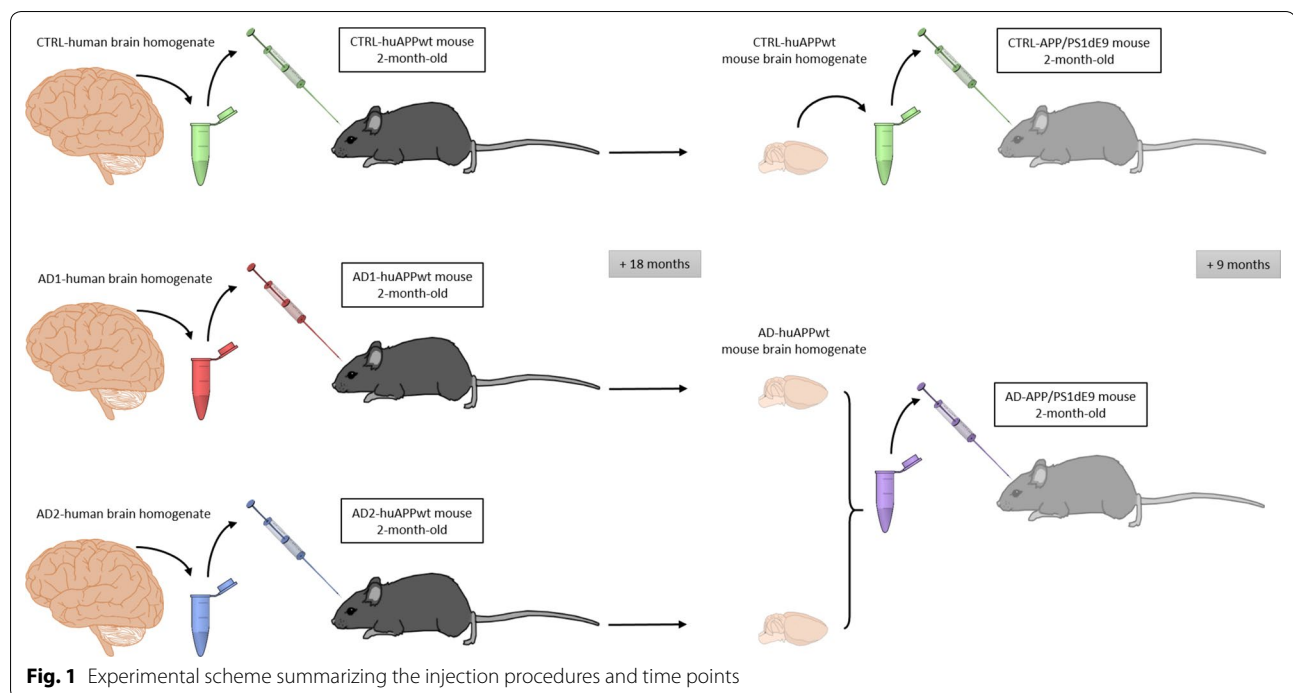
All animal experiments were conducted in accordance with the European Community Council Directive 2010/63/ECC. Animal care was in accordance with institutional guidelines and experimental procedures were approved by local ethical committees (APAFIS 2015062412105538 v1; ethics committees CEtEA-CEA DSV IdF N°44, France). They were performed in a facility authorized by local authorities (authorization #D92-032-02), in strict accordance with recommendations of the European Union (2010-63/EEC), and in compliance with the 3R recommendations. Animal care was supervised by a dedicated veterinarian and animal technicians. Animals were housed under standard environmental conditions (12-h light-dark cycle, temperature:  $22 \pm 1^{\circ}\text{C}$  and humidity: 50%) with ad libitum access to food and water.

### Animals and overall experimental plan

#### Transgenic mouse models

The overall experimental plan is described in Fig. 1.

First, three experimental groups were initially created for experiments involving female huAPP<sub>wt</sub> mice. These transgenic animals express a wild type form of the  $\beta$ -amyloid peptide precursor (A $\beta$ PP) [16]. Mice involved in this study were heterozygous. These mice do not display any A $\beta$  deposits even at late age [15]. HuAPP<sub>wt</sub> mice were stereotaxically inoculated, in the hippocampus, at 2 months of age with AD brain



homogenates from the two different AD patients (AD-huAPP<sub>wt</sub>, n=6 for AD1, n=6 for AD2) or with control human brain homogenate (CTRL-huAPP<sub>wt</sub>, n=8). Their brains were collected at 20 months of age (18 months post-inoculation) and used for histological and biochemical analyses. Data from huAPP<sub>wt</sub> mice inoculated with AD brain homogenates were pooled for statistical analysis. We thus compared two groups of animals, CTRL-huAPP<sub>wt</sub> (n=8) and AD-huAPP<sub>wt</sub> (n=12). Brains from huAPP<sub>wt</sub> mice were also used to prepare hippocampal homogenates for secondary injection into APP<sub>swe</sub>/PS1<sub>dE9</sub> mice. Two homogenates were prepared. The first one was made from the hippocampi of huAPP<sub>wt</sub> mice inoculated with either AD1 (n=6) or AD2 (n=6) that were pooled to serve as a single homogenate. The second one was issued from the hippocampi of huAPP<sub>wt</sub> mice inoculated with CTRL brains (n=8). The APP<sub>swe</sub>/PS1<sub>dE9</sub> transgenic mice express mutated forms of both human A $\beta$ PP (APP<sub>swe</sub>: KM670/671NL) and presenilin 1 (deletion of exon 9) at high levels all throughout the brain and present with amyloid plaques and amyloid angiopathy [4]. Two experimental groups were followed-up: APP<sub>swe</sub>/PS1<sub>dE9</sub> mice inoculated with brain homogenates from AD-huAPP<sub>wt</sub> mice (AD-APP<sub>swe</sub>/PS1<sub>dE9</sub>, n=6) or from CTRL-huAPP<sub>wt</sub> mice (CTRL-APP<sub>swe</sub>/PS1<sub>dE9</sub>, n=5). The mice were stereotactically injected, in the hippocampus, at 2 months of age. Their brains were collected at 11 months of age (9 months post-inoculation).

#### **Stereotaxic injections and mouse brain collection**

Inoculations were performed bilaterally in the dorsal hippocampus (AP - 2 mm, DV - 2 mm, L  $\pm$  1 mm [17]). The animals were anaesthetized by an intraperitoneal ketamine-xylazine injection (Imalgène 1000, Merial, France (1 mg/10 g); 2% Rompun, Bayer Healthcare, Leverkusen, Germany (0.1 mg/10 g)) and placed in a stereotaxic frame (Phymep, France). Respiration rate was monitored and body temperature was maintained at 37  $\pm$  0.5  $^{\circ}$ C with a heating blanket during surgery. After making a midline incision of the scalp, burr holes were drilled in the appropriate location. Bilateral intrahippocampal injections of 2  $\mu$ L 10% brain homogenates were performed with a 26-gauge needle. The surgical area was cleaned before and after surgery (iodinate povidone, Vetedine, Vetoquinol, France), the incision sutured, and the animals placed in an incubator (temperature 25  $^{\circ}$ C) and monitored until recovery from anesthesia.

Animals were euthanized with an overdose of sodium pentobarbital (100 mg/kg intraperitoneally), followed by intracardiac perfusion with phosphate-buffered saline (PBS, Gibco, ThermoFisher Scientific, France) for APP<sub>swe</sub>/PS1<sub>dE9</sub> mice only. Indeed, to preserve soluble A $\beta$  species at best in the brain of huAPP<sub>wt</sub> mice initially inoculated with human brain homogenates, we decided not to drain their brains with PBS. The left hemisphere was post-fixed with 4% paraformaldehyde in PBS for histological analysis. The right hemisphere was dissected to extract the hippocampus, which was immediately

snap-frozen in liquid nitrogen and stored at  $-80^{\circ}\text{C}$  for biochemical analysis and homogenate preparation.

#### **huAPPwt mouse brain homogenate preparation**

Hippocampi from huAPP<sub>wt</sub> mice were sonicated 6 times (cycle 0.5, amplitude 30%, Heidolph, Entraigues sur la Sorgue, France) in Dulbecco's PBS (10% m/m). They were then homogenized using ceramic beads (CK14-KT03961-1-003.2) and a Precellys 24 tissue homogenizer (Bertin Instrument, France) at 5000 rpm for 20 s. Samples were vortexed for 2 min, sonicated for 5 s (cycle 1, 40 amplitude units, 80 W) and centrifugated at 3000 g for 5 min. The supernatant was aliquoted and stored at  $-80^{\circ}\text{C}$ . Samples were extemporaneously sonicated 20 times (cycle 0.5, 20 amplitude units) before injection in APP<sub>swe</sub>/PS1<sub>dE9</sub> mice. A fraction of all the huAPP<sub>wt</sub> mouse hippocampal homogenates, either AD- or CTRL-inoculated, were pooled to prepare the two homogenates injected in the brains of APP<sub>swe</sub>/PS1<sub>dE9</sub> mice.

#### **Immunohistochemistry and microscopic image analysis**

The 4% paraformaldehyde post-fixed hemispheres were cryoprotected using 15% and 30% sucrose solutions. Series of brain coronal sections (40- $\mu\text{m}$ -thick) were cut on a sliding freezing microtome (SM2400, Leica Microsystems). The floating histological serial sections were preserved in a storage solution (30% glycerol, 30% ethylene glycol, 30% distilled water, and 10% phosphate buffer) at  $-20^{\circ}\text{C}$  until use. Serial sections of the entire brain were stained for the evaluation of A $\beta$  pathology (4G8 immunohistochemistry and Congo red staining). For 4G8 immunohistochemistry brain sections were rinsed with PBS, pre-treated with 70% formic acid for 3 min (only for biotinylated-4G8) and then incubated in 0.3% hydrogen peroxide for 20 min. Sections were then blocked with PBS-0.2% Triton (Triton X-100, Sigma, St Louis, MO, USA) and 4.5% normal goat serum (NGS) for 30 min before overnight incubation with biotinylated-4G8 at  $4^{\circ}\text{C}$  (1:500; Biologend Covance #SIGNET-39240, monoclonal). The sections stained were rinsed with PBS and then incubated with ABC Vectastain (Vector Labs) before diaminobenzidine tetrahydrochloride (DAB) revelation (DAB SK4100 kit, Vector Labs). For Congo red staining, sections were pretreated with 1% NaOH in 80% EthOH saturated with NaCl for 30 min. Then, they were immersed in the same solution saturated with Congo red for 30 min. Image of stained sections were digitized with a Zeiss Axio Scan.Z1 (Zeiss, Jena, Germany) whole slide imaging microscope at X20 (0.22  $\mu\text{m}$  in plane resolution). Sections stained for A $\beta$  or Congo red were blindly analyzed using ImageJ software [18]. A $\beta$  deposits were segmented from 4G8-immunostained sections by applying a threshold (value of 100) on the blue component of

the 8-bit images. A $\beta$  burden was evaluated as the percentage of surface occupied by the 4G8 staining inside delineated regions of interest as well as the number of plaques per unit of surface. They were quantified in four regions: the hippocampus, parietal cortex, entorhinal cortex, and a region that follows the virtual ventricle that borders the alveus of the hippocampus towards the lateral ventricle. In the hippocampus, ROI definition was based on manual drawing following the region shape. In the parietal and entorhinal cortices, it relied on circles of constant diameter. For the alveus, ROIs were ribbons of 88  $\mu\text{m}$  wide centered on the alveus (one per section, all labelled sections per mouse, selection brush tool from ImageJ). Four to seven sections were used for each animal depending on the number of available sections. Scientists who performed the analyses were blinded to the inoculation groups. Evaluations from Congo-red stained sections used similar methods (but with a threshold of 90), based on the green component of the 8-bit images. As lesions were more discrete, ribbons used for alveus ROIs were 35  $\mu\text{m}$  wide. Labelling from structure with a diameter inferior to 7  $\mu\text{m}$  were excluded from the quantification to avoid measures of background signal.

#### **Quantification of A $\beta$ by immunoassays**

Hippocampal extracts from both mouse strains were homogenized in Dulbecco's PBS (10% m/m) and sonicated 6 times (cycle 0.5, 30% amplitude). They were incubated with a lysis buffer at a final concentration of 50 mM Tris HCl pH7.4, 150 mM NaCl, 1% Triton X-100 supplemented with protease and phosphatase inhibitor cocktails, and sonicated again as previously described. Samples were centrifugated at 20,000 g for 20 min at  $+4^{\circ}\text{C}$ , the supernatant was collected as the soluble fraction and stored at  $-80^{\circ}\text{C}$  until use. A $\beta$  was measured by an electrochemiluminescence (ECL)-linked immunoassay (Meso Scale Discovery, MSD). The MSD V-PLEX A $\beta$  peptide panel 1 (6E10) kit was used according to the manufacturer's instructions. Briefly, samples were diluted 10-fold or 25-fold in the provided dilution buffer, respectively for soluble and insoluble fractions. Meanwhile, 96-well plates pre-coated with capture antibodies against A $\beta$ x-40 and A $\beta$ x-42 were blocked for 1 h and washed three times according to the manufacturer instructions, at room temperature. The SULFO-TAG anti-A $\beta$  6E10 detection antibody solution was then added to the wells and co-incubated with the diluted samples or calibrators at room temperature with shaking for 2 h. After washing, MSD Read Buffer T was added to the wells and the plate was read immediately on a MSD Sector Imager 2400. Data were analyzed using the MSD DISCOVERY WORKBENCH software 4.0. Internal samples were used



for quality control of the assay performance and inter-plate variability. All samples and calibrators were run in duplicates.

### Statistics

Statistical analysis was performed using GraphPad Prism software, version 8, using a Mann-Whitney test (one-tailed). Data are shown on scattered dot plots with median and interquartile range.

## Results

### Human Alzheimer's disease brain extracts induce a slight amyloid pathology in huAPP<sub>wt</sub> mice

We bilaterally inoculated brain extracts from clinically and pathologically confirmed AD patients into the hippocampus of huAPP<sub>wt</sub> mice. A brain extract from a non-AD patient was used as control. In a previous study, we demonstrated that, 4 months after inoculation, APP<sub>swe</sub>/PS1<sub>dE9</sub> mice inoculated with the same AD brain extracts display increased amyloid plaque deposition and higher level of biochemically detectable A $\beta$  as compared to mice inoculated with a CTRL human brain extract [5].

Using 4G8 biotinylated antibodies or Congo red, we did not detect any A $\beta$  or amyloid deposits in the cortex or hippocampus of the huAPP<sub>wt</sub> mice whether they were inoculated with human AD- or CTRL-brains. A clear labelling for A $\beta$  was however detected in 4G8-stained sections in the region surrounding the alveus of almost all the mice inoculated with the AD brains (Fig. 2a–c). It consisted of diffuse extracellular deposits that did not adopt the morphology of plaques and were not present around blood vessels (Fig. 2c). This labelling was not detectable in the CTRL-inoculated mice (Fig. 2e–f). Congo-red stained sections did not reveal any amyloid deposits in AD- or CTRL-inoculated mice (Fig. 2g–h). Quantification of 4G8 sections confirmed the significantly higher A $\beta$  load in AD-inoculated mice as compared to CTRL-inoculated mice (Fig. 2d,  $U=9$ ;  $p=0.001$ ) and only 2/12 AD-inoculated mice did not display obvious A $\beta$  load. Biochemical analysis of huAPP<sub>wt</sub> mouse hippocampus extracts demonstrated similar amounts of soluble A $\beta$ <sub>1-42</sub> ( $U=26$ ;  $p=0.11$ ) or A $\beta$ <sub>1-40</sub> ( $U=32.50$ ;  $p=0.26$ ) in both AD and CTRL groups (data not shown).

### Induction of amyloid pathology in APP<sub>swe</sub>/PS1<sub>dE9</sub> mice after inoculation of brain samples from huAPP<sub>wt</sub> mice primarily inoculated with AD brains

Hippocampal homogenates from AD-huAPP<sub>wt</sub> or CTRL-huAPP<sub>wt</sub> mice were stereotaxically injected in the hippocampus of APP<sub>swe</sub>/PS1<sub>dE9</sub> mice (AD-APP<sub>swe</sub>/PS1<sub>dE9</sub> or CTRL-APP<sub>swe</sub>/PS1<sub>dE9</sub>). Nine months post-inoculation, as expected, 4G8-positive A $\beta$  plaques were detected in the hippocampus and cortex of both AD-APP<sub>swe</sub>/PS1<sub>dE9</sub>

(Fig. 3a, b) and CTRL-APP<sub>swe</sub>/PS1<sub>dE9</sub> (Fig. 3c, d) animals. A clear labelling for A $\beta$ , in the form of plaques, was also detected in the region surrounding the alveus of almost all the AD-APP<sub>swe</sub>/PS1<sub>dE9</sub> mice, and to a lower extent of CTRL-APP<sub>swe</sub>/PS1<sub>dE9</sub> mice. The morphology of the A $\beta$  deposits observed in the alveus differed in the APP<sub>swe</sub>/PS1<sub>dE9</sub> compared to that seen in the huAPP<sub>wt</sub> mice. In the APP<sub>swe</sub>/PS1<sub>dE9</sub> A $\beta$  formed plaques while it was more diffuse in AD-huAPP<sub>wt</sub> mice (Fig. 2a, b). However, as for AD-huAPP<sub>wt</sub> mice, A $\beta$  was not deposited within blood vessels of the APP<sub>swe</sub>/PS1<sub>dE9</sub> mice (Fig. 3h). Quantification of 4G8-stained histological sections revealed an increased A $\beta$  load (Fig. 3e, Mann-Whitney test,  $U=1$ ,  $p=0.004$ ) and an increase in the number of A $\beta$  plaques per surface unit (Fig. 3f, Mann-Whitney test,  $U=3$ ,  $p=0.015$ ) in the regions surrounding the alveus of the AD-APP<sub>swe</sub>/PS1<sub>dE9</sub> mice as compared to CTRL-APP<sub>swe</sub>/PS1<sub>dE9</sub> mice. These plaques were not different in size ( $U=10$ ,  $p=0.2$ ). There was not a statistically significant difference in A $\beta$  load in the hippocampus (Fig. 3g,  $U=11$ ,  $p=0.3$ ), parietal cortex (not shown,  $U=14$ ,  $p=0.5$ ) or entorhinal cortex (not shown,  $U=13$ ,  $p=0.4$ ) of these two groups. The number of A $\beta$  plaques per surface unit was also not different between these two groups in these regions (not shown,  $U>10$ ,  $p>0.2$ ). Staining with Congo red detected amyloid plaques in the hippocampus and cortex of AD-APP<sub>swe</sub>/PS1<sub>dE9</sub> animals (Fig. 3i) or CTRL-APP<sub>swe</sub>/PS1<sub>dE9</sub> animals (Fig. 3j). Some amyloid plaques were also detected in the region surrounding the alveus of almost all the mice. Whatever the regions, congophilic plaques were however less numerous and visible than 4G8-labelled plaques. Unlike for 4G8 staining, quantification of Congo red stained sections did not show differences between the two groups of APP<sub>swe</sub>/PS1<sub>dE9</sub> animals either in regions surrounding the alveus ( $U=10$ ,  $p=0.2$ ) or in other regions as the hippocampus ( $U=9$ ,  $p=0.2$ ) or parietal cortex ( $U=13$ ,  $p=0.4$ ). Soluble A $\beta$ <sub>1-42</sub> and A $\beta$ <sub>1-40</sub> were assayed in the hippocampus of the APP<sub>swe</sub>/PS1<sub>dE9</sub> animals inoculated with AD- or CTRL-huAPP<sub>wt</sub> mouse brain homogenates. No differences were found between the two groups of animals (not shown, A $\beta$ <sub>1-42</sub>:  $U=11$ ,  $p=0.3$ ; A $\beta$ <sub>1-40</sub>:  $U=12$ ;  $p=0.3$ ).

## Discussion

Human AD-brain extracts were inoculated in the hippocampus of huAPP<sub>wt</sub> mice that express human wild-type A $\beta$ PP gene. We showed that, 18 months after inoculation, there was no induction of cortical or hippocampal A $\beta$  deposits. However, extracts from the apparently A $\beta$ -deposit-free hippocampus of these AD-inoculated animals induced A $\beta$ -deposition in APP<sub>swe</sub>/PS1<sub>dE9</sub> mice 9 months after inoculation. This suggests

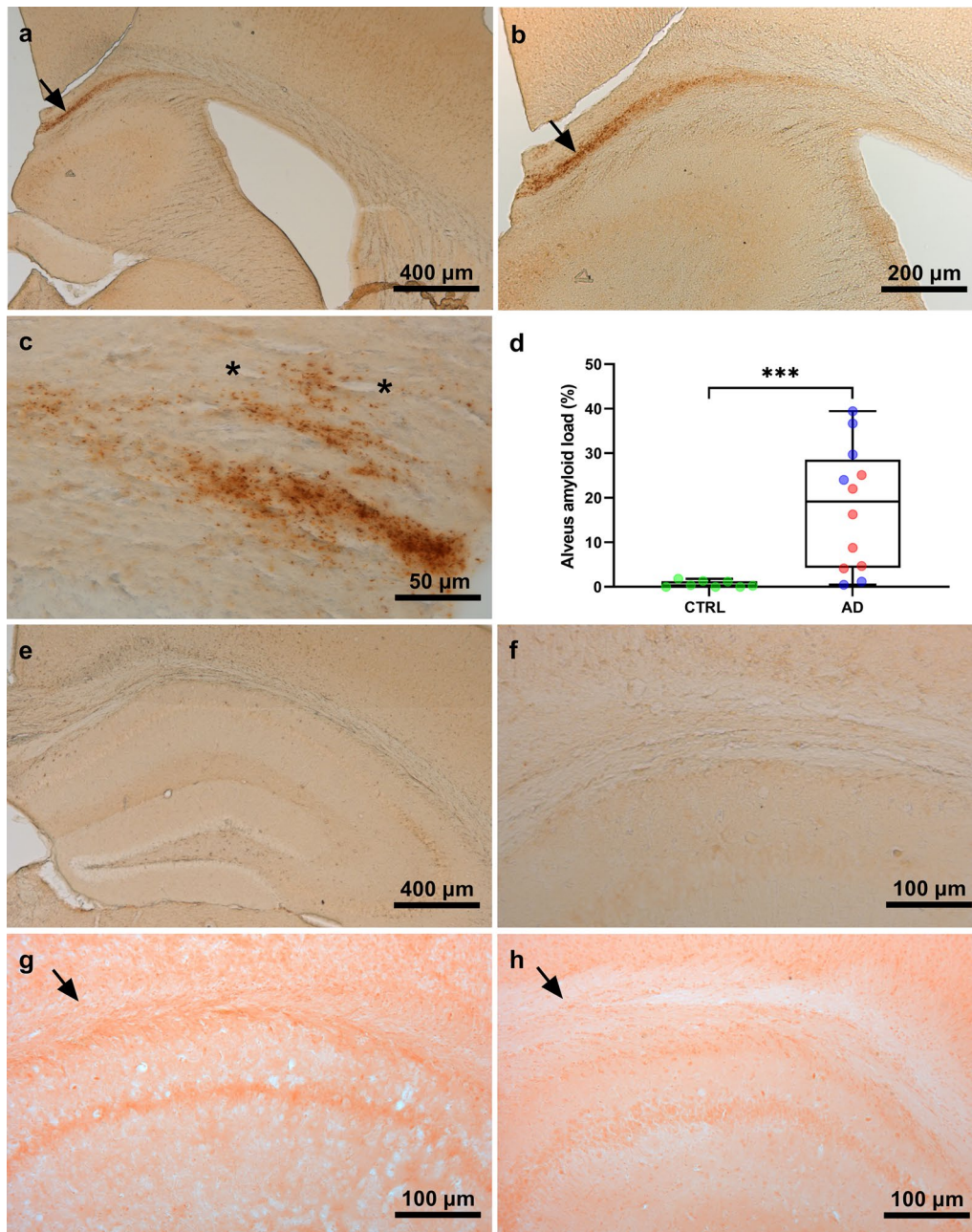


**Fig. 2** Detection of A $\beta$  in the huAPP<sub>wt</sub> mice inoculated with AD or CTRL brain. Mice inoculated with human brain homogenates were euthanized 18 months after the inoculation. Brain sections were stained with anti-A $\beta$  (4G8-biotinylated) antibody. Staining was detected in the region surrounding the alveus of almost all the mice inoculated with the AD brains (**a–c**, arrows) but not the CTRL-brains (**e–f**). There was no staining in the hippocampus or cortex of the inoculated mice. 4G8 staining was not observed in the close vicinity of blood vessels (asterisk) as shown in a mouse inoculated with AD brain extract (**c**). Congo red did not stain any deposits in the inoculated mice, as shown in the alveus of an AD- (**g**) or CTRL-inoculated animal (**h**). 4G8-labeling was quantified in the alveus (**d**). First, regions of interest corresponding to the alveus were defined as ribbons of 88  $\mu$ m wide centered on the virtual ventricle that borders the alveus of the hippocampus. Amyloid burden in this region was defined, using a thresholding method, as the percentage of surface occupied by the 4G8-staining inside the regions of interest. This analysis showed significant difference between CTRL and AD mice ( $U = 9; p = 0.001$ )

(See figure on next page.)

**Fig. 3** Increased A $\beta$  deposition in the alveus of 11-month-old APP<sub>swe</sub>/PS1<sub>dE9</sub> mice inoculated with AD-huAPP<sub>wt</sub> brain homogenate. APP<sub>swe</sub>/PS1<sub>dE9</sub> mice were inoculated with apparently amyloid deposit-free hippocampus extracts from huAPP<sub>wt</sub> mice previously inoculated with human brain homogenates and euthanized 18 months after the inoculation. A $\beta$  (biotinylated 4G8) stained brain sections from the APP<sub>swe</sub>/PS1<sub>dE9</sub> mice showed plaques in the hippocampus of all mice (**a–d**). A $\beta$  deposition was also seen in regions surrounding the alveus of the mice inoculated with AD-huAPP<sub>wt</sub> brains (**a–b**, arrows). 4G8 staining did not involve blood vessels (asterisk) as highlighted here in a mouse inoculated with AD-huAPP<sub>wt</sub> (**h**). 4G8-positive load (**e**) and the number of plaques per surface unit (**f**) were significantly increased in the region surrounding the alveus of AD-APP<sub>swe</sub>/PS1<sub>dE9</sub> mice compared to the CTRL-APP<sub>swe</sub>/PS1<sub>dE9</sub> ( $U = 1, p = 0.004^{**}$ , and  $U = 3, p = 0.015^*$ , respectively). **g** Amyloid load was not different in the hippocampus of AD-APP<sub>swe</sub>/PS1<sub>dE9</sub> and CTRL-APP<sub>swe</sub>/PS1<sub>dE9</sub> mice ( $U = 11, p = 0.3$ ). Congo red stained brain sections from the APP<sub>swe</sub>/PS1<sub>dE9</sub> mice showed amyloid plaques (arrows) in the hippocampus and cortex of mice from AD (**i**) and CTRL groups (**j**)

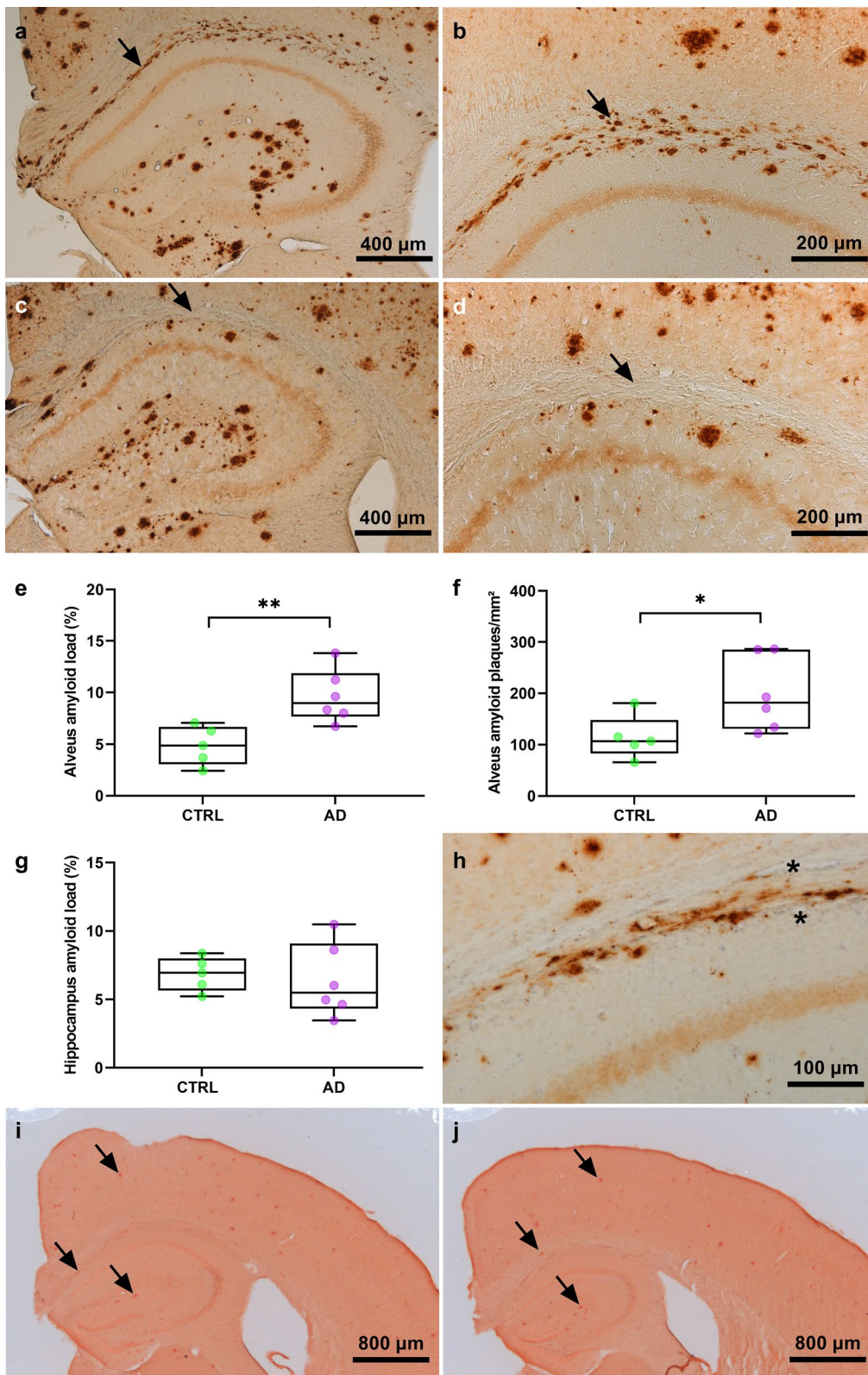
that A $\beta$  seeds, able to foster A $\beta$  deposition, were present in the hippocampus of huAPP<sub>wt</sub> without being easily detectable.

Several studies have shown that the inoculation of human brains containing A $\beta$  seeds can accelerate cerebral amyloid plaque occurrence in mouse models or primates [5, 14]. The ability to induce cerebral A $\beta$ -amyloidosis experimentally highly depends on the hosts and the inoculated samples [14]. Inoculation of human brains in hosts that overexpress A $\beta$ PP (i.e. in specific transgenic mice) leads to an acceleration of A $\beta$  plaque occurrence. In particular, in a previous study, we showed that inoculation to APP<sub>swe</sub>/PS1<sub>dE9</sub> mouse models of amyloidosis of the human AD brain extracts used in the current study induced A $\beta$  depositions 4 months after the inoculation [5]. Studies in primates that have a natural expression of A $\beta$ PP (100% homology with the human gene) showed that sparse A $\beta$  deposits can also be induced following inoculation of A $\beta$  seeds [5]. A previous study in huAPP<sub>wt</sub> mice that express the human wild-type A $\beta$ PP gene, which never develop A $\beta$  plaques spontaneously, showed sparse A $\beta$  deposition in the cortex and hippocampus in 40% of the animals 9 months post inoculation, in 65% of the animals 15 months post inoculation and in 100% of the animals 19 months post inoculation [15]. In our hands, small diffuse A $\beta$  deposits were detected in the region surrounding the alveus, but Congoophilic amyloid plaques were not detected. The lower detection of A $\beta$  deposits in our study as compared to the previous study [15] might be related to a different preparation of the human samples, and potentially different sonication procedures.

We wondered why A $\beta$  accumulation occurred in regions surrounding the alveus. Several articles reported A $\beta$  deposition in this region after intrahippocampal inoculation of human AD-brain homogenates [2, 5, 11, 14, 21], amyloid-positive mouse brains [7, 14, 20, 22] or synthetic A $\beta$  species [19, 20]. The presence of abnormal protein deposits in this region was also reported after inoculation of prion homogenates in the thalamus/brain midline with a needle that crossed the parietal cortex, the lateral ventricle and the hippocampus [6]. It was

suggested that the orientated disposition of white matter fibers in this area might provide an efficient path for the diffusion from the inoculation sites towards the lateral ventricles to clear pathological proteins [13].

One of the critical questions to prevent iatrogenic transmission of amyloid concerns the propensity of the donor to induce A $\beta$ -deposits or amyloidosis. Studies in transgenic mouse models of A $\beta$ -amyloidosis proved that amyloid plaque-positive brains from non-demented subjects are able to induce cerebral A $\beta$ -amyloidosis [2] while amyloid plaque-negative human brain samples were not able to induce A $\beta$ -amyloid pathology [2]. Here, we show that homogenates from hippocampi free of A $\beta$  plaques can induce A $\beta$  deposition when injected into APP<sub>swe</sub>/PS1<sub>dE9</sub> mice. We hypothesize that the huAPP<sub>wt</sub> hippocampi from mice previously inoculated with AD brain extracts probably contained very low amount of A $\beta$  seeds. Indeed, even if A $\beta$ -deposits were not detected in the hippocampus, they were detected in the alveus that juxtaposes the hippocampus. This small amount of A $\beta$  did not lead to A $\beta$  plaque occurrence or stronger A $\beta$  detection by biochemical analysis of A $\beta$ <sub>1-40</sub> or A $\beta$ <sub>1-42</sub> in the hippocampi of huAPP<sub>wt</sub> animals. However, these samples could induce an increase A $\beta$  deposition in regions surrounding the alveus, 9 months post inoculation after their inoculation in the hippocampus of APP<sub>swe</sub>/PS1<sub>dE9</sub> mice. Evidence for A $\beta$  deposition was provided by the increase in A $\beta$  burden as well as the increase in the number of A $\beta$ -plaques. This clearly outlines that brains with minimal amount of A $\beta$  are able to induce A $\beta$  deposition. Furthermore, a recent study showed long-term resilience (180 days) of transmissible but barely detectable A $\beta$  seeds in A $\beta$ PP null mice previously inoculated with the brain of mouse models of amyloidosis [23]. The study was based on inoculation of A $\beta$ -containing brain extracts issued from very old transgenic mice with high amyloid load in A $\beta$ PP null mice that cannot produce A $\beta$  proteins. These mice were analyzed up to 6 months after inoculation and only slight A $\beta$  accumulation (pg/ml range) could be detected by ultra-sensitive techniques in their brains. When these brains were intracerebrally inoculated



in 3-month-old APP23 mice (harboring the APP<sub>swe</sub> (APP KM670/671NL) transgene), they accelerated A $\beta$ -deposition as early as 4 months after their inoculation, thus suggesting the long resilience—at least, up to 6 months— of the contaminating forms of A $\beta$  [23]. This means that exogenous A $\beta$  seeds from transgenic mice can remain in the brain at levels below routine detection, retain their pathogenicity in A $\beta$ PP null mice, i.e. in the absence of replication, and therefore have extreme longevity. Unlike this latter study, our experiment was based on the inoculation of human (and not mouse) brain extracts. We speculate that the pathology developed in the APP<sub>swe</sub>/PS1<sub>dE9</sub> mice may reflect a dual process based on the resilience of initial seeds and/or on the nucleation of the A $\beta$  from the huAPP<sub>wt</sub> mice. Congophilic plaques were however not modulated by the inoculation of AD-huAPP<sub>wt</sub> brain extracts. In any case, this study shows that very small amounts of A $\beta$  seeds presumably issued from the human brain samples are able to induce an A $\beta$  pathology. Nonetheless, the limitations of some ELISA kits to detect very low amounts of A $\beta$  peptide are pointed out by some authors. We cannot rule out that A $\beta$  would have been detected with more sensitive tools as Simoa technology. Unfortunately, we did not have any sample left to test this hypothesis. Based on our data, it is reasonable to suggest that soluble forms of A $\beta$  can act as seeds that are able to induce A $\beta$  aggregation in recipient hosts. This is consistent with previous data showing that supernatant from full brain extracts have a strong ability to induce A $\beta$  aggregation while containing only low level (0.05%) of the brain A $\beta$  pool [12].

Aside from sporadic and genetic forms of AD, iatrogenic transmissions are “new” ways to transmit an AD-related amyloid pathology. These iatrogenic transmissions can be based on surgical procedures and/or inoculation of cadaver brain extracted hormones. Elucidating the risk factors is critical to organize prevention procedures. Here, we outline that even small amounts or undetectable A $\beta$  seeds can induce A $\beta$  deposits in a recipient host. Previous studies have recommended the systematic use of prion diseases preventive measures in neurosurgery and the exclusion of patients with AD from donor programs. Since, as suggested by our results, A $\beta$  deposit-negative samples can also induce A $\beta$  pathology, it may be useful to also recommend prudence with samples from donors who could present unsuspected A $\beta$  deposits.

#### Acknowledgements

The project was funded by France-Alzheimer and Vaincre Alzheimer associations as well as the CEA bottom-up program. It was performed in a core facility supported by/member of NeurATRIS - ANR-11-INBS-0011. We thank the donors and the Brain Donation Program of the “The Brainbank Neuro-CEB Neuropathology Network” run by a consortium of Patient Associations: ARSLA

(association for research on amyotrophic lateral sclerosis), CSC (cerebellar ataxias), Fondation ARSEP (association for research on multiple sclerosis), France DFT (fronto-temporal dementia), Fondation Vaincre Alzheimer, France Parkinson, with the support of Fondation Plan Alzheimer and IHU A-ICM for providing the brain samples used in this study.

The Neuro-CEB Neuropathology network includes: Dr Franck Letournel (CHU Angers), Dr Marie-Laure Martin-Négrier (CHU Bordeaux), Dr Maxime Faisant (CHU Caen), Pr Catherine Godfraind (CHU Clermont-Ferrand), Pr Claude-Alain Maurage (CHU Lille), Dr Vincent Deramecourt (CHU Lille), Dr Mathilde Duchesne (CHU Limoges), Dr David Meyronnet (CHU Lyon), Dr André Maudes de Paula (CHU Marseille), Pr Valérie Rigau (CHU Montpellier), Dr Fanny Vandenbos-Burel (Nice), Pr Charles Duyckaerts (CHU PS Paris), Pr Danielle Seilhean (CHU PS, Paris), Dr Susana Boluda (CHU PS, Paris), Dr Isabelle Plu (CHU PS, Paris), Dr Serge Milin (CHU Poitiers), Dr Dan Christian Chiforeanu (CHU Rennes), Pr Annie Laquerrière (CHU Rouen), Dr Béatrice Lannes (CHU Strasbourg).

#### Author contributions

Ch.G., F.P., and M.D. contributed to the study conception and design. N.N.N. provided the human brain samples. N.N.N., A.S.H., S.B. and Ch.G. characterized the human brain samples. Ch.G., C.I.G., M.G., S.L. performed the inoculations in mice. A.S.H., F.P., S.L. designed and performed the immunohistological analysis in animals. A.S.H., C.I.G. performed biochemical analysis in mice. A.S.H. and M.D. wrote the manuscript. All authors commented on previous versions of the manuscript. All authors read and approved the final manuscript.

#### Conflict of interest

The authors declare no conflict of interest.

#### Author details

<sup>1</sup> Laboratoire des Maladies Neurodégénératives, Université Paris-Saclay, CEA, CNRS, 18 Route du Panorama, 92265 Fontenay-aux-Roses, France. <sup>2</sup> Molecular Imaging Research Center, CEA, 18 Route du Panorama, 92265 Fontenay-aux-Roses, France. <sup>3</sup> Paris Brain Institute, Alzheimer’s and Prion Diseases Team, CNRS, UMR 7225, INSERM 1127, Sorbonne University UMR75, Paris, France. <sup>4</sup> Laboratoire Neuropathologie Raymond Escourrolle, Pitié, APHP, Salpêtrière Hospital, Sorbonne University, 47, Blvd l’Hôpital, 75651 Paris Cedex 13, Paris, France. <sup>5</sup> Neuro-CEB Neuropathology Network Network: Plate-Forme de Ressources Biologiques, Bâtiment Roger Baillet, Hôpital de la Pitié-Salpêtrière, 47-83 boulevard de l’Hôpital, 75651 Paris Cedex 13, France.

Received: 7 October 2020 Accepted: 15 November 2020

Published online: 30 November 2020

#### References

- Banerjee G, Adams ME, Jaunmuktane Z, Lammie GA, Turner B, Wani M, Sawhney IMS, Houlden H, Mead S, Brandner S, Werring DJ (2019) Early onset cerebral amyloid angiopathy following childhood exposure to cadaveric dura. *Ann Neurol* 85:284–290. <https://doi.org/10.1002/ana.25407>
- Duran-Aniotz C, Morales R, Moreno-Gonzalez I, Hu PP, Soto C (2013) Brains from non-Alzheimer’s individuals containing amyloid deposits accelerate Abeta deposition in vivo. *Acta Neuropathol Commun* 1:76. <https://doi.org/10.1186/2051-5960-1-76>
- Duyckaerts C, Sazdovitch V, Ando K, Seilhean D, Privat N, Yilmaz Z, Peckeu L, Amar E, Comoy E, Maceski A, Lehmann S, Brion JP, Brandel JP, Haik S (2018) Neuropathology of iatrogenic Creutzfeldt-Jakob disease and immunoassay of French cadaver-sourced growth hormone batches suggest possible transmission of tauopathy and long incubation periods for the transmission of Abeta pathology. *Acta Neuropathol* 135:201–212. <https://doi.org/10.1007/s00401-017-1791-x>
- Garcia-Alloza M, Robbins EM, Zhang-Nunes SX, Purcell SM, Betensky RA, Raju S, Prada C, Greenberg SM, Bacskai BJ, Frosch MP (2006) Characterization of amyloid deposition in the APP<sub>swe</sub>/PS1<sub>dE9</sub> mouse model of Alzheimer disease. *Neurobiol Dis* 24:516–524. <https://doi.org/10.1016/j.nbd.2006.08.017>
- Gary C, Lam S, Herard AS, Koch JE, Petit F, Gipchtein P, Sawiak SJ, Caillierez R, Eddarkaoui S, Colin M, Aujard F, Deslys JP, Network FN, Brouillet E, Buée L, Comoy EE, Pifferi F, Picq J-L, Dhenain M (2019) Encephalopathy induced

- by Alzheimer brain inoculation in a non-human primate. *Acta Neuropathol Commun*. <https://doi.org/10.1186/s40478-019-0771-x>
6. Gibson PH (1986) Distributions of amyloid plaques in four regions of the brains of mice infected with scrapie by intracerebral and intraperitoneal routes of injection. *Acta Neuropathol* 69:322–325. <https://doi.org/10.1007/BF00688311>
  7. Hamaguchi T, Eisele YS, Varvel NH, Lamb BT, Walker LC, Jucker M (2012) The presence of Abeta seeds, and not age per se, is critical to the initiation of Abeta deposition in the brain. *Acta Neuropathol* 123:31–37. <https://doi.org/10.1007/s00401-011-0912-1>
  8. Herve D, Porche M, Cabrejo L, Guidoux C, Tournier-Lasserre E, Nicolas G, Adle-Biasset H, Plu J, Chabriat H, Duyckaerts C (2018) Fatal Abeta cerebral amyloid angiopathy 4 decades after a dural graft at the age of 2 years. *Acta Neuropathol* 135:801–803. <https://doi.org/10.1007/s00401-018-1828-9>
  9. Jaunmuktane Z, Mead S, Ellis M, Wadsworth JD, Nicoll AJ, Kenny J, Launchbury F, Linehan J, Richard-Loendt A, Walker AS, Rudge P, Collinge J, Brandner S (2015) Evidence for human transmission of amyloid-beta pathology and cerebral amyloid angiopathy. *Nature* 525:247–250. <https://doi.org/10.1038/nature15369>
  10. Jaunmuktane Z, Quaegebeur A, Taipal R, Viana-Baptista M, Barbosa R, Koriath C, Scot R, Mead S, Brandner S (2018) Evidence of amyloid-beta cerebral amyloid angiopathy transmission through neurosurgery. *Acta Neuropathol* 135:671–679. <https://doi.org/10.1007/s00401-018-1822-2>
  11. Kane MD, Lipinski WJ, Callahan MJ, Bian F, Durham RA, Schwarz RD, Roher AE, Walker LC (2000) Evidence for seeding of beta-amyloid by intracerebral infusion of Alzheimer brain extracts in beta-amyloid precursor protein-transgenic mice. *J Neurosci* 20:3606–3611. <https://doi.org/10.1523/JNEUROSCI.20-10-03606.2000>
  12. Langer F, Eisele YS, Fritsch SK, Staufienbiel M, Walker LC, Jucker M (2011) Soluble Abeta seeds are potent inducers of cerebral beta-amyloid deposition. *J Neurosci* 31:14488–14495. <https://doi.org/10.1523/JNEUROSCI.3088-11.2011>
  13. Manson JC, Jamieson E, Baybutt H, Tuzi NL, Barron R, McConnell I, Somerville R, Ironside J, Will R, Sy MS, Melton DW, Hope J, Bostock C (1999) A single amino acid alteration (I01L) introduced into murine PrP dramatically alters incubation time of transmissible spongiform encephalopathy. *EMBO J* 18:6855–6864. <https://doi.org/10.1093/emboj/18.23.6855>
  14. Meyer-Luehmann M, Coomaraswamy J, Bolmont T, Kaeser S, Schaefer C, Kilger E, Neuenschwander A, Abramowski D, Frey P, Jaton AL, Vigouret JM, Paganetti P, Walsh DM, Mathews PM, Ghiso J, Staufienbiel M, Walker LC, Jucker M (2006) Exogenous induction of cerebral beta-amyloidogenesis is governed by agent and host. *Science* 313:1781–1784. <https://doi.org/10.1126/science.1131864>
  15. Morales R, Duran-Aniotz C, Castilla J, Estrada LD, Soto C (2012) De novo induction of amyloid-beta deposition in vivo. *Mol Psychiatry* 17:1347–1353. <https://doi.org/10.1038/mp.2011.120>
  16. Mucke L, Masliah E, Yu GQ, Mallory M, Rockenstein EM, Tatsuno G, Hu K, Kholodenko D, Johnson-Wood K, McConlogue L (2000) High-level neuronal expression of abeta 1-42 in wild-type human amyloid protein precursor transgenic mice: synaptotoxicity without plaque formation. *J Neurosci* 20:4050–4058. <https://doi.org/10.1523/JNEUROSCI.20-11-04050.2000>
  17. Paxinos G, Franklin KBJ (2001) *The mouse brain in stereotaxic coordinates*. Academic Press, Cambridge
  18. Schneider CA, Rasband WS, Eliceiri KW (2012) NIH Image to ImageJ: 25 years of image analysis. *Nat Methods* 9:671–675. <https://doi.org/10.1038/nmeth.2089>
  19. Stohr J, Condello C, Watts JC, Bloch L, Oehler A, Nick M, DeArmond SJ, Giles K, DeGrado WF, Prusiner SB (2014) Distinct synthetic Abeta prion strains producing different amyloid deposits in bigenic mice. *Proc Natl Acad Sci USA* 111:10329–10334. <https://doi.org/10.1073/pnas.1408968111>
  20. Stohr J, Watts JC, Mensinger ZL, Oehler A, Grillo SK, Dearmond SJ, Prusiner SB, Giles K (2012) Purified and synthetic Alzheimer's amyloid beta (Abeta) prions. *Proc Natl Acad Sci USA* 109:11025–11030. <https://doi.org/10.1073/pnas.1206555109>
  21. Watts JC, Condello C, Stohr J, Oehler A, Lee J, DeArmond SJ, Lannfelt L, Ingelsson M, Giles K, Prusiner SB (2014) Serial propagation of distinct strains of Abeta prions from Alzheimer's disease patients. *Proc Natl Acad Sci USA* 111:10323–10328. <https://doi.org/10.1073/pnas.1408900111>
  22. Watts JC, Giles K, Grillo SK, Lemus A, DeArmond SJ, Prusiner SB (2011) Bioluminescence imaging of Abeta deposition in bigenic mouse models of Alzheimer's disease. *Proc Natl Acad Sci USA* 108:2528–2533. <https://doi.org/10.1073/pnas.1019034108>
  23. Ye L, Fritsch SK, Schelle J, Obermuller U, Degenhardt K, Kaeser SA, Eisele YS, Walker LC, Baumann F, Staufienbiel M, Jucker M (2015) Persistence of Abeta seeds in APP null mouse brain. *Nat Neurosci* 18:1559–1561. <https://doi.org/10.1038/nn.4117>

## Publisher's Note

Springer Nature remains neutral with regard to jurisdictional claims in published maps and institutional affiliations.

Ready to submit your research? Choose BMC and benefit from:

- fast, convenient online submission
- thorough peer review by experienced researchers in your field
- rapid publication on acceptance
- support for research data, including large and complex data types
- gold Open Access which fosters wider collaboration and increased citations
- maximum visibility for your research: over 100M website views per year

At BMC, research is always in progress.

Learn more [biomedcentral.com/submissions](https://biomedcentral.com/submissions)





## ANNEX II – SCIENTIFIC PRODUCTION

---

### Publications

**Lam S.**, Petit F., Hérard AS., Boluda S., Eddarkaoui S., Guillermier M., The Brain Bank Neuro-CEB Neuropathology Network, Buée L., Duyckaerts C., Haïk S., Picq J.L., Dhenain M. Transmission of amyloid-beta and tau pathologies is associated with cognitive impairments in a primate. *Acta Neuropathologica Communications* 9: 165 (2021). <https://doi.org/10.1186/s40478-021-01266-8>.

**Lam S.**, Boluda S. Hérard AS. Petit F., Eddarkaoui S., Cambon K., The Brainbank Neuro-CEB Neuropathology Network, Picq JL., Buée L., Duyckaerts C., Haïk S., Dhenain M. Cognitive, synaptic and neuropathological changes in Alzheimer’s brain-inoculated mice. Submitted & Available on BioRxiv: <https://www.biorxiv.org/content/10.1101/2021.04.06.438654v1>.

Hérard AS., Petit F., Gary C., Guillermier M., Boluda S., Garin C., **Lam S.**, Dhenain M. Induction of amyloid- $\beta$  deposits from serially transmitted, histologically silent, A $\beta$  seeds issued from human brains. *Acta Neuropathologica Communications*. 30;8(1):205 (2020). <https://doi.org/10.1186/s40478-020-01081-7>.

Gary C., **Lam S.**\*, Hérard A.S.\*, Koch J.E., Petit F., Gipchtein P., Sawiak S.J., Caillierez R., Eddarkaoui S., Colin M., Aujard F., Deslys J.P., French Neuropathology Network, Brouillet E., Buée L., Comoy E.E., Pifferi F.\*, Picq J-L\*, Dhenain M. Encephalopathy induced by Alzheimer brain inoculation in a non-human primate. *Acta Neuropathologica Communications*. 7: 126 (2019). <https://doi.org/10.1186/s40478-019-0771-x>.

### Posters

**Lam S.**, Stimmer L., Boluda S., Hérard AS., Petit F., Duyckaerts C., Delatour B., Haïk S., Dhenain M. Evaluation of Alzheimer’s disease heterogeneity through human brain inoculations in a mouse model of amyloid and tau lesions. The 15th International Conference on Alzheimer’s & Parkinson’s Diseases. March 2021.

**Lam S.**, Boluda S., Hérard AS., Petit F., Eddarkaoui S., Canbon K., Picq JL., Buée L., Duyckaerts C., Haïk S., Dhenain M. Tau-seeded pathology induced by human brain inoculation in a mouse model of amyloidosis is the main culprit for synaptic and cognitive deficits. The Brain Conference. March 2021.

**Lam S.**, Boluda S., Hérard AS., Petit F., Duyckaerts C., Delatour B., Haïk S., Dhenain M. Heterogeneity of Alzheimer’s disease: Insight from a novel mouse model of amyloid and tau lesions based on human brain inoculations. Alzheimer’s Association International Conference. July 2020.



Dhenain M., **Lam S.**, Gary C., Herard AS., Koch JE., Petit F., Gipchtein P., Sawiak SJ, Caillierez R., Eddarkaoui S., Colin M., Aujard F., Deslys JP., French Neuropathology Network, Brouillet E., Buée L., Comoy EE., Pifferi F., Picq JL. Iatrogenic transmission of Alzheimer's disease: Evidence based on experimental inoculation of Alzheimer's brains into a primate. Alzheimer's Association International Conference. July 2020.

### **Invited oral communications**

**Lam S.**, Boluda S., Hérard A.-S., Petit F., Duyckaerts C., Haïk S., Dhenain M. Hétérogénéité de la maladie d'Alzheimer: étude dans un nouveau modèle murin d'amyloïdose et de tauopathie induites par inoculation de cerveau humain. Société Française de Neuropathologie. January 2020. Paris.

Dhenain M., Gary C., **Lam S.**, Herard AS., Koch JE., Petit F., Gipchtein P., Sawiak SJ., Caillierez R., Eddarkaoui S., Colin M., Aujard F., Deslys JP., French Neuropathology Network, Brouillet E., Buée L., Comoy EE., Pifferi F., Picq JL. Transmission iatrogène de la maladie d'Alzheimer: Eléments de preuves basés sur l'inoculation expérimentale de cerveaux Alzheimer à un primate. Société Française de Neuropathologie. January 2020. Paris.

Gary C., **Lam S.**, Herard A.S., Koch J. E., Petit F., Gipchtein P., Sawiak S., Caillierez R., Eddarkaoui S., Colin M., Aujard F., Deslys J.P., French Neuropathology Network, Brouillet E., Buée L., Comoy E.E., Pifferi F., Picq J-L., Dhenain M. Transmission of cerebral lesions and of a neurodegenerative process by Alzheimer brains. Séminaire du Grenoble Institute of Neuroscience. December 2019.

Gary C., **Lam S.\***, Herard A.S.\*, Koch J.E., Petit F., Gipchtein P., Sawiak S.J., Caillierez R., Eddarkaoui S., Colin M., Aujard F., Deslys J.P., French Neuropathology Network, Brouillet E., Buée L., Comoy E.E., Pifferi F.\*, Picq J-L\*, Dhenain M. Transmission of cerebral lesions and of a neurodegenerative process by Alzheimer brains. Séminaire annuel 2019 des programmes transversaux de compétences et du programme exploratoire Bottom-Up du CEA. November 2019. Grenoble.

Gary C., **Lam S.\***, Herard A.S.\*, Koch J.E., Petit F., Gipchtein P., Sawiak S.J., Caillierez R., Eddarkaoui S., Colin M., Aujard F., Deslys J.P., French Neuropathology Network, Brouillet E., Buée L., Comoy E.E., Pifferi F.\*, Picq J-L\*, Dhenain M. Transmission of cerebral lesions and of a neurodegenerative process by Alzheimer brains. 8èmes rencontres de la Fondation Alzheimer. November 2019. Paris

## ANNEX III – ABSTRACT

---

La maladie d'Alzheimer (MA) se caractérise par l'agrégation intracérébrale de protéines  $\beta$ -amyloïde (A $\beta$ ) et tau mal conformées, ainsi que par des processus neuroinflammatoires et neurodégénératifs menant à des troubles cognitifs. Des études observationnelles réalisées chez l'Homme suggèrent que les pathologies A $\beta$  et tau sont transmissibles de manière similaire aux maladies à prions, notamment à la suite d'une exposition iatrogène à des composants ou des outils chirurgicaux contaminés par des agrégats d'A $\beta$  et de tau (Duyckaerts et al., 2018; Jaunmuktane et al., 2021, 2015b). Expérimentalement, la démonstration d'une telle transmission a largement été mise en évidence chez des modèles rongeurs transgéniques surexprimant des gènes humains mutés, et après inoculation de protéines pathologiques d'origine synthétique ou dérivées d'échantillons cérébraux (Clavaguera et al., 2013; Iba et al., 2013; Meyer-Luehmann et al., 2006; Stöhr et al., 2012). Ces modèles représentent des outils intéressants pour mieux comprendre la physiopathologie de la MA et caractériser les mécanismes impliqués dans le développement et la progression des lésions de la MA. Cependant, les impacts fonctionnels et neuronaux associés à la transmission des pathologies A $\beta$  et tau, ainsi que les relations entre ces marqueurs de la MA demeurent mal connus.

Le premier objectif de cette thèse a été d'étudier les relations entre les lésions de la MA dans un modèle murin bien caractérisé, produisant des niveaux élevés d'A $\beta$  et exprimant des niveaux physiologiques de la protéine tau murine endogène. Nous avons montré que l'inoculation intracérébrale d'extraits de cerveaux issus de patients atteints de la MA induit des pathologies A $\beta$  et tau dans ce modèle. L'inoculation d'extraits cérébraux issus de patients avec différentes formes sporadiques de la MA entraîne différents niveaux d'altérations cognitives associées à des pertes synaptiques. Ces atteintes synaptiques étaient corrélées avec la sévérité de la pathologie tau et avec une réduction de l'activité microgliale, soulignant ainsi leur contribution dans les processus neurodégénératifs associés à la MA et mettant en avant l'origine multifactorielle des déficits cognitifs.

A ce jour, de nombreuses questions subsistent concernant l'impact d'une transmission iatrogène des pathologies A $\beta$  et tau chez l'Homme. Le deuxième objectif de cette thèse a ainsi été d'évaluer les conséquences fonctionnelles, morphologiques et histopathologiques de l'inoculation d'extraits de cerveaux issus de patients atteints de la MA chez le primate

microcèbe (*Microcebus murinus*). Nous avons montré que cela induit une encéphalopathie caractérisée par des altérations cognitives, une atrophie cérébrale associée à une perte de neurones et des altérations de l'activité neuronale, en l'absence de pathologies A $\beta$  et tau marquées. Cette étude est la première à mettre en évidence des dysfonctions neuronales et cognitives suite à l'inoculation d'extraits de cerveaux MA chez un primate.

Le diagnostic de la MA repose sur la présence d'A $\beta$  et tau s'agrégant et se propageant de manière stéréotypée dans le cerveau. Ainsi, le troisième objectif de cette thèse a été d'évaluer chez le microcèbe l'impact lésionnel suite à l'inoculation d'extraits de cerveaux MA selon une nouvelle procédure visant à améliorer les potentiels de nucléation et de propagation des agrégats d'A $\beta$  et tau présents dans les échantillons. Cela a permis d'induire l'apparition systématique de dépôts A $\beta$  et tau à proximité du site d'injection, ainsi que leur propagation vers des régions interconnectées plus distantes. De plus, une altération progressive des performances cognitives et une atrophie cérébrale ont été rapportées. Ces résultats ont été répliqués avec deux types d'extraits de cerveaux MA. Cette étude est la première à mettre en évidence chez un primate la transmission de signes cliniques de la MA, tels que des troubles cognitifs et une atrophie du cerveau, ainsi que des lésions A $\beta$  et tau caractéristiques de la maladie. Ce travail renforce ainsi l'hypothèse d'une possible transmission des pathologies A $\beta$  et tau chez l'Homme et suggère qu'une telle transmission peut également être associée à des atteintes morphologiques et cognitives. Ces données appellent de ce fait au renforcement des mesures de décontamination préventives et à la surveillance des patients soumis à un risque de transmission iatrogène des pathologies A $\beta$  et tau. Enfin, nos données suggèrent que le microcèbe inoculé avec des extraits de cerveau MA est un modèle pertinent pour explorer la physiopathologie de la MA et pourrait permettre une meilleure translation des études de la préclinique vers la clinique.



**Titre :** Transmission de la pathologie Alzheimer à des modèles murins et primates : des protéinopathies aux atteintes neuronales et cognitives

**Mots clés :** maladie d'Alzheimer, transmission expérimentale, modèles animaux, primate,  $\beta$ -amyloïde, tau

**Résumé :** La maladie d'Alzheimer (MA) se caractérise par l'agrégation cérébrale de protéines  $\beta$ -amyloïde (A $\beta$ ) et tau mal conformées, ainsi que par des processus neuroinflammatoires et neurodégénératifs menant à des troubles cognitifs. Des études chez l'Homme et des modèles animaux suggèrent que les pathologies A $\beta$  et tau sont transmissibles de manière similaire aux prions. L'impact neuronal et cognitif de cette transmission et les relations entre les marqueurs de la MA sont mal connus. Ce travail étudie la transmission de la pathologie Alzheimer dans des modèles murins et primates après inoculation cérébrale d'extraits cérébraux de patients MA. Premièrement, nous avons montré que l'inoculation de cerveau Alzheimer dans un modèle murin d'amyloïdose entraîne des pathologies A $\beta$  et tau, une microgliose et dans certains cas, des atteintes synaptiques et cognitives. La perte synaptique et les troubles cognitifs étaient associés à la pathologie tau, à une réduction de l'activité microgliale et, de manière plus modérée, aux lésions A $\beta$ .

Ensuite, nous avons montré pour la première fois chez un primate que l'inoculation de cerveau Alzheimer entraîne des dépôts A $\beta$  et tau chez le microcèbe (*Microcebus murinus*), ainsi que des troubles cognitifs et fonctionnels, une atrophie cérébrale et une perte neuronale.

En conclusion, ces travaux montrent que les pathologies A $\beta$  et tau, des pertes synaptiques/neuronales et des signes cliniques majeurs peuvent être expérimentalement transmis à des modèles murins et primates. Ces modèles offrent de nouvelles opportunités pour caractériser la MA et explorer de nouveaux biomarqueurs et thérapies. De plus, nos données expérimentales soulignent l'impact potentiel d'une transmission des pathologies A $\beta$  et tau en matière de troubles cognitifs et d'atrophie cérébrale. L'évaluation systématique des biomarqueurs de la MA reflétant ces aspects de la pathologie chez des patients à risque de développer des lésions A $\beta$  et tau d'origine iatrogène devient ainsi indispensable.

**Title:** Transmission of Alzheimer pathology in murine and primate models: from proteinopathies to neuronal and cognitive impairments

**Keywords:** Alzheimer's disease, experimental transmission, animal models, primate,  $\beta$ -amyloid, tau

**Abstract:** Alzheimer's disease (AD) is characterized by the cerebral aggregation of misfolded  $\beta$ -amyloid (A $\beta$ ) and tau proteins, along with neuroinflammatory and neurodegenerative processes leading to cognitive deficits. Evidence in humans and animal models indicates that A $\beta$  and tau pathologies can be transmitted, in a manner akin to prion diseases. However, the neuronal and cognitive impacts of such transmission and the relationships between AD pathological hallmarks are still unclear. The current work evaluated the transmission of AD pathology in murine and primate models after the intracerebral inoculation of human AD brain extracts. First, we demonstrated that AD brain extract inoculation into an A $\beta$  plaque-bearing mouse model induces A $\beta$  pathology, Alzheimer-like tau-positive lesions, microgliosis and, in some animals, synaptic loss and cognitive deficits. Synaptic and cognitive impairments were associated with tau pathology, microglial activity

reduction and to a lesser extent with A $\beta$  deposition.

Then, we showed for the first time in a primate that AD brain inoculation induces widespread A $\beta$  and tau pathologies in mouse lemurs (*Microcebus murinus*). It also leads to cognitive and functional impairments, cerebral atrophy and neuronal loss.

In conclusion, our data show that both A $\beta$  and tau pathologies can be experimentally transmitted in murine models and in primates, along with synaptic/neuronal loss and significant clinical signs. These models offer new opportunities to characterize AD pathophysiology and explore new biomarkers and therapeutics. Additionally, our experimental data outline the possible impacts of A $\beta$  and tau transmissions in terms of cognitive impairments and cerebral atrophy. A systematic monitoring of AD biomarkers evaluating these aspects of the pathology in patients at risk of A $\beta$  and tau iatrogenic transmission is thus urgently needed.